

Cranfield University, Silsoe Campus

National Soil Resources Institute (NSRI) – Engineering

This thesis is submitted in fulfilment of the requirements for the
award of degree of Doctor of Engineering (EngD)

By

Kieron Eatough

Academic year – 2002

Tractive performance of 4x4 tyre treads on pure sand

Supervisor – Dr. James L. Brighton

Presented on 31st December 2002

ProQuest Number: 10832281

All rights reserved

INFORMATION TO ALL USERS

The quality of this reproduction is dependent upon the quality of the copy submitted.

In the unlikely event that the author did not send a complete manuscript and there are missing pages, these will be noted. Also, if material had to be removed, a note will indicate the deletion.



ProQuest 10832281

Published by ProQuest LLC (2018). Copyright of the Dissertation is held by Cranfield University.

All rights reserved.

This work is protected against unauthorized copying under Title 17, United States Code
Microform Edition © ProQuest LLC.

ProQuest LLC.
789 East Eisenhower Parkway
P.O. Box 1346
Ann Arbor, MI 48106 – 1346

Abstract

School: Cranfield University, Silsoe Campus, NSRI

Student: Kieron Eatough

Degree: Engineering Doctorate

Title: Tractive performance of 4x4 tyre treads on pure sand

This thesis examined the difficulties of generating traction from 4x4 (light truck) tyres in pure sand conditions. Investigations conducted in the Cranfield University Soil Dynamics Laboratory measured the tractive performance of a range of production and prototype 4x4 tyre tread patterns to quantify the effect of tread features upon tractive performance. The investigation also quantified the amount of sand displacement instantaneously occurring beneath the tyre, by a novel application of radio frequency identification (RFID) technology, which determined sand displacements to an accuracy of ± 5.5 mm. A limited number of normal contact stress measurements were recorded using a TekScan normal pressure mapping system. This technology was employed in a new manner that allowed pressure distributions to be dynamically recorded on a deformable soil surface.

Models were developed or adapted to predict rolling resistance, gross thrust of a tyre and the gross thrust effect due to its tread. Net thrust was predicted from refined versions of equations developed by Bekker to predict gross thrust and rolling resistance. These were modified to account for dynamic tractive conditions. A new tread model proposed by the author produced a numerical representation of the gross thrust capability of a tread based on factors hypothesised to influence traction on loose sand. This allowed the development of a relationship between the features of the tread and its measured gross thrust improvement (relative to a plain tread tyre), from which a total relationship was developed. The tread features were also, in combination with the wheel slip, related to the sand displacements and net thrusts simultaneously achieved.

The sand displacement results indicated that the majority of the variation in displacement between the different treads occurred in the longitudinal (rearward) direction. This effect was influenced by the wheel slip, as increased slip caused greater displacements, so the differences between the treads were greater at higher slips. The treads that generated the highest relative displacements also derived the higher gross thrusts (up to +5% extra gross thrust compared to a plain tread), although at the higher slips this also caused increased sinkage. As sinkage increased, the rolling resistance increased at a faster rate than the gross thrust, and thus the net thrust reduced. To prevent this effect the wheel slip should be limited to a maximum of 20% at low forward speeds (approximately 5 km/h).

Current market forces dictate that the biggest benefit that tyre manufacturers could offer in desert market regions would be to optimise road-biased tyres to suit loose sand conditions. The modelling developed indicated that this could be achieved by maximising the number of lateral grooves (and thus lateral edges) featured on a tread, however care would have to be exercised so as not to compromise the necessary on-road capability. The models could also be used to quantifiably determine from a choice of possible tyre treads, the tread that would offer most traction on pure loose sand.

Acknowledgements

The author would like to thank the sponsors, in particular EPSRC, for their financial support, which enabled this work to be undertaken. The technical assistance and advice received from numerous people at Land Rover, Dunlop and Goodyear was important in the research achieving a successful outcome. Thanks are particularly due to John Kellett and Eddie Franklin of Land Rover who supported the project throughout and Ian Kemp of Dunlop who made a positive impact during uncertain times.

The support and guidance received from John Kilgour, Prof. Dick Godwin and Dr. Mike Hann and other academic staff at the Silsoe Campus has been very useful and welcome throughout the project. Particular thanks go to Dr. James Brighton for his thoughtful supervision, continuous support and considerable effort over the whole project.

Thanks are also due to the technical staff at the Silsoe Campus, especially Roy Newland and Tony Reynolds who assisted in conducting much of the experimental work, and who provided the benefit of their expertise on many instances. I am also grateful to the workshop staff for their support in producing, or repairing, numerous components, often at short notice, whilst always providing a sense of humour.

This research would not have been achieved without the assistance of Marcus Oliver. This came on many levels, from conducting experiments and manufacturing test equipment, to processing data and scrutinising results and ideas, all of this was appreciated. Thank you also for a continued friendship outside of work.

The most thanks must go to my fiancée Frances Tubb, who has provided continuous support and encouragement from the outset of the project, particularly during the most frustrating and challenging stages. A special thank you is also necessary for the continued support and understanding shown over most evenings and weekends during the final six months, which made this thesis possible.

Table of Contents

TABLE OF FIGURES	VII
TABLE OF PLATES	XIV
TABLE OF TABLES	XVI
LIST OF SYMBOLS.....	XVII
LIST OF ABBREVIATIONS	XX
1 INTRODUCTION	1
2 AIM AND OBJECTIVES	5
2.1 AIM.....	5
2.2 OBJECTIVES	5
2.3 PROJECT METHODOLOGY	6
3 LITERATURE REVIEW	7
3.1 INTRODUCTION.....	7
3.2 BASIC TYRE EVALUATION.....	8
3.2.1 Basic Tyre Relationships.....	8
3.2.2 Features of a Sand Tyre.....	10
3.2.3 Implications of the Engineering Features of Desert Sand.....	13
3.2.4 Tyre Evaluation Using Slip-Pull Curves.....	14
3.2.5 Indications from a Simple Off-Road Tyre Field Investigation.....	16
3.3 MEASUREMENT OF SOIL (SAND) DISTURBANCE.....	16
3.3.1 Glass Sided Tanks and Visible Markers	17
3.3.1.1 <i>Paints, dyes, films and layers</i>	19
3.3.2 Particles Inserted in a Soil Profile.....	19
3.3.2.1 <i>Metal detection</i>	21
3.3.3 RFID Technology	22
3.3.4 The Implications of Other Sand Flow Investigations	23
3.4 PRESSURE/ STRESS SENSING	24
3.4.1 Pressure/ Stress Sensing from the Sand (Soil).....	24
3.4.2 Pressure/ Stress Sensing from the Tyre.....	25
3.4.2.1 <i>Pressure cells in/ on the tyre tread</i>	25
3.4.2.2 <i>Conductive rubber</i>	29
3.4.2.3 <i>TekScan pressure sensing system</i>	30
3.4.3 Findings of Oida <i>et al.</i>	31
3.5 TRACTION MODELS.....	34
3.5.1 Analytical Models.....	34
3.5.2 Empirical Models.....	34
3.5.3 Semi-Empirical Models.....	37

3.5.3.1	<i>Prediction of tractive pull</i>	39
3.5.3.2	<i>Derivation of the soil deformation modulus (K)</i>	40
3.5.3.3	<i>Contact area prediction</i>	42
3.5.3.4	<i>Other thrust prediction methods</i>	45
3.5.3.5	<i>Prediction of rolling resistance</i>	46
3.5.3.6	<i>An analysis of 4x4 performance on sand</i>	47
3.5.3.7	<i>Bekker's prediction for wheeled and tracked vehicles (from Wong)</i>	50
3.5.4	Finite Element Mathematical Models.....	53
3.6	TYRE TEST RIGS.....	55
3.6.1	Fixed Slip Test Rigs.....	55
3.6.2	Variable Slip Test Rigs.....	55
3.7	SUMMARY OF LITERATURE REVIEW.....	57
4	MARKET SURVEY AND REVIEW	59
4.1	MARKET SURVEY METHODOLOGY.....	59
4.2	MARKET SURVEY RESULTS.....	60
4.2.1	The Profile of Prospective Purchasers of Off-road Tyres.....	61
4.2.2	Properties Identified as Important for Off-road Tyres.....	62
4.2.3	Respondents' Perceptions of Tyre Brands.....	64
4.2.4	Likelihood of Purchasing Secondary Performance Off-Road Tyres.....	65
4.2.5	Interest in Automatic Central Tyre Inflation Systems (CTIS).....	65
4.3	IMPLICATIONS OF THE MARKET SURVEY RESULTS.....	65
5	TRACTION SURFACE EVALUATION	68
5.1	SOIL ASSESSMENT.....	68
5.1.1	Determination of <i>K</i> (Soil Deformation Modulus).....	70
5.1.2	Determination of Bekker Plate Sinkage Values.....	71
5.1.3	Comparison of the Experimental Soil Preparations.....	72
5.2	SAND COMPARISON ANALYSIS.....	78
5.3	ANALYSIS OF THE DA80F SAND.....	84
5.3.1	Determination of <i>K</i> (Sand Deformation Modulus).....	85
5.3.2	Determination of Bekker Plate Sinkage Values.....	86
6	TYRE EVALUATION APPARATUS AND METHODOLOGY	87
6.1	THE SOIL DYNAMICS LABORATORY (SDL).....	87
6.2	TEST TYRES.....	88
6.3	FIXED SLIP TEST RIG.....	90
6.3.1	Design of the Fixed Slip System.....	90
6.3.2	Derivation of Tractive Forces.....	94
6.3.2.1	<i>Free-rolling rolling resistance</i>	94
6.3.2.2	<i>Gross thrust, net thrust and rolling resistance</i>	94
6.3.3	Test Rig Instrumentation.....	95
6.3.3.1	<i>EORT calibration</i>	97

6.3.3.2	<i>Tension link calibration</i>	98
6.3.3.3	<i>LVDT (sinkage) calibration</i>	99
6.3.3.4	<i>Tacho-generator (fifth wheel) calibration</i>	99
6.3.3.5	<i>Rotary encoder (wheel speed) calibration</i>	100
6.4	FIXED SLIP TESTS ON SOIL	102
6.4.1	Treatments Investigated	102
6.4.2	Experimental Results	103
6.4.2.1	<i>Effect of inflation pressure</i>	104
6.4.2.2	<i>Effect of soil bulk density</i>	105
6.4.2.3	<i>Effect of tread pattern</i>	109
6.4.3	Summary of Results	110
6.5	FIXED SLIP TESTS ON SAND	111
6.5.1	Experimental Results	112
6.5.2	Fluctuations within the Traction Results.....	115
6.5.3	Limitations of the Fixed Slip System.....	118
6.6	THE VARIABLE SLIP TEST RIG	119
6.6.1	Operating Characteristics of the Variable Slip Rig	121
6.7	COMPARISON (VERIFICATION) TESTS ON SOIL	123
6.7.1	Variable Slip Test Results	124
6.7.2	Methodology for Test Rig Performance Comparisons	126
6.7.3	Test Rig Comparison Results	128
6.8	COMPARISON (VERIFICATION) TESTS ON SAND	130
6.8.1	Variable Slip Test Results	130
6.8.2	Test Rig Comparison Results	132
6.9	A FULL VEHICLE TEST ON SAND	134
7	SAND FLOW MEASUREMENT APPARATUS AND METHODOLOGY . 137	
7.1	SAND AND RFID TAG DISPLACEMENT ASSESSMENT	137
7.1.1	Bench Sand Flow Evaluations.....	137
7.1.1.1	<i>RFID Tag and sand flow assessment methodology</i>	137
7.1.1.2	<i>Tag/ sand flow assessment results</i>	139
7.2	FULL SIZE SAND DISPLACEMENT MEASUREMENT RIGS	141
7.2.1	Tag Position Placement.....	141
7.2.2	Tag Position Location	147
7.2.3	Tag Position Measurement Apparatus	147
7.2.4	Accuracy and Repeatability of Tag Placement and Measurement	153
7.3	POSITION OF THE TAG GRID IN THE THRUST (SLIP) CYCLE	157
7.4	VERIFICATION OF THE SUITABILITY OF THE TEKSCAN SYSTEM 158	
7.4.1	6911 mat.....	159
7.4.2	5051 mat.....	160
7.4.3	6300 mat.....	162

7.4.4	TekScan Measurement Capabilities.....	163
7.4.5	Attachment of the TekScan Mats to the Tyres	163
8	INVESTIGATION OF NORMAL STRESSES UNDER TYRES	167
8.1	EXPERIMENTAL TREATMENTS	167
8.2	PRESSURE MEASUREMENT RESULTS	167
8.2.1	Pressure Map Construction Procedure	167
8.2.2	Experimental Results	169
8.2.2.1	Plain tread (PT)	169
8.2.2.2	Lateral tread (LAT)	170
8.2.2.3	Longitudinal tread (LON).....	171
8.2.2.4	45° Backward facing tread (45B).....	171
8.3	DISCUSSION OF THE RESULTS	172
9	SAND DISPLACEMENT INVESTIGATION	174
9.1	TEST TREATMENTS.....	174
9.2	SAND DISPLACEMENT TEST RESULTS.....	175
9.2.1	Horizontal Net Thrust Results	176
9.2.2	Wheel Slip and Wheel Sinkage Results	178
9.2.3	Longitudinal (X-axis) Displacements	180
9.2.4	Lateral (Y-axis) Displacements	185
9.2.5	Vertical (Z-axis) Displacements.....	189
9.2.6	Peak Net Thrusts.....	193
9.3	ROLLING RESISTANCE TESTS.....	194
9.4	SUMMARY OF THE RESULTS	195
9.4.1	Combined Sand Displacements	195
9.4.2	Tread Effects.....	198
9.4.3	Tyre Body (Carcass) Effects	199
10	MODELLING OF SAND – TYRE INTERACTION.....	201
10.1	VARIABLES REQUIRING TRACTION MODELLING	201
10.2	MODEL FORMATION.....	202
10.2.1	Gross Thrust	202
10.2.2	Rolling Resistance	206
10.2.3	Mathematical Description of the Tyre Treads.....	208
10.2.4	Calculation of the Volume of Sand Flow.....	210
10.3	PROOF OF THE MODEL COMPONENTS.....	211
10.3.1	Rolling Resistance	211
10.3.2	Gross Thrust – Tyre Effects	213
10.3.3	Gross Thrust – Tread Effects.....	214
10.3.4	Volume of Displaced Sand.....	219
10.4	THRUST COMPONENTS DURING THE SAND DISPLACEMENTS	220

10.5	APPLICATION OF THE NET THRUST MODEL.....	222
10.6	RELATIONSHIP OF THE NET THRUST MODEL COMPONENTS	226
10.6.1	Thrust – Slip Relationships and Sand Displacement Results.....	229
10.7	TREAD EFFECTS, GROSS THRUSTS AND DISPLACEMENTS	230
10.8	APPLICATION OF THE MODELLING TO PRODUCTION TREADS... ..	232
10.8.1	235/70 R16 Treads.....	232
10.8.2	255/55 R19 Treads.....	237
10.9	IMPROVEMENT OF THE TREAD FACTOR MODEL	241
10.10	PERFORMANCE INDICATED BY THE MODELLING	242
11	DISCUSSION OF THE PROJECT FINDINGS	245
11.1	TEST EQUIPMENT AND METHODOLOGIES.....	245
11.1.1	Traction Test Rigs.....	245
11.1.2	Sand Displacement Assessment Methodology.....	246
11.2	MODELLING CAPABILITIES	247
11.3	TYRE PERFORMANCE.....	248
11.3.1	Cyclical Slip and Thrust Behaviour	248
11.3.2	Sand Displacements	249
11.3.3	Tread Effects.....	250
11.3.4	Contact Patch Pressure Distributions	252
11.3.5	Combination of the Effects Upon Performance.....	253
11.4	TYRE RECOMMENDATIONS AND IMPLICATIONS.....	255
12	CONCLUSION.....	259
12.1	TRACTION MODELLING	259
12.2	TYRE PERFORMANCE AND DESIGN IMPLICATIONS	260
12.3	NOVEL INVESTIGATIVE TECHNIQUES.....	261
13	FUTURE RECOMMENDATIONS.....	262
14	REFERENCES	264
	APPENDIX 1 – RFID TECHNOLOGY AND PRODUCTS	273
	APPENDIX 2 – TEKSCAN SYSTEM DATA AND INFORMATION.....	277
	APPENDIX 3 – MOTOR SHOW QUESTIONNAIRE – OCT. 1998.....	280
	APPENDIX 4 – TRANSLATIONAL SOIL SHEAR TEST RESULTS.....	285
	APPENDIX 5 – CALCULATION OF K (SOIL DEF. MODULUS)	286
	APPENDIX 6 – PLATE SINKAGE TESTS ON SOIL.....	292
	APPENDIX 7 – DENSITY AND MOISTURE CONTENT STATISTICS	300

APPENDIX 8 – CONE INDEX STATISTICS (SOIL)	309
APPENDIX 9 – SLED FRICTION ANOVA RESULTS	314
APPENDIX 10 – TRANSLATIONAL SAND SHEAR RESULTS	317
APPENDIX 11 – SAND DENSITY RESULTS	318
APPENDIX 12 – CONE INDEX STATISTICS (REPLICATE SAND)	319
APPENDIX 13 – CALCULATION OF K (SAND DEF. MODULUS).....	322
APPENDIX 14 – PLATE SINKAGE TESTS ON SAND	328
APPENDIX 15 – TEST RIG DRAWINGS	337
APPENDIX 16 – TEST RIG INSTRUMENTATION	340
APPENDIX 17 – PULSE COUNTER CIRCUIT (WHEEL SPEED)	341
APPENDIX 18 – VARIABLE SLIP RIG PERFORMANCE.....	342
APPENDIX 19 – MATHEMATICS OF THE MEASURING FRAME.....	344
APPENDIX 20 – TRIAL COLUMN INSERTION RESULTS	346
APPENDIX 21 – TRIAL GRID INSERTION RESULTS.....	349
APPENDIX 22 – TEKSCAN DATA SHEETS AND RESULTS.....	353
APPENDIX 23 – SAND DISPLACEMENT STATISTICS.....	357
APPENDIX 24 – MODELLING SPREADSHEETS	358
APPENDIX 25 – CALCULATION OF TREAD COEFFICIENTS.....	359
APPENDIX 26 – DISPLACED SAND VOLUMES.....	367
APPENDIX 27 – MODELLING NET THRUST RESULTS	368

Table of Figures

Figure 3.1 – The relative effect of seven tyre factors upon a 4x4 tyres ability to generate traction on desert sand, i.e. increased diameter is three times more effective than shoulder notches (Note: scores are relative, not percentages)	9
Figure 3.2 – Tyre performance requirements for 4x4 vehicles in five worldwide markets	11
Figure 3.3 – Tyres demonstrating sipes and shoulder notches	12
Figure 3.4 – Typical slip-pull curves generated by Goodyear from full vehicle tests of off-road tyres	14
Figure 3.5 – General slip-pull curves for illustration, from Wismer & Luth	15
Figure 3.6 – A circular three-axis stress transducer	27
Figure 3.7 – A normal pressure transducer	28
Figure 3.8 – A schematic of the combination stress transducer with sonic emitters	28
Figure 3.9 – Stress distributions along the tyre-soil contact surface at a sideslip angle of 20°; at 3 slips: — = -29.7%, - - - = 12.2%, - · - · - = 66.8%	32
Figure 3.10 – Distribution of thrust (+ ve) and rolling resistance (– ve) components along the contact surface at slips of 8.2% (left) and 53.5% (right) at 10° sideslip	33
Figure 3.11 – Variations in dynamic weight (W), thrust/ weight ratio (H/W) and rolling resistance/ weight ratio (R/W) with slip	33
Figure 3.12 – A typical plot of pressure (ρ) against sinkage (z) for 3 plate widths (b) from plate sinkage tests	38
Figure 3.13 – A diagram illustrating how soil deformation modulus, K , is determined.	40
Figure 3.14 – A diagram of the position of the forces acting on a driven wheel operating on soft terrain	43
Figure 3.15 – Forces, torque and stresses acting on a driven rigid wheel	45
Figure 3.16 – A graph of contact stress characteristics beneath a tyre on sand	48
Figure 3.17 – A diagram of the forces acting on a tractive tyre in sand	49
Figure 3.18 – A method for measuring compressive sand fracture	49
Figure 4.1 – The relative importance of five off-road tyre factors as indicated by off-road drivers	62
Figure 4.2 – The relative importance of five off-road tyre performance factors as indicated by off-road drivers	63
Figure 4.3 – Typical smooth (left) and chunky (right) treaded tyres	64
Figure 5.1 – Particle size distribution graphs for a number of global and local sand samples and a sandy loam soil	69
Figure 5.2 – The relationships between the contact area and K_I for the sandy loam soil under different normal tyre loads	70
Figure 5.3 – The soil densities achieved for the 1170 kg/m ³ soil preparations created during the fixed slip tests	73

Figure 5.4 – The soil densities achieved for the 1270 kg/m ³ soil preparations created during the fixed slip tests.....	73
Figure 5.5 – The soil densities achieved for the 1400 kg/m ³ soil preparations created during the fixed slip tests.....	74
Figure 5.6 – The moisture contents achieved for the 1170 kg/m ³ soil preparations created during the fixed slip tests	74
Figure 5.7 – The moisture contents achieved for the 1270 kg/m ³ soil preparations created during the fixed slip tests	75
Figure 5.8 – The moisture contents achieved for the 1400 kg/m ³ soil preparations created during the fixed slip tests	75
Figure 5.9 – Cone index readings recorded for different 1170 kg/m ³ soil bin preparations over the duration of all testing	77
Figure 5.10 – Cone index readings recorded for different 1270 kg/m ³ soil bin preparations over the duration of all testing	77
Figure 5.11 – Cone index readings recorded for different sand preparations in the soil bin over the duration of all testing	85
Figure 5.12 – The relationships between contact area and K_t for the DA80F sand under different normal tyre loads	86
Figure 6.1 – A schematic diagram of the layout of the fixed slip test rig	91
Figure 6.2 – The deflected sinkage of a wheel	96
Figure 6.3 – EORT calibration graph.....	97
Figure 6.4 – Tension link calibration graph	98
Figure 6.5 – LVDT calibration graph	99
Figure 6.6 – Tacho-generator calibration graph	100
Figure 6.7 – Rotary encoder calibration graph	101
Figure 6.8 – Gross and net forces generated by the plain tread tyre on 1170 kg/m ³ soil across a range of discrete slips and inflation pressures.....	104
Figure 6.9 – Rolling resistances and depths of sinkage generated by the plain tread tyre on 1170 kg/m ³ soil across a range of discrete slips and inflation pressures	105
Figure 6.10 – Gross and net forces generated by the plain tread tyre inflated to 1.10 bar across a range of discrete slips and soil preparations.....	106
Figure 6.11 – Rolling resistances and sinkage generated by the plain tread tyre inflated to 1.10 bar across a range of discrete slips and soil preparations.....	106
Figure 6.12 – Gross and net forces generated by the plain tread tyre inflated to 3.10 bar across a range of discrete slips and soil preparations.....	107
Figure 6.13 – Rolling resistances and sinkage generated by the plain tread tyre inflated to 3.10 bar across a range of discrete slips and soil preparations.....	108
Figure 6.14 – Gross and net forces generated on 1170 kg/m ³ soil across a range of discrete slips by six different tread pattern tyres inflated to 1.10 bar	109
Figure 6.15 – Rolling resistances and sinkage generated on 1170 kg/m ³ soil across a range of discrete slips by six different tread pattern tyres inflated to 1.10 bar	110

Figure 6.16 – Gross and net thrusts, rolling resistances and deflected sinkages generated by the PT tyre operating at 1.10 bar on sand	113
Figure 6.17 – Gross and net thrusts, rolling resistances and deflected sinkages generated by the G82 tyre operating at 1.10 bar on sand	114
Figure 6.18 – The PT tyre tractive performance when operated at an intended 10% slip (inflation pressure 1.10 bar and static normal load 632 kg) on sand	115
Figure 6.19 – PT tyre tractive performance when operated at a nominal 50% slip (inflation pressure 1.10 bar and static normal load 632 kg) on sand	116
Figure 6.20 – G82 tyre tractive performance when operated at a nominal 50% slip (inflation pressure 1.10 bar and static normal load 632 kg) on sand	116
Figure 6.21 – Two cycles of data generated by the G82 tread inflated to 1.10 bar with a 650 kg static normal load (as described in section 1.1.1)	122
Figure 6.22 – Typical results generated by the variable slip test rig operating the PT tyre inflated to 3.10 bar on 1170 kg/m ³ soil	125
Figure 6.23 – Typical regions of decreasing slip (indicated by lengths ‘X’)	127
Figure 6.24 – Comparative results for the net thrusts and sinkages generated by a PT tyre inflated to 3.10 bar operated on both the fixed and variable slip rigs across a slip range on 1170 kg/m ³ soil	129
Figure 6.25 – Comparative results for the net thrusts and sinkages generated by a PT tyre inflated to 3.10 bar operated on both the fixed and variable slip rigs across a slip range on 1270 kg/m ³ soil	129
Figure 6.26 – Traction data produced using the PT tread inflated to 1.10 bar and a static normal load of 650 kg on the variable slip test rig on sand	131
Figure 6.27 – Traction data produced using the G82 tread inflated to 1.10 bar and a static normal load of 650 kg on the variable slip test rig on sand	131
Figure 6.28 – Tractive performance traces from a full 4x4 vehicle test where the vehicle’s right side was operated on the sand surface	135
Figure 7.1 – The chosen tag grid positions in the sand profile (in mm)	142
Figure 7.2 – A schematic plan view of the tag placement equipment showing the location of the zero point	145
Figure 7.3 – The calibration graphs for the three drawstring transducers	149
Figure 7.4 – A schematic plan view of the tag location measurement equipment showing the location of the zero point (as per the placement frame) and the positive measurement axes	149
Figure 7.5 – A schematic plan and side view of the measuring frame showing the three drawstrings and the two triangles these created (soil bin and sand omitted)	151
Figure 7.6 – A schematic plan and side view of the measuring frame and the distances into which the drawstring lengths were transformed	151
Figure 7.7 – The positions of some of the tags during the assessment of the accuracy of the combined system	156
Figure 7.8 – The typical slips within the thrust/ slip cycle at which the three tag grids were positioned so as to be struck at three different slips	157

Figure 7.9 – The relationship between the contact area (white) and the 3 mm band of contact length (blue) over which the 6911 TekScan mat could potentially measure stress	159
Figure 7.10 – Mean normal stress distributions along the contact length as measured by the 6911 TekScan mat	160
Figure 7.11 – The relationship between the contact area (white) and the 112 mm band of contact length (blue) over which the 5051 mat measured stress	161
Figure 7.12 – Mean normal stress distributions along the contact length as measured by the 5051 TekScan mat	161
Figure 7.13 – Mean normal stress distributions along the contact length as measured by the 6300 TekScan mat	162
Figure 7.14 – The TekScan mat bonded to the LAT tread prior to rubber encapsulation	165
Figure 7.15 – The relative location of each TekScan mat in the 180 mm wide tread region of each of the six different treads.....	166
Figure 8.1 – Normal stresses recorded through the contact patch of the PT tread	169
Figure 8.2 – Normal stresses recorded through the contact patch of the LAT tread	170
Figure 8.3 – Normal stresses recorded through the contact patch of the LON tread....	171
Figure 8.4 – Normal stresses recorded through the contact patch of the 45B tread	172
Figure 9.1 – An illustration of typical tag displacements that occurred as the tag grids were struck at the three different slips (Note: the three positive axes of tag displacement, shown as X, Y and Z)	174
Figure 9.2 – Mean values of net thrust recorded at the three slip treatments for the six different treads	177
Figure 9.3 – Mean values of wheel slip recorded at the three slip treatments for the six different treads	178
Figure 9.4 – Mean values of deflected wheel sinkage recorded at the three slip treatments for the six different treads	179
Figure 9.5 – Mean tag displacements in the X direction across the grid for all tyre treads and slips (as viewed from beneath a tyre along the line of travel)	181
Figure 9.6 – Mean tag displacements in the X direction for tag positions across the grid for all treads at the three levels of slip (again viewed from beneath a tyre along the line of travel)	182
Figure 9.7 – Mean tag displacements in the X direction for tag depth levels down the grid for all treads at the three levels of slip (side view)	183
Figure 9.8 – Smoothed mean tag displacements in the X direction for all the grid locations and slips to allow comparison between the six treads (same viewpoint as previous figures).....	184
Figure 9.9 – A two-dimensional plot of mean tag displacements in the Y direction for all grid locations, treads and slips (viewed along the direction of wheel travel)	186
Figure 9.10 – Two-dimensional plots of mean tag displacements in the Y direction for all grid locations and treads at the three slips (viewed along direction of travel)	187

Figure 9.11 – Two-dimensional plots of mean tag displacements in the Y direction for all grid locations and slips for the six treads (viewed along direction of travel)	188
Figure 9.12 – A two-dimensional plot of mean tag displacements in the Z direction for all grid locations, treads and slips (viewed along the direction of wheel travel)	190
Figure 9.13 – Two-dimensional plots of mean tag displacements in the Z direction for all grid locations and treads at the three slips (viewed along direction of travel)	191
Figure 9.14 – Two-dimensional plots of mean tag displacements in the Z direction for all grid locations and slips for the six treads (viewed along direction of travel)	192
Figure 9.15 – Mean net thrusts derived from the three replicate tests of each tread, and associated mean values of slip and sinkage that occurred simultaneously	193
Figure 9.16 – The relationship between deflected wheel sinkage and rolling resistance across all treatments on sand	195
Figure 9.17 – The different sand profile displacement patterns that occurred	196
Figure 9.18 – A diagram showing how slip governed the void size left by the tyre and hence the sand's Y displacement as it re-filled the void.	197
Figure 10.1 – The derivation of the dynamic deflected wheel sinkage	203
Figure 10.2 – The relationship between contact length and vertical tyre acceleration.	204
Figure 10.3 – The relationship between contact width and vertical tyre acceleration.	205
Figure 10.4 – The relationship between tyre contact width and rut width.....	207
Figure 10.5 – A typical tread pattern identified with the variables used to determine its tread coefficient	209
Figure 10.6 – A representation of the methodology used to determine the volume of sand displacement	211
Figure 10.7 – A comparison of experimental rolling resistance results and predicted rolling resistance results	212
Figure 10.8 – A comparison between experimental and predicted gross thrust results for the plain tread tyre inflated to 1.10 bar operated on 1170 kg/m ³ soil.....	213
Figure 10.9 – Gross thrusts achieved by the PT tread during the displacement experiments.....	215
Figure 10.10 – Gross thrusts achieved by the LON tread during the displacement experiments.....	215
Figure 10.11 – Gross thrusts achieved by the 45F tread during the displacement experiments.....	216
Figure 10.12 – Gross thrusts achieved by the 45B tread during the displacement experiments.....	216
Figure 10.13 – Gross thrusts achieved by the LAT tread during the displacement experiments.....	217
Figure 10.14 – The relationship between tread coefficients and the percentage extra thrust that each tread was capable of generating over a plain tread tyre...	218

Figure 10.15 – Mean volumes of sand displaced at the eighteen slip and tyre treatments plotted with corresponding values of net thrust.....	219
Figure 10.16 – Gross thrust and rolling resistance data from the sand displacement experiments; treatments ordered by the magnitude of gross thrust	221
Figure 10.17 – Experimental net thrust results plotted against predicted net thrusts calculated for the PT tread.....	222
Figure 10.18 – Experimental net thrust results plotted against predicted net thrusts calculated for the LON tread	223
Figure 10.19 – Experimental net thrust results plotted against predicted net thrusts calculated for the 45F tread	223
Figure 10.20 – Experimental net thrust results plotted against predicted net thrusts calculated for the 45B tread.....	224
Figure 10.21 – Experimental net thrust results plotted against predicted net thrusts calculated for the LAT tread.....	224
Figure 10.22 – A comparison plot of experimental and predicted net thrust results	225
Figure 10.23 – A plot of experimental and predicted net thrusts for the PT tyre inflated to 1.10 bar operating on the 1170 kg/m ³ soil.....	226
Figure 10.24 – The components of the gross thrust prediction, based upon PT results recorded during the sand displacement experiments	227
Figure 10.25 – The relationships between sinkage and predictions of both the gross thrust and rolling resistance made using the PT experimental results	228
Figure 10.26 – Net thrusts produced by the combination of gross thrusts and rolling resistances, based upon PT results from the sand displacement experiments	229
Figure 10.27 – The relationship between the volume of sand displacement caused by the treads and the gross thrusts achieved	231
Figure 10.28 – The relationships between the tyre treads and the sand displacements	232
Figure 10.29 – Experimental net thrust results plotted against predicted net thrusts calculated for the G82 tread	234
Figure 10.30 – Experimental net thrust results plotted against predicted net thrusts calculated for the Wrangler HP tread.....	234
Figure 10.31 – Experimental net thrust results plotted against predicted net thrusts calculated for the Wrangler UG tread.....	235
Figure 10.32 – A comparison plot of experimental and predicted net thrust results for the production treads	236
Figure 10.33 – The relationships between the tyre treads and the sand displacements for all the treads.....	237
Figure 10.34 – Experimental net thrust results plotted against predicted net thrusts calculated for the Diamaris tread.....	238
Figure 10.35 – Experimental net thrust results plotted against predicted net thrusts calculated for the Wrangler HP (255) tread	239
Figure 10.36 – Experimental net thrust results plotted against predicted net thrusts calculated for the TG31 tread	239

Figure 10.37 – A comparison plot of experimental and predicted net thrust results for the production treads.....240

Figure 10.38 – The relationship between tread coefficient and percentage extra gross thrust relative to a PT tyre for all the tyres.....242

Table of Plates

Plate 1.1 – A photograph of an immobilised Land Rover Discovery in Dubai desert sand conditions	2
Plate 3.1 – The Goodyear G82 sand tyre.....	10
Plate 3.2 – Typical forward and rearward sand failure patterns beneath a narrow plain rigid wheel.....	17
Plate 3.3 – A soil profile with paint markers developed by Trein.....	20
Plate 3.4 – The handheld RFID scanner (a <i>Pocket Reader</i>) and a data tag used for the experiments (the tag's code is visible on the scanner's screen)	22
Plate 3.5 – A fully assembled SST.....	24
Plate 3.6 – Stress sensors mounted to the outside of a plain tread tyre.....	25
Plate 3.7 – An agricultural tyre mounted with diaphragm type pressure cells.....	26
Plate 3.8 – A TekScan pressure sensing system.....	30
Plate 3.9 – One side of a 5101 TekScan pressure sensitive mat showing the parallel horizontal piezo-electric gel lines.....	31
Plate 5.1 – The rubber bases of the sliding friction test sleds	81
Plate 6.1 – A rear view of the soil bin and processor unit (mounted with the variable slip single wheel tester)	87
Plate 6.2 – The three standard production tyres supplied	89
Plate 6.3 – Left: A comparison in diameter between the two G82 tyres supplied; Right: the laser cut 235/70 R16 G82 tread and a 235/70 R16 plain tread blank....	89
Plate 6.4 – The symmetrical hand cut tread designs; the forward (F) and backward (B) facing nomenclature was applied as if the tyres were rolling towards the reader.....	90
Plate 6.5 – The fixed slip test rig mounted to the soil processor operating on a firm sandy loam soil	92
Plate 6.6 – A view of the opposite side of the fixed slip test rig	93
Plate 6.7 – The rotary encoder, signal cables and cable storage drum mounted to the test rig	96
Plate 6.8 – A front view of the soil processor, diesel engine and sub-frame	120
Plate 6.9 – The new components fitted to create the hydraulically driven variable slip test rig.....	120
Plate 7.1 – The tank of sand to which dyed sand strips and then twenty data tags were added, together with a Ø12 mm tine that was used to disturb the sand....	138
Plate 7.2 – The flow patterns of dyed sand strips and tags after disturbance.....	139
Plate 7.3 – The flow patterns of dyed sand and tags after further excavation.....	140
Plate 7.4 – The location of the remaining tags and dyed sand	140
Plate 7.5 – The data tag placement frame	143
Plate 7.6 – The placement frame insertion bracket.....	144
Plate 7.7 – A plan view of the frame zero point on the tag measurement frame.....	145

Plate 7.8 – The data tag insertion process 146
Plate 7.9 – The tag position measurement frame positioned over a sand tank..... 148
Plate 7.10 – The three drawstring transducers mounted to the measuring frame..... 150

Table of Tables

Table 2.1 – The stages of the project methodology	6
Table 5.1 – Particle size analysis of the sandy loam soil	68
Table 5.2 – Average soil densities produced for the three soil preparations during the plate sinkage tests and appropriate dry base moisture contents	71
Table 5.3 – Bekker pressure sinkage coefficients for the three soil preparations	72
Table 5.4 – Mean soil density preparations and moisture contents	76
Table 5.5 – Descriptions of the assessed sand samples	79
Table 5.6 – Weightings used for sand ranking analysis	79
Table 5.7 – Results from the translational shear box tests	80
Table 5.8 – Results from the sliding sand-rubber friction tests.....	82
Table 5.9 – The weighted percentage differences of the local sand sample scores (relative to the Dubai sand)	83
Table 5.10 – Bekker pressure sinkage coefficients for the sand preparation	86
Table 6.1 – Fixed slip tests treatments investigated on the sandy loam soil (note: colour coding indicates the different groups of variables investigated)	102
Table 6.2 – The variables investigated in the fixed slip tests on the sand	112
Table 6.3 – The bands of slip that were used to produce mean values	127
Table 7.1 – The results from the carpenters square calibration measurements.....	154
Table 9.1 – The test variables for the sand displacement investigation for the prototype treads inflated to 1.10 bar	175
Table 9.2 – A sample section of the overall results table showing the experimental data and headings that were entered into Genstat	176
Table 9.3 – The treads grouped by the tractive performance variations they caused ...	180
Table 9.4 – The tractive performance trends produced by the different treads.....	199
Table 10.1 – Tread coefficients for the five prototype treads tested during the sand displacement experiment	210
Table 10.2 – Percentage extra gross thrust outputs that were achieved by the five prototype treads at 100mm sinkage	217
Table 10.3 – Tread factors determined for the five prototype treads.....	219
Table 10.4 – Tread coefficients and factors determined for the production treads	233
Table 10.5 – Tread coefficients and percentage extra gross thrusts achieved by the 255/55 R19 production treads.....	238
Table 10.6 – Tread coefficients and gross thrust benefits of the production treads	241

List of Symbols

This list details commonly used symbols used throughout the whole text. It does not include specific symbols from several equations detailed only in the literature review, which are listed with a full explanation of the relevant symbols, because different authors use conflicting symbols to represent the same set of variables.

<u>Symbol</u>	<u>Full Description</u>
\varnothing	Diameter
α	Gradient of tangent to shear stress / shear displacement curve
α	Terms from Bekker resistance prediction equations
α_e	Angle of the groove edge
δ	Tyre deflection
ε	Terms from Bekker resistance prediction equations
ϕ	Angle of internal shearing resistance
γ	Soil density
ρ	Normal pressure (stress) typically below a sinkage plate
ρ_{gcr}	Critical ground pressure
τ	Shear stress
ω	Angular velocity of the wheel
A	Contact area
a	Acceleration
A^D	Dynamic contact areas ($w^D \times l^D$)
b	Contact patch width
b	Minimum sinkage plate width
b_{tr}	Deflected tyre width
c	Cohesion
C	Cone Index
d	Tyre diameter
D	Undeflected tyre diameter
E_n	Edge number

<u>Symbol</u>	<u>Full Description</u>
G	Sand penetration resistance gradient
g	Acceleration due to gravity (9.81 m/s ²)
g'	Dynamic vertical load adjustment factor
G_{ey}	Revised sand penetration resistance gradient
G_n	Groove number
H	Thrust
h	Tyre section height (unloaded)
H_{max}	Maximum thrust
i	Slip
j	Shear deformation (displacement)
K	Soil deformation modulus
k_ϕ	Empirically measured Bekker soil deformation coefficient
k_c	Empirically measured Bekker soil deformation coefficient
K_e	Representation number for tyre carcass
K_{py}	Terms from Bekker resistance prediction equations
K_{pc}	Terms from Bekker resistance prediction equations
l	Contact patch (shear) length
l^D	Dynamic contact length
L_e	Length of groove edge
L_{fu}	Fraction of tread unit length
L_g	Length of a groove type
M	Mobility number
m	Mass
n	Empirically measured Bekker soil deformation coefficient
n	Number of different groove types
N_γ	Terzaghi soil coefficient
N_c	Tyre numeric for clay
N_c	Terzaghi soil coefficient
N_q	Terzaghi soil coefficient
N_s	Tyre numeric for sand
N_{sey}	Revised tyre numeric for sand

<u>Symbol</u>	<u>Full Description</u>
P	Pull
Q	Normal load on axle
Q_g	Quantity of grooves of each particular groove type
Q_{te}	Total number of groove edges
r	Rolling radius of wheel
R	Resistance
R_b	Bulldozing resistance
R_c	Compaction resistance
R_f	Tyre carcass flexing resistance
RR	Rolling Resistance
T_c	Tread coefficient
T_f	Tread factor
T_n	Tread number
TV_r	Tread: void ratio
V_a	Actual travel speed
V_t	Theoretical travel speed ($r\omega$)
W	Normal load on axle
w^D	Dynamic contact width
W_{ff}	Fraction of full tread width
W_g	Width of a groove type
z	Plate (or wheel) sinkage
Z_{def}	Deflected wheel sinkage
Z_r	Tyre sinkage

List of Abbreviations

<u>Abbreviation</u>	<u>Full Description</u>
A-D	Analogue to Digital
CCD	Charge Couple Device
CFD	Computational Fluid Dynamics
CTIS	Central Tyre Inflation System
DA80F	Product code for the replicate sand
DAC	Digital / Analogue Conversion
DC	Direct Current
EORT	Extended Octagonal Ring Transducer
EPSRC	Engineering and Physical Sciences Research Council
FE / FEA	Finite Element / Finite Element Analysis
FPS	Frames per second
GTC*L	Goodyear Technical Centre in Luxembourg
IPOT	Image Processing and Optical Technology
LVDT	Linear Variable Displacement Transducer
NIAE	National Institute of Agricultural Engineering
OEM	Original Equipment Manufacturer
RDC	Region of Direct Contact
RF / RFID	Radio Frequency / Radio Frequency Identification
RHS	Rectangular Hollow Section
RS	Radio Spares
SDL	Soil Dynamics Laboratory (Cranfield University Silsoe)
SIMS	School of Industrial Manufacturing Science
SST	Soil Stress State Transducer
SUV	Sports Utility Vehicle
Tread G82	Goodyear Sand Tread
Tread G90	Goodyear Off-road Military Mud Tread
Tread HP	Goodyear Wrangler HP Tread
Tread LAT	Lateral Prototype Tread
Tread LON	Longitudinal Prototype Tread

<u>Abbreviation</u>	<u>Full Description</u>
Tread PT	Plain Tread (Slick or Blank)
Tread UG	Goodyear Wrangler Ultra-Grip Tread
Tread xxB	Prototype Tread (xx degrees rearward)
Tread xxF	Prototype Tread (xx degrees forward)
U.A.E.	United Arab Emirates
WES	Waterways Engineering Station

1 INTRODUCTION

It is no longer sufficient, nor economically sustainable, for well developed automotive markets to produce a basic car to just get people from A to B. Across the consumer vehicle range the automotive industry is becoming ever-increasingly competitive as the market becomes more demanding. This is especially true in ‘newer’ market segments, such as the SUV (Sports Utility Vehicle) sector, also termed the 4x4, or light truck, market. To maintain sales in this premium brand environment, vital customer value must be added by delivering high performance, high specification vehicles. The desires of several motor vehicle and tyre manufacturing companies to maintain their commercial positions as leading manufacturers of high performance off-road products led to this project’s sponsorship.

Alongside EPSRC, who provided much of the funding for this study, Land Rover (BMW) provided the initial company sponsorship, whilst Goodyear Technical Centre in Luxembourg (GTC*L) provided technical assistance. Both companies wished to develop a greater understanding of the factors that contribute to 4x4 tyres offering good mobility on loose desert sands, which cover approximately one-seventh of the world’s land mass¹, and more importantly, which are commonly located adjacent to the potential future growth markets for motor vehicles in the developing world². The sponsors also wished to identify modifications that could be made to existing tyre designs and/ or vehicle systems to further improve the mobility of Land Rover vehicles.

In desert conditions it is a tyre’s limited ability to develop net positive traction that limits vehicle performance. For Land Rover to maintain its brand and market position as the manufacturer of “the best 4x4 by far” its products must be capable of achieving superior off-road performance over competitor vehicles, as once mobility is lost then any vehicle becomes of little use, whatever its brand. Whilst limits to a vehicle’s ability will always exist, such circumstances are potentially very damaging for a brand image built on its product’s off-road capabilities.

As the tyre is the limiting factor in these conditions, Land Rover only has indirect control over the main component governing its product (and brand) performance,

makes it difficult to ensure that the premium performance tyre that is desired is always available to Land Rover. To help address this situation Land Rover wished to collaborate with both a tyre manufacturer and a University. Their aim was to develop a clearer understanding of sand traction mechanics for 4x4 vehicles, whilst allowing closer integration of tyre and vehicle development.

Goodyear's participation was driven by their brand image being enhanced when their products are fitted to high-performance vehicles. Closer involvement with an OEM (original equipment manufacturer) also provided increased opportunities to understand the OEM requirements and market their products. Increased OEM custom also generates more secondary purchases from end-users. Additionally, in recent years no tyre manufacturer has conducted any significant quantity of research on off-road desert tyres³, thus the project offered Goodyear an opportunity to develop a competitive advantage.



Plate 1.1 – A photograph of an immobilised Land Rover Discovery in Dubai desert sand conditions⁴

Due to various circumstances over the course of the project the roles of the two sponsors became reversed, and for a period during the protracted changeover Dunlop

Tyres Ltd, Fort Dunlop, Erdington, UK, replaced GTC*L as sponsors. Despite these changes, the project's focus remained on identifying the interactions between a tyre (tread) and sand surface that enable useful traction to be generated, and determining if, and how, the governing factors in the interaction could be altered to reduce the likelihood of vehicle immobility occurring in the manner shown in Plate 1.1.

Generating net positive traction on pure sand can be difficult, especially if the sand is in a loose state. Desert sand conditions can vary from firm to weak depending upon the local conditions. Often the sand medium results from the deposition of large quantities of loose sand by aeolian processes over many years. The extreme diurnal temperature fluctuations (and associated evaporation/ dew formation) encountered in desert regions cause the top sand layer to form a stronger crust that overlies weak structured, loose sand⁵. The stronger crust is more capable of bearing vehicle weight and thus allowing vehicle mobility, however once the crust is breached the vehicle is then forced to operate in weaker sand conditions. It is these weaker conditions that are most likely to immobilise the vehicle, and hence the conditions that warrant the most study.

In these conditions it is important to extend the barriers of mobility as far as possible. Through its many years of off roading experience Land Rover has learnt that tyre choice is vital to maximising mobility. However, whilst both sponsors can identify good performing tyres for sand environments through extensive field-testing, they have not identified exactly which tyre features actually generate the high tractive performance³. This is sometimes highlighted when end-users fit different replacement tyres that did not demonstrate impressive performance during company testing⁶, but which the user either know, feel or believe, enable the vehicle to deliver greater performance over the standard fitment. These choices are particularly important, as end-user experience in its totality far exceeds that of the manufacturers, whose test programmes are operated under cost and time constraints. The manufactures are therefore often unable to identify when particular tyre (and vehicle) features are suited to specific local conditions.

If the factors governing a tyre's performance, in particular the tread, which is often the biggest difference between different manufacturers' tyres, were modelled then the

potential performance of different tyre designs could be evaluated from the design office by the manufacturers, who are increasingly relying upon FEA (finite element analysis), CFD (computational fluid dynamics) and dynamic analysis software packages to fully model vehicle behaviour in the virtual environment. This type of evaluation is used because it removes some field-testing costs, whilst also reducing the development time scale, which achieves further indirect cost savings. Developing a tyre performance model necessitated both a model and actual test results against which the model's predictions could be benchmarked, thus physical traction experiments were required. These provided a basis for the understanding of the contact interactions, which enabled the tyre and tread performance prediction models to be developed, and test data for validation purposes.

2 AIM AND OBJECTIVES

2.1 AIM

To determine the relationships between tractive force, sand displacement and tread pattern for light truck (4x4) tyres generating traction from pure sand.

2.2 OBJECTIVES

1. Develop instrumentation and methodologies for the measurement of tyre tractive performance and three-dimensional sand particle movement underneath tyres.
2. Determine the effect of tread pattern upon the three-dimensional sand disturbance and tractive performance generated at low forward speeds across a slip range.
3. Develop empirical or computational models of the relationships between tread pattern features, sand flow and traction.
4. To identify developments for 4x4 tread designs for desert conditions to improve traction and determine the commercial implications of the proposed changes.

2.3 PROJECT METHODOLOGY

Project management procedures were adopted for the study to ensure that it was delivered within the time, budget and quality constraints that were fixed at the outset. Seven key project phases were defined, as listed in Table 2.1.

Table 2.1 – The stages of the project methodology

No.	Component	Deliverable
1	Literature review.	A critical review of current applicable traction knowledge and applicable tyre test methodologies.
2	Traction surface analysis.	Quantification of the differences in the traction (engineering) properties of a range of sand and soil traction mediums.
3	Design and development of instrumentation.	Instrumentation systems and test methodologies to allow the measurement of three-dimensional sand displacements and normal stresses beneath 4x4 tyres.
4	Tyre test rig construction.	An instrumented test rig suitable for the tractive evaluation of 4x4 tyres in the soil bin environment to enable slip-pull graphs to be generated.
5	Measurement of tyre tractive performance and associated sand displacement.	Tyre traction and sand displacement results from the range of treatments tested, which were suitable for the development and validation of the models.
6	Modelling of tractive force and sand displacement relationship.	A prediction model for tyre tractive performance and sand displacement, based on both tyre and tread characteristics, which was capable of predicting traction on loose sand for a given tread and other treatments.
7	Evaluate the commercial implications of the findings.	An evaluation of the recommendations for sand tyre design from a commercial viewpoint.

3 LITERATURE REVIEW

3.1 INTRODUCTION

The need for the research arose because both tyres and sand have complex characteristics. A tyre is a heterogeneous, discontinuous composite, made from cords, wires and elastomers, with complex elastic, plastic and viscous properties, which under operates under mechanical and thermal stress⁷. No test equipment capable of measuring all tyre properties in a satisfactory and reproducible way is currently available and no theoretical model exists to predict all tyre properties, whilst the partial models that do exist are very complex and mathematically demanding⁷. In short, whilst tyre manufacturers have a very good knowledge of on-road tyre mechanics, they do not completely understand how a tyre functions in all environments.

The complexity of sand arises because in its naturally occurring state it too is a heterogeneous material, comprised of quartz particles and other minerals of varying size combined with varying sizes of air pores, depending upon its compaction. As many different sand types exist in comparison to the quantity of different road pavements, thus modelling tyre performance and surface interaction is considerably more complicated for sand surfaces than for road pavements. Until recently 4x4 tyre/ soil interaction represented only a small and complex part of the tyre market, thus comparatively less money and effort was expended on understanding its mechanics, in comparison to the resources spent upon understanding tyre behaviour on wet tarmac³. Therefore a gap in knowledge exists in this subject area.

Both sponsors wished to address the general lack of test procedures, apparatus or models that could simply and universally describe the performance capabilities of new, or development, tyres in sand. Any partial substitutes for the extensive subjective handling tests necessarily conducted at present to determine the optimum vehicle and tyre combinations have the potential to generate significant cost savings. Additionally, the automotive industry has a growing need for greater statistical information to more accurately model the effects of different tyres within the totality of vehicle simulation and modelling⁸. Additional comments by Williams⁹ confirmed both those needs. Hence,

minimal increase in rolling resistance for a similar increase in contact area⁵. Extra contact length also gives a greater shear length from which greater tractive capability can be extracted.

The tractive improvements gained by increasing the tyre diameter, and hence the contact length, are demonstrated by Figure 3.1, taken from a body of research by Goodyear Ltd.¹² The most significant tyre factor tested to produce increased performance was outside diameter, which was shown to be three times more effective than the next most significant improvement on desert sand. The need to use large diameter, uniformly loaded wheels was also recorded by Garbari¹³ who investigated methods of reducing motion resistance. He also suggested reducing carcass rigidity and tread curvature, whilst maintaining tyre height.

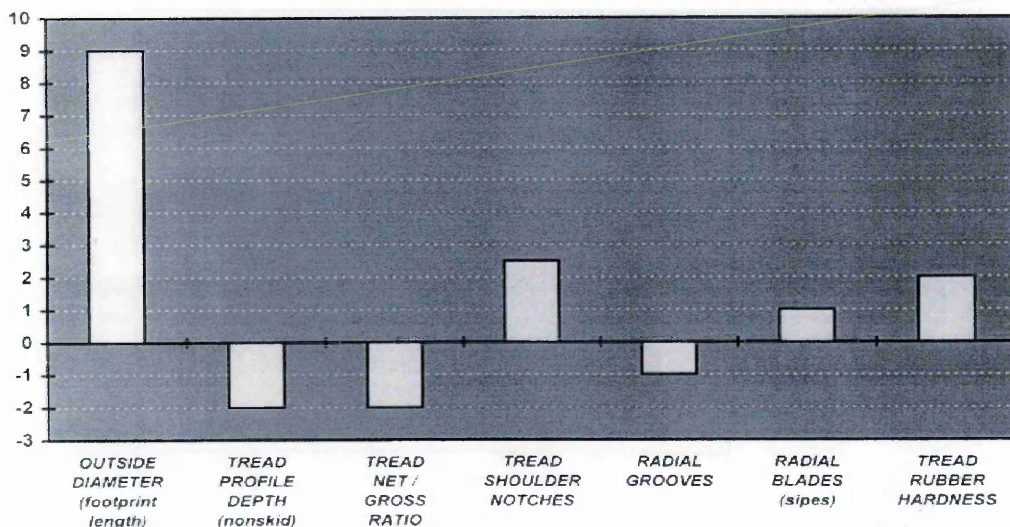


Figure 3.1 – The relative effect of seven tyre factors upon a 4x4 tyres ability to generate traction on desert sand, i.e. increased diameter is three times more effective than shoulder notches (Note: scores are relative, not percentages)¹²

Physical constraints, such as the wheel arch, limit a continuous increase in tyre outside diameter and whilst a trend of small increases in 4x4 tyre diameters have occurred, they are already close to the maximum level achievable without major vehicle re-styling. Even with a fixed tyre size, extra contact length (tractive performance) can be achieved by a simple reduction in tyre pressure. Wang & Reece¹⁴ proved that pneumatic tyres offered lower rolling resistances than rigid tyres and that as pneumatic tyre inflation

pressures reduced, resistances decreased even further. They also showed that these effects were more pronounced under higher normal loads¹⁴. This is why 4x4 tyres are commonly operated on sand at 1.10 bar to 1.25 bar (16 psi to 18 psi), or even as low as 0.97 bar (14 psi) in emergencies^{3,6}. Below these pressures the risk of the tyre unseating from the rim increases markedly. To maximise the benefit from operating at reduced pressures tyre material must be available to increase the contact patch size under deformation, thus greater benefit is derived from lower inflation pressures if larger aspect ratio (section height) tyres are used¹⁵.

As both tyre outside diameter and operating pressure are constrained by other requirements, this study concentrated on 235/70 R16 tyres, the standard Land Rover Discovery specification, operating at 1.10 bar. Although less than the maximum available section height (aspect ratio) the contact patch of these tyres still significantly increased with deformation.

3.2.2 Features of a Sand Tyre

The tests undertaken to produce Figure 3.1 proved that Goodyear's best performing 4x4 tyre in a sand environment was the G82³, as shown in Plate 3.1.



Plate 3.1 – The Goodyear G82 sand tyre

This style of radial 7.50 R16 tyre is similar to those produced by other manufacturers for desert environments e.g. Michelin XS, through being taller and narrower than 235/70 R16 tyre's these already exploit the benefits of increased diameter and large section height. This has mainly occurred because these tyres have developed from those designed for 4x4 vehicles for desert operations during, and just after, the Second World War³. Features were adopted because they functioned well in the desert, rather than because a well-developed fundamental analysis warranted their inclusion.

Although the tyre size has been retained over time, many of the other features of these tyres have been refined. The large tread features of the G82 spread the tyre load reducing the likelihood of it digging through the stronger sand surface crust⁵. The large tread blocks also assist in achieving reasonably even stress (pressure) distributions, which prevents any portion of sand being over-stressed. The block shape and spacing compress the sand in 'cups' that enhance flotation and traction⁵, although the exact nature of this process is unknown. Whilst bias-ply tyres enhance this action¹⁵, both sponsors did not wish these tyres considered, as they would not be fitted to modern vehicles because of their reduced on-road capabilities, e.g. reduced stability. Additionally, Ataka & Yamashita¹⁵ (1995) who developed Figure 3.2, indicated that the challenge currently faced in the U.A.E. market is to produce radial tyres capable of achieving the same level of performance on sand as bias-ply tyres.

	H. Sp. Endur.	H. Sp. Stab.	LRR	Low Noise	Rid. Comf.	Steer. Stab.	Wet Perf.	Mud Perf.	Sand Perf.	Snow Perf.
Japan			○	⊙	⊙	⊙	○			⊙
N. America			⊙	○	⊙	⊙	○	○		⊙
Europe	⊙	⊙		⊙	⊙	⊙	⊙			⊙
Australia				○	⊙	⊙		⊙		
Mideast	⊙	⊙		○	⊙	⊙			⊙	

Note: ⊙ = Very important performance. ○ = Important performance.

Figure 3.2 – Tyre performance requirements for 4x4 vehicles in five worldwide markets¹⁵

The G82 tyre does not feature sipes (small tread block features shown in Figure 3.3). Whilst offering small increases in performance, as shown in Figure 3.1, these would cause significant extra tread wear as sand particles trapped between the sipes cut rapidly into the tread³. The G82 tyre features shoulder notches, visible in Plate 3.1, to further

enhance traction, as indicated by Figure 3.1. These features, typified by the design in Figure 3.3, allow soil on the side of a rut to also be sheared by the tyre, thus more pull is generated without a significant increase in resistance¹².

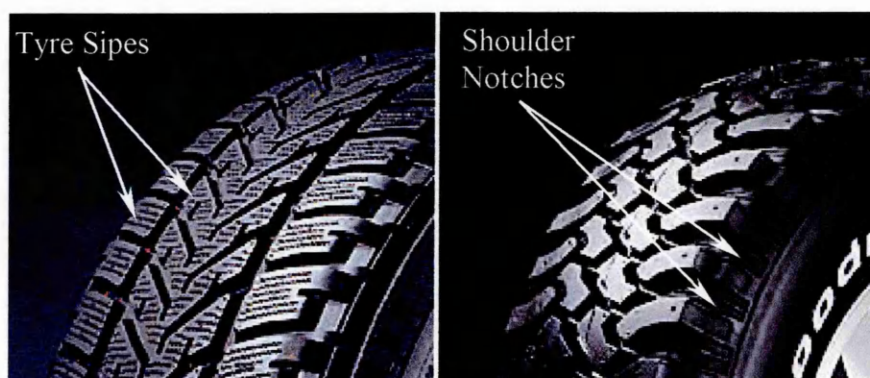


Figure 3.3 – Tyres demonstrating sipes and shoulder notches

Although sand tyres have broadly similar features, tests have shown that differences exist between the levels of tractive performance offered, even when identical sizes are compared⁶. This is caused by a combination of the two main features of a tyre, construction and tread pattern. Dunlop staff guided the project towards the study of the effect of tread upon tractive performance on sand¹⁶, as understanding this element would contribute the greater impact to the development of future tyres, particularly when assessing suitability of on-road treads for off-road use.

This decision was reinforced by another compromise faced in 4x4 tyre fitment. Land Rover has found that drivers in the Middle East market favour using a single set of tyres for on and off-road driving for both work and leisure, due to simplicity, and cost reasons. This was notably highlighted in an episode of ‘Driven’¹⁷, filmed around the infamous ‘Big Red’ sand dune in Dubai, where weekend entertainment consists of challenges amongst friends to see whose 4x4 can most easily scale the dune, before driving home on highways using identical vehicle set-ups. The tyres fitted must therefore compromise to offer adequate performance in both instances. Most critically the vehicle must repeatedly perform safely and predictably at high on-road speeds. As this behaviour is mainly determined by a tyre construction it was undesirable to seek to alter tyre construction to solely suit the off-road environment. Any prototype tyres

tested were therefore made to the same construction as a Goodyear Wrangler HP tyre, a universal 4x4 tyre designed for high-speed on road use, but with an off-road soil and mud capability.

In summary, the sponsors had greatest interest in the effect of tyre tread pattern components upon off-road sand performance, as the mechanics by which traction is generated in this situation are not fully understood by the design engineers³. Treads are necessarily optimised to achieve on-road performance, whilst it is hoped that good off-road performance will simultaneously be achieved. If an understanding of the mechanics of different tread pattern features on loose sand were developed, it would potentially allow treads developed for on-road performance to be simultaneously adjusted to include (or omit) features that would achieve (or inhibit) good off-road sand performance.

3.2.3 Implications of the Engineering Features of Desert Sand

Zhuang *et al.*¹⁸ demonstrated that the shear strength of dry loose sand on the surface of a profile is almost zero, but as depth increases, and hence the confining (normal) stress increases, then the sand shear strength also gradually increases. Furthermore increasing the confining stress, or decreasing the void ratio, caused the strength of surface sand to be increased considerably, although the internal friction angle was reduced¹⁸. Additionally as the compressibility of loose sand is low (less than 4%) any sand failure will result in plastic flow¹⁸.

Liu¹¹ used this sand behaviour to describe the effect of interaction by vehicle running gear. During interaction a small load will produce local plastic deformation at the surface that is limited by the increased shear strength found with increased depth¹¹. As the shear strength is limited, the horizontal plastic flow under the wheel forms the dominant pattern of failure when a wheel is driven on sand¹⁹. This was proved in experiments¹⁹, where it was shown that for one set of experimental conditions lateral sand flow accounted for 40% of the total sinkage and longitudinal flow 60% of the total sinkage. Once sinkage occurred the lateral component of normal stress acting on the driven wheel resisted the motion of the tyre. This was the maximum force faced, as the

normal stress acted in the direction of the sand's greatest bearing capacity. Therefore as sinkage grew, rolling resistance increased rapidly, causing further slip sinkage and even greater rolling resistance, which further exacerbated the problem¹¹. To address these relationships a tyre must confine sand flow away from the tyre (limiting sinkage), whilst exploiting the stronger vertical bearing capacity¹¹. Thus a tread that could control sand displacement would potentially improve tractive ability.

3.2.4 Tyre Evaluation Using Slip-Pull Curves

At $GTC \cdot L^3$ a number of different variables that may influence tyre traction on a variety of off-road surfaces (such as those shown in Figure 3.1) have been investigated using both single and double instrumented vehicle pull tests. The single vehicle tests were used for handling evaluation and were therefore subjective, whilst the double vehicle test provided quantitative measures of tractive performance, such as slip-pull graphs, as shown by Figure 3.4.

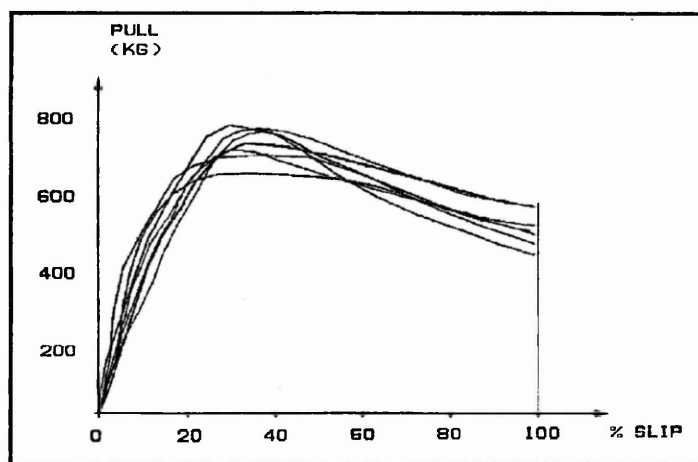


Figure 3.4 – Typical slip-pull curves generated by Goodyear from full vehicle tests of off-road tyres³

The use of variations of the double vehicle tests, or single vehicles and bespoke towed test rigs, are both widely accepted test methodologies. These have been extensively employed for conducting testing to produce slip-pull graphs, which are used as an accepted way of comparing tyre performance²⁰; where slip (i) is defined by equation 2.

$$i = \left(1 - \frac{V_a}{V_t} \right) \quad (2)$$

Where: V_a = actual travel speed V_t = theoretical travel speed = $r\omega$
 r = rolling radius of wheel ω = angular velocity of the wheel

A slip-pull curve describes a tyre's performance envelope. Typically a graph will show the pull (thrust) of a vehicle (tyre) across the full range of slips (0-100%) for any set of tyre and soil treatments. As no useful traction is achieved at 0% or 100%, graphs more commonly describe traction from about 5% to 80% slip. However, the full range of skid and slip can be plotted for completeness, as shown by Figure 3.5.

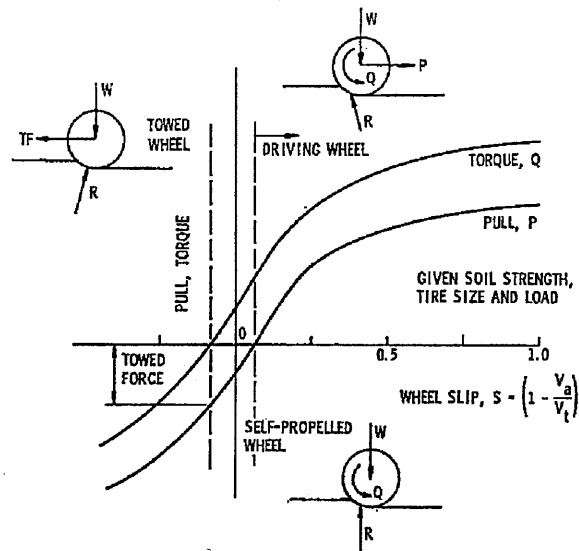


Figure 3.5 – General slip-pull curves for illustration, from Wismer & Luth²¹

Results can either be generated for a whole vehicle, or if a single wheel tester is used, for an individual wheel. In both instances vehicles separate from those being tested are required to provide a resistance to enable slip to be generated. Thrust results are recorded for either several passes testing at a range of discrete wheel slips, or for a single test run conducted with a varied slip sweep range. Gross, or net, thrust results may be plotted for tyre analysis and comparison.

3.2.5 Indications from a Simple Off-Road Tyre Field Investigation

Piper²² conducted an investigation examining the tractive performance of a variety of tyres, both production and experimental, operating on sand at Cainhoe sand quarry, near Silsoe, UK, at discrete inflation pressures ranging from 1.10 bar to 2.76 bar. This work involved the development and testing of an experimental methodology for outdoor tyre evaluation with 4x4 vehicles. This author gave assistance during the testing, and thus observed first hand the processes of sand traction for a Land Rover vehicle and a range of different treaded tyres. Piper's work showed that his methodology was effective, but the experimental results were not extensive enough to support dependable conclusions, although the following trends were shown²²:

1. Different treads influenced the rate of wheel sinkage.
2. The relationship between pull and tyre inflation pressure was not consistent with the typically accepted theory that lower pressure equals greater pull.

If, as was indicated, tread pattern influences the rate of sinkage by influencing slip sinkage, then the potential exists to optimise tread to reduce sinkage, and hence rolling resistance. Perara²³ proposed a possible explanation why, in contrary to accepted wisdom, the measured pulls were not necessarily increased with reduced inflation pressure. When operating at very low inflation pressures the tyre carcass may become squarer, and hence act more like a bulldozer blade with increased rolling resistance²³. However, this conclusion contradicts a vast body of anecdotal evidence from experienced 4x4 desert drivers⁵ and must therefore remain doubtful.

3.3 MEASUREMENT OF SOIL (SAND) DISTURBANCE

If soil deformation can be measured then it can be directly related to the traction generated by a tyre. Strain is a more direct measurement than stress, being directly related to the deformation experienced. Several authors have investigated both variables on soil, with early methods documented by Gill & Vanden Berg²⁴. During tyre immobilisation sand flow occurs in every plane so to measure the tread effect upon sand displacement an ability to identify, mark and measure sand displacements in three-dimensions was required. The options examined were:

1. Directly measure displacements by recording the path of individual sand grains.
2. Insert particles into the sand to act as dummy grains that could displace with the sand, without impeding any disturbance. After disturbance the displacements of the dummy particles and hence the sand would be measured.

3.3.1 Glass Sided Tanks and Visible Markers

Direct measurement or photography of soil particles offers a good insight into soil behaviour beneath a tyre, as Gliemeroth²⁵, who dug a pit alongside the path of a wheel and photographed the motion of a soil marker during vehicle passage demonstrated. Payne²⁶, who quantified soil deformation caused by a simple tillage tool using visible marker filaments, and Bekker²⁷, who studied vertical soil movement under grouser plates both demonstrated that the use of glass sided plates simplified this approach. Wong & Reece²⁸ and Wong²⁹ also used these methods to investigate the longitudinal flow of sand under a rigid wheel. Their work utilised a glass sided soil bin and tested a number of different wheel speed conditions e.g. towed, driven, locked, skid and slip.

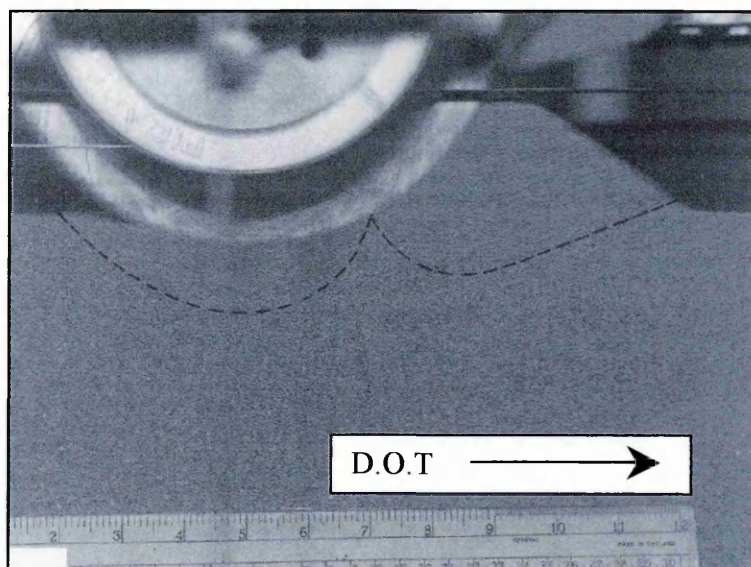


Plate 3.2 – Typical forward and rearward sand failure patterns beneath a narrow plain rigid wheel²⁹

A scaled rigid wheel was used as it was assumed that tyre deformation on sand was not significant. However, the results of current associated investigations³⁰ have shown that this definitely only occurs at pressures exceeding 1.72 bar to 2.07 bar (25 psi to 30 psi).

The failure patterns produced by the various treatments were filmed through a glass plate, as Plate 3.2 demonstrates. Using these techniques the authors^{28,29} investigated and measured forward and rearward failure patterns beneath wheels. Their findings are further discussed in section 3.3.4.

More recently new technology has allowed this technique to be further developed. Shikanai *et al.*³¹ used a photographic technique to measure deformation beneath scaled rigid wheels in a 2 m long, glass sided, soil tank, previously used for the assessment of tractive performance^{32,33}. Their technique used Ø5 mm markers made from 25 µm thick polyester film with fine crosshairs printed on their surface. Sand grains were glued to one face, which forced the markers to displace with any sand deformations, whilst the opposite faces were attached to the glass plate with 15 mm spacings using a moisture film. Between 200 and 300 markers were placed whilst the tank was filled with sand. The side of the tank was photographed before, during, and after passage by the rigid wheel. The photographs were analysed using a two-axis table and a microscopic CCD camera, which allowed accurate measurement of the markers' positions. This system allowed the marker (and assumedly the sand) displacement to be accurately and reliably measured, although no proof that the markers truly followed the sand flow was stated. The data they gathered was used to improve the accuracy of several FEA analyses³¹.

Applications of these techniques were investigated in discussions between Marantz³⁴ and the author, and at the Image Processing and Optical Technology (IPOT) Exhibition 2000 and Machine Vision 2000. These investigations confirmed that camera technology with frame per second (fps) speeds capable of recording particle displacements, was potentially available to the author through the EPSRC instrumentation hire pool. Hardware existed that was capable of capturing and digitising such photographs in real time for interpretation on a PC. However, although some generic software packages were available that could translate these into tracks of particle displacements these would require a significant level of custom programming to make them suitable for this particular application. Also two other problems rendered the use of glass-sided bins inappropriate:

1. Assumptions concerning friction losses of the soil against the glass, and soil containment by the glass must always be made²⁴.
2. Soil displacement is limited to only the vertical or longitudinal directions. For the purposes of this research project the effect of lateral movement was very important, because of the lateral flow effect upon sinkage noted by Liu¹¹.

Thus other methods of measuring deformation using in-situ particles were investigated.

3.3.1.1 Paints, dyes, films and layers

The use of different materials and/ or colours to differentiate between different sand layers was considered. Plastic or foil films were discounted, as they would severely impede any sand flow. Also Cranfield University experience³⁵ had shown that pressure film, as manufactured by Pressurex, yielded poor results in a soil profile because localised stress differentials between soil particles were below the film's sensitivity.

Attempts were made to paint sand particles, but even aerosol paints caused the particles to agglomerate, which was unacceptable. On a small-scale sand could be dyed using a solution of potassium permanganate to produce coloured sand with matching physical properties. Consideration was given to using coloured sand regions throughout the profile, but whilst these would have produced good visual patterns, it would have been very difficult to measure grain displacements in a repeatable manner. Furthermore the test sand would gradually have been contaminated with coloured sand making measurements after each test repetition more difficult.

3.3.2 Particles Inserted in a Soil Profile

To measure sand disturbance in three-dimensions insertion of identifiable and retrievable particles into the sand mass would be required instead. Previous Cranfield University experience³⁵ indicated that any particles used would have to be less than $\varnothing 7$ mm to be carried by the sand flow. For disturbance to be characterised throughout a portion of sand then the insertion of some form of numbered grid pattern with individually identifiable particles would be necessary.

Methods employed by various authors to track soil movement using particles inserted into the soil were studied. Abebe *et al.*³⁶ used lime powder markers. Woods & Wells³⁷ used filaments of white marble granules to track deformation in a segmented soil bin, which allowed vertical soil profiles to be exposed. To tackle inadequacies in these techniques Spoor & Trein^{38,39} developed an improved methodology whereby filaments of white paint were deposited across the soil profile during its construction. Following a treatment, the soil was profiled to expose nodal grids that were photographed through a glass plate, see Plate 3.3, and then digitised to determine the x – y coordinates for each node. The accuracy obtained by this method was ± 3 mm. Although recent advances in digital image analysis techniques have reduced the time necessary for such analyses, as Yu *et al.*⁴⁰ proved, unfortunately it remains impossible to successfully profile cohesionless soil (sand).

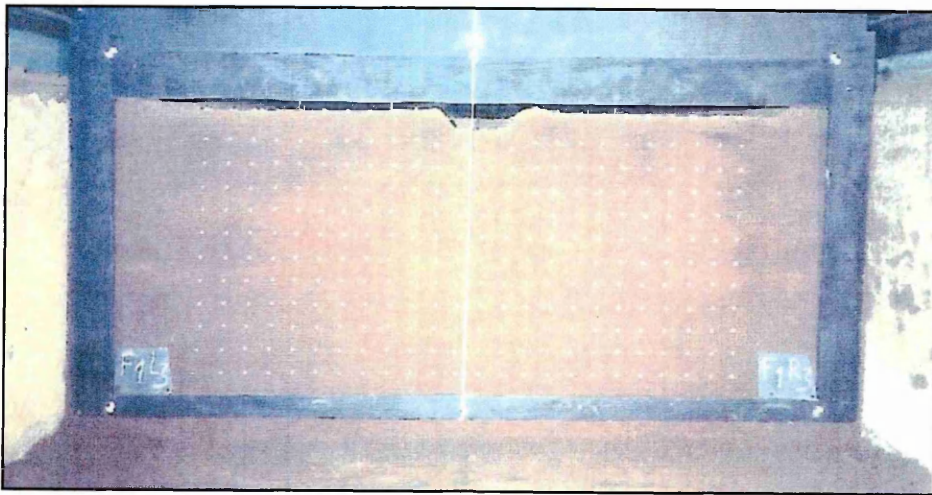


Plate 3.3 – A soil profile with paint markers developed by Trein³⁹

Wells *et al.*⁴¹ and Xing *et al.*⁴² described a laboratory system used to construct soil profiles and measure three-dimensional soil deformations. The soil bin used was formed from ten modules 0.91 m long x 1.22 m wide x 0.91 m deep that bolted together³⁷. Over the bin ran a powered carriage and small pneumatic wheel tester of the form described by Burt *et al.*⁴³ and Wells & Buckles⁴⁴. Wells *et al.*'s⁴¹ methodology evaluated soil deformation by precisely measuring the displacement of visible soil profile markers using a sonic digitiser. Xing *et al.*⁴² later refined the measurement technique by using digital image analysis. In both cases the markers used were 25.4 mm lengths of $\text{Ø}6.4$

mm white polypropylene rod. Milled templates were used to insert these markers into the soil profile at pre-set depths co-planar with the bin section joints, thus constructing a grid within the profile. After a treatment the bin modules were separated to reveal the new positions of the markers, which were then measured. The markers could be positioned in the soil to within ± 0.5 mm and their subsequent positions could be measured to within ± 0.5 mm.

It would have been possible to code such markers, but again locating such markers without disturbing the sand flow patterns after displacement, would have been difficult in cohesionless sand, particularly if their locations were unknown. Additionally the authors^{41,42} did not explain how the markers would be located in the profile if they were exposed to significant longitudinal disturbance, nor did they state how accurately the markers tracked the true soil disturbance. As both glass plate and profiling techniques were unsuitable for this project, but the need for a simple method of measuring sand displacement with high accuracy remained³¹, other methods were investigated.

3.3.2.1 Metal detection

Some authors^{45,46} have used lead particles to record deformation within sand by tracking them using an X-ray machine. The process provided measurements with high accuracy, but the response time of the X-ray process meant that only slow deformations could be tracked. Coupled with the fact that the Cranfield University laboratory facilities (section 6.1) use a sunken soil bin, the X-ray process was unsuitable for this project.

Instead, the use of metal detection technology to locate steel particles in the sand was considered. Several manufacturers and distributors of personal metal detectors were contacted. They stated that whilst the proposed application was theoretically possible, the following issues would be relevant:

1. Steel reinforcement in the soil bin walls would considerably reduce detector sensitivity, thus particles would have to exceed $\text{Ø}50$ mm to remain detectable.
2. The steel processor unit would further reduce the sensitivity of any detector.

Clearly commercially available detectors were unsuitable. Therefore the merits of smaller-scale detectors were investigated. A hand-held household pipe, and wire

detector (*Tracker*), and a miniature metal detector kit (from RS components) were tested upon steel ball bearings of Ø3 mm, Ø5.5 mm, Ø10 mm and Ø15 mm.

Both detectors offered similar performance, being able to detect all of the bearings on the soil surface. However, the detecting ability of these devices decreased markedly with an increase in ball bearing depth in the soil profile. Beyond depths of 20 mm none of the bearings could be located, and a Ø5.5 mm bearing could not be located deeper than 12 mm. As 12 mm was too shallow to realistically enable a grid of such particles to be located after tyre passage, and bigger ball bearings were unlikely to follow the sand displacement, the application of metal detection technology was abandoned.

3.3.3 RFID Technology

RFID (Radio Frequency IDentification) systems have two parts, transmitters (chips or tags) and receivers (scanners). Generally the tags electronically store individual ID codes, and possibly extra product information, which the scanners can read from the tags. Both active and passive tags are available. The passive tags are smaller as their power is transmitted by the scanner's signal, before being re-radiated. A fuller description is provided in Appendix 1.

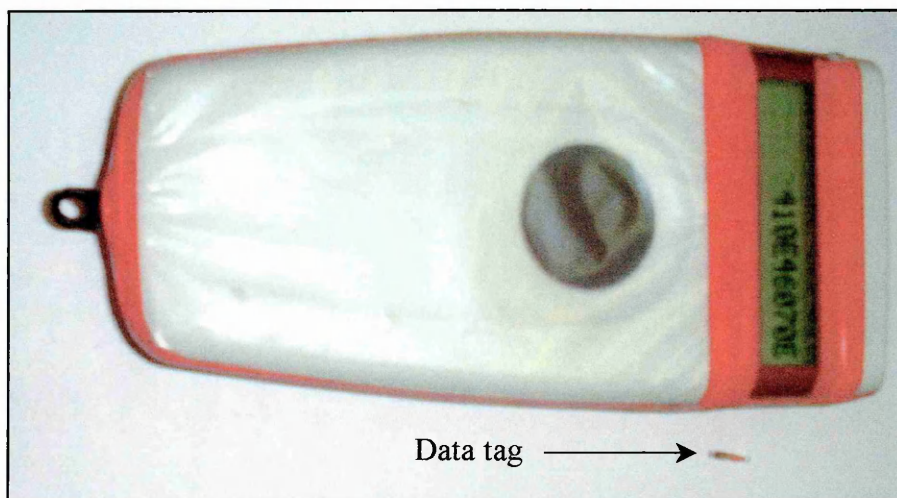


Plate 3.4 – The handheld RFID scanner (a *Pocket Reader*) and a data tag used for the experiments (the tag's code is visible on the scanner's screen)

Destron-Fearing manufacture the smallest commercially available coded tags. These are supplied in glass capsules \varnothing 2 mm by 12 mm long, with each tag containing a unique 10 to 16 digit alphanumeric code, see Plate 3.4 and Appendix 1. Predominantly they are used for the tagging of wildlife and pets. Both the size and construction made these potentially suitable particles, so their performance was investigated (section 7.1).

3.3.4 The Implications of Other Sand Flow Investigations

From their investigations, which were initially upon dry sand, but later on clay, Reece & Wong²⁸ and Wong²⁹ drew the following conclusions. Soil failure was a three-dimensional phenomenon, rather than a two-dimensional occurrence, upon which contemporary theory was based. Their studies demonstrated that soil was displaced partly sideways and partly longitudinally. Unless the wheel was operating at 100% slip or 100% skid, then forward and rearward longitudinal failure, and flow, planes existed beneath the wheel, see Plate 3.2, with the changeover in direction occurring at the point of maximum radial (normal) stress. The location of this point was dependent upon both the wheel width and slip, and increased slip caused the point to move forwards. The formation and location of these failure planes conformed to the basic principles of soil mechanics, being bounded by logarithmic spirals and straight lines such that the soil ahead of the tyre failed forwards and outwards, whilst that soil failing rearwards was simply driven backwards by the stresses formed at the sand-tyre interface.

Whilst a tyre on sand would have an initial sinkage due to a bearing capacity failure, tyre slippage would increase this sinkage further by driving sand rearwards. The authors^{28,29} termed this phenomenon '*slip sinkage*' and showed that it increased as wheel slip increased. As well as causing extra wheel sinkage this event also caused '*rut recovery*', whereby the sand being forced rearwards filled the rut left behind the tyre.

Zhuang *et al.*¹⁹ also noted forward and rearward failure zones under tyres. Additionally they also showed that the magnitude of the forward zone increased with increased sinkage, and that the backward zone enlarged with increased slip. This led the authors¹⁹ to investigate methods of confining both side and longitudinal sand flows by using rigid paddle-type plates fitted to the outside of tyres. These consisted of two flanges to stop

side flow, with different configurations of longitudinal plates added between the flanges to constrain longitudinal flow. The results showed that by controlling the sideward and longitudinal sand flow, the sinkage and thus rolling resistance could be reduced¹⁹. Unfortunately, such large flanges have no on-road practicality.

3.4 PRESSURE/ STRESS SENSING

3.4.1 Pressure/ Stress Sensing from the Sand (Soil)

Way *et al.*^{47,48} utilised soil stress state transducers (SST's) to investigate soil stresses beneath agricultural tyres in soil conditions, to relate them, and in turn load and inflation pressure, to soil compaction. Nichols *et al.*⁴⁹ further developed these transducers, which work by measuring six soil pressure components on six appropriately orientated diaphragm-type strain gauge transducers, see Plate 3.5, which allows the stress-state at any point in a soil to be described. Whilst SST's worked well in soils the method of embedding the transducers in the soil was critical⁴⁸, because incorrect readings were obtained if the soil was not returned to a condition comparable to the original state. Another drawback of using these devices for this project was their size, which Plate 3.5 illustrates is approximately 6 cm x 8 cm⁴⁹, so these could not be used in a sand profile without significantly interfering with any sand displacement.

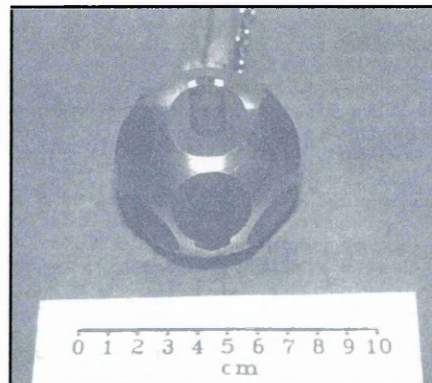


Plate 3.5 – A fully assembled SST

Pressure transducers mounted in the soil were also utilised by Hammel⁵⁰ in an investigation into soil stress distributions under lugged agricultural tyres. These transducers consisted of oil filled cylinders whose pressures were measured with piezo-

resistive pressure sensors. The transducers were inserted from a trench to avoid soil disturbance and they too adequately measured the normal stresses. However, again the outer dimensions of such devices precluded their use in this project and therefore tyre-mounted sensors were potentially more useful.

3.4.2 Pressure/ Stress Sensing from the Tyre

3.4.2.1 Pressure cells in/ on the tyre tread

Stress transducers embedded in the carcass of a smooth rubber tyre, see Plate 3.6, were utilised by Gill and Vanden Berg²⁴ to measure normal stress distributions on several soils. They found that better knowledge of the transducer position, and hence stress location, occurred when the transducers were embedded in the tyre rather than the soil, which also eliminated any prior soil disturbance. Whilst good agreement was shown between pressures measured on the tyre and pressures recorded by sensors on a non-yielding surface below the tyre, significant transducer developments were identified as necessary to improve robustness and more closely match the sensor and tyre rigidity/flexibility before this application could be progressed²⁴.

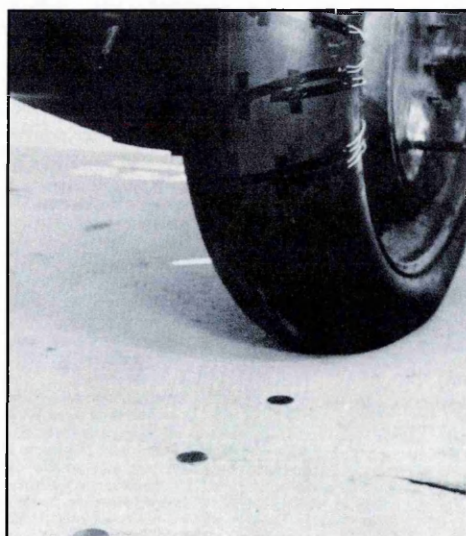


Plate 3.6 – Stress sensors mounted to the outside of a plain tread tyre²⁴

Similar experiments to investigate normal stresses on soil using transducers incorporated in smooth treads were conducted by Freitag *et al.*⁵¹. Trabbic *et al.*⁵²

extended such work to examine normal stresses under agricultural tyres by embedding a number of diaphragm type pressure cells in the tread blocks, see Plate 3.7. This enabled the collection of results throughout a contact patch.



Plate 3.7 – An agricultural tyre mounted with diaphragm type pressure cells⁵¹

However, Plate 3.7 shows that this application required the use of a large number of sensors (in the order of 20), which each required power and signal channels, and thus a connecting module greater in diameter than a 4x4 wheel. Electronic technology has developed considerably since the research and with modern A-D technology and slip rings, or RF transmitters, similar devices could now be fitted to a 4x4 wheel, although problems with wheel balancing would remain. The cost and unknown durability of such items precluded their use in this project.

Burt *et al.*⁵³ also incorporated pressure cells into treads to measure normal pressure distributions beneath agricultural tyres. Developing this approach further Oida *et al.*⁵⁴ investigated stress distributions in the wheel-soil contact area, through measuring stress distributions in the normal, lateral and longitudinal directions at the interface. Their use of stress transducers developed by Krick⁵⁵ and shown in Figure 3.6 enabled the tyre tractive performance to be determined for the treatments they tested.

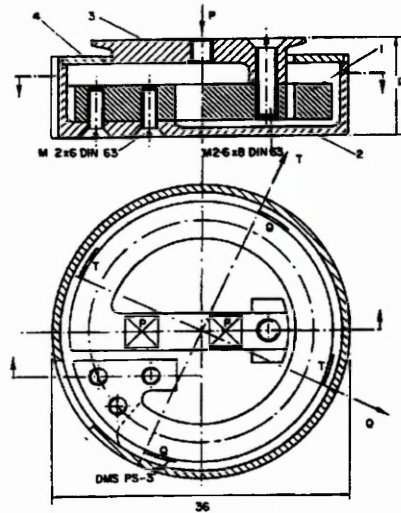


Figure 3.6 – A circular three-axis stress transducer

Transducers were attached to circular core sections of either rigid or pneumatic tyres. The sections (and embedded sensors) were reattached to the treads and the tyres tested on rigid and sand surfaces. This technique worked well in agricultural tyres and allowed the magnitude and variance of contact stresses to be determined across the contact patch. Longitudinal stresses were shown to increase with slip, and stress distributions were shown to vary as the contact patch altered between the two surfaces.

This methodology was refined further by Oida *et al.*⁵⁶ in their investigation into contact patch shape, tyre sinkage (including entry and exit angles), and three-dimensional stress distributions in the contact patch. They attached only one transducer to a deformable tyre, but it was neither stated how, nor where, on the tyre. This device enabled the authors⁵⁶ to dynamically measure normal, lateral and longitudinal stress transitions at the tyre contact for varying slip treatments, from which they calculated tractive forces. The implications of this research will be discussed in section 3.4.3. This work demonstrated the capability of such sensors to measure stresses beneath a tyre. However, to simultaneously measure stresses across the contact width, a significant number of such sensors would be required. Manufacturing and fitting these to the range of intended test treads would have been too costly and time-consuming for this project.

Smith *et al.*⁵⁷ developed another similar transducer for embedding in the treads of forestry skidders, which was capable of measuring the interface normal stress. This

consisted of a strain gauged pressure transducer incorporated in a fluid housing. It used the piston and cylinder mechanism indicated in Figure 3.7 to transmit the stress.

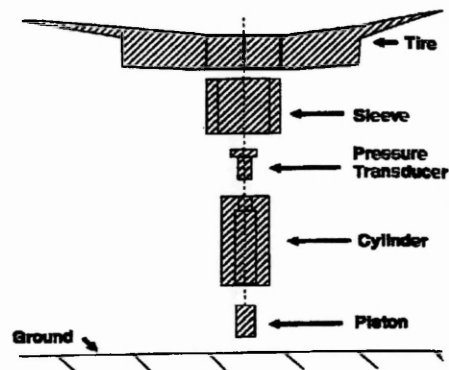


Figure 3.7 – A normal pressure transducer⁵⁷

Burt *et al.*^{58,59} investigated contact stresses by fitting a combination of transducers into the lugs of agricultural tyres. The apparatus shown in Figure 3.8 was placed in the tyre cavity, and was capable of measuring normal and tangential stresses at low forward speeds.

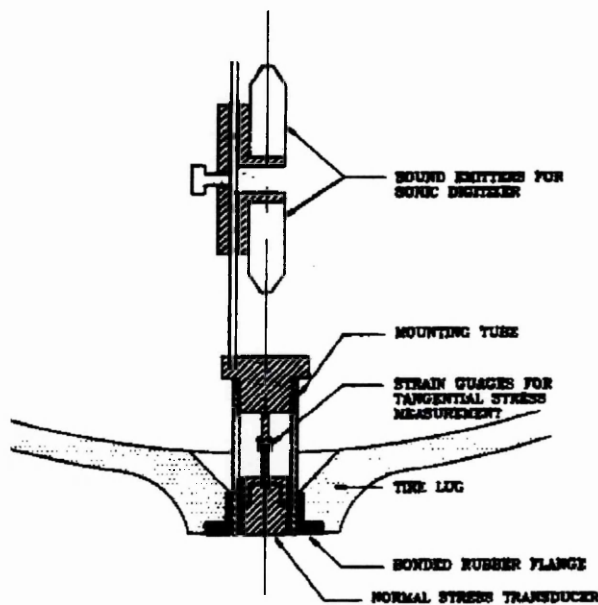


Figure 3.8 – A schematic of the combination stress transducer with sonic emitters⁵⁸

The normal stress was measured by a proprietary pressure cell mounted at the interface, whilst the tangential stresses were measured by strain gauges mounted on a cantilever beam that extended into the tyre cavity. The orientation of the whole transducer, and

hence the direction of the stresses, was determined by the sonic emitter and digitiser system. This combination transducer was able to accurately measure the magnitudes and directions of normal and tangential stresses at the soil-tyre interface for agricultural tyres. However, it could not be applied to 4x4 tyres because of the size of the existing format. Uncertainty also existed over the ability of this device to operate in the noisy soil laboratory conditions.

In summary, stress transducers capable of measuring stresses between a tyre and soil exist, but many of these have been developed for agricultural tyres featuring deeper and more rigid treads, and greater voids between the tyre and rim. Thus some transducers are too large for application to 4x4 tyres, and most other devices would greatly alter a 4x4 tyre's tread stiffness. The use of pressure cells requires many transducers for measurement across the contact area, which in turn necessitates numerous signal (and in some cases power) connections routed off the tyre, which is in itself a technical challenge. A different method of measuring stresses across the contact patch of a range of different treaded tyres was therefore sought.

3.4.2.2 Conductive rubber

Assegdow⁶⁰ investigated the use of embedded conductive rubber transducers to measure tyre contact stresses, by manufacturing transducers from conductive elements mixed with a rubber compound. During bench tests the transducer outputs become non-linear during unloading and suffered from hysteresis effects. Haresign⁶¹ subsequently investigated the use of proprietary conductive rubber transducers fitted inside rubber grouser plates to measure normal and shear stresses during operation. As the transducers' resistivities returned slowly to zero after load was removed these were ineffective. The author considered inserting commercially available conductive rubber tube into treads to create stress transducers, but rejected this approach due to the difficulties noted above. Instead the use of a TekScan pressure sensing system⁶² (see Appendix 2) was considered.

3.4.2.3 TekScan pressure sensing system

This system is a normal pressure measurement device that both Goodyear and Dunlop have used extensively to measure pressure distributions beneath tyres on hard surfaces. Their measurements have frequently been coupled with under tyre photography through glass plates allowing them to confirm the measuring ability of the system^{3,16}. The system consists of piezo-electric pressure sensitive mats, which are connected to a computer card fitted inside a PC computer via a cable, as shown in Plate 3.8.

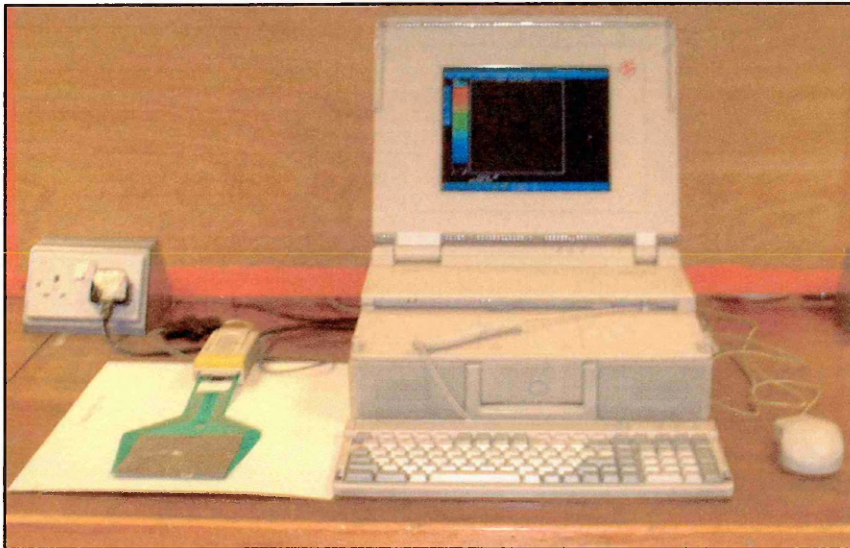


Plate 3.8 – A TekScan pressure sensing system

The mats are formed from two thin sheets of Mylar both of which have piezo-electric gel applied in appropriate formations of parallel lines. One mat half has horizontal lines; whilst the other has vertical lines, see Plate 3.9, so when the two halves are bonded together a gel lattice is produced within the mat. The PC runs bespoke TekScan pressure sensing software such that when a load is applied to a connected mat, the compressed piezo-electric elements create electrical signals that are sensed by the computer card, and related to load by the software. The lattice of the mat allows the computer software to determine the touching nodes, and hence determine the location of the load. Each mat type has different dimensions and pressure ratings. Therefore each mat requires a different computer software ‘map’ program to correctly correlate any recorded nodal pressures to their physical location.

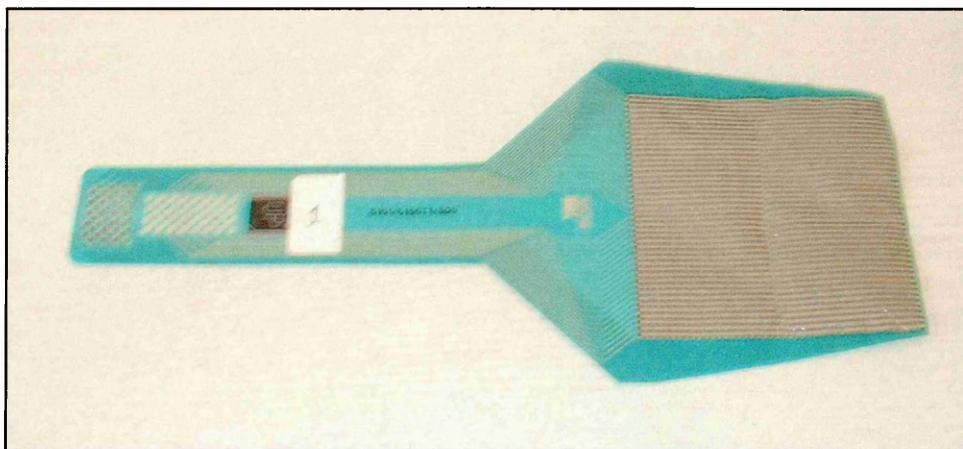


Plate 3.9 – One side of a 5101 TekScan pressure sensitive mat showing the parallel horizontal piezo-electric gel lines

If the position of a mat mounted to a tyre were known, then the normal stress acting on the tyre during contact could be measured and located. Each mat's thin construction allows it to be deformed around tread features, and they are relatively cheap, costing between £80 and £120 each. This system was identified as being capable of measuring normal stresses at the tyre interface as this project required, but it remained necessary to fully quantify the capability of a system borrowed from Dunlop Ltd. to dynamically record contact stresses. The investigation is detailed in section 7.4.

3.4.3 Findings of Oida *et al.*⁵⁴

Using their stress sensor Oida *et al.*⁵⁴ measured three-dimensional stresses beneath a small pneumatic wheel (4.50 – 5 4PR) across a range of discrete wheel slips and angles of sideslip. The experiments were conducted on a standard dry silica sand, $\phi = 38^\circ$, $c = 0$, specific gravity = 1.33 g/cm³, particle diameter 0.3 mm to 1.2 mm. Figure 3.9 shows a typical set of results. It was noted that the drive mechanism caused the downward tyre load to significantly vary as the input torque varied. To tackle this issue and produce useful results the recorded stresses were normalised, by dividing the thrust unit by the acting axle load, which was calculated from the measured vertical stresses. The normalised results showed that the maximum measured normal stress decreased with increased slip, whilst the maximum longitudinal stress slightly increased when slip was increased⁵⁴.

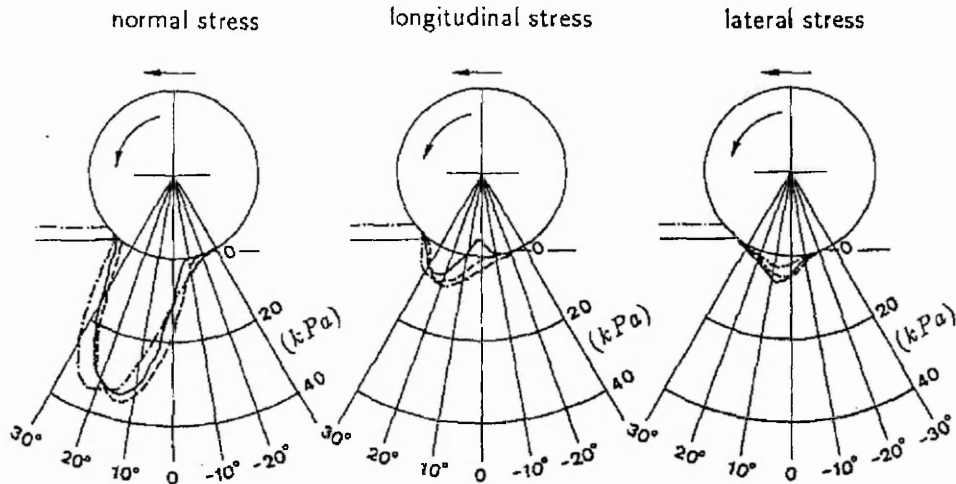


Figure 3.9 – Stress distributions along the tyre-soil contact surface at a sideslip angle of 20°; at 3 slips: — = -29.7%, - - - = 12.2%, - · - · = 66.8%⁵⁴

Using their stress results the authors⁵⁴ calculated the vertical wheel load, thrust, rolling resistance, wheel torque and side force using assumptions about the tyre contact patch shape and dimensions. Figure 3.10 shows the thrust, the rolling resistance and the deduced net pull distributions calculated for two slips. Through the first part of the contact the net pull was negative i.e. rolling resistance > thrust, then as the angle through the contact patch increased the net thrust became positive. However, integration of the total net pull revealed it was only marginally positive, i.e. in both cases the tyre was barely mobile on the sand surface used.

The authors⁵⁴ also produced Figure 3.11, which showed that generally dynamic weight increased with slip, although great spread occurred in the results. Additionally, as would be expected, the normalised thrusts increased with increased slip. Simultaneously the normalised rolling resistances marginally increased with slip, up to about 70% slip, before then reducing as slip continued to increase. However, the normalisation of these results made it difficult to compare them to existing theory²⁰, which would predict a curved slip-pull graph. Additionally if a line of net thrust were computed from the plotted H/W (normalised thrust) and R/W (normalised rolling resistance) values, then positive normalised net pull (net pull/W) was only achieved above 20% slip, and significant levels of normalised net pull only occurred above 70% slip.

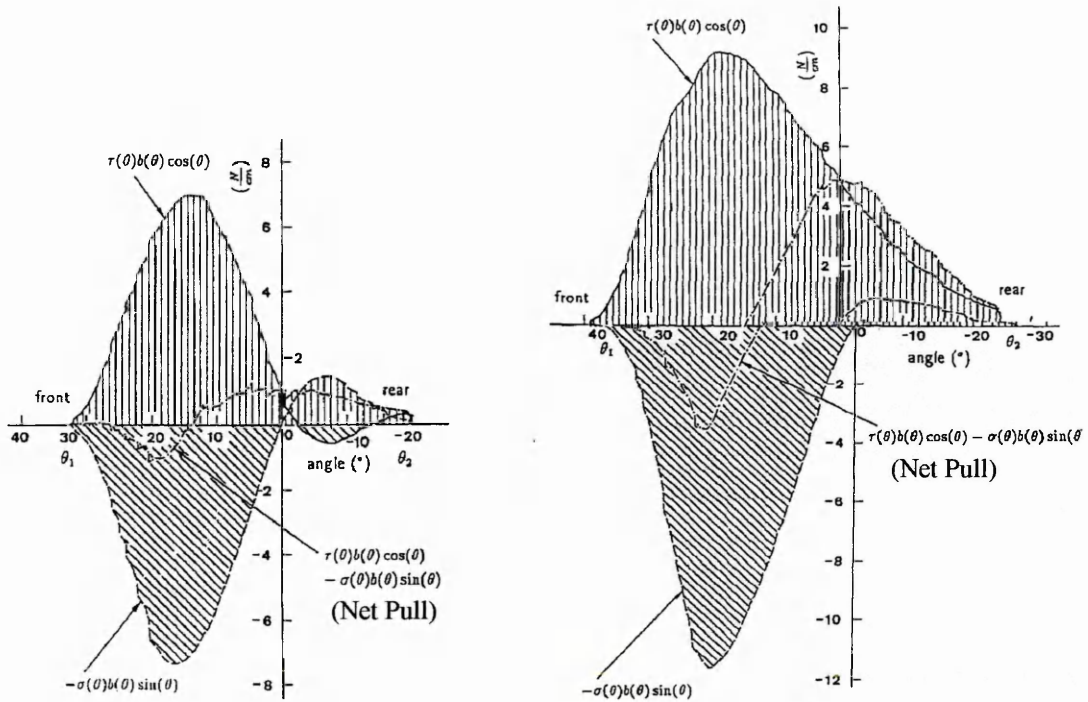


Figure 3.10 – Distribution of thrust (+ ve) and rolling resistance (– ve) components along the contact surface at slips of 8.2% (left) and 53.5% (right) at 10° sideslip⁵⁴

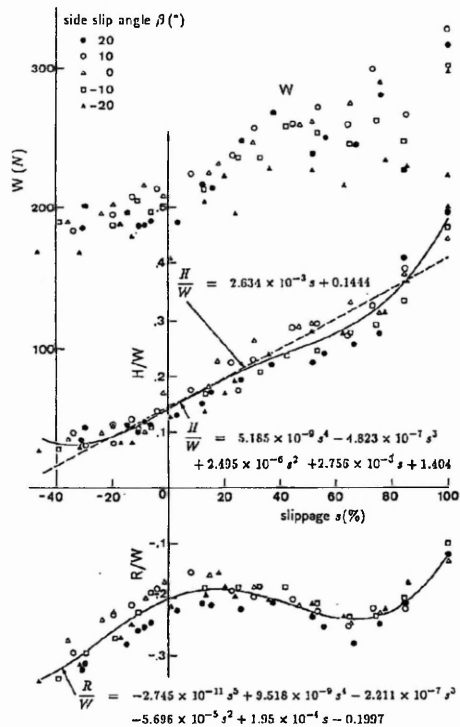


Figure 3.11 – Variations in dynamic weight (W), thrust/ weight ratio (H/W) and rolling resistance/ weight ratio (R/W) with slipp⁵⁴

3.5 TRACTION MODELS

3.5.1 Analytical Models

The theory of plastic equilibrium assumes that terrain behaves like a rigid, perfectly plastic material. Wong⁶³ states that this is suitable for dense sand and similar materials (though unsuitable for many other terrains) encountered. However, the theory is concerned with the prediction of the maximum load to cause failure and not soil deformation, thus its application to this work is of limited potential. Solutions for two-dimensional problems have been achieved, but a move to three-dimensional problems would greatly complicate such solutions⁶³. Although current levels of computing power render this less of an issue, the application of this theory remains limited.

Baladi and Rohani⁶⁴ developed a mathematical model for calculating the motion resistance, sinkage, drawbar-pull, torque and the side force for a flexible tyre on a deformable surface from predicted normal and shear stress distributions. However, the model was only partially validated and contradicted some authors' previous results⁶⁴, so its further application is doubtful. Generalising the development such methods Wong⁶³ states "theoretical models currently available have not been developed to a point that can be considered practically useful for the prediction of tyre performance in the field".

3.5.2 Empirical Models

The complex interactions between an off-road vehicle and the terrain, outlined in the previous section, make this a difficult situation to analytically model. This has led to empirical methods to describe vehicle mobility being developed. The U.S. Army Corps of Engineers Waterways Experiment Station (WES) developed the most cited technique using this approach. Their system sought to provide a quick assessment of the trafficability of terrain in a 'go' or 'no go' manner, and it involved the use of a standardised cone penetrometer to derive a cone index (CI) value, reflecting the combined shear and compressive characteristics of the soil. The value of such models arises from the simplicity of only measuring one soil strength parameter^{65,66}, which has allowed certain dimensionless tyre performance parameters to be empirically correlated with mobility numbers (or tyre numerics) based on CI readings. From his work at WES

Freitag⁶⁷ developed the following tyre numerics for clay (N_c) and sand (N_s) for operation on purely cohesive or frictional soil, equations 3 and 4 respectively.

$$N_c = \frac{C(bd)}{W} \times \sqrt{\frac{\delta}{h}} \quad (3)$$

$$N_s = \frac{G(bd)^{\frac{3}{2}}}{W} \times \frac{\delta}{h} \quad (4)$$

Where: C = cone index G = sand penetration resistance gradient
 b = tyre width d = tyre diameter
 W = tyre load h = tyre section height (unloaded)
 δ = tyre deflection

Turnage⁶⁸ (1972) produced a tyre mobility number, M , (equation 5) that enhanced equation 3 to more accurately consider the wheel properties.

$$M = \frac{Cbd}{W} \sqrt{\frac{\delta}{h}} \times \frac{1}{\left(1 + \frac{b}{2d}\right)} \quad (5)$$

Dwyer et al. developed this equation further⁶⁹ during their investigation of the performance of a range of tractor drive tyres operated in a range of field conditions. Wismer and Luth^{21,70} used equation 3, to formulate equation 6, which predicted the net pull of off-road wheeled vehicles on agricultural (not pure frictional) soils, and C_N became a wheel numeric that was a function of tyre diameter and section width, as well as the CI value, which represented topsoil strength.

$$\frac{P}{W} = 0.75 \left(1 - e^{-0.3C_N i}\right) - \left(\frac{1.2}{C_N} + 0.04\right) \quad (6)$$

Where: P = pull W = dynamic wheel load $C_N = CIbd/W$
 CI = cone index averaged over top 150 mm (6 in.) of soil
 b = tyre width d = tyre diameter i = wheel slip

Whilst CI values can easily be obtained, the adequacy of empirical models to fully and accurately predict mobility remains controversial. As with any empirical method, predictions cannot be accurately extrapolated beyond the conditions from which results were derived. Additionally cone penetrometer resistance depends greatly upon the cone design and its method of use⁷¹. For instance, Reece & Peca⁷² indicated that whilst the methodology is useful for remoulded frictionless clay soil, it is inadequate for characterising sand mobility properties. Wang & Reece¹⁴ also showed that performance prediction using N_s was inadequate for free-rolling tyres on a variety of sands.

Following this publication¹⁴, Turnage⁷³ re-examined a sizeable portion of the WES experimental data. He concluded that for better accuracy in predicting tyre performance upon any given sand of given moisture content, additional laboratory testing alongside penetrometer readings was required. Therefore the original concept of a single test to determine the properties of coarse-grained soils became insufficient. Gee-Clough⁷⁴ had also reported that predictions of certain tyre performance parameters on sand from the cone penetrometer/ mobility number approach were insufficiently accurate. In response to all of these issues Turnage⁷³ proposed a revised numeric N_{sey} , shown on equation 7, where the variables remained common to equations 4, except for G_{ey} , which replaced G and introduced the effects of sand grain median diameter and sand compactibility, which and to be quantified by laboratory investigations.

$$N_{sey} = \frac{G_{ey} (bd)^{\frac{3}{2}}}{W} \times \frac{\delta}{h} \quad (7)$$

This gave improved prediction over a broader range of sand types, however, the surrounding debate meant that extensive geo-technical testing and analysis, including in-situ measurement, sample acquisition and laboratory testing were necessary to accurately define the properties of any sand⁷⁵. This all renders the philosophy of a single measurement inadequate and questions the usefulness of this empirical method for sand⁶³. Additionally the action of the cone penetrometer bears little analogy to that of a traction wheel, a fact investigated by Dwyer *et al.*⁷⁶ who compared the ability of a cone penetrometer and a soil shear meter to measure soil parameters. They concluded that the

soil shear meter, or plate sinkage tests, provided better estimates of a coefficient of traction than cone penetrometer readings⁷⁶. Alcock & Wittig also noted this criticism⁷⁷. From this weight of negative evidence it was concluded that semi-empirical prediction models should be studied instead.

3.5.3 Semi-Empirical Models

These methods have their roots in many years of work at the Land Locomotion Laboratory under Bekker^{20,78,79,80,81}, who introduced the concept of Bevameter (Bekker Value Meter) tests to measure terrain properties. Bevameter tests have two parts, vertical plate penetration tests and horizontal plate shear deformation tests, which are meant to represent the two types of soil failure beneath a tyre (or track). Test results can then be respectively described by equations 8 and 9. Many authors have used equation 8 as a basis for estimating vehicle sinkage, and thus motion resistance from ground compaction, whilst equation 9 has been used to predict thrust forces generated from shear beneath a wheel or similar object.

$$\rho = \left(\frac{k_c}{b} + k_\phi \right) z^n \quad (8)$$

Where: ρ = normal pressure beneath the plate (load/ area)
 k_c, k_ϕ & n = empirically measured soil deformation defining constants
 b = minimum plate dimension (be it width for a rectangular plate, \square , or diameter for a circular plate, O ,)
 z = plate sinkage

Note: these apply for all subsequent equations of this type, unless otherwise stated.

$$\tau = (c + \rho \tan \phi) (1 - e^{-j/K}) \quad (9)$$

Where: τ = shear stress c = cohesion ρ = normal stress
 ϕ = angle of shear resistance j = shear deformation
 K = soil deformation modulus

And where: $(c + \rho \tan \phi) = \tau_{max}$

To determine the soil defining constants in equation 8 (k_c , k_ϕ & n), it is necessary to conduct several plate sinkage tests with different plate sizes. When $\log \rho$ is plotted against $\log z$ a series of straight lines are obtained as shown by Figure 3.12, and the gradient of these lines equals the constant n . To determine k_c and k_ϕ the intercepts of the lines on the $\log \rho$ axis must then be plotted against $1/b$. These points will form a new line with a gradient of k_c , and the intercept, at $1/b = 0$, equals k_ϕ .

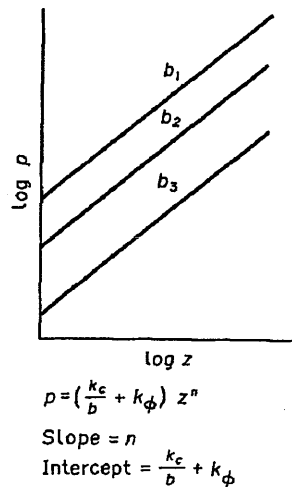


Figure 3.12 – A typical plot of pressure (ρ) against sinkage (z) for 3 plate widths (b) from plate sinkage tests⁸²

Following their investigations of soil stress distributions and displacements beneath moving rigid wheels Onafeko & Reece⁸³ and Wong & Reece^{84,85} noted inadequacy in the prediction ability of equation 8⁸⁶. Whilst providing good prediction at low contact pressures, and hence low sinkages, as soil loading increased the predictions became inadequate. This was because extra horizontal loading reduced the capability of the soil to carry vertical loads, which in turn caused extra slip sinkage. To account for this equation 10, which utilised z , b and n from equation 8, but which introduced different (but similar) soil coefficients k'_c and k'_ϕ was proposed⁸⁶.

$$\rho = \left(ck'_c + \gamma bk'_\phi \right) \left(\frac{z}{b} \right)^n \quad (10)$$

Where: c = cohesion γ = soil density

Although improved prediction was achieved from equation 10, Wong⁶³, who has considerable experience of using both prediction equations for a range of mineral soil types (including sand), stated that “both the Bekker and Reece equations may be used to characterise the pressure sinkage relationships of mineral terrains” and that “both equations can provide an acceptable fit to measured data”. Therefore the simpler, and more universally employed, Bekker equation was utilised as a basis for prediction within this project. Further evidence for the use of the Bekker equation comes from Ziani & Biarez’s investigation of pressure sinkage on loose sand⁸⁷. They showed that for very loose, to average density sand, bearing capacity prediction using equation 11 (a simplified version of Bekker’s equation) gave suitably representative results.

$$\rho = kz^n \quad (11)$$

Where: $k = \text{constant}$

A modified version of Equation 11 was utilised by Ji *et al.*⁸⁸ to describe the effect of different loading patterns upon plate sinkages in dry sand. They found that the use of both inclined loads, and inclined plates, affected pressure sinkage relationships⁸⁸. They modified equation 11 to account for the angled loading by including extra terms and presented a single set of traction results to prove their new theory. Unfortunately a single set of results did not provide a sufficiently rigorous assessment of the methodology to justify its utilisation. Therefore the more accepted equation 8 was used.

3.5.3.1 Prediction of tractive pull

Based upon Bekker’s work (equation 9), Janosi & Hanamoto⁸⁹ proposed equation 12, where thrust, P , is assumed to act similarly to the shear force, F , in a horizontal plane under the traction device, where F is dependant upon the slip and soil deformation relationships. This methodology gave good estimations of the tractive effort/ slip characteristics and the maximum traction achievable for both tracked and wheeled vehicles⁸⁹. “Although many other researchers have subsequently developed a wide variety of differing models, this approach has remained both popular and durable because it is based upon related mechanical principles”⁹⁰.

$$P = F \left[1 + \frac{K}{il} \left(e^{-\frac{l}{K}} - 1 \right) \right] \quad (12)$$

Where: K = soil deformation modulus i = slip
 l = shear (contact) length $F = (Ac + W \tan \phi)$
 A = contact area c = cohesion
 W = vertical axle load ϕ = soil internal friction angle

3.5.3.2 Derivation of the soil deformation modulus (K)

K is defined as the ratio of maximum shear stress (τ_{\max}) and the slope of the tangent to the curve drawn from the origin on a soil shear stress-displacement curve. Yong *et al.* related the relationship to equation 9, from which they derived equation 13⁹¹, in which j equals displacement and α equals the slope of the tangent at the origin of the shear stress versus displacement curve, see Figure 3.13.

$$\left. \frac{d\tau}{dj} \right|_{j=0} = \frac{\tau_{\max}}{K} = \tan \alpha \quad (13)$$

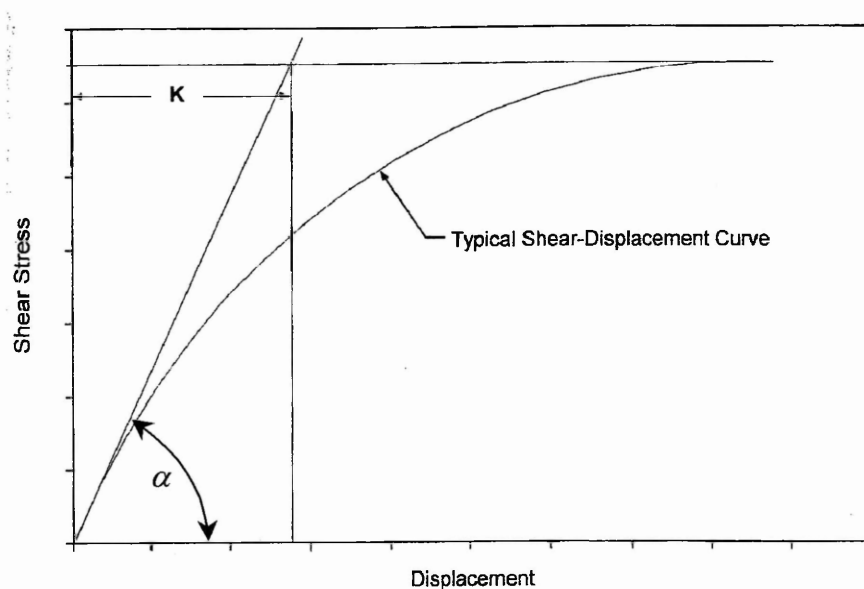


Figure 3.13 – A diagram illustrating how soil deformation modulus, K , is determined⁷¹

Generally values of K have been assumed to be constant for a particular type of soil⁹¹. However, Godbole *et al.*⁹² found that K varies linearly with the amount of normal stress acting on a sample, stating this finding by the relationship shown as equation 14.

$$K = K_0 - C_k \sigma \quad (14)$$

Where: K_0 = a constant for a particular soil type σ = normal stress
 C_k = the slope of the graph K vs. σ

The authors⁹² went further to propose a model, shown by equation 15, in which K values depended upon contact area, shear stress and normal stress.

$$K^2 = C_\alpha A \left(\frac{\tau}{\sigma} \right)^{C_I} \quad (15)$$

Where: C_α = an experimental coefficient A = contact area
 C_I = an appropriate exponent

When this equation was applied to a situation with two identical soils experiencing similar normal stresses over different areas the relationship changed to that shown by equation 16, where K_1 and K_2 are values corresponding to the different areas A_1 and A_2 respectively⁹². Application of this equation allowed K values to be scaled from direct shear apparatus test results to represent those applicable for the vehicle situation.

$$\frac{K_1}{K_2} = \sqrt{\left(\frac{A_1}{A_2} \right)} \quad (16)$$

The purpose of the authors' research⁹² was to compare predicted and measured dynamic traction ratios (P/W). K_1 values were measured on a direct shear-testing machine of area A_1 and converted into K_2 values using equation 16. These were then applied to equation 17 (equation 12 re-arranged), from which dynamic traction ratio predictions were obtained.

$$\frac{P}{W} = \left(\frac{A}{W} c + \tan \phi \right) \left[1 + \frac{K}{il} \left(e^{-\frac{l}{K}} - 1 \right) \right] \quad (17)$$

These predictions were compared against dynamic traction ratios measured from tests on soil using a single wheel tester, described by Alcock & Wittig⁷⁷, fitted with a 6.7 x 15 tyre inflated to 55 kN/m² which represented area A_2 . Shear stresses were derived from measured torque values and a calculated contact patch area, which was derived from the tyre width multiplied by the measured contact length. This assumed a rectangular contact patch, which was shown to be sufficiently accurate for the contact investigated. No difference was found between K values measured in the field and calculated from the laboratory readings, therefore the theoretical scaling was assumed to be valid⁹². Although not unequivocally stated by the authors this suggests that direct shear laboratory results are adequate to predict K values beneath a known tyre contact area for field conditions, providing the normal stress conditions are comparable.

3.5.3.3 Contact area prediction

Having stated their methodology for determining K values Godbole *et al.*⁹² utilised equation 17 to determine wheel thrust. To do this accurately they developed further the models of Krick⁵⁵ for the determination of tyre contact patch geometries. Thus the rectangular contact area was described by equation 18⁵⁵.

$$A = 4C_A f \sqrt{DS} \quad (18)$$

Where: $C_A = 1$ for hard soil, or $C_A > 1$ for soft soil
 $f =$ tyre deflection $D =$ tyre diameter $S =$ tyre section height

Krick⁵⁵ defined the deflection (f) as being a function of S and a tyre numeric, T . Due to inadequacy in these methods Godbole *et al.*⁹² replaced T with T' a modified numeric expressed by equation 19.

$$T' = \frac{pDS}{W} \quad (19)$$

Where: $p =$ inflation pressure $W =$ axle load

The results of their analysis allowed this equation to be used to develop the empirical relationship for tractor tyres shown by equation 20. More generally this equation can be expressed in the form $f/S = Q(T')^{-m}$, where the constants Q and m vary due to alterations in the tyre size under consideration.

$$\frac{f}{S} = 0.54(T')^{-0.79} \quad (20)$$

Wulfsohn & Upadhyaya⁹³ have also conducted extensive field tests upon agricultural tyres using a single wheel tester (described in section 3.6.2) to develop prediction equations for both traction and compaction, see equations 21 and 22, and Figure 3.14.

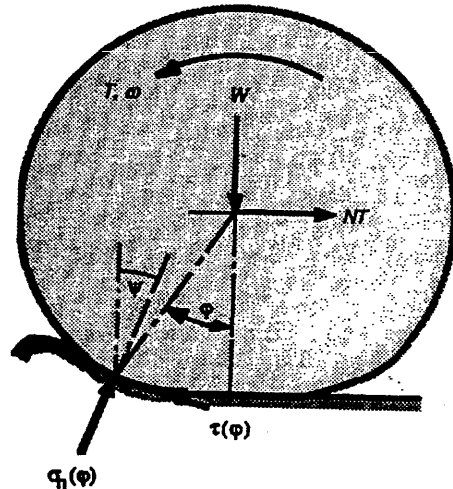


Figure 3.14 – A diagram of the position of the forces acting on a driven wheel operating on soft terrain⁹³

$$\text{Net traction} = NT = \int_A \{ \tau(\varphi) \cos \psi - \sigma_n(\varphi) \sin \psi \} dA \quad (21)$$

$$\text{Dynamic axle load} = W = \int_A \{ \tau(\varphi) \sin \psi - \sigma_n(\varphi) \cos \psi \} dA \quad (22)$$

Where: τ = shear stress at contact surface σ_n = normal stress at contact surface

ψ = angle between surface normal and vertical at any point on contact surface

φ = angle from tyre axle vertical line to the point on contact surface

A = area of the soil tyre contact surface

To fully utilise these equations the contact patch dimensions were required. This led Upadhyaya & Wulfsohn⁹⁴ to develop mathematical expressions for two-dimensional agricultural tyre contact patch areas on rigid surfaces. Later these were enhanced to determine three-dimensional soil-tyre contact profiles for agricultural tyres operating on deformable soil^{95,96}, which were related to the tyres' tractive performances⁹⁷. The three-dimensional prediction method involved the measurement of incremental arc lengths at discrete locations along the contact length⁹⁵. This prediction was derived from measurements made using wire and cable potentiometers placed in the soil to measure the soil deformation at the interface. As would be expected the three-dimensional representation produced the best traction predictions, achieving a correlation coefficient value of 0.7, when compared against actual measured net traction values⁹⁶.

From their testing Upadhyaya *et al.*⁹⁸ determined traction equations capable of defining gross and net thrust coefficients produced by agricultural tyres, based on five semi-empirical coefficients. However, these were related to cone index readings and proved inadequate. Thus a device was developed to measure soil sinkage and shear parameters⁹⁹, allowing the five coefficients to be related to directly measured soil characteristics¹⁰⁰. Latterly Upadhyaya *et al.*¹⁰¹ developed simplified equations. Whilst these theories are important in terramechanics their suitability for application to this situation was unknown because only agricultural (tractor) tyres were evaluated when operating on typical agricultural soils (clays and loams). In contrast Bekker's equations have been validated for tyre sizes and soil conditions appropriate to this study.

Although knowledge of contact area dimensions is important for traction prediction this project overlooked the methods outlined above and instead used the more relevant results recorded by a contemporary Cranfield University EngD student³⁰. His research investigated the dynamic behaviour of 4x4 contact patches for identical tyres and related them to tyre performances. He did this by fitting drawstring potentiometer measurement devices inside the tested tyres to allow dynamic measurement of contact patch areas on sand³⁰. To hasten both researcher's test programmes the investigations were conducted jointly where possible, so identical tyre and soil treatments were investigated. Thus, for the purposes of traction prediction, contact patch dimensions

relevant to this project were drawn directly from Oliver's measurements³⁰ and a separate contact area prediction model was not required.

3.5.3.4 Other thrust prediction methods

Reece⁸⁶ postulated that developments of Bekker's models were needed to account for bow wave effects, which altered both the contact patch dimensions and thus the points of action of forces between the soil and the tyre. He therefore proposed the following theory to predict both the radial (normal) stresses and tangential (shear) stresses beneath a rigid wheel⁸⁶. The radial stresses in the forward region of failure σ_1 , were predicted by equation 23, whilst the radial stresses in the rearward region of failure σ_2 , were predicted by equation 24. Plate 3.2 shows typical forward and rearward failure zones, whilst Figure 3.15 shows the nomenclature for equations 23 and 24. Equation 25 was proposed to predict the shear stresses around the rim⁸⁶.

$$\sigma_1(\theta) = (k_1 + k_2 b) \left(\frac{r}{b} \right)^n (\cos \theta - \cos \theta_1)^n \quad (23)$$

$$\sigma_2(\theta) = (k_1 + k_2 b) \left(\frac{r}{b} \right)^n \left[\cos \left(\theta_1 - \theta \left(\frac{1 - (c_1 + c_2 i)}{c_1 + c_2 i} \right) \right) - \cos \theta_1 \right]^n \quad (24)$$

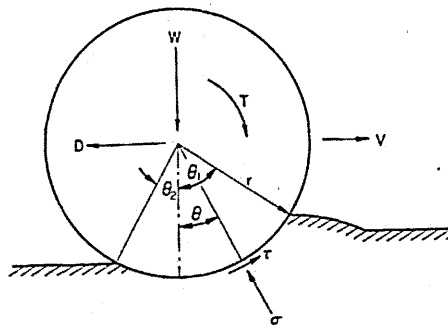


Figure 3.15 – Forces, torque and stresses acting on a driven rigid wheel⁸⁶

$$\tau(\theta) = (c + \sigma(\theta) \tan \phi) \left(1 - e^{-r/k[(\theta_1 - \theta) - (1-i)(\sin \theta_1 - \sin \theta)]} \right) \quad (25)$$

Using these three equations, additional relationships were developed to predict sinkage and drawbar pull. However, besides knowledge of the soil properties and plate sinkage coefficients, values for the coefficients used to determine the point of maximum stress beneath the wheel c_1 and c_2 were also required, along with stress measurements at the rim. If these were known this theory provided good prediction for the full range of slips and associated wheel sinkages⁸⁶. This study would not measure shear stresses around the wheel and thus the theory was not applied.

3.5.3.5 Prediction of rolling resistance

Whilst it is generally agreed that equation 12 can be used to predict the thrust produced by a wheel, much debate has occurred on the subject of rolling resistance prediction. Originally Bekker²⁰ proposed the following equation (26) to describe the rolling resistance (R) of a towed rigid wheel running upon homogeneous soils, where the pressure sinkage terms described in equation 8 applied.

$$R = \frac{(3W)^{\left(\frac{2n+2}{2n+1}\right)}}{(3-n)^{\left(\frac{2n+2}{2n+1}\right)} (n+1)(k_c + bk_\phi)^{\left(\frac{1}{2n+1}\right)} d^{\left(\frac{n+1}{2n+1}\right)}} \quad (26)$$

Gee-Clough¹⁰² compared results from equation 26 to results that he had previously calculated using modified versions of Bekker's equations¹⁰³. He concluded that his own theory was only applicable to narrow wheels (more typical of agricultural tyres) operating in sandy soil, and that neither theory accurately predicted the performance of wide wheels in sand. Hetherington & Littleton¹⁰⁴ studied these issues and derived their own formula, equation 27, to describe the rolling resistance of a towed rigid wheel on granular (sand) soil, based upon the energy expended to form a unit length of rut.

$$R = \left(\frac{2W^4}{bd^2 \gamma N_q} \right)^{1/3} \quad (27)$$

Where: R = Rolling Resistance

W = Normal axle load

b = Wheel breadth

d = Wheel diameter

γ = Bulk unit weight of sand

This theory was more suited to the narrow wheel (small b : d ratio) application, which is more akin to long thin footings being pressed into soil. Besides the numerical constant this was actually a special case of Bekker's equation, where $n = 1$ and $(k_c / b + k_\phi) = N_q \gamma$, where N_q was from Terzaghi's bearing capacity solution for a rough foundation on a weightless, cohesionless soil. Application of the theory showed good agreement between measured and predicted results for the range of conditions tested.

Later Bekker re-evaluated the tyre motion resistance problem, with the benefit of a vast experience in the field. His most detailed methods of performance prediction, which are suitable for a range of wheeled and tracked vehicles are detailed in section 3.5.3.7, which is a précis from a summary his report¹⁰⁵ by Wong⁶³.

3.5.3.6 An analysis of 4x4 performance on sand

Ataka & Yamashita¹⁵ developed, and conducted in-situ testing of, the following theory for tyres that would typically be found on 4x4 utility vehicles operating in the U.A.E. The sand tractive force, ST , was defined by equation 28, where equation 29 described H .

$$ST = H - R \quad (28)$$

Where: H = traction force R = rolling resistance of the sand.

$$H = C_A \times K_1 \quad (29)$$

Where: C_A = the tyre contact area (length x width)

K_1 = the shearing stress of the sand under the tyre ($\sigma \tan \phi$)

Thus K_1 was related to ϕ , which the authors related to the void ratios of the three sands that they tested. The authors¹⁵ also showed that the shearing stress of the sand in the contact patch, τ , increased proportionally with the normal contact stress, σ , as the contact area decreased, until a certain critical stress, σ_1 , was reached.

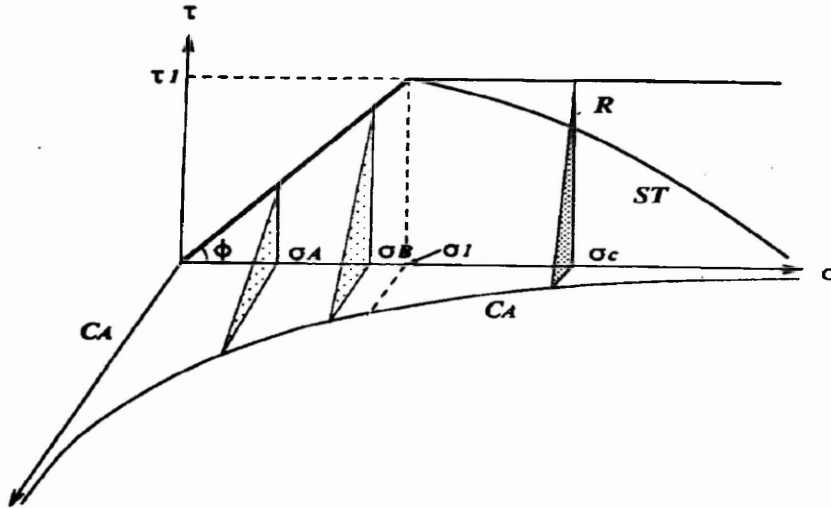


Figure 3.16 – A graph of contact stress characteristics beneath a tyre on sand¹⁵

Once σ_1 was exceeded then the sand beneath the tyre could not support the excessive load, and hence moved aside and rose ahead of the tyre. Thus the shearing stress achieved a constant critical value of τ_1 , whilst the sand rising ahead of the tyre increased the resistance force R . Figure 3.16 represents this conceptual analysis, from which equation 29 was developed into equations 30 and 31, to describe the two possible stress states beneath the wheel¹⁵.

$$\text{If } (\sigma \leq \sigma_1) \text{ then:} \quad H = C_A \times \sigma \tan \phi \quad (30)$$

$$\text{Else if } (\sigma > \sigma_1) \text{ then:} \quad H = C_A \tau_1 \quad (31)$$

R was described as the force required to compressively fracture the sand in front of the tyre. This was translated into a mathematical expression equation 32.

$$R = K_2 C_W L_R (\theta_L - \theta_V) \quad (32)$$

Where: K_2 = compressive fracture force of sand ahead of the tyre

C_W = contact width

L_R = static loaded radius measured in laboratory on sand

θ_L & θ_V = Angles from the horizontal to the sand, see Figure 3.17 and equations 33 and 34 (measured statically in the laboratory)

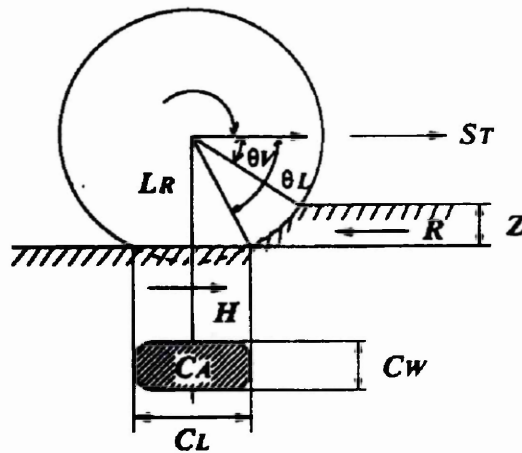


Figure 3.17 – A diagram of the forces acting on a tractive tyre in sand¹⁵

$$\theta_L \approx \cos^{-1} \left(\frac{C_L}{2L_R} \right) \tag{33}$$

$$\theta_V \approx \sin^{-1} \left\{ \frac{(L_R - Z)}{L_R} \right\} \tag{34}$$

Where: C_L = contact length L_R = deflected radius
 Z = tyre deflected sinkage

K_2 values were determined from data collected during desert testing. This was done by measuring the depth of sinkage of a mass dropped onto the sand, Y , proportional to the height from which it was dropped, h , relative to the sinkage that occurred due to its own weight when placed on the sand, X , see Figure 3.18. Equation 35 was then used.

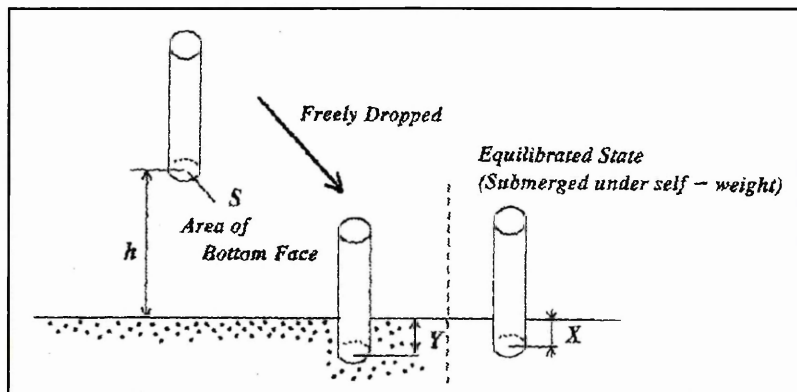


Figure 3.18 – A method for measuring compressive sand fracture¹⁵

$$K_2 = \frac{mg(h+Y)}{S(Y-X)} \quad (35)$$

These authors¹⁵ developed a simplified method of determining the resistances and gross thrusts generated by 4x4 tyres in desert conditions and they demonstrated good comparison between predicted values and experimental results. However, these were only determined on a ranked index basis comparing the time taken for each tyre treatment to accelerate a vehicle from standstill over 50 m. As only a limited number of tests were conducted this approach was not rigorously evaluated, but more disappointingly no data was presented comparing the predictions of gross thrust and rolling resistance (or net pull) against actual measured values from the field trials. Thus despite the promising nature of this work further, more rigorous, analysis is necessary before it can become accepted theory.

3.5.3.7 Bekker's prediction for wheeled and tracked vehicles (from Wong⁶³)

Although not without its criticisms, it has been generally agreed that Janosi & Hanamoto's⁸⁹ equation for predicting thrust is applicable for pneumatic tyres, as shown by section 3.5.3.2. The manner in which rolling resistance is calculated is more disputed. Study of different researcher's theories has shown that a universally suitable model has yet to be developed. In the absence of such a model it is proposed that this project will utilise the methods described by Bekker¹⁰⁵, whose study of terramechanics has most rigorously investigated the tractive effects of many tyre sizes and varieties upon all of the common soil types. Though weaknesses exist when comparison is made between his proposed methods and the mechanisms by which traction is generated, the durability of this approach, which has been employed in many studies, is testament to its usefulness. This approach is presented below:

(1) Net Thrust: Gross thrust – rolling resistance

(2) Horizontal force (Gross Thrust) prediction: Use Janosi & Hanamoto's equation, detailed in this document as equation 12⁸⁹.

(3) Rolling Resistance prediction: Depending upon its pressure and the ground's stiffness then a tyre will either operate in a rigid (un-deformed) mode or an elastic (deformed) mode. At low pressures 1.10 bar (16 psi) it will always operate elastically, however between 1.10 bar and 3.10 bar (45 psi) a changeover will occur at the critical pressure (ρ_{gr}), which was defined by the following equation (36) proposed by Wong⁶³.

$$\rho_{gr} = \left[\frac{k_c}{b} + k_\phi \right]^{\left\{ \frac{1}{2n+1} \right\}} \left[\frac{3W}{(3-n)b_{tr}\sqrt{D}} \right]^{\left\{ \frac{2n}{2n+1} \right\}} \quad (36)$$

Where: b = minimum plate dimension (be it width, \square plate, or diameter, \circ plate)
 k_c, k_ϕ & n = empirically measured coefficients from plate sinkage tests
 W = normal axle load b_{tr} = deflected tyre width
 D = un-deflected tyre diameter

Above ρ_{gr} then the tyre will operate rigidly, whilst below ρ_{gr} elastic operation will occur. The rigid or elastic mode of operation governs the number of components used in the rolling resistance prediction model:

(3a) Rigid mode:

R_c = Compaction resistance
 R_b = Bulldozing resistance

(3b) Elastic mode:

R_c = Compaction resistance
 R_b = Bulldozing resistance
 R_f = Tyre carcass flexing resistance

(3a) Rolling Resistance – Rigid operation mode = ($R_c + R_b$)

R_c – Compaction resistance

$$R_c = b_{tr} \left(\frac{Z_r^{n+1}}{n+1} \right) \left(\frac{k_c}{b} + k_\phi \right) \quad (37)$$

Where: b_{tr} = rut width created by tyre Z_r = tyre sinkage
 k_c, k_ϕ & n = empirically measured coefficients from plate sinkage tests
 b = minimum plate dimension (be it width, \square plate, or diameter, \circ plate)

R_b – Bulldozing Resistance

This is analogous to the force due to passive earth pressure acting on a retaining wall. However, there are two conditions that can apply: ‘General’ and ‘Local’ failure. The assumed failure has great consequences for the forces predicted, however, Bekker¹⁰⁵ states that, “in most cases there is no indication if soil failure takes place through the general or local shear.” Thus uncertainty exists of which sets of Terzaghi ‘ N ’ factors should be used for prediction, and hence both cases are presented.

General Failure

$$R_b = b_{tr} (czK_{pc} + 0.5z^2\gamma K_{py}) \quad (38)$$

Where the constants are as above except for:

γ = soil density

$$K_{pc} = (N_c - \tan \phi) \cos^2 \phi \quad (39)$$

$$K_{py} = \left(\frac{2N_\gamma}{\tan \phi} + 1 \right) \cos^2 \phi \quad (40)$$

Where N_c and N_γ are Terzaghi bearing capacity factors for General shear failure.

Local Failure (assumed for loose soils)

$$R'_b = b_{tr} (0.67czK'_{pc} + 0.5z^2\gamma K'_{py}) \quad (41)$$

Again constants are as before except for:

$$K'_{pc} = (N'_c - \tan \phi') \cos^2 \phi' \quad (42)$$

$$K'_{py} = \left(\frac{2N'_\gamma}{\tan \phi'} + 1 \right) \cos^2 \phi' \quad (43)$$

Where N'_c and N'_γ are Terzaghi factors for Local shear failure and:

$$\tan \phi' = \frac{2}{3} \tan \phi \quad (44)$$

(3b) Rolling Resistance – Elastic operating mode = $(R_c + R_b + R_f)$

R_c – Compaction resistance

$$R_c = b_{tr} \left(\frac{Z_e^{n+1}}{n+1} \right) \left(\frac{k_c}{b} + k_\phi \right) \quad (45)$$

Where: b_{tr} = rut width created by tyre

Z_e = Tyre sinkage

k_c, k_ϕ & n = empirically measured coefficients from plate sinkage tests

b = minimum plate dimension (be it width, \square plate, or diameter, O plate)

R_b – Bulldozing Resistance

This prediction is common to both operating modes and therefore the equations presented for rigid operation should be used.

R_f – Tyre Carcass Flexing Resistance

$$R_f = [3.581b_{tr}D^2\rho_g\varepsilon(0.0349\alpha - \sin 2\alpha)] / \alpha(D - 2\delta) \quad (46)$$

Where: D = tyre diameter

δ = tyre deflection

$$\rho_g = P_g = \left[\frac{k_c}{b} + k_\phi \right]^{1/(2n+1)} \left[\frac{3W}{(3-n)b_{tr}\sqrt{D}} \right]^{2n/(2n+1)} \quad (47)$$

$$\alpha = \cos^{-1}[(D - 2\delta) / D] \quad (48)$$

$$\varepsilon = 1 - e^{(-k_e\delta/h)} \quad (49)$$

Where: h = Section height $K_e = 7$ for radial tyres

3.5.4 Finite Element Mathematical Models

More recently as computing performance and capability has increased some authors have pursued the use of FE models to predict tractive tyre performance and tyre effects on the soil, i.e. compaction. Yong & Fattah¹⁰⁶ (1976) were amongst the first authors to apply the finite element method to terramechanics using energy calculations to predict soil deformation beneath, and drawbar pull of, a rigid wheel but the descriptions of soil material properties and boundary conditions were inherently limited.

Oida¹⁰⁷ (1984) developed FE methods further to better account for soil properties, which were not well described by off-the-shelf products, thereby addressing some of the weaknesses in Yong & Fattah's¹⁰⁶ model. Oida's¹⁰⁷ model showed good prediction of wheel sinkage on a sandy loam soil and Regli *et al.*¹⁰⁸ developed an FE model to predict the tractive performance for, and soil deformation beneath, lugged agricultural tyres for limited conditions. Whilst model predictions correlated well to measured values at low slips (up to 20%) considerable error occurred above 30% slip. The authors stated this as being due to "big deformations causing significant inaccuracies in the FE program"¹⁰⁸.

A more recent FE sand-tyre interaction model by Liu *et al.*¹⁰⁹ produced useful prediction of tyre traction, but only for a specialised set of conditions. Particular limitations were the use of two-dimensional solid wheels (discs) and poor representation of the contact pressure and friction force along the tyre-soil interface. More significantly "local failure and significant amounts of sand flow under moving tyres cannot be modelled adequately by the conventional finite element method"¹⁰⁹. Thus the model's performance deteriorated with increased slip, indicating that such methods would be inappropriate to provide predictions at the high slips of approximately 75% that would form part of this investigation.

Despite all the advances, the modelling of tyres and soil by the FE approach remains complex. It is possible to produce models to predict performance where small soil strains occur, but FE methods struggle to solve problems involving large soil displacements. There is also the issue of developing models that are suitably complex to accurately model a given situation. At the initiation of this project (1998) Goodyear were developing a dynamic FE tyre model capable of replicating low speed revolutions on a non-deformable surface with an accuracy suitable for their purposes. This required a supercomputer for its solution. In the light of this evidence it was beyond this project's capabilities to deliver an FE type model capable of providing useful predictions for a tyre operating at high slips on loose deformable sand.

3.6 TYRE TEST RIGS

3.6.1 Fixed Slip Test Rigs

Publications by Uffelman¹¹⁰ and Reece & Wills¹¹¹ detailed systems developed for their experimental tyre investigations and the generation of slip-pull curves. Both systems operated with a similar principle, whereby fixed wheel (or track) slips were generated using anchored cables that wrapped around variable sized drums (or chain drives), which in turn connected to the wheel. The test tyre was mounted on a framework that was driven away from the anchor point using either a tractor or a towed trolley, thereby inducing wheel slip. Measuring the forces within the system allowed the tyre thrust and rolling resistance to be determined. These machines offered the researchers versatility and simplicity at a low cost. Latterly Del Rosario¹¹² designed a system that generated good experimental results by adapting these principles for use in a soil bin situation.

The one drawback of these systems was that, either the slip (drum size) had to be changed before each test run to generate results across the full slip range, or else a variable diameter drum had to be utilised. Variable size drums were achievable as Soehne¹¹³ demonstrates, however, it was difficult and costly to manufacture such items, especially if a large diameter was required. Thus, more commonly, a number of discrete drum sizes or gear ratios were utilised to overcome this issue.

3.6.2 Variable Slip Test Rigs

Truly adequate variable slip tyre traction test rigs were not developed until around the 1940's¹¹⁴, when the N.I.A.E. were simultaneously developing a single wheel tester¹¹⁵. This device was structured around a tractor that underwent a bespoke re-design to include an electric motor to apply a controlled torque to the separate test wheel mounted behind the tractor. The wheel frame mounting used parallel linkages and Hooke's joints to avoid weight transfer between the two sections, a criticism of earlier devices.

The advantages of this device¹¹⁵ were that it was able to quickly measure thrusts across a range of slips for a given tyre, and because it was mounted on a tractor it was extremely mobile and could be used on any surface. The experiments conducted with

the device showed that it worked well, however, the design was complex, expensive and had been time consuming to perfect. Despite this, the advantages that could be achieved in the timely completion of a test programme by being able to speedily change the tyre slip, through a separately controllable wheel drive, were clearly apparent.

Billington¹¹⁶ described the further development of this apparatus as it was improved to form the N.I.A.E. Mark II single wheel tester. 52 kW (70 hp) hydrostatic transmissions were fitted as they best provided the high power and controllable drives necessary for both the tractor and test wheels. Again the test frame was connected to the tractor by parallel linkages to avoid weight transfer between the two units, whilst strain gauged units were fitted appropriately to measure the thrust produced by the wheel. Wheel speeds were measured by tacho-generators, whilst wheel torque was measured using a strain-gauged transducer. This equipment was successfully used to investigate the tractive performance of a range of agricultural tyres on a variety of agricultural surfaces.

Upadhyaya *et al.*^{117,118} described the development of another type of single wheel tester undertaken by staff at the University of California, Davis to allow the investigation of soil-tyre interaction. This took the form of a mobile soil bin with a drive unit that could be operated in either a draft, or slip control mode. It consisted of two 12 m tracks mounted on either side of a front and rear trailer, which allowed easy location of the device in a field. A carriage with a test wheel, powered by a hydrostatic drive, ran along the tracks. Changing the pressure in a load cylinder controlled the vertical tyre load. Variation to the hydrostatic controls allowed a tyre to be tested across the full slip range, although this required several test runs. A range of instrumentation was fitted to the device to measure the carriage and wheel speeds and sinkages, thereby allowing a full picture of the traction interactions to be developed.

Keen^{119,120,121} described various traction investigations that were undertaken using a single wheel tester that was developed at Harper Adams University College, Shropshire, UK. This single wheel device was designed to mimic a quarter of a high-speed tractor through the inclusion of a suspension between the wheel and the supported mass. It was mounted to a tractor three-point linkage and driven through a 44 kW diesel Land Rover

engine and gearbox. The tractor forward speed controlled ground speed, and varying the Land Rover engine speed controlled the wheel slip. This worked well across the low slip range that was investigated (up to 25%). The tester was instrumented to measure thrust, through a strain gauged parallel linkage, thus allowing slip-pull curves and wheel sinkages to be determined. Good agreement was shown¹¹⁹ between thrust values measured by this device and the prediction equations proposed by Janosi and Hanamoto⁸⁹. Accelerometers were also fitted to the test rig and used to measure the vertical accelerations that were incorporated into Keen's later research^{120,121}.

The most capable of the single wheel testers discussed have a high mobility allowing them to operate upon a range of soil surfaces. However, even the most basic systems using cable drums are very capable of producing results from which slip-pull curves can be constructed. Although more costly, variable hydrostatic transmissions allow much greater experimental flexibility, as a full range of wheel slips can be quickly tested. Study of all of these devices indicated that instrumentation and data recording systems should be fitted to allow the determination of the following tractive variables:

1. Tractive Force (Thrust) and (or) Rolling Resistance.
2. Test wheel rotational speed
3. Drive unit ground speed.
4. Wheel sinkage.
5. Wheel slip (derived from measurements 2 and 3).
6. Angular wheel position
7. Tyre deflection
8. Normal and longitudinal stress at the interface

3.7 SUMMARY OF LITERATURE REVIEW

The completed literature review enabled the required stages of the project to be more clearly identified and planned. Initially it was necessary to understand the market requirements for performance off-road tyre products, which would necessitate a market survey. Then to enable the tyre performance to be modelled using adaptations of Bekker's predictive methodologies outlined above it would be necessary to collect raw data that could be used to develop and validate the models. A further model would have

to be developed to allow the required tread pattern to be related to the tyre performance. The development of this would also require experimental results.

To enable experimental results to be collected it was necessary to develop an instrumented test-rig and experimental methodology capable of measuring the tractive performance data outlined in section 3.6 in the Cranfield University Soil Dynamics Laboratory. Additionally the performance of both the TekScan stress measuring system and the RFID tag sensing system required evaluation in terms of their new intended applications before they could be adopted for the main investigations into pressure distributions and particularly sand displacements beneath the tyres. Tractive performance data was also recorded during these investigations so that the prediction capabilities of the proposed tyre performance models could be assessed for the dynamic sand traction environment created in the SDL.

4 MARKET SURVEY AND REVIEW

Before any tyre performance investigations were conducted, it was necessary to investigate the implications of optimising 4x4 tyre treads to suit off-road environments from the perspective of 4x4 end-users (drivers). If the tyre (and vehicle) products currently available to them already delivered capabilities that exceeded their requirements, then further tread developments and enhanced modelling techniques would be unnecessary and unwarranted. A customer questionnaire was identified as being the most effective way to evaluate the market's views upon a range of tyre issues related to off-road and on-road performance. When this was jointly designed and undertaken with Marcus Oliver³⁰, during the early stages of both projects, the author was considering conducting tyre traction investigations on a range of off-road surfaces. Therefore a set of results from which the implications of off-road tyre requirements could be assessed for a range of off-road surfaces, not just sand environments, was required. These implications were considered for both of the sponsoring manufacturers.

4.1 MARKET SURVEY METHODOLOGY

The requirement to understand a range of views of end-users meant that the questionnaire had to be universally applicable to a range of 4x4 drivers and it had to sample an audience with a wide range of driving habits, skills etc. This meant that it could not be conducted at a specialised off-roading event, so instead it was undertaken at the 1998 International Motor Show, held in October at the NEC, Birmingham, UK, for the following reasons:

- It would attract large numbers of prospective 4x4 tyre customers, from diverse backgrounds, including overseas visitors.
- The event is the UK's premier car show.
- Its proximity to the Land Rover Solihull site, allowed use of their Driving Experience site (a dedicated off-road promotional training track). This greatly assisted identifying existing, and potential, Land Rover customers, and therefore prospective performance 4x4 tyre purchasers, as guests invited to the Driving Experience were either existing Land Rover customers, or had a strong interest in owning a Land Rover.

The questionnaire used, see Appendix 3, was designed to survey people who drove a variety of vehicles upon a range of on-road and off-road surfaces, from ice to desert sand, for a range of purposes. A significant number of the questions were designed to be open-ended, so that a range of individual views could be sampled from respondents. In particular the questionnaire was intended to determine:

1. The market's perception of the performance of existing 4x4 tyres.
2. What would be the important factors if respondents were considering purchasing high performance off-road tyres?
3. The likelihood of respondents to purchase a second set of dedicated off-road tyres for their 4x4 vehicles if they offered extra performance over existing tyres on a particular surface.

The questionnaire was also designed to record:

1. People's personal profiles, to determine the sex, age, geographical location, socio-economic group and vehicles driven both on and off-road by respondents.
2. Data questions, to determine opinions, particularly those related to cost, value and relative importance, for a range of tyre related issues.
3. Response triangulation, for analysis of the truthfulness and/or bias of answers.

The questionnaire was conducted at the Driving Experience for the show's duration whilst the respondents waited for their promotional trip around the track. The wait could take up to 30 minutes, which allowed time for people to fully participate with the questionnaire. Respondent's participation was sought on a purely random basis as they entered the waiting area. A total of 369 questionnaires were fully completed, however, the results of respondents whose replies contained three or more contradictory answers (about 3%) were not included in the analysis.

4.2 MARKET SURVEY RESULTS

The questionnaires were individually examined and the responses entered into an Excel spreadsheet, which allowed the results to be easily sorted and grouped. The results were then analysed to find trends and factors contained within the replies. The respondents were segmented into separate groups of purely on-road drivers, on and off-road drivers

and 'serious' off-road drivers by employing recognised methods^{122,123}. 'Serious' off-road drivers were those people who were the most frequent and knowledgeable off-road drivers, be it through work or leisure, for example Land Rover enthusiasts, hill farmers and landowners. This last segment were of most interest because they owned the greater quantity of 4x4 vehicles, had the most valid opinions based upon their real experience, and because they were the drivers most likely to purchase second sets of dedicated 4x4 off-road tyres to supplement existing road biased tyres. This group accounted for 12% of all respondents, and 46% of the respondents who partook in some form off-road driving. Analysis of the replies from the off-road drivers and 'serious' off-road drivers produced the following results.

4.2.1 The Profile of Prospective Purchasers of Off-road Tyres

Within the UK these drivers were concentrated in Yorkshire and Humberside, the East and West Midlands, and the South East. However, these results were biased by the proximity of these locations to the Motor Show. Typically these people drove off-road in muddy environments, although some people drove on beach sand. The off-road drivers from overseas accounted for 7% of respondents, but this quantity was too small to identify patterns in their geographical locations. 65% of these drivers did their off-roading in rocky (semi-desert) or sand environments, though often off-roading only involved driving on dirt tracks and trails, for which universal (compromise) treads were generally fitted.

The respondents in the 'serious' group were either in the Middle or Skilled working classes and exclusively male drivers (as no women questioned undertook any form off-road driving, although this cannot be representative of the whole off-roading population). The ages of likely purchasers ranged from 26-50. Predominantly these respondents drove off-road for recreation and leisure and they were well informed about the importance of tyre choice for such ventures. Both the respondents from the UK and overseas stated that they were keen that their vehicles should be fitted with high-performing tyres when they were undertaking off-roading, although 80% of tyre fitments were actually compromises that offered an adequate level of on-road performance. These statements were confused by the respondents' relative perceptions

of what constituted a high-performing tyre, and their inability to universally quantify high (or low) levels of off-road tyre performance.

4.2.2 Properties Identified as Important for Off-road Tyres

As expected the two main factors that influenced the purchase of off-road tyres were the cost and the perceived potential performance benefits, although the frequency and level of off-road driving undertaken were also important. Off-road tyre requirements were analysed in greater detail and the data collected was used to construct the graphs shown below. The data questions required people to rank five tyre factors in order of importance. If each factor were viewed as equally important all the factors scored 20%, thus scores above (below) 20% indicated the relative importance (un-importance) of the factor. The most important property for an off-road tyre was unanimously its performance; see Figure 4.1, and this choice came at the expense of aesthetics, which were viewed, as being of minimal importance. Five tyre performance factors were also separately analysed to establish what were the key factors, see Figure 4.2. Grip (potential thrust) was of most importance, although handling also rated highly.

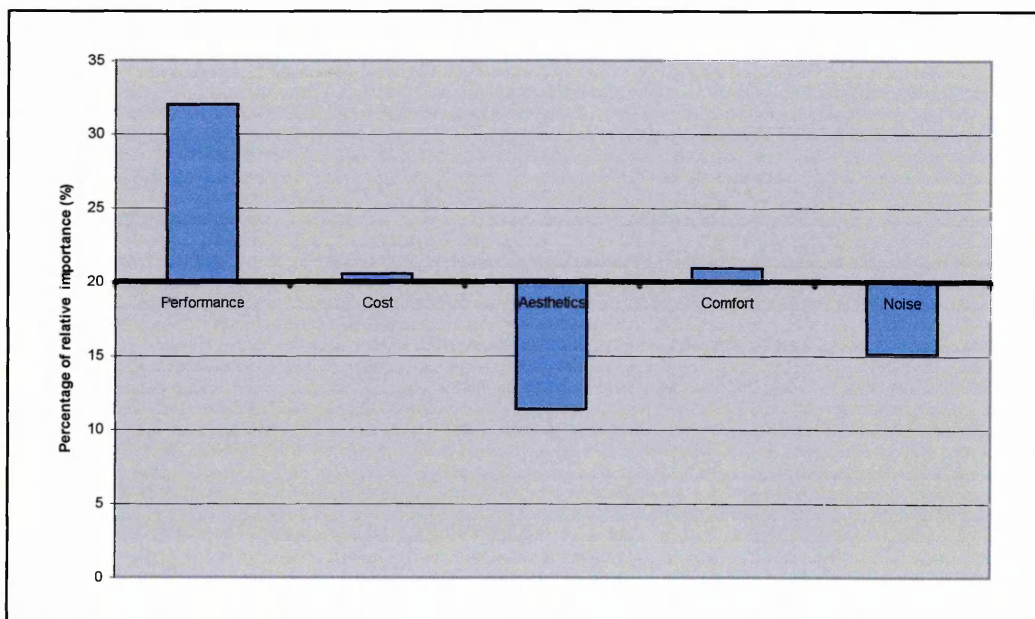


Figure 4.1 – The relative importance of five off-road tyre factors as indicated by off-road drivers

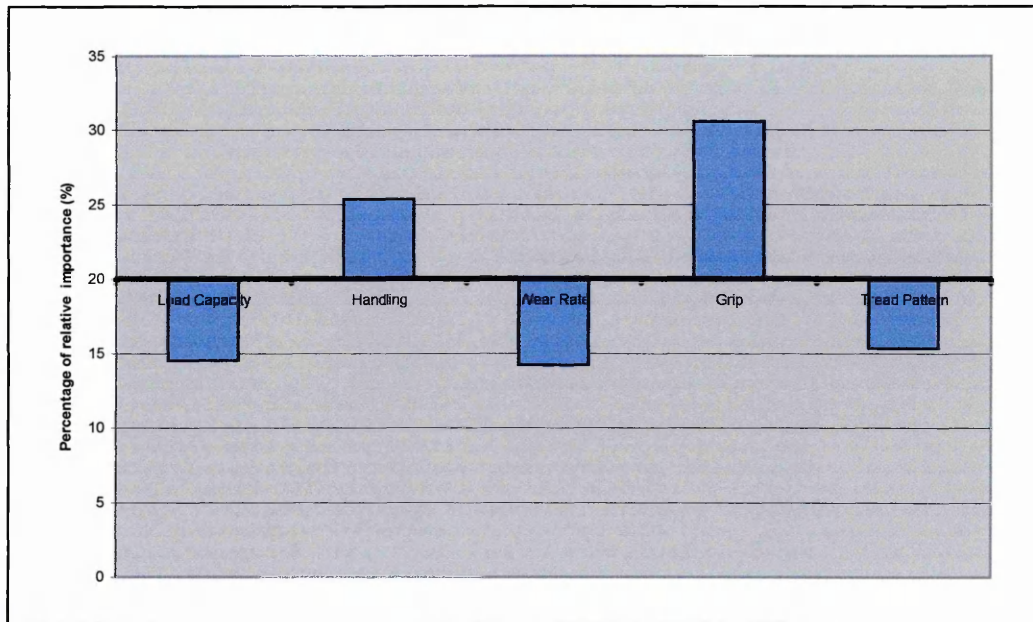


Figure 4.2 – The relative importance of five off-road tyre performance factors as indicated by off-road drivers

From the pictorial analysis that formed part of the questionnaire it was established that the tyre that respondents most wanted fitted to their vehicles would be a low profile (61% of respondents), wide section (90%), treaded tyre with a black sidewall and plain black lettering (93%). It was interesting to note that conflict existed in off-road driver's minds between their stated desire that tyres should not compromise on delivering good off-road tractive performance and their wishes for their vehicles to look aesthetically pleasing e.g. sporty and trendy. People indicated that the tyres they wanted fitted to their vehicles were wide (90% of respondents) and low profile (61% of respondents). This conflicts with the types of tyres capable of producing the highest levels of grip and performance in desert conditions e.g. narrow, high profile tyres.

Respondents' opinions were also divided over the type of tread they wished their tyres to have, with 64% desiring a smooth tread, whilst 34% favoured a chunky tread pattern. Typical treads of this nature are shown in Figure 4.3. This split in opinion arose due to whether people typically used their vehicles on-road or off-road. The off-road drivers felt that a chunky tread was required, as this would allow the tyre to perform well off-road (which is certainly true on mud). The more seasoned 4x4 drivers also felt that such treads made 4x4 vehicles 'look the part' and hence were more desirable. In contrast on-

road drivers favoured smooth treads, partly because they offered better performance and partly for aesthetic reasons i.e. they looked more like car tyres.



Figure 4.3 – Typical smooth (left) and chunky (right) treaded tyres

4.2.3 Respondents' Perceptions of Tyre Brands

The questions from which these results were derived asked people to name a tyre brand that offered a particular variable, i.e. value, but no brands were suggested when the question was posed. The results showed a split in tyre brands favoured by off-road and on-road drivers, for off-road drivers B.F. Goodrich, Michelin and Pirelli found particular favour from a performance viewpoint. However, a significant number of drivers (30%) did not have any preference. 11% of all the drivers stated they had no opinion of a particular brand offering good performance, whilst 27% had no opinion of a particular brand offering good value. Hence, no individual off-road tyre brand was seen to offer significantly better performance, or occupy a dominant market position.

When answering brand related questions people generally relied heavily on personal perception rather than factual information. Possibly all available tyres offer very similar characteristics and performance, although this seems unlikely given the diversity within the tyre market. It is more likely that any advantages of a particular tyre are poorly marketed, either because it is hard to quantify and effectively communicate the exact benefits, or perhaps because the manufacturers are unaware of possible benefits. Also

each tyre probably only performs well in particular circumstances, thus different tyres will better suit different driving habits.

4.2.4 Likelihood of Purchasing Secondary Performance Off-Road Tyres

For infrequent off-road driving, one set of tyres offering an off/ on-road compromise was considered adequate. Only the most 'serious' (frequent and skilled) off-road drivers would consider purchasing a second set of dedicated off-road tyres, for example 81% of the overseas off-road drivers stated that they would seriously consider purchasing a second set of dedicated tyres. Respondents would generally not be willing to pay more for a set of high performance, dedicated 4x4 off-road tyres than sets of currently available 4x4 tyres cost; approximately £400 a set (excluding the rims).

Offers put to respondents were considered much more in terms of cost, than extra tyre performance. However, most respondents stated that if significant measurable performance advantages of a high performance off-road tyre could be demonstrated over and above the performance levels of existing tyres, then they would consider justifying the purchase of a second set of tyres for use purely off-road. When choosing secondary specialist off-road tyres the ease of interchange between the two sets of tyres was also important. Whereas noise would only become a deterring issue (inhibitor) if off-road tyres had to be driven at high-speed on-road, for example, getting to and from the off-roading locations in Dubai¹⁷.

4.2.5 Interest in Automatic Central Tyre Inflation Systems (CTIS)

Interest existed in the fitment of a self-sensing tyre inflation system as an extra vehicle feature, providing its cost did not exceed £1000. Respondents indicated that a specification of such a system and its merits would be required before a true value of its worth could be estimated (such a specification was not supplied with the questionnaire).

4.3 IMPLICATIONS OF THE MARKET SURVEY RESULTS

A market interested in purchasing off-road tyres offering better tractive performance was identified. However, consumers are quite ignorant about the relative performance

abilities of different tyre makes and brands. Individual views are predominantly based upon subjective personal experience, influenced by opinions expressed in the motoring press. This is understandable given that no simple and effective means of tyre comparison is publicly available, however, it can lead to conflicting opinions developing between manufacturers and drivers. Franklin⁶ commented that in the Middle Eastern market the Dunlop TG35 tyre was perceived to offer performance advantages, which may be true in a particular driver's circumstances, however, Land Rover's official off-road testing had not shown this tyre to significantly outperform any other products on the market. These findings demonstrated that the lack of a unified measure of tyre performance across a range of conditions, and no simple way of communicating tyre test data to the general public, prevents them knowing which tyres offer the "best" performance.

The serious off-road drivers were capable of picking a tyre that would offer good off-road performance if fitted to their vehicles. However, this statement was contradicted by a desire to purchase and fit tyres that "looked good" on their vehicles. Low profile tyres, which are typically considered to 'look good', do not allow a vehicle to achieve its maximum potential traction, as tyre deformation, and hence the contact patch length is limited. This conflict is seen in the Middle Eastern market where 4x4 vehicle image is viewed as very important by the wealthy 4x4 owning classes^{6,17}. Land Rover has traditionally erred towards fitting tyres able to generate high levels of off-road (and where possible on-road) performance ahead of those that 'look good'⁶. However, recently competitor 4x4 vehicles, e.g. BMW X5, have been optimised for the on-road situation, which has partially been achieved by the fitment of lower profile, wider tyres, which also happen to 'look good'. The success of such vehicles has placed increased pressure upon Land Rover to justify (compromise) its tyre fitments, so that sales are not jeopardised⁶. Tyre tread was also shown to govern the vehicle aesthetics, but the exact patterns were unclear as different customers favour different treads. However, if significantly greater tyre performance could be generated then most consumers would disregard the style of the treads, and be satisfied with the performance gain.

Currently Land Rover's tyre testing mainly involves large quantities of subjectively marked, and loosely controlled, field trials⁹. This process could be improved if a more objective test method capable of speedily determining a single measure of a tyre's potential tractive performance were developed. It would not be cost-effective to develop a significantly better performing tyre if this ability cannot be clearly demonstrated to the market, to justify a premium price tag. The development of a model to relate tyre (and tread) parameters to vehicle performance could allow potential performance improvements to be directly communicated to the public. The results indicated that 21% of the 4x4 vehicle owning/ driving market would seriously consider purchasing a second set of dedicated high performance 4x4 off-road tyres. However, any interest was highly cost dependant and to justify any extra cost over the price of existing tyres then significant performance gains would have to be demonstrated.

5 TRACTION SURFACE EVALUATION

5.1 SOIL ASSESSMENT

Initial trials of the traction capabilities of the tyre test rigs were conducted on a sandy loam soil. The properties of this were measured using the following techniques.

1. Particle size analysis¹²⁴
2. Triaxial tests¹²⁵
3. Translational shear tests¹²⁶

The particle size analysis results, Table 5.1 and Figure 5.1, showed agreement with results from previous authors^{127,128,129} who used the SDL extensively in their research. The other tests determined a cohesion (c) of 8.4 kN/m² and an angle of internal shear resistance (ϕ) of 28° at 9.5% moisture content and an initial dry bulk density of 1265 kg/m³, see Appendix 4. Again this showed good agreement with the same previous authors^{127,128,129} who measured the following ranges of values: $c = 7$ kN/m² to 8.8 kN/m² and $\phi = 23^\circ$ to 29° for similar soil conditions.

Table 5.1 – Particle size analysis of the sandy loam soil

Soil Constituent	Mean Fraction (%)
Coarse Sand	6.4
Sand	22.4
Fine Sand	27.5
Silt	30.3
Clay	13.4

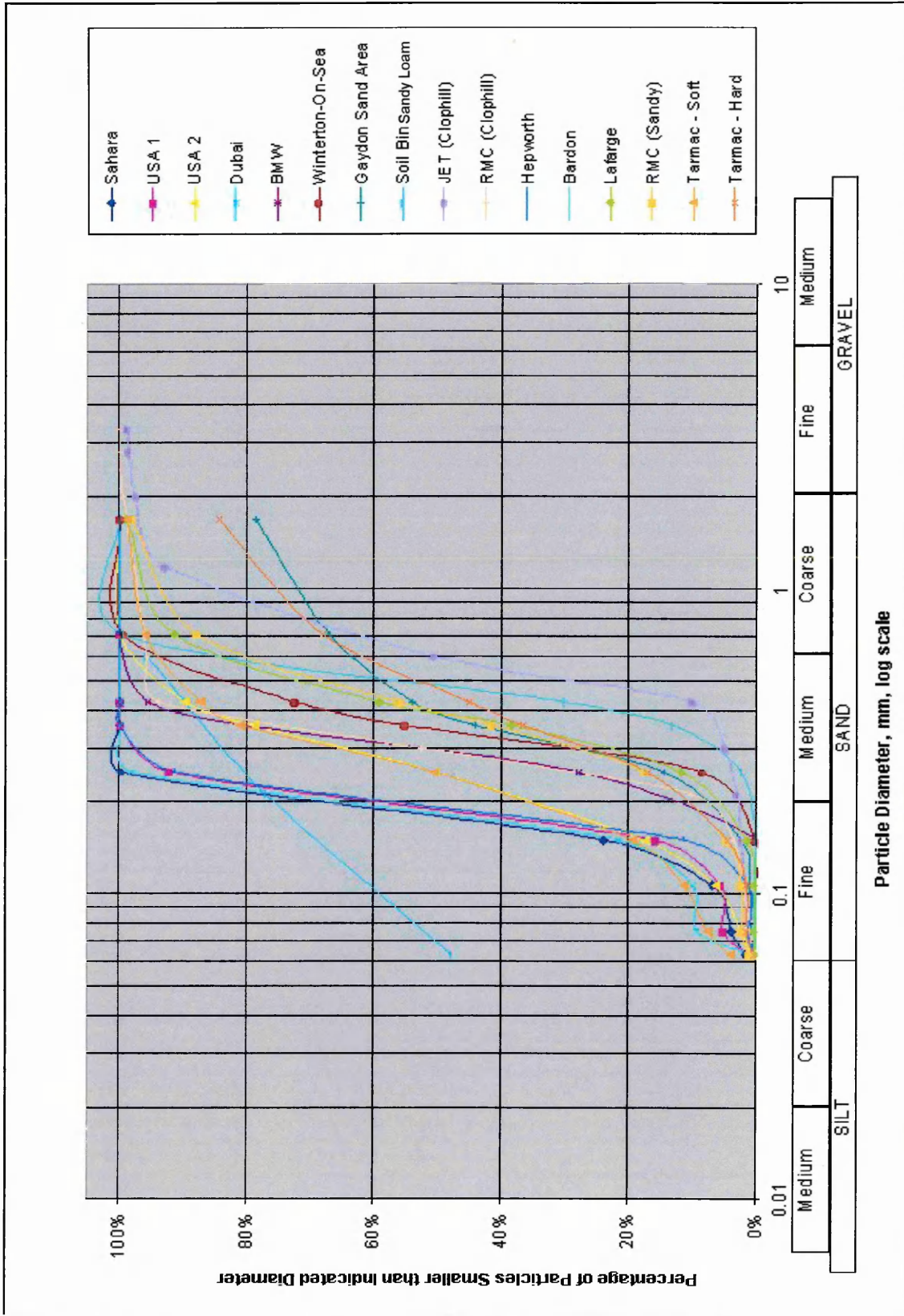


Figure 5.1 – Particle size distribution graphs for a number of global and local sand samples and a sandy loam soil

5.1.1 Determination of K (Soil Deformation Modulus)

Values of K were determined in the manner outlined in the literature review. Full details and results of the process are detailed in Appendix 5. Shear box tests for the sandy loam soil showed a linear relationship between σ and K , as described by equation 50.

$$K = 0.00003\sigma + 0.001 \quad (50)$$

Equation 16 $\left\{ \frac{K_1}{K_2} = \sqrt{\left(\frac{A_1}{A_2} \right)} \right\}$ showed that for soils experiencing similar normal

stresses, but over varying areas A_1 (tyre contact) and A_2 (shear box), then K_1 could be derived from knowledge of K_2 , which was described by equation 50. However, it was only possible to determine a range of K_1 values for any given normal load, because as the contact area increased then both the normal stress, which was used to compute of K_2 , and the ratio $A_1:A_2$ altered. Therefore several analyses were required to produce the results shown in Figure 5.2, which detail how the relationships between the K_1 values and tyre contact areas varied for different normal loads.

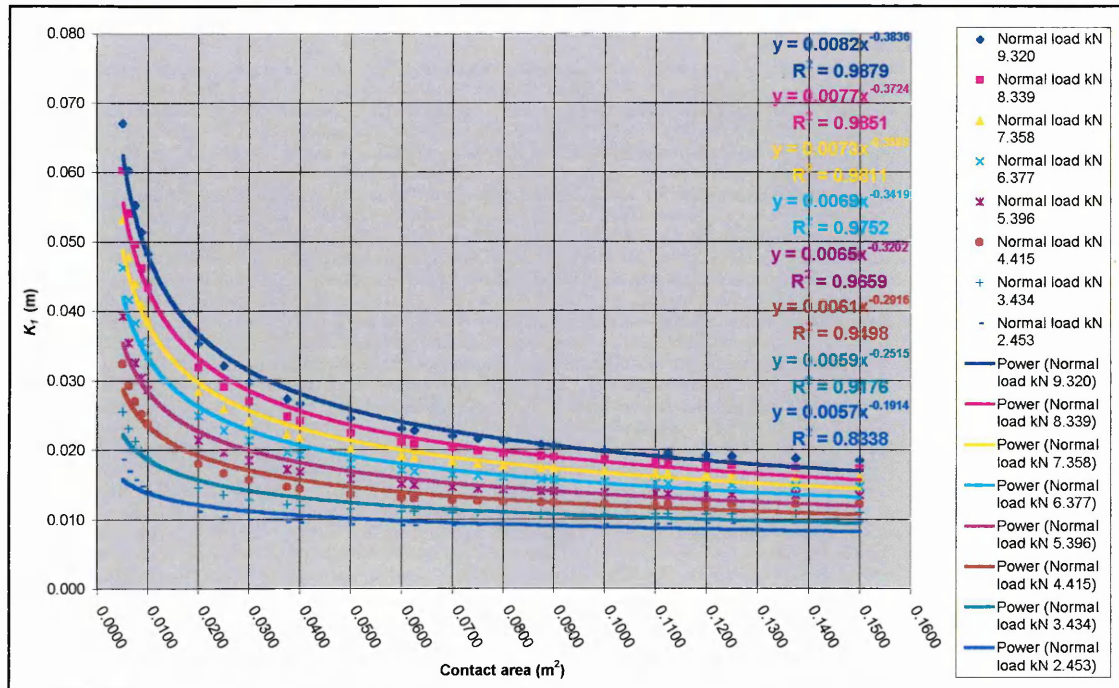


Figure 5.2 – The relationships between the contact area and K_1 for the sandy loam soil under different normal tyre loads

The relationships described in Figure 5.2 allowed a value of K for beneath a tyre to be calculated for any combination of tyre contact area and normal load on the sandy loam soil.

5.1.2 Determination of Bekker Plate Sinkage Values

This process also followed the methodology outlined in the literature review, with full details and the results recorded in Appendix 6. Tests were conducted on the sandy loam soil using four different sized plates upon the three different density preparations used for the subsequent experiments. These surfaces were produced in the following manner. The top 600 mm of soil was scraped from the surface, being loosened in the process. Buckets of soil were then carried back to the start of the bin, before being scraped level at a depth of 50 mm. This process was repeated until the soil profile was returned to its original depth. This produced the first soil preparation '*poured and scraped*'. The other two preparations involved the surface, once scraped level, then being rolled level with a Ø600 mm steel roller. This rolling was either conducted once for each layer for the '*poured, scraped and 1 roll*' preparation, or four times for the '*poured, scraped and 4 rolls*' preparation. After each rolling a small spiked roller was run over the surface to break the pan and ensure bonding and cohesion to the next overhead layer. Soil densities and moisture contents produced for each preparation are shown in Table 5.2. These are typical of the soil characteristics produced throughout the testing.

Table 5.2 – Average soil densities produced for the three soil preparations during the plate sinkage tests and appropriate dry base moisture contents

Soil Poured and scraped			Soil Poured, scraped and 1 roll			Soil Poured, scraped and 4 rolls		
Rep no.	Dry bulk density kg/m ³	Moisture content %	Rep no.	Dry bulk density kg/m ³	Moisture content %	Rep no.	Dry bulk density kg/m ³	Moisture content %
1	1185	9.3	1	1309	8.5	1	1408	8.9
	1201	8.4		1280	8.6		1372	8.1
	1239	7.7		1239	8.8		1358	8.0
	1243	8.4		1320	8.8		1391	8.4
	1129	8.7		1276	8.9		1377	9.2
2	1090	9.0	2	1229	8.8	2	1402	9.7
	1163	9.2		1268	8.8		1425	10.1
	1176	9.4		1234	9.4		1386	9.4
	1132	8.7		1240	9.1		1430	10.4
	1190	9.0		1248	9.8		1370	9.0
3	1092	9.7	3	1267	9.6	3	1408	9.6
	1211	9.3		1247	9.5		1400	10.1
	1148	9.4		1295	9.4		1433	9.6
	1179	9.6		1314	9.3		1361	9.6
	1080	10.0		1219	9.2		1402	9.6
Av.	1164	9.1	Av.	1266	9.1	Av.	1395	9.3

Five readings were taken from each soil preparation, which was randomly chosen for this assessment throughout the duration of the plate sinkage experiments. The results from the pressure sinkage experiments, shown in Appendix 6, produced the values for the Bekker soil coefficients shown in Table 5.3.

Table 5.3 – Bekker pressure sinkage coefficients for the three soil preparations

Soil coefficient	kc	$k\phi$	n
Poured and scraped	10.2	417	0.793
Poured, scraped and 1 roll	16.7	954	0.444
Poured, scraped and 4 rolls	28.1	1529	0.397

5.1.3 Comparison of the Experimental Soil Preparations

During the traction tests soil density and moisture content were recorded at random intervals during the testing on each of the three soil preparations. Three readings of both soil density and moisture content were recorded every time that the soil preparation was measured. These results are presented on the following graphs Figure 5.5 – 1170 kg/m³, Figure 5.4 – 1270 kg/m³ and Figure 5.5 – 1400 kg/m³ (density readings) and Figure 5.6 – 1170 kg/m³, Figure 5.7 – 1270 kg/m³ and Figure 5.8 – 1400 kg/m³ (moisture contents). As well as the three readings, all of the graphs also detail the mean results for each preparation tested, and the overall mean and SED for each density preparation. These values were derived from the statistics presented in Appendix 7. The total number of soil preparations produced at each particular density governed the number of sets of triplicate results that were recorded for each preparation at each soil density, i.e. only three 1400 kg/m³ soil preparations were experimented upon, so only three sets of readings could be recorded.

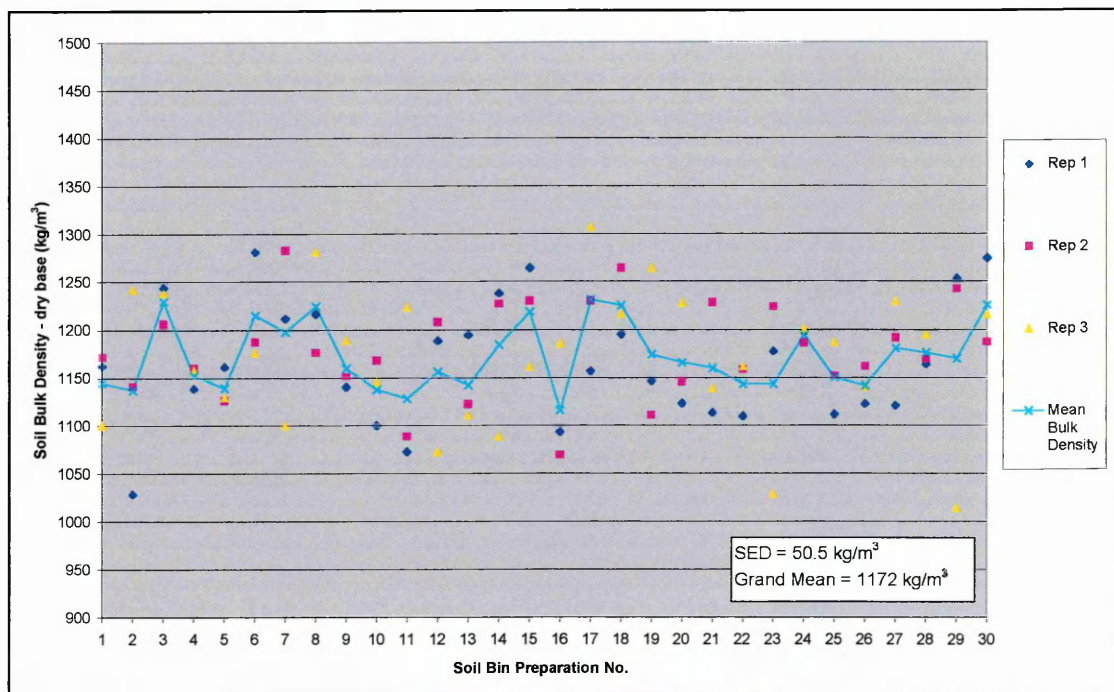


Figure 5.3 – The soil densities achieved for the 1170 kg/m³ soil preparations created during the fixed slip tests

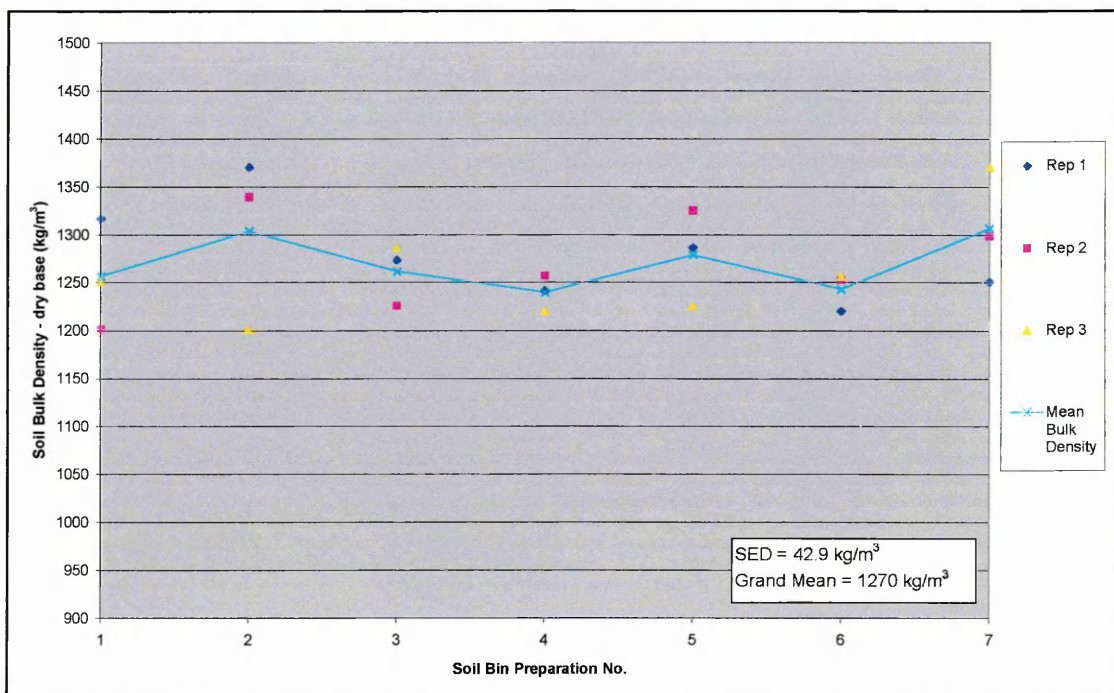


Figure 5.4 – The soil densities achieved for the 1270 kg/m³ soil preparations created during the fixed slip tests

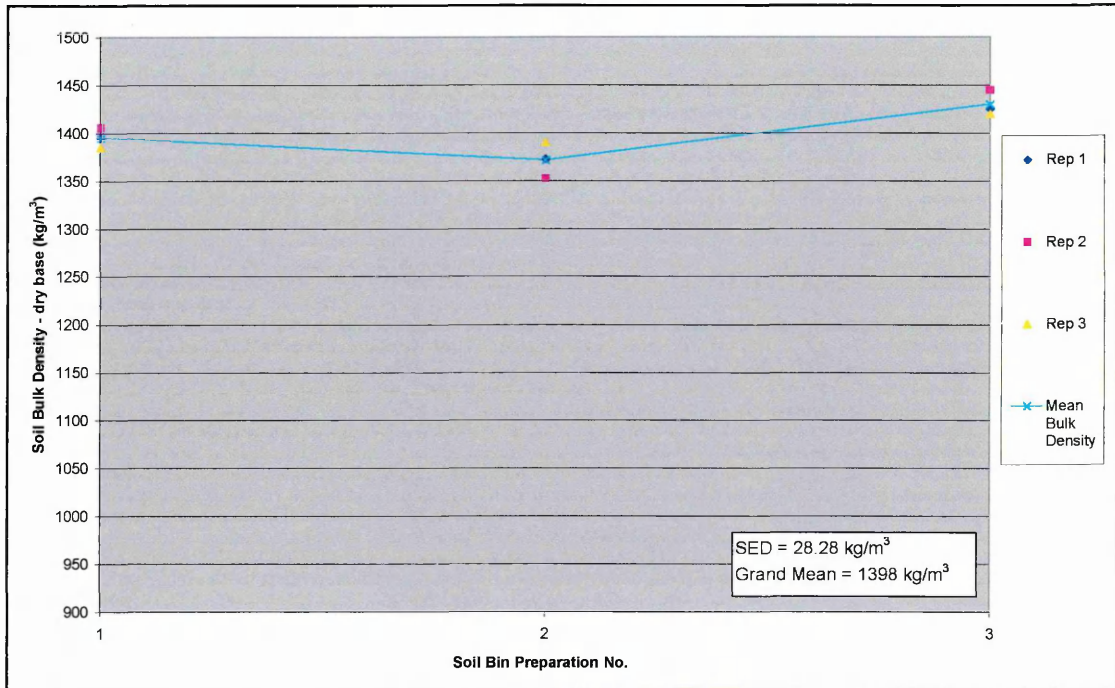


Figure 5.5 – The soil densities achieved for the 1400 kg/m^3 soil preparations created during the fixed slip tests

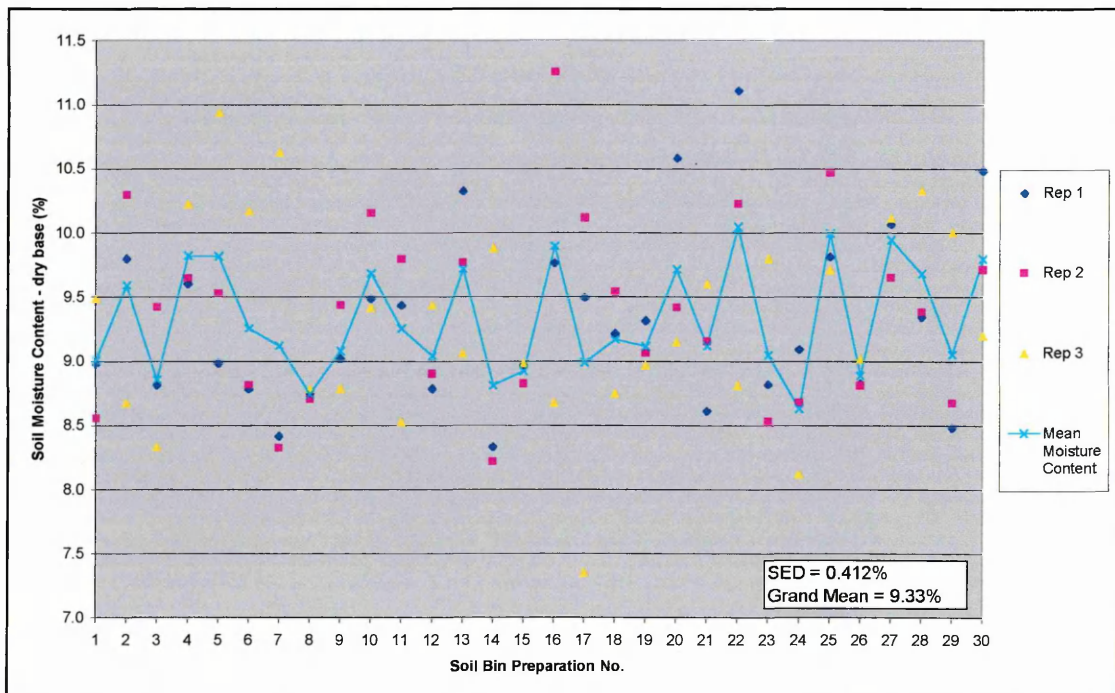


Figure 5.6 – The moisture contents achieved for the 1170 kg/m^3 soil preparations created during the fixed slip tests

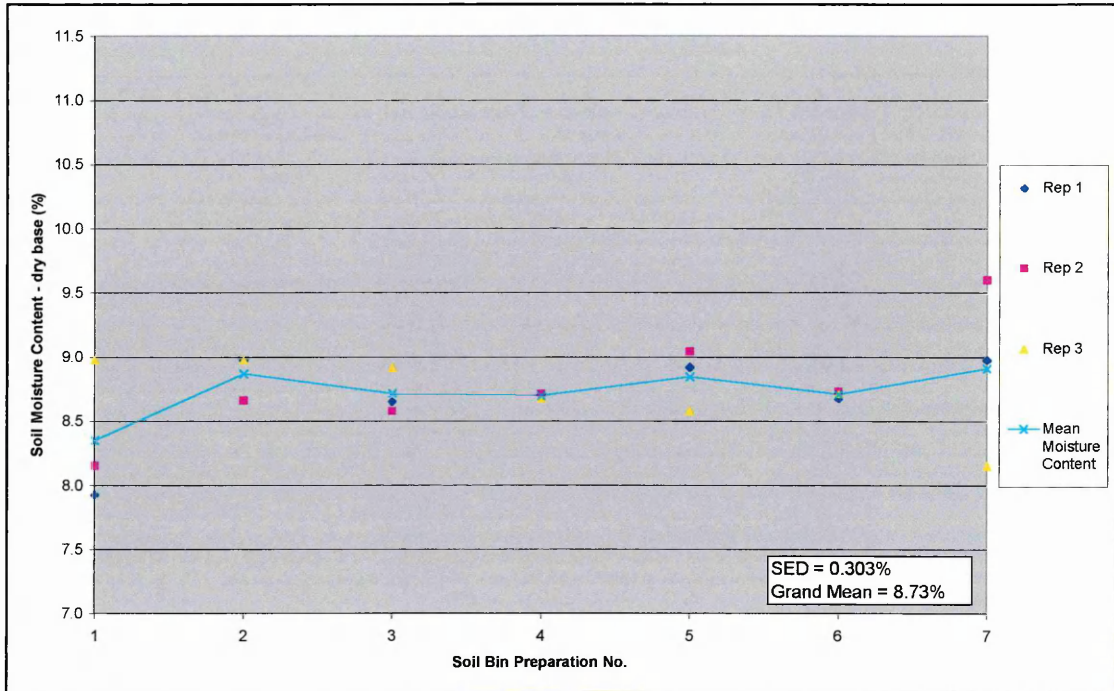


Figure 5.7 – The moisture contents achieved for the 1270 kg/m³ soil preparations created during the fixed slip tests

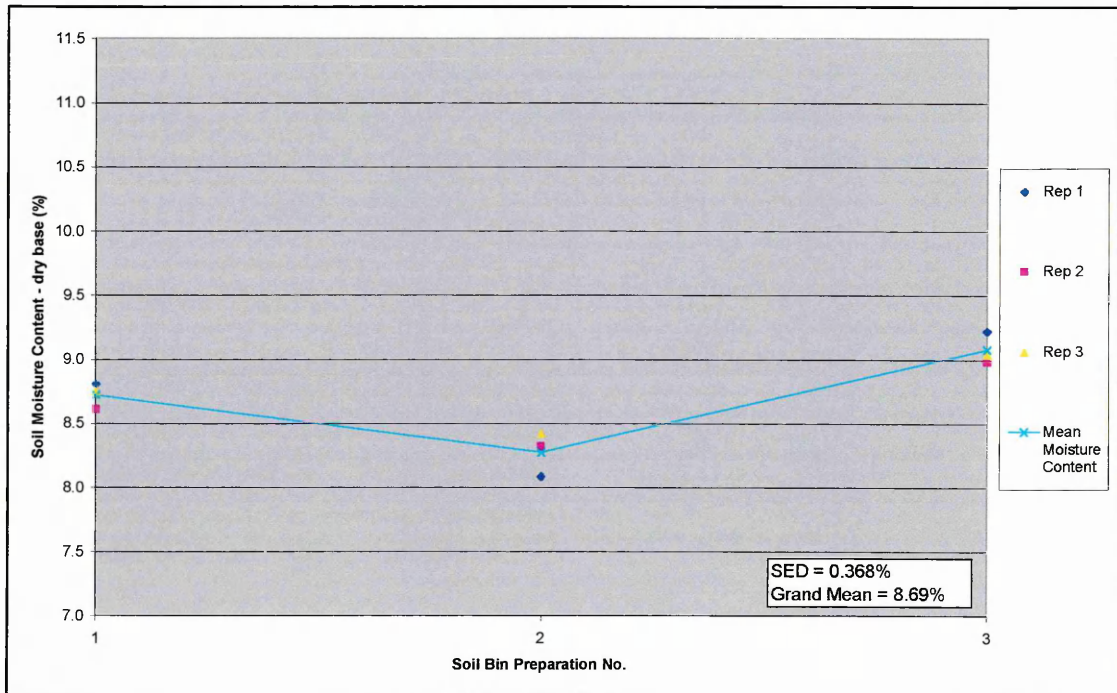


Figure 5.8 – The moisture contents achieved for the 1400 kg/m³ soil preparations created during the fixed slip tests

The overall means produced from these results, shown in Table 5.4, indicated that the three different soil densities were achieved at consistent moisture contents. Study of the standard errors of the difference of the means (SED) values and data distributions show that consistent density preparations were achieved over time. Further evidence of the consistency of the soil preparations achieved can be seen in the close agreement between these results and those detailed in Table 5.2.

Table 5.4 – Mean soil density preparations and moisture contents

Soil Preparation	Soil Density (dry base)	Moisture Content (dry base)
No. of rolls	kg/m ³	%
0	1172	9.3
1	1270	8.7
4	1398	8.7

Cone Index (CI) readings were measured using a standard 30° cone penetrometer during the tests to ensure consistent soils (and sand) preparations were achieved. For sand and the 1170 kg/m³ soil preparation the cone had a base area of 1035 mm², whilst on the firmer soils (1 and 4 rolls) a 280 mm² base cone was used. In both cases this was inserted at the recommended rate of 30 mm/s. Each penetration was averaged across the readings recorded for the top 150 mm of soil to produce the average CI value.

Figure 5.9 and Figure 5.10 show CI readings that were recorded for a number of the 1170 kg/m³ and 1270 kg/m³ density soil preparations over the duration of all the testing on soil. Again SED's and grand means are presented, which were determined from the statistics presented in Appendix 8. The results indicated that for both preparations, as was expected, good repeatability was maintained over time. Insufficient tests were conducted upon the 1400 kg/m³ soil to allow a similar analysis to be conducted. The three sets of readings that were recorded produced an average CI reading of 948.3 kN/m² ±20 kN/m².

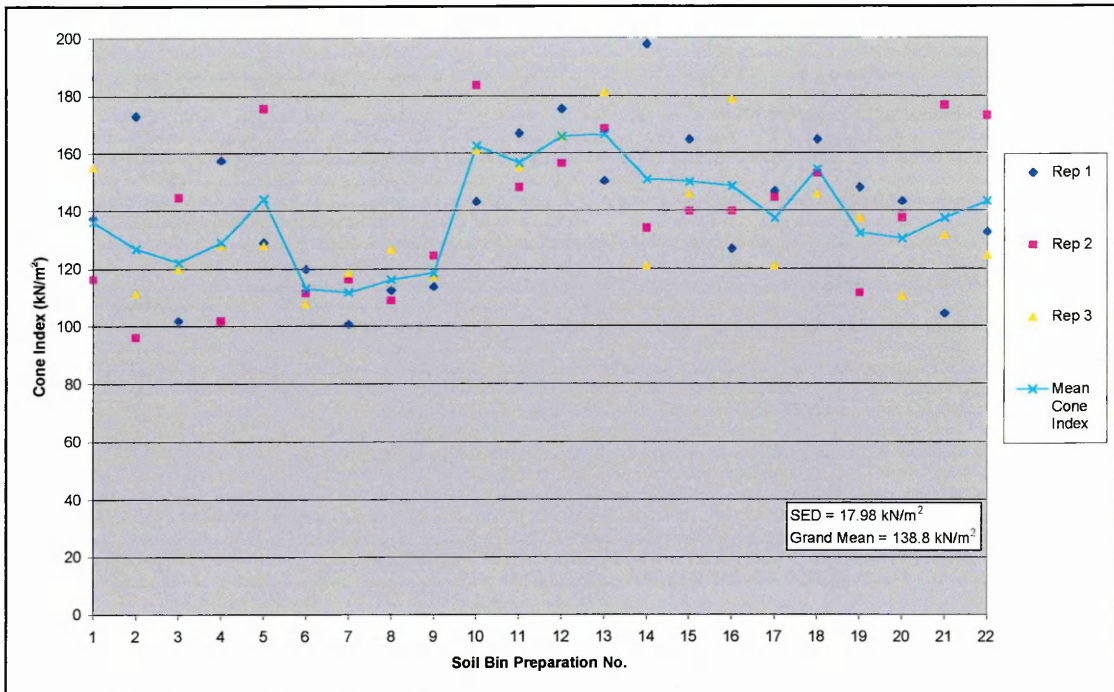


Figure 5.9 – Cone index readings recorded for different 1170 kg/m³ soil bin preparations over the duration of all testing

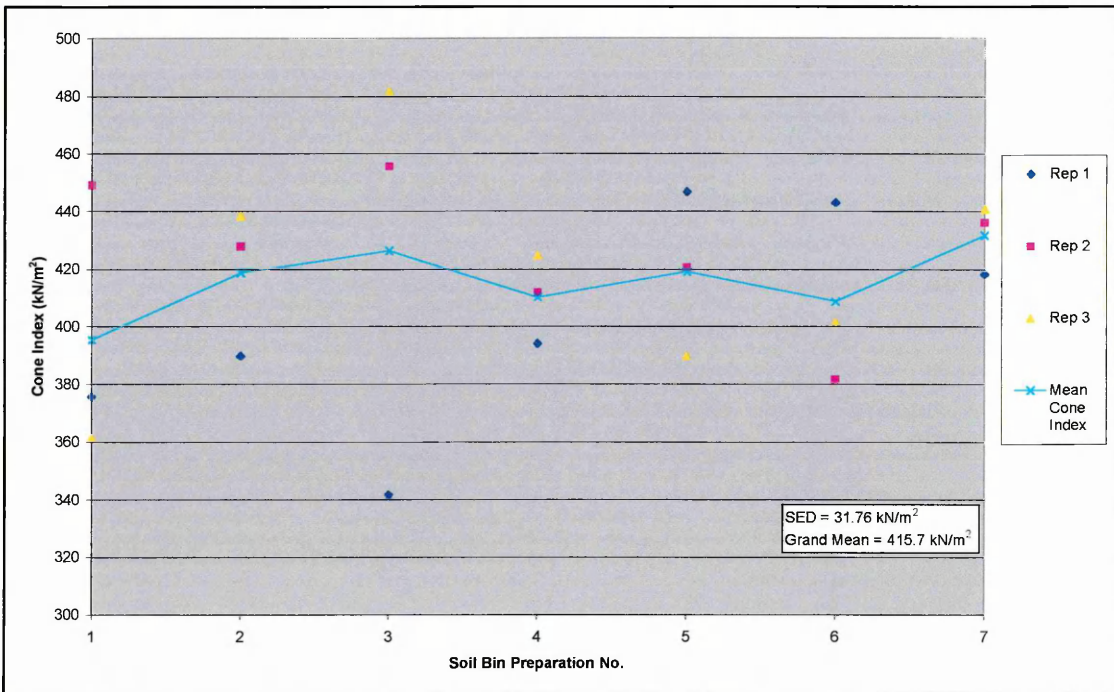


Figure 5.10 – Cone index readings recorded for different 1270 kg/m³ soil bin preparations over the duration of all testing

5.2 SAND COMPARISON ANALYSIS

This assessment was conducted to find sand that could be used in the soil bin to produce replicate desert sand conditions. The conditions to be replicated were pure loose sand, the conditions from which it is most difficult to generate net positive traction. The sand type that it was desired to replicate was from the Dubai region of the United Arab Emirates (U.A.E.), which was selected because it is an important market for Land Rover products in the Middle East. To facilitate the sand analysis and comparison programme Land Rover supplied sand samples from a number of global desert regions. This allowed variations in their properties to be determined. A variety of sand and sandy soil samples were collected from a number of local quarries for comparison. All of the samples listed in Table 5.5 were tested with moisture contents < 1%). They were subjected to following tests (which determined four values):

1. Particle size analysis – to determine particle distribution.
2. Translational shear box – to determine the internal friction angle and cohesion.
3. Sliding sand-rubber friction – to determine both the angle of sand-rubber friction and the adhesion.

A weighted ranking based upon percentage differences between each of the four measured values for the Dubai sand sample and for the locally sourced comparison (replicate) sands allowed the differences between the samples to be quantified. The weightings used for the process are shown in Table 5.6. These values were selected based upon their perceived relative importance in firstly governing sand flow (i.e. particle size) and secondly tyre traction (friction angles) and tread effects. A mean weight diameter assessment¹³⁰ was conducted to transform the particle size distribution results into percentage results suitable for this analysis.

The particle size distribution analysis, recommended by Bagnold¹³¹, was conducted using a set of British Standard soil sieves¹²⁴. The results of this analysis, shown in Figure 5.1 (page 69), demonstrated that the three true desert sands (Dubai, Sahara and USA 1) all had very similar, and considerably smaller particle size distributions, than the majority of the other sands tested because of their aeolian formation processes. Only the sand from the Hepworth Mineral Company had a similar particle size distribution.

Table 5.5 – Descriptions of the assessed sand samples

<u>Global Sand Types</u>		
Name	Location	Type
Dubai	Dubai Desert.	Pure loose desert sand – <i>Ideal Sand</i> .
USA 1	Imperial Dunes.	Pure loose desert sand.
USA 2	Imperial Dunes.	Loose desert sand, with larger stones.
Sahara	Sahara Desert.	Pure loose desert sand.
BMW	Mireval Sand Track, Southern France.	Loose beach sand, sourced from south coast of France.
Winterton-on-sea	Winterton Beach, UK	Loose beach sand.
<u>Local Sand Types</u>		
Name	Location	Type
Jet (Hanson) Clophill	Sand quarry, Clophill, Beds, UK.	Loose sand and silt mix, as quarried.
RMC Clophill	Sand quarry, Clophill.	Loose sand and silt mix, as quarried.
Hepworth Mineral & Chemical (DA80F)	Sand quarry, Heath and Reach, Beds, UK.	Pure loose sand, washed, sieved and sized, and dried.
Bardon Aggregates	Sand quarry, Heath and Reach.	Pure loose sand washed and dried.
Tarmac – Hard (WCS)	Sand quarry, Sandy, Beds, UK.	Pure loose sand, washed coarse state.
Tarmac – Soft	Sand quarry, Sandy.	Loose sand and silt mix, as quarried.
Lafarge Aggregates	Sand quarry, Sandy.	Pure loose sand, as quarried.
RMC Sandy	Sand quarry, Sandy.	Pure loose sand, as quarried.
<u>Comparison Sand & Soils</u>		
Name	Location	Type
Gaydon Sand Track	Gaydon, Warks, UK.	Soil and builders sand mix.
Coarse Builders Sand	Jewson Builders Merchant.	As supplied.
Fine Builders Sand	Jewson Builders Merchant.	As supplied.
Silsoe Sandy Loam	Silsoe Soil Bin.	Locally occurring soil.

Table 5.6 – Weightings used for sand ranking analysis

Criterion	Weighting
Particle size distribution	0.50
Sand / rubber shear angle	0.25
Sand / sand shear angle	0.15
Adhesion	0.10

Translational shear box tests, as described by Day¹³², were used to determine the internal friction angles (ϕ), as triaxial tests are generally unsuitable for cohesionless soils¹³², and because Taylor¹³³ had demonstrated that differences in results obtained for sand samples using different apparatus were not significant. These tests also determined values of c (cohesion) for the samples with a soil component. The results, in Table 5.7, showed that variations in the value of ϕ between all the samples were limited to 5°.

Table 5.7 – Results from the translational shear box tests

Sand Type	Angle of Internal Shear Resistance (ϕ)	Cohesion (c)
	Degrees	kN/m ²
RMC – Clophill	36.6	3.22
Gaydon	36.7	0
RMC – Sandy	36.9	0
Bardon	37.2	0
Hepworth	37.5	0
Coarse Builders Sand	37.8	0
Jet – Clophill	38.2	8.05
Tarmac Soft	38.5	1.11
Imperial USA 1	39.0	0
Winterton-on-sea	39.1	0
BMW Mireval	39.4	0
Lafarge	39.5	0
Fine Builders Sand	40.5	0
Sahara	40.5	0
Tarmac WCS	40.5	0
Dubai	40.6	0
Imperial USA 2	41.5	0

The sliding sand-rubber friction tests conducted were versions of friction tests described by Gill & Vanden Berg²⁴, using a methodology developed by Godwin & Lovelace¹³⁴. These were conducted using sand trays across which five different rubber-bottomed sleds with a range of discrete loads were towed at a constant rate. Simultaneously the forces required to pull each sled were recorded from a spring force balance. Each sled was 150 mm long by 100 mm wide, with a 45° by 30 mm lip. The rubber bases used, shown in Plate 5.1, were all of a similar hardness to tread rubber but with different

groove patterns to allow any effects from different tread and sand interactions to be gauged. The rubber formed a smooth base (A), lateral grooves (B), longitudinal grooves (C) and 45° angles forwards (D) and rearwards (E). The two angled patterns were positioned so that the apex ran along the longitudinal centre of the sleds.

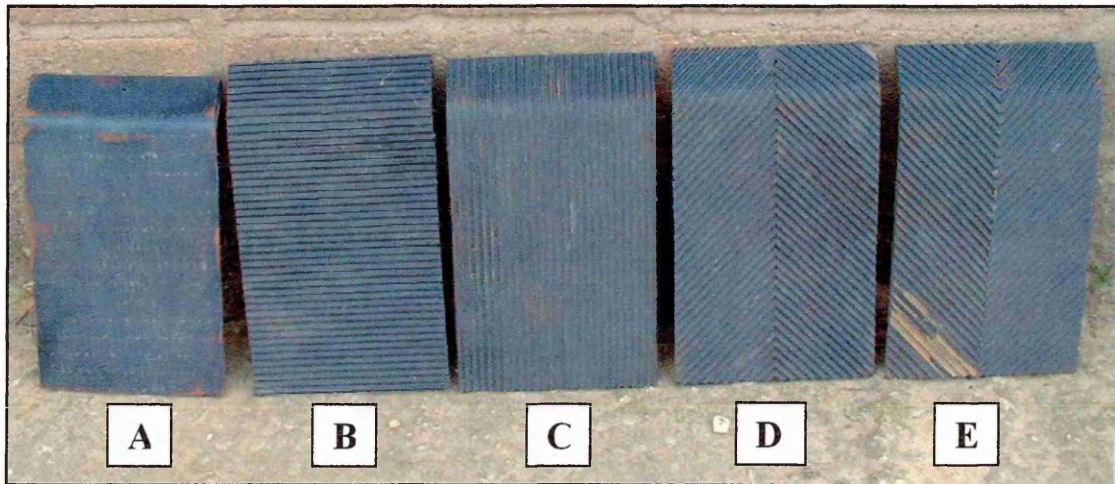


Plate 5.1 – The rubber bases of the sliding friction test sleds

The results of the sliding friction tests are shown in Table 5.8. When analyses of variance were conducted upon these results, see Appendix 9, no significant difference existed between the mean results of sand-rubber friction angles (δ) for different treads at the 99% confidence level. The analyses of variance showed that the different treads significantly affected the mean values of adhesion recorded. The adhesion results from sleds B, D and E, which generated the greatest adhesions (total mean of 108 N/m²), showed no significant difference at the 95% confidence level, but these adhesions were significantly greater than the adhesions produced by sleds A (mean 34 N/m²) and C (mean 81 N/m²), which were themselves both significantly different. Thus treads that most opposed the sleds' directions of travel produced the greatest adhesions, although variation in force was small. Therefore because tread type influenced the disturbance of loose sand it remained necessary to quantify this effect for the full-size situation, where the small differences would potentially increase to become significant effects.

Table 5.8 – Results from the sliding sand-rubber friction tests

Sled Type	Sled A		Sled B		Sled C		Sled D		Sled E	
Sled Pattern Front (to) Rear	(Smooth)		F () R		F (====) R		F (<<<<) R		F (>>>>) R	
	Angle of Sand – Rubber Friction (δ)	Adhesion (a)	Angle of Sand – Rubber Friction (δ)	Adhesion (a)	Angle of Sand – Rubber Friction (δ)	Adhesion (a)	Angle of Sand – Rubber Friction (δ)	Adhesion (a)	Angle of Sand – Rubber Friction (δ)	Adhesion (a)
Sand Type	Degrees	N/m ²								
RMC – Clophill	26.7	52	28.8	115	30.0	71	29.3	108	28.7	114
Gaydon	26.6	21	27.9	113	29.5	47	26.8	131	27.6	116
RMC – Sandy	26.9	15	28.2	126	29.1	77	28.9	109	27.9	123
Bardon	24.9	57	27.5	112	26.1	106	26.4	127	24.6	118
Hepworth	25.6	42	24.8	119	25.3	110	25.8	109	25.7	111
Coarse Bdrs Sand	27.2	56	29.2	115	28.1	99	29.0	121	29.2	107
Jet – Clophill	24.8	68	28.3	75	25.2	91	25.3	116	24.7	130
Tarmac Soft	26.8	20	27.0	139	27.9	99	28.6	123	28.6	123
Imperial USA 1	26.9	36	29.9	86	31.1	58	30.0	85	29.2	94
Winterton-on-sea	27.2	13	32.6	49	29.2	66	30.2	76	29.3	94
BMW Mireval	27.3	30	28.0	84	26.9	83	27.5	95	26.5	110
Lafarge	27.0	23	27.6	134	27.9	98	28.4	113	27.7	125
Fine Bdrs Sand	25.3	71	25.7	119	27.5	72	25.8	107	25.9	110
Sahara	27.8	13	29.4	99	30.1	61	30.0	83	29.3	94
Tarmac WCS	25.5	30	26.8	127	27.7	69	26.8	123	26.5	130
Dubai	27.4	19	29.2	99	28.5	80	29.9	89	30.0	82
Imperial USA 2	27.0	18	29.4	105	28.6	82	29.0	96	28.8	103

All of the (δ) and (a) results shown in Table 5.8 were averaged to produce a single number to simplify the weighted percentage difference comparison. For each of the four measured variables shown in Table 5.9, the Dubai sand results were taken as a 100% value. The difference between each of the four 100% values and each comparison sands' values were expressed in percentage terms, and each percentage difference was

multiplied by the appropriate weighting from Table 5.6 to produce a score. The four variable scores were totalled to give an overall mark for each sand type. Thus the closer the mark was to zero, the closer the match between the Dubai and comparison sand.

Table 5.9 – The weighted percentage differences of the local sand sample scores (relative to the Dubai sand)

Sand Type	Particle Size			Sand – Rubber Friction Angle			Sand – Sand Friction Angle			Adhesion			Overall Mark (Sum of scores)
	Mean Weighted Diameter	δ (Degrees)	ϕ (Degrees)	a (N/m ²)	% Difference	Weighting (wt)	Score (% x wt)	% Difference	Weighting (wt)	Score (% x wt)	% Difference	Weighting (wt)	
Bardon	271	0.5	135.5	11	0.25	2.75	8	0.15	1.20	133	0.1	13.3	152.8
BMW	100	0.5	50.0	6	0.25	1.50	3	0.15	0.45	54	0.1	5.4	57.4
Hepworth	16	0.5	8.0	12	0.25	3.00	8	0.15	1.20	96	0.1	9.6	21.8
Lafarge	248	0.5	124.0	4	0.25	1.00	3	0.15	0.45	58	0.1	5.8	131.3
RMC – Clophill	128	0.5	64.0	1	0.25	0.25	10	0.15	1.50	109	0.1	10.9	76.7
RMC – Sandy	264	0.5	132.0	3	0.25	0.75	9	0.15	1.35	32	0.1	3.2	137.3
Tarmac Soft	99	0.5	49.5	4	0.25	1.00	5	0.15	0.75	56	0.1	5.6	56.9
Tarmac WCS	444	0.5	222.0	8	0.25	2.00	0	0.15	0.00	70	0.1	7.0	231.0
Winterton-on-sea	173	0.5	86.5	2	0.25	0.50	4	0.15	0.60	4	0.1	0.4	88.0

The sand obtained from Hepworth Mineral & Chemical Company (code number DA80F) gave the closest match because of the similarity between both sets of particle distribution results. Particle size was the variable in which the greatest variation between the samples occurred, and that which had the greatest weighting. Hence close agreement had a big impact. The DA80F sand, which was supplied in a sieved and dried state, was thus used to produce a replicate loose desert sand condition.

5.3 ANALYSIS OF THE DA80F SAND

The previous section showed that the DA80F sand had the following properties:

- Particle size $\sim 0.1 \text{ mm} < \text{over } 97\% \text{ of grains } > 0.4 \text{ mm}$.
- Angle of internal resistance (ϕ) (sand-sand shear) $\sim 37.5^\circ$ (Appendix 10).
- Cohesion (c) $\sim 0 \text{ kN/m}^2$ (as would be expected for frictional sand).
- Angle of sand-rubber friction $\sim \approx 25.5^\circ$ (mean value).
- Adhesion (a) $\sim 98 \text{ N/m}^2$ (mean value).

Further properties of this sand, which was always used at a moisture content of less than 1%, were also measured. The density of the sand was measured as $1485 \text{ kg/m}^3 \pm 12 \text{ kg/m}^3$ by weighing the mass of a tin of a known volume (approximately 0.015 m^3) filled with loosely poured sand. To mimic the manner in which the sand was prepared in the soil bin (*poured and scraped*), and therefore its experimental density, excess sand was added to the tin before being levelled. This was repeated three times. The small density variation occurred because of the low compactibility of a material with similar particle sizes. To ensure that the sand was not being compacted during the traction tests, density readings were taken from the top sand layers using density rings at random intervals over the duration of all the testing. These results (see Appendix 11) showed that a mean sand density of $1482 \text{ kg/m}^3 \pm 21 \text{ kg/m}^3$ was recorded, which agreed closely with the bench test value.

The torsional shear strength of the sand mass was measured in-situ in the soil bin using two different shear vane devices, both of which were used to test the surface strength. Five different sand preparations were tested and ten readings were recorded each time. These devices recorded the surface sand torsional shear strength as being $1.25 \text{ kPa} \pm 0.25 \text{ kPa}$. Cone Index (CI) readings were also recorded at random intervals during all the testing on sand to further investigate any variation in the sand strength properties between different preparations. This provided a simple comparison between the sand preparations to ensure the expected levels of repeatability were maintained. The results from these tests can be seen in Figure 5.11, and the associated statistics are presented in Appendix 12. The first eight preparations were tested when the sand was used in the sand tank, whilst the other results were recorded when the full soil bin was used. These

results provided further evidence of the good repeatability achieved between the sand preparations.

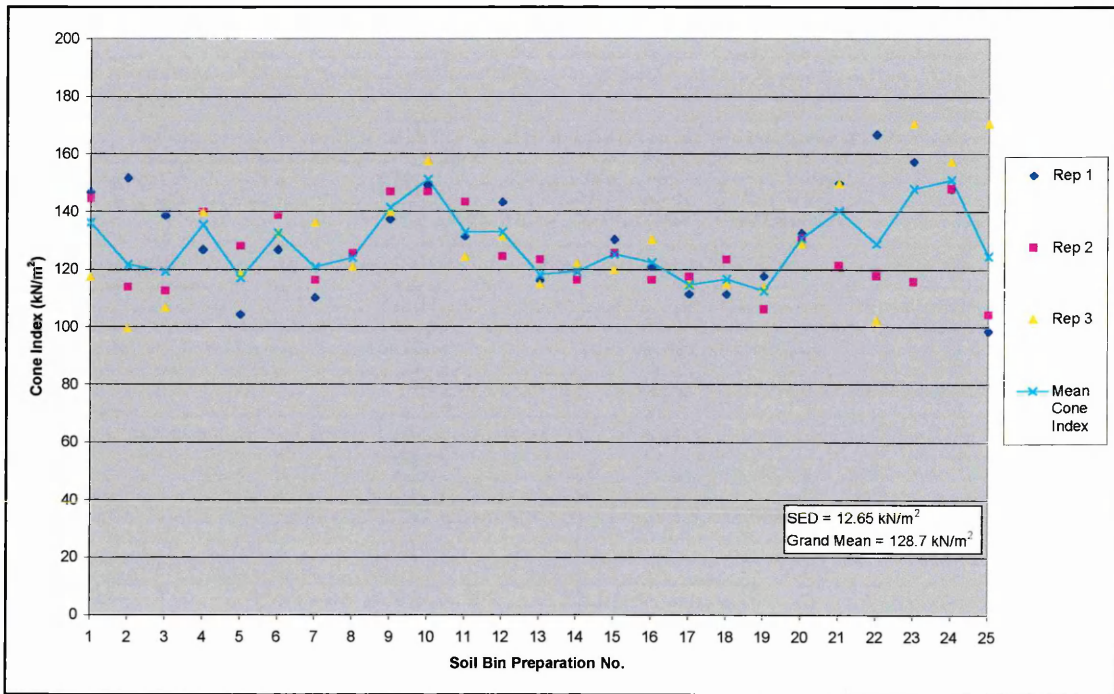


Figure 5.11 – Cone index readings recorded for different sand preparations in the soil bin over the duration of all testing

5.3.1 Determination of K (Sand Deformation Modulus)

Again values of K were determined in the manner outlined previously, with a full account of the process and results detailed in Appendix 13. The sand shear box test results produced a linear relationship between σ and K , described by equation 51.

$$K = 0.00009\sigma \quad (51)$$

Again Equation 16 $\left\{ \frac{K_1}{K_2} = \sqrt{\left(\frac{A_1}{A_2} \right)} \right\}$ was used to relate A_1 (the tyre contact area),

A_2 (the shear box area) and K_2 (described by equation 51) to allow derivation of K_1 . Again it was only possible to determine a range of K_1 values for each given soil load, so a range of relationships between the tyre contact area and values of K_1 , which are shown in Figure 5.12, were again developed. These allowed a K value to be calculated for

beneath a tyre for all combinations of tyre contact area and normal load produced during the testing on sand.

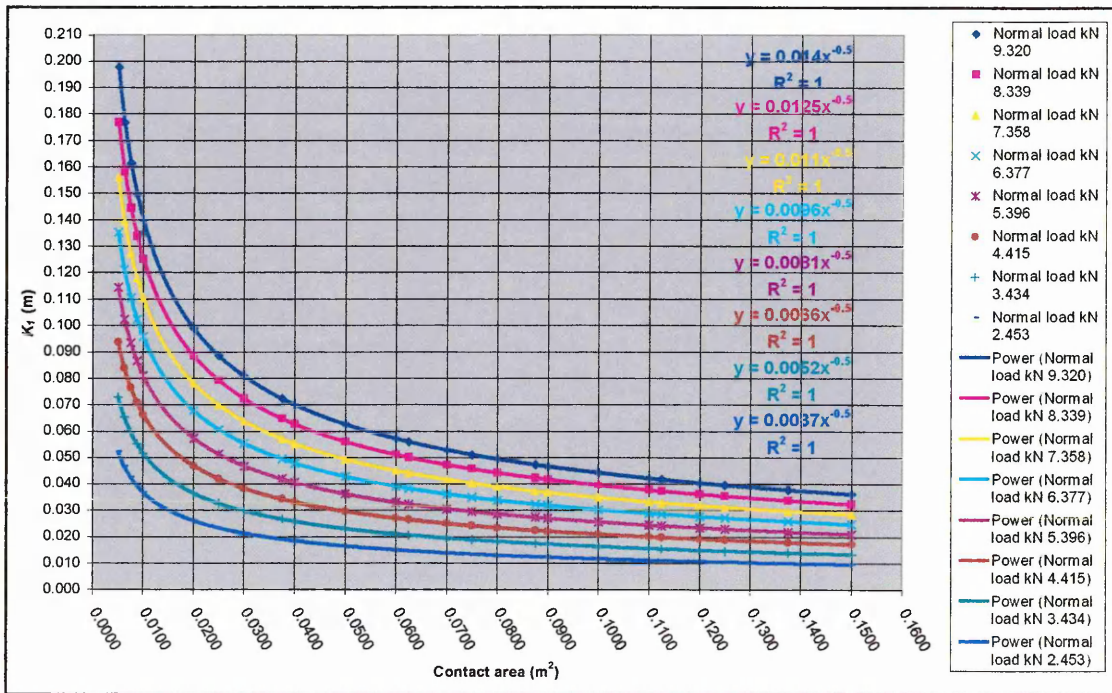


Figure 5.12 – The relationships between contact area and K_f for the DA80F sand under different normal tyre loads

5.3.2 Determination of Bekker Plate Sinkage Values

These values were also determined following the methodology outlined in the literature review. The full details of this process and the results that were generated are presented in Appendix 14. These tests used three different plate sizes on the experimental sand preparation (*poured and scraped*). The pressure sinkage results produced the Bekker soil coefficients shown in Table 5.10.

Table 5.10 – Bekker pressure sinkage coefficients for the sand preparation

Sand Coefficient	kc	$k\phi$	n
Value	65.0	1329	0.885

6 TYRE EVALUATION APPARATUS AND METHODOLOGY

6.1 THE SOIL DYNAMICS LABORATORY (SDL)

The experiments were all conducted in the Cranfield University at Silsoe laboratories. The traction tests all used the Soil Dynamics Laboratory (SDL) soil bin and soil processor facilities. These consist of a custom built, semi-automated soil bin and soil processor unit. The use of such soil tanks, or bins, for traction and tillage studies removes the inherent variability found in field conditions, allowing uniform soil conditions to be obtained following careful preparation¹³⁵. This allows investigations of soil behaviour under conditions of prescribed physical properties which would be difficult, if not impossible, to achieve under “field” conditions¹³⁶.



Plate 6.1 – A rear view of the soil bin and processor unit (mounted with the variable slip single wheel tester)

The soil bin is a sub-surface concrete tank 20 m long, 1.7 m wide and 1 m deep¹³⁷. On top of this tank run the rails that guide the main processor unit, see Plate 6.1, which contains the hydraulically operated soil engaging blades, bucket and grabs, and rollers to enable a variety of soil preparations to be produced. To the rear of this unit is fitted an adjustable mounting plate for attaching test equipment. The whole unit is moved by a cable drive system, which is operated by an electro-hydraulically controlled winch drum¹³⁸. The maximum forward velocity of the processor unit is approximately 8 km/h.

Attached to the mounting plate was an Extended Octagonal Ring Transducer (EORT)¹³⁹, which was used to measure horizontal and vertical forces applied between the processor unit and any attached drive systems. Each of the three channel outputs from the EORT was passed through an individual strain gauge conditioning module (Strainstall Model 91C), which produced a stabilised 9.2 V supply for each particular wheatstone-bridge circuit on the EORT. The strain gauge module amplified the μV return output from each circuit, such that a voltage output proportional to load could be determined. The strain gauge module also allowed any offsets, from gauge inconsistency or static load to be removed.

6.2 TEST TYRES

To investigate the effect of tread pattern upon tractive performance a range of different treaded tyres were used. The production tyres selected were standard Goodyear products, which are shown in Plate 6.2. These were a Goodyear HP Wrangler (HP), an on-road/ mud biased tyre and a Goodyear Wrangler Ultra-Grip (UG), a winter on-road/ mud biased tyre, both of which were supplied in the 235/ 70 R16 size, and a G82, as described in section 3.2.2, which was supplied as a 7.50 R16 (its only manufactured size). The differences in section width and outside diameter of these two sizes can be clearly seen in Plate 6.2 and Plate 6.3. To ensure comparable results between the G82 tread and the 235/70 R16 treads, a 235/70 R16 G82 tread was required. This tyre was a bespoke prototype produced by Goodyear by being laser cut on to a plain tread blank (slick), which produced the tyre shown in Plate 6.3. The blank used was of the same rubber, construction and size as the 235/70 R16 Goodyear Wrangler HP.

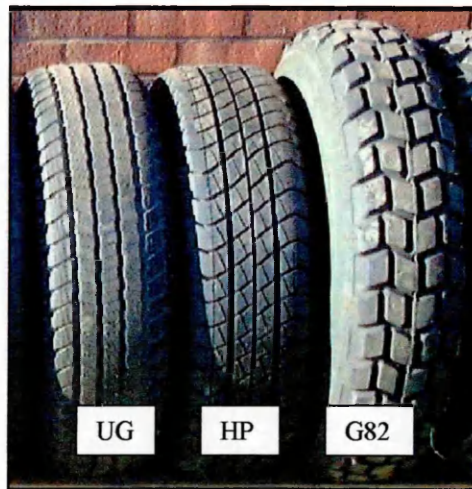


Plate 6.2 – The three standard production tyres supplied



Plate 6.3 – Left: A comparison in diameter between the two G82 tyres supplied; Right: the laser cut 235/70 R16 G82 tread and a 235/70 R16 plain tread blank

The tread effect investigation required tyres with simpler tread patterns. Therefore several prototype treads with basic parallel grooved patterns were designed. These were hand cut on to extra identical plain tread (PT) blanks by Dunlop staff. The tread depths for all hand cut treads were 11 mm, as per the HP tyre, and their tread block/ void width spacings were determined by the following requirements:

- The necessity to maintain tread: void ratios of approximately 60%: 40%.
- The width of the longitudinal tread design.
- The circumference of the lateral and 45° tread designs.
- The necessity to produce complete treads around each tyre diameter.

These requirements produced tread widths of 45 mm and void spacings of 30 mm for all the treads. The tread patterns featured a range of tread angles from longitudinal (LON), through 45° forward facing (F) to lateral (LAT) and back again to the LON tyre. All these treads are shown in Plate 6.4.



Plate 6.4 – The symmetrical hand cut tread designs; the forward (F) and backward (B) facing nomenclature was applied as if the tyres were rolling towards the reader

6.3 FIXED SLIP TEST RIG

A fixed (constant) slip test rig was developed so that slip-pull curves could be constructed by running a series of tests across a range of discrete slips for a given set of tyre treatments. The rig development and the later experimentation was aided by Oliver³⁰, because both authors could record different, but relevant, measurements from a single investigation. This allowed the efficient completion of both test programmes.

6.3.1 Design of the Fixed Slip System

The rig was designed to mount to the soil processor unit using a pin joint, which allowed the wheel sinkage to freely vary as required. Between the processor unit and the joint was an EORT, which was used to measure horizontal force acting between the two frames. The rig consisted of a RHS frame structure on to which a Land Rover hub and half-shaft assembly were mounted. An adjustable tie-bar mounted between the frame and the hub controlled the alignment of the wheel.

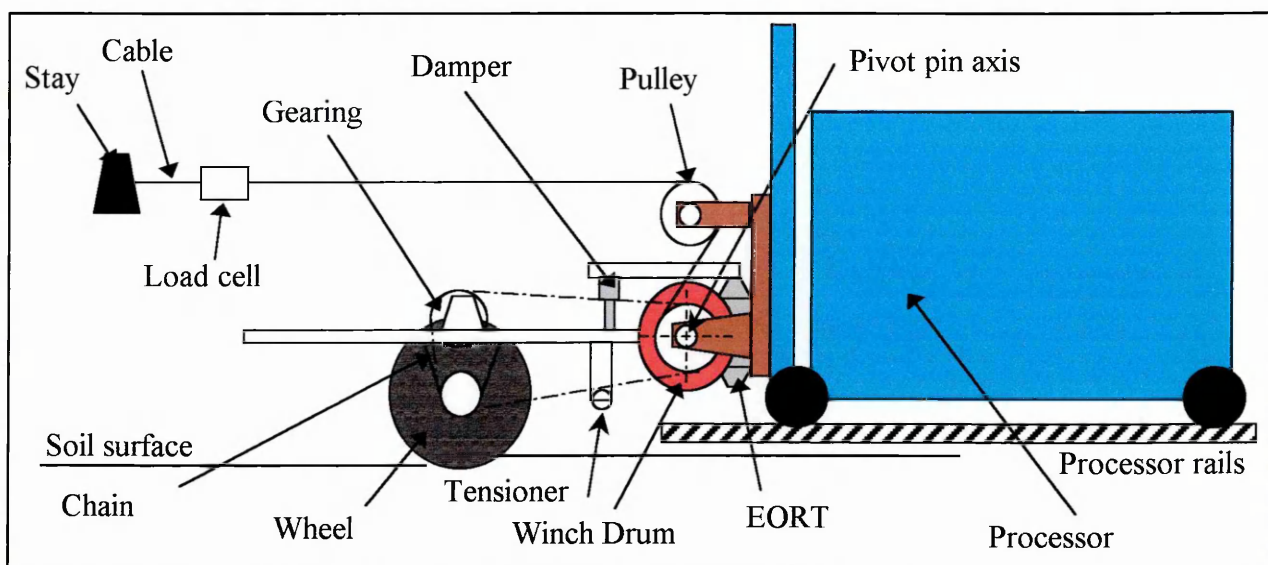


Figure 6.1 – A schematic diagram of the layout of the fixed slip test rig

The basic rig dimensions are shown in Appendix 15. The wheel hub's half-shaft was shortened and had a taper-lock sprocket fitted to supply drive to the wheel. A 25 mm (1") simplex chain drive connected the hub sprocket to the drum sprocket, via an idler sprocket and tensioning mechanism, as shown in Figure 6.1. The shaft to which the drum sprocket was mounted was on the same axis as, but offset from, the pivot pin. Mounted to these was a fixed diameter drum around which a $\text{Ø}12$ mm multi-core steel cable was wound. Plumber blocks attached the drum shaft to a frame mounted on the processor, which stopped forces being directly transmitted to the EORT, see Plate 6.5. The other end of the cable was attached to a load cell (tension link), which was in turn attached to a fixed anchor stay at the end of the bin.

Extra static load (normally equivalent to 650 kg – $\frac{1}{4}$ of a laden Land Rover Discovery) was mounted on the rig's weight platforms. This was adjusted to achieve the correct vertical load acting on the wheel, which was measured with the frame attached to the processor and the wheel supported with a load strap, which was connected to an overhead crane through a load cell. The load was distributed around the frame so that it was evenly balanced about the tyre centre-line on all axes, as Plate 6.5 illustrates.

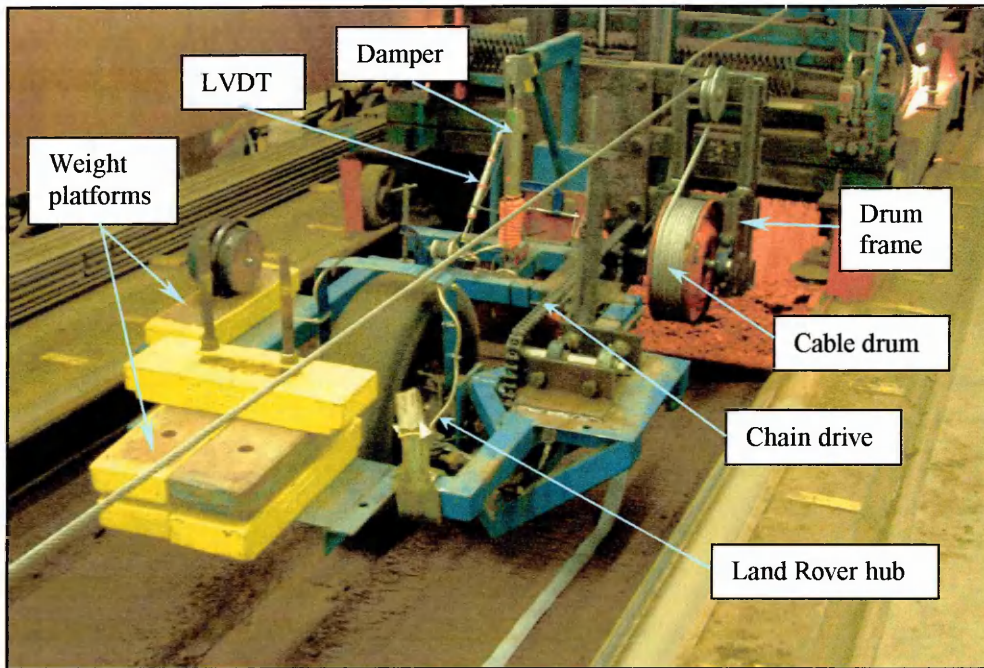


Plate 6.5 – The fixed slip test rig mounted to the soil processor operating on a firm sandy loam soil

It was found that the vertical deflection of the test frame varied due to fluctuations in wheel slip (sinkage). To minimise this effect a damper was fitted between the frame and a separate bracket, as shown in Plate 6.5 and Plate 6.6. The bracket was mounted between the pin joint and the EORT so that any forces that it bore were kept within the measurement system. The bracket positioned an Enidine AD720M, 200 mm stroke, variable rate control (damper) vertically over the test frame. The damping, which was independently variable in tension and compression, was set at approximately 295 kNs/m in both directions. This achieved an angular damping of 18 kNms/rad (equivalent to a damping ratio of 0.7). The fitment of the damper minimised the vertical displacement fluctuations and thus ensured good contact between the tyre and the ground at all times. To prevent sand ingress the damper's arm was encapsulated in a rubber sleeve.

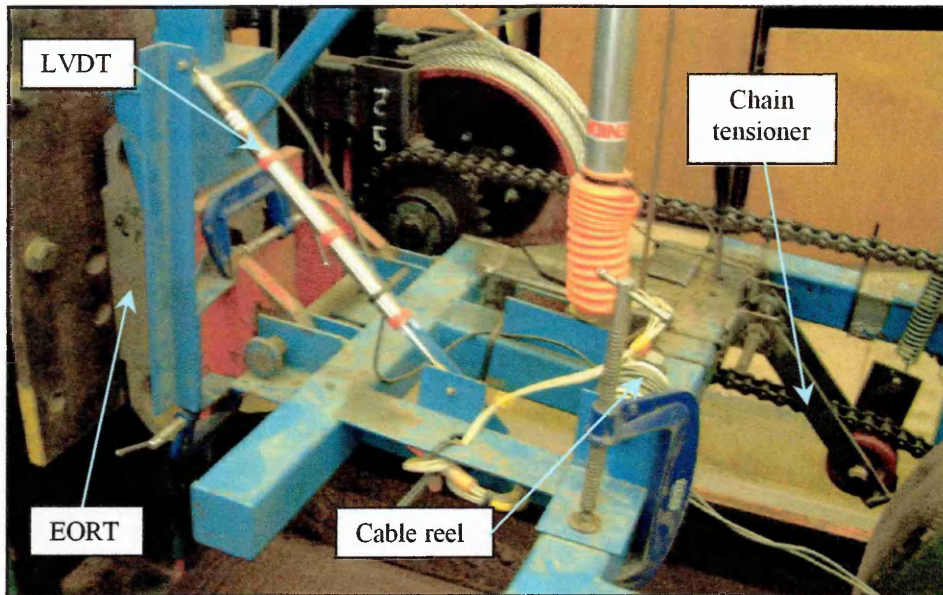


Plate 6.6 – A view of the opposite side of the fixed slip test rig

Prior to each test run the appropriate tyre was mounted to the hub using a 406 mm (16") split rim and set at the correct pressure. The wheel was then rotated, which pulled the cable taught as the frame was lowered onto the soil, so that both it and the cable ran horizontal. As the processor unit was driven along the bin, cable was pulled off the drum at a rate equivalent to the forward speed. The chain drive transformed this motion into a rotational wheel speed. Using different sprocket ratios between the drum and the wheel allowed different wheel speeds, and hence different wheel slips to be achieved. The fixed relationship between the sprockets achieved a fixed slip ratio irrespective of the processor's forward travel speed, though it was found that the actual achieved slip varied from the intended value. This was not vital as the slip was calculated for every treatment. The variation could only be determined retrospectively after a test, as its effect was governed by the treatments tested.

The test rig had been intended to be capable of testing any tyre or soil treatments at slips of between 10% and 70%. However, it was found that excessive momentary peak forces could be generated within the system, so the operational envelope was constrained to below a maximum of 50% slip on the looser (1170 kg/m^3 and 1270 kg/m^3) soils and 25% slip on firmest (1400 kg/m^3) soil.

6.3.2 Derivation of Tractive Forces

6.3.2.1 Free-rolling rolling resistance

The test rig could be used to measure a tyre's free-rolling rolling resistance by removing the drive chain and disconnecting the cable. Towing the frame along the bin, with the wheel freewheeling, allowed the rolling resistance to be determined from the tension force induced on the EORT as the forward motion of the wheel was resisted.

6.3.2.2 Gross thrust, net thrust and rolling resistance

The gross thrust produced at the wheel was proportional to the tension in the cable and was measured by the tension link. Although it ran through sprockets, the system was comparable to two drums mounted on one shaft, such that a torque produced on one drum by tension acting at its radius would be directly proportional to the torque produced in the shaft and on the other drum's radius. Changing sprocket ratios (slips), tyre radii and slight chain losses (calculated from the force required to pull cable from the drum with the wheel suspended) complicated the basic analogy, so Excel was used to account for these factors and compute the actual gross thrusts generated.

The net wheel thrust pushed the test rig forwards, which produced a compressive force at the EORT. However, because the drive chain was mounted on either side of the EORT, as the wheel was turned the chain tension also compressed the EORT. As with the gross thrust, the chain tension effect depended upon the sprocket ratios and the cable tension. Therefore the net force was calculated from the EORT horizontal force reading minus the extra chain tension force (a proportion of the cable force). The rolling resistance was calculated from the difference between the gross and net thrusts.

Tension in the drive chain produced a lifting effect of the whole frame. This was minimised by routing the chain close to the height of the pivot point, but the static weight of the frame had to be increased from 650 kg to 730 kg to achieve a wheel load of 650 kg when the tyre was producing thrust. As the cable tension varied, because the tyre switched between slipping and gripping the surface, the vertical load acting on the

wheel also varied. This value had to be determined retrospectively but at $650 \text{ kg} \pm 20 \text{ kg}$ ($\pm 3\%$) it was deemed to be negligible.

6.3.3 Test Rig Instrumentation

The instrumentation devices used (detailed in Appendix 16) were all connected to the data logging and power supply equipment via long lengths of earthed signal cable. This gave direct connection, yet still enabled wheel travel along the full soil bin length. The output signals inputted into a 16-channel analogue capture unit that was wired directly to a PC mounted data capture card. The PC ran DasyLab, a Windows/ GUI based data logging software, within which dedicated logging programmes were written to capture the appropriate readings from each test run. After capture the data files were imported into Excel for post-processing.

Cable tension was measured by a tension link. The signals from the strain gauges in this unit were inputted in to the same Strainstall conditioning module used to process the EORT outputs. With this test rig only the EORT horizontal force readings were used during the analysis of the results, as throughout the testing no significant variation occurred in the recorded moments and vertical forces. This was acceptable because the test frame's pivot point was positioned to force the frame to operate horizontally during traction by estimating for load and slip sinkage effects. Thus when the wheel dug into the ground the frame ran approximately level. The recorded variation in sinkage was insufficient to significantly alter the horizontal alignment, and all the horizontal thrust components were always recorded.

The wheel sinkage was determined using an LVDT (Linear Variable Displacement Transducer) fitted between the processor unit's mounting plate and the test rig, as shown in Plate 6.6. This was positioned and calibrated to measure any variation in frame height relative to the frame's horizontal position, thereby always recording a true sinkage height irrespective of the distance between the soil and pivot pin, a distance that was set and measured before each test. As part of Oliver's investigation³⁰ three drawstring transducers were fitted inside the tyre to measure tyre deflection. The results

from these devices allowed the tyre deflection to be subtracted from the measured sinkage to derive a true value of deflected tyre sinkage, see Figure 6.2.

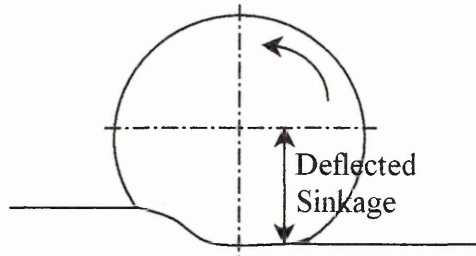


Figure 6.2 – The deflected sinkage of a wheel

The forward speed of the processor unit was measured using a ‘fifth-wheel’, which ran along the carriage rails. Attached to the wheel was a tacho-generator that produced a voltage output proportional to the wheel speed, and hence the processor’s forward speed. The test wheel’s rotational speed was measured using a rotary encoder that attached onto a threaded shaft that extended from the internal thread of the wheel hub, as shown in Plate 6.7. Also mounted on the shaft was a drum of signal cable to carry all the signals to and from the rotating wheel.



Plate 6.7 – The rotary encoder, signal cables and cable storage drum mounted to the test rig

The pulse signal output from the encoder was inputted into a purpose built pulse counter circuit (detailed in Appendix 17), which transformed the pulses into a voltage output proportional to the pulse frequency (the wheel’s angular velocity). Subtracting the mean

tyre deflection (measured with the drawstring transducers) from the undeflected radius calculated the rolling radius. During subsequent analyses, multiplication of the rolling radius and angular velocity allowed actual wheel forward speeds to be derived. Both the processor and wheel forward speeds were then used to derive the wheel slip (see equation 2). An inductive switch was also mounted to the hub, whilst a screw was attached to the rim of the brake disc to trigger the switch at each wheel revolution. This device allowed the number and timing of the wheel revolutions during each test run to be calculated, which in turn allowed wheel rotational speed, calculated from the encoder pulses, to be verified.

6.3.3.1 EORT calibration

The EORT was connected to the strain gauge module, which was in turn connected to the data logger. One face of the EORT was placed on flat concrete. Calibrated weights were then loaded on the other face at set time intervals. During this process the data logger constantly recorded the EORT output. Afterwards sections of logged data were determined for each loading and a mean voltage was calculated for each data section.

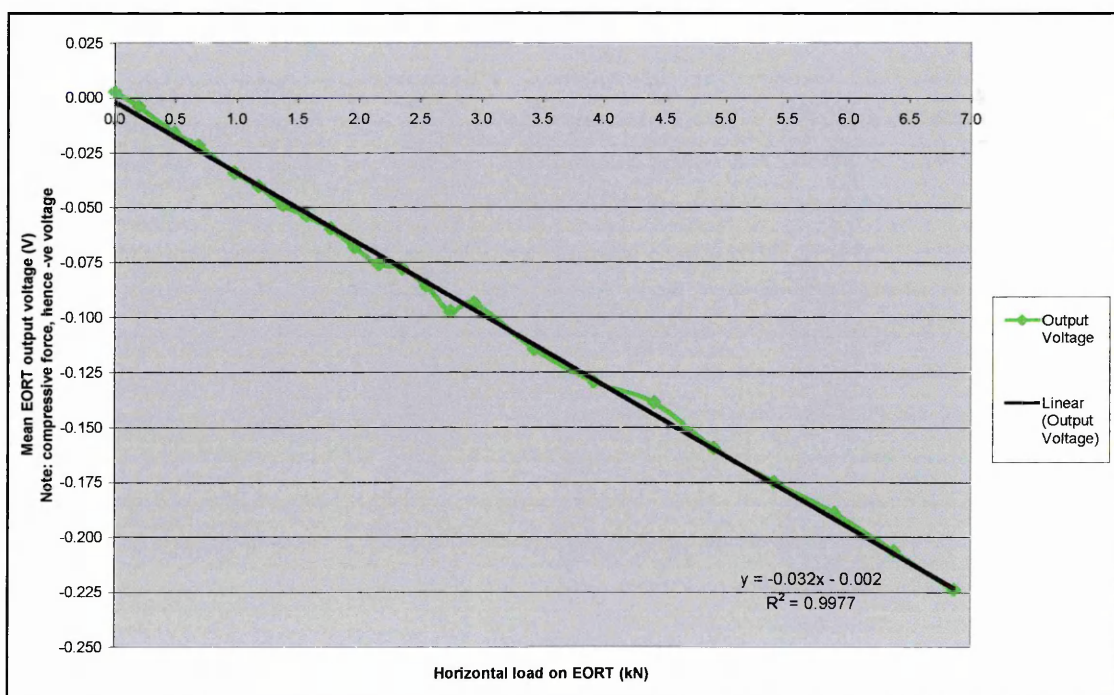


Figure 6.3 – EORT calibration graph

All the mean values were plotted against load to produce the calibration line shown in Figure 6.3. From this calibration the measurement accuracy was determined as being ± 0.09 kN. The equation of this trendline, and the calibration trend lines calculated for the rest of the instrumentation (see below), were used later in the analysis in Excel to convert the logged voltages into SI units.

6.3.3.2 Tension link calibration

This calibration was conducted by suspending one end of the tension link from a crane. A digital load cell fitted with a set of chain links was mounted on the other end of the link. This set-up allowed weights to be suspended on the tension link to provide a load, whilst the true weight was read from the load cell. Connection was made to the strain gauge module, which allowed constant logging of the tension link output as the weight was increased. Mean voltages were then derived for each loading by using the same method as described in the previous paragraph. When plotted these produced the calibration trendline shown in Figure 6.4, from which a measurement accuracy of ± 0.11 kN was determined.

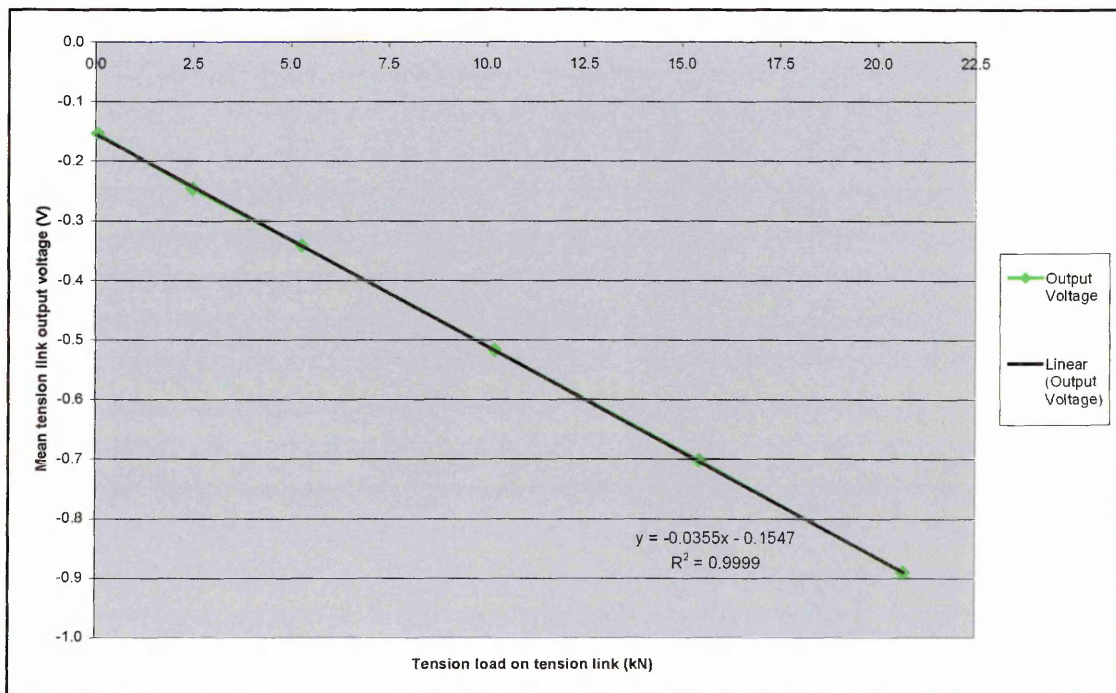


Figure 6.4 – Tension link calibration graph

6.3.3.3 LVDT (sinkage) calibration

To conduct this calibration the LVDT was wired to the data logger and a 10 V DC supply. The test rig frame was then set horizontal above a flat concrete floor using a spirit level. A second spirit level was taped to the tyre so that it protruded horizontally beneath the tyre. This allowed the tyre to be rotated to keep the second level positioned at the lowest most point on the tyre, which in turn facilitated the accurate measurement of the height of this point above the floor with a steel rule. The frame was raised from its minimum to maximum height in discrete measured steps. Simultaneously the LVDT's output was recorded on the data logger. Again mean voltages were derived for each discrete height and when plotted against the measured heights they formed the calibration trendline shown in Figure 6.5. This device had a measurement accuracy of ± 3.5 mm.

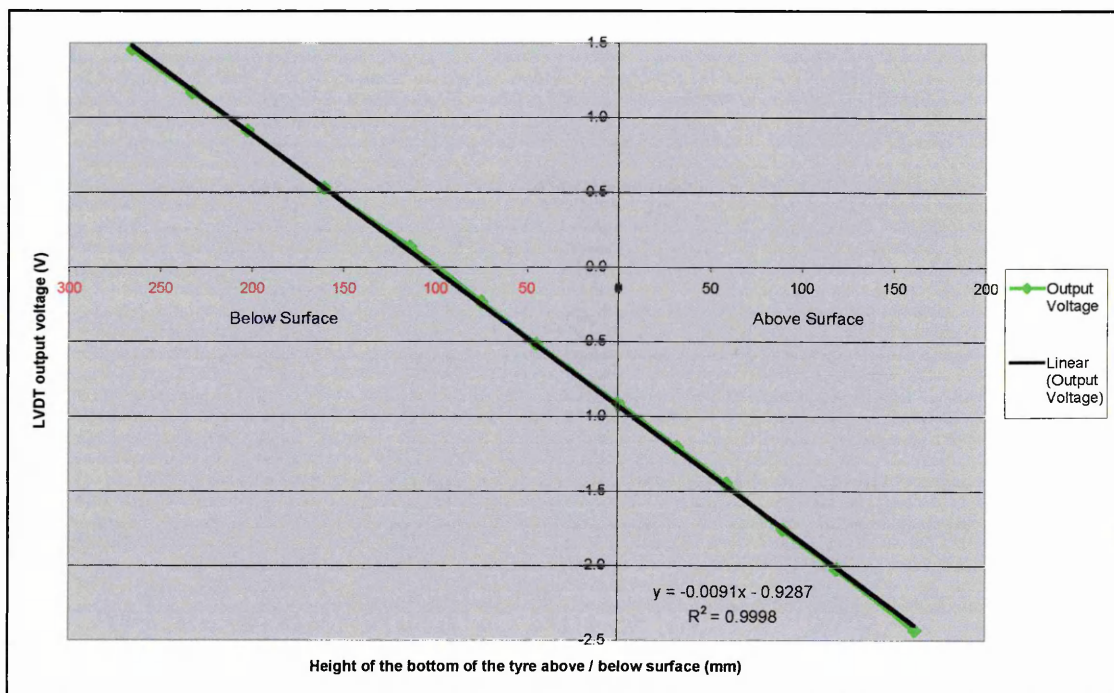


Figure 6.5 – LVDT calibration graph

6.3.3.4 Tacho-generator (fifth wheel) calibration

The tacho-generator wheel was connected to the data logger and the test rig suspended off the ground. A 9 m length was marked out alongside the soil bin and the processor unit was run along the bin at nine different constant speeds ranging from 0.8 m/s to 2.7

m/s. The time taken for a fixed point on the processor cover the 9 m was timed and used to determine the processor unit's velocity. Simultaneously the tacho-generator output was logged and later used to derive a mean voltage output for the period of constant speed. The voltages were then plotted against speed to derive the calibration line shown in Figure 6.6, from which the measurement accuracy was determined as ± 0.012 m/s.

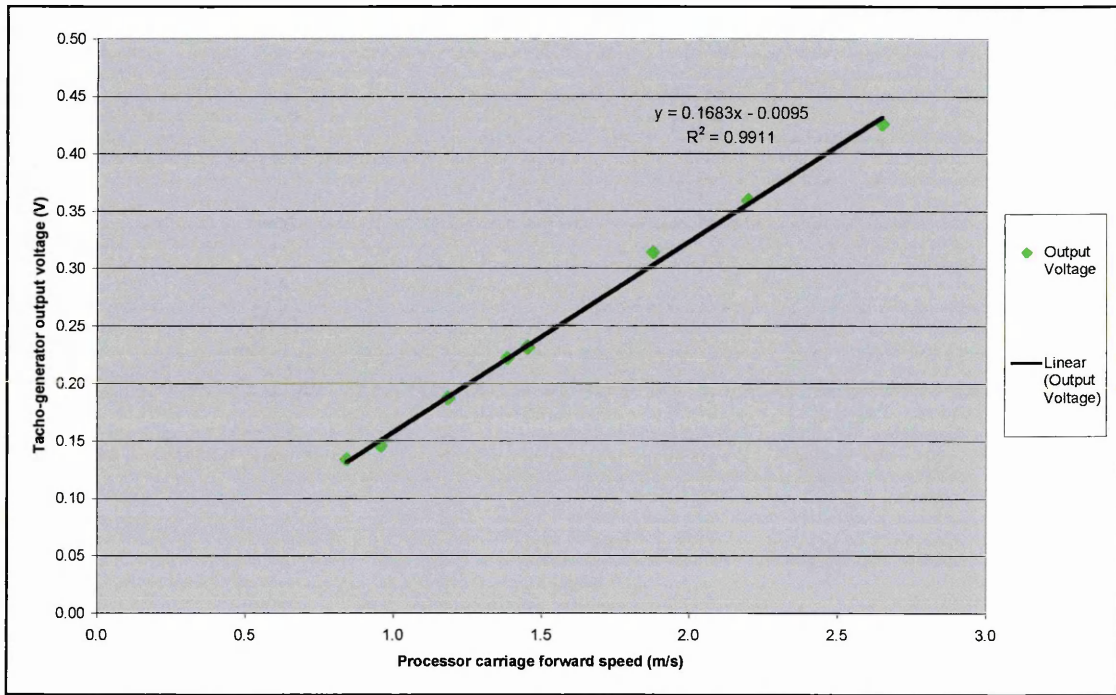


Figure 6.6 – Tacho-generator calibration graph

6.3.3.5 Rotary encoder (wheel speed) calibration

The rotary encoder was supplied with a 7 V DC voltage and its output was connected to the pulse counter circuit, which was in turn connected to the data logger. The test rig was suspended off the ground and the wheel was rotated at a constant speed. The wheel speed was measured with a hand-held optical rev counter, which counted twelve pieces of reflective tape stuck at 30° spacings around the outer edge of the wheel rim, and provided a digital read-out of the rotational speed. The wheel was rotated at a range of speeds and a rotational speed measurement taken each time the wheel achieved a constant speed. Simultaneously the voltage output from the counter circuit was logged. A mean voltage was derived for each constant speed and all of the data was then plotted

to derive the calibration trendline shown in Figure 6.7. This calibration produced a measurement accuracy of ± 1.3 rpm.

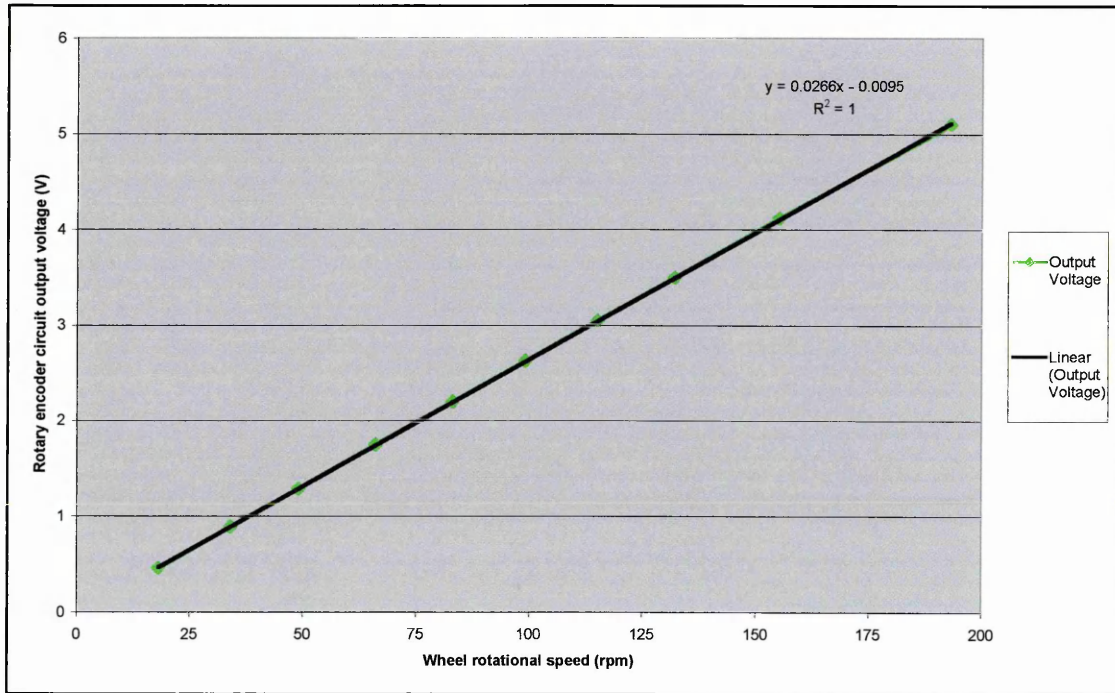


Figure 6.7 – Rotary encoder calibration graph

6.4 FIXED SLIP TESTS ON SOIL

6.4.1 Treatments Investigated

The first tests that were conducted were undertaken using a sandy loam soil in the soil bin, which was used at one of the three density preparations described in section 5.1 (1170 kg/m³, 1270 kg/m³ or 1400 kg/m³). The different treatments tested are shown in Table 6.1. These treatments were investigated in different groups, as indicated by the colour coding in Table 6.1, i.e. the red groups were the treatments which investigated tread effects, and the pink those which investigated pressure effects etc. Plate 6.3 shows the different 235/70 R16 tread patterns tested. The discrete slip targets in Table 6.1 were the slips that the sprocket choices were intended to achieve, not the slips actually achieved, which differed slightly from these values. A range of tyre loads was achieved over the different discrete slips, because of variations in the chain tension, which caused the small variations in the vertical load.

Table 6.1 – Fixed slip tests treatments investigated on the sandy loam soil (note: colour coding indicates the different groups of variables investigated)

Tyre Tread	Discrete Slip Targets	Tyre Pressure	Tyre Load Achieved	Soil Preparation
Type	%	bar (psi)	kN	kg/m ³
PT	10, 15, 20, 30, 50, 70	1.10 (16)	6.425 to 6.572	1170
PT	10, 15, 20, 30, 50, 70	1.38 (20)	6.425 to 6.572	1170
PT	10, 15, 20, 30, 50, 70	2.07 (30)	6.425 to 6.572	1170
PT	15, 20, 40, 50	3.10 (45)	6.425 to 6.524	1170
PT	15, 20, 40, 50	3.10	6.425 to 6.524	1270
PT	10, 15, 20, 30, 50	1.10	6.425 to 6.524	1270
PT	10, 15, 20	1.10	6.425 to 6.524	1400
45F	10, 15, 20, 30, 50	1.10	6.425 to 6.524	1170
45B	10, 15, 20, 30, 50	1.10	6.425 to 6.524	1170
G82	10, 15, 20, 30, 50	1.10	6.425 to 6.524	1170
LAT	10, 15, 20, 30, 50	1.10	6.425 to 6.524	1170
LON	10, 15, 20, 30, 50	1.10	6.425 to 6.524	1170

These tests were not thoroughly replicated, as some replication of the results was achieved during each test-run and because this was a pilot experiment that was conducted to:

1. Confirm the operation of the test rig.
2. Check that the slip-pull results generated agreed with accepted theory²⁰, thus validating the methodology used with the fixed-slip test rig.
3. Determine if variations in slip-pull performance occurred between different tyre treatments, and if they were measurable.

6.4.2 Experimental Results

Slip-pull curves were used for tyre comparisons. These were constructed from measurements recorded over a series of test runs conducted across a range of discrete fixed slips. The following variables were plotted on the slip-pull graphs:

1. Gross thrust
2. Rolling resistance
3. Net thrust (calculated from 1 & 2)
4. Deflected sinkage (accounting for both tyre and ground deformation)

Thus four values (one for each variable) were plotted at each discrete slip value generated by each different test run, i.e. five test runs would produce five discrete sets of data on each curve. Results were only calculated from the central periods of each test-run, when the rig operated at a constant forward speed, mechanically set at 1.4 m/s (≈ 5 km/h), and hence when it achieved a consistent wheel slip. The value plotted for each variable was a mean value of all the data recorded for that variable during the period of constant speed during the test-run. This process was undertaken for all four variables for all of the test-runs conducted. The results for each treatment effect presented in the following sub-sections are shown on two pairs of graphs, which use the following coding system to identify the results; i.e. TREAD, PRESSURE, SOIL DENSITY, i.e. *PT 1.38 1170*, would indicate a plain tread tyre inflated to 1.38 bar operating on 1170 kg/m³ soil.

6.4.2.1 *Effect of inflation pressure*

Figure 6.8 shows the gross and net thrusts that were achieved, whilst Figure 6.9 details the deflected sinkage and rolling resistance results. The gross thrusts increased from around 3 kN up to 4.5 kN as slip increased from 10% to 50%. Above 50% slip the gross thrust reduced as the slip increased further until at 70% slip only 3 kN of thrust was achieved. Variations in tyre pressure did not generate any notable patterns in the gross thrust results. This was because the tyres had all been operated on an easily deformed surface, as the sinkage results in Figure 6.9 proved. This allowed a long contact patch to be generated across the tested pressure range, which in turn allowed long shear displacements, and hence high gross thrusts, to be achieved in all instances.

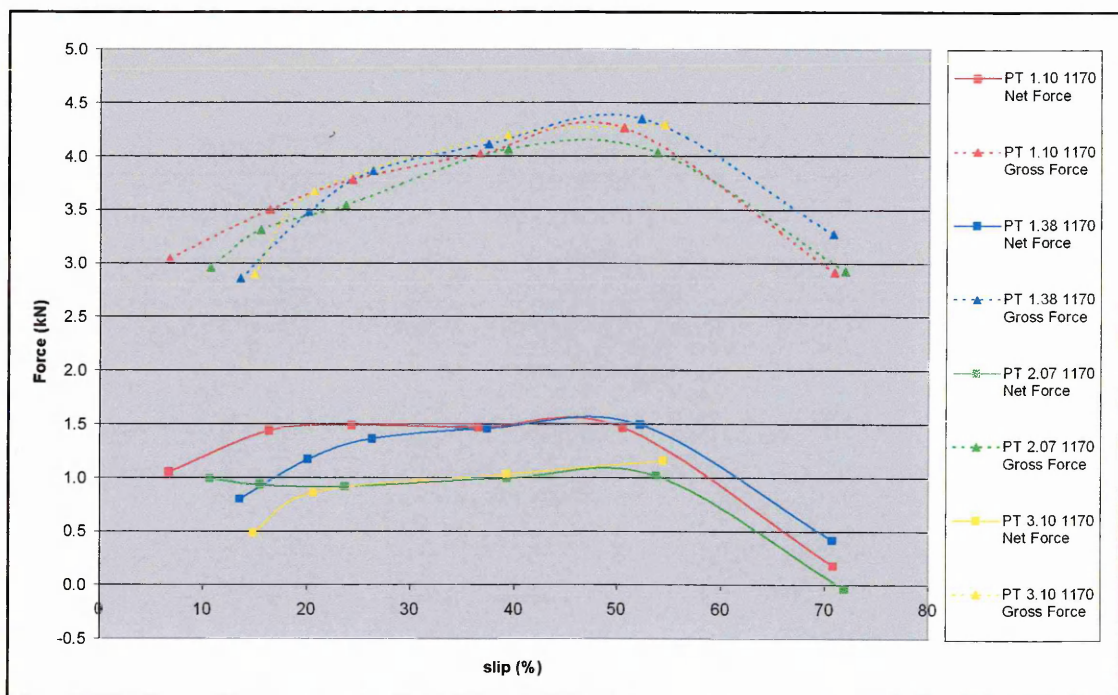


Figure 6.8 – Gross and net forces generated by the plain tread tyre on 1170 kg/m³ soil across a range of discrete slips and inflation pressures

The results in Figure 6.9 confirmed that sinkage increased with slip, as would be expected due to slip sinkage effects. This extra sinkage caused the rolling resistance to also increase with slip. The inflation pressure influenced this relationship, as at lower pressures the contact area was greater, which reduced the sinkages of the lower pressure tyres. Therefore at equivalent slips the lower pressure tyres produced up to 0.5 kN less resistance. These rolling resistance trends affected the net thrusts achieved at different

tyre pressures, such that the tyres typically generated 0.5 kN ($\approx 50\%$) extra net thrust when operated at the lower inflation pressures of 1.10 bar and 1.38 bar, compared to the thrusts achieved at 2.07 bar and 3.10 bar. These results demonstrated the capability of the test methodology to conduct, and measure differences between, traction performance tests for different tyre treatments.

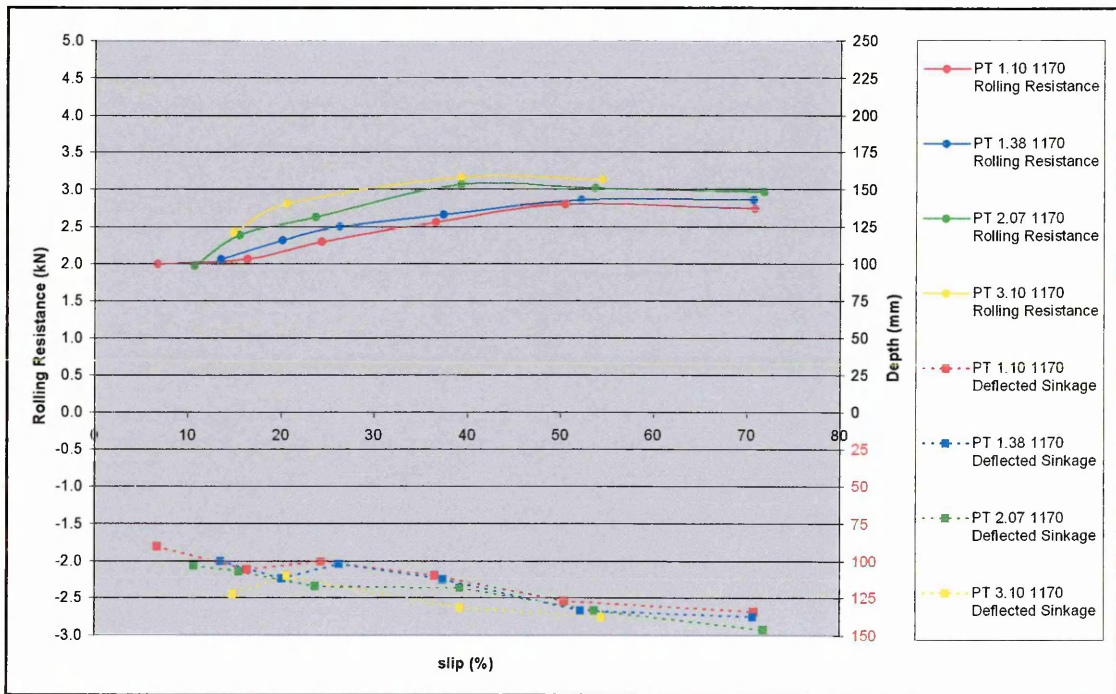


Figure 6.9 – Rolling resistances and depths of sinkage generated by the plain tread tyre on 1170 kg/m^3 soil across a range of discrete slips and inflation pressures

6.4.2.2 Effect of soil bulk density

This was investigated at two different inflation pressures. Figure 6.10 and Figure 6.11 show the results for the PT tyre when operated at a 1.10 bar (16 psi) inflation pressure on the three soil preparations. Whilst, Figure 6.12 and Figure 6.13 show the performance of the same tread operated at 3.10 bar (45 psi), but this was only conducted on the two weaker preparations due to restrictions caused by the performance capability of the test rig. Figure 6.10 showed that typically higher gross thrusts were achieved as soil strength (density) was increased, except below 20% slip where higher gross thrusts were achieved on the 1170 kg/m^3 soil than on the 1270 kg/m^3 soil.

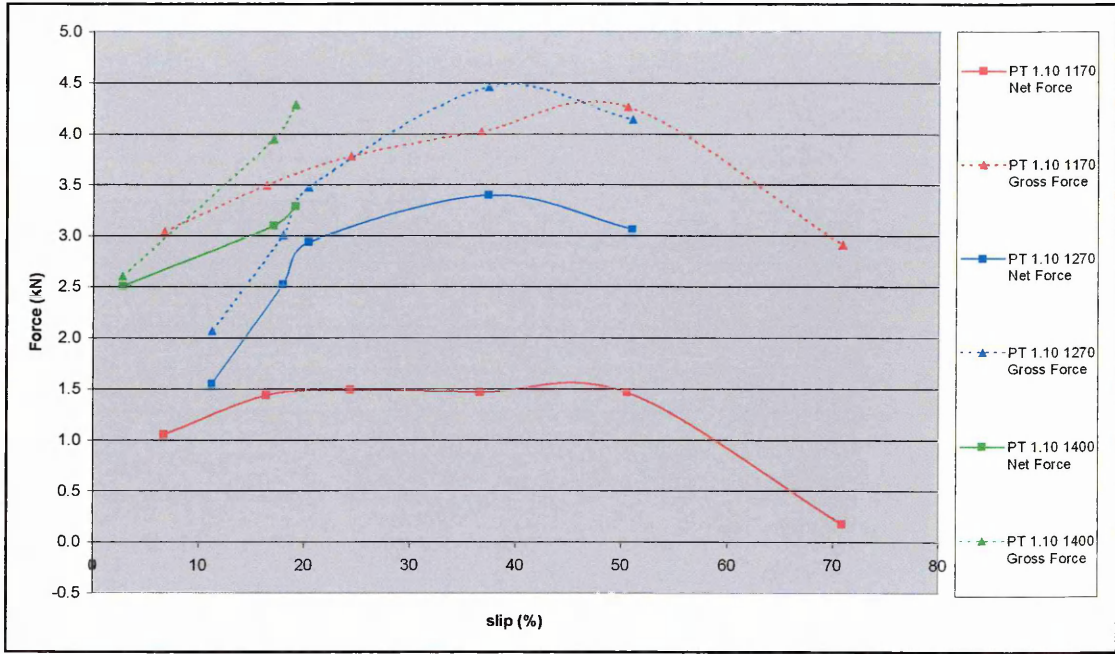


Figure 6.10 – Gross and net forces generated by the plain tread tyre inflated to 1.10 bar across a range of discrete slips and soil preparations

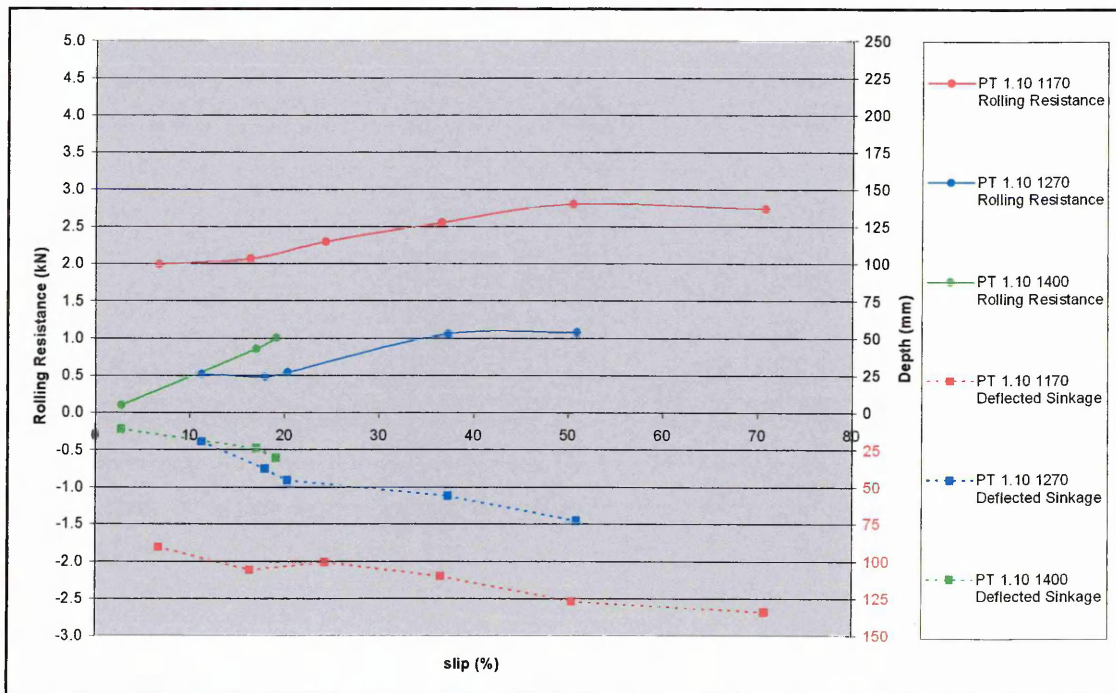


Figure 6.11 – Rolling resistances and sinkage generated by the plain tread tyre inflated to 1.10 bar across a range of discrete slips and soil preparations

Figure 6.11 showed that strong correlation again existed between the tyre sinkage and the associated rolling resistance. As expected the sinkage increased with both decreased

soil strength and increased slip. This contributed to resistances of up to 1 kN on the 1400 kg/m³ soil, between 0.5 kN and 1.1 kN on the 1270 kg/m³ soil and between 2 kN and 2.8 kN on the 1170 kg/m³ soil. The combination of the trends in the gross thrusts and rolling resistances greatly affected the net thrusts achieved on the different surfaces, such that the peak net thrusts were approximately 3.4 kN on the 1400 kg/m³ and 1270 kg/m³ soil and 1.6 kN on the 1170 kg/m³ soil. Greater net thrusts would probably have been generated on the 1400 kg/m³ soil had the test rig's capability not been limited to below 20% slip). For the 1170 kg/m³ and 1270 kg/m³ soils the amount of net thrust generated tailed off above slips of 40% to 50%.

The gross thrusts achieved when operating at inflation pressures of 3.10 bar, shown in Figure 6.12, indicated that approximately 1 kN of extra gross thrust was generated on the 1170 kg/m³ soil, as opposed to the 1270 kg/m³ soil, over the range of slips that the investigation evaluated. This pattern differed from the thrusts generated when the tyres were operated at 1.10 bar because at 3.10 bar the tyre became virtually rigid (i.e. its deflection approached zero).

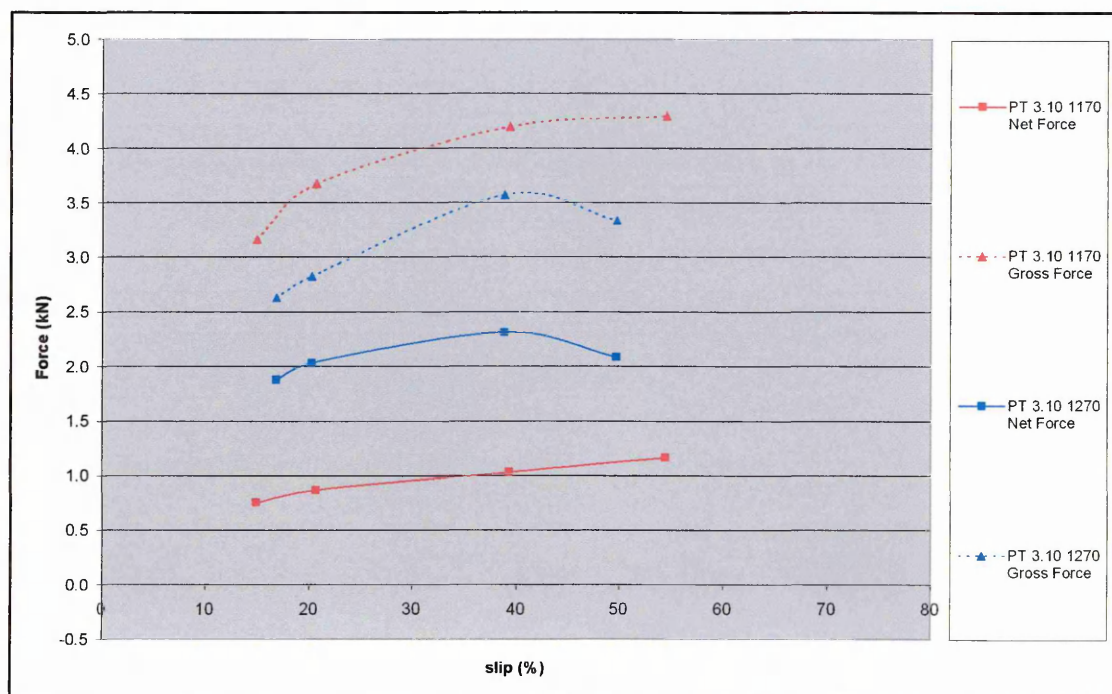


Figure 6.12 – Gross and net forces generated by the plain tread tyre inflated to 3.10 bar across a range of discrete slips and soil preparations

As such the tyre's contact length (ability to generate gross thrust) was mainly governed by the tyre sinkage. Figure 6.13 showed that approximately 50 mm extra sinkage occurred on the softer surface, which therefore increased the contact length and allowed extra thrust to be generated even though the soil was weaker (before the local strength was increased by the tyre load). Again sinkage was closely related to rolling resistance, thus the extra sinkage on the weaker soil also caused increased resistance. This relationship occurred at both 3.10 bar and 1.10 bar, but because of the extra sinkage that occurred at 3.10 bar (due to the reduced contact area) higher peak rolling resistances of up to 1.3 kN (1270 kg/m³) and 3.2 kN (1170 kg/m³) were recorded.

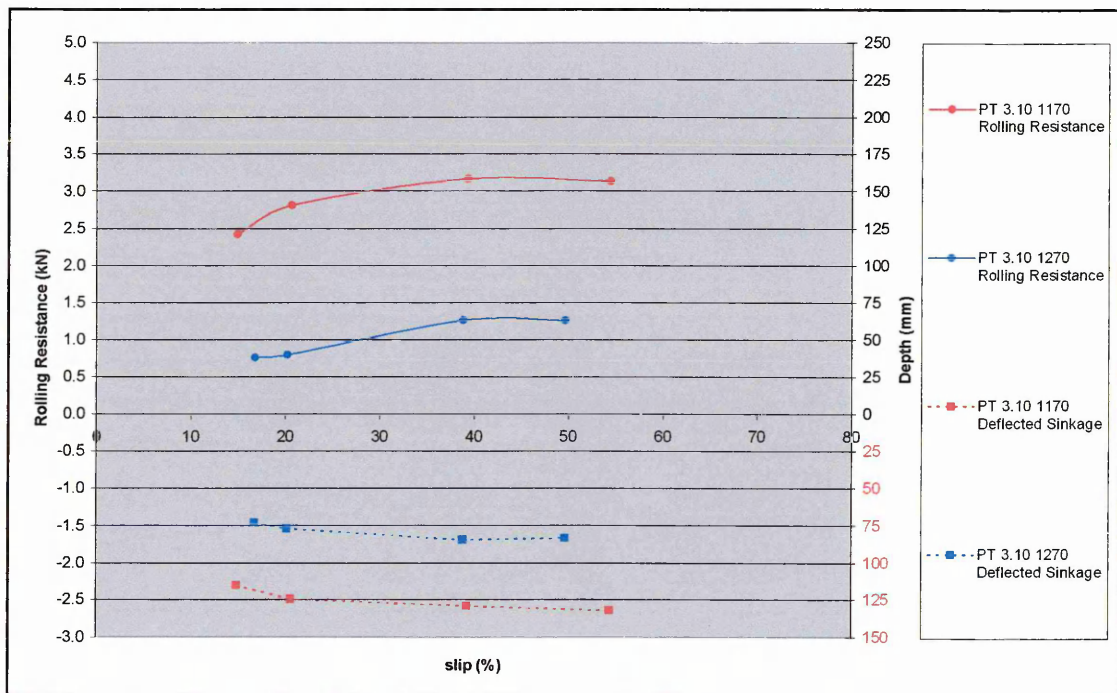


Figure 6.13 – Rolling resistances and sinkage generated by the plain tread tyre inflated to 3.10 bar across a range of discrete slips and soil preparations

The combination of these effects meant that the net thrusts generated across the slip range were again greatly influenced by the variations in sinkage, which governed both the gross thrust and resistance generated on the two different surfaces. Thus, the net thrust firstly increased with increased slip, before again levelling off at higher slips. This meant that peak net thrusts of 2.3 kN and 1.2 kN on the 1270 kg/m³ and 1170 kg/m³ soils respectively (at a 3.10 bar inflation pressure). This compared to peak net thrusts of 3.4 kN and 1.6 kN that were generated at inflation pressures of 1.10 bar,

which proved that a net thrust benefit is achieved when operating at reduced inflation pressures on deformable terrain. Therefore the test rig could measure differences produced in tractive performance by operating at different inflation pressure and soil strength treatments.

6.4.2.3 *Effect of tread pattern*

The results generated by the different treads are shown in Figure 6.14 and Figure 6.15. The range of gross thrusts varied from 2.6 kN at approximately 10% slip, to a maximum of 4.7 kN at between 30% and 50% slip. A disparity existed between the gross thrusts recorded for the PT and all of the other treads, such that the PT generated a reduced gross thrust between 20% and 40% slip, which was greater than the experimental error of ± 0.18 kN. The other variations in the recorded gross thrusts were probably due to experimental variability, rather than measured performance differences, but because the experiments were not replicated this could not be statistically determined.

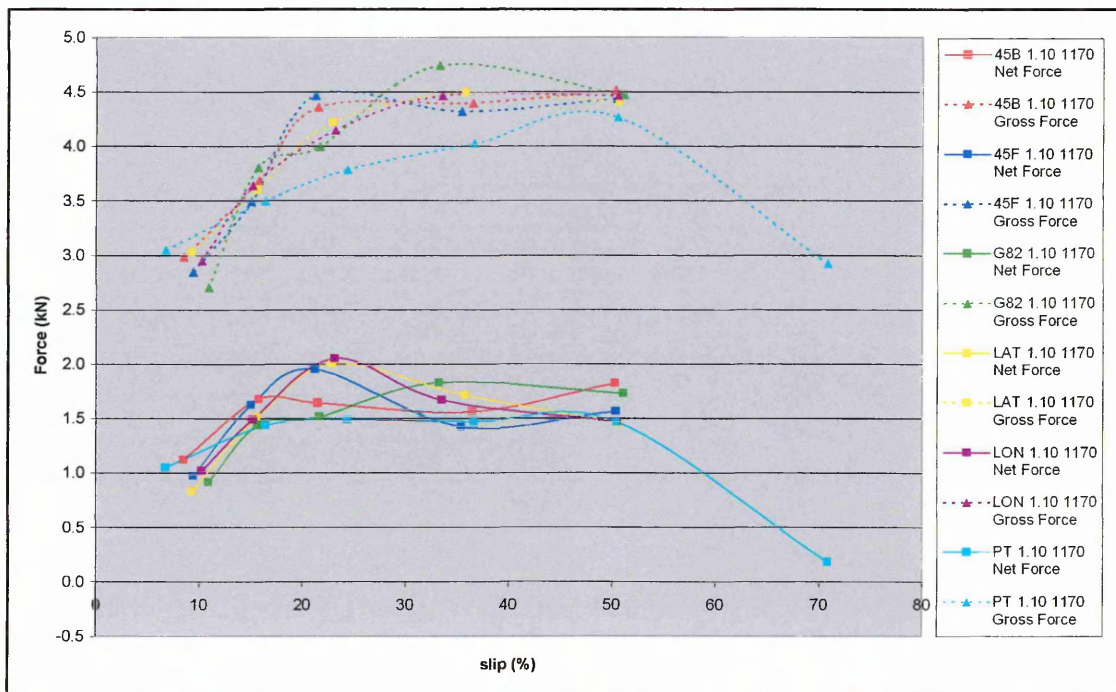


Figure 6.14 – Gross and net forces generated on 1170 kg/m^3 soil across a range of discrete slips by six different tread pattern tyres inflated to 1.10 bar

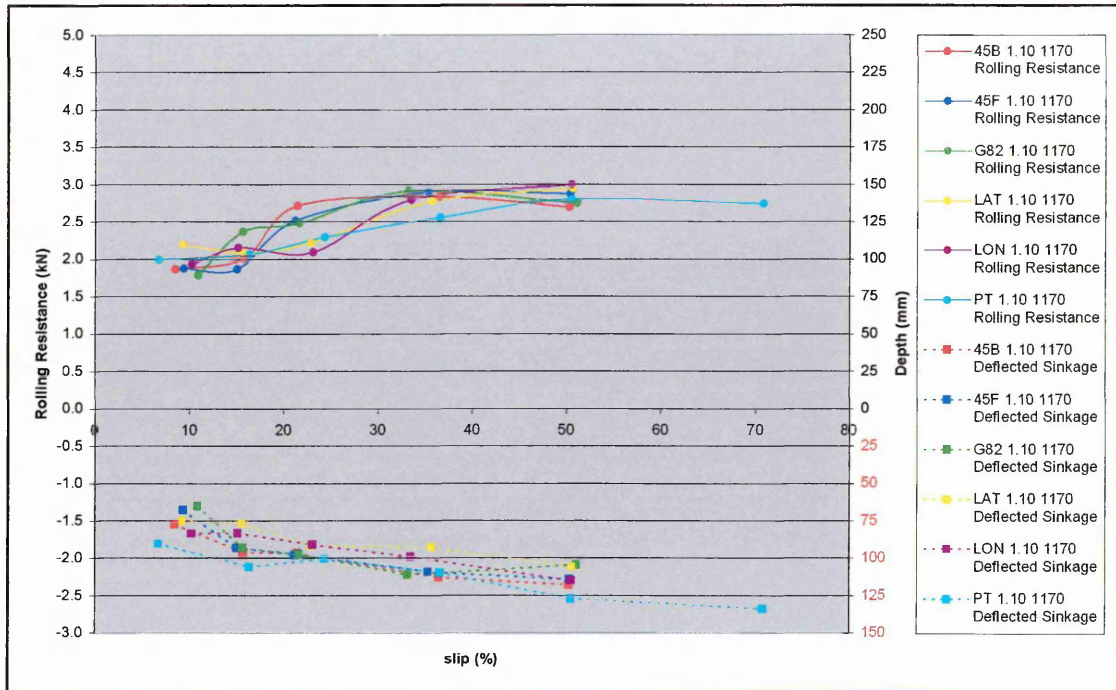


Figure 6.15 – Rolling resistances and sinkage generated on 1170 kg/m³ soil across a range of discrete slips by six different tread pattern tyres inflated to 1.10 bar

Tyre sinkage again increased from 75 mm to 130 mm with increased slip, thus due to the previously noted relationship between sinkage and rolling resistance, resistance correspondingly increased from 1.8 kN up to 3 kN. Additionally, the treads that sank the least generated the lowest rolling resistances. The resulting trends in the net thrusts were that at approximately 10% slip, all the treads generated about 1 kN of thrust. As the slip increased the net thrusts generated by all the treads increased to approximately 1.5 kN at 15% slip. Some of the treads' performances then became consistent at 1.5 kN, whilst the others (LON, LAT & 45F) generated greater peak net thrusts of up to 2 kN at around 25% slip. From 30% to 50% slip the variation in net thrust between all the treads reduced to 1.6 kN \pm 0.2 kN.

6.4.3 Summary of Results

The test system and methodology were capable of generating results that agreed with accepted traction theory predictions^{20, 28} and typical results³ i.e. increased net thrust was generated with increased slip, before levelling off or decreasing once in excess of 30% slip. This pattern occurred because between 20% and 50% slip, the gross thrust

increased asymptotically with extra slip, whilst the increase in rolling resistance with increased wheel slip (extra slip sinkage) was approximately linear. Between 55% and 70% slip the gross thrust decreased markedly, whilst the rolling resistance continued to increase, thus considerably less net thrust was achieved. Also more net thrust was generated with reduced tyre inflation pressure, or increased soil density. In both cases this occurred because the sinkage was reduced, as the gross thrust potential increased.

The trends between the tread patterns were insufficiently clear for detailed conclusions to be drawn. However, notable differences existed between the net thrusts generated by the different treads across the range of slips. Even though the variations caused between the treads were at their maximum 0.45 kN, this was important. For instance, a potential difference of 0.2 kN acting at each corner of a vehicle would equate to 0.8 kN of extra thrust, which could potentially change a 'no-go' situation into a 'go' situation. Thus further study of the effects of tread pattern on tyre performance on sand was justified, to enable the potential benefits of different tread features to be understood.

6.5 FIXED SLIP TESTS ON SAND

In addition to the verification (rig comparison) tests conducted on the sandy loam, similar tests were conducted upon the replicate sand to act as a pilot study to enable the sand displacement boundaries to be quantified prior to their attempted measurement and to investigate the tyre performance on sand. These tests investigated the treatments detailed in Table 6.2. Again these tests were not thoroughly replicated because it was a pilot study, but a limited replication of the results was derived from the repetitive results that occurred over the course of each test-run. Instead the available experimental time was devoted to investigating the maximum possible range of variables.

These tests were conducted using a sand tank that was 6 m long x 1 m wide x 0.6 m deep. This was sufficiently large to prevent any significant edge effects occurring during the testing, which was confirmed as none of the sand displacements reached either the base or the sides of the tank.

Table 6.2 – The variables investigated in the fixed slip tests on the sand

Tyre Tread	Desired Discrete Slips	Tyre Pressure	Static Tyre Load	Sand Preparation
Type	%	bar (psi)	kN	Type
PT	10, 15, 25, 35, 50	1.10 (16)	4.47	Poured and scraped
PT	10, 15, 25, 35, 50	1.10	5.36	Poured and scraped
PT	10, 15, 25, 35, 50	1.10	6.20	Poured and scraped
PT	10, 15, 25, 35, 50	1.10	7.30	Poured and scraped
G82	10, 15, 25, 35, 50	1.10	4.47	Poured and scraped
G82	10, 15, 25, 35, 50	1.10	5.36	Poured and scraped
G82	10, 15, 25, 35, 50	1.10	6.20	Poured and scraped
G82	10, 15, 25, 35, 50	1.10	7.30	Poured and scraped

The tank limited test runs to 5.3 m, which meant that between 1¾ and 2 wheel revolutions could be achieved at a constant forward speed of 5 km/h. The tank was located centrally in the soil bin with its rim set co-planar to the ground level, and it was brim-filled with dry, loosely poured, replicate sand with a density of $1480 \text{ kg/m}^3 \pm 15 \text{ kg/m}^3$. The following process of sand preparation was used before each test run:

1. Raking repositioned the previously disturbed sand evenly over the tank.
2. The sand was then disturbed to a greater depth over the full tank length by using the rake on its side, in a tine-like fashion.
3. Excess fresh sand was added to one end of the tank to replace any displaced sand and the surface was levelled to the rim by running a full-width wooden board over the tank.

6.5.1 Experimental Results

The results generated by the PT and G82 treads during the fixed slip tests are shown in Figure 6.16 and Figure 6.17 respectively. The same methodology of analysis, detailed in section 6.4.2, was used to generate a set of individual mean values to represent the data recorded for each variable over the duration of the whole test-run.

At low slips (between 5% and 15%) the net thrusts generated by both treads were either slightly positive (below 1 kN), or in some cases negative (immobile). However, in all instances as the slip increased, then greater immobility occurred, with peak negative net thrusts of up to -2 kN achieved. The increased immobility occurred because the rate by which rolling resistance increased with extra sinkage (caused by the increased slip) exceeded the corresponding increase in gross thrust that the extra sinkage also generated.

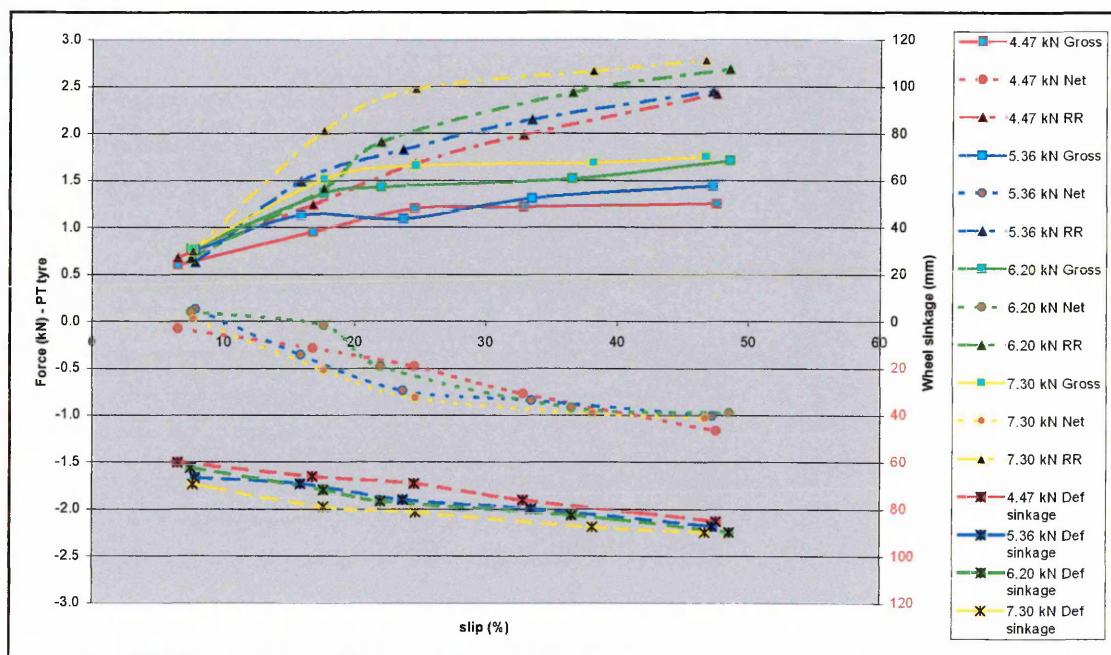


Figure 6.16 – Gross and net thrusts, rolling resistances and deflected sinkages generated by the PT tyre operating at 1.10 bar on sand

Both treads generated extra gross thrust with increased normal load, however, the extra load also increased the wheel sinkage, which increased the rolling resistance, which in turn nullified the extra thrust being generated. These dependant relationships blurred the trends between the variables, but it was noted that to maximise traction on this loose sand at the 5 km/h forward speed that was investigated, slip had to be limited to below approximately 15% slip.

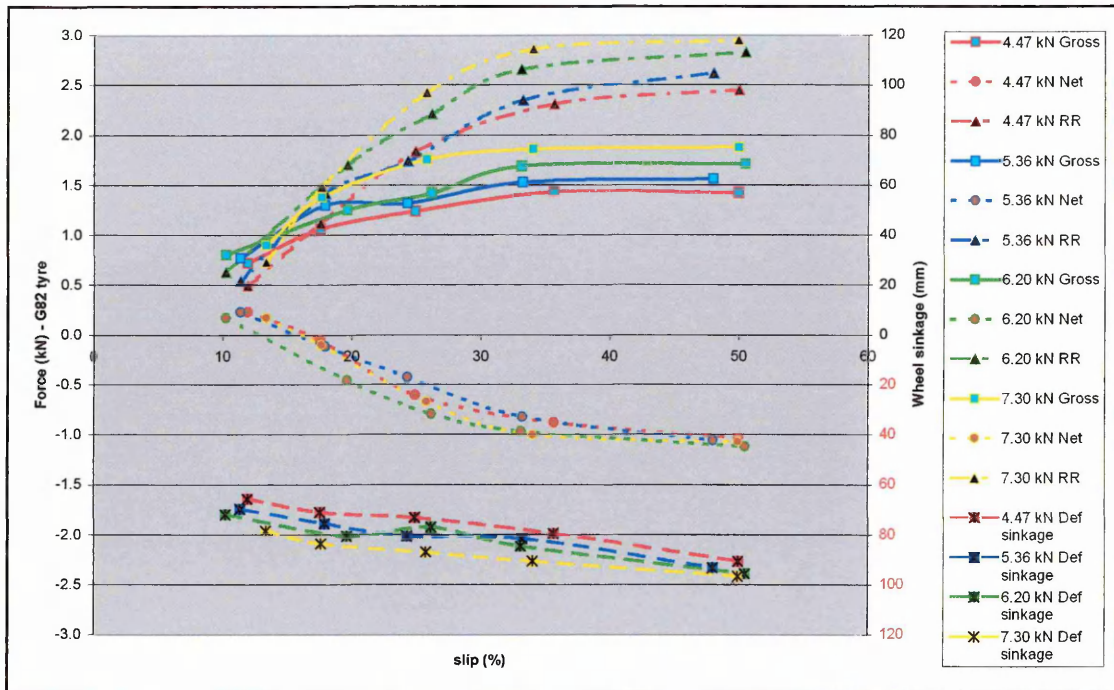


Figure 6.17 – Gross and net thrusts, rolling resistances and deflected sinkages generated by the G82 tyre operating at 1.10 bar on sand

The G82 tread developed the higher gross thrusts of the two treads across the slip range for all load conditions. It achieved thrusts of between 0.4 kN to 0.9 kN at 10% slip and between 1.4 kN and 1.9 kN at higher slips. Whilst the PT developed similar gross thrusts at 10% slip, its range of peak thrusts was between 1.2 kN and 1.8 kN. The G82 also produced slightly higher rolling resistances, of approximately between +0.05 kN and +0.3 kN across the range of treatments.

For both treads the rolling resistance increased as the sinkage (influenced by the wheel slip) increased. However, the G82 tread operated deeper so it generated higher rolling resistances. When considered in combination these trends meant that both treads produced similar levels of net thrust, mostly achieving mobility below 15% slip, but as the slip (sinkage) increased, the net thrust reduced because the rolling resistance correspondingly increased. Closer examination of the net thrust results revealed that the G82 tread produced the higher positive net thrusts, when performing at its best, but it also produced slightly more negative net thrusts (greater immobility) at the higher slips, because it operated at slightly deeper sinkages.

6.5.2 Fluctuations within the Traction Results

The trends presented in section 6.5.1 demonstrated important relationships between the traction variables, but the data presented was insufficiently detailed to convey all of the relationships that were experienced during the testing. The use of mean values to convey the test results had been used because for the results on the soil this had been valid, as the variables recorded had been reasonably consistent. This consistency carried across to the low slip tests on sand, as the example shown in Figure 6.18 indicates, so therefore a single mean value accurately represented the magnitude of each variable that was recorded over the duration of the test, which was why this methodology was used to produce the results in section 6.5.1.

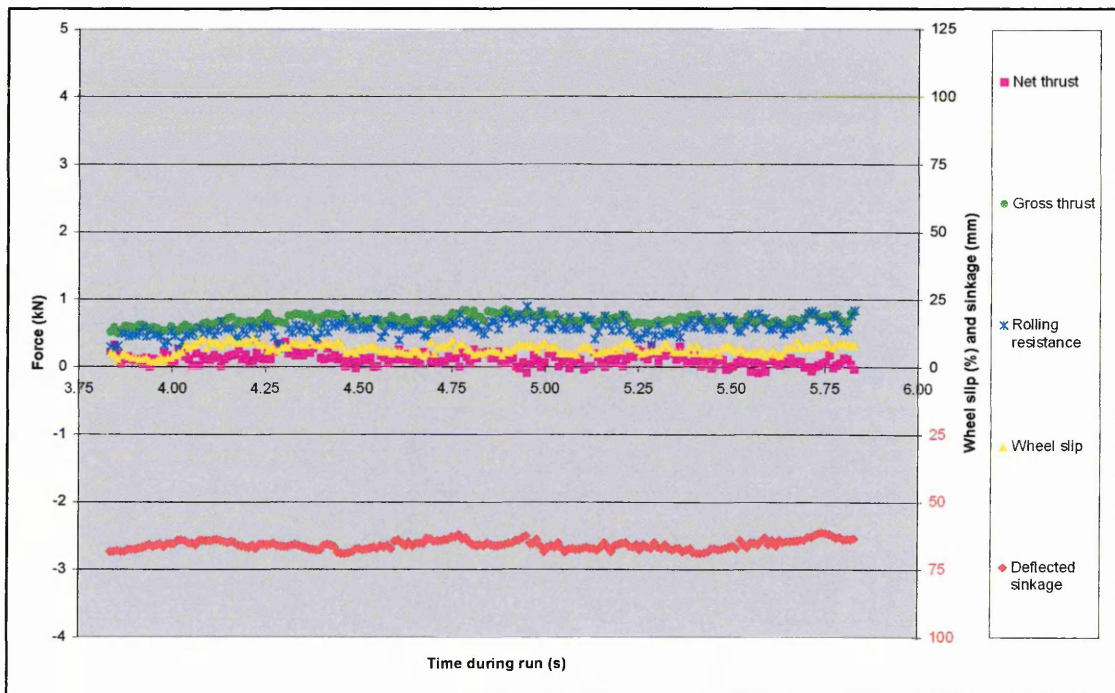


Figure 6.18 – The PT tyre tractive performance when operated at an intended 10% slip (inflation pressure 1.10 bar and static normal load 632 kg) on sand

Although this methodology was employed to allow mean values to be produced from all of the results, it was found that when the test rig was operated on the sand at higher slips above 30%, and especially around 50% slip, different trends were experienced which meant that the use of mean values did not represent all relationships that were recorded within the data. Results typical of the maximum variation recorded for the five traction variables during the testing are shown in Figure 6.19 (PT) and Figure 6.20 (G82).

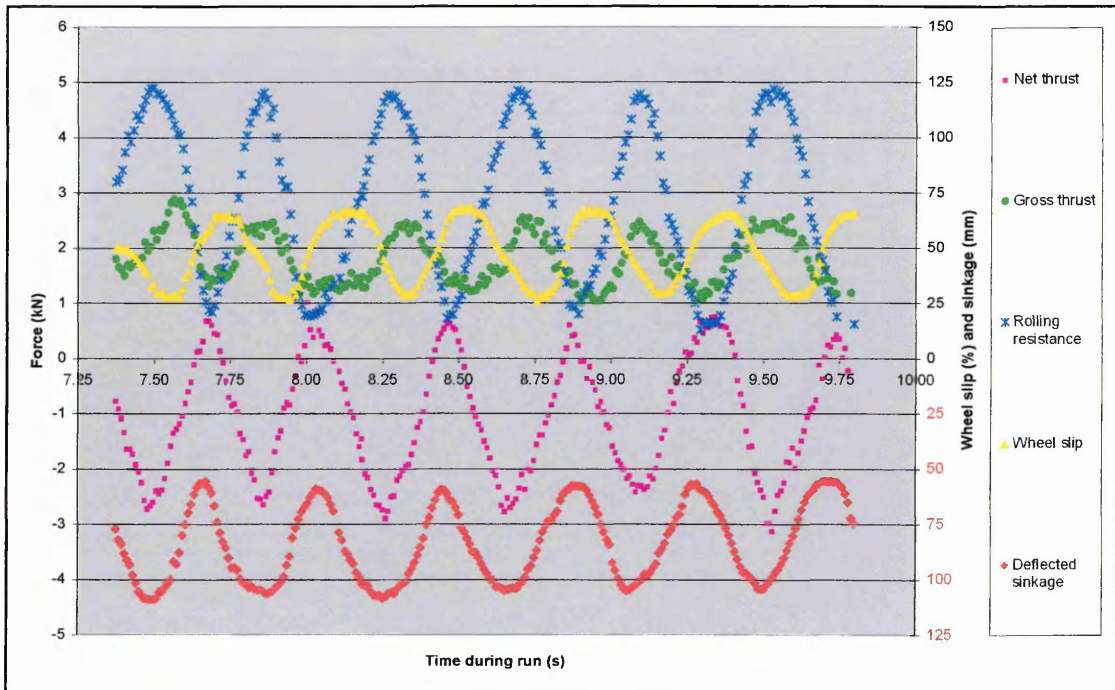


Figure 6.19 – PT tyre tractive performance when operated at a nominal 50% slip (inflation pressure 1.10 bar and static normal load 632 kg) on sand

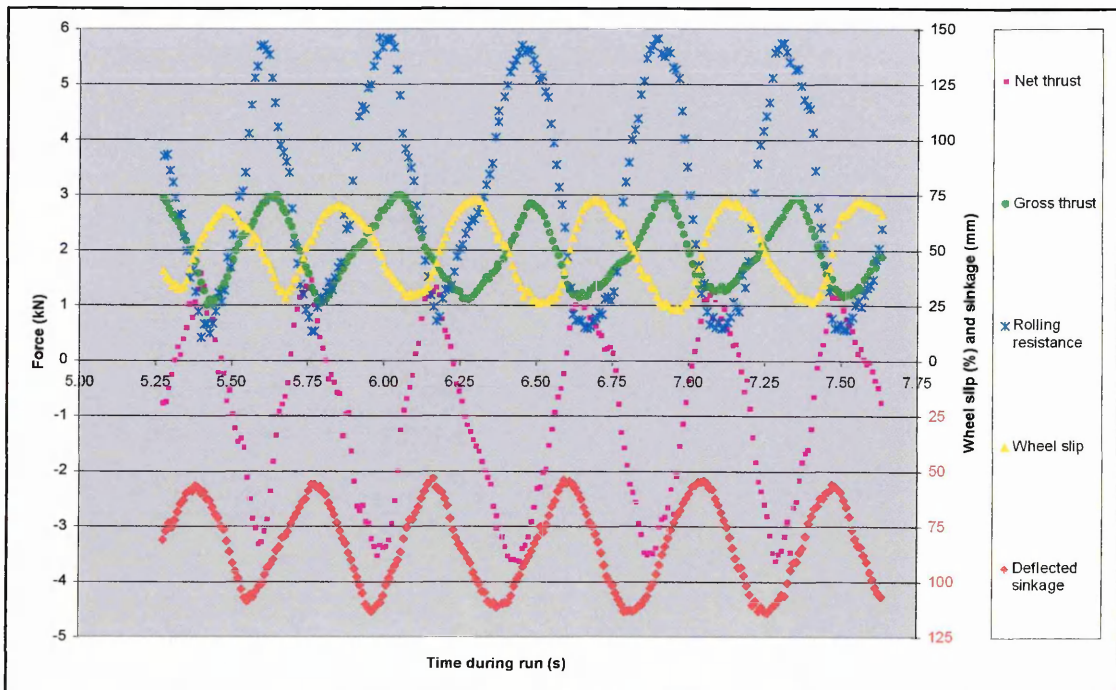


Figure 6.20 – G82 tyre tractive performance when operated at a nominal 50% slip (inflation pressure 1.10 bar and static normal load 632 kg) on sand

When these are compared to Figure 6.18 (note: both sets of data are presented on identical Y-axes), the wide variation between the sets of results becomes evident. The changes in the rig performance occurred because large variations in the performance of the test wheel were caused at the higher slips. These occurred because of the varying wheel slip, which caused the sand displacement to vary, which in turn altered the slip sinkage of the wheel (note: increased slip caused increased sinkage and vice versa). As the sinkage varied, it produced vertical accelerations of the test rig, which altered the normal load acting on the wheel and thus the gross thrust potential. The varying sinkage of the wheel also increased (or reduced) the contact length, further influencing its gross thrust potential. Although the rig behaviour fluctuated, strong positive correlations were still experienced between wheel sinkage and the associated rolling resistance. These relationships made the mean value approach insufficient to represent and study these results, so a more thorough explanation was required.

The mechanics of the fixed slip system meant that gross thrust was always directly proportional to the chain tension. As the sand was sheared, the torque within the system, which was caused by friction at the interface, was rapidly translated into rotational momentum. If more torque was created in the system, then more gross thrust was achieved, hence why the gross thrust was directly proportional to the sinkage and normal load. As the sinkage reduced, the torque contained within the system was rapidly released causing the wheel speed to increase. As the cycle progressed this caused wheel slips in excess of the intended setting to be produced, as the minimum sinkage was reached. This in turn caused high levels of sand displacement to occur, which consequently once again increased the wheel sinkage. As the sinkage (and torque) once again increased, due to reduced slip, the net effect was that the maximum wheel sinkage (and tyre immobility) was achieved. Normally tyre immobilisation would have occurred, but instead the combination of continued wheel torque and the test rig's (processor's) forward motion drove the tyre up the opposing sand ridge. This action increased the cable tension and subsequently the wheel slip, which forced the thrust cycle to become a repetitive cyclical event.

The combination of the wide variations in the gross thrusts and rolling resistances greatly influenced the net thrust results. Whilst the mean results had recorded the tyres producing approximately -1 kN of net thrust, the true net thrusts varied from between 1 kN to -3 kN over a test run. Peak net thrust was achieved where both minimum gross thrust and rolling resistance occurred, as then the gross thrust exceeded the resistance. Thereafter as sinkage increased, the rate of increase in resistance with increased sinkage, exceeded the rate of increase in gross thrust, and thus the net thrust became increasingly worse.

Comparison of the relative performance of the two treads operating at 50% slip showed that the peak sinkage of the G82 was deeper than the PT, which resulted in it generating higher rolling resistances, and therefore achieving the peak negative net thrusts of either tread. The G82 also generated higher gross thrusts when operating at the minimum sinkages, which caused this tread to also generate the higher peak positive net thrusts as well. Therefore again the G82 showed that it would achieve either the peak positive, or peak negative, net thrusts (mobility, or immobility) depending upon at which point in the thrust-slip cycle it was operating

The changeover from steady behaviour (at low slips), to the fluctuating behaviour (at higher slips) was driven by increased slip altering the tyre sinkage. These events were confidently related to the shear interactions between the tyres and sand, as the same fluctuating behaviour had only been experienced to a minor extent at high slips during the soil tests, which tested similar tyre treatments (except the surface). These tests indicated that wheel sinkage, which was caused by sand displacement that was driven by the magnitude of slip, governed the mobility of the tyre. Therefore for mobility to be increased it was necessary to understand what type of sand displacements were caused by the wheel slip, before any possible methods to address them could be considered.

6.5.3 Limitations of the Fixed Slip System

These results demonstrated the capability of the fixed slip system to conduct traction experiments, but the key drawback of the system's operation was that to produce one useful slip-pull curve for each treatment, at least five test runs were required. Whilst

each run took about ten seconds, the soil preparation and all of the subsequent measurements meant that theoretically approximately five hours of testing were required to produce one curve (depending upon the soil preparation tested). However, the initial test programme had progressed at a slower rate because the necessity to change the test tyres, deflection transducers, or sprocket ratios to achieve the necessary treatments took longer than planned. Also the time-consuming necessity to check that the sprockets were correctly aligned prior to each test-run had wasted a considerable amount of testing. These time losses meant that the drive system needed to be altered prior to the main experiments.

It had also been discovered that some of the drive system components failed when the rig was operated above certain slip limits on the firm soils, when the maximum gross thrusts were achieved. Thus before a more detailed, replicated test programme to examine the tractive effects of tread on sand across a wide range of slip treatments could be efficiently conducted the rig required re-designing. This necessity presented an opportunity to re-evaluate the operation of the whole system. As the instrumentation and the logging hardware and software had proved capable of accurately and repeatedly measuring the required traction variables these systems were not altered. Instead the re-design concentrated on the drive system with the following two priorities in mind:

1. To provide a quicker method of slip variation, thus allowing greater flexibility and efficiency in the experimental work.
2. To reduce the stresses on the drive components in the system.

6.6 THE VARIABLE SLIP TEST RIG

As well as the instrumentation systems, the main framework, hub unit, load platforms and damper were all carried over to the new rig. The most obvious solution to providing a flexible, and easily adjustable, method of changing the wheel slip was the adoption of a hydraulic drive system. A variable flow system allowed easy adjustment of the motor speed, and hence the wheel speed, and mounting the motor on the test frame closer to the hub reduced the stresses generated in the system, whilst higher input drive speeds reduced the torques transmitted by some of the components.



Plate 6.8 – A front view of the soil processor, diesel engine and sub-frame

The system consisted of a four-cylinder 50 kW diesel engine with a hydraulic pump and motor. The engine and pump were mounted on a sub-frame that bolted onto the front of the processor unit. These items can be seen in Plate 6.8. The output and return flows from the pump were fed along two $\text{\O}25$ mm (i/d) hydraulic hoses that ran along the processor. These powered a 12 kW motor mounted on the front end, hub side corner of the test rig, which is visible in Plate 6.9.

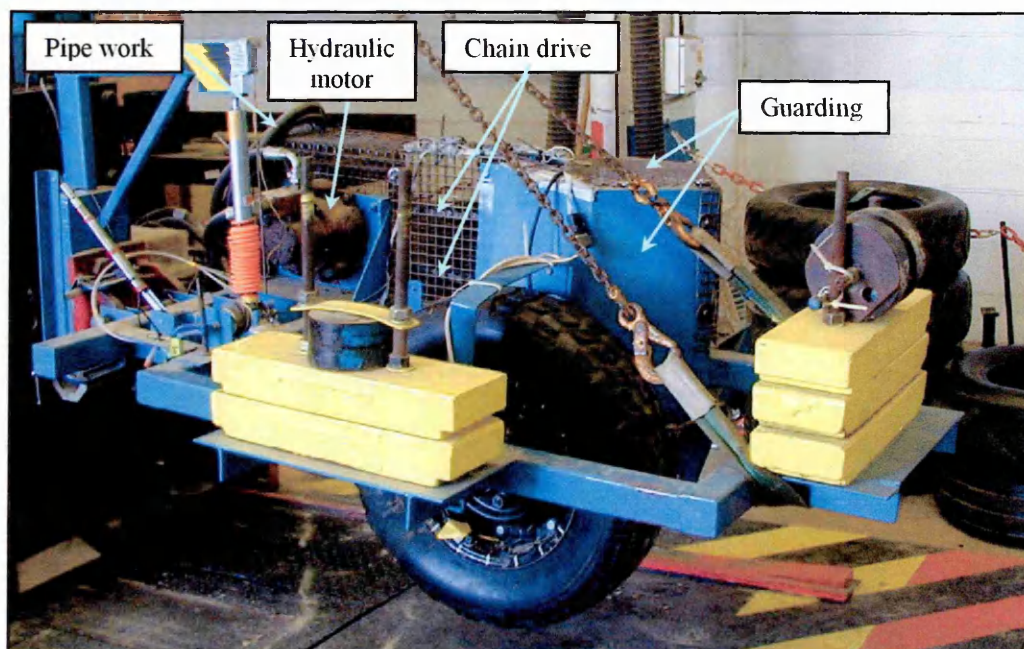


Plate 6.9 – The new components fitted to create the hydraulically driven variable slip test rig

A manually operated flow divider was mounted on the processor between the pump and the motor. This enabled oil to be directed away from the motor and thus, to a degree, allowed its speed to be controlled and easily adjusted. Some speed control could also have been achieved by changing the engine (pump) speed, but test runs were always conducted at full throttle to maximise the system pressure. The location of the divider meant that a desired slip could be manually selected prior to each test run, but it could not be adjusted during a test run. At a processor forward speed of 5 km/h the new design could theoretically achieve a wheel slip range of 10% to 80%. This capability was confirmed by static tests, which are described in Appendix 18.

Mounting the motor on the test rig meant the rig's sinkage (and that of the test wheel) was unrestricted. It also removed the necessity to deduct the chain tension readings from the EORT readings, which now solely represented the net thrust generated by the tyre (tread). However, this change removed the ability to determine both the gross thrust and rolling resistance produced during each test run. Instead, to derive a gross thrust from the wheel it was necessary to separately measure the rolling resistance (using the procedure outlined in section 6.3.2) and add it to the net thrust. The net thrust remained the most useful value to use for tyre comparison as it described the overall mobility.

6.6.1 Operating Characteristics of the Variable Slip Rig

When it was used for traction tests this test rig produced a fluctuating range of the slip, sinkage and net thrust results. It was easiest to understand the relationships between the slip, the sinkage and net thrust by considering a single cycle from a test run. Figure 6.21 presents such a section of data, with numbered dashed lines that relate to the stages through the cycle and the following explanation:

1. At this position the wheel slip was at its lowest, whilst the wheel was rising above its median depth. The low wheel slip, and thus low rearward sand displacements meant that the wheel continued to rise up the sand ahead of it. This reduced the negativity of the net thrust because the reducing sinkage reduced the rolling resistance.

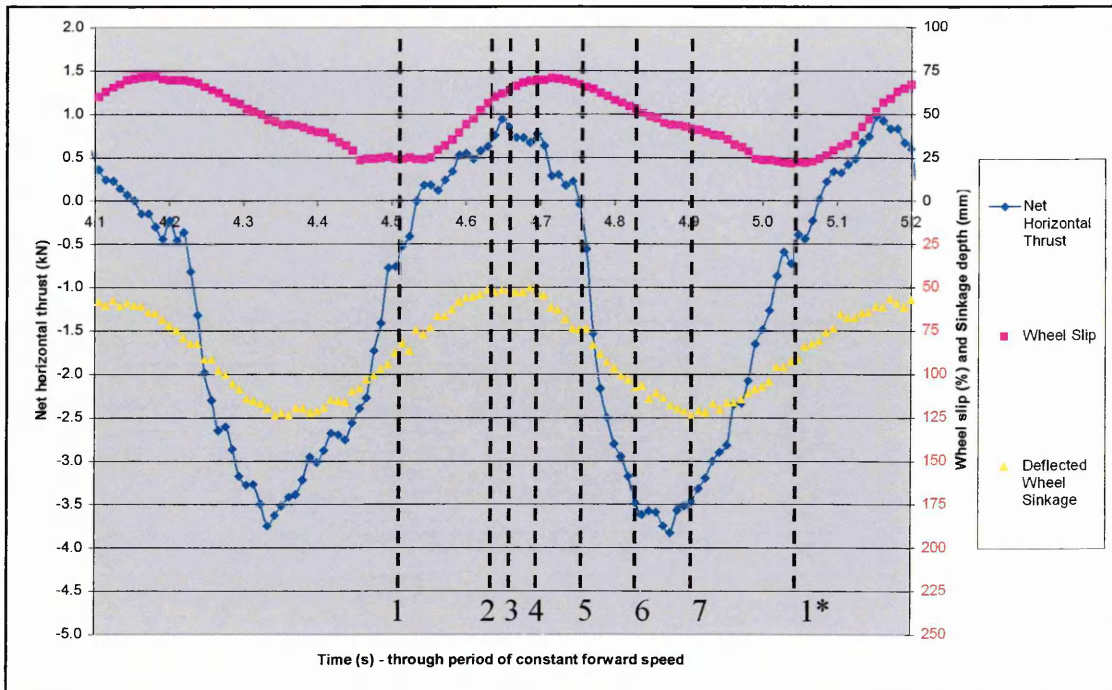


Figure 6.21 – Two cycles of data generated by the G82 tread inflated to 1.10 bar with a 650 kg static normal load (as described in section 6.8.1)

2. The continued effects of low wheel slip and the processor's forward motion caused the sinkage, and thus the rolling resistance, to continue to reduce, thus the net thrust output continued to increase. As the wheel slip rapidly increased thereafter the peak net thrust occurred at this point in the cycle (50% slip).
3. The sinkage reached a minimum value, as the increasing slip caused extra rearward sand displacements, but despite the increasing slip, a reduced contact length and normal load (caused by the rig's upward acceleration) limited the net thrust output.
4. The maximum wheel slip was now reached. Thus larger rearward sand displacements and associated increases in sinkage (and hence rolling resistance) were triggered, thus net thrust continued to reduce.
5. The high slip (and the processor's resistance) continued to cause aggressive digging and large rearward sand displacements by the tyre. This caused rapidly increasing sinkage and rolling resistance, and therefore the net thrust generated became increasingly negative, despite the high slip maintaining high gross thrust.
6. The continued high, but reducing, slip caused the wheel sinkage to increase further, so that the deepest sinkages and maximum resistances were achieved. Coupled to minimum slips the peak negative net thrust was thus achieved.

7. The peak sinkage was quickly reached as the low slip reduced the rearward sand movements, so continued tyre rotation and forward displacement of the processor forced the tyre to begin climbing out of the sand. The reducing sinkage (rolling resistance) allowed the net horizontal thrust to increase and the tyre returned to stage 1*. Thereafter the cycle of passing from mobility to immobility due to high slips was once again repeated.

This understanding related both the drivers of, and the responses to, the relationships between the wheel slip, sinkage and net thrust. It also allowed the effect upon the net thrust of both, the variations in dynamic normal loading, and the positive relationship between tyre sinkage and the associated rolling resistance to be understood. This understanding allowed the importance of the effect of sand displacement (sinkage) upon tyre mobility to be realised. This enabled the sections of the thrust cycle where sand displacement measurements were required to enable the quantification of this effect to be identified (see section 7.3).

6.7 COMPARISON (VERIFICATION) TESTS ON SOIL

The re-design meant that the effectiveness and suitability of the variable slip rig had to be evaluated against the performance of the fixed slip test rig. It was particularly important to compare net thrusts and sinkages produced across a slip range when using the variable slip rig, against those that had been produced at discrete slips (within the same slip range) by the fixed slip rig. If agreement occurred between the two sets of results (for the same treatments), then the variable slip test rig could be confidently used for the future tests. Tests were conducted using the variable slip rig to obtain results for the following treatments:

- PT tread inflated to 3.10 bar (thereby minimising any tyre deflection effects),
- 1170 kg/m³ and 1270 kg/m³ soil density preparations,
- A static normal load of 650 kg,
- A variable slip range that encompassed discrete slips of 15%, 20%, 40% and 50%, i.e. the discrete slips tested by the fixed slip tests.

The results from these tests were compared to results generated when testing the following treatments with the fixed slip rig (before its modification):

- PT inflated to 3.10 bar,
- 1170 kg/m³ and 1270 kg/m³ soil density preparations,
- Static normal loads of 350 kg, 450 kg, 550 kg, 650 kg, 750 kg and 850 kg,
- Target discrete slips of 15%, 20%, 40% and 50%.

6.7.1 Variable Slip Test Results

It was found that when the variable slip test rig was set to achieve a nominal slip of 50% it produced results that were comparable to the results that the fixed slip rig had produced on the sand when operated at high slips, i.e. a variable thrust-slip cycle was produced, which created vertical accelerations of the rig. Therefore the flow divider did not make the test rig produce a constant slip value, but rather a consistent range of wheel slips, which would typically fluctuate from 15% to 70% wheel slip, as the typical results presented in Figure 6.22 for an intended 50% slip setting indicate.

As well as fluctuating slips and sinkages, the results showed that the net thrusts also altered considerably over the course of a test-run. The wheel slip fluctuations caused the significant variations in wheel sinkage that were experienced, and thus (due to the relationships noted in section 6.4) they indirectly controlled the rolling resistance.

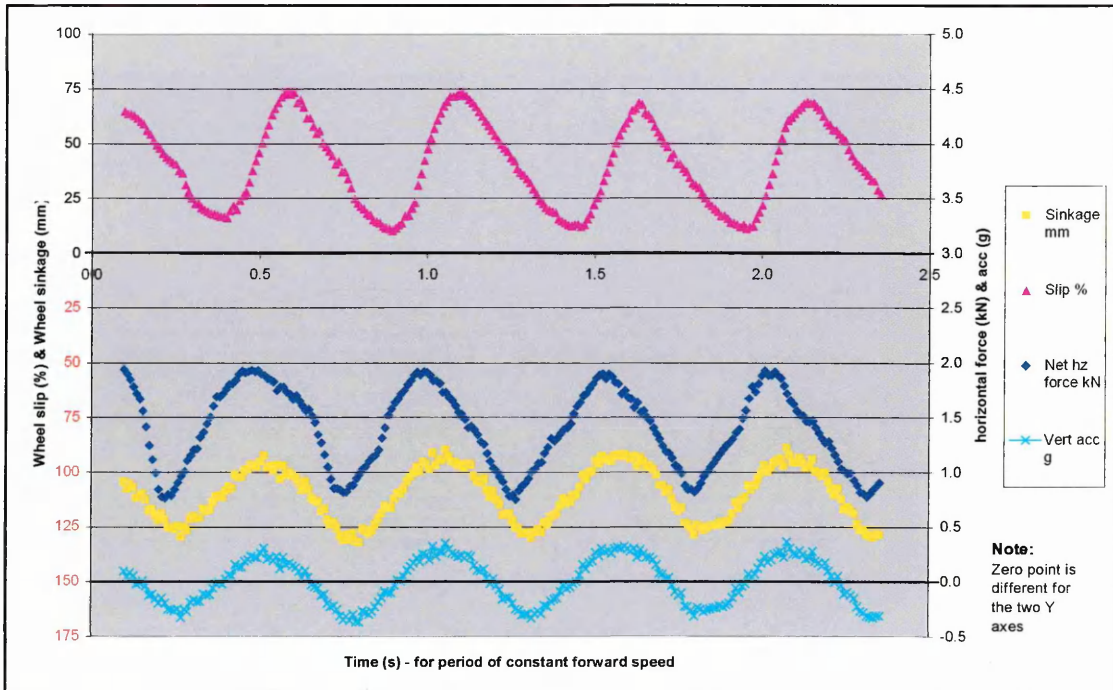


Figure 6.22 – Typical results generated by the variable slip test rig operating the PT tyre inflated to 3.10 bar on 1170 kg/m³ soil

The relationship between sinkage and slip was partially self-reinforcing because as sinkage increased, the slip reduced. As the slip reduced, so to did the disturbance (removal) of the soil beneath the tyre, and thus the sinkage increased at a reducing rate. However, the increasing resistance reduced the net thrust output, such that ‘in the field’ the tyre would have rapidly approached immobility. In this application the soil processor, which could be likened to vehicle momentum, instead partially towed the driving wheel forwards, which forced it to rise out of the soil. This action effectively re-commenced the test conditions and allowed the slip to once again increase.

These relationships meant that once steady forward velocities, and therefore slips, were achieved, each test run produced five, or more, repetitions of the mechanism of excessive slip causing tyre immobility. Only four cycles are shown on Figure 6.22 so that the relationships are clearly visible. This meant that a single test run replicated the passage from mobility to immobility that the project intended to study. Thus replication of each treatment was generated within each test-run, which allowed greater confidence to be derived from the results.

This methodology introduced a drawback, as the frame's height constantly varied due to the fluctuating sinkage. This caused vertical acceleration of the test rig, such that the static normal tyre load of 6.377 kN was either increased, or decreased, depending upon the location in the thrust cycle. However, the adjustment to the normal load could be derived by using the equation $F = ma$, where a (gravitational acceleration) was increased (or reduced) by a factor, g' , to represent the acting acceleration. The acting acceleration a' (in m/s^2) was derived from the displacement, s , by using the relationship $a' = \frac{d^2s}{dt^2}$. Dividing a' by 9.81 produced the acting g' factor. This was applied as follows; if the g' factor was calculated as +0.2, then the dynamic normal tyre load would equal; $650 \times (9.81 \times (1 + 0.2)) = 7.652$ kN. Dynamic normal load fluctuations were experienced up to $\pm 0.5a$, over all the testing, which equated to a range of mass from 325 kg to 975 kg. Figure 6.22 shows the typical cyclical nature of these variations. Quantifying this effect allowed the rigs to be compared when the same normal loads were acting upon the tyres.

6.7.2 Methodology for Test Rig Performance Comparisons

Useful suitable comparisons could only be made between results taken when similar treatments were tested on both rigs. As only the normal load and wheel slip were deliberately varied, achieving this need was simplified. The results from the variable slip test runs used for comparison with those from the fixed slip tests were taken over the period of decreasing wheel slip, as the high slip caused the wheel to dig into the soil, which generated gross thrust, but which also increased the rolling resistance, causing immobility to be approached. Typical data regions used for the comparison are shown in Figure 6.23. Data outside these regions was ignored for this comparison.

The variable slip test rig produced results similar to those shown by Figure 6.23 on both soil preparations. From these results five or six consecutive regions of decreasing slip were selected from each test run's period of constant forward speed and all of the net thrusts, sinkages, slips and g' factors that occurred in those regions were noted. The selected results for each test run were grouped and ordered by ascending slip value.

Mean values of net thrust, sinkage and dynamic normal load were then calculated for each of the eight slip ranges detailed in Table 6.3.

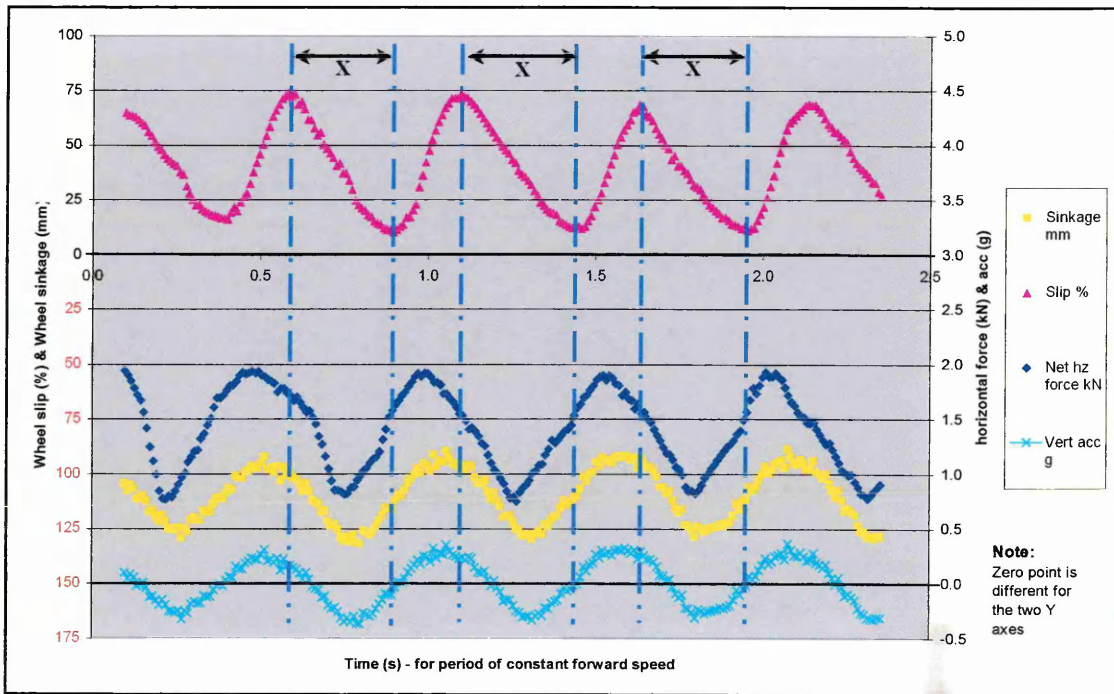


Figure 6.23 – Typical regions of decreasing slip (indicated by lengths ‘X’)

Table 6.3 – The bands of slip that were used to produce mean values

Variable slip rig	Fixed slip rig	Both rigs
Range of slip	Discrete slip	Typical normal load
%	%	Mean dynamic load (closest static load to 50 kg)
5 – 12.49	10	604 (650)
12.5 – 17.49	15	533 (550)
17.5 – 22.49	20	504 (550)
22.5 – 27.49	25	428 (450)
27.5 – 34.99	30	541 (550)
35 – 44.99	40	659 (650)
45 – 54.99	50	771 (750)
55 - 70	60	886 (850)

Table 6.3 also details the mean dynamic normal loads that occurred within each slip range. These are tallied to the nearest static normal load treatment that was tested on the

fixed slip rig, i.e. for a mean dynamic load of 604 kg (variable slip), the nearest static load tested using the fixed slip rig was 650 kg. The mean net thrusts and sinkages measured using the variable slip rig were plotted against appropriate sets of results recorded with the fixed slip rig. Appropriate results were selected by using mean results from the constant speed sections of the tests (section 6.4) with normal load and discrete slip conditions that matched the data presented in Table 6.3, e.g. at a discrete slip of 40% results recorded with a 750 kg normal load were used. Undeformed tyre sinkages were used for the comparison, as the drawstring transducers were not fitted for the variable slip runs.

6.7.3 Test Rig Comparison Results

The results for the tests on the 1170 kg/m³ soil are presented in Figure 6.24, and those for the 1270 kg/m³ soil in Figure 6.25. Generally, agreement existed between the results from the two test rigs with all the results being of comparable magnitudes. The closest agreement occurred in the net thrust results. Agreement occurred between the sinkages, but more variation occurred between results across the slip range. Broadly both test rigs extracted similar tractive performances from the same treatments and in both cases the tyres operating on the firmer surface generated lower sinkages, and thus higher net thrusts, as traction theory would predict²⁰.

When the results were more closely examined to determine the cause of the variations, it was noted that the fixed slip rig results displayed the classical trends of small increases in net thrust with increased slip, whereas the variable slip rigs' results displayed some differing trends, with all the results having slightly 'U' shaped profiles. Initially the sinkage increased with slip, as would be expected, but above 40% slip it then decreased with increased slip. Differences also occurred in the associated net thrust results, such that higher net thrusts were achieved at the higher and lower slips.

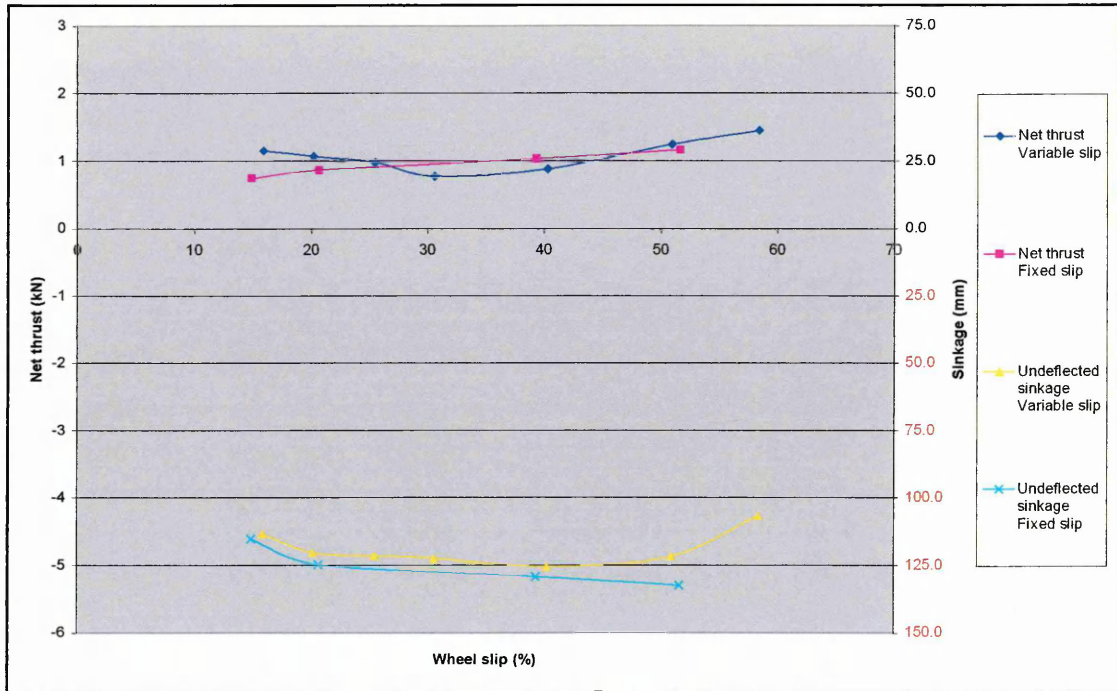


Figure 6.24 – Comparative results for the net thrusts and sinkages generated by a PT tyre inflated to 3.10 bar operated on both the fixed and variable slip rigs across a slip range on 1170 kg/m³ soil

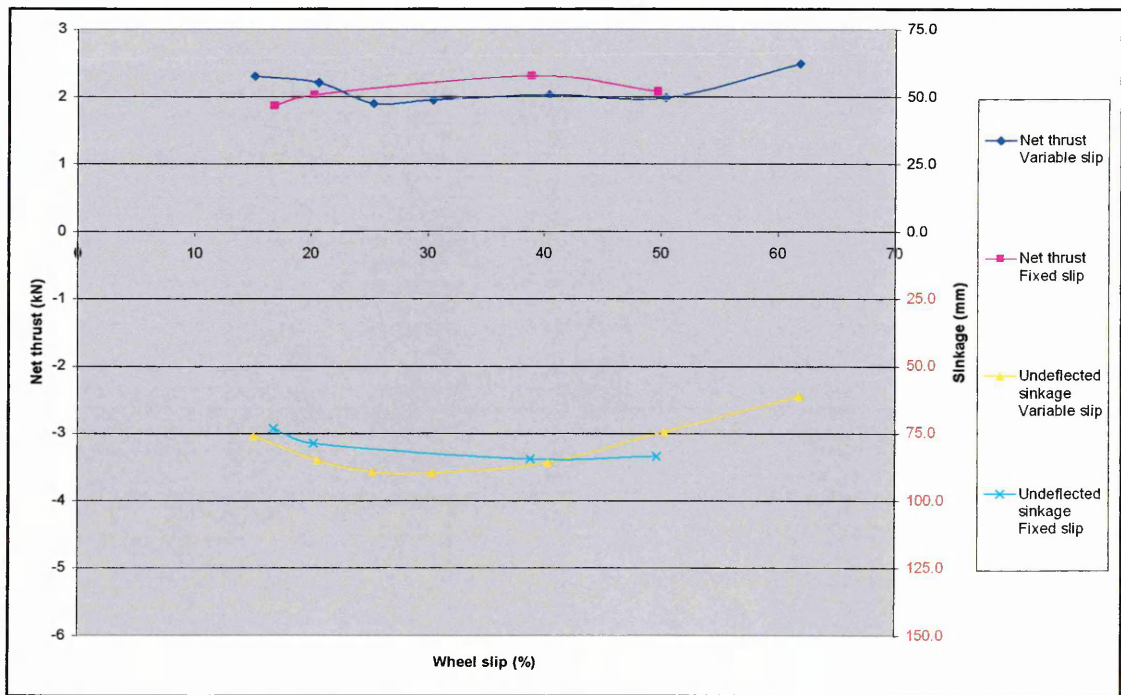


Figure 6.25 – Comparative results for the net thrusts and sinkages generated by a PT tyre inflated to 3.10 bar operated on both the fixed and variable slip rigs across a slip range on 1270 kg/m³ soil

When initially studied the variable slip results appeared to contradict accepted traction theory, their cause, which was more complex, did not. It was demonstrated earlier that net thrust was closely governed by the associated wheel sinkage, such that at higher sinkages increased rolling resistances significantly reduced net thrust. As the variable slip rig developed varying sinkage results, this relationship was again important. The net thrusts were greater at the lower and higher slips, because when these slips were occurring the lower wheel sinkages were experienced. The varying sinkage that the rig generated therefore skewed the results that were generated, blurring the trends between the interacting variables.

6.8 COMPARISON (VERIFICATION) TESTS ON SAND

Although agreement was shown on soil, it was more important that agreement between the two test rigs was demonstrated when their performance on sand was considered. This followed a similar pattern to the comparison on soil, i.e. results recorded for the same treatments on both test rigs were compared. Although the fixed slip test rigs had been undertaken in a sand tank, the variable slip test used the whole soil bin. All subsequent traction experiments continued to use the whole soil (sand) bin as well. The previous comparison had shown that a range of treatments had to be tested to produce suitable results to allow good comparisons to be made. The fixed slip tests had investigated the treatments detailed on Table 6.2. The variable slip tests undertaken used the PT and G82 treads inflated to 1.10 bar, with static normal loads of 650 kg, forward travel speeds of 5 km/h and nominal slip settings of 50%. Three replicates were undertaken for each tread.

6.8.1 Variable Slip Test Results

Typical results from a single replicate for both the PT and G82 are presented respectively in Figure 6.26 and Figure 6.27. Results with comparable magnitudes and phase relationships for all the measured variables were recorded for the three replicates undertaken for both tread patterns. The variable slip rig caused the tyre to repeatedly pass from being mobile to immobile over the course of a test run, as had been noted when the fixed slip rig had operated on the sand.

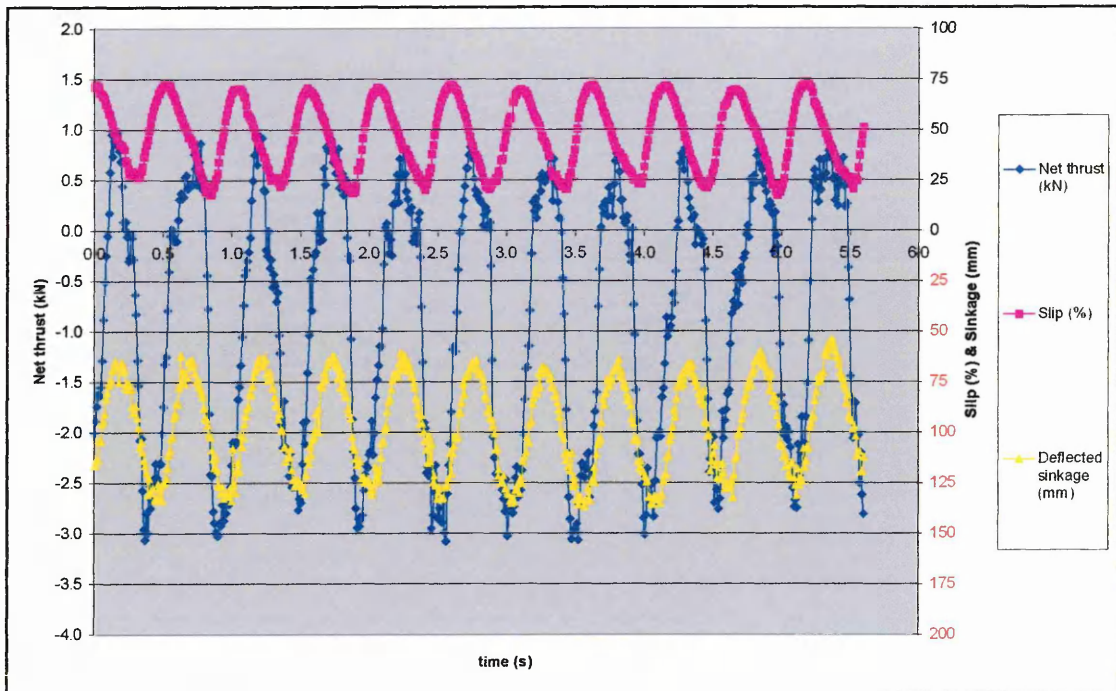


Figure 6.26 – Traction data produced using the PT tread inflated to 1.10 bar and a static normal load of 650 kg on the variable slip test rig on sand

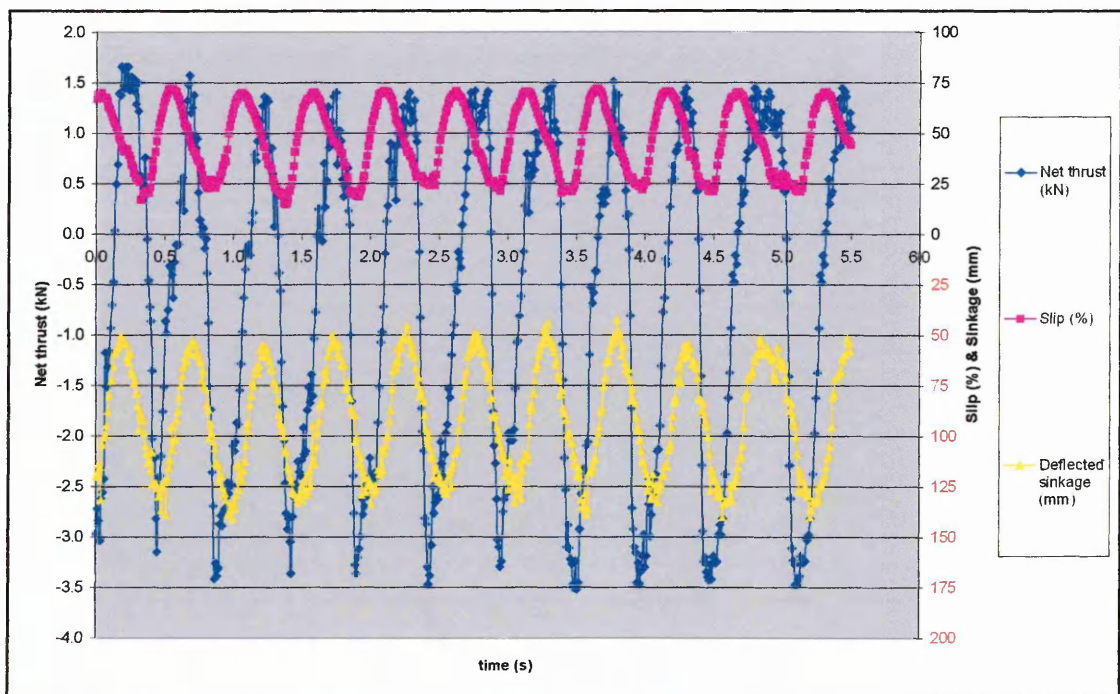


Figure 6.27 – Traction data produced using the G82 tread inflated to 1.10 bar and a static normal load of 650 kg on the variable slip test rig on sand

As the test rig caused the tyre to pass from a mobile to immobile situation it once again produced cyclical results for each measured variable. Good repeatability was achieved between each test-run in terms of the magnitudes of all three variables, which reduced the probability of the results occurring by chance. This meant that comparisons could be drawn between the results within each test run, as well as across test runs.

For both treads the wheel slip cycled between 15% and 75%, whilst the deflected tyre sinkage varied in a sinusoidal manner between approximately 40 mm and 130 mm. Net thrust varied between 1 kN and -3.1 kN for the PT and 1.5 kN and -3.5 kN for the G82. Maximum experimental variations of ± 0.25 kN, ± 15 mm and $\pm 2.5\%$ were recorded from peak-to-peak for net thrust, deflected sinkage and slip respectively over each test run. The variations between the replicate results for each tread were also within these boundaries. Again the net thrusts produced by the G82 tread again exhibited the greater range of variation, compared to the PT results, as was previously noted in section 6.5.1 (fixed slip results). It achieved more positive net thrusts, when performing at its best, and providing good traction. However, when the immobility situation (the worst net thrust performance) occurred the PT created less negative net thrust, or less opposition to the forward progress of a vehicle.

6.8.2 Test Rig Comparison Results

This comparison directly compared the performance of the two test rigs when they were both operating at nominally intended slips of 50%, which was when the treatments were most similar. The results recorded using the PT tread are presented in Figure 6.19 and Figure 6.26, whilst results for the G82 tread are shown in Figure 6.20 and Figure 6.27. When these graphs were compared, again considerable agreement was noted between the results for both treads, including broadly similar time periods for the cyclical behaviour of between 0.4 s and 0.5 s.

The variable slip rig produced a range of wheel slips from 15% to 75%, whilst for the other rig this range was 20% to 70% slip. Both rigs produced a similar pattern of cyclical slip variations. Similar patterns were also demonstrated between the sinkage results, although the variable slip rig caused both treads to operate about 20 mm deeper

when maximum sinkage was produced. At the minimum sinkages produced both rigs caused sinkages of approximately 55 mm. The variation in depth at maximum sinkage may have been caused by the difference in the test tanks, or because of the difference in the length of the test runs, as when the full bin was used the rig had longer to settle into its rhythm, which possibly allowed greater sinkages to develop.

Each tread developed different net thrusts, as described previously, but when these were compared between the two rigs, it was noted that the ranges of net thrusts were again similar. Thus both rigs were capable of deriving similar levels of tractive performance from the tyres under investigation. Although small differences were achieved between each oscillation effects for both test rigs, it was concluded that overall the oscillation effects were similar for both systems. Generally the individual differences were not significant, as where practicable, mean data from a number of oscillations or test-runs would be considered when comparing the tyre (tread) tractive performance. The similarities between the results for both tyre treatments indicated that the consistently fluctuating results were not generated solely by a particular drive mechanism, and were instead mainly the result of the sand/ tyre interaction and sand displacement. The use of the processor to provide a fixed resistance influenced this behaviour, but it was not the main driver in the relationships.

For a completely accurate comparison to have been achieved, in the manner attempted, it would have been necessary to design and develop a methodology to prevent wheel sinkage, whilst still allowing complete tyre-soil contact to be maintained, irrespective of the wheel slip. Whilst such a design may have been possible, to produce suitable apparatus would have been a major distraction from the project's objectives. Instead, it was more beneficial to take the agreement demonstrated between the sets of results from the two rigs as sufficient proof that the variable slip rig was capable of conducting realistic and useful tractive performance tests. Additionally, as the operation of the variable slip rig produced a number of immobilisation events over a single test run, the effect of tread upon mobility (or immobility) on sand could be more thoroughly investigated.

As the effect of these relationships upon the tyre mobility remained of interest, further testing was continued with the variable slip rig because of its ability to produce greater consistency in the results, due to its ability to more smoothly apply the variations in torque that occurred, and because it allowed a particular test schedule to be completed faster. Improvements to the design of the variable slip rig also meant that an unlimited range of tyre and surface treatments could be studied during the further investigations. Using this rig meant that it was impossible to produce traditional slip-pull curves from the results, as the slip-pull inter-relationship was always complicated by the varying sinkage, which controlled both the rolling resistance and the contact length. This complication was tackled by the modelling that was developed, which allowed the performance of the treads to be compared, so it was not an obstacle to the investigations.

6.9 A FULL VEHICLE TEST ON SAND

A separate project undertaken by Cranfield University staff and Land Rover¹⁴⁰ generated some limited traction test data for a full vehicle operating on the replicate sand in the soil bin. The testing used a V8 Land Rover Discovery Series 2 fitted with 235/70 R16 Goodyear HP Wrangler tyres inflated to 1.24 bar. The right side of the vehicle drove on the sand, whilst the left side operated on sealed concrete. A full vehicle width beam was mounted to the rear chassis. Tension links attached at either end of the beam allowed independent net thrust measurement along each side of the vehicle. Wheel speed was measured from pulses off the ABS sensors and the true forward speed was measured with ground radar. The wheel slip was derived from these two readings.

The tension links were connected to a beam that attached to a winch drum mounted on a static tractor, via a winch cable. As the Discovery was driven forwards the tension began to retard the vehicle, the throttle was incrementally increased until it was fully open, which gave an increasing slip profile. As the tyres on the sand became buried, the throttle was released and so the slip declined. A plot of the net thrusts achieved by the right side tyres, with both the differential locks and the traction control disengaged, is shown in Figure 6.28.

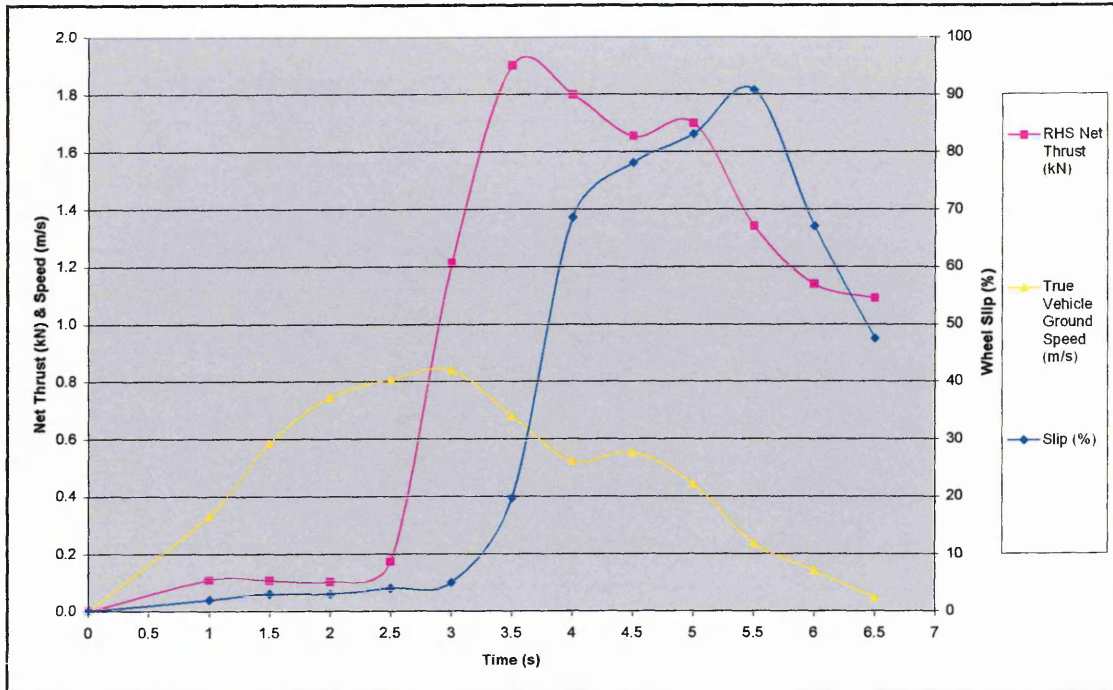


Figure 6.28 – Tractive performance traces from a full 4x4 vehicle test where the vehicle’s right side was operated on the sand surface

The peak net thrust was achieved at 20% slip, after which the net thrust continued to decline, as the slip first continued to increase and then decrease. The lack of any sinkage data prevented these results from being properly compared with the fixed slip test results, but one important point of comparison existed. Although at a slower forward speed (of approximately 3 km/h), the test achieved the peak net thrust of 1.95 kN (approximately 1 kN per tyre) early in the test run when the sinkage would have been minimal and mainly due to the sands bearing capacity. This value compared favourably with the results generated from the previous test rig trials discussed above when the tyres were operating at their minimum sinkages. During the traction tests on the sand using the PT tyre, peak net thrusts of approximately 0.85 kN were recorded. Being un-treaded tyres it would be expected that these would produce less thrust, therefore it could be concluded that favourable agreement between a vehicle test and rig tests could be achieved.

This agreement provided further proof of the validity of the results generated by both of the test methodologies. Full vehicle tests were not used for all the testing, as it was desirable to remove any suspension effects from the system. Also the vehicle was too

wide to fully operate in the soil bin, so variations in the heights of the bin and sand caused the vehicle tilt. Additionally it would not have been possible to operate safely on the dissimilar surfaces without the requirement for steering inputs, which would have added another dimension to the complex interactions experienced. Further testing was therefore conducted with the variable slip test rig for the pressure and sand displacement investigations as this had proved to be the most useful test device.

7 SAND FLOW MEASUREMENT APPARATUS AND METHODOLOGY

7.1 SAND AND RFID TAG DISPLACEMENT ASSESSMENT

7.1.1 Bench Sand Flow Evaluations

The initial investigations into the suitability of the RFID system were conducted in small sand masses. The first trial investigated the abilities of the two available RFID scanners (Appendix 1) to detect the Ø2 mm x 12 mm long tags in a sand mass. The more powerful scanner detected tags up to 150 mm deep, but this greater range became a hindrance when trying to locate several closely spaced tags, because interfering signals from the tags ‘confused’ the scanner, and so it would not register any of the tags. Hence the smaller scanner, see Plate 3.4, which could locate tags up to 100 mm to 125 mm deep was more suitable. The variance in the range of detection occurred because variations in the orientations of the tags affected the scanner’s sensitivity.

The tags were entered into a small sand mass (approximate size 400 mm x 300 mm x 300 mm), which was then disturbed laterally. The small size of the tags appeared to allow them to flow with the sand mass, although this was not definitely confirmed at this stage. It was established that by scanning over a buried tag from several directions its location in plan view could be closely determined, such that the tag would lie centrally in the region over which it could be detected. It was also found that because the mass of a tag was greater than that of a sand grain, the overlaying sand layers could be gently sucked off a tag (using a vacuum tube) to reveal the tag’s location without disturbing its position, which could then be measured. These promising results made it necessary to evaluate the flow relationship between the tags and the sand, to check that the tags would flow exactly with surrounding sand grains, thus making them suitable as markers for tracking sand flow.

7.1.1.1 RFID Tag and sand flow assessment methodology

The aim of this experiment was to quantify if the tags would flow with the sand. For this assessment a quantity of dyed replicate sand (achieved using potassium

permanganate) with identical mechanical properties to the original sand was used. A tank was filled with ‘normal’ replicate sand to a depth of 40 mm and levelled. Strips of dyed sand were added on to this surface. These were initially 2 mm wide with 6 mm spacings and depths of 1.5 mm, as Plate 7.1 illustrates, although they settled fractionally wider where the twenty data tags were positioned upon them. Ten tags were positioned in pairs on top of the first five strips of dyed sand, with their ends meeting centrally along the tank’s centre line. The remaining ten tags were paired on the other five coloured sand bands, but instead a 12 mm gap (6 mm either side of tank’s centre line) was left between their ends, see Plate 7.1. The tank was then filled to a depth of 80mm with ‘normal’ sand by a fine sieve to limit the sand deposition, so that possible disturbances to the positions of the tags and coloured sand were minimised. A cylindrical tine of $\text{Ø}12$ mm was then pulled along the tank’s centre line at a depth of 80 mm. This subjected the sand and tags to a three-dimensional crescent type soil failure.



Plate 7.1 – The tank of sand to which dyed sand strips and then twenty data tags were added, together with a $\text{Ø}12$ mm tine that was used to disturb the sand

7.1.1.2 Tag/ sand flow assessment results

Afterwards the sand above the dyed strips and tags was carefully removed using a $\varnothing 3$ mm i/d tube, which was attached to a vacuum cleaner suction hose. This enabled sand to be removed without disturbing the flow pattern of the dyed sand and tags. This initially revealed the flow patterns shown in Plate 7.2, where ten tags from one side of the tank and three tags from the other side were visible. The tags had translated with the dyed sand longitudinally, laterally, and vertically, and had orientated themselves along the flow lines of the dyed sand. The breaks in the flow lines on the left hand side of Plate 7.2 were caused by a rule used to record the disturbance, not the action of the tine.

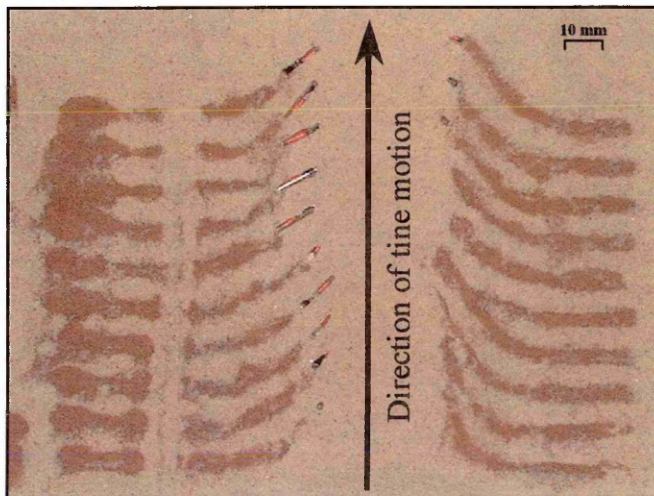


Plate 7.2 – The flow patterns of dyed sand strips and tags after disturbance

The sand mass was then excavated further until the flow patterns and fifteen tags visible in Plate 7.3 appeared. The tags not located had initially been directly in front of, and to the right hand side of the tine, thus it had been expected for them to appear in the area indicated in Plate 7.3. The sand's flowing behaviour made it impossible to excavate any more of the profile without disturbing the positions of the fifteen tags and the associated sand, so their relative positions were measured. The maximum deviation in displacement from either end of these fifteen tags compared to the associated dyed sand was measured as ± 1.5 mm (in all three planes). These fifteen tags and associated sand were then removed to allow further excavation.

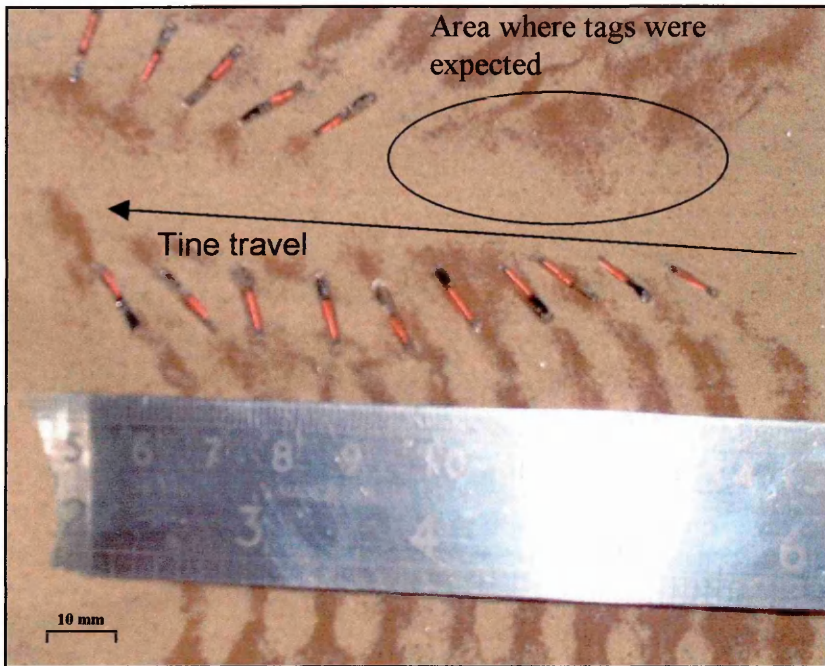


Plate 7.3 – The flow patterns of dyed sand and tags after further excavation

Based upon the type of disturbance to which they were subjected, it was thought that the five remaining tags would be found adjacent to their partner tags, but located slightly lower in the sand mass, but this did not occur. As the sand was excavated a number of dyed particles were found, but these were dispersed and mixed with the original sand, indicating they had experienced a different displacement. After removing 10 mm of sand the remaining five tags were uncovered in the pattern shown in Plate 7.4.

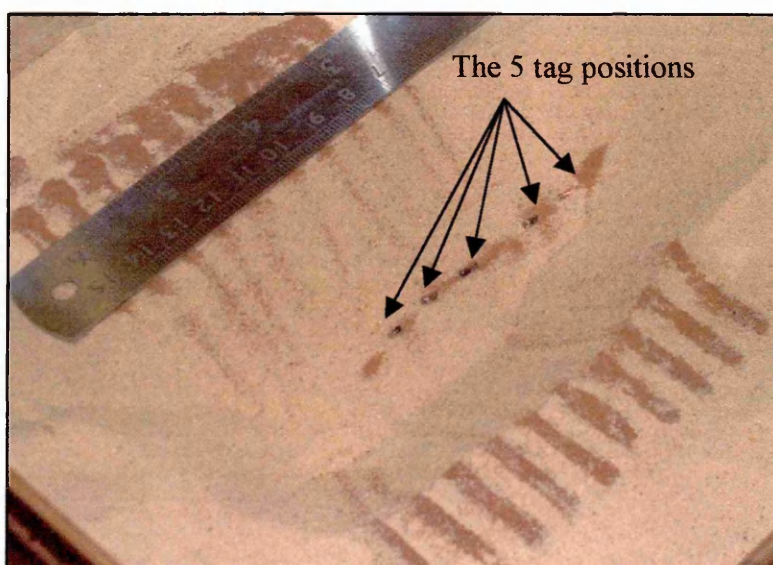


Plate 7.4 – The location of the remaining tags and dyed sand

Whilst dyed sand could be seen around these tags, the flow patterns previously noted were not evident. This was partly because a quantity of the dyed particles had been unavoidably removed during the deeper excavation, and partly as the differing displacement had mixed the sand making it harder to identify the dyed flow lines. Thus the positions of the remaining five tags and the dyed sand could not be completely reconciled to their original starting positions, in the same manner that was possible for the other fifteen tags. However, distances equivalent to the original spacings had been maintained between the tag positions and each tag had orientated identically, additionally analysis of the tags' ID numbers showed that they had remained in the correct order. Therefore, although the sand displacement was not as predicted the tags had followed the flow of the sand, which was most evident from the way that they orientated with the flow.

In combination these results showed proof that the data tags would travel closely with the movement of surrounding sand during the disturbance of a sand mass. Therefore this RFID system offered the best potential to measure sand flow of any considered methodologies because:

1. Three-dimensional sand flow could occur.
2. The tags flowed with the sand allowing sand movement to be recorded.
3. The small size of the tags meant that they did not impede the sand flow.
4. The individual coding made each tag identifiable.
5. Location in a sand mass could be achieved to allow subsequent measurement.

7.2 FULL SIZE SAND DISPLACEMENT MEASUREMENT RIGS

7.2.1 Tag Position Placement

The novel use of the data tags to record three-dimensional sand displacement necessitated the development of a methodology to achieve accurate placement and measurement of their positions in a sand profile, which would vary fractionally in height (up to 7 mm). The preliminary driven wheel tests showed that across the complete slip range the sand displacement was contained within an 800 mm wide (400 mm each side of the tyre centre line) and 400 mm deep region of sand. The test tyres for

which sand displacement would be measured were all symmetrical, so a vertical grid of tags that covered a 400 mm x 400 mm region from the tyre centre line was selected, as illustrated in Figure 7.1. These tag positions were selected for the following reasons:

1. The tags along the 400 mm spacing boundaries served to confirm that no disturbance occurred beyond this limit.
2. A varied concentration of the tags allowed more to be stationed closer to the wheel where the greatest variation in disturbance was expected to occur.
3. To facilitate a statistical analysis the pattern of concentration was identical on both axes.
4. It was difficult to accurately position tags closer than 25 mm.
5. This was considered the minimum number of tags that could be placed, whilst allowing a sufficiently accurate picture of the sand displacement to be gauged.

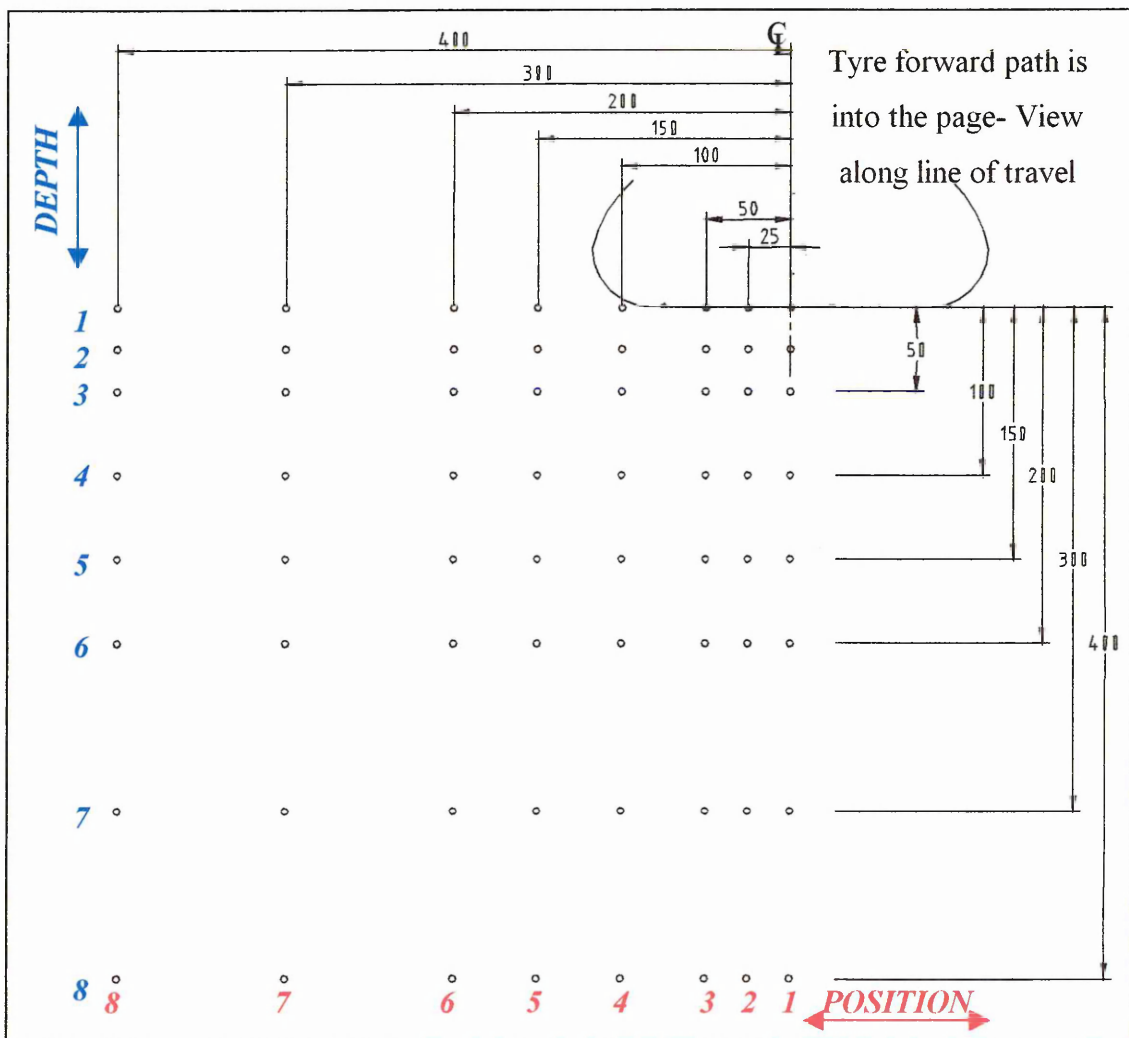


Figure 7.1 – The chosen tag grid positions in the sand profile (in mm)

If a soil with cohesion had been used, then a template could have been used to construct the tag grids during construction of the soil profile. This was not possible with the replicate sand because its ‘flowing’ nature meant the profiles could not be constructed in defined layers and hence another insertion method was required. The selected method involved the use of a 6 mm o/d, 3 mm i/d and 780 mm long hollow copper tube that could be pushed into the sand, after which a tag would be pushed down the tube so that it reached the required depth in the sand.

To achieve the correct position of the tube in the soil bin a placement frame was designed. This consisted of a RHS beam that spanned the bin, as shown in Plate 7.5. Two legs welded to the beam straddled one of the yellow metal plate markers that ran alongside the bin to give longitudinal location. Two further legs fitted closely inside the bin rails to give lateral location, and vertical location was achieved directly off the rails. Mounted to the beam was a triangular track with graduated length markings. The track’s mountings allowed it to be set coplanar with the bin’s vertical and horizontal axes.

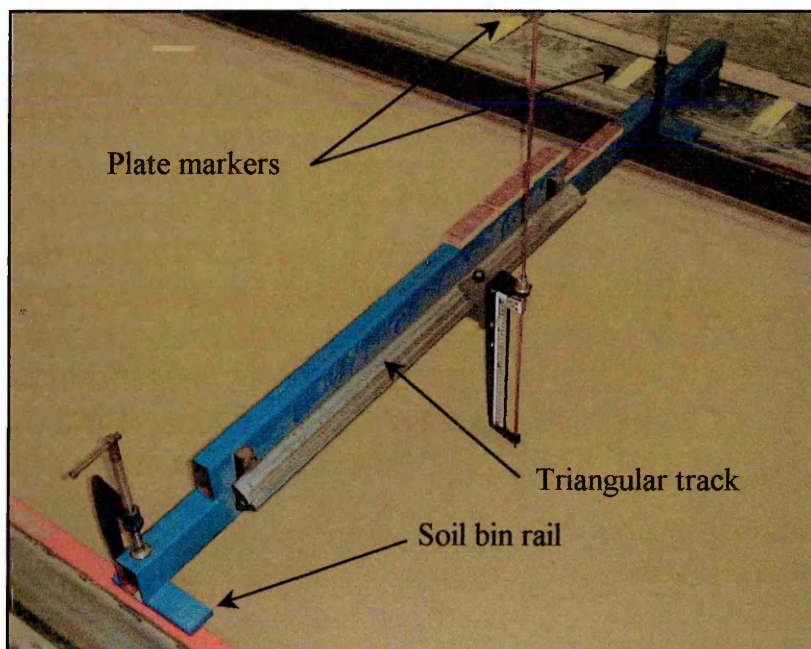


Plate 7.5 – The data tag placement frame

A 325 mm tall bracket fitted with a screw fastener ran along the triangular track as Plate 7.6 illustrates. Extending from the top and bottom of the bracket were two arms that contained concentric $\text{Ø}6.05$ mm i/d bushes. These enabled the tube to be slid through the bracket in the vertical plane. Mounted to this bracket was a locking mechanism to hold the tube at a particular depth. This was measured against a graduated scale using a sliding vernier pointer, also shown in Plate 7.6. The pointer also housed a $\text{Ø}6.05$ mm i/d bush (to fit the tube) and a locking mechanism.



Plate 7.6 – The placement frame insertion bracket

The placement frame was always positioned to straddle the correct soil bin marker and arranged perpendicular to the carriage rails, before being fastened with two G-clamps. This was necessary so that the measurement zero point, which was the intersection of the beam and rail, shown by Figure 7.2 and Plate 7.7, was consistently set. To produce a tag grid a bridge was placed alongside the frame for the operator. The centre line of the tyre's passage was determined and the tube carrier bracket was slid across to the appropriate lateral position for the first tag column, where it was locked in place.

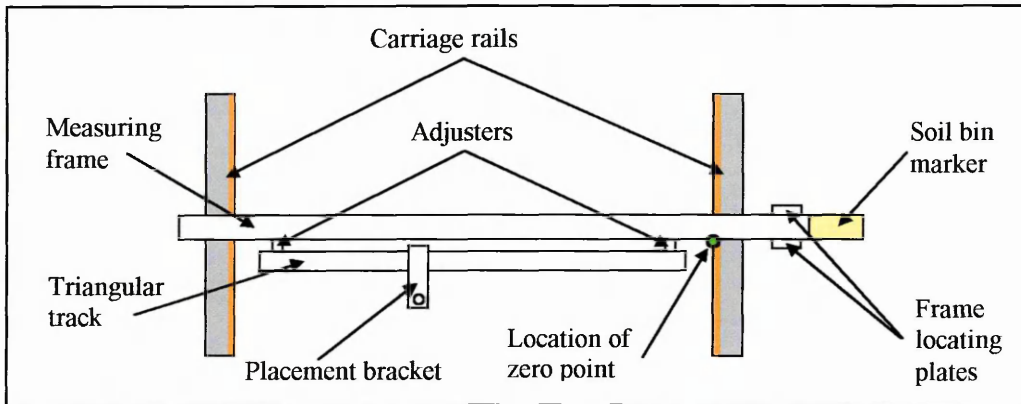


Figure 7.2 – A schematic plan view of the tag placement equipment showing the location of the zero point

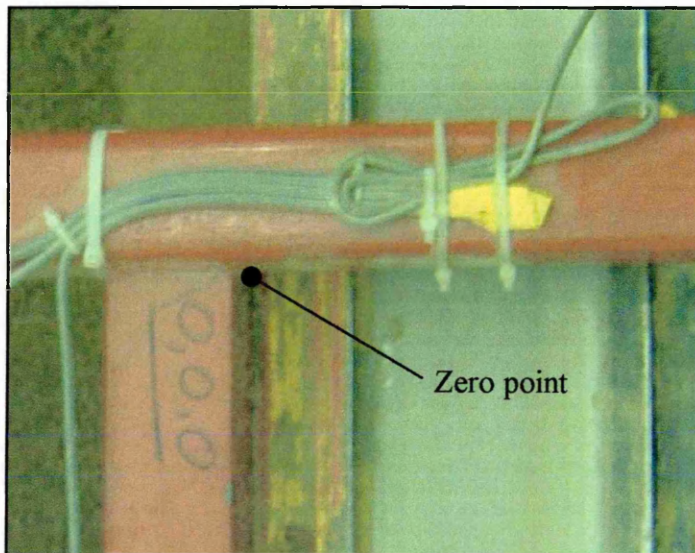


Plate 7.7 – A plan view of the frame zero point on the tag measurement frame

An 820 mm long, $\text{Ø}2.75$ mm steel rod with a threaded end was fitted inside the tube. This had a nut fitted to the threaded end of the bar that positioned the bottom of the rod level with the bottom of the tube and assisted in the insertion of both items. The rod and tube were pushed level with the bottom arm and the sliding pointer was locked onto the tube. The rod and tube were then pushed down to touch the sand surface and locked in place. The difference in height was read and noted in the Excel spreadsheet that was used to record every set of tag grid positions. This measurement accounted for the 7 mm variation in the height that was experienced between different sand preparations. The bottom of the tube was held level with the sand, whilst the pointer was re-adjusted to

zero. Both the rod and tube were then pushed vertically down by 300 mm and locked, the pointer was raised 100 mm and then the rods were inserted a further 100 mm (making 400 mm deep in total).

The inner rod was then withdrawn from the tube and a tag was inserted, as shown in Plate 7.8 (left hand). Prior to insertion each tag's code was noted in the same Excel spreadsheet against its grid position location. A 6 mm spacer (half a tag length) was slid onto the rod before it was re-inserted. The rod was then used to push the tag to the correct depth, as shown in Plate 7.8 (right hand), after which both the tube and rod were withdrawn upwards by the appropriate height, thus leaving the tag at the correct depth and positioning them at the correct height to insert the next tag. Eight repetitions of this process created one vertical column of tags. After a column of tags was inserted the bracket was moved to the next position and the insertion process was repeated, until all 64 tags in the grid were inserted.

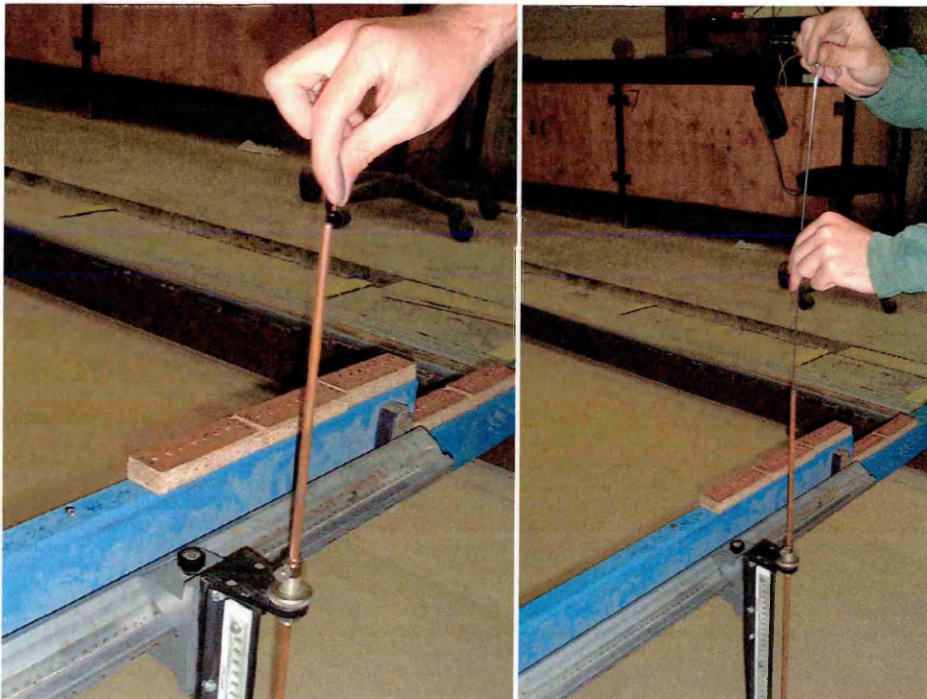


Plate 7.8 – The data tag insertion process

7.2.2 Tag Position Location

After the tyre had passed over the tags and disturbed them the tags were scattered across a wide area of sand, and were, in the majority, buried beneath the sand surface. To locate the tags the bridge was again placed over the surface to prevent further sand disturbance, then the scanner was methodically passed over the sand until the location of one or more tags was pinpointed, at which point the overlying sand was removed to reveal each tag. This was done using an industrial vacuum cleaner that had a $\text{Ø}1$ mm hole mesh clamped over the end of the hose. This allowed sand passage but prevented the tags from being accidentally sucked into the vacuum.

Employing this method meant that on 98% of occasions, the sand could be removed from around the tag to sufficiently expose its centre for measurement whilst not disturbing its location. When a tag was accidentally picked up and trapped by the mesh it could often be repositioned in its original location, as this remained evident in the sand. If this was not possible then no measurement was taken. As the tags were found their code number was recorded, which assisted in locating the remaining tags. As the tags were found their positions were measured using the apparatus described in section 7.2.3. Once all the tags were found and measured for a region of sand, they were removed and then another region was scanned and the excavation and measurement process was repeated.

7.2.3 Tag Position Measurement Apparatus

The following criteria were important for the system used to measure the tag positions:

- It had to be sufficiently rigid to provide accurate measurement, yet light enough to be lifted over the bin.
- It had to be simple and quick to use to hasten the location process.
- Its framework could not impede scanning for the tags
- It had to locate from the same bin marker points as the placement frame.

A welded steel framework that comprised two RHS beams that spanned the bin, as shown by Plate 7.9 was designed. One beam was fitted with two plates that straddled

the soil bin markers to give identical longitudinal location to the placement frame. Two right angle sections fitted closely inside the bin rails to give lateral location, and between the beams to give the correct longitudinal spacing. Vertical location was again achieved from the bin rails; thus measurements by the placement and measurement apparatus were directly comparable. During placement the measuring frame was also adjusted to be perpendicular to the rails prior to secure fastening with G-clamps.

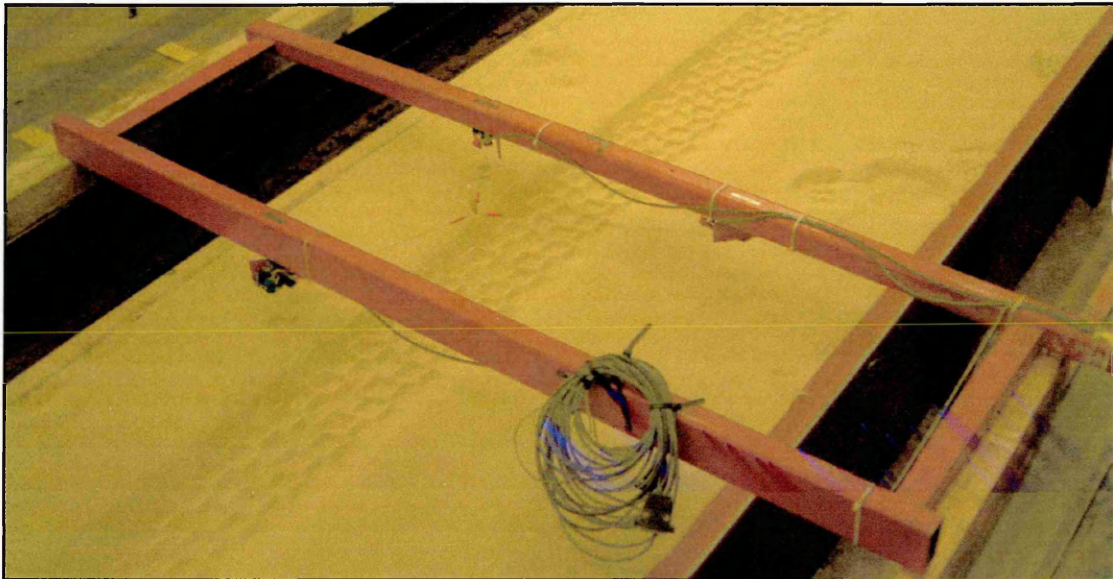


Plate 7.9 – The tag position measurement frame positioned over a sand tank

Three 1 m drawstring transducers fitted with multi-turn high accuracy potentiometers were used to perform the measurement. Pulling wire (the drawstring) from each transducer turned the potentiometer, which altered its resistance. Applying 12 V DC voltages across the devices produced voltage outputs proportional to the wire extensions. Calibrations were performed on each transducer against the wire extension from the outlet face. The extension was measured to an accuracy of ± 0.5 mm along a bench using a 1 m rule, whilst the output voltage was simultaneously recorded by the data logging system. The calibration results for the three transducers are shown in Figure 7.3, which also presents the calibration equations that were used when calculating the tag positions.

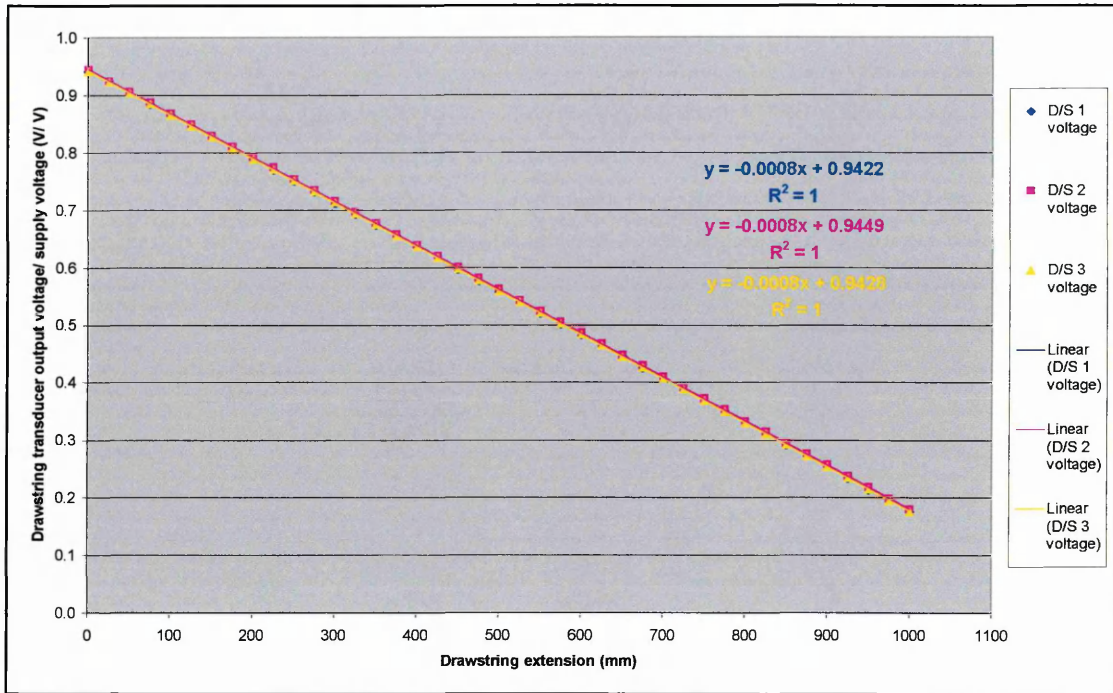


Figure 7.3 – The calibration graphs for the three drawstring transducers

The three transducers were mounted to thin plates welded to the RHS beams, which were positioned so that the transducers formed an ‘L’ shape beneath the frame as shown on Figure 7.4 and Plate 7.10.

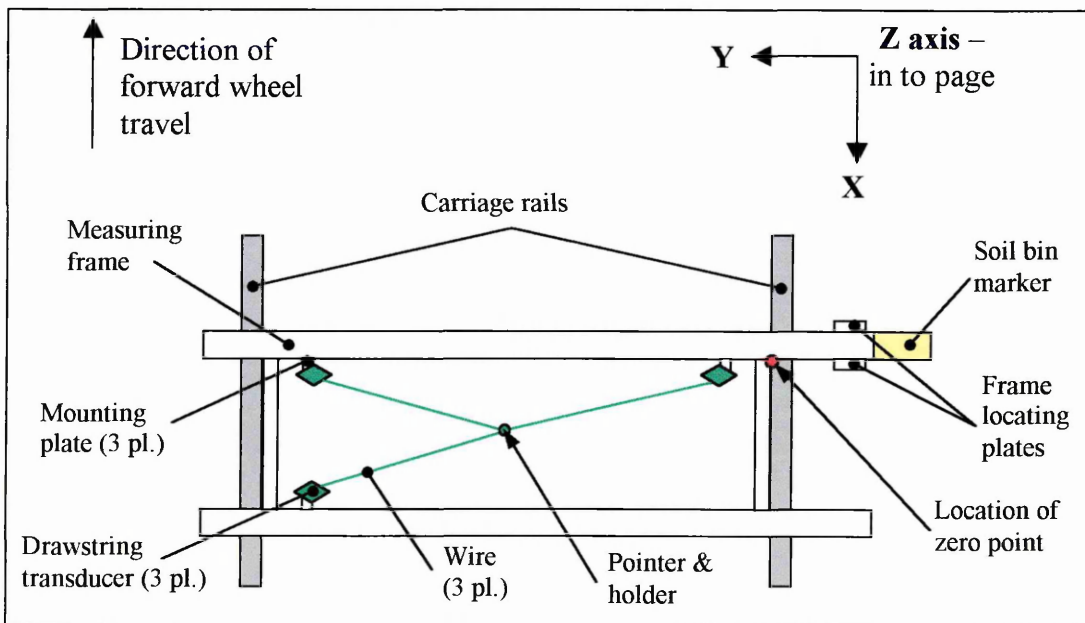


Figure 7.4 – A schematic plan view of the tag location measurement equipment showing the location of the zero point (as per the placement frame) and the positive measurement axes

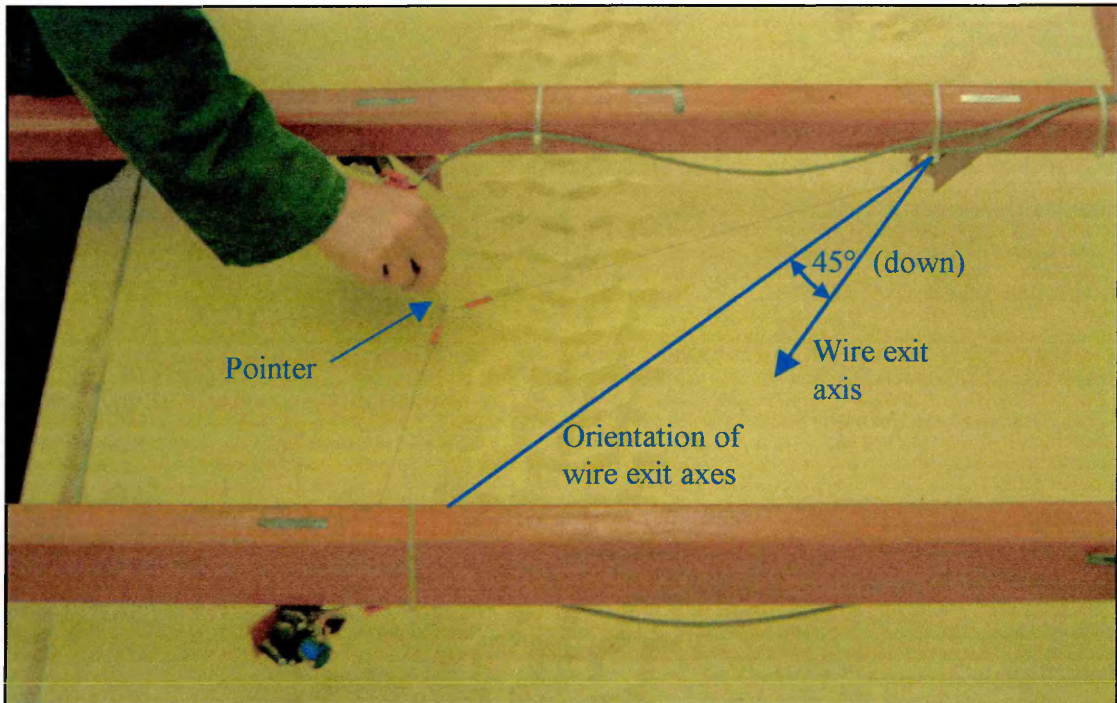


Plate 7.10 – The three drawstring transducers mounted to the measuring frame

The plates and transducers were mounted so that the wire exit axes pointed 45° downwards from the horizontal, as indicated in Plate 7.10. They were also orientated so that the wire exit axes passed through the opposite corner of an imaginary rectangle, of which the locations of the transducers formed three (of the four) corners. The ends of the three drawstring wires were connected together by being glued into three small holes drilled close to the point of a $\varnothing 4$ mm pointer. A $\varnothing 12$ mm nylon holder was attached to the opposite end of the pointer to allow control over its position. The transducers' mountings allowed the measurement of an area of sand larger than the region in which tag displacement in the Y and Z directions had occurred during the pilot study. Quantification of tag displacement in the X direction outside of the frame's measurement range was achieved by moving the frame to the next soil bin marker, as the measurement ranges overlapped.

Moving the pointer altered the drawstring extensions (and hence voltages), and thus by using the calibrations shown above in Figure 7.3 the three string lengths could be calculated. Pythagoras's theorem was used to calculate orthogonal coordinate measurements along the X, Y and Z-axes, shown in Figure 7.4, from the three string

lengths, and these co-ordinates were determined relative to the zero point of both frames. These were calculated using Excel in the following manner, and a full explanation is in Appendix 19. When the drawstrings were extended they created two triangles between themselves, shown as triangles A and B in Figure 7.5. These existed across all three planes as the view of triangle A on the side elevation illustrates.

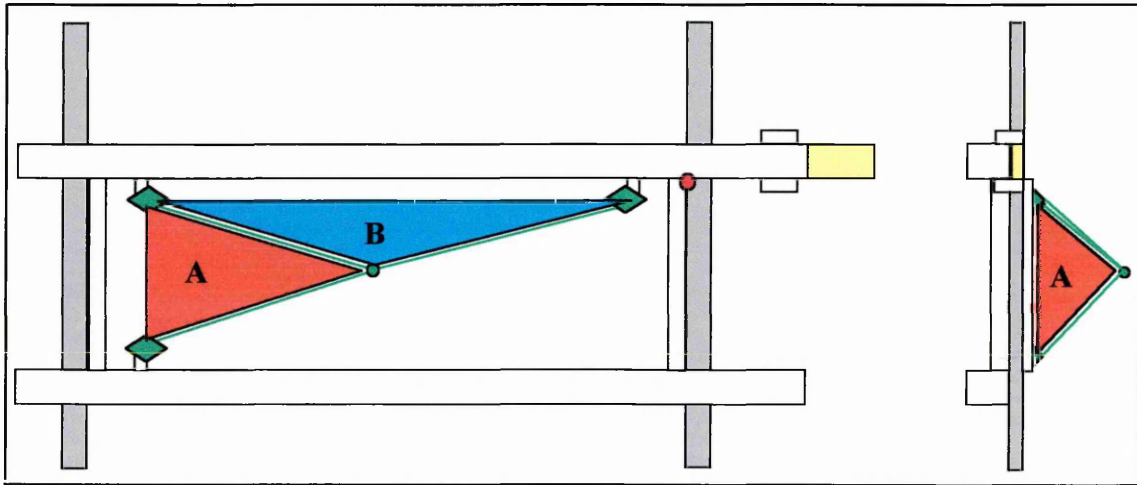


Figure 7.5 – A schematic plan and side view of the measuring frame showing the three drawstrings and the two triangles these created (soil bin and sand omitted)

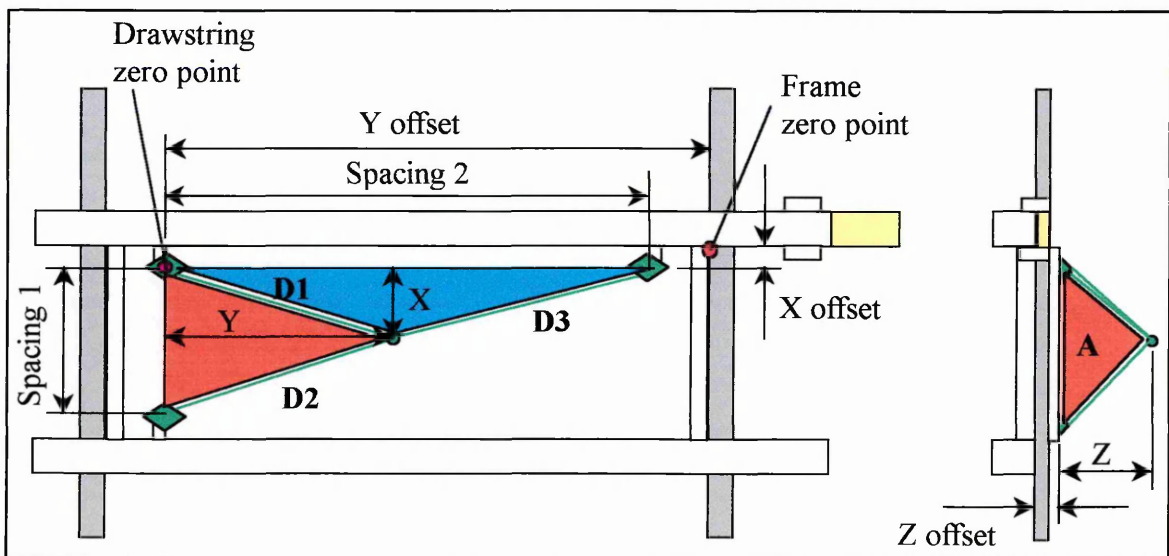


Figure 7.6 – A schematic plan and side view of the measuring frame and the distances into which the drawstring lengths were transformed

The values of X and Y, shown in Figure 7.6, were calculated first. X was determined from two Pythagoras calculations upon drawstring lengths D1 & D2 and Spacing 1.

Likewise Y was calculated from D1, D3 and Spacing 2. Then by using D1, X and Y the spreadsheet performed two further Pythagoras calculations to deduce Z. Thus Cartesian distance readings of X, Y and Z from the pointer tip to the drawstring zero point were calculated. To adjust these to give correct measurements of the pointer's tip relative to the frame zero point (identical for both frames) the spreadsheet then added (or for Y subtracted) the distances X, Y and Z to (or from) the three offset distances between the drawstring zero point and frame zero points, see Figure 7.6.

For this system to work accurately it was vital that besides determining the drawstring lengths sufficiently accurately, which was possible from the calibrations, the relative positions of the zero points and the transducer locations also had to be accurately measured. These measurements were made on a triple-axis measurement device at the Cranfield School of Industrial and Manufacturing Science (SIMS). This device was able to measure to within ± 0.001 mm the position of the three string entry points and each drawstring's zero point relative to the frame zero point. The three transducers were set so that their exit points were level to within ± 0.06 mm of the X-Y plane that ran along both beams and through the frame zero point. An investigation of this error upon the measurement sensitivity showed that it did not significantly compromise the accuracy of the position calculation. The 'L' shape achieved did not form a perfectly true rectangle, so the slight error of 0.6° was corrected using an extra trigonometrical calculation in the spreadsheet to maintain the required accuracy of calculation.

All three transducers were supplied with 12 V DC and their outputs were separately logged on a Toshiba laptop PC using DasyLab data logging software. The signals were inputted into the PC via a Strawberry Tree DAC pad. They were post-processed in Excel. A push-button switch with a 3 V battery circuit was fitted to another signal channel. The software logged continuously over the duration of the tag searches but the switch was only activated when the pointer was correctly positioned to measure a tag position. An Excel file later used the switch inputs to automatically identify the correct sections of logged data, which enabled the relevant data to be sorted prior to the mathematical calculations.

To minimise measurement errors, between eight and thirteen separate output voltages were logged at each tag position. The spreadsheet averaged all of these to produce a single output voltage for each drawstring transducer for each tag position. The spreadsheet then calculated the X, Y and Z co-ordinates (relative to the frame zero point) for each tag location. The spreadsheet was designed to flag up an error if impossible co-ordinates, or co-ordinates for too many tag locations were calculated. This allowed the original data to be investigated and corrected.

The list of order in which the tags (ID numbers) were located was then tallied against the list of generated X, Y and Z co-ordinates. The list of tag ID numbers and their corresponding starting grid locations was also copied into the spreadsheet. These two sets of data and positions were then tallied against each other, by using the tag ID numbers as a reference. This allowed the displacements in the X, Y and Z directions to be computed. To study the displacements, and to double-check the outputs, each tag's starting position and its displacement vector was plotted in AutoCAD for every grid. This also allowed any apparent errors to again be corrected as necessary. Although the mathematical calculations would always provide accurate measurements, providing the string lengths were correctly calculated, it was necessary to determine the system's measurement accuracy.

7.2.4 Accuracy and Repeatability of Tag Placement and Measurement

To assess the accuracy of the measurement apparatus a three-dimensional item of known dimensions was placed in the soil bin and some of its dimensions were measured using the measurement frame. The item used was a medium sized carpenters square (arms of 350 mm by 250mm). Before its placement all the carpenters square's dimensions were measured on a granite bench using a calibrated height gauge. The square was then positioned firmly in the soil at depth of approximately 650 mm. This distance was greater than any expected tag disturbance, so any inaccuracy in the tag measurements would be less than the accuracy determined in the investigation.

The square was clamped in a position in the soil so that it was randomly angled to the frame, but so that the positions of three points at opposite ends of its structure (termed

X, Y & Z) could be easily determined relative to constant points on the measurement frame, e.g. they were directly below one face or corner. The locations of these three points were accurately measured using a combination of rules, squares and clamps. This allowed the position of these three points to be determined to ± 1 mm along each of the orthogonal axes. Once this was complete seven corner points of the carpenters square (termed X, Y, Z, P, Q, R & S) were measured using the measurement frame. To assess the measurement repeatability, two of the corners (X & Y) were each measured another four times, making a total of fifteen measurements. The orthogonal co-ordinates of each of these points were determined using the spreadsheet calculations as described above.

Next the measurement frame and square were drawn in their relative positions in AutoCAD. The square was initially drawn on a flat plane, as it had been measured on the bench, before being correctly orientated so that the positions of the appropriate three points (X, Y & Z) matched the locations relative to the zero point that were achieved when it was positioned. This transposition also automatically orientated the four other measured points (P, Q, R & S) to their correct locations. The locations of all the measured corners were read from the AutoCAD drawing and compared against the spreadsheet's calculated (measured) values. Table 7.1 shows the variations between the location of the seven corners and the measurements made using the measuring frame.

Table 7.1 – The results from the carpenters square calibration measurements

Point	initial location from bin 0,0,0 (mm)			position from frame 0,0,0 (mm)			Difference in position (mm)		
	in x	in y	in z	in x	in y	in z	in x	in y	in z
X1	-3.18	1018.79	659.32	-2.70	1020.01	659.83	0.48	1.23	0.50
X2	-3.18	1018.79	659.32	-2.02	1020.16	660.37	1.16	1.37	1.04
X3	-3.18	1018.79	659.32	-2.22	1019.04	660.36	0.96	0.26	1.04
X4	-3.18	1018.79	659.32	-2.56	1019.88	659.92	0.62	1.09	0.59
X5	-3.18	1018.79	659.32	-1.78	1020.10	660.13	1.40	1.31	0.81
Y1	25.70	1020.03	687.29	25.70	1019.86	687.28	0.00	-0.17	-0.01
Y2	25.70	1020.03	687.29	26.41	1021.01	687.89	0.71	0.98	0.60
Y3	25.70	1020.03	687.29	26.41	1019.33	687.71	0.71	-0.50	0.42
Y4	25.70	1020.03	687.29	26.90	1020.87	687.28	1.20	0.84	-0.01
Y5	25.70	1020.03	687.29	26.78	1020.31	688.33	1.08	0.28	1.04
Z	-85.27	711.01	545.37	-82.37	713.97	548.14	2.90	2.96	2.76
P	-83.01	673.24	544.71	-80.42	676.01	547.31	2.59	2.77	2.59
Q	45.64	716.65	672.13	42.81	716.98	670.86	-2.83	0.34	-1.27
R	47.90	679.22	671.47	50.03	681.55	673.29	2.13	2.33	1.82
S	46.17	678.59	681.33	46.74	681.53	681.43	0.57	2.94	0.10

The maximum measuring error was ± 3.0 mm in any of the three orthogonal planes. Over the maximum measured length (1020 mm) ± 3.0 mm represented an error of $\pm 0.3\%$. The measurement repeatability was shown to be within ± 1.5 mm.

To confirm that the tag placement apparatus actually positioned tags at the intended depths, six, single tag column, trial insertions were undertaken in 25 mm spacings down to a depth of 400 mm. The tags were then excavated and their depths were measured using calipers, a square and a rule (accuracy of ± 1 mm). After four different attempts a suitable methodology was established that was capable of achieving the correct height positioning. This was accurate to ± 2.5 mm at the lower depths (350 mm to 400 mm), and to ± 1.5 mm for the tags closest to the surface, as shown in Appendix 20.

To determine the accuracy of the combined (placement and measurement) system three complete sets of tag grids (64 tags) were placed in the sand using the placement frame. These were not disturbed but instead immediately excavated. Figure 7.7 shows the tag positions of the three grids part way through this process at a depth of 300 mm. As each tag was found its position was measured using the measurement frame. From the results that were recorded, it was found that the total errors due to placement and measurement were ± 5.5 mm in any direction from the expected tag position, as shown in Appendix 21. This was equivalent to an error of $\pm 1.4\%$ over the maximum measured range. The error in repeatability for a single position was determined to be ± 3.5 mm. Part of this error was introduced by the way that the tag was measured, as when the pointer was held against the middle of the tag (obvious by a change in colour) this unavoidably introduced a 1 mm offset error (due to the tag's diameter) for which no compensation could be made, due to the continuously changing orientations of the tags.

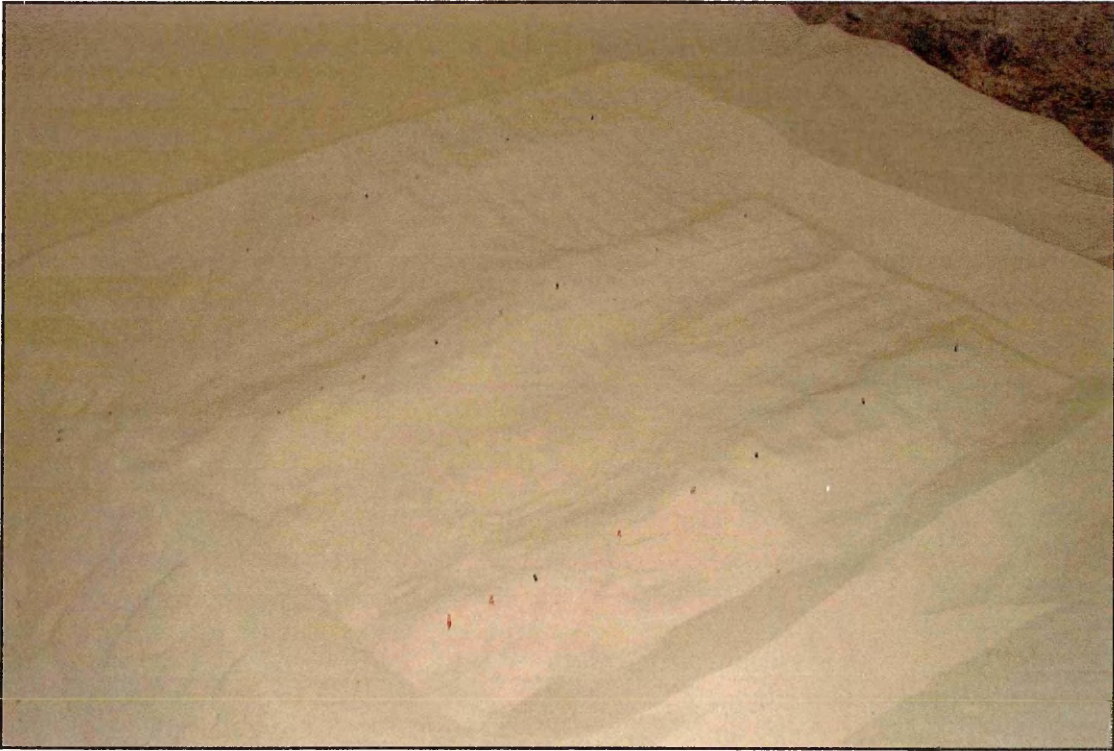


Figure 7.7 – The positions of some of the tags during the assessment of the accuracy of the combined system

During the sand and tag displacement evaluation experiment, the results of which are discussed later in section 9, the combined accuracy was continually assessed. This was calculable because the positions of the tags in row 8 and column 8 (400 mm from the tyre centre line) were never disturbed by the sand displacement. Therefore their positions could be monitored to ensure that accurate tag placement was achieved throughout the experiment. It was noted that for repeated treatments the error in placement accuracy increased to -7.5 mm (instead of -5.5 mm) in the upward vertical (Z) direction, as the placement apparatus occasionally failed to achieve the correct positioning at this depth. This was only recorded at the lower depth levels and the majority of the tags were placed and located more accurately than this, as an average error of ± 4.1 mm in all directions was achieved.

7.3 POSITION OF THE TAG GRID IN THE THRUST (SLIP) CYCLE

Based upon the understanding of the traction process developed during the pilot study (section 6.8.2), it was decided that the sand displacement measurements would be conducted at the positions in the thrust cycle represented in Figure 7.8. The chosen grid positions enabled measurement as the tyres passed from a typically mobile situation (at low slip), through maximum mobility, just prior to maximum slip, before reaching maximum immobility at a medium slip. These positions allowed the high sand displacements that caused the tyres to become immobile to be quantified against the sand displacements that occurred at lower slips, whilst representing the best achievable compromise between the number of tags placed and the quantity of measurements recorded. These three wheel slips at which displacement was recorded were 70% (H), 40% (M) and 15% (L), as indicated on Figure 7.8.

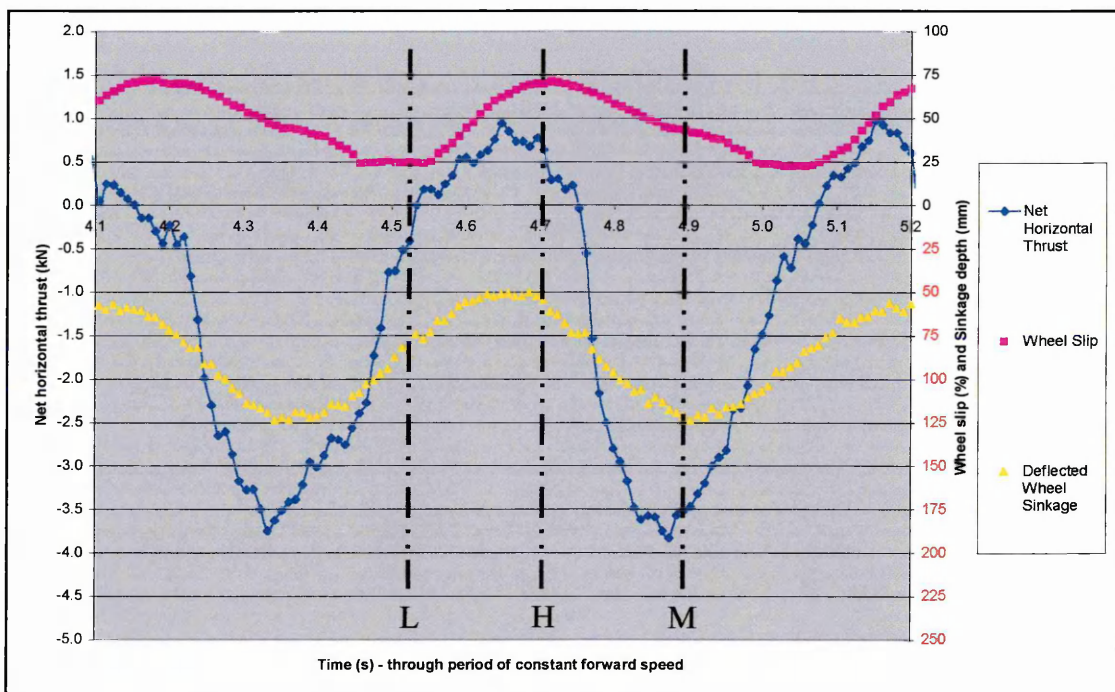


Figure 7.8 – The typical slips within the thrust/ slip cycle at which the three tag grids were positioned so as to be struck at three different slips

At each point of measurement the tags were positioned in a grid of the form shown in Figure 7.1 and each of the 64 positions was referred to using the 1 to 8 numerical reference system. Thus the tag on the surface directly under the tyre centre line was at 'Position across 1, Depth level 1', and the tag placed directly underneath, 400 mm

lower was at '*Position across 1, Depth level 8*'. Each of the three grids had to be positioned so that it was struck at the appropriate wheel slip treatment over each test run. Previous results showed that the whole thrust/ slip cycle described in Figure 6.21 consistently occurred over a distance of 600 mm \pm 15 mm and that the three chosen slip conditions were equally distributed over this length. Therefore by employing consecutive 200 mm grid spacings, it was guaranteed that each grid would be struck at one of the three target slips, even though the actual slip treatment received by each grid would only be determined in the subsequent analysis.

To assist the identification of the slip value a steel block was placed co-incident with each tag grid. As the processor passed over each of the three blocks a micro-switch was triggered which sent a voltage signal to the data logger. These pulses identified the value of wheel slip that was occurring as each grid was struck. The subsequent experimental results proved that the spacings achieved the desired effect as the grids were consistently struck at the sets of intended slips to an accuracy of \pm 5% slip.

7.4 VERIFICATION OF THE SUITABILITY OF THE TEKSCAN SYSTEM

To determine the TekScan pressure sensing system's suitability to this application, the performances of the three most potentially suitable pressure mats were evaluated. These were the 5051 mat, the 6300 mat and the 6911 mat. All of these are shown in Appendix 22. Variants of each mat with a 0 kPa to 690 kPa (0 to 100 psi) range were selected. Before each mat could record useful data it had to be calibrated. A bespoke air bladder load device was used to apply a known, equally distributed load to all of each mats' sensing nodes. Once this load was applied the computer software could conduct both a calibration (adjusting the displayed output to represent the applied pressure) and an equilibration (balancing the pressures equally across the cells).

Each mat was then subjected to three replicated free wheel rolling test runs in the soil bin at a 1 m/s travel speed using a PT 235/70 R16 tyre and split rim inflated to 2.21 bar (32 psi) and mounted on a Land Rover hub with a 650kg normal load. For easy positioning and changeover the mats they were securely fastened within plastic sleeves glued to the tyre. The soil used was a flat and very compact sandy loam (approximately

1420kg/m³). This was sufficiently hard so that the soil deflection was negligible (1 to 3 mm), whilst approximately 25 mm of tyre deflection occurred. This produced a contact area of 0.042 m² (200 mm wide x 210 mm long), which was determined statically from a chalk dust outline, thus with a 6.38 kN normal load, a nominal normal stress of 152 kN/m² was produced beneath the tyre (neglecting carcass stiffness effects). The TekScan system was set to log at 50Hz, which produced approximately eleven sets of logged data from the contact event for every wheel revolution. Thus the 5 revolutions that formed each test run produced 55 useful sections of logged data from a total of 570 sections, although the area of contact patch that was logged was dependant on each mat's size and its position.

7.4.1 6911 mat

This mat was positioned with the four fingers equi-spaced on the longitudinal centre line of the tyre's circumference. The mat was flattened to the tyre's surface, thus forming a gap of 16 mm between each finger and 23 mm between each sensing pad. Thus potentially the mat could record stress along a 3 mm wide band of the tyre, as indicated by the shaded area in Figure 7.9. Although these mats were only capable of measuring a small area, they were potentially useful for very precise applications.

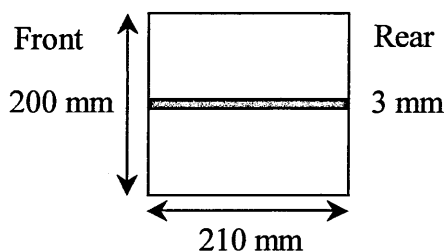


Figure 7.9 – The relationship between the contact area (white) and the 3 mm band of contact length (blue) over which the 6911 TekScan mat could potentially measure stress

The 55 sets of results from each of the 3 replications undertaken are detailed in Appendix 22. Interlacing the results recorded from different stages of the tyre's angular rotation allowed the mean stress distributions along the contact area to be derived. However, because each section of logged data only accounted for a very small portion

of the contact length it was impossible to produce a complete representation for the total contact length. Thus despite data from all three replicates being used to develop the greatest possible quantity of results, which are shown in Figure 7.10, gaps occurred where stress was not recorded. Elsewhere stress distributions of between 153 kN/m^2 and 160 kN/m^2 were recorded which, for the assumed contact area, equated to a normal load of between 655kg and 685kg, which agreed with the 650kg applied normal load. Some of the extra stress was due to the carcass stiffness increasing the ground pressure, whilst the rest was caused by the mat's sensitivity to small point loads caused by stones and grit particles etc. This created pressure spikes in the data that skewed the results.

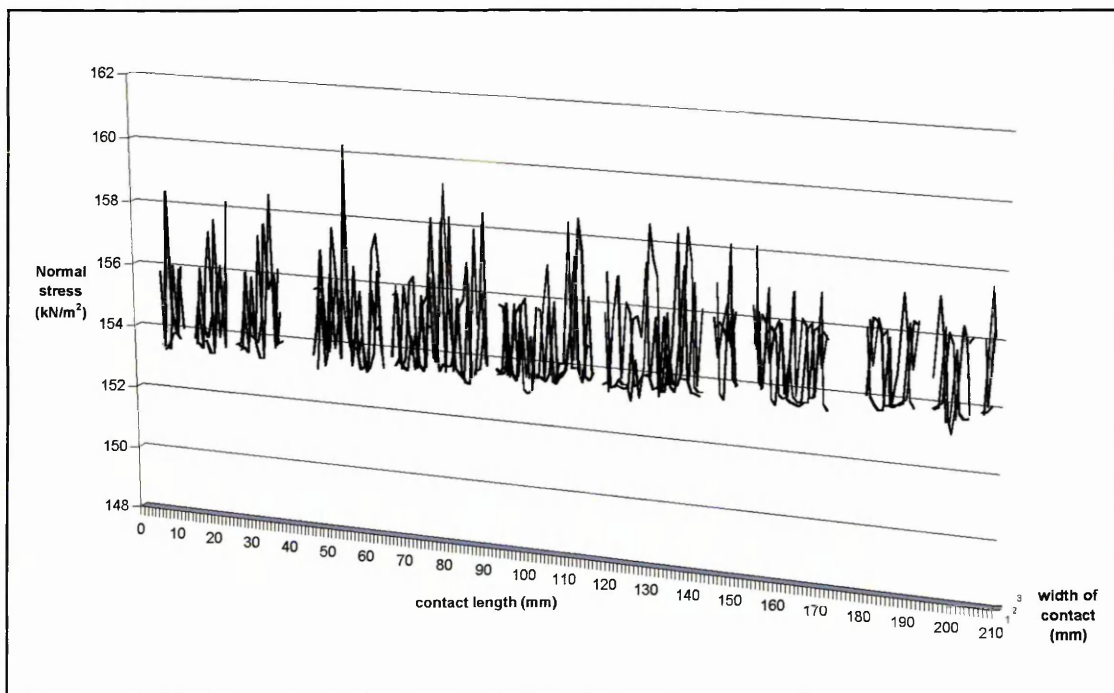


Figure 7.10 – Mean normal stress distributions along the contact length as measured by the 6911 TekScan mat

7.4.2 5051 mat

This mat was also equi-spaced about the tyre's longitudinal centre line, allowing it to potentially record stresses along a 112 mm wide band of the contact length, as indicated in Figure 7.11. This mat's larger coverage meant that more overlap existed between the eleven data readings recorded during each wheel revolution, so a complete plot of the mean stress distributions across the measured region could be generated.

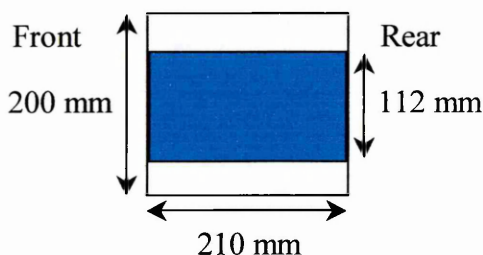


Figure 7.11 – The relationship between the contact area (white) and the 112 mm band of contact length (blue) over which the 5051 mat measured stress

The actual results are also detailed in Appendix 22, but these have been shortened to facilitate their inclusion, thus they only include the mean results for the periods when the mat was in contact with the ground. Again it was necessary to use all three sets of results to provide overlapping sets of angular results to allow the complete stress plot shown in Figure 7.12 to be constructed. The results showed stresses ranging from 152 kN/m² to 166 kN/m² (650 kg to 698 kg), which agreed with the data presented in section 7.4.1. Again a combination of carcass stresses and random peak stresses due to point loads accounted for the extra load.

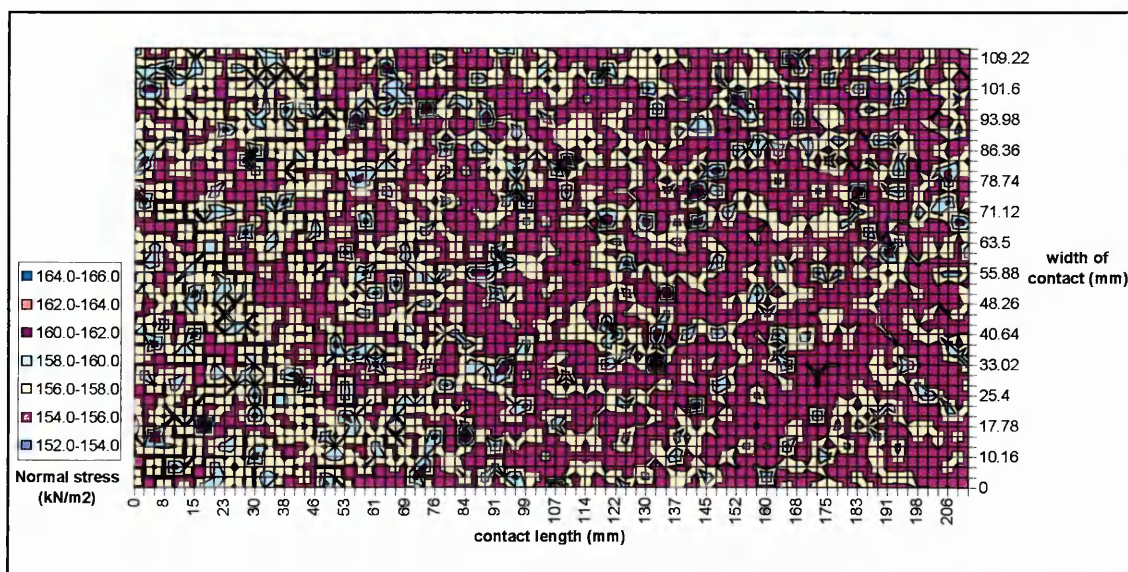


Figure 7.12 – Mean normal stress distributions along the contact length as measured by the 5051 TekScan mat

7.4.3 6300 mat

This mat's extra length meant that it could be positioned to cover the full contact width. Although narrower than the previous mat, sufficient width was available for overlap to exist between the 11 data sections recorded during each wheel rotation. Thus mean stress distributions could be determined across the whole contact area. The mean stress distributions could be determined across the whole contact area. The mean contact results from this test, which were shortened in the manner described in section 7.4.2, are detailed in Appendix 22. Once again all three sets of replicate results had to be used to generate the plot of stress distributions shown in Figure 7.13. In this instance stresses of between 152 kN/m^2 and 162 kN/m^2 (equivalent to 650 kg and 694 kg, if a 0.042 m^2 contact patch was assumed) were recorded, which agreed well with the stresses measured using the other two mats.

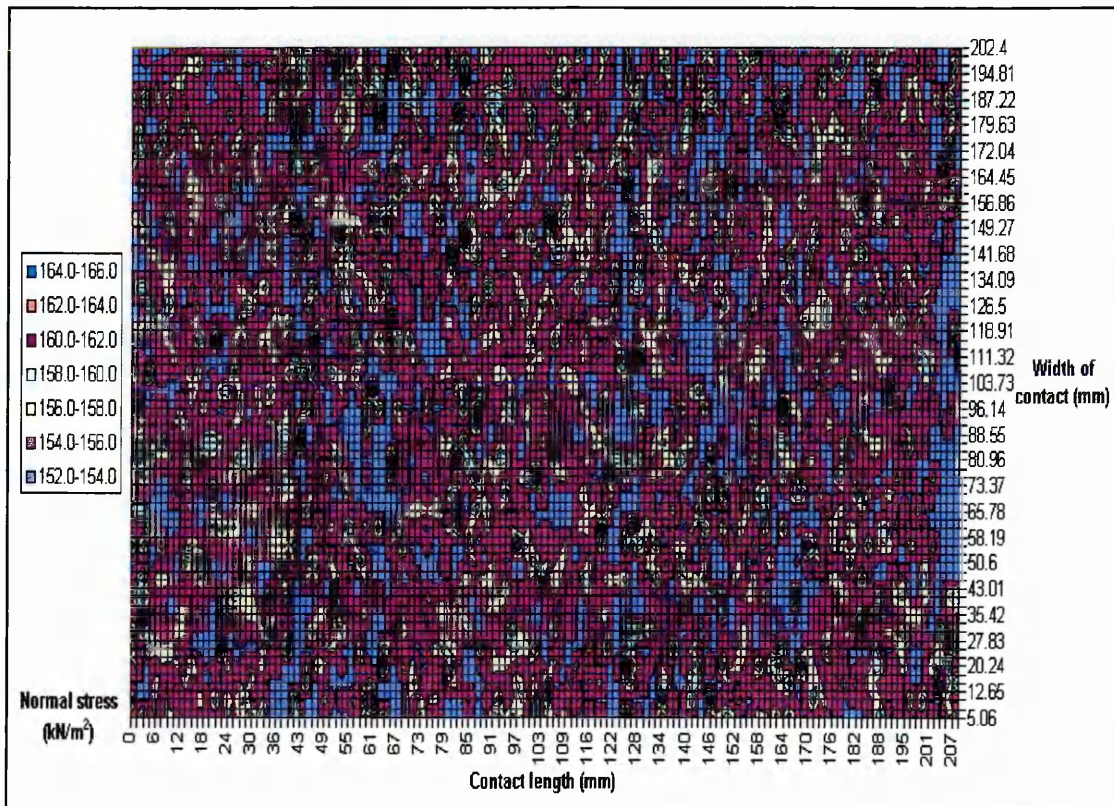


Figure 7.13 – Mean normal stress distributions along the contact length as measured by the 6300 TekScan mat

7.4.4 TekScan Measurement Capabilities

The dynamic normal stress results calculated from this trial showed good agreement with the expected stress of 152 kN/m² in all instances. Some slightly higher stresses were also recorded, but these were caused by a combination of the tyre carcass stress and extreme point loads. As the surface tested upon was comparatively rigid and the forward speed was relatively low, no significant pressure distribution variations due to tyre and surface interactions were recorded across the contact areas of any of the mats. Instead the results that were derived were more closely related to the static situation as approximately consistent pressure distributions were recorded, although slight pressure reductions were noted at the rear of the patches, where contact with the ground reduced as the tyre lifted off.

It was concluded that the TekScan system could be used for normal stress measurements when attached to a tyre. The 6300 strip-sensor achieved the best results because it covered the biggest contact width and it enabled the closest location of the connection block to the axle, which reduced the likelihood of large sinkages causing the mats to tear. Additionally the 6300 mat could be successfully moulded around the prototype treads' linear tread features. A caveat remained over the manufacturer's advice that sensing performance would deteriorate under high shear stresses, as these were not examined in this investigation. This could potentially be addressed if the mats were protected with a thin covering capable of bearing the shear stresses. This would also have to be flexible to match the tyre deformation so as not to distort the normal stress patterns.

7.4.5 Attachment of the TekScan Mats to the Tyres

Six 6300 'L' shaped strip sensors, rated for pressures up to 690 kPa (100 psi) were attached to six differently treaded prototype tyres using the following procedure:

1. Each mat was individually calibrated and equilibrated (prior to attachment).
2. The appropriate section of each tyre was sanded to produce a flat, but roughened, surface and then cleaned with a spirit fluid.

3. The underside of the each mat was bonded to the appropriate tread using an activated cyanoacrylate.
4. Thin patches produced from a two-pack self-curing (vulcanising) rubber compound purchased from Pang Rubber Ltd. were attached over the mat to provide mechanical protection. This compound was designed for repairing tyre cuts and punctures so its deformation properties matched those of tread rubber.
5. Prior to curing the compound was very malleable, which allowed the patches to be shaped around the tread features and pressed firmly into the tread rubber, which had been painted with the appropriate chemical activator solution, which chemically bonded them to the tread rubber.

The symmetry of the treads enabled only half of each tread face to be covered, yet the correct orientation had to be achieved so that each mat also reached the connection block on the wheel rim. Figure 7.14 demonstrates the necessary orientation of the connecting leg towards the rim so that a metal bracket mounted on the wheel studs could be used to securely retain the TekScan connecting block. Each mat's exact position varied slightly to accommodate each tread's individual features, as Figure 7.15, which illustrates flattened versions of each tread and the mat position demonstrates. Approximately 90 mm from the centre line the tread merged into the tyre shoulder so the mats were bent around the tyre contours at this point, as Figure 7.14 demonstrates. This transition was omitted from Figure 7.15 as only poor results were recorded from these regions, so they were ignored.



Figure 7.14 – The TekScan mat bonded to the LAT tread prior to rubber encapsulation

After curing of the rubber compound the mats were all tested to ensure satisfactory function. When a known normal load was applied to each tyre on a flat concrete surface (i.e. a constant contact area) the appropriate pressure to ($\pm 5\%$) was displayed by the TekScan system. Some small pressures (up to 120 N/m^2) were recorded on each tyre's shoulder under zero loads. These insignificant pressures arose as the mats had been attached whilst the tyres were off their rims, and under inflation the tyre carcasses slightly stressed the mats at the shoulder. However, this effect did not compromise the abilities of the mats to measure normal stresses across the central 90 mm width of tread that was of interest.

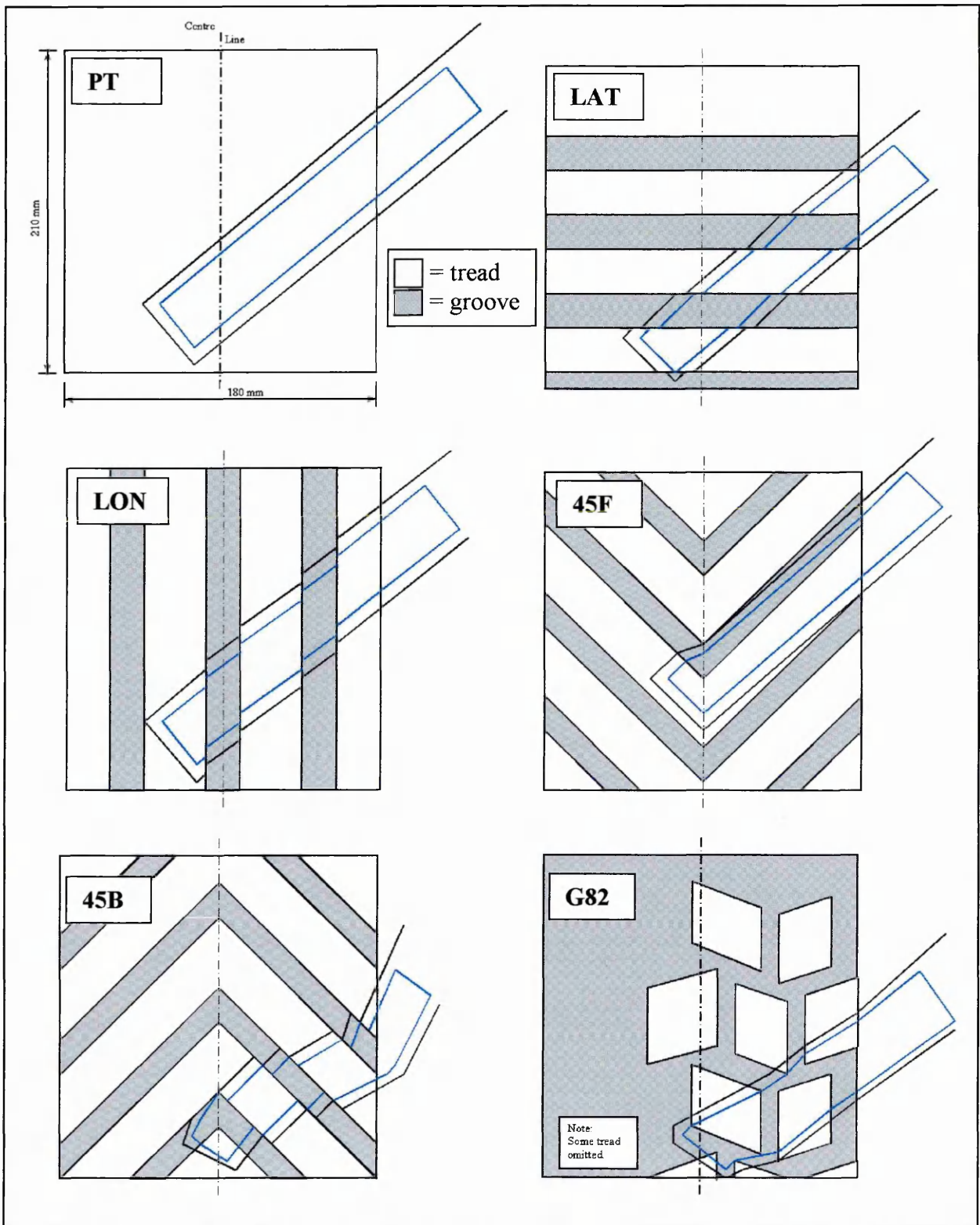


Figure 7.15 – The relative location of each TekScan mat in the 180 mm wide tread region of each of the six different treads

8 INVESTIGATION OF NORMAL STRESSES UNDER TYRES

8.1 EXPERIMENTAL TREATMENTS

The test runs were all conducted upon the previously described poured and rolled sand preparation over the full soil bin length at a constant 5 km/h forward speed. A nominal 50% slip was selected, which achieved the same cyclical thrust – slip fluctuations described in section 6.9. The other treatments were as previously detailed for other experiments, i.e. 1.10 bar inflation pressure and the five prototype treads (PT, LON, LAT, 45B & 45F shown in Plate 6.4), except for the TekScan system's logging speed, which was increased to its 100 Hz maximum setting.

It had been intended to record three test-run replications of the pressure distributions beneath each of the six tread patterns. Unfortunately the quality of the outputs from the mats on the prototype tyres deteriorated much quicker than had been expected. The constant flexing and high strains quickly damaged the mats' electrical connections, so that large holes appeared in the data. The poor longevity of the mats limited the amount of useful results that could be collected, and thus data was only collected for the LON tread (over 1¼ test runs), and the PT, LAT and 45B treads (over 2 complete test runs).

8.2 PRESSURE MEASUREMENT RESULTS

8.2.1 Pressure Map Construction Procedure

The poor mat longevity meant that sufficient data was only available to produce detailed results for a single region of the thrust cycle. The position in the thrust cycle chosen for the pressure distribution analysis was the period of maximum slip (maximum potential sand displacement), which was of greatest interest because this was where the most excessive tyre sinkage and resulting immobility was caused. Oliver's³⁰ drawstrings measured an approximately rectangular contact area with a length of 390 mm ±10 mm for this part of the thrust cycle.

The recorded results were used to produce pressure maps of the form shown in Figure 8.1, which described the variations in pressure on the contact patch at a single moment

in the thrust cycle. Each pressure mat was derived through a lengthy analysis procedure conducted using Excel. The TekScan system recorded all the test results in long data streams. Each stream had to be individually analysed to isolate the sections of data where the mat had experienced an applied pressure (ground contact). These readings (in psi) were then translated from pressures at isolated mat locations angled across the tyre (due to the mat positions – see Figure 7.14) into pressures (in kPa) at appropriately defined grid locations around the tyre circumference that were square (perpendicular) to the longitudinal axis.

The sections of contact data appropriate to the high slip region of the thrust cycle were then identified and isolated by considering the micro-switch outputs. All of the isolated sections (bands) of data were appropriately positioned along a single timeline to represent each angular position through the contact event, which allowed overlaps between the results to be identified. Any overlapping pressure readings were spliced together by calculating a mean value. Thus a single pressure value was determined for each grid location (angular position) by combining readings from different wheel revolutions at the correct cyclical position to cover all of the angular positions. As only small sections of data were recorded during each wheel revolution, all the recorded data had to be combined to enable continuous snapshots of the pressure distributions beneath each tread for a single moment in the thrust cycle to be produced. Thus as each map was the product of data from six or more wheel revolutions only a small likelihood of any chance influence skewing the results was small

The contact region was considered flat, as this was simpler to represent than the true complex curved profile. Each tread was featured on the plots, but it was only possible to derive sufficient data to accurately record the pressures experienced on the normal tread faces and not those on the groove sides (faces). The mapping was confined to the 180 mm tread width because of the measurement inconsistencies on the tyre shoulder. The position of all the mats only allowed pressures to be recorded for just over half of the tread, as the pink boxes indicate, however, maps of the whole contact area were easier to interpret, so the recorded pressures were reflected about the tyre centre line for the regions where stress was not measured. The estimated errors created by the process used

to calculate the stress distributions combined with the measurement errors produced a total error of $\pm 8\%$.

8.2.2 Experimental Results

8.2.2.1 Plain tread (PT)

At the point in the thrust cycle under consideration an average reduction of the normal load by 10% occurred, which equated to a dynamic load of 585 kg. If this load were assumed to act on a 390 mm long x 230 mm wide contact area (full tyre width), then the expected pressure would be 64 kPa. The average pressure recorded in Figure 8.1 was 62.9 kPa, however the actual pressures were unevenly distributed.

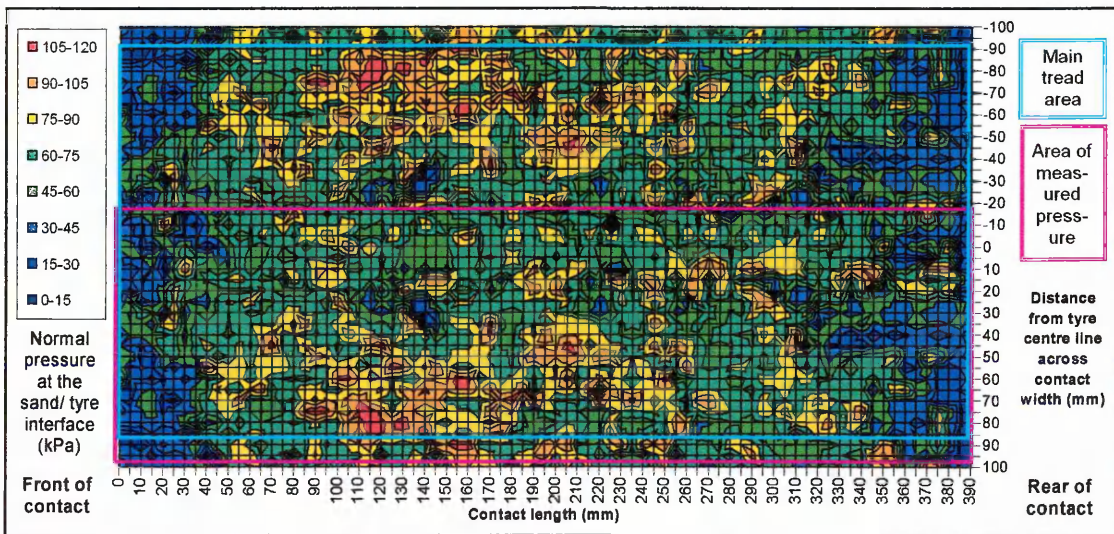


Figure 8.1 – Normal stresses recorded through the contact patch of the PT tread

Peak pressures up to 120 kPa were recorded at certain points on the tread, with the highest pressures noted over the second quarter of the contact length (between 100 mm and 200 mm) and at the edge of the tread, in proximity to the tyre shoulder. These are positions where other authors^{24, 54, 81} have shown the majority of tyre load to be borne. As expected, reduced pressures were noted at the contact patch entry and exit points. Slightly reduced pressures were also noted along the central tread width (30 mm to -30 mm), in comparison to the higher pressures experienced at the edge of the contact patch. Again the sensitivity to point loads produced a number of high peak pressures randomly distributed over the contact region. The typical mean tractive performance data recorded

for the period appropriate to Figure 8.1 was a slip of 61%, a net thrust of 0.37 kN and a deflected sinkage of 59 mm.

8.2.2.2 *Lateral tread (LAT)*

Figure 8.2 shows that the LAT tread results displayed broadly similar patterns to the PT results. An average pressure of 62.2 kPa was recorded and the pressures were again unevenly distributed. Pressure was again reduced in the entry and exit regions. Pressure was also reduced over the length of the central contact region although this was less pronounced. The maximum pressures again occurred in the second quarter of the contact length, but high pressures were also recorded in the third quarter (200 mm to 300 mm). Although the pressure patterns were broadly similar to the PT, the tread influenced the recorded results. The recorded pressures were greater on the edges of the tread features that were closer to the front of the contact, i.e. the edge that contacted the sand last. The typical mean tractive performance data recorded for the period appropriate to Figure 8.2 was a slip of 65%, a net thrust of 0.53 kN and a deflected sinkage of 69 mm.

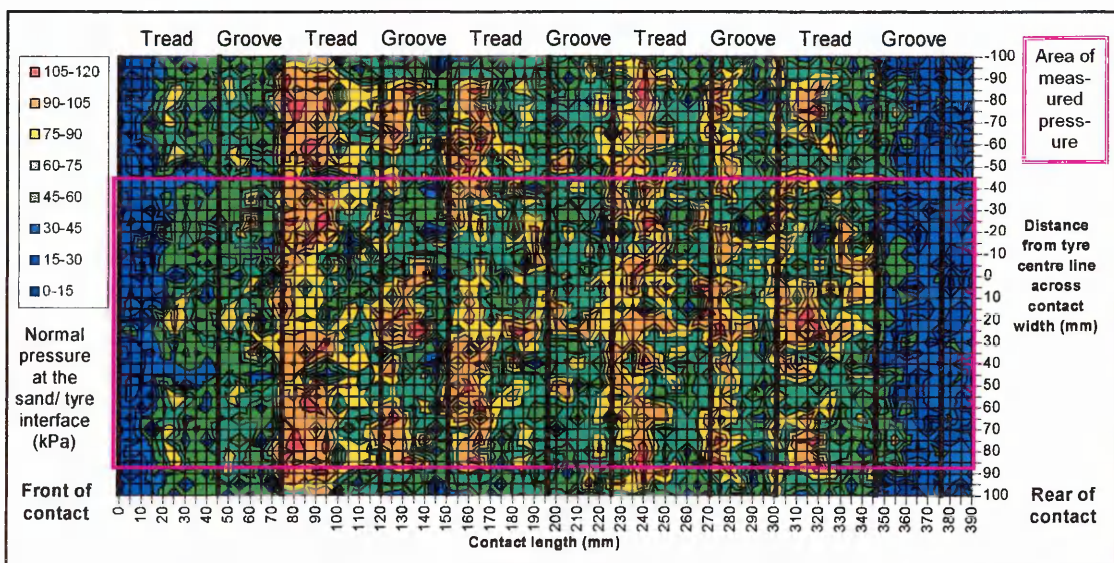


Figure 8.2 – Normal stresses recorded through the contact patch of the LAT tread

8.2.2.3 Longitudinal tread (LON)

Similar pressure distributions were also noted for the LON tread (Figure 8.3), with an average pressure of 62.9 kPa recorded. The relevant recorded performance data was a slip of 62%, a net thrust of 0.42 kN and a deflected sinkage of 58 mm. Again reduced pressures occurred at the entry and exit points, and a pressure reduction was noted along the central tread portion, though it only occurred over the rear half of the contact. Increased pressures again mainly occurred in the second quarter of the contact, though high pressures were also noted in the third quarter of the contact length. These general trends were influenced by the tread pattern, such that the average recorded pressures were greater on the treads than in the grooves. This was probably skewed because the treads were the more prominent features and because they struck the sand first.

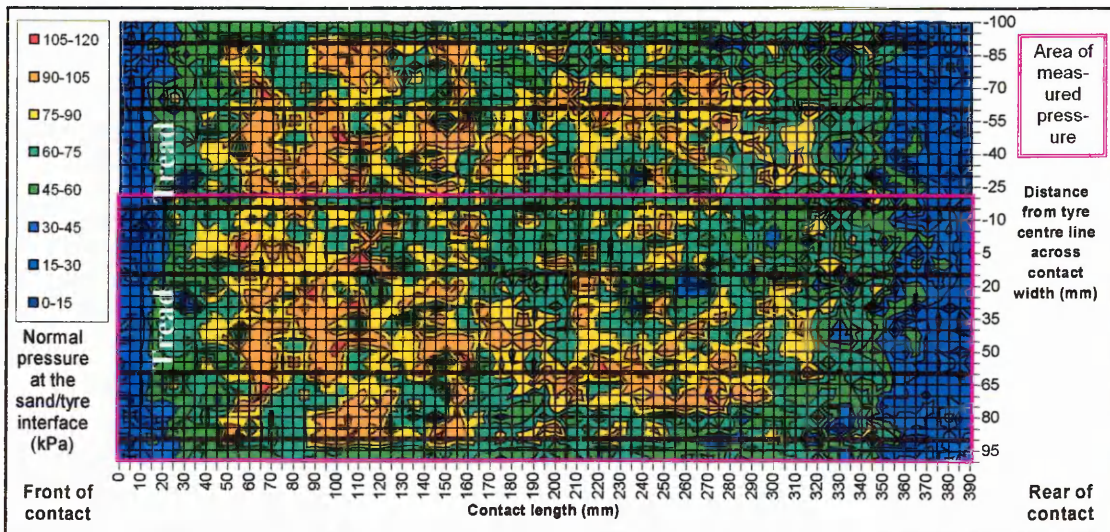


Figure 8.3 – Normal stresses recorded through the contact patch of the LON tread

8.2.2.4 45° Backward facing tread (45B)

The typical mean performance data achieved by the 45B tread was a slip of 64%, a net thrust of 0.56 kN and a deflected sinkage of 65 mm. Figure 8.4 demonstrates that the same general pressure patterns were experienced for this tread, as had been noted for the other treads, although this was disguised by the regions for which no results could be determined. An average pressure of 61.9 kPa occurred over the regions where data was recorded. Again pressures were reduced at both the entry and exit points, but this tread did not exhibit a pressure reduction along the central tread band. As for the previous

treads the higher pressures were mainly concentrated in the second quarter of the contact length, although these too spread to the third quarter. The gaps in the data disguised the pressure patterns along the treads, but it was noted that pressure increased at the points (apexes) of the angled grooves.

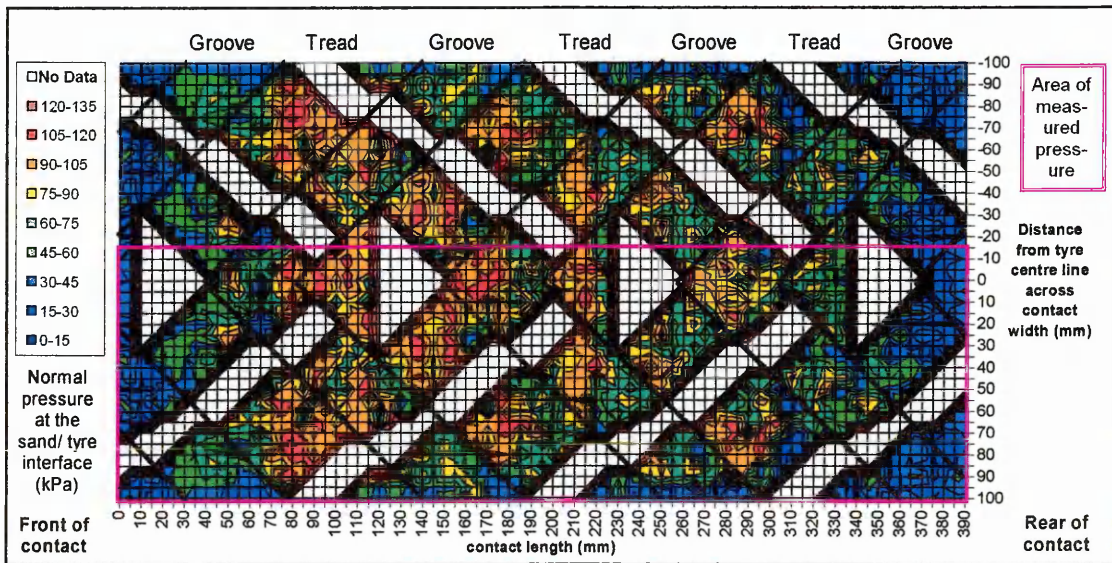


Figure 8.4 – Normal stresses recorded through the contact patch of the 45B tread

8.3 DISCUSSION OF THE RESULTS

Ignoring the influence of the treads, similar pressure distribution patterns trends were shown for all of the treads. Although approximately correct average pressures were recorded, these were not evenly distributed across the treads. Wide variations in the pressure distributions occurred over the contact length, with reduced pressures noted at the tyre entry and exit points, and increased pressures noted over the second quarter (and possibly the third quarter) of the contact length. Both of these patterns agree with typical pressure distributions on loose surfaces described by a number of previous authors^{24, 54, 81}. Pressure also tended to be reduced along the central width of the contact area and increased closer to the shoulder region, which was caused by variations in the carcass stiffness over the contact width.

Although the pressure distribution patterns recorded were generally similar the different tread patterns each influenced the results that were recorded. This was because the tread influenced the direction of the sand flow. For the LON tread this meant higher pressures

were recorded on the tread, rather than in the groove, but the tread had little influence over the direction of the sand flow. Contrastingly the LAT tread significantly altered the sand flow due to its perpendicular treads. This caused sand to be concentrated in the groove, thus as the tread drove further sand off the tread the pressure on the front face of the tread increased as the sand trapped by the groove resisted the extra sand displacement. The action 45B tread forced sand into the apexes of the tread features and this concentrated the sand flow, which caused the higher pressures, to be recorded in these sections of the tread features.

The limited quantity of results meant that the pressure distributions could only be determined for a single point in the thrust – slip cycle, so the conclusions that could be drawn from the results were limited and could not be related to the changes in the measured sand displacements. The results proved that wide pressure distributions were experienced beneath the tyres and the treads altered the distributions of the pressures, therefore the tread would affect the patterns of sand displacement generated beneath the tyres.

9 SAND DISPLACEMENT INVESTIGATION

9.1 TEST TREATMENTS

This investigation was conducted to quantify sand displacements beneath differently treaded tyres. To provide a context to the investigation Figure 9.1, which is a view from above and behind some typical tag positions, looking along the line of wheel travel, is presented. It provides an illustration of typical tag displacements that the methodology recorded. The relative tag (and grid) spacings and the tag displacements in Figure 9.1 are all correctly scaled relative to the wheel dimensions. The three sets of coloured coded vectors indicate the tag displacement vectors that were experienced at the three different slips. The grid positions used to position the data tags for this experiment were those positions detailed in Figure 7.1.

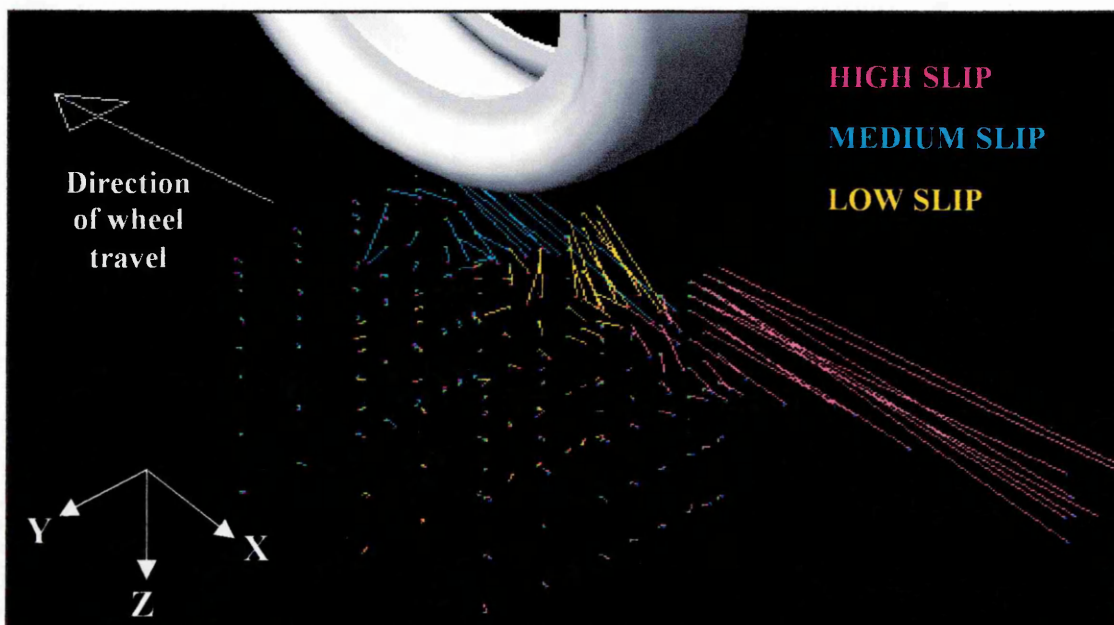


Figure 9.1 – An illustration of typical tag displacements that occurred as the tag grids were struck at the three different slips (Note: the three positive axes of tag displacement, shown as X, Y and Z)

The investigation treatments used for the sand displacement investigation are shown in Table 9.1, where 'X' marks each treatment (test) combination. The combination of treatments amounted to 18 tests, each of which was replicated 3 times, making a total of 54 sets of measurements. These were conducted in a standard randomised block design.

The G82 tread was used as a benchmark tread, whilst the other treads allowed an investigation of the effects of tread angle upon displacement and tractive performance.

Table 9.1 – The test variables for the sand displacement investigation for the prototype treads inflated to 1.10 bar

	TREAD	1	2	3	4	5	6
SLIP		G82	PLAIN	LON (0)	45F (45)	LAT (90)	45B (135)
1	15%	X	X	X	X	X	X
2	40%	X	X	X	X	X	X
3	70%	X	X	X	X	X	X

The test runs were all conducted upon the previously described poured and rolled sand preparation over the full soil bin length at a constant speed of 5 km/h. The hydraulics were set to provide a nominal 50% slip, which achieved the same thrust fluctuations demonstrated in section 6.9. This allowed the three desired slips to be achieved in one test run, so through correct positioning of the tag grids the test schedule could be completed in eighteen test runs. The testing measured the sand displacement beneath the different treads at the chosen slips, whilst simultaneously recording the associated net thrusts and sinkages, so that all of these performance variables could be related.

9.2 SAND DISPLACEMENT TEST RESULTS

All of the results from the testing were compiled on a single spreadsheet that matched the recorded tag displacements to their associated sets of traction data. The top section of this table is shown in Table 9.2. A multiple analysis of variance was then conducted using the Genstat statistical programme to determine which of the variables were significant, and at what level. Any relationships that showed an F probability (F pr.) value above the 95% level of confidence (F pr. < 0.05) were taken as significant. Further analysis was then conducted upon the mean values that the statistical analysis

generated to determine what the significant trends indicated. In the following analysis the means were graphed to aid comprehension and either an SED (Standard Error of the Difference of the Means) value or LSD (Least Significant Difference) value was included as appropriate. The full statistical analysis is presented in Appendix 23.

Table 9.2 – A sample section of the overall results table showing the experimental data and headings that were entered into Genstat

Test runs conducted										down = -ve		
treatment number 1 to 54	Bin prep number 1 to 18	Tyre type lon, lat, g82 pt, 45f, 45b	Wheel slip just H, M, L	Repetition number 1 to 3	Position lateral 8 no's	Position vertical 8 no's	Change in Position in x (mm)	Change in Position in y (mm)	Change in Position in z (mm)	Horizontal Force kN	Wheel Slip %	Wheel Depth mm
Runs	Bin	Tyre type	Slip	Block	Position	Depth	X move	Y move	Z move	Force	Slip	Depth
1	1	G82	M	1	1	1	342.70	-0.88	114.64	-2.817	40.5	-123.5
1	1	G82	M	1	2	1	345.51	12.88	113.04	-2.817	40.5	-123.5
1	1	G82	M	1	3	1	198.35	4.08	63.27	-2.817	40.5	-123.5
1	1	G82	M	1	4	1	*	*	*	-2.817	40.5	-123.5
1	1	G82	M	1	5	1	3.25	-53.06	39.15	-2.817	40.5	-123.5
1	1	G82	M	1	6	1	-6.81	1.18	-2.54	-2.817	40.5	-123.5
1	1	G82	M	1	7	1	-7.74	2.02	-3.48	-2.817	40.5	-123.5
1	1	G82	M	1	8	1	-8.17	1.19	-1.82	-2.817	40.5	-123.5
1	1	G82	M	1	1	2	154.40	-0.93	56.92	-2.817	40.5	-123.5
1	1	G82	M	1	2	2	150.83	8.80	58.59	-2.817	40.5	-123.5
1	1	G82	M	1	3	2	155.73	11.97	44.55	-2.817	40.5	-123.5
1	1	G82	M	1	4	2	33.78	-32.41	22.24	-2.817	40.5	-123.5
1	1	G82	M	1	5	2	50.90	90.62	25.64	-2.817	40.5	-123.5
1	1	G82	M	1	6	2	-6.91	2.33	-4.57	-2.817	40.5	-123.5
1	1	G82	M	1	7	2	-7.35	2.01	-4.11	-2.817	40.5	-123.5
1	1	G82	M	1	8	2	-7.72	1.09	-2.53	-2.817	40.5	-123.5

9.2.1 Horizontal Net Thrust Results

The mean net thrust results that were recorded at the particular instances when the tags were struck are shown on Figure 9.2. The net thrust output correlated with both the value of slip and the tyre type ($F_{pr} = 0.003$). The largely negative net thrusts that were recorded indicated that in the majority of cases the rolling resistance exceeded the gross thrust. No correlation existed for the tag location in the tag grid, as the same value of thrust and slip was recorded against every tag location for each individual treatment (set of tag grid results). At the low slips the net thrusts achieved were between -0.25 kN and -0.6 kN, whilst the maximum thrusts (achieved at the highest slips) were between 0.6 kN and -0.15 kN. The lowest thrusts that were achieved, which were -2 kN to -3 kN occurred at the medium slips.

This data confirmed that the tags were struck at the intended positions in the thrust/ slip cycle. As this was instantaneous data, it must be considered in this context, i.e. although a high slip momentarily achieved a high net thrust, the longer-term sinkage effect that

would subsequently cause the tyre to be immobilised, if the high slip was maintained, was temporarily overlooked. These tractive inter-relationships will be described fully in section 10.

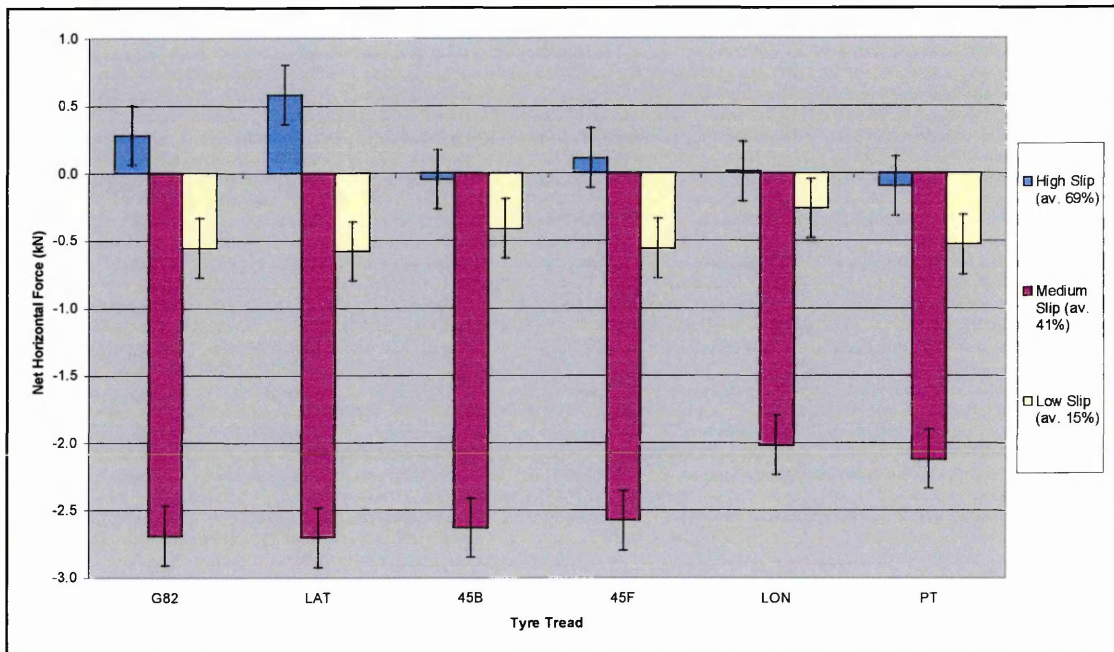


Figure 9.2 – Mean values of net thrust recorded at the three slip treatments for the six different treads

Significant differences occurred between the highest and lowest mean thrust generated by the six treads at both the medium and high slip treatments, but the differences between the peak thrusts and the median thrusts at each slip treatment were not significant. For example, at high slip the difference in the thrust from the LAT tread (the maximum thrust) and from the PT tread (the minimum thrust) was significant, however, the difference between the thrust from either of these treads and the median thrust produced by the 45F tread was not significant. In general the G82 and LAT treads produced both the highest levels of positive net thrust and the most negative levels of negative net thrust, whilst the opposite effects were achieved by the PT and LON treads. The thrust outputs from the 45B and 45F treads fell between these two extremes. These relationships agreed with the trends noted earlier, as the G82 consistently produced more extreme peak thrusts (both positive and negative) than were achieved by the PT.

9.2.2 Wheel Slip and Wheel Sinkage Results

The mean slips generated at each slip condition were: High – 69%, Medium – 41% and Low 15%. As Figure 9.3 demonstrates significant variation was achieved between each slip condition (F pr. <0.001), with mean slips of 70%, 40% and 18% generated, which meant slips close to the desired slip treatments were achieved. Unexpectedly, significant variation (F pr. 0.052) also occurred between the slips at which each tread operated at each slip treatment. This variation was less than $\pm 3\%$ of the mean slip and was caused by differences generated at the contact tread by the different tread patterns, because the test equipment settings remained unchanged throughout the testing. This enabled the tread to influence the torque at the wheel (the slip), as the torque output from the test rig was not directly controlled. The variation was such that typically the G82 and LAT treads typically operated at the higher slips up to 3% above the mean value, whilst the PT tread and LON tread typically operated at slips up to 3% lower than the mean value.

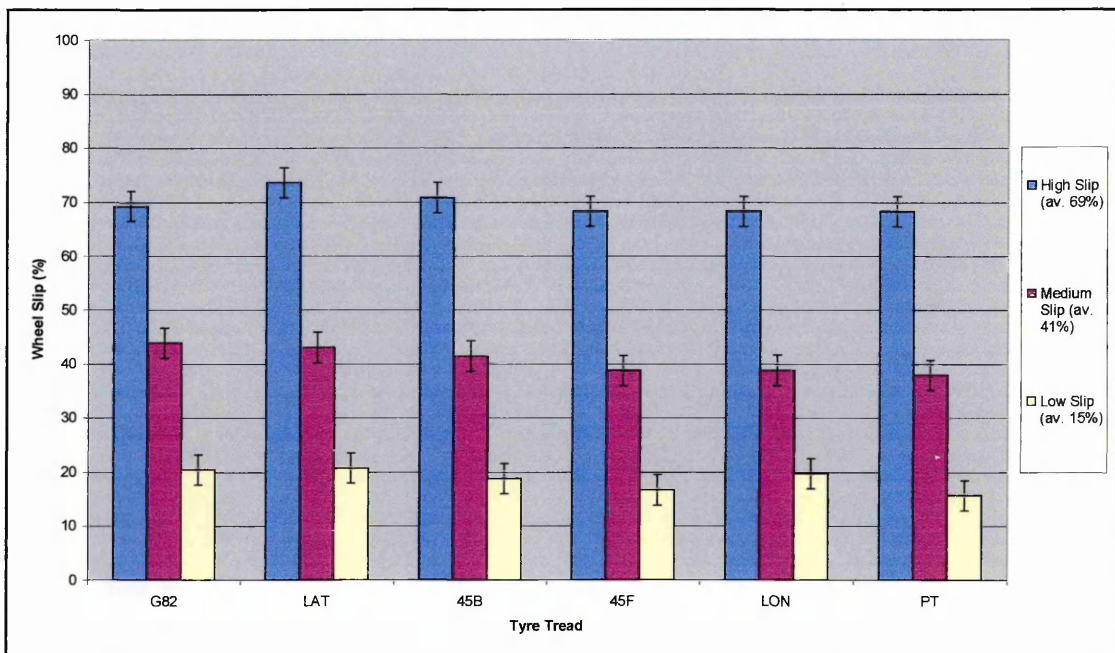


Figure 9.3 – Mean values of wheel slip recorded at the three slip treatments for the six different treads

Only slip had a significant (F pr. <0.001) effect upon any variation in the deflected wheel sinkage, as Figure 9.4 illustrates. Whilst sinkage variations between the treads were not significant at the high and low slips, significant differences in the sinkages of

the treads did occur at the medium slips (occurrences of maximum sinkage). These were such that the PT tread exhibited the least sinkage, whilst the LAT and 45B treads sank the most.

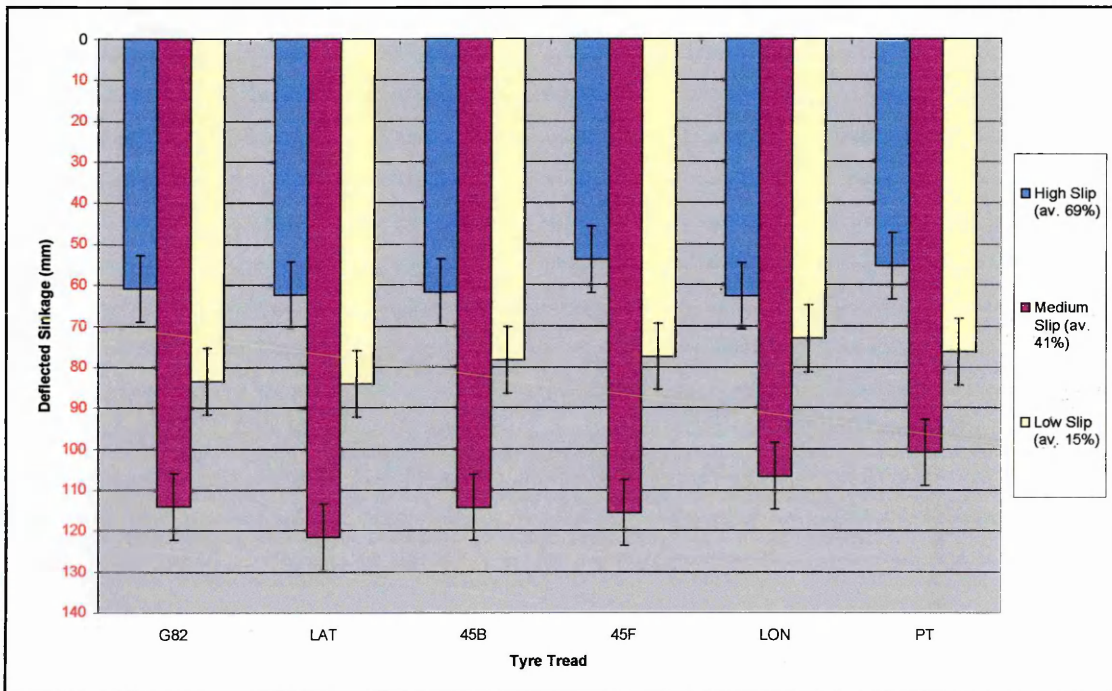


Figure 9.4 – Mean values of deflected wheel sinkage recorded at the three slip treatments for the six different treads

The data above showed agreement with the previous results, such that irrespective of the tyre tread pattern, the slip had a significantly greater impact upon the tractive performance than any of the treads were capable of achieving at any point in the thrust/slip cycle. The net thrust variations that occurred due to the slip (see Figure 9.2), over the influence of the tread, were caused by a combination of the following effects:

1. The different levels of slip that occurred (i.e. H, M and L) caused different levels of gross thrust to be generated.
2. The relationships noted in previous sections, which showed that the slip controlled the sinkage of the tyre, which consequently changed the rolling resistance as the sinkage varied.
3. The vertical displacement of the test apparatus, which altered the vertical load at the tyre interface increasing (or decreasing) the gross thrust capability.

As well as the major performance differences that were caused by the tyre slip (noted above) differences also existed between the tractive performances that the different treads achieved, although these were considerably more limited. To simplify the relationships that the results indicated, the tread performances were characterised and grouped across all of the slip treatments in the following manner, as shown in Table 9.3.

Table 9.3 – The treads grouped by the tractive performance variations they caused

Treads	Net Thrust (Rolling Res.)	Wheel Slip	Wheel Sinkage <i>Only significant at max. sinkage</i>
G82 & LAT	Greatest extremes i.e. Greatest positive thrusts and greatest negative thrusts	Operated at higher slips (typically median +2.5%)	Trend towards greater sinkages
45F & 45B	Median +ve & -ve thrusts	Median slips	Median sinkages
LON & PT	Least extremes i.e. Lowest Thrusts and Least Rolling Resistances	Operated at lower slips (typically median -2.5%)	Trend towards lesser sinkages

Whilst the differences between the sinkages of the treads at the three different slips were not generally significant, the trends indicated that different levels of rolling resistance would have acted in each case. However, the magnitudes of the differences between the tread's sinkages, which would have been influenced by the slip variations, would not have been solely sufficient to cause the variations noted, therefore the different treads must have achieved different net thrusts because of how they interacted with the sand.

9.2.3 Longitudinal (X-axis) Displacements

All the factors in the statistical analysis i.e. Slip, Tyre Type, Tag Position (*across the grid*) and Tag Depth (*down the grid*) had a significant effect (range of F pr. <0.001 to 0.022) on the sand displacements in the X direction. Figure 9.5 shows the mean displacements that were recorded for all of the treatments. This diagram demonstrated that all the sand (tag) displacement that occurred beneath the tyres in the X direction was restricted to a block of sand extending 150 mm outwards from the tyre centre line and 250 mm downwards beneath the sand surface.

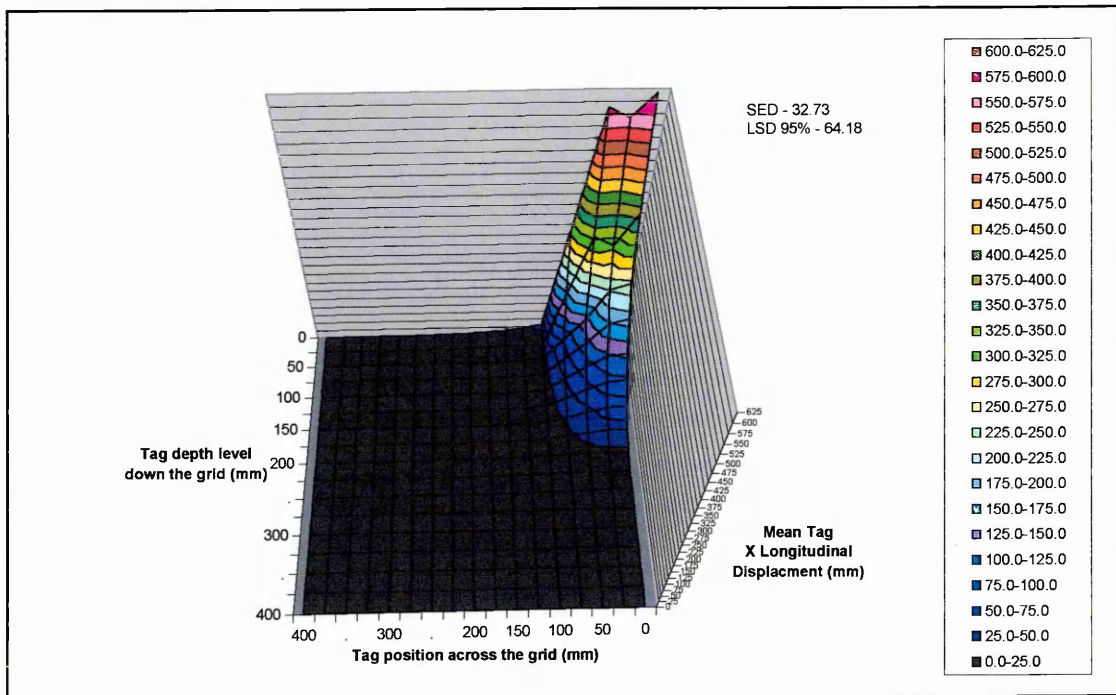


Figure 9.5 – Mean tag displacements in the X direction across the grid for all tyre treads and slips (as viewed from beneath a tyre along the line of travel)

The mean displacement within the identified region (150 mm x 250 mm) was all rearwards and reduced in a parabolic fashion as depth increased. The displacements were of high magnitude for the three tag positions directly under the tread (0, 25 and 50 mm across). The magnitude of displacement was reasonably consistent between these three positions at each of the depth layers, but the displacement rapidly reduced to less than 40 mm at positions more than 100 mm across from the wheel centre line.

The results also indicated that the amount of slip significantly affected the magnitudes and locations of the sand displacements. Figure 9.6 showed the relationships between slip, tag position across the grid and mean sand displacement. Within the 150 mm band noted above (directly under the tyre), higher slip produced higher rearward displacements, such that the mean displacements across all treatments for tag positions 1, 2 and 3 were approximately 300 mm at high slip, but these reduced to 125 mm at medium slip and 75 mm at low slip.

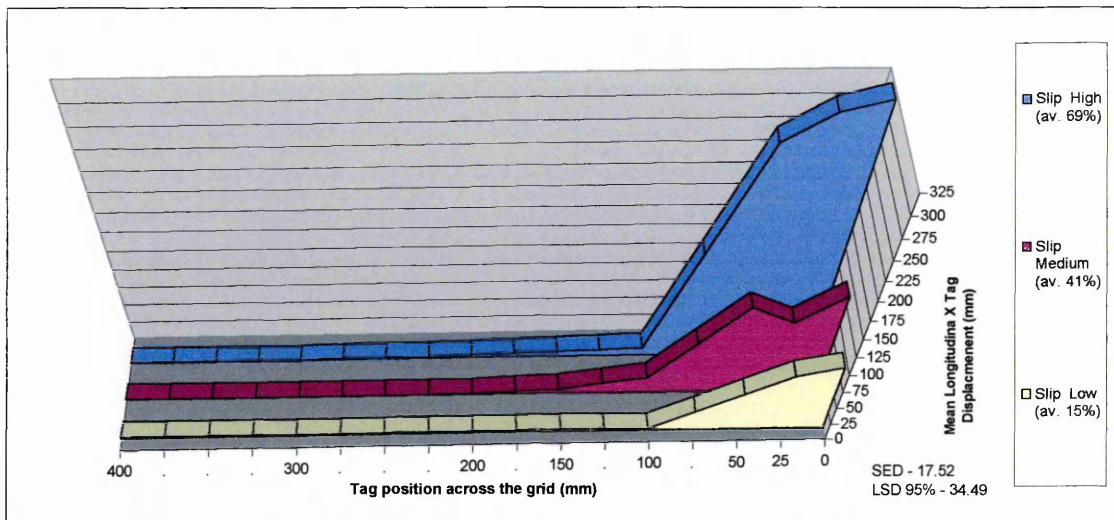


Figure 9.6 – Mean tag displacements in the X direction for tag positions across the grid for all treads at the three levels of slip (again viewed from beneath a tyre along the line of travel)

Figure 9.7 displays how the rearward sand displacements varied with both the slip and tag depth level down the grid. The displacement pattern was distributed such that at all of the slips, the displacements typically reduced in a parabolic manner as depth increased. Again the higher displacements were achieved at higher wheel slips, although this effect only extended 200 mm down from the surface, below which no significant variation in displacement was experienced. The variations between the displacements at low and medium slips were only significant at the surface, but the displacements caused by the high slips were all significantly different from the other two slip treatments down to the 200 mm cut-off.

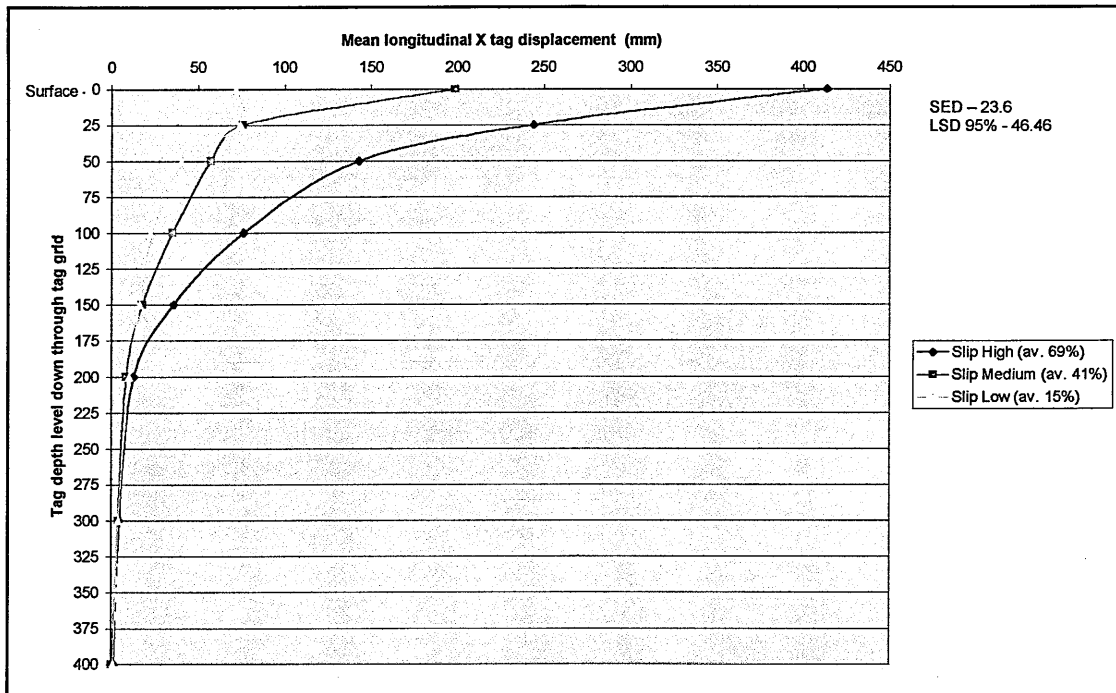


Figure 9.7 – Mean tag displacements in the X direction for tag depth levels down the grid for all treads at the three levels of slip (side view)

Figure 9.8 compared the differences between the rearward sand displacements caused by the six treads. In this instance the displacements were averaged across the three slip conditions to produce mean results. In all cases the displacements again occurred within the 150 mm x 250 mm region noted above, although the majority of the displacements occurred within a 100 mm x 200 mm region. However, closer analysis revealed that the significant variations in the displacements that occurred between the treads were actually confined within the top 100 mm x 100 mm portion of this area, located directly under the tyre, where direct contact with the sand occurred. Within this 100 mm x 100 mm region (hereafter termed the Region of Direct Contact, or RDC) all of the treads produced their maximum displacements at the surface, and as the depth in the profile increased all of the displacements again reduced in parabolic manner.

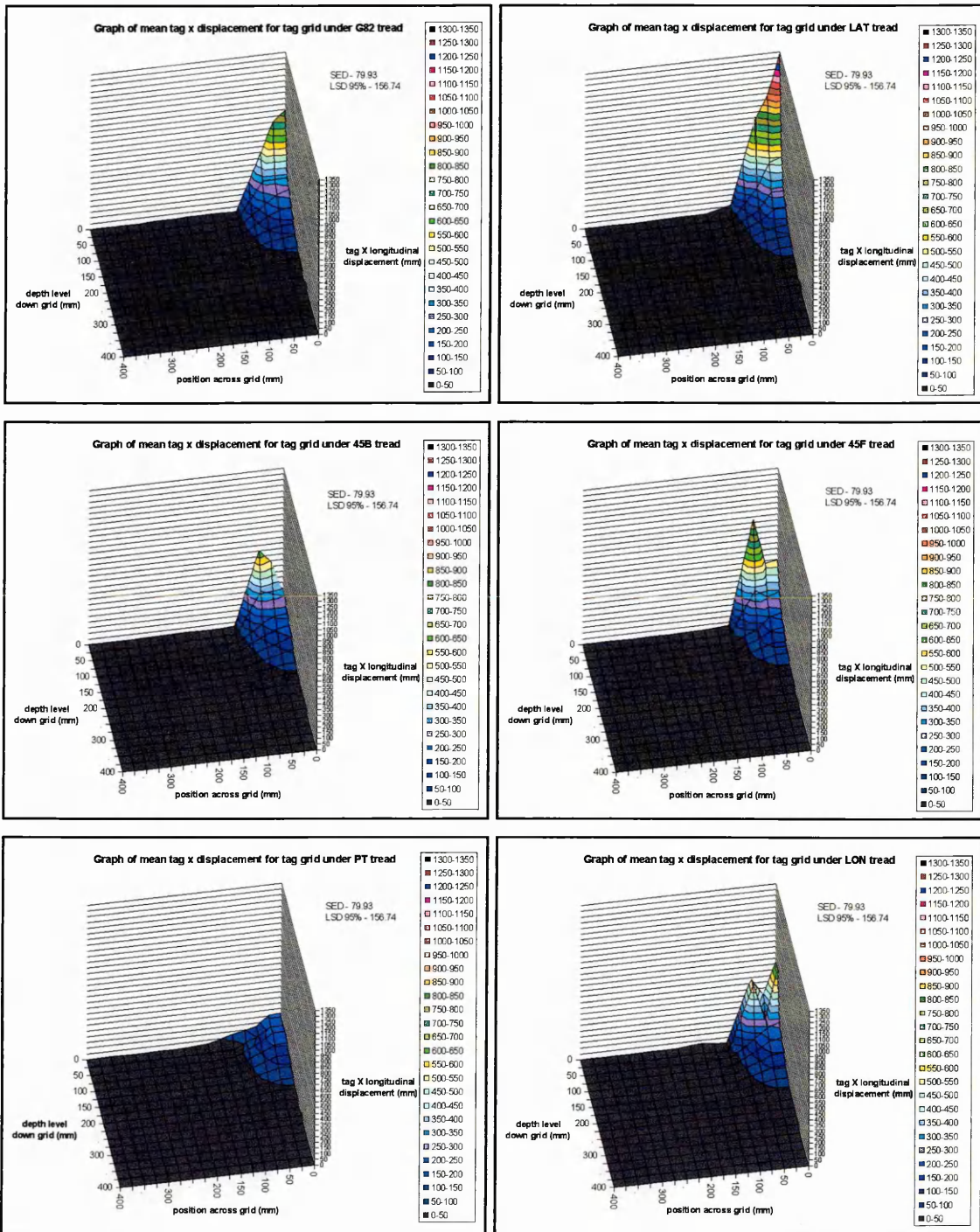


Figure 9.8 – Smoothed mean tag displacements in the X direction for all the grid locations and slips to allow comparison between the six treads (same viewpoint as previous figures)

The data in Figure 9.8 indicated that the PT tread exhibited the lowest displacements, achieving a peak mean rearward displacement of 250 mm within the RDC. The other treads all exhibited larger, but differing displacements within the RDC. To more closely

analyse the relationship between the tread types and mean rearwards displacements, the mean displacement pattern produced by the PT was used as a base value that occurred due to the test treatments and conditions. Thus any displacement in the RDC in excess of 250 mm (PT) was due to each tyre's individual tread features. As part of this process the graphs in Figure 9.8 were grouped in the same three tread pairs identified in Table 9.3 (G82 and LAT, 45B and 45F, LON and PT).

The LAT tread generated the most rearwards disturbance, due to its 'paddle' type tread, and the G82 tread caused similar displacement patterns, but of a slightly lower magnitude. For both these treads the peak displacements occurred directly under the wheel centre line and they reduced as the distance from this point increased. In contrast, the 45B and 45F treads exhibited their peak displacements 50 mm across from the centre line, whilst they displayed reduced displacements directly under the centre line. The LON was the treaded tyre that exhibited the least amount of displacement, with a displacement pattern similar to the pattern of the 45F tread. Although the locations of the peak displacements varied across the surface, all of the displacement patterns decayed in the same exponential manner as the depth in the profile increased.

9.2.4 Lateral (Y-axis) Displacements

In terms of Y displacements (note: positive Y displacement = movement away from the tyre centre line) tread was not a significant factor by itself; however, it became significant when it was considered in combination with each of the other factors e.g. wheel slip, tag position (*across the grid*), and tag position (*down the grid*), each of which was individually very significant (F pr. <0.001). Thus, variation in Y displacement was more closely linked to these other test factors, rather than the tread. Figure 9.9 shows the variations in the mean sand displacements due to the grid positions for all of the tests. The coloured regions of the following two-dimensional (surface) plots indicate the magnitude of mean displacement experienced by the sand in that region, for instance in Figure 9.9 the sand located 50 mm across and 50 mm down was displaced between 7.5 mm and 15 mm towards the tyre centre line (i.e. in the negative Y direction).

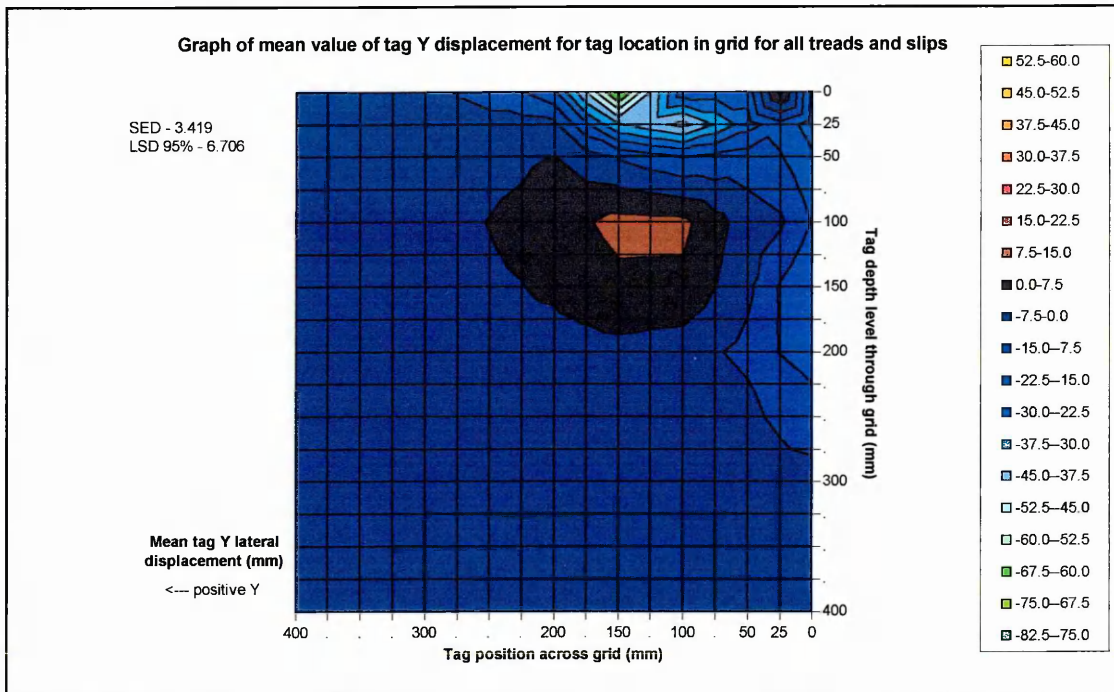


Figure 9.9 – A two-dimensional plot of mean tag displacements in the Y direction for all grid locations, treads and slips (viewed along the direction of wheel travel)

Figure 9.9 showed that nearly all of the displacements in the Y direction were contained within a portion of sand that extended 275 mm across from the tyre centre line and 275 mm down from the sand surface. It also highlighted that the sand originally located from 0 mm to 100 mm from the tyre centre line and up to 275 mm deep typically finished up being displaced towards the tyre centre line by around 20 mm (up to 275 mm deep). The sand in the top 50 mm (0 mm to 50 mm layer) of sand located between 100 and 150 mm across from the centre line was also displaced towards the tyre centre line, but these displacements were much larger (approximately 75 mm). The top 25 mm layer of sand located between 150 mm and 200 mm across from the centre line also experienced displacement towards the centre line. In contrast, the sand located between 100 mm and 150 mm deep and between 100 mm and 150 mm across from the tyre centre line experienced small movements away from the centre line.

Again the slip significantly altered the magnitudes of sand displacement, as Figure 9.10 demonstrated, although the patterns of displacement that occurred at each slip remained similar to the trends noted above. These were such that within the lower layers of the sand located between 0 mm and 100 mm across from the tyre centre line, about 20 mm

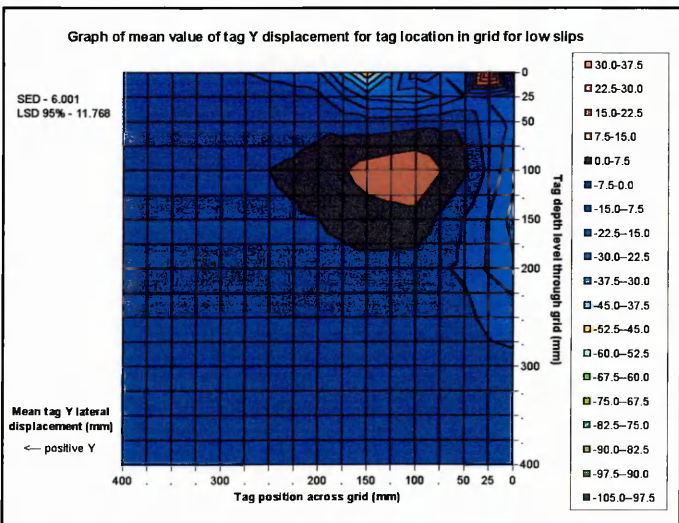
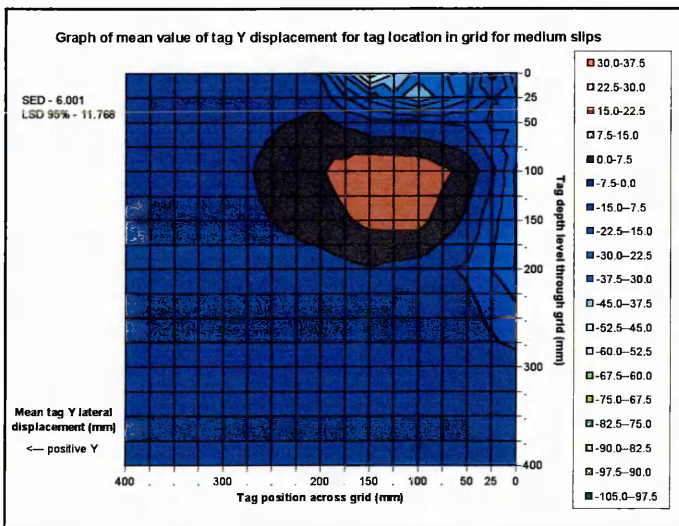
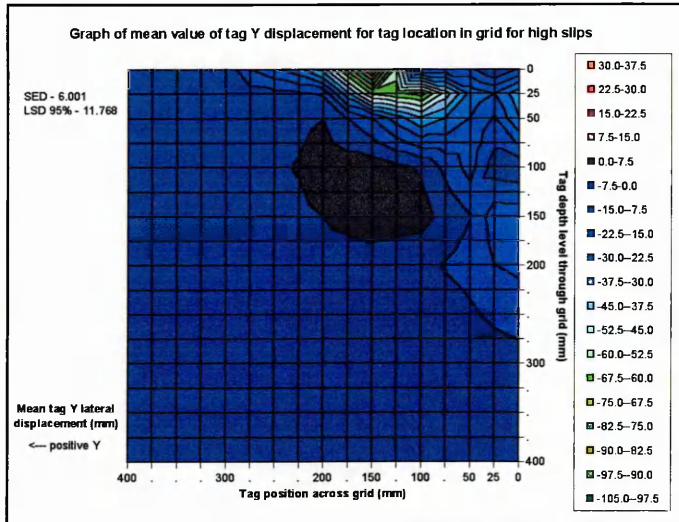


Figure 9.10 – Two-dimensional plots of mean tag displacements in the Y direction for all grid locations and treads at the three slips (viewed along direction of travel)

of negative sand displacement (movement away from the tyre) was experienced. The size of the displacements became increased as proximity to the surface increased. Their magnitude also increased as the distance from the tyre centre line increased, up to 150 mm from the centre line. They then decreased until the 275 mm horizontal boundary was met. These displacements were all predominantly towards the tyre.

The displacement patterns at low and medium slips were both similar, except at the medium slip, as the magnitude of displacement that occurred over the surface layers increased. Differences of a greater significance arose at the high slips. These variations were concentrated in the sand regions between 100 mm and 150 mm from the centre line, where as slip increased, the displacement grew from approximately 50 mm to 100 mm.

To compare the variations in displacement caused by the treads, the results were once again paired into the same three tread sets. The results, shown in Figure 9.11, indicated that the only significant differences between the treads occurred in the 0 mm to 50 mm deep and the 0 mm to 100 mm wide portion of sand directly under the tyres. Outside this region the displacements were consistent with the overall patterns outlined above.

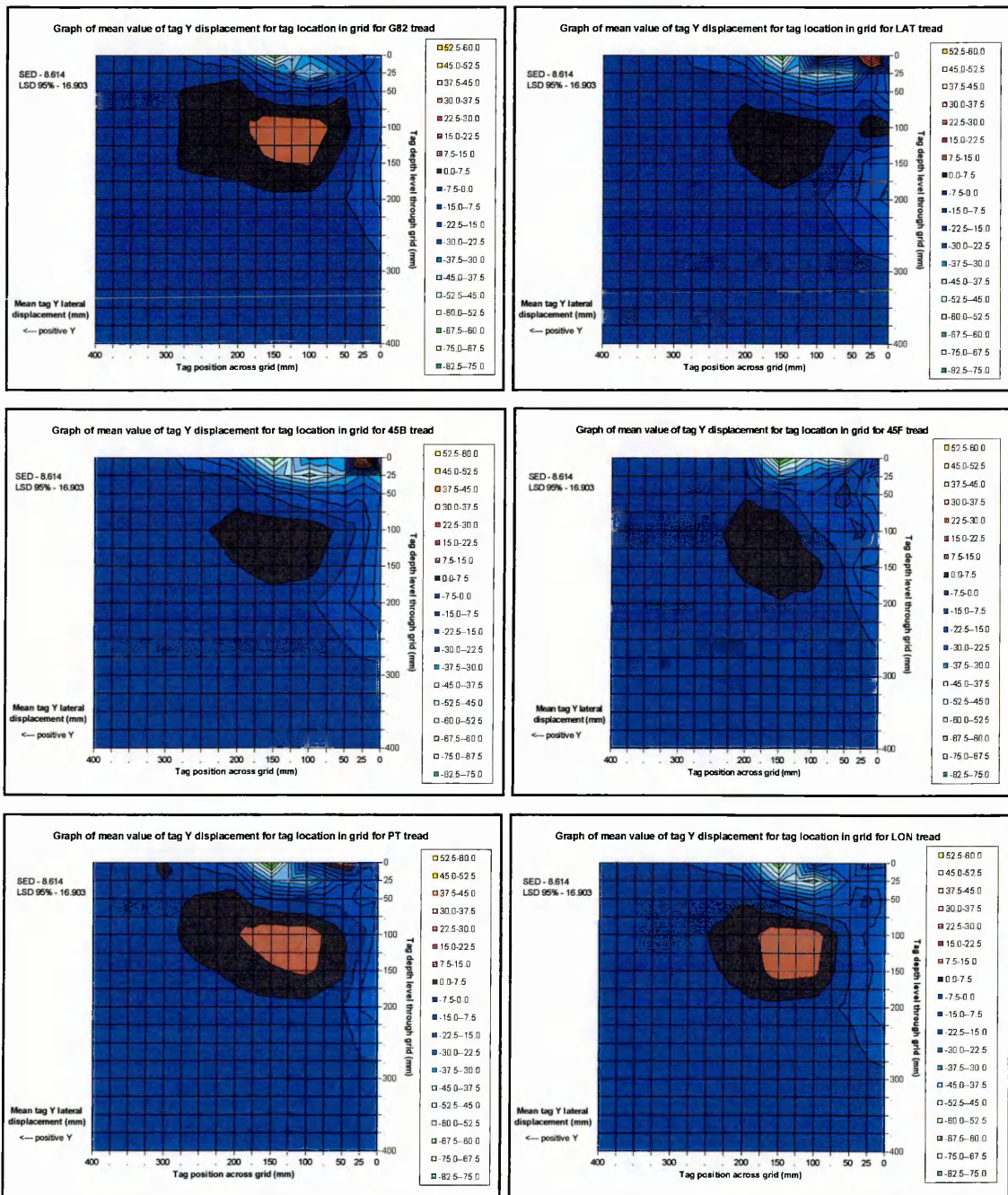


Figure 9.11 – Two-dimensional plots of mean tag displacements in the Y direction for all grid locations and slips for the six treads (viewed along direction of travel)

Again the treads only caused differing disturbances over the portions of sand with which they had direct contact. Although the different treads caused different displacements within the 50 mm wide x 100 mm deep region of sand, the limited number of results recorded within this region did not allow any patterns to be determined. Also, in reality the differences in the displacements were only of small magnitudes (being between 20 mm and 30 mm). Thus it was the tyre carcass that was responsible for most of the Y displacements, i.e. those that were common between treads, whilst the tread only had a minor influence over the variations in the Y displacement and these were concentrated in the sand closest to the tyre.

9.2.5 Vertical (Z-axis) Displacements

The same factors were significant for the Z (vertical movement) analysis as had been for the Y analysis, i.e. wheel slip, and tag vertical and horizontal tag position (all F pr. <0.001). Again tread was only significant when considered in combination with the other factors (F pr. <0.001 to 0.034). Figure 9.12 indicated that the displacements in the X direction were also limited within the same 275 mm x 275 mm region of sand. The downward displacements from the surface in the sand located between 125 mm and 200 mm across from the tyre centre line occurred because of the sand flow effects explained in section 9.2.4, where the most significant sand flows were those from this region which moved back towards the tyre. Contrastingly the sand in the lower layers of this band of sand was forced to rise slightly as the tyre load caused a crescent shear failure across the cross-section of sand. This upward displacement added further impetus to the later failure of the sand back into the void left by the tyre, which was highlighted the Y and Z displacement results.

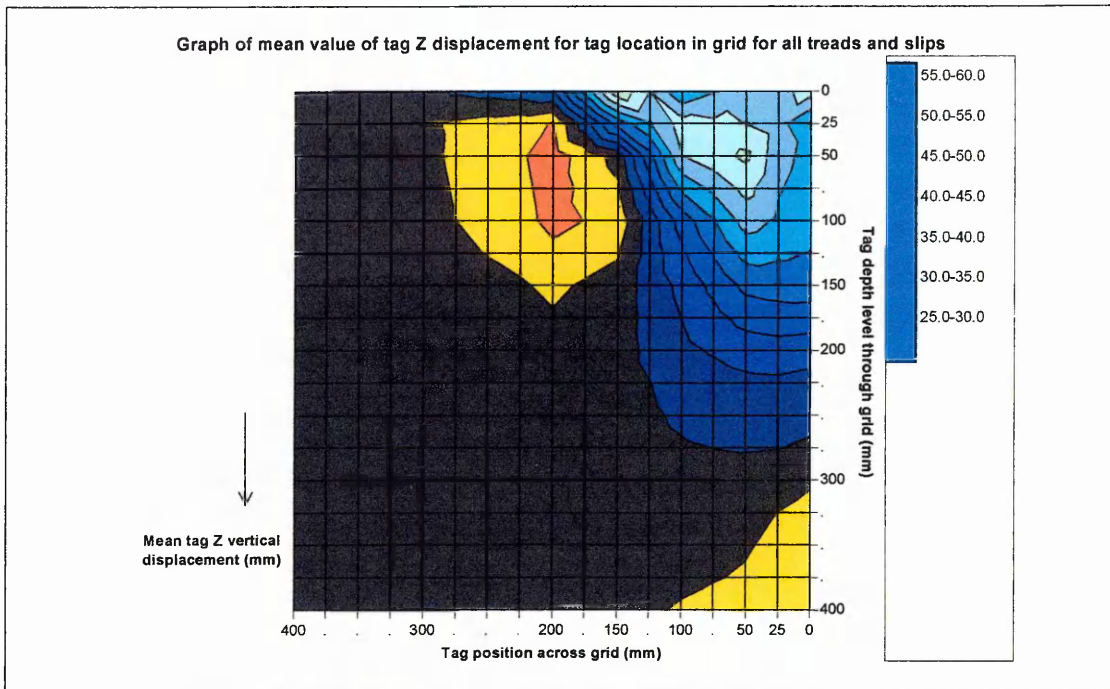
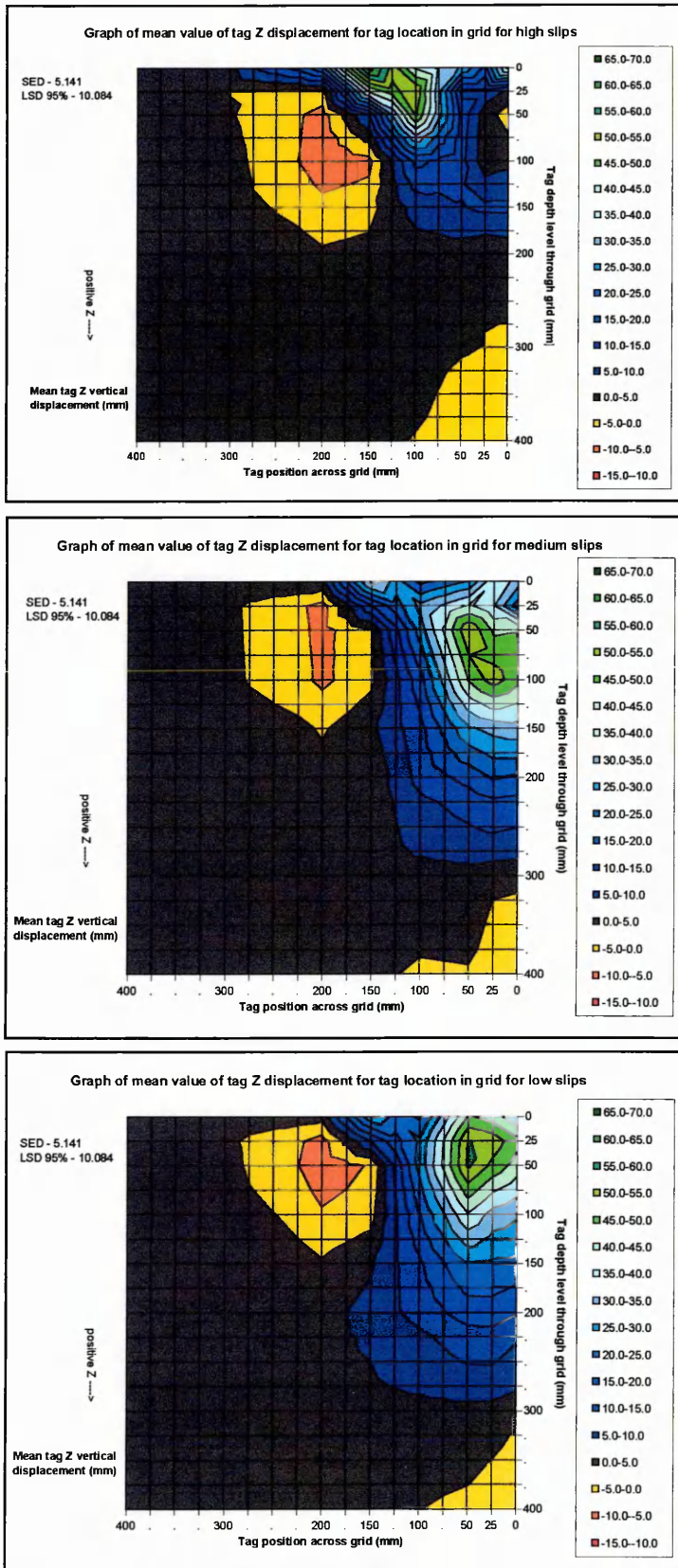


Figure 9.12 – A two-dimensional plot of mean tag displacements in the Z direction for all grid locations, treads and slips (viewed along the direction of wheel travel)

In the portion of sand directly beneath the tyre (0 mm to 100 mm across from the centre line) the displacement effects were different. In this region the compressive forces from the tyres caused all the sand to undergo downward displacements of a magnitude that was equal across each profile layer, but which reduced in magnitude in a parabolic manner as the depth in the profile increased. In this direction (vertical) the accuracy of the tag measurement apparatus diminished slightly at the furthest measurement extremes, which resulted in slight sand displacements (up to ± 6 mm) being recorded close to the boundaries of the plots that were not caused by the tyres.

Figure 9.13 indicated that increased wheel slip also significantly increased the Z displacements, but as with the Y displacement results, extra slip increased the magnitude, and not the pattern, of sand disturbance. Thus when the slip increased from low to medium levels the upper layers of sand (tags) still underwent downward displacements, but these displacements were of a reduced magnitude.



At high slips the pattern of displacement changed even more significantly, as even lower downward sand displacements were caused, and consequently the depths to which these movements were experienced reduced considerably (although this was partially caused by the minimum tyre sinkage that occurred at this point in the thrust cycle). Therefore because the displacements changed and became increasingly rearward as the wheel slip increased, the magnitude of downward displacement that was experienced consequently reduced to compensate for this change in direction.

Figure 9.14 shows the effect of tread upon displacement. Again it was the tyre carcass (body) that caused most of the disturbance, so therefore the tread effect was limited.

Figure 9.13 – Two-dimensional plots of mean tag displacements in the Z direction for all grid locations and treads at the three slips (viewed along direction of travel)

The variation in displacement caused by the tread again only occurred in the region of sand with closest contact to the tyre (the same 100 mm x 100 mm of sand noted earlier). The tread did not alter the pattern of displacement in this region, as it only influenced the magnitudes of the disturbances. However, again the limited amount of variation in displacement meant that no patterns could be determined amongst the treads.

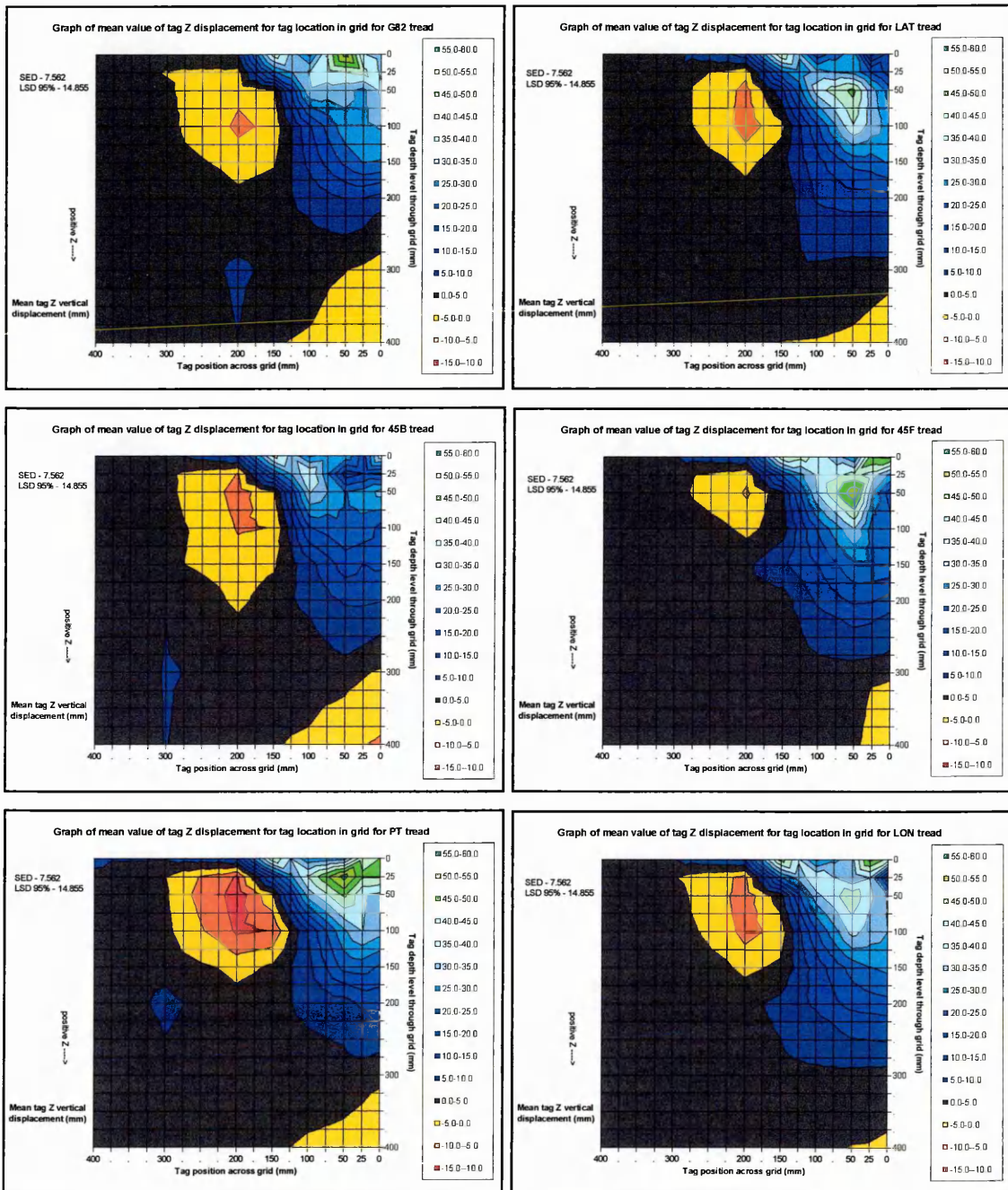


Figure 9.14 – Two-dimensional plots of mean tag displacements in the Z direction for all grid locations and slips for the six treads (viewed along direction of travel)

9.2.6 Peak Net Thrusts

Figure 9.15 shows both the mean net thrusts, and the associated mean values of slip and deflected sinkage at which they occurred. This data shows the mean values for each tread and variable (i.e. slip). These were calculated by taking the means of the results produced as all the peak thrusts produced during the thrust/ slip cycles were generated (typically over ten cycles). These were averaged across all three replicate test runs that were conducted for each tread. The peak net thrusts generated occurred out of phase to when the tag displacements and other associated values considered so far were recorded, thus they have been calculated separately.

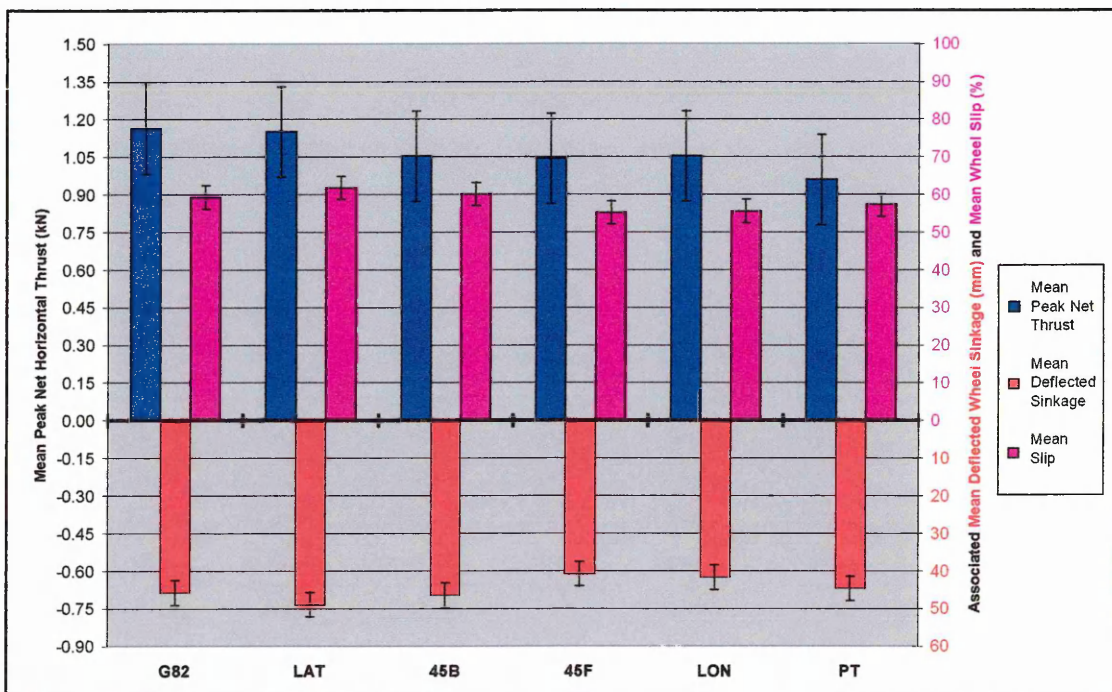


Figure 9.15 – Mean net thrusts derived from the three replicate tests of each tread, and associated mean values of slip and sinkage that occurred simultaneously

No significant difference existed between the mean peak net thrusts that were recorded, as the LSD's of the results were greater than the differences between them, therefore all the treads were potentially capable of generating the same peak net thrusts. However, these results only consider a single moment in the thrust cycle, and thus they do not convey the relationships noted from the more comprehensive analysis above, which showed that different treads produced greater (or lesser) envelopes of positive net thrust during a particular test run. Although the trends were not significant, it was again noted

that the thrusts produced placed the treads into the same ranked pairs that were noted previously in Table 9.3. These results also only consider the net thrusts, not the actual gross thrusts produced by the treads.

The majority of the differences between the treads in terms of the slip and sinkage at which they operated were not significant. However, the lowest mean slip at which peak thrust occurred was noted as the 45F tread. This tread also operated at a reduced sinkage compared to the other treads. It is likely that the reduced slip was partially caused because slightly less sand was being excavated from beneath the tyre as the slip was reduced, but the magnitude of this effect was limited. Although the results were not generally significant between the treads, trends still existed within the results that showed agreement with those noted in Table 9.1.

9.3 ROLLING RESISTANCE TESTS

A number of rolling resistance tests were conducted at different stages of the project using 235/70 R16 tyres with a range of treads, including the six prototype treads. These were all conducted at inflation pressures between 1.10 and 1.38 bar. In total 37 test runs were conducted using both test rigs upon the replicate sand, in both the sand tank and the full soil bin. The sinkage was adjusted by applying different normal loads.

The resistances recorded were averaged across periods of each individual run where a continuous magnitude of sinkage was experienced, and 137 mean values of resistance (and corresponding sinkages) were derived. As expected, the results showed a strong correlation between wheel sinkage and rolling resistance. When plotted these results took the form shown in Figure 9.16 and the trendline plotted through the data took the form of equation 52.

$$Y = 0.0004x^2 - 0.0106 \quad (52)$$

Where: Y = Rolling resistance x = sinkage (described as negative)

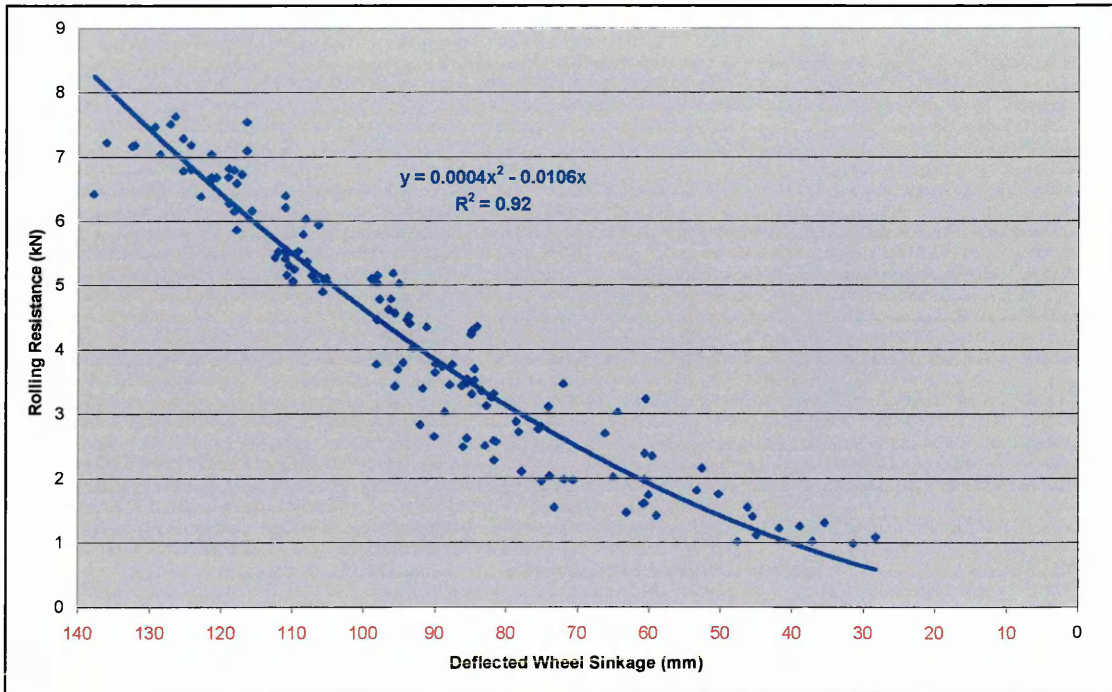


Figure 9.16 – The relationship between deflected wheel sinkage and rolling resistance across all treatments on sand

9.4 SUMMARY OF THE RESULTS

9.4.1 Combined Sand Displacements

The size of the regions of the sand profile in which the sand disturbances that occurred were experienced are summarised in Figure 9.17. This also details the directions in which the displacements noted in each region occurred. It should be remembered that these effects were also duplicated on the other side of the tyre. In the region of direct contact (RDC) the displacements occurred in all three directions (X, Y and Z), but the patterns were unclear as the limited number of data points and the close contact between the sand and the tyre tread blurred the differences between the significant displacements.

The displacement patterns suggested that the positive lateral (Y) displacements noted in the sand region between approximately 100 mm and 150 mm from the tyre centre line and 100 mm to 200mm deep in the middle of the sand profile were caused by the bow wave effect that pushed through the profile ahead of the tyre, thereby forcing the sand

outwards. However, this effect resulted in a minimal displacement, as it was only short lived because the tyre passed quickly forwards.

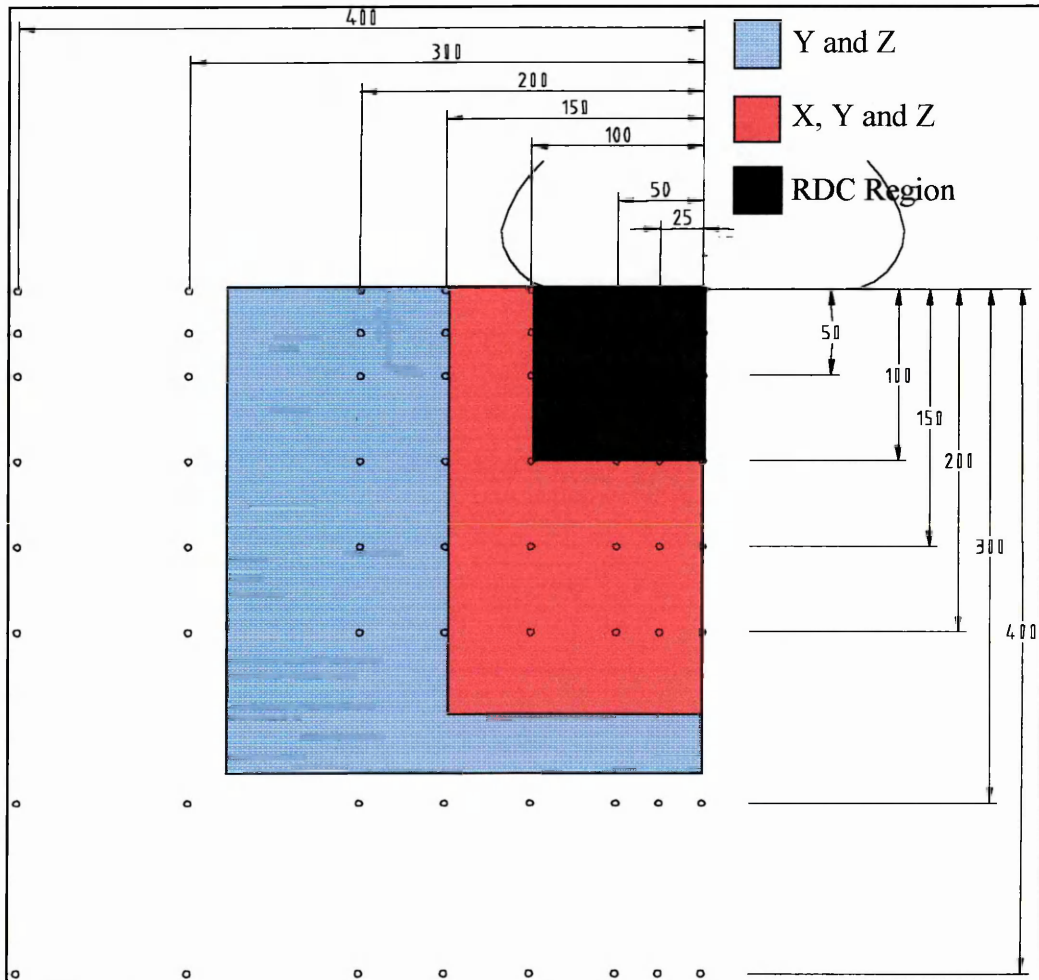


Figure 9.17 – The different sand profile displacement patterns that occurred

As each tyre drove itself forwards it simultaneously forced a large quantity of sand rearwards (as the X displacement results demonstrated). This rearward movement created a void in the sand, alongside which an inherently unstable sandbank (located in columns 100, 150 and 200 mm) was formed. As the tyre subsequently moved forwards this bank failed and fell back towards the tyre centre line, causing the main lateral (Y) displacement patterns. Figure 9.18 illustrates this effect, where lines have been included to indicate the depth of the tyres when they struck the tags for each slip treatment. These lines have been extended to indicate the typical shear planes that were formed through the sand bank.

This figure has been adjusted to account for the different magnitudes of rearward sand displacement that were achieved at each of the slip levels, as well as the depth at which the tyre was operating. For example, when high slips occurred the tyres were operating at low sinkages, but when the quantity of rearward sand displacement noted by the X displacement results was also considered, the rut left by the tyre was considerably greater.

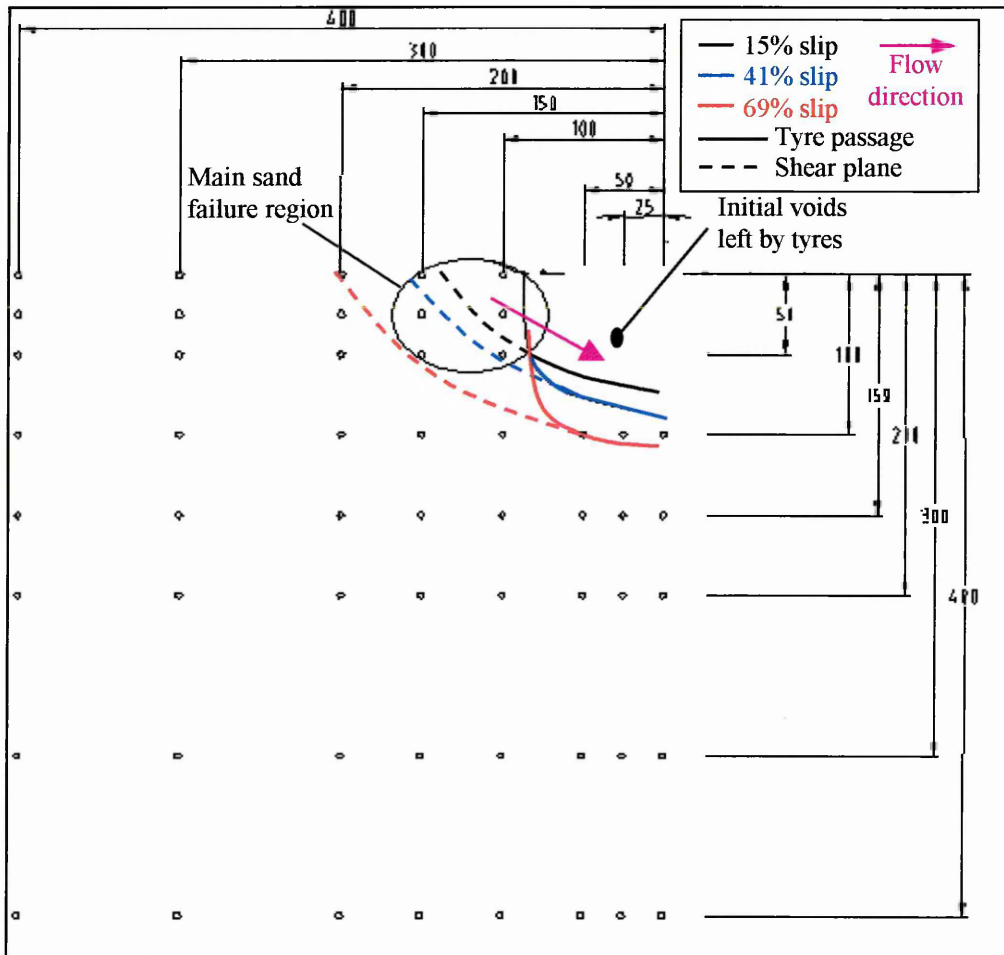


Figure 9.18 – A diagram showing how slip governed the void size left by the tyre and hence the sand's Y displacement as it re-filled the void.

The magnitudes of the different rearward displacements generated at the different slip treatments greatly influenced the rut recovery effect, particularly at high slips, when it significantly reduced the size of the void left behind by the tyre. Thus in all cases the void remaining behind the tyre was always greatly influenced by the magnitude of slip

(rut recovery) occurring directly ahead of it. These effects were also considered when Figure 9.18 was constructed.

Additionally the vertical (Z) displacement results indicated that the mean depths at which the sand was left after traction were higher than the sinkages at which the tyres operated at each considered point in the thrust cycle. This was partially due to the rut recovery effect that occurred, due to sand displacement in the longitudinal (X) direction, which replaced some of the sand in the void left behind the slipping (excavating) tyre. It was also partially due to sand moving into the tyre void as the sand alongside the rut failed. These combined effects meant that the sand from the top layers of the profile (0 mm to 50 mm deep) became mixed as it moved either rearward or sideward and the volume increased, which meant that the surface layers finished their displacement at a position that was above the lower sinkage to which they had been forced whilst producing traction.

9.4.2 Tread Effects

The tread effect in both the lateral (Y) and vertical (Z) displacement directions all occurred within the RDC region. Whilst differences did occur between the treads these affected only small quantities of sand, such that in both directions the effects of any variations were small, and the limited number of tags located in this region produced insufficient data to allow any precise trends to be determined. Contrastingly the tread pattern significantly affected the mean longitudinal (X) displacements across all the treads and with a much greater magnitude. The PT produced the minimum displacement in this direction, which was taken as the 'base' displacement caused by the tyre. The other treads all produced similar patterns of displacement, although the magnitude of these varied significantly depending upon the tread pattern, whilst all of the variation in magnitude occurred in the RDC.

As the tyre tread only very significantly affected both the net thrusts that were produced by the treads and the longitudinal (X) displacements noted in the RDC, then the net thrust variations produced by the treads must be dependant upon the magnitude of rearward sand displacement. This could have affected either (or both) the gross thrust or

the rolling resistance produced by the tread, but these effects were not considered until section 10, as neither factor was directly measured during this section of the investigation. Therefore to allow the relationships between the different effects that were noted between the treads to be better understood the results have been summarised in Table 9.4. This has sought to generalise all of the results that have been presented, by taking the trends indicated by the majority of the results, rather than concentrating upon specific isolated results. The effects of these trends is also considered in section 10.

Table 9.4 – The tractive performance trends produced by the different treads

Treads	Net Thrust	Wheel Slip	Wheel Sinkage <i>Only significant at max. sinkage</i>	Rearward sand displacements
G82 & LAT	Greatest extremes i.e. greatest positive peak thrusts and greatest negative peak thrusts	Operated at higher slips (typically median+2.5%)	Trend towards greater sinkages	Greatest mean displacements (over 900 mm peak)
45F & 45B	Median +ve & -ve thrusts	Median slips	Median sinkages	Median displacements
LON & PT	Least extremes i.e. lowest maximum thrusts and least negative peak thrusts	Operated at lower slips (typically median -2.5%)	Trend towards smaller sinkages	Lowest mean displacements (below 600 mm peak)

9.4.3 Tyre Body (Carcass) Effects

The tread effect was only minor compared to that produced by the main body (construction) of the tyre (i.e. the PT tyre) and particularly the slip had a very large impact on the results. The common tyre factors (i.e. the size and construction) were responsible for producing the basic levels of performance, and therefore most of the displacement patterns shown in Figure 9.17. The typical displacements experienced were caused by sand being driven rearwards from directly beneath the tyre, however, this effect only occurred within the red region shown on Figure 9.17. The displacements in the lateral (Y) and longitudinal (Z) directions, which occurred consistently

irrespective of the tread pattern, affected a much greater region of the sand. In the central region of the sand profile (between 100 mm and 200 mm on both axes) the sand was pushed slightly upwards and laterally away from the tyre by a combination of the bow-wave and shear failure effects. In contrast, directly underneath the tyre, below 150 mm deep, the traction forces simply forced the sand downwards and slightly laterally inwards toward the tyre centre line as it was sheared to generate traction.

The sand in the surface layers that bordered the tyre rut underwent much greater magnitudes of lateral flow towards the tyre, with a downwards element, as the sand failed into the void left by the rearwards, and upwards, displacement of sand from the RDC by the slipping tyre. The sand displacements along all three axes were shown to be closely inter-related, such that an increase in displacement in one direction normally caused a reduction in displacement along a different axis. However, these basic relationships were greatly influenced by the slip at which the tyre was operated. In particular, increased slip caused the sand displacement to change from being downwards and rearwards to being mostly rearwards. Simultaneously the greater slip disturbed a greater volume of sand, which left greater voids behind each tyre, which resulted in greater lateral sand flow back into the void due to sand failure.

10 MODELLING OF SAND – TYRE INTERACTION

The modelling was conducted to relate the tyre tread, sand flow and tyre performance, to produce a predictive performance tool. This process used measured results from the experimental tests that were undertaken and applied these in combination with Bekker's prediction methods. His work, and other useful related work, was outlined in section 3.5.3. Most of the equations listed in section 3.5.3 (8 to 17 and 36 to 49) were used during this modelling, although they were adapted and developed to improve the accuracy of prediction for the sand environment.

10.1 VARIABLES REQUIRING TRACTION MODELLING

The modelling sought to relate the quantity of sand flow produced by a tyre to the tread pattern and from knowledge of the quantity of sand flow produced, as well as the tyre size, tread pattern and sinkage, predict the net thrust that the tyre (and tread) would generate. Thus modelling had to account for a number of different variables:

1. Tyre characteristics, particularly size, construction, inflation pressure and most importantly the tread features.
2. The quantity of sand flow produced by the tyres, which was linked to the tread features, wheel slip and wheel sinkage.
3. The net thrust produced by the tyres. This was derived by two elements that required modelling separately:
 - a. Gross Thrust
 - b. Rolling Resistance

These elements were determined using Bekker's prediction methods, although the author customised these to suit this situation.

4. Gross thrust was modelled using an adaptation of equation 12 (page 40).
5. Rolling resistance was modelled using the methodology detailed in section 3.5.3.9.

Where possible actual values of the relevant variables recorded during the tests were used in the models to produce more accurate outputs.

10.2 MODEL FORMATION

Complete details of the full Excel representations of the following proposed models are presented in Appendix 24.

10.2.1 Gross Thrust

The modelling of the gross thrust was based upon equation 12

$$P = F \left[1 + \frac{K}{il} \left(e^{-\frac{l}{K}} - 1 \right) \right] \quad (12)$$

Where:	K = soil deformation modulus	i = slip (%)
	l = shear (contact) length (m)	$F = (Ac + W \tan \phi)$ (kN/m ²)
	A = contact area (m ²)	c = cohesion (kN/m ²)
	W = vertical axle load ~ (kN)	ϕ = soil internal friction angle (°)

The values of K , c and ϕ derived in section 5 were used to represent the traction surface. Different values were used for sand or soil. Values of slip used for the model were taken from the test results. If the tests had produced consistent (not cyclical) results, then W , l and A would have been constants. As the testing had produced considerable vertical accelerations, the model had to properly account for these dynamic variations and the three inter-related effects they had on the traction variables.

All of the test runs were assessed to examine the vertical acceleration behaviour. This was derived from the deflected sinkage (accounting for tyre deflection that was recorded by the drawstring transducers). Plotting the acceleration against time produced consistently cyclical relationships that peaked between +0.5g and -0.5g. This was equivalent to a dynamic load change of $\pm 50\%$, which was centred about the mean deflected wheel sinkage. The model was adapted such that the load W was replaced with W^D , which represented the dynamic load. This was equivalent to the static mass (m) multiplied by a vertical load adjustment factor g' , thus for the dynamic situation g' varied between 4.905 and 14.715 ($9.81 \times 1 \pm 0.5$). The following process determined the actual value used. All the sinkage data for a dynamic case was averaged to derive the

mean sinkage. The mean sinkage was then deducted from the actual sinkage to produce the ‘dynamic sinkage’, as demonstrated in Figure 10.1.

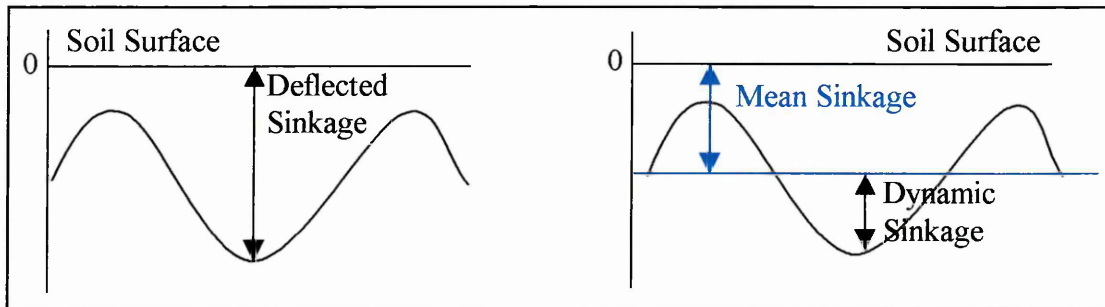


Figure 10.1 – The derivation of the dynamic deflected wheel sinkage

A spreadsheet was used to determine the maximum and minimum dynamic sinkages, which occurred simultaneously with the occurrence of the maximum and minimum loads. Thus the +50% and –50% load adjustment were applied respectively. The remaining dynamic sinkages that occurred between the peaks were awarded a proportionate value equivalent to the sinkage, i.e. if the maximum dynamic sinkage was +50 mm, then a dynamic sinkage of +25 mm was equated to +25% load increase. As the sinkage variations were consistently cyclical, this method was a simple, but sufficiently accurate method to derive this value. Had the variations not been consistent then this term would have been replaced by a differential calculation.

Contact lengths were derived from Oliver’s results³⁰. When placed on the sand with a static normal load of 650 kg, the typical contact length was 390 mm. To produce a useful dynamic relationship, measured contact lengths recorded over a test run were plotted against corresponding vertical accelerations (an equivalent representation of the dynamic normal load) that were calculated using the procedure outlined above. This procedure allowed the variations due to wheel slip and sinkage to be included when the contact lengths were determined. This process produced the relationship shown in Figure 10.2, which expressed contact length variations with acceleration, from which the expression of the trend line was used to represent the relationship between the variables. The equation of the trendline was re-arranged to form an identical mathematical representation, equation 53, which shows how the actual variables fitted into the equation.

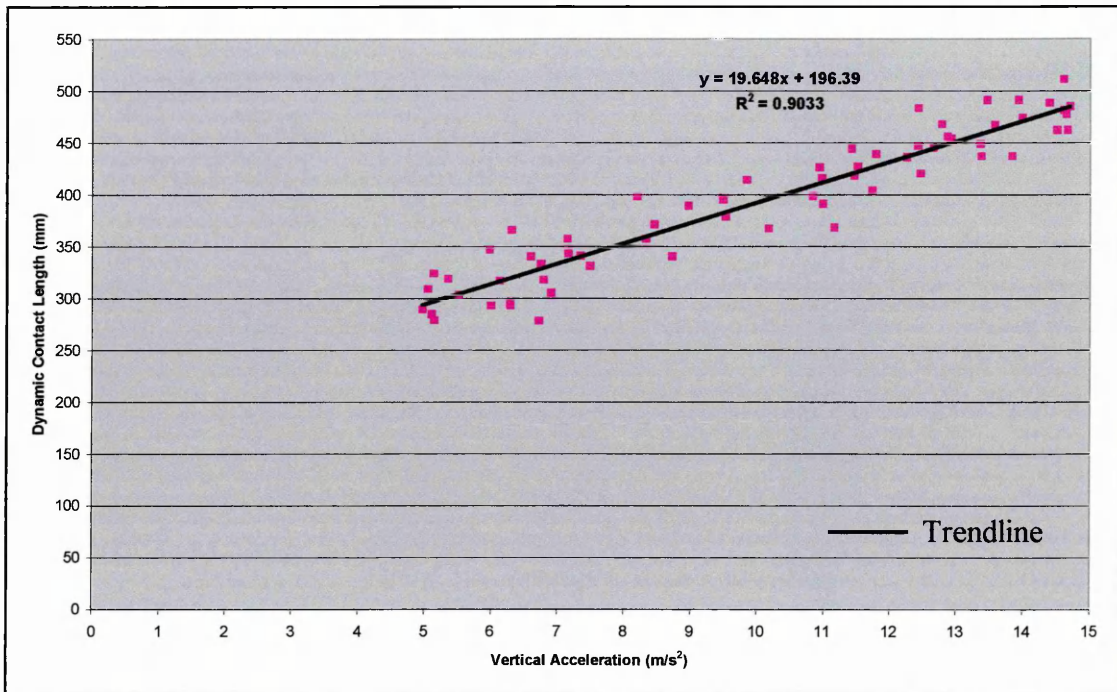


Figure 10.2 – The relationship between contact length and vertical tyre acceleration

$$l^D = \frac{l}{2} + 2g(g') \quad (53)$$

Where: l^D = dynamic contact length l = standard contact length (390 mm)
 g = vertical acceleration due to gravity (9.81 m/s²)
 g' = acting vertical acceleration ($g \pm 50\%$)

A similar process was then applied to determine the dynamic contact width, which was based on the standard tyre width of 235 mm. Contact width data was plotted against the calculated dynamic vertical accelerations to produce the relationship shown in Figure 10.3. Again the trendline produced by the data was used to develop a relationship that would use the calculated acting vertical acceleration to predict a dynamic contact width, which would account for slip and sinkage variations. The expression of the trend line was again used to develop an identical mathematical relationship between the considered variables, which took the form of equation 54.

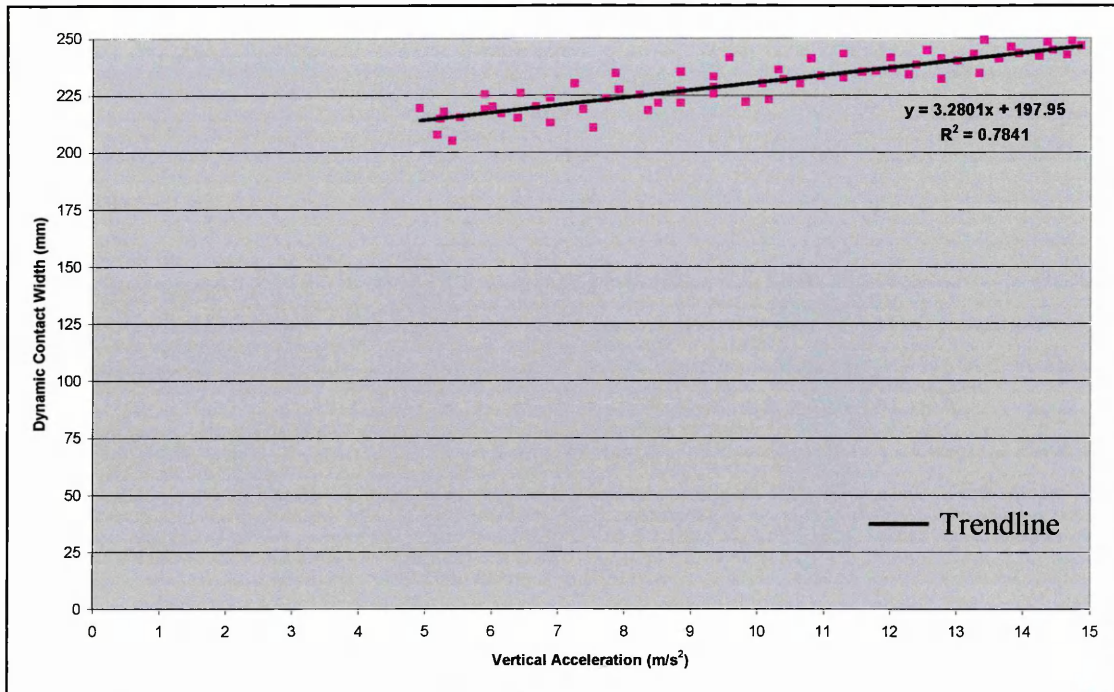


Figure 10.3 – The relationship between contact width and vertical tyre acceleration

$$w^D = \frac{6w}{7} + \frac{g}{3}(g') \quad (54)$$

Where: w^D = dynamic contact width w = tyre width (235 mm)
 g = vertical acceleration due to gravity (9.81 m/s²)
 g' = acting vertical acceleration ($g \pm 50\%$)

Therefore the gross thrust prediction was based upon equation 55.

$$GT = \left[1 + \left(\frac{T_f}{100} \right) \right] \left\{ \left(A^D c + W^D \tan \phi \right) \left[1 + \frac{K}{il^D} \left(e^{-\frac{l^D}{K}} - 1 \right) \right] \right\} \quad (55)$$

Where: A^D = dynamic contact area ($w^D \times l^D$) c = cohesion
 W^D = dynamic vertical axle load ($m \times g'$) i = slip
 ϕ = sand (soil) internal friction angle l^D = dynamic contact length
 K = soil deformation modulus T_f = tread factor

As the equations to calculate the value of K were dependent upon the size of the contact area to which they were related, a series of logic statements were added to the model so that the correct equation for K was always used. The tread factor term T_f was added to

the equation to allow a percentage increase in the thrust prediction to account for any variation in thrust produced by the tread designs, as the equation by itself accounted for a plain tread tyre. The value of this factor depended upon the gross thrust output produced by the tread. This was determined from the experimental results in a process that will be detailed subsequently.

10.2.2 Rolling Resistance

The calculation of the rolling resistance of the treads was determined by using the process detailed in equations 36 to 49 (section 3.5.3.9). The model was designed to automatically calculate the critical pressure and check the mode of operation (rigid or elastic). It then included the correct terms for the particular case. When inflated to 1.10 bar the tyre always operated elastically, but the inclusion of all the possible terms increased the model's flexibility to be used for other cases. The mode of operation governed the terms included in the calculation (see below).

Rigid mode:

R_c = Compaction resistance

R_b = Bulldozing resistance

Elastic mode:

R_c = Compaction resistance

R_b = Bulldozing resistance

R_f = Tyre carcass flexing resistance

The following equations are based upon Bekker's work, as noted above. However, because these were customised to suit this particular application, they are all fully detailed below, with the source and nature of the new terms that were introduced (or replaced) identified.

R_c – Compaction resistance

$$R_c = w^D \left(\frac{Z_{def}^{n+1}}{n+1} \right) \left(\frac{k_c}{w} + k_\phi \right) \quad (56)$$

Where: w^D = Dynamic contact width (equivalent to rut width)

Z_{def} = Recorded experimental deflected tyre sinkage

k_c , k_ϕ & n = empirically measured coefficients from plate sinkage tests

w = tyre width (equivalent to minimum plate dimension)

R_b – Bulldozing Resistance

This is analogous to passive earth pressure acting on a retaining wall. Bekker states that this can take either a General or Local form. It was found that the general expression (equations 38, 39 and 40) gave good agreement with the sand results, whereas when the model was applied to the loose soil environment the local force prediction (equations 41 to 44) gave considerably better agreement with the recorded results instead. Again the sinkage data used was the experimental deflected tyre sinkages recorded during each individual test run. The rut width (b_{tr}) generated by the tyre could only be measured after wheel passage. Measurements of the width of the tyre tracks were matched to the appropriate tyre contact width, as shown in Figure 10.4.

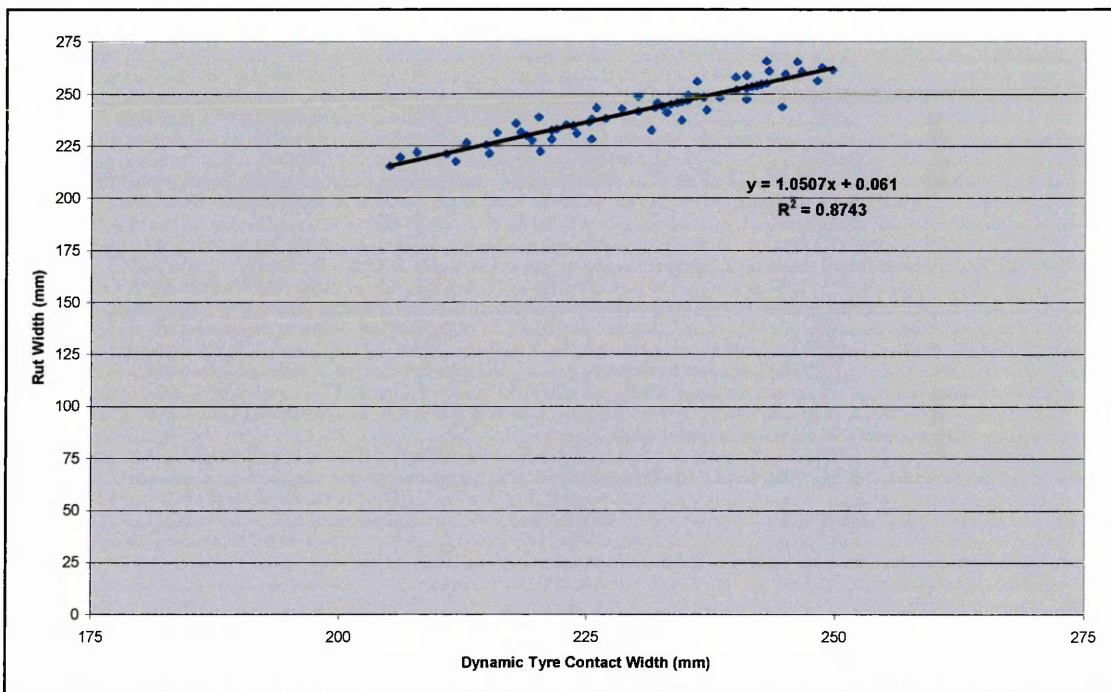


Figure 10.4 – The relationship between tyre contact width and rut width

The relationship produced between the two variables was approximated to produce equation 57, which was used in the modelling to again consider the dynamic effects.

$$b_{tr} = w^D \times 1.05 \quad (57)$$

R_f – Tyre Carcass Flexing Resistance

The expression shown as equation 46 was used in its original form to predict this extra resistance force. The correct tyre values were used in the model as appropriate i.e. tyre

diameter (735 mm) and section height (164.5 mm), and data from the actual test runs was included where appropriate. To prevent over-complication of this calculation an average tyre deflection of 40 mm was used in the calculation, as it was only a small force of approximately 0.2 kN, so this only introduced a small error into the calculation.

Net Thrust

Net thrust was derived from gross thrust minus rolling resistance.

10.2.3 Mathematical Description of the Tyre Treads

To allow the tyre tread to be modelled a mathematical description of the tread patterns was required, as no such model existed, the author developed one to suit this purpose. As the five treaded prototype tyres all shared identical tread/ void ratios, the model could not utilise different relatively sized areas of shear, so instead it was focused upon the features of the leading tread edge and the orientation of these to the longitudinal direction of travel. The expressions and coefficients used were developed on an iterative basis and included terms relative to the tread features. The expression developed took the following form (equation 58):

$$T_c = (0.8T_n + G_n + 0.2E_n) - 0.555 \quad (58)$$

Where: T_c = tread coefficient T_n = tread number (eq. 59)

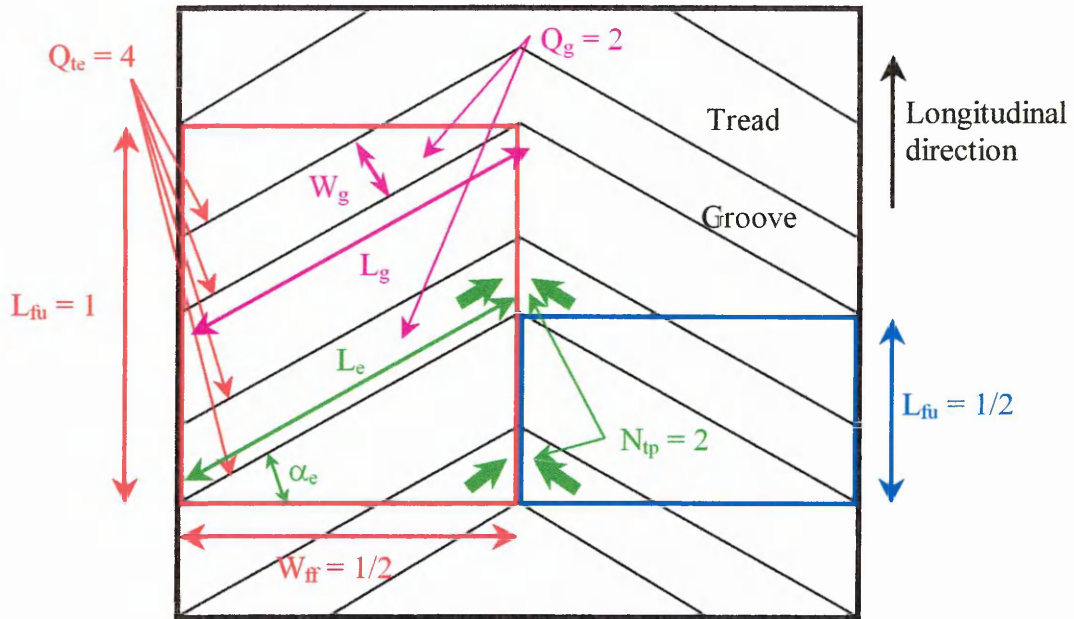
G_n = groove number (eq. 60) E_n = edge number (eq. 61)

To aid understanding of the following formulae, a basic tread pattern illustrating the location of each variable used in the equations is included in Figure 10.5. The variables have been colour coded to aid identification. When applying the equations grooves or sipes that were less than 5 mm wide were ignored and curved tread block faces were approximated to straight angular tread faces.

$$T_n = \ln(Q_{te} \times TV_r \times W_{ff} \times L_{fu}) \quad (59)$$

Where: Q_{te} = total number of groove edges TV_r = Tread: Void ratio

W_{ff} = fraction of full tread width L_{fu} = fraction of tread unit length



Simple tread, so $n = 1$ as only one groove type is present

Figure 10.5 – A typical tread pattern identified with the variables used to determine its tread coefficient

$$G_n = \left(\frac{\sum_0^n (W_g \times L_g \times Q_g) \times W_{ff} \times L_{fu}}{10000} \right) \quad (60)$$

Where: W_g = width of the groove type (mm)
 L_g = length of the groove type (mm)
 Q_g = total number of grooves of the groove type
 n = number of different groove types

$$E_n = \ln \left[1 + \left(\left[5N_{tp} + \left(\frac{\sum_0^n (L_e \sin \alpha_e \times Q_e)}{20} \right) \right] \times W_{ff} \times L_{fu} \right) \right] \quad (61)$$

Where: L_e = length of the groove edge (mm)
 α_e = angle of the groove edge (longitudinal = 0° , lateral = 90°)
 Q_e = total number of groove edge of the groove type
 n = number of different groove types
 $N_{tp} = \sum \text{positive flow points} - \sum \text{negative flow points}$

Note for equation 61: A positive flow point is a tread location where sand is forced together, i.e. the apex of a backward vee, whilst a negative flow point is where the tread forces sand apart, i.e. from one channel to two channels.

Equation 58 was applied to the five prototype treads used during the sand displacement experiment and it produced the tread coefficients shown in Table 10.1. Full details of this calculation are in Appendix 25.

Table 10.1 – Tread coefficients for the five prototype treads tested during the sand displacement experiment

Tread Type	Tread Coefficient
PT	0.00
LON	2.50
45F	4.64
45B	5.06
LAT	5.62

10.2.4 Calculation of the Volume of Sand Flow

It was necessary to calculate the volume of sand that had been displaced during the sand flow experiments from the recorded sand displacements. This process was simplified to include only longitudinal displacements, which had been related to gross thrust output. These were contained within the region of sand 100 mm across from the tyre centre and 200 mm down from the surface. This region encompassed four tag positions across the grid and six tag grid positions down the grid. Adjoining tag positions within this region were linked to form a series of rectangular grids, with a total area of three grids across by five grids deep. A representative volume of displacement from each grid was determined from the four displacements that were recorded for the four corner points. This was done by an adaptation of the trapezium rule, as demonstrated by Figure 10.6.

This was such that the four displacements were averaged to produce a mean displacement (h), which was then multiplied by the base area of the rectangle (ab) to produce a value equivalent to the total volume of sand displaced within the region of interest. This process was repeated for each of the fifteen rectangular grids and these

were summed to produce a total volume of sand displacement caused by a tyre treatment.

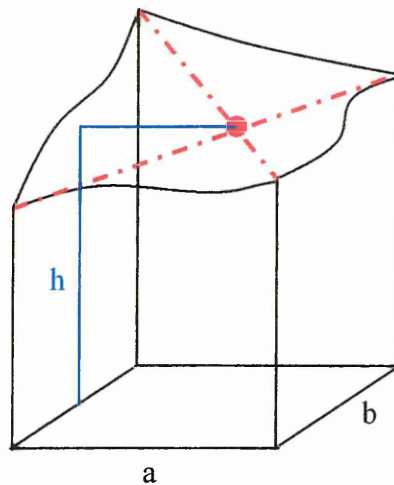


Figure 10.6 – A representation of the methodology used to determine the volume of sand displacement

During the experiment each treatment was tested three times. The repetitions were averaged to calculate the mean volume of sand displacement for each of the eighteen tread and slip treatments that were tested. This calculation of the volume of displaced sand necessarily assumed that the sand flow had been laminar, even though it was suspected that this had not occurred in the top region of the sand under consideration. The calculated volume of sand displacement was doubled to account for a whole tyre.

10.3 PROOF OF THE MODEL COMPONENTS

10.3.1 Rolling Resistance

The model terms detailed above (section 10.2.2) were entered into an Excel spreadsheet, in conjunction with a contact area for a 650 kg load, and the dynamic elements of the model were set to be non-operational. Then suitable ranges of wheel sinkages were entered into the model and corresponding rolling resistances were predicted. The results from this process are shown as the predicted data in Figure 10.7. This figure also includes the data (and trendline) from the rolling resistance tests, which was shown in Figure 9.16, to allow comparison of the prediction and actual data. Appendix 24 details these results more fully.

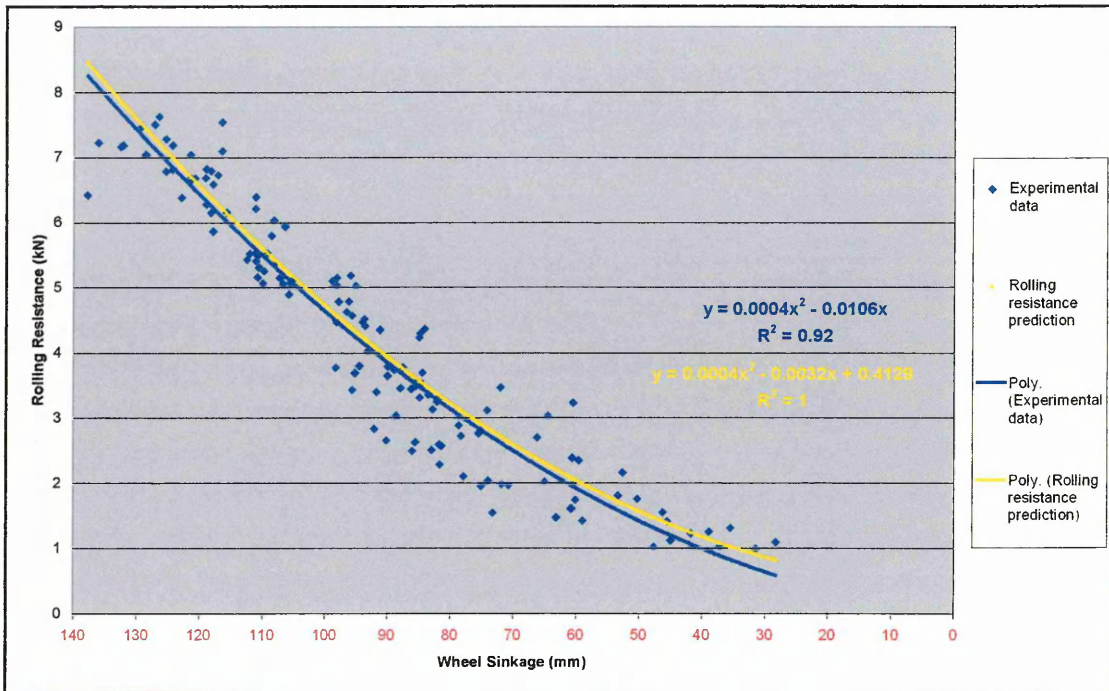


Figure 10.7 – A comparison of experimental rolling resistance results and predicted rolling resistance results

Therefore for the particular set of tyre and sand operating conditions that were modelled the rolling resistance could be summarised by equation 62, which was an equation that provided a more simple prediction of rolling resistance for these specific conditions, by representing all the Bekker equations by a single equation.

$$\text{Rolling Resistance} = 0.0004Z_{def}^2 - 0.0032Z_{def} + 0.4129 \quad (62)$$

Where: Z_{def} = Deflected wheel sinkage (negative)

Figure 10.7 shows that good agreement occurred between the experimental and predicted resistance results. Therefore the rolling resistance prediction could be used with high confidence to predict the level of resistance faced by a tyre at a known level of deflected wheel sinkage. The variation introduced below 40 mm did not affect this work, as the tyres always operated deeper than 40 mm, therefore the maximum error was 7%, though most predictions were more accurate.

10.3.2 Gross Thrust – Tyre Effects

To evaluate the accuracy of the model's gross thrust predictions it was necessary to compare these against measured gross thrust data. Gross thrusts were only measured experimentally when the fixed slip test rig was used. The application of this rig on the sand was limited, so only a few runs with fluctuating results were produced. The most extensive tests undertaken with this test rig were conducted on the sandy loam soil, testing the PT tyre inflated to 1.10 bar on 1170 kg/m^3 density soil, this data was therefore used for the comparison. Appropriate soil description data was entered into the model and the tread coefficient was set at 1 (the value for a PT tyre). The dynamic terms were adjusted to account for the semi-static situation. The results of this procedure are shown in Figure 10.8.

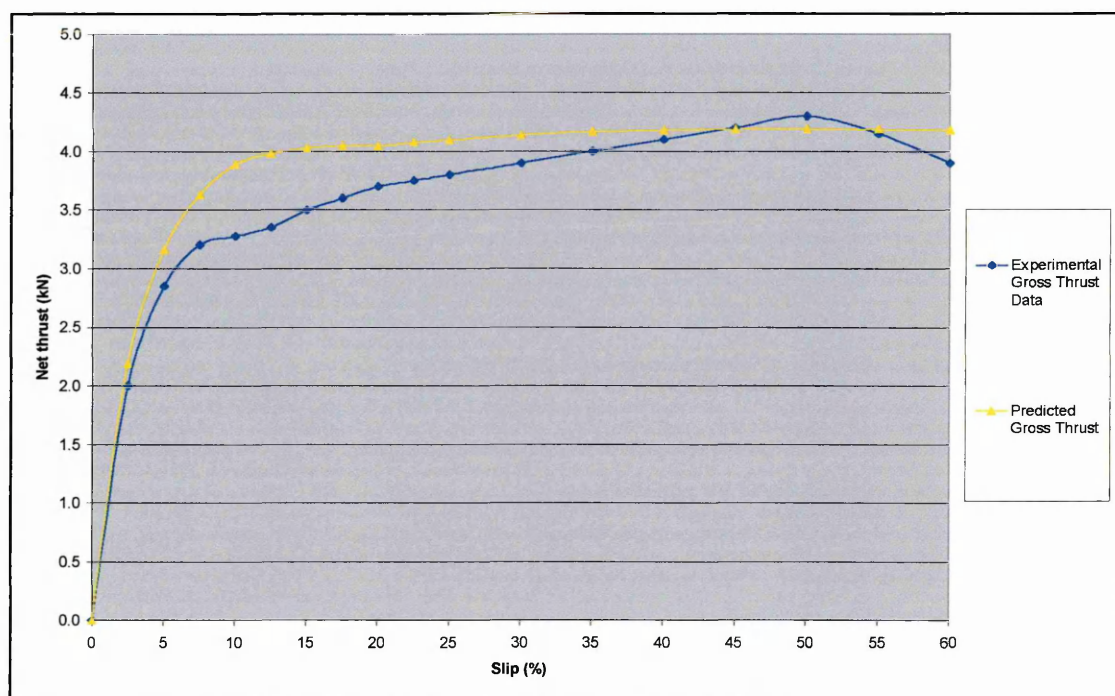


Figure 10.8 – A comparison between experimental and predicted gross thrust results for the plain tread tyre inflated to 1.10 bar operated on 1170 kg/m^3 soil

A good level of agreement was shown between the predictions and the actual results. The model was most inaccurate between approximately 8% and 18% slip (up to a 20% error). At the higher slips between 20% and 65%, where the majority of the modelling was conducted the error was significantly reduced to a maximum of 8%. It was therefore concluded that the adjusted model continued to offer good tyre thrust

predictions. Thus as the original authors of the model validated the model across a wide range of soil conditions, it was also equally applicable to modelling the gross thrust output on sand when the appropriate sand engineering values were employed.

10.3.3 Gross Thrust – Tread Effects

The majority of the tests conducted on the sand used the variable slip test rig, therefore only the wheel slip, wheel sinkage and the net thrust were recorded. To allow the effect of the tread patterns to be calculated, with reference to the gross thrust outputs, a method was devised to calculate gross thrusts from the experimental net thrust results. Rolling resistances calculated from the sinkage data were added to the experimental net thrust data to produce gross thrust results. The close agreement between the predicted and actual rolling resistance results allowed this calculation to be conducted with a high degree of accuracy. This was conducted for all the different experimental tread patterns for all the thrust slip data that was recorded during the displacement experiments.

To allow these results to be compared, a method of achieving representative comparison between the treads was required. Due to the inter-related elements that occurred between the thrust, slip and sinkage during the experiments, a holistic approach was used. Comparison was achieved by normalising the data in terms of deflected tyre sinkage. Using wheel sinkage minimised the errors in this process, because the variations in gross thrust were more sensitive to changes in sinkage, rather than wheel slip. The calculated (predicted) gross thrust output was plotted against the deflected wheel sinkage for the five prototype treads.

To calculate the effect of the tread upon the thrust, linear trend lines were fitted through the data. As zero gross thrust would occur at zero sinkage, as contact with the ground would cease, these were orientated through the origin. Linear trend lines were used to provide a simple approximation to the relationships. With any variations in thrust due to sinkage accounted for, then the difference between the thrusts was due to variations in the tread. Therefore the relative gradients of the trend lines equated to relative gross thrust benefits derived from the different treads. The results of this process are shown in Figure 10.9 to Figure 10.13, for the different tread patterns.

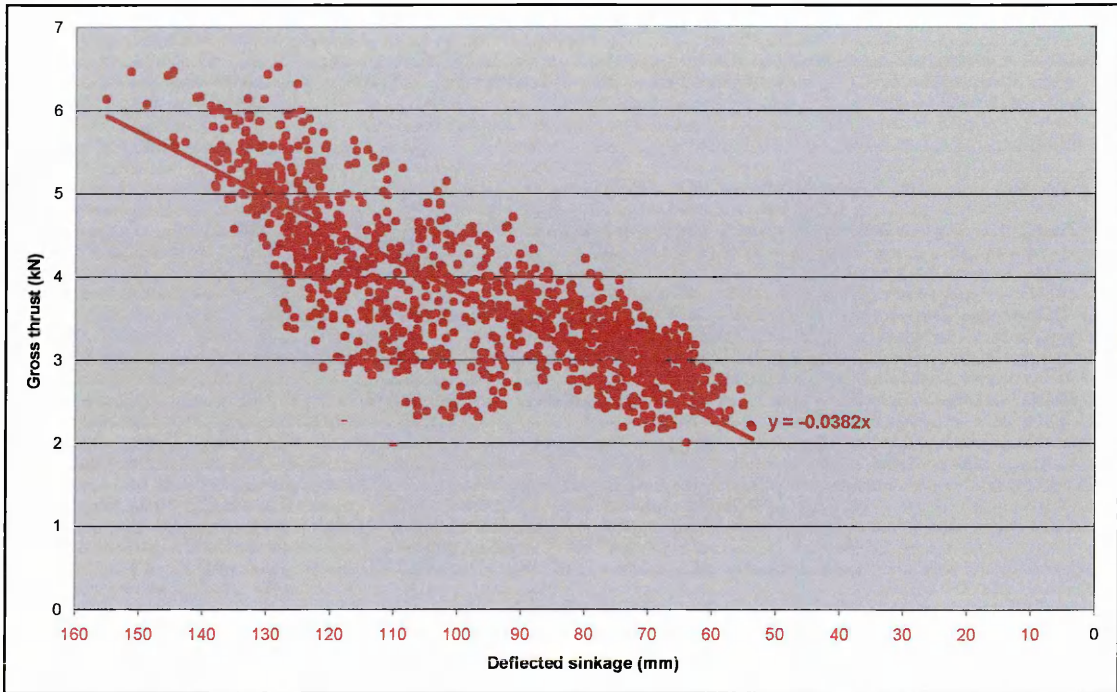


Figure 10.9 – Gross thrusts achieved by the PT tread during the displacement experiments

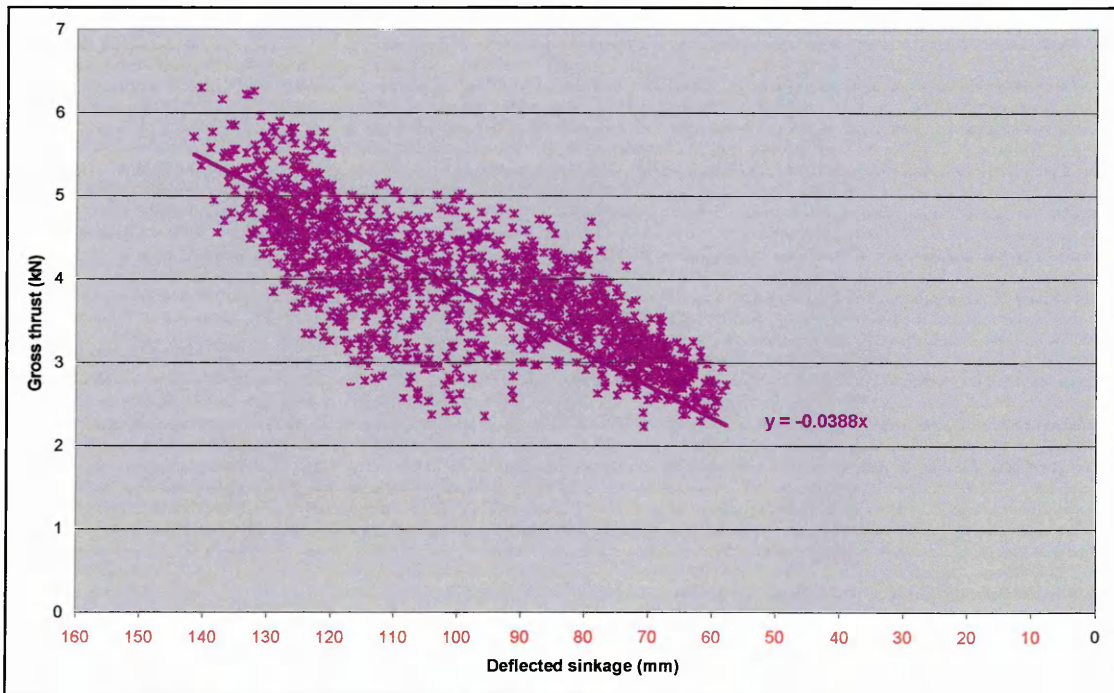


Figure 10.10 – Gross thrusts achieved by the LON tread during the displacement experiments

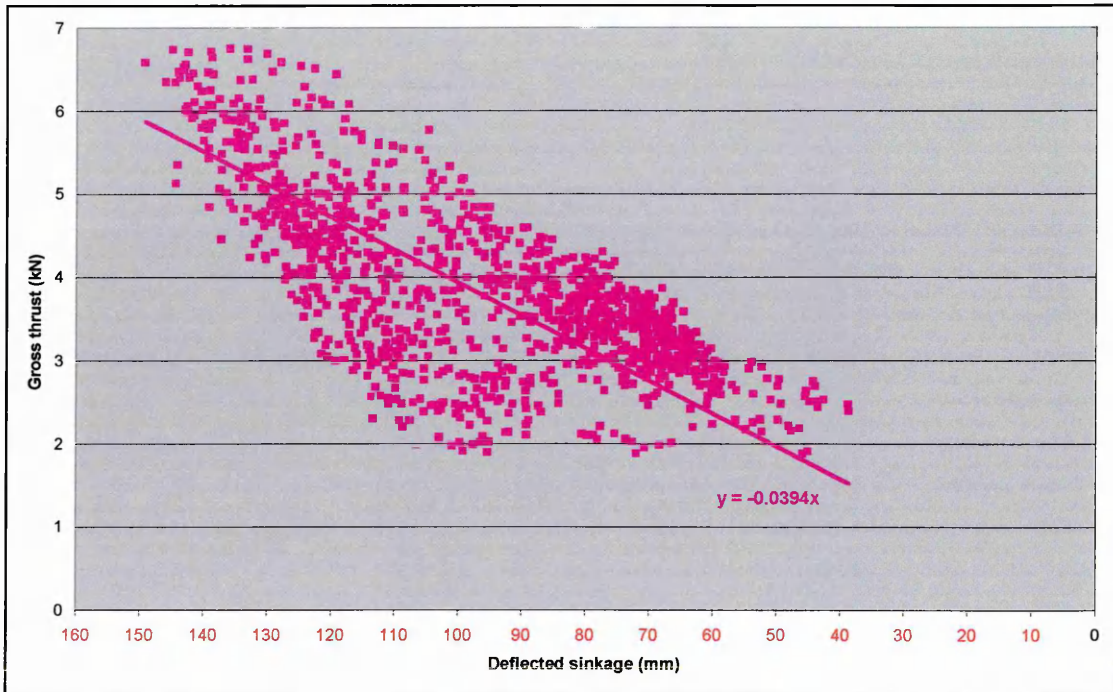


Figure 10.11 – Gross thrusts achieved by the 45F tread during the displacement experiments

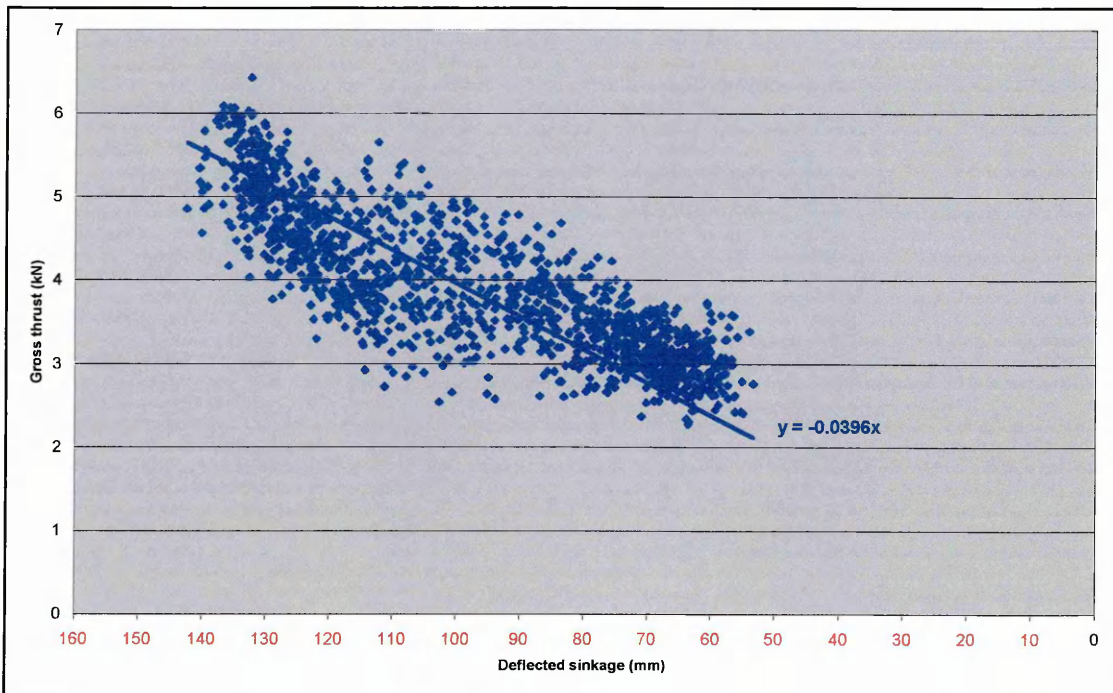


Figure 10.12 – Gross thrusts achieved by the 45B tread during the displacement experiments

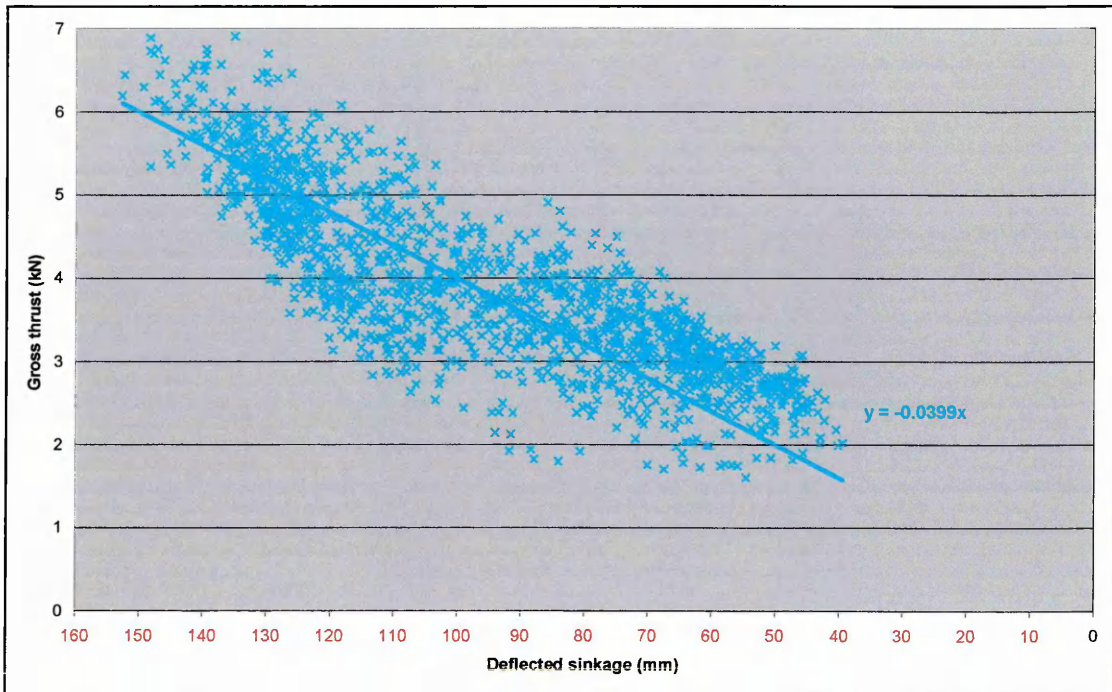


Figure 10.13 – Gross thrusts achieved by the LAT tread during the displacement experiments

The equations of the trend lines were used to predict gross thrusts at an arbitrary sinkage of 100 mm (though any realistic depth could have been used). The thrust produced by the plain tread (the lowest thrust) was taken as the baseline and the extra thrust above the baseline produced by the other treads was calculated in percentage terms. The results of this analysis can be seen in Table 10.2.

Table 10.2 – Percentage extra gross thrust outputs that were achieved by the five prototype treads at 100mm sinkage

Tread Type	Tread Coefficient	% Extra Gross Thrust
PT	0.00	0.00
LON	2.50	1.57
45F	4.64	3.14
45B	5.06	3.66
LAT	5.62	4.45

The treads were ordered by the percentage increase in gross thrust and it was noted that this order matched both the order of the tread coefficients and the order in which the treads had been grouped based upon the tractive performances recorded when the tag grids had been struck, as shown in Table 9.4. Thus although the relationships were not statistically significant, they were sufficient to be noticeable and re-confirm the trends

that were noted during the earlier analysis. Additionally, a consistent relationship was demonstrated between the tread coefficient and the percentage extra gross thrust that each tread was capable of generating over the performance of the plain tread. The data shown in Table 10.2 was plotted to determine the nature of the relationship between the two sets of tread descriptor values. This produced the relationship shown in Figure 10.14 and detailed as equation 63.

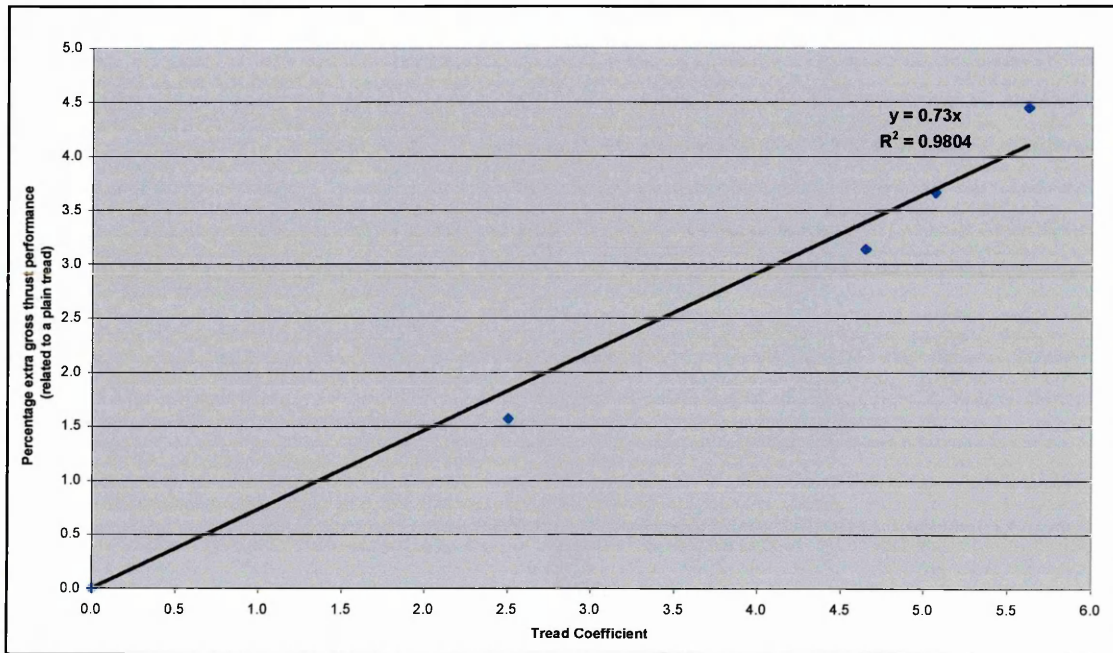


Figure 10.14 – The relationship between tread coefficients and the percentage extra thrust that each tread was capable of generating over a plain tread tyre

$$\% \text{ thrust increase} = 0.73T_c \quad (63)$$

Where: T_c = tread coefficient

Once this relationship was established then it was straightforward to replace the % thrust increase by T_f (the tread factor), which was a part of equation 55 (the gross thrust model). Thus for a given tread, represented by a tread coefficient, then the percentage extra thrust that it would generate on the sand surface with the adopted tyre treatments could be predicted and used to model gross thrust output for a range of conditions. Therefore the following tread factors (factors of gross thrust increase due to tread) were determined from the calculated tread coefficients, using equation 63.

Table 10.3 – Tread factors determined for the five prototype treads

Tread Type	Tread Coefficient	Tread Factor
PT	0.00	0.00
LON	2.50	1.83
45F	4.64	3.39
45B	5.06	3.70
LAT	5.62	4.10

10.3.4 Volume of Displaced Sand

The volumes of measured sand displacements were calculated using the process outlined above in section 10.2.4 (also see Appendix 26). This produced the results shown in Figure 10.15, where the volumes of sand displaced were matched to the corresponding net thrusts, which were recorded simultaneously as the displacement occurred. The net thrust data is shown in greater detail in Figure 9.2, whilst corresponding data for instantaneous wheel slips and depths of deflected wheel sinkage are shown in Figure 9.3 and Figure 9.4 respectively.

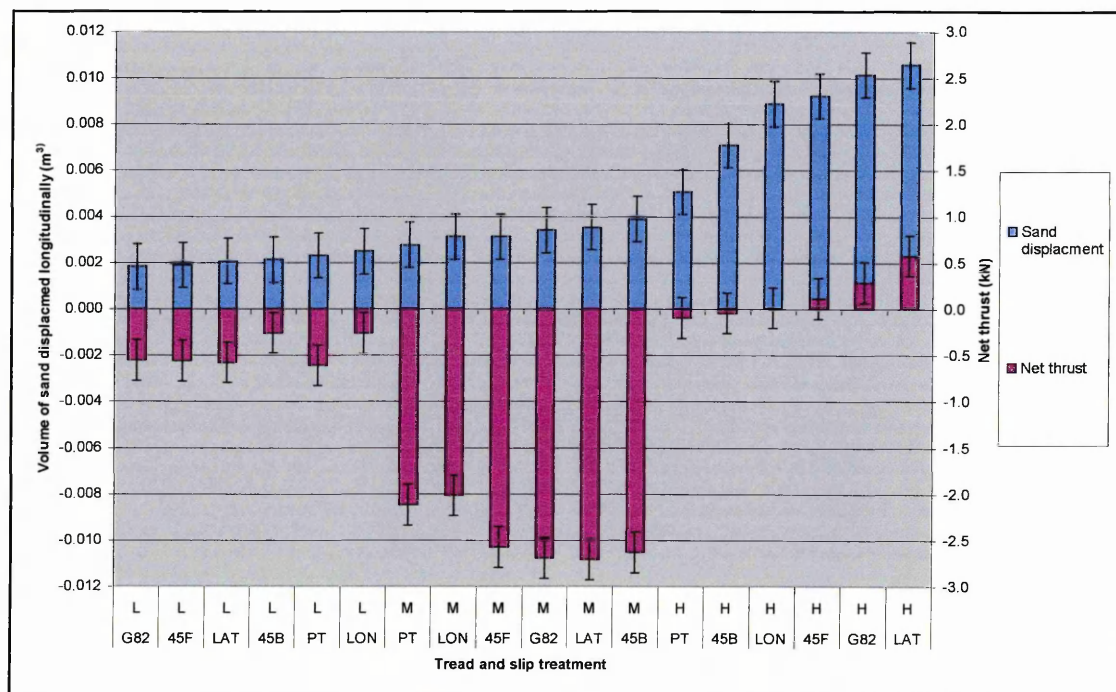


Figure 10.15 – Mean volumes of sand displaced at the eighteen slip and tyre treatments plotted with corresponding values of net thrust

Figure 10.15 shows that increasing slip caused increasing sand displacement, although within both the low treatments and the medium treatments the differences between the

volumes of displacement were not significant. However when the displacements that occurred during the high slips treatments were considered, significantly different volumes of sand were displaced by the treads. For the relationships to be fully understood it was necessary for instantaneous gross thrusts and rolling resistances to be considered as well, because this data was produced from snap shots of a dynamic situation, thus no valid operational recommendations could be inferred from Figure 10.15 in isolation, because the load and sinkage conditions varied at different slip treatments.

10.4 THRUST COMPONENTS DURING THE SAND DISPLACEMENTS

The same procedure outlined above was applied to the net thrust results recorded during the sand displacement experiments, i.e. rolling resistance predications based on the recorded sinkages were used to predict the gross thrusts acting when the displacements were measured. Thus gross thrust data could be produced from the net thrust data shown in Figure 10.15 and related to the corresponding volumes of displacement shown in Figure 10.15. This process produced the thrust data shown in Figure 10.16, where the treatments have been ordered by the magnitude of calculated gross thrust.

This process showed that wheel slip did not solely influence the gross thrust output from the treads, as generally the lowest gross thrusts occurred during the high slip (and low sinkage) section of the thrust cycle, whilst the highest gross thrusts occurred during the medium slip (and high sinkage) section. The data also highlighted that producing a high gross thrust was insufficient to guarantee good net thrust, as when operating at the medium slip condition, although the highest gross thrusts were generated, these did not translate into the maximum net thrusts, because the tyres also generated considerably greater rolling resistances than at any other point in the cycle. Additionally within each slip set of slip treatments the treads with higher tread coefficients generated higher gross thrusts than the treads with lower tread coefficients.

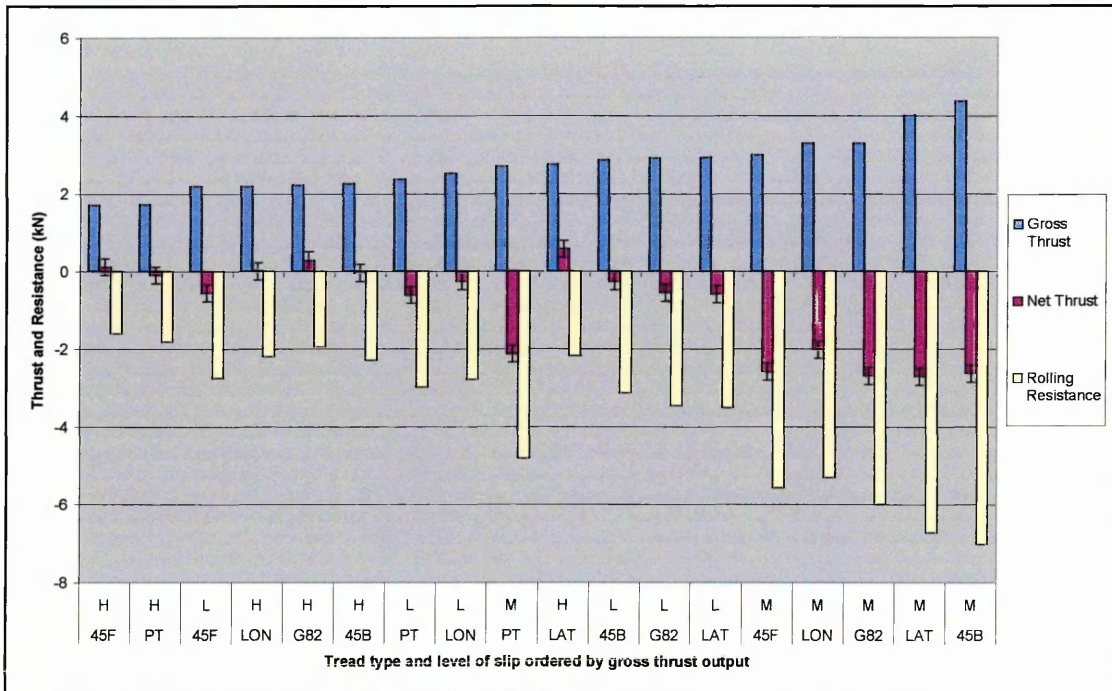


Figure 10.16 – Gross thrust and rolling resistance data from the sand displacement experiments; treatments ordered by the magnitude of gross thrust

When this data is considered, it must be remembered that the detailed slip treatments were those acting when the tags were struck, and not those responsible for the tyre being at that particular point in the slip cycle, because slips acting earlier in the thrust-slip cycle were mainly responsible for the subsequent wheel sinkage. This point, and its implications, will be explained in greater detail in the following sections. These will also link the calculated gross thrusts to the measured sand displacements.

10.5 APPLICATION OF THE NET THRUST MODEL

To better understand the relationship between the thrust components the elements of the predictive model were considered. For this to be appropriate the validity of the model had to be assessed when it was used to predict net thrusts based upon the data recorded during the sand displacement experiments. Gross thrust and rolling resistance predictions were used to predict net thrusts, which were then compared against the recorded net thrusts. For the model to provide a good representation of the results it had to be able to account for the large variations in wheel slip, sinkage and vertical acceleration, as well as the tyre tread treatments used during the experiments. To allow comparison of the differences in performance between each tread one test run was modelled for each tyre tread, and the tread factor equation (63) was used to introduce the tread effects into the gross thrust model. This evaluation was conducted for all five of the prototype treads. The results are shown in Figure 10.17 to Figure 10.21. The details of the modelling calculations for all similar plots, on the accompanying data CD, are listed in Appendix 27. These are presented in order of the tread factor rankings, starting with the lowest scoring tread, the PT tyre.

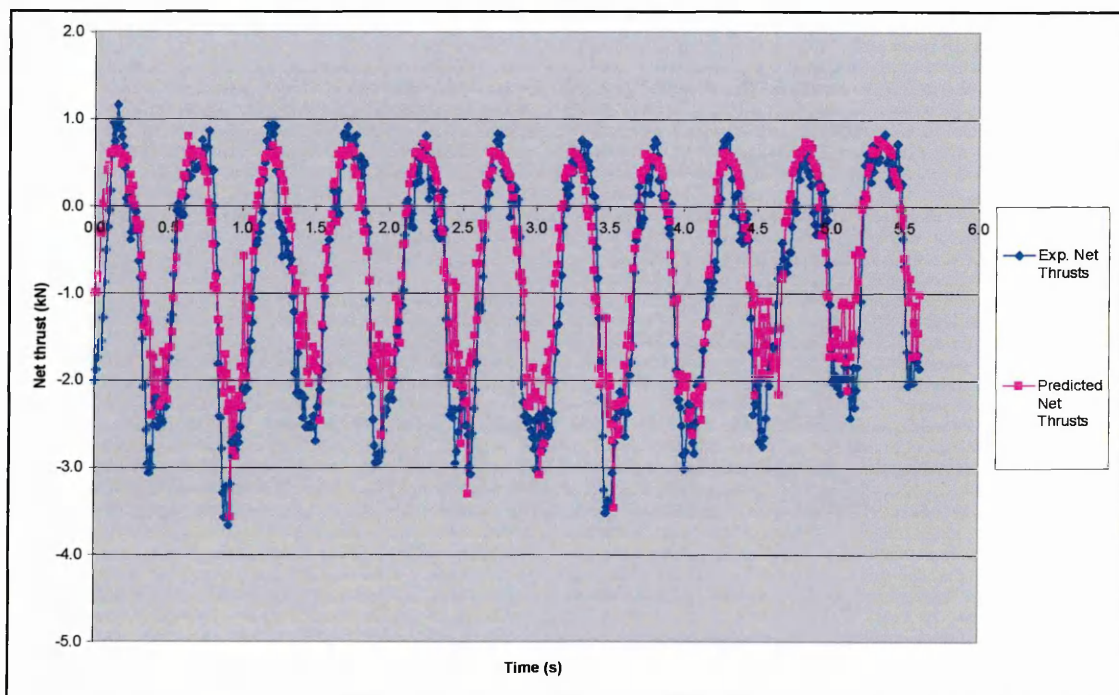


Figure 10.17 – Experimental net thrust results plotted against predicted net thrusts calculated for the PT tread

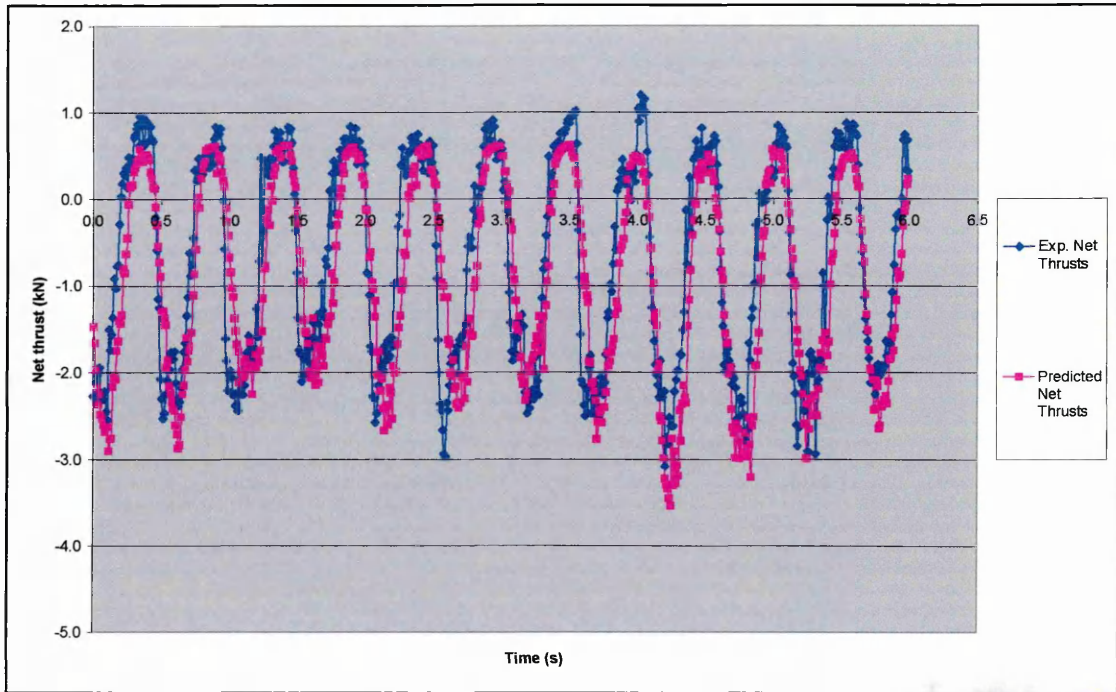


Figure 10.18 – Experimental net thrust results plotted against predicted net thrusts calculated for the LON tread

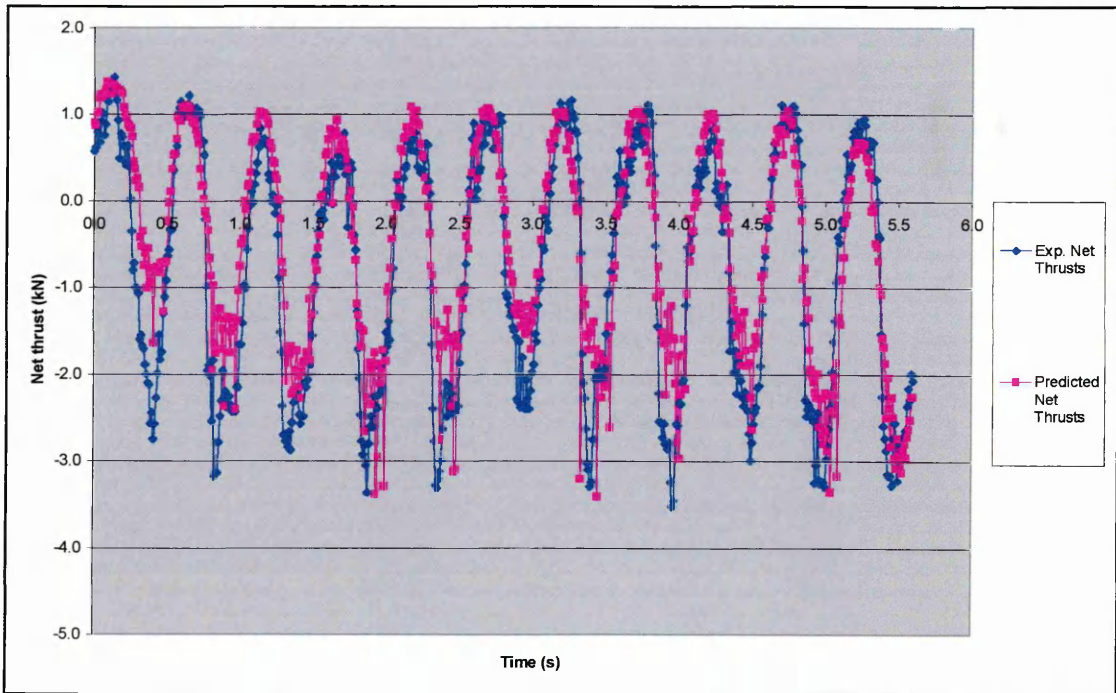


Figure 10.19 – Experimental net thrust results plotted against predicted net thrusts calculated for the 45F tread

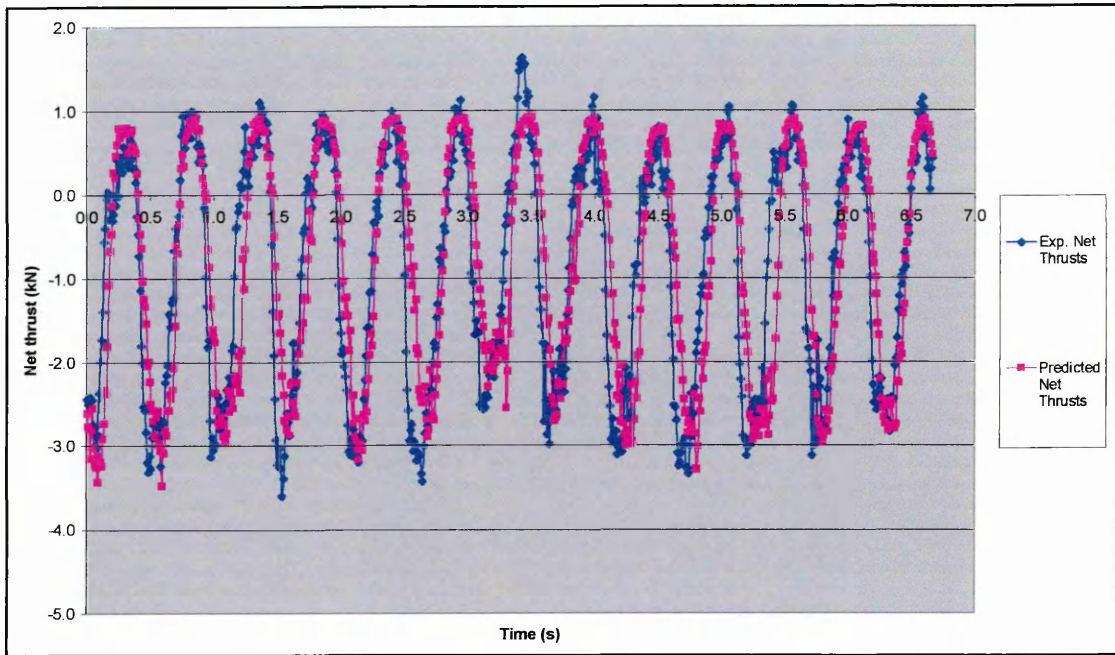


Figure 10.20 – Experimental net thrust results plotted against predicted net thrusts calculated for the 45B tread

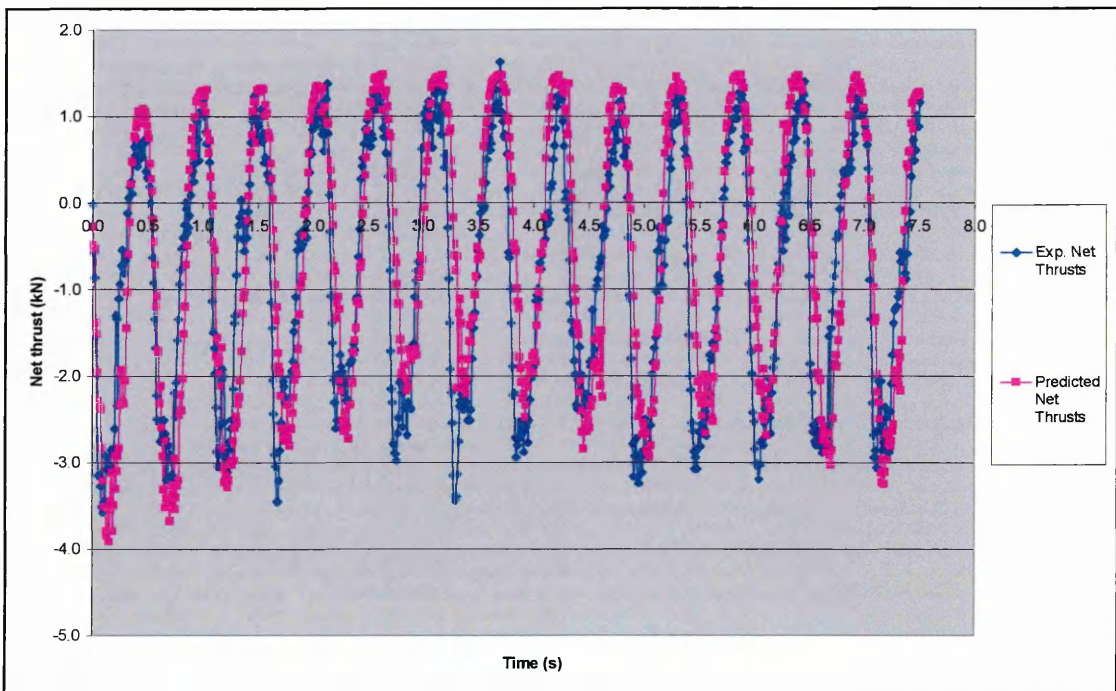


Figure 10.21 – Experimental net thrust results plotted against predicted net thrusts calculated for the LAT tread

The predicted results showed reasonable agreement with the experimental results for all of the tread patterns, and the inclusion of the tread factor suitably adjusted the predicted results to account for the effect of the tread pattern. Most importantly the model

adequately predicted the wide cyclical variations in the net thrusts that had been experienced over the course of a test-run, due to the fluctuations in slip, sinkage and load. To better quantify the agreement, all of the predictions were plotted against the actual net thrust data, with the results shown in Figure 10.22. The trend line applied to the data passed through the origin, with an R^2 value of 0.7 indicating that reasonable agreement was achieved, particularly when the complexity of the situation was considered. The weakness of the model was indicated by the gradient of the trend line being approximately 0.79, which indicated that the model tended to under predict the experimental data at the thrust extremes, particularly for predictions of the peak negative net thrusts that were recorded.

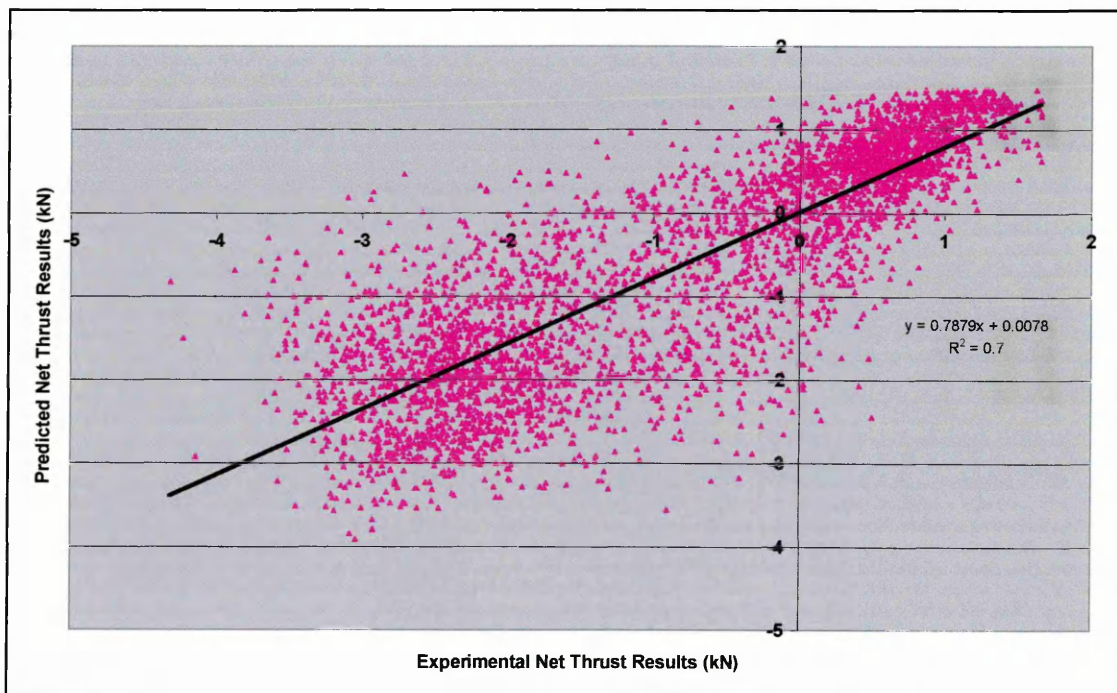


Figure 10.22 – A comparison plot of experimental and predicted net thrust results

To confirm the applicability of the model across different soil types, modelling of the net thrusts achieved on the soil was also attempted, although only for a single case of the PT tyre inflated to 1.10 bar operating on the weakest soil condition. The relevant soil variables were changed to the values determined in section 5 in both the gross thrust and rolling resistance models, and corresponding experimental tractive performance data (slips and sinkages) was applied to the models. Again the prediction was plotted against the experimental net thrust data, which is shown in Figure 10.23 (see also

Appendix 27). Good agreement occurred once more, which demonstrated that the model was, as Bekker's work had indicated, applicable to a range of soil conditions.

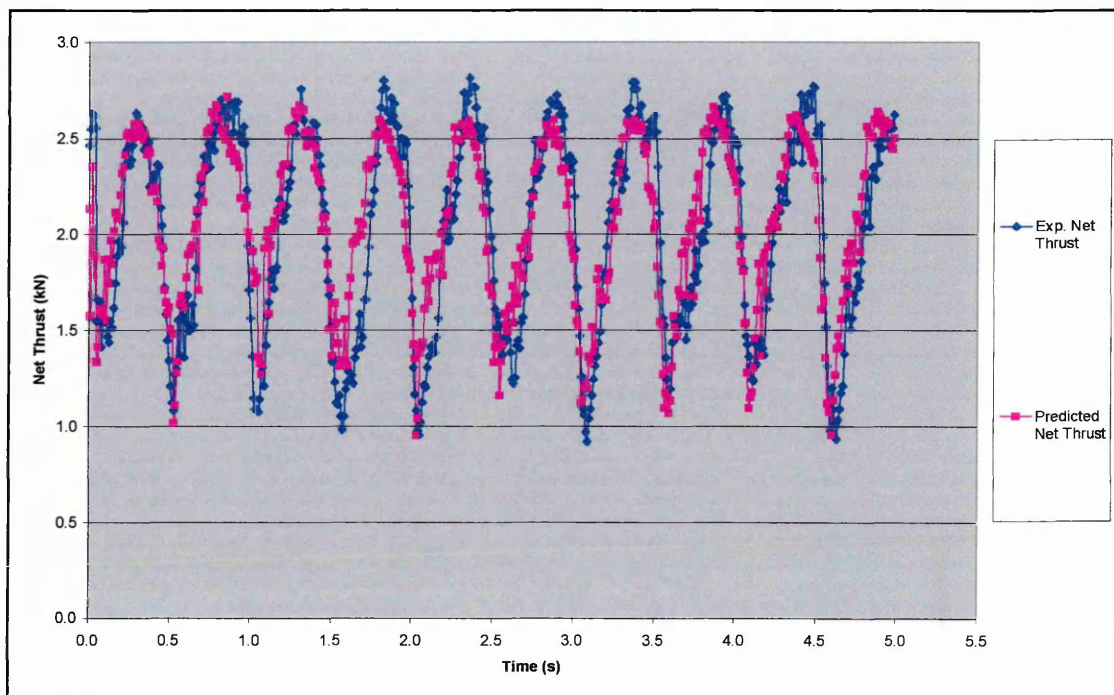


Figure 10.23 – A plot of experimental and predicted net thrusts for the PT tyre inflated to 1.10 bar operating on the 1170 kg/m^3 soil

10.6 RELATIONSHIP OF THE NET THRUST MODEL COMPONENTS

The capability to accurately model the forces experienced during the slip thrust cycle allowed events occurring over its duration to be clearly identified, which in turn allowed a better understanding of the tractive behaviours occurring during this complex event. Figure 10.24 and Figure 10.26 highlighted these complex inter-relationships between the different factors. Figure 10.24 showed the relationship between the component parts of the gross thrust output.

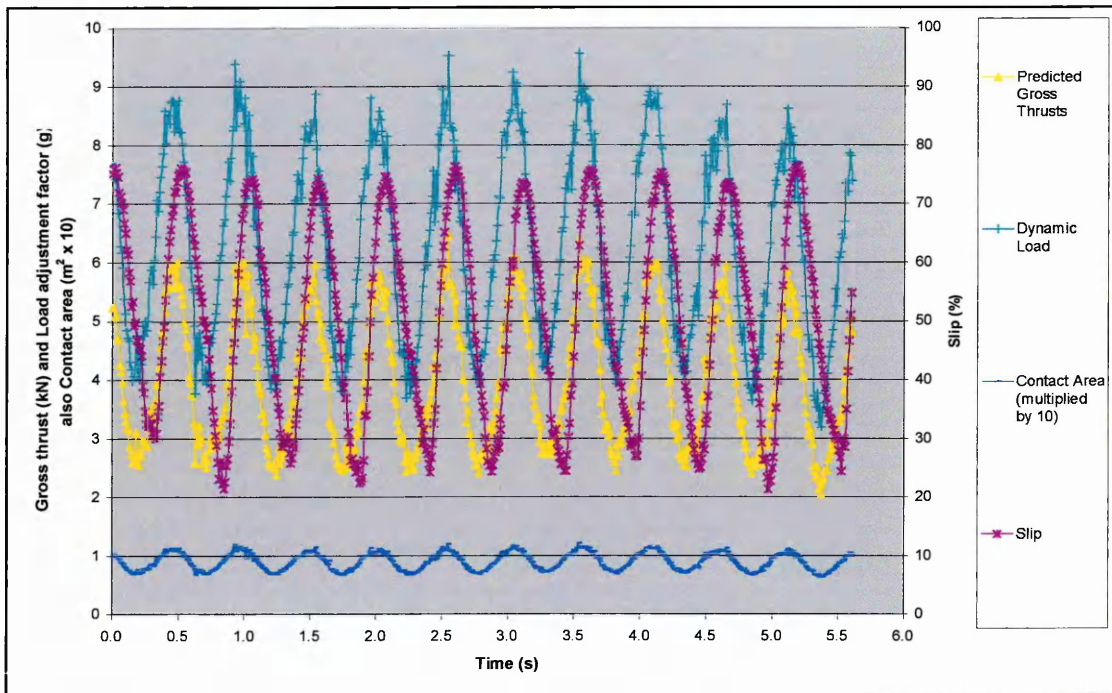


Figure 10.24 – The components of the gross thrust prediction, based upon PT results recorded during the sand displacement experiments

The relationships were such that the peak gross thrust occurred at the peak load, which corresponded to the peak contact area. Although they were slightly out of phase with the peak slips, the slips at which they occurred were sufficiently high to generate high thrusts. As expected the peak minimum gross thrusts were generated by a simultaneous combination of minimum loading, contact area and slip. The rolling resistance was mainly related to the wheel sinkage, therefore as the sinkage increased, so to did the resistance.

It had been expected that the peak net thrust would occur simultaneously with the peak gross thrust. This proved not to be the case. Instead the net thrust output was controlled to a much greater extent by the fluctuating rolling resistance. Maximum gross thrust and rolling resistance were both achieved at maximum sinkage and vice versa. At low sinkages the gross thrust exceeded the rolling resistance and hence positive net thrust was achieved. However, as the rate of increase in resistance with increased sinkage exceeded the rate of increase in thrust due to increased sinkage, negative net thrust (immobility) was achieved as the sinkage increased. These relationships are shown in Figure 10.25, which has again used a holistic approach and plotted predicted results for

all of the load and slip conditions that were experienced over the course of a test run. The variation in the gross thrust predictions depend upon if the wheel slip was increasing when the thrust was predicted.

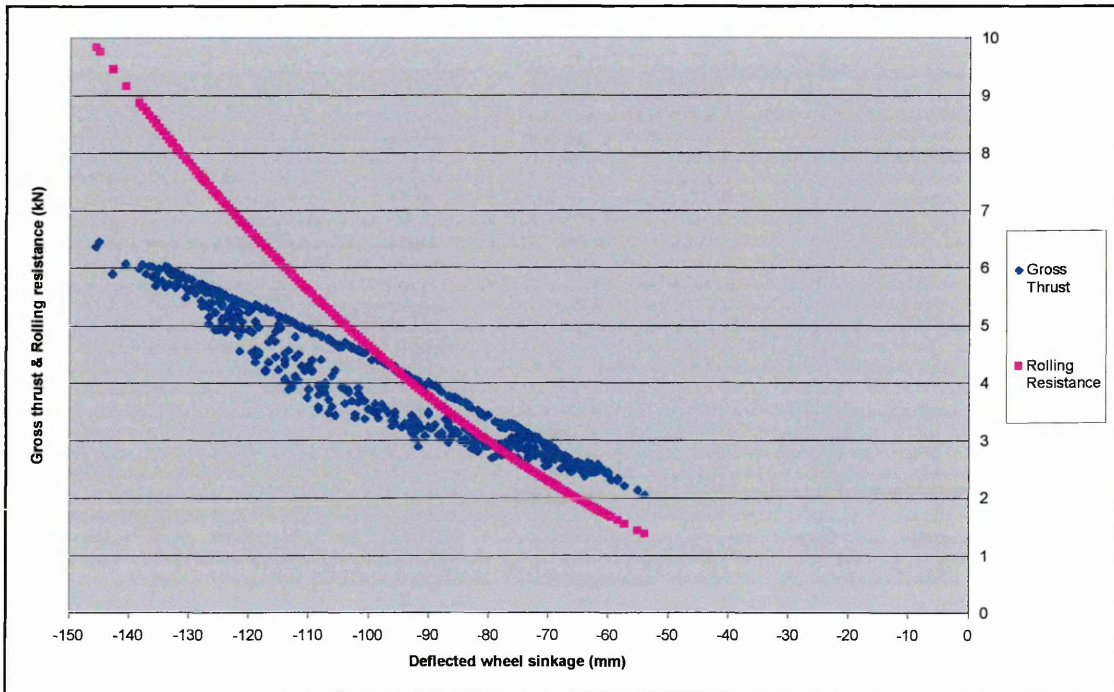


Figure 10.25 – The relationships between sinkage and predictions of both the gross thrust and rolling resistance made using the PT experimental results

Therefore contrary to expectation, maximum net thrust was actually achieved at minimum sinkage (coincident with reduced sinkage, load and contact area), as the gross thrust achieved exceeded the rolling resistance, and hence positive net thrust was achieved. These relationships are more fully illustrated in Figure 10.26.

The gross thrust trends occurred because of the increased loading and contact area that occurred, as the sinkage increased, which allowed extra thrust to be generated. Additionally the rolling resistances were also closely related to the sinkage of the treads. The key to these relationships lay in the cause of the tyre sinkage. If the tyre was statically placed on the sand, then a limited amount of sinkage was experienced. However, as the wheel was ‘slipped’ to derive traction then slip sinkage removed sand from beneath the tyre, which in turn caused the tyre to sink further into the ground.

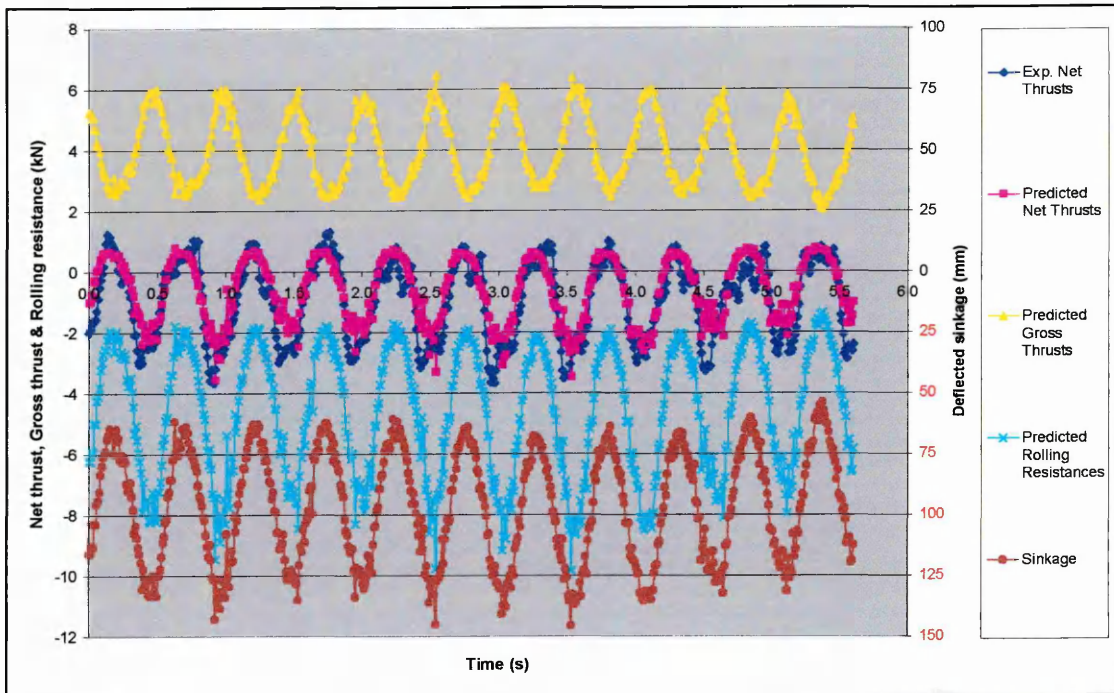


Figure 10.26 – Net thrusts produced by the combination of gross thrusts and rolling resistances, based upon PT results from the sand displacement experiments

Although slip was necessary to achieve traction, on this surface most of the thrust had been yielded before 15% slip was exceeded. Therefore, for the range of slips under consideration, extra slip produced only a limited increase in gross thrust. This extra thrust was far outweighed by the extra increase in rolling resistance generated due to the increased slip sinkage. Demonstrating these relationships confirmed the suspicion that to maximise traction on this surface, slip had to be minimised (to below approximately 20%). This would prevent excessive sand removal from beneath the tyre, and therefore prevent excessive sinkage, which caused the excessive resistance that the tyre was incapable of overcoming. Hypothetically, if a mechanism to prevent wheel sinkage could be found then operating at maximum slip would be advantageous, as the instantaneous results indicated.

10.6.1 Thrust – Slip Relationships and Sand Displacement Results

The instantaneous net thrusts recorded with the sand displacements (Figure 10.16) appeared contradictory (as noted in the previous section), as they could be used to infer that the tyre should be operated at high or low slips, not medium slips. It is wrong to infer that high slips were best from such instantaneous results, as they do not convey the

very large sinkages (resistances) that the high slips generated immediately after they occurred. These effects become obvious once constant streams of data generated over full test runs were considered, because as the previous section noted, the instantaneous data recorded during the displacement experiments neither accounted for the dynamic nature of the relationships, nor the effect of slip upon the subsequent sinkage.

The instantaneous slip results did not account for the preceding slip (slip sinkage), though this slip was directly responsible for the sinkage of the wheel when the instantaneous displacement and tractive measurements were recorded. These effects were instead considered when the whole test runs were considered. Therefore although the results indicated that the high slips were potentially capable of generating the highest net thrusts. They failed to properly demonstrate that this benefit was only momentary as the slip sinkage that was generated quickly immobilised the tyre, an effect that was properly explained once the model could be applied to complete sets of results.

10.7 TREAD EFFECTS, GROSS THRUSTS AND DISPLACEMENTS

The theoretical derivation of gross thrust allowed the sand displacements calculated for the treads to be related to the derived gross thrusts (i.e. the data shown in Figure 10.16). This data was plotted as Figure 10.27. This graph indicated that two different types of displacement had occurred. The two patterns were separated by the slip treatments at which the treads had operated, such that between the high and medium slip conditions the sand displacement had changed significantly. At low and medium slips higher net thrusts were generated, from smaller volumes of sand displacement. At higher slips significantly greater sand displacements produced lower thrusts, because the dynamic load (and contact area) were reduced. This allowed the treads to throw the surface layers of sand rearwards after they were sheared, which resulted in the larger sand displacements that occurred even though lower gross thrusts were generated.

'Low' slips still achieved sufficient slip to release a large proportion of the potential shear force from the sand and thus good gross thrust was achieved. Despite the difference in thrust, Figure 10.27 showed that these were altered by the tread pattern,

such that the treads that generated the higher gross thrusts (had the higher tread factors) also tended to generate larger sand displacements (slip sinkages). This therefore accounted for why these treads developed both the higher rolling resistances and higher gross thrusts.

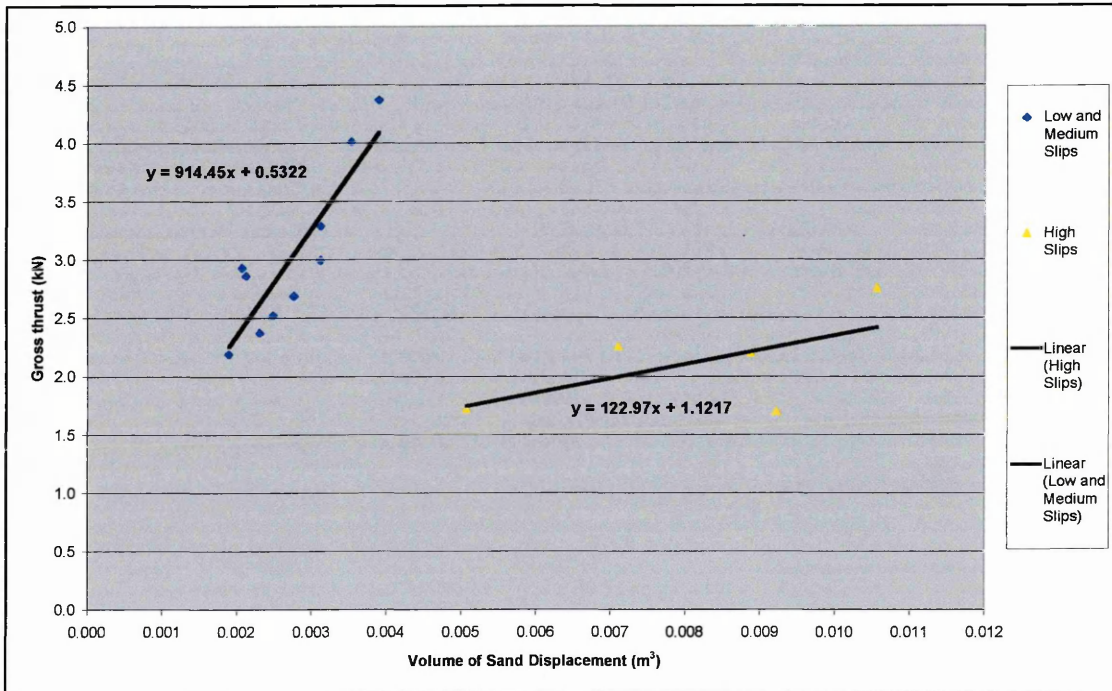


Figure 10.27 – The relationship between the volume of sand displacement caused by the treads and the gross thrusts achieved

To allow a better analysis of the sand displacements, they were separated by the slip treatment at which they were achieved and the tread factor. These results are shown in Figure 10.28. As Figure 10.27 had indicated the relationships at low and medium slips were hardly significant, although the trends indicated that at low slips the higher tread factor treads displaced less sand, but as the medium slip was reached then the treads with a higher tread factor caused greater sand displacements, which was directly linked to higher thrusts they had achieved. At the high slips the relationship became significant, such that much higher volumes of displacement were achieved by the higher thrust potential (tread factor) treads.

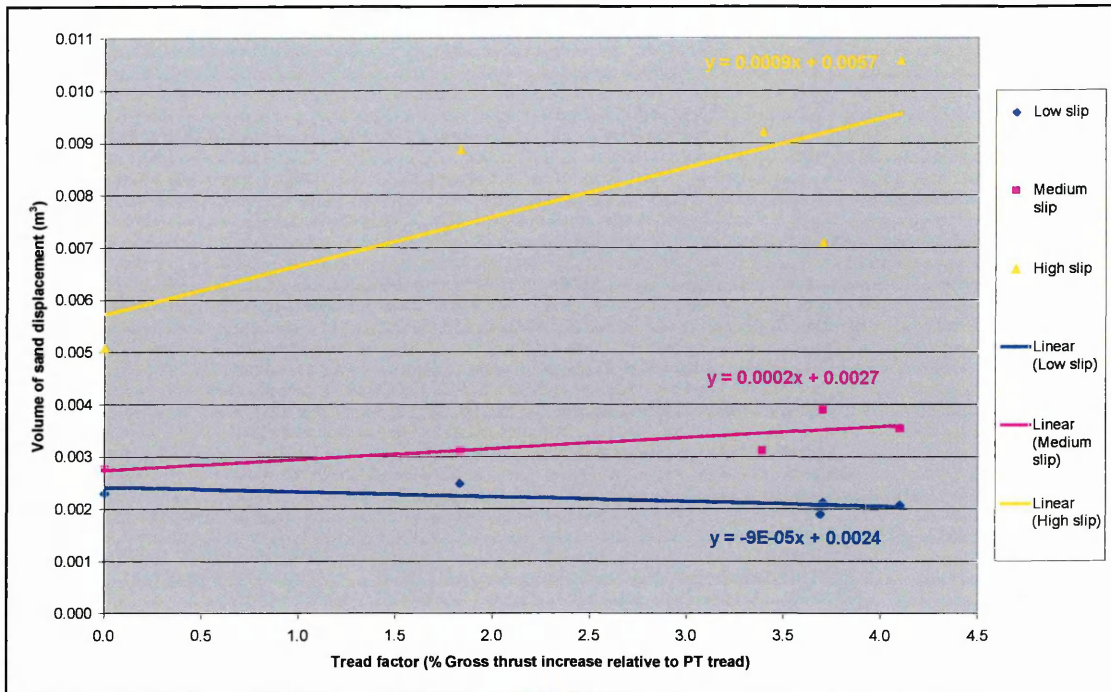


Figure 10.28 – The relationships between the tyre treads and the sand displacements

10.8 APPLICATION OF THE MODELLING TO PRODUCTION TREADS

10.8.1 235/70 R16 Treads

The modelling methodology was applied to three 235/70 R16 production treads, a G82, a Wrangler HP and a Wrangler Ultra-Grip, shown on Plate 6.2 and Plate 6.3, to assess its prediction capability against measured net thrust results. The G82 tread tested was cut on a 235/70 R16 blank, as the prototype tread had been, so the standard 7.50 R16 production tyre was not used. The G82 tread results to which the predictions were compared were from one of the replicates recorded during the sand displacement experiments. The results for the other two treads were from test runs conducted at a preliminary stage of the investigation using the variable slip rig in the full soil (sand) bin, whilst the damper settings were being optimised. Therefore the net thrusts were less consistent because the wheel sinkage was more variable. All three treads were inflated to 1.10 bar and run at nominal slips of 50%, which caused the typical cyclical thrust-slip behaviour to occur in all instances.

The tread patterns were individually analysed to determine the values of their tread coefficients, which are shown in Table 10.4. Where the treads featured inconsistent tread lengths (due to noise abatement design techniques) average tread lengths and widths were determined for the calculation. The previously determined relationship between tread coefficient and tread factor (equation 63) was used to calculate tread factors for the production treads, which are shown in Table 10.4. The full calculations are detailed in Appendix 25.

Table 10.4 – Tread coefficients and factors determined for the production treads

Tread Type	Tread Coefficient	Tread Factor
PT	0.00	0.00
G82	6.65	4.85
HP	5.27	3.85
UG	4.39	3.20

These calculations allowed the gross thrust benefit due to the tread (tread factor) to be used for the prediction of the gross thrust. The tractive data recorded over each test run was inputted into the model and net thrusts were predicted. These were individually plotted against the measured net thrusts for each tread; see Figure 10.29 to Figure 10.31 (and also Appendix 27). The cyclical distribution of the results was similar to the patterns noted for the prototype treads, which indicated that relationships similar to those determined for the prototype treads had occurred between the different inter-related traction variables.

The peak thrust results showed that the G82 tread was capable of achieving more thrust than the other two treads. This was not unexpected as the tread is specifically intended for desert conditions. However, it was interesting to discover that it is the tread pattern, as well as the construction of the production tyre, that is responsible for its good off-road performance. The other two treads (HP and UG) achieved performances equivalent to the 45° angle prototype treads, with the HP developing slightly more thrust. As expected, because it is intended for use in winter climates, the UG achieved the worst tractive performance.

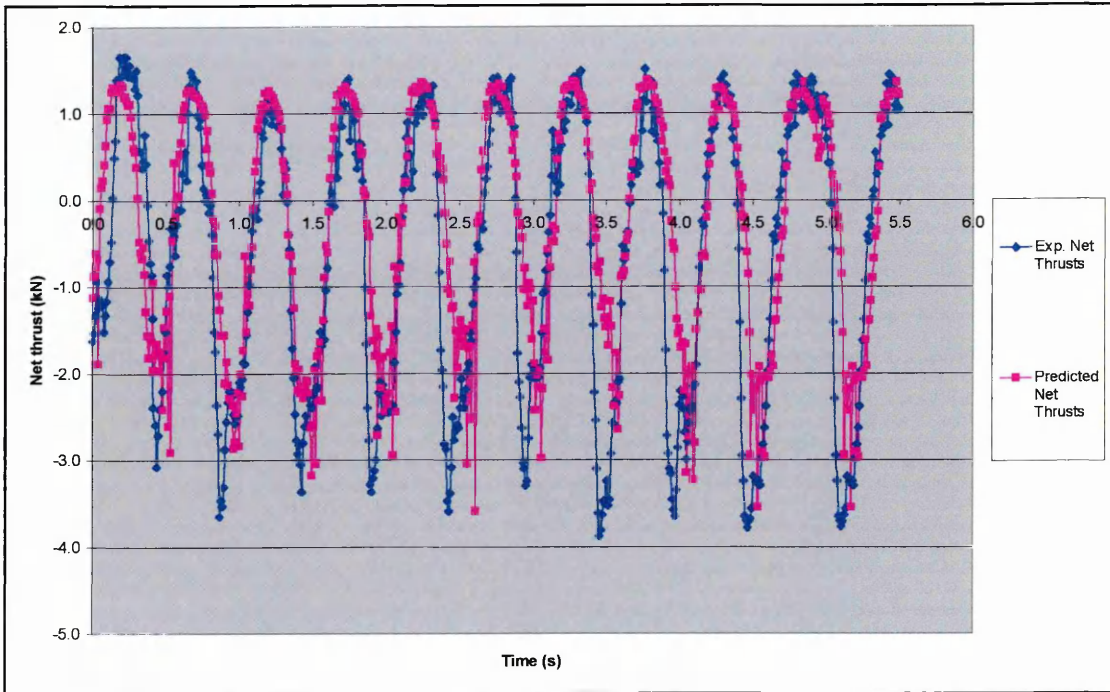


Figure 10.29 – Experimental net thrust results plotted against predicted net thrusts calculated for the G82 tread

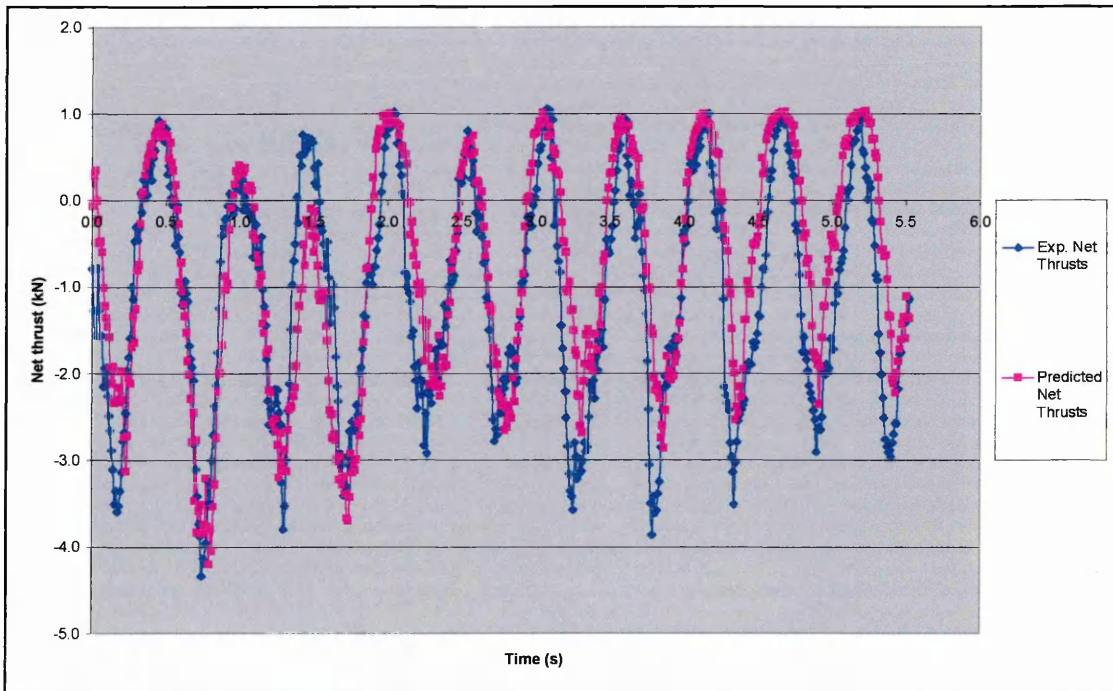


Figure 10.30 – Experimental net thrust results plotted against predicted net thrusts calculated for the Wrangler HP tread

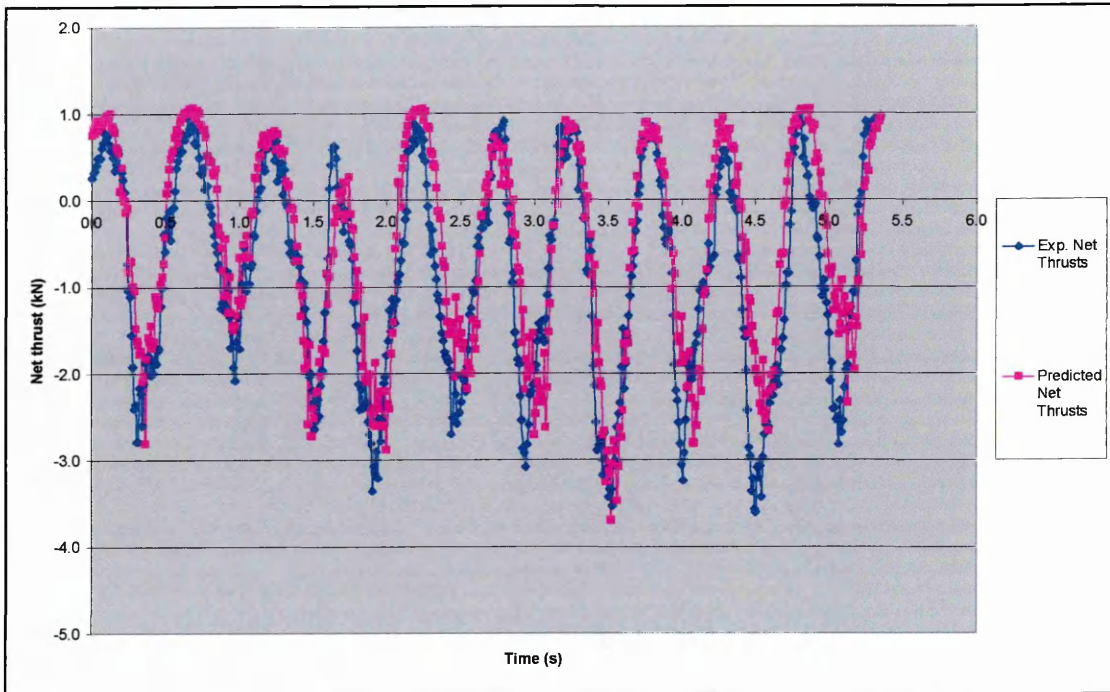


Figure 10.31 – Experimental net thrust results plotted against predicted net thrusts calculated for the Wrangler UG tread

These results indicated that the application of the modelling techniques to production treads was valid, and that good predictions of the amount of thrust that a tread could achieve on this surface were possible. To further assess the quality of the predictions all of the data from the previous three figures was plotted in Figure 10.32 and a trendline was added. The trendline of the data showed close agreement with the trendline in Figure 10.22, which applied the same process to the prototype treads. A gradient of 0.79 was again recorded, which meant that the model continued to under predict the peak thrusts, especially the peak negative net thrusts. Overall though, the predictive model again offered reasonable net thrust predictions of the experimental results. This further proved the applicability of the techniques that had been used.

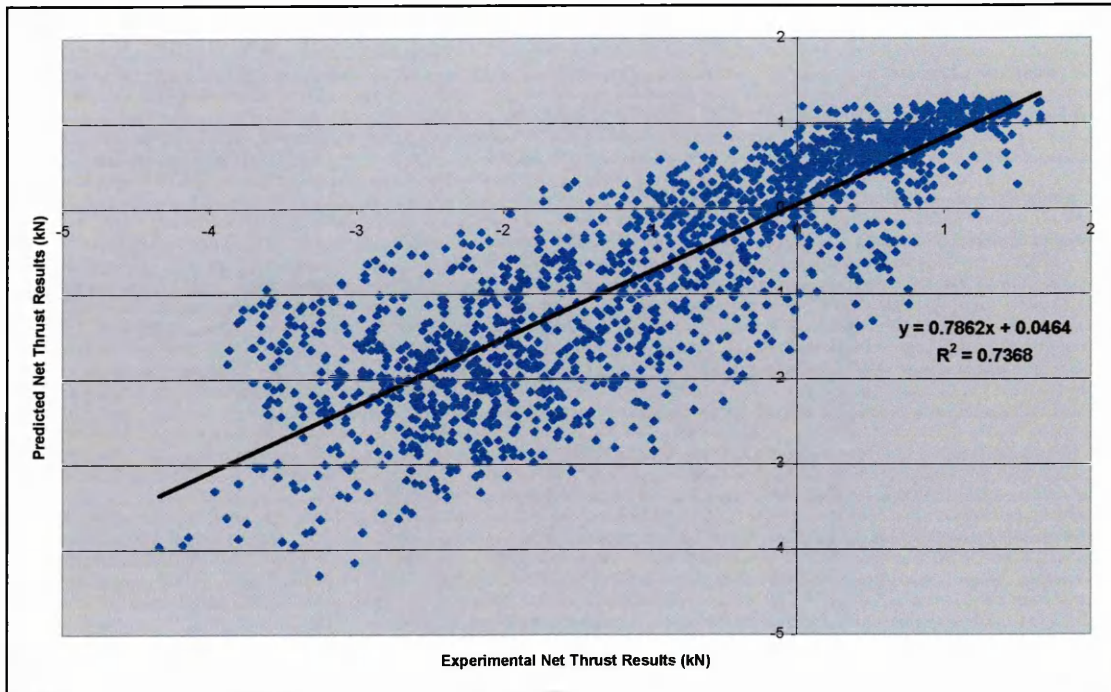


Figure 10.32 – A comparison plot of experimental and predicted net thrust results for the production treads

The sand displacement results recorded for the G82 tread were also analysed. This was done in the same manner adopted for the other prototype treads, thus the thrusts and displacements were plotted with the data shown in Figure 10.28 (section 10.7). This produced the results shown in Figure 10.33. Comparison of the two graphs showed that the inclusion of the G82 results did not alter the equations of the trend lines, i.e. the trends in the data were continuous. Therefore the conclusions noted regarding the relationships between the tread factors and the volumes of sand displaced by the treads remained unchanged from those stated in section 10.7, i.e. as slip was increased the treads with higher tread factors caused increasingly greater sand displacements to occur. The effect meant that any increased sinkage, caused by extra displacement, caused the treads to face increased rolling resistance, which mostly exceeded the additional thrust developed from the extra displacement.

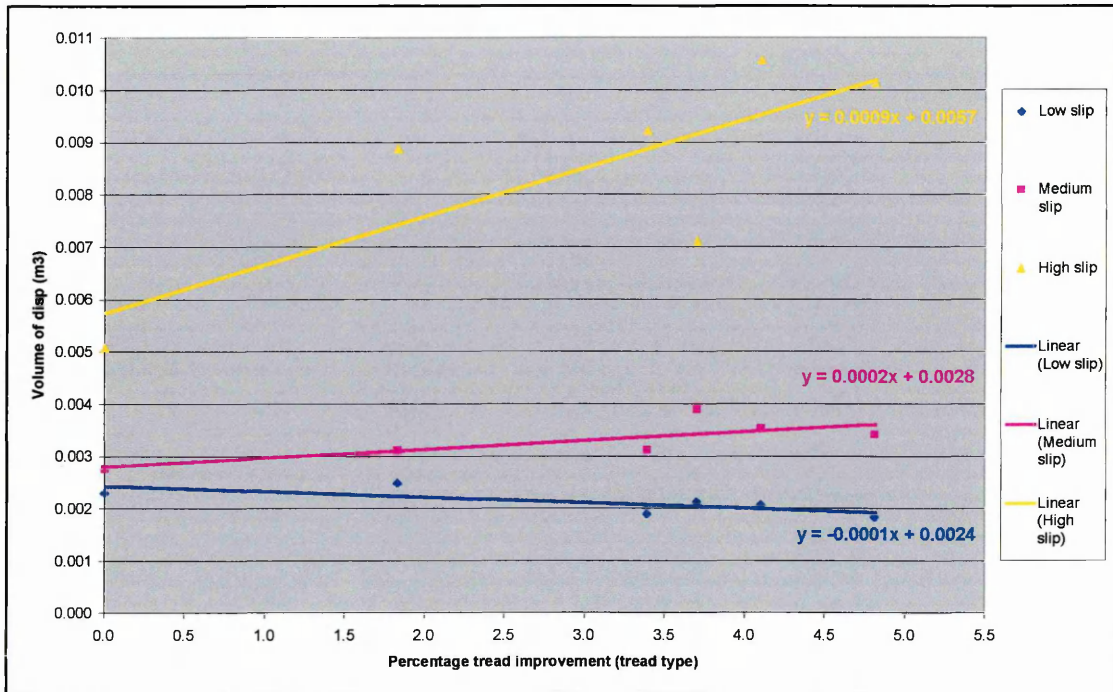


Figure 10.33 – The relationships between the tyre treads and the sand displacements for all the treads

10.8.2 255/55 R19 Treads

A limited number of traction tests were conducted on some 255/55 R19 tyres featuring potential production treads that were supplied by Land Rover. This made it possible to assess the application of the modelling techniques to these differently sized treads and tyres. The treads that were tested were a Michelin Diamaris, a Goodyear Wrangler HP (same tread as 235 tyre) and a Dunlop TG31; these were termed DIA, HP and TG respectively. The test runs used the variable slip test rig on sand in the full soil bin. All the treads were inflated to 1.10 bar and run at nominal slips of 50%. Again similar cyclical slip/ thrust was experienced.

The analysis detailed in section 10.8.1 was again used to analyse the results from these treads, with one adjustment. For the previous applications, the thrust due to the tread was compared to the thrust achieved by a similarly sized PT tyre. In this instance a suitable plain tread was not available for testing, so comparison results were not available. Therefore a gross thrust value had to be calculated instead. This was achieved by using the model to estimate the gross thrust capability of a 255/55 R19 plain treaded tyre. The prediction indicated that the larger PT tyre would generate approximately

103.5% of the gross thrust achieved by the 235/70 R16 PT tyre. This provided a baseline tread effect against which the effect of the other treads could be calculated, so that the validity of the predictions could be ensured. The tread representation model was used to predict tread coefficients for the three tested treads, and equation 63 was used to predict the tread factors. This produced the results shown in Table 10.5, which are detailed in Appendix 25.

Table 10.5 – Tread coefficients and percentage extra gross thrusts achieved by the 255/55 R19 production treads

Tread Type	Tread Coefficient	Tread Factor
PT	0.00	0.00
DIAMARIS	5.29	3.86
HP	5.27	3.84
TG31	4.04	2.95

These values were used in the net thrust predictions for the three treads, which produced the results shown in Figure 10.34 to Figure 10.36 (see also Appendix 27). These results showed that similar cyclical patterns of performance were derived from these tyres (treads) as had been achieved from the smaller tyres.

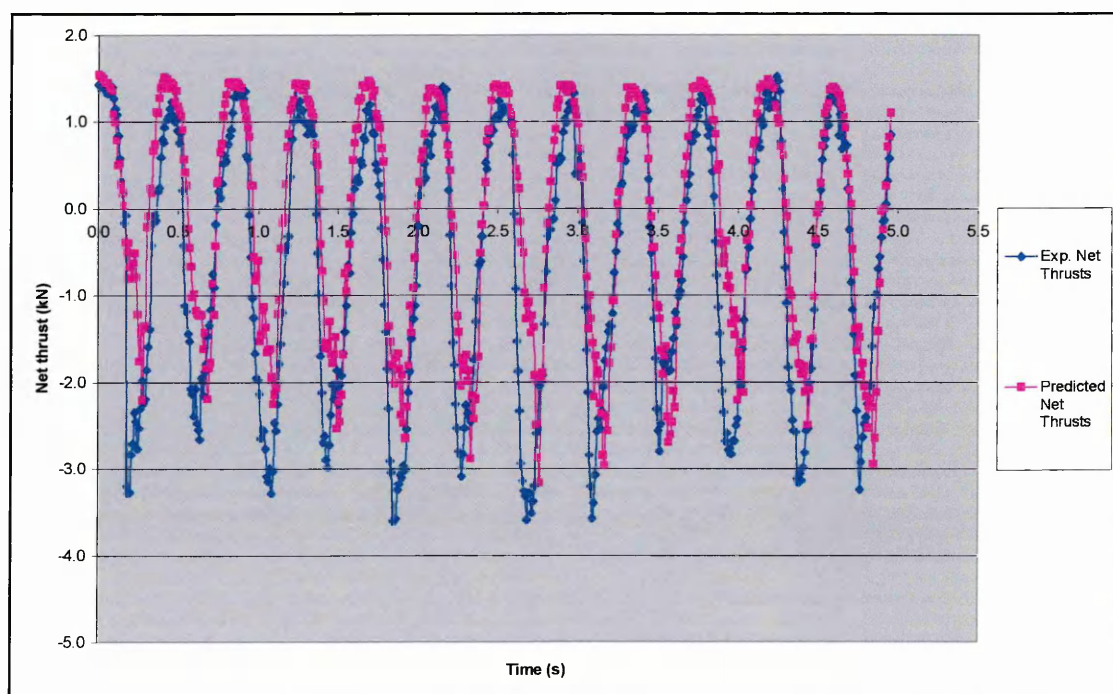


Figure 10.34 – Experimental net thrust results plotted against predicted net thrusts calculated for the Diamaris tread

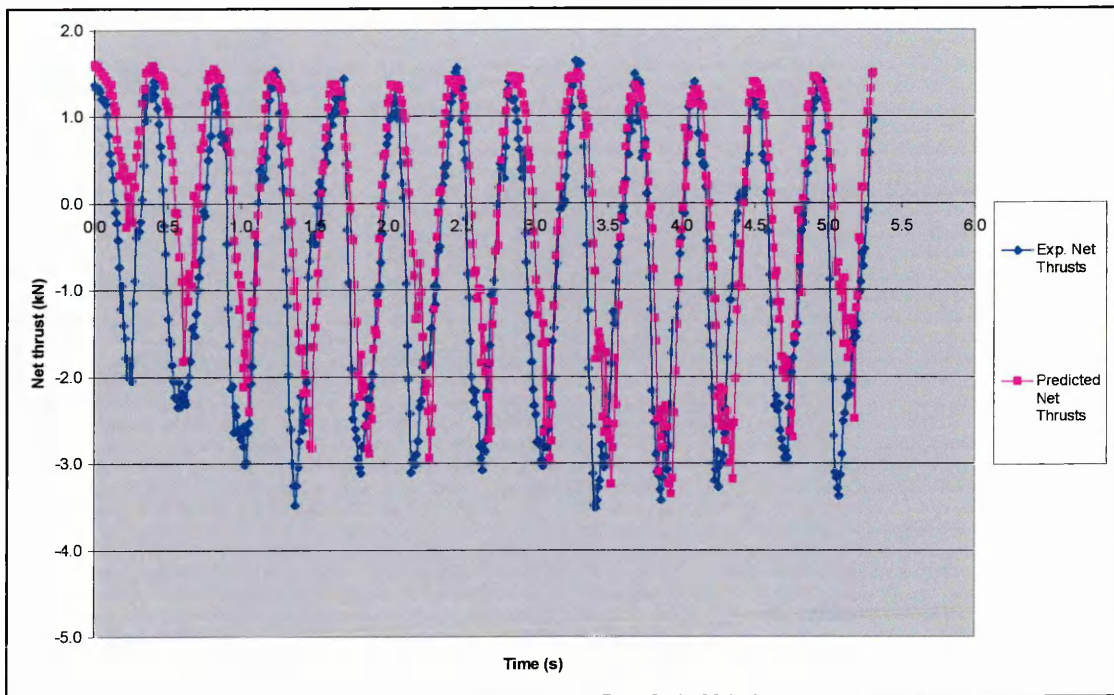


Figure 10.35 – Experimental net thrust results plotted against predicted net thrusts calculated for the Wrangler HP (255) tread

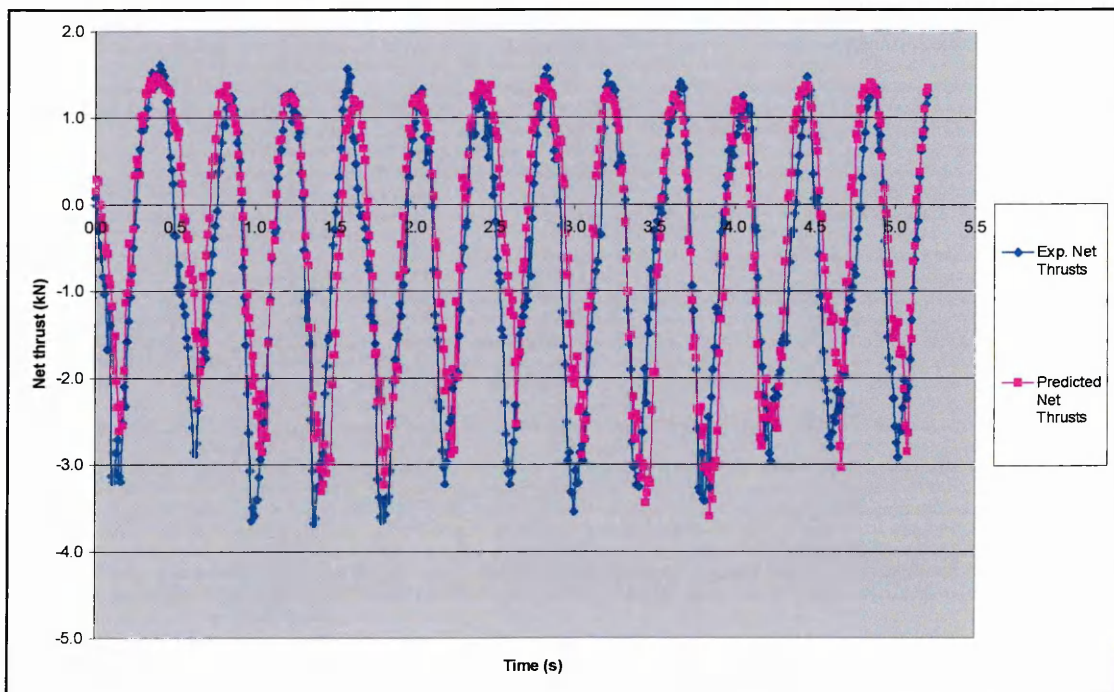


Figure 10.36 – Experimental net thrust results plotted against predicted net thrusts calculated for the TG31 tread

The results showed that as expected the increased tyre size had allowed higher gross thrusts to be generated by the tyres, which had resulted in higher peak positive net thrusts being generated by these tyres (treads). Similar negative net thrusts were achieved by the two tyre sizes, as although the larger tyre generated higher gross thrust, its extra width also created increased rolling resistance, thus the overall effect was that the two forces approximately nullified each other.

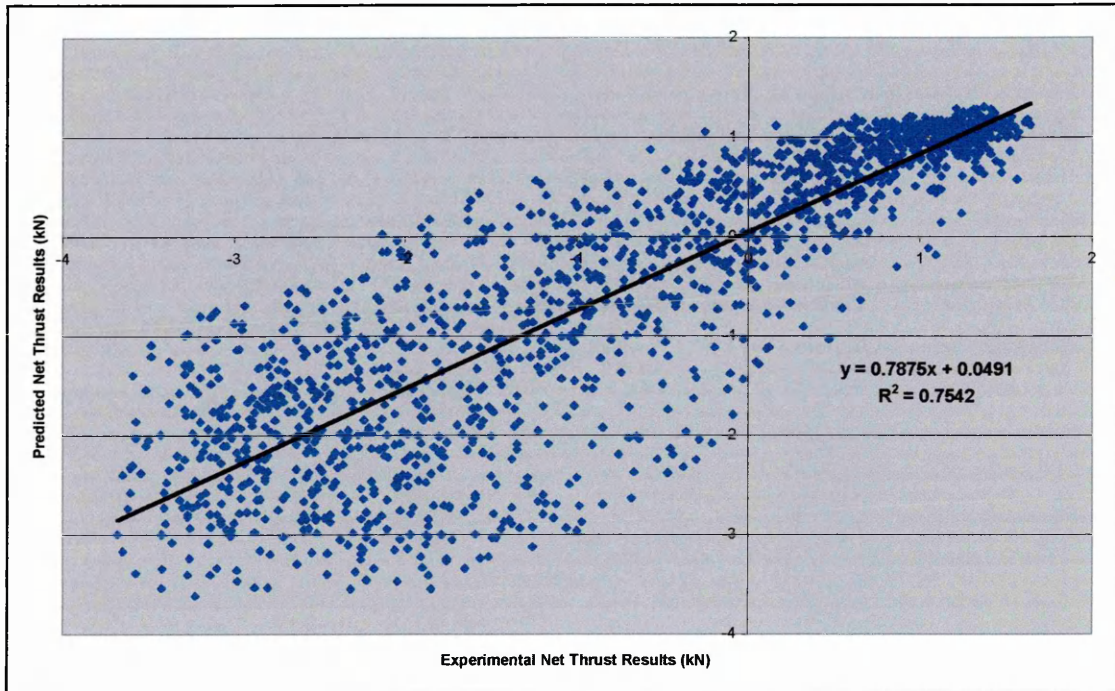


Figure 10.37 – A comparison plot of experimental and predicted net thrust results for the production treads

The predictions were again plotted against the experimental results to assess their quality, as shown in Figure 10.37. The same patterns were once again noted, i.e. a gradient of 0.79 and the trendline passing through the origin, so again the peak forces were under predicted. These results further confirmed the applicability of the modelling techniques to provide reasonable net thrust predictions for the dynamic events that had been experienced. They also demonstrated that the models were applicable to a greater range of production treads and tyre dimensions on this sand surface.

10.9 IMPROVEMENT OF THE TREAD FACTOR MODEL

The data that had been used in the previous section to validate the predictive model was also used to improve the tread coefficient vs. tread factor relationship (equation 64). This enabled the predictive capability of this to be confirmed for the maximum range of treads, which added greater robustness to its prediction capability. For each of the production treads the gross thrust was predicted from the experimental net thrusts by adding rolling resistances predictions based upon the sinkage, following the same process that was used to derive equation 64. This allowed the gross thrusts produced by the different treads to be quantified. When these results were compared to the results for the PT tyres the gross thrust benefit derived by each tread was quantified. These results were tallied against the tread coefficients calculated for each tread, as detailed in Table 10.6.

Table 10.6 – Tread coefficients and gross thrust benefits of the production treads

Tread Type	Tread Coefficient	% Extra Gross Thrust
PT	0.00	0.00
TG31	4.04	2.56
UG	4.39	2.88
HP (235)	5.27	3.40
HP (255)	5.27	4.10
DIAMARIS	5.29	3.85
G82	6.65	5.24

This data was plotted with all of the values calculated for the prototype treads, which were detailed in Table 10.2 and Figure 10.14. Plotting all these values formed Figure 10.38, and a trend line was fitted through the data to describe the relationship between the two tread descriptors. This showed that the thrust effect due to tread remained similar across the range of different tyre sizes and treads, so the production tread predictions had been accurate. However, the equation of this trendline (equation 65) provided a more accurate relationship between the tread coefficient and tread factor, thus it should replace equation 64 in the prediction methodology.

$$T_f (\% \text{ thrust increase}) = 0.7239T_c \quad (65)$$

Where: T_f = tread factor T_c = tread coefficient

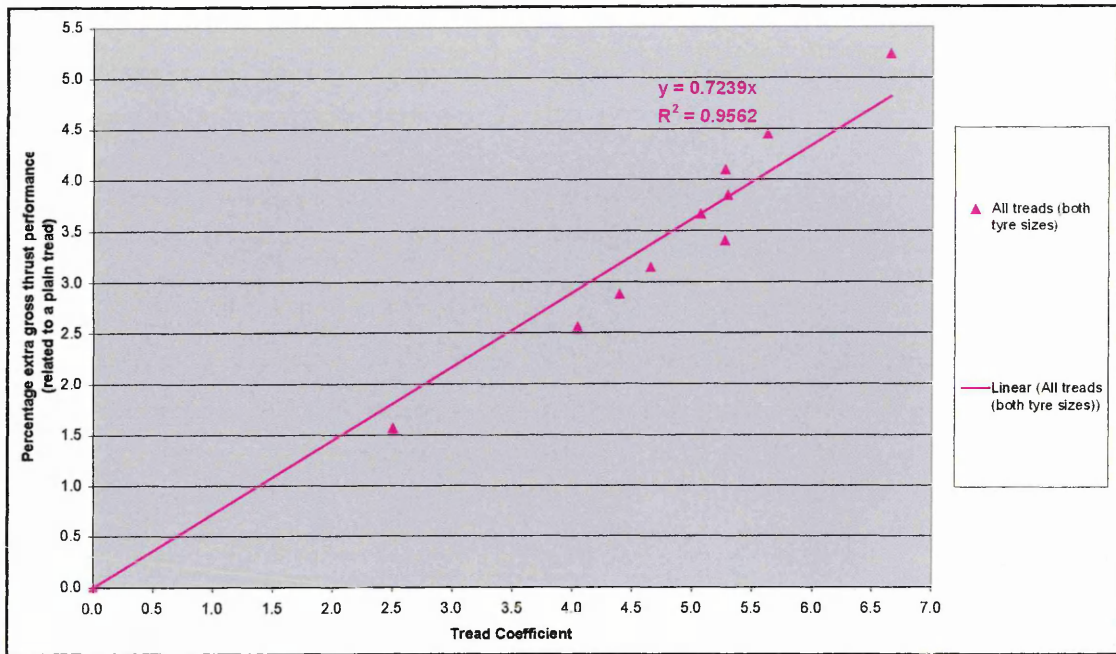


Figure 10.38 – The relationship between tread coefficient and percentage extra gross thrust relative to a PT tyre for all the tyres

10.10 PERFORMANCE INDICATED BY THE MODELLING

The modelling (equation 55) primarily allowed the prediction of a base level of gross thrust from a plain treaded tyre for a range of tyre dimensions and soil surfaces. In the first instance Bekker, and a number of other related authors, have validated these semi-empirical models across a wide range of conditions. This work proved that this model is applicable to the loose sand conditions upon which the bulk of the testing occurred. The work also proved that the model (equation 55) could be improved to account for the dynamic effects of vertical oscillations of the wheel, which significantly improved its predictive capability. Theoretically the validity of predictions using this improved methodology will remain valid for any soil, so long as the conditions considered are within the boundaries of the model identified by Bekker.

Theoretical calculation of the percentage extra thrust recorded for the different tread pattern on desert sand was achieved by the development of both the tread coefficient model (equation 58) and the tread factor term (the thrust increase caused by a tread). These allowed each tread pattern's features to be related to the extra gross thrust it generated in excess of the gross thrust achieved by a plain tread tyre operating under a

similar treatment. This model showed good agreement with the recorded results (see Figure 10.38).

The relationships confirmed by the model (equation 55) showed that within the 15% to 80% slip range the dynamic normal load and related contact area of the tyre had a more significant impact on the gross thrust generated than the slip. However, the wheel slip was directly related to the sand displacement, and thus more crucially, the sinkage of the tyre, because as the slip sinkage increased, so too did the rolling resistance. As high slips (of approximately 55% to 70%) occurred at small sinkages and loads, the failure of the surface layers of sand changed from being purely sheared (as occurred at lower slips) to being sheared and having the surface layers thrown rearwards. This change in caused extra sand to be removed from beneath the tyres at high slips, as greater displacements were achieved, which subsequently left the tyres facing considerably greater rolling resistances.

The resistance faced due to the resulting high sinkage far exceeded the gross thrust capabilities of any of the evaluated tyres treads and thus the tyres were placed in an immobile condition. Thus although operating the tyres at high slips momentarily yielded high net thrusts, they rapidly became immobilised thereafter. Thus to achieve maximum tractive performance on this surface at the forward speeds, the slip should be limited to below 20% slip, so as to prevent excessive sand disturbance. This requirement is not necessarily valid at higher forward speeds, where vehicle momentum and the position of the tyre relative to its bow-wave would influence the tyre performance. This conditions could possible prevent a wheel with limited slip from achieving maximum thrust, but these conditions were not investigated.

If a volume of sand displacement were known for a particular tread pattern in combination with its tread factor, and corresponding values of wheel slip, sinkage and load, then this could be used to predict the gross thrust and rolling resistance produced by the tread, and thus the net thrust. However, it is very time consuming to quantify sand displacement and thus it is easier to use the thrust prediction model (equation 55) and tread factor model (equation 58) to achieve the same prediction, providing the

necessary engineering coefficients for the soil surface that are used in the model are known.

As it is based on Bekker's prediction methods, the proposed methodology is also potentially applicable to other sandy surfaces, but this should be confirmed by additional traction tests to record data against which model predictions could be judged. It would be necessary to test a PT tread and at least two other treads on appropriately sized tyres to establish the tread factor vs. tread coefficient relationship for the new surface (following section 10.8.1 as a methodology route map). These should be treads expected to produce average and high levels of performance on that surface. Once the relationship is established it would be straightforward to develop desk-based performance predictions for any treads under consideration, by using the tread factors to predict the gross thrust benefit of the new treads. Such a study would also allow further confidence to be placed in the tread representation models and confirm the application of the methodology to a boarder range of situations.

11 DISCUSSION OF THE PROJECT FINDINGS

11.1 TEST EQUIPMENT AND METHODOLOGIES

11.1.1 Traction Test Rigs

Two test rigs were developed during the project to allow the completion of the traction investigations. Two fundamentally different drive mechanisms were used for these, but both achieved similar patterns of tractive performance on both the soil and sand surfaces. The similarities between the tractive performances derived from the two rigs were most striking when they were operated at higher wheel slips. In particular, in terms of the consistency of the relationships developed between the wheel slip, sinkage, and contact area. These relationships indicated that the treatments tested had affected both the gross thrust and rolling resistances generated by the tyres, which in combination governed the overall net thrust output. The net thrusts generated varied between approximately +1.2 kN and -4 kN on the sand surface in both instances. The similarities in the performance (behaviour), and comparative tests conducted on both the soil and sand, confirmed that the results were related to the thrust interaction between the surface and the tyre tread and not a particular drive system.

The variable slip (hydrostatic) drive was used for the majority of the testing, as it provided several replications of a wheel passing from a mobile to immobile situation due to the large sand displacements. It was also more operationally flexible when changing the intended band of wheel slip. Typically ranges of slip of approximately 50% to 60% slip were achieved, which enabled the investigation of the tyre behaviour across a range of conditions (from 15% to 75% wheel slip). The variable sinkage behaviour that occurred did so because of the combination of the varying wheel slip and the constant forward motion of the test rig. This was partially self-reinforcing as it caused the normal load acting on the tyre to vary dynamically, but this allowed a tyre's interaction with the sand to be studied across a range of tractive conditions, rather than a single case, so a greater range of results were collected. Additionally the repetitive cycles of the test rig allowed more results to be produced from a single test run, so more significance could be derived from the test results.

The use of the University soil bin facilities enabled the testing to be conducted in a controlled environment with a degree of consistency that would be impossible to replicate in any field environment. The repeatability provided by the test methodology allowed the results to be easily compared to establish their variance. However, the complex interlinked nature of the results made the production of a simple method of tyre (tread) performance comparison, such as a slip-pull graph, difficult. Therefore the modelling techniques developed had to firstly allow the effects of the inter-relationships between the slip, sinkage, load and tread pattern upon the net thrust that was generated to be understood. Secondly, they had to allow the tread pattern and its effect upon the performance to be quantified in a manner that allowed comparative evaluations.

11.1.2 Sand Displacement Assessment Methodology

This measurement methodology was developed specifically for this project. For the tag movements to be accurately determined, both the tag placement locations and their final positions (displacements) had to be accurately determined. All the equipment developed by the author for this purpose was proved to be suitably accurate for the task (positioning and measurement accuracy ± 5.5 mm). The placement equipment was particularly effective in the X-Y plane, but its accuracy reduced in the vertical plane as it occasionally failed (approximately 1% of occasions) to release the tags at the correct depth and instead positioned them up to 5 mm too high. Although adequate for the tests conducted, this apparatus would need re-designing if significantly deeper tag placements were required to prevent deflection of the rods during installation.

The key benefit that the tag measurement frame delivered for the investigations, when used with Excel, was a fast and simple method of transforming the three-dimensional tag positions into real Cartesian disturbance measurements relative to a fixed reference point. A more automated insertion process could hasten the overall operation, but this would not avoid the largest time absorbing factor necessary to produce accurate results, which was the painstaking tag excavation process.

The data tags proved to be a reliable and accurate method of recording the movement of particles within a sand mass. The main criticisms of this methodology were threefold.

Firstly, it was not possible to accurately place sufficient tags to comprehensively record the disturbance patterns that occurred in close proximity to the tyre tread, due to the complex disturbances that occurred. Secondly, it was very time consuming to accurately place, uncover and measure the tag positions. Finally, it could not determine the exact trajectories of the particles, so they were assumed to follow vector paths, even though this was thought to be unlikely.

The merits of this system do not lie in a large-scale application outside a research environment, but in its ability to provide otherwise unobtainable data, which allowed a superior empirical quantification of the magnitude of three-dimensional sand disturbance caused by a 4x4 tyre, without constraining or interrupting the resulting sand flow. This in turn allowed the successful development and validation of model predictions. In the future this approach will be useful to confirm the CFD sand displacement models that will undoubtedly be developed to replicate traction situations.

11.2 MODELLING CAPABILITIES

To enable the gross thrust effect of the tread (and tyre) to be considered, it had to be derived from the net thrust results recorded during the sand displacement experiments. This was achieved by calculating a resistance to add to the net thrusts ($NT + RR = GT$). The good agreement that occurred between measured resistances and those predicted by the rolling resistance model across the range of sinkage experienced (maximum error of 7%) enabled resistances to be predicted for each net thrust result (see Figure 10.7). This allowed suitably accurate gross thrust data to be derived from the data recorded from the full duration of each test run, for both the driven and towed-driven conditions. These were compared against gross thrust predictions produced by the modified equations and agreement was noted. The combination of the measured net thrusts and the rolling resistance predictions therefore enabled gross thrusts to be calculated. These were shown to give close agreement with the predicted gross thrusts (maximum error $\pm 8\%$).

The tread model (equation 58) developed by the author (in the absence of a recognised method) produced quantitative representations of the tread patterns, which were termed tread coefficients. These allowed the theoretical longitudinal gross thrust benefits of the

treads to be calculated for the sand environment, based upon the treads' features (see Appendix 25). The evaluations of the differences in the gross thrusts (tread factors) that the prototype treads were capable of achieving showed the ranked order of treads (by thrust) matched the ranked hierarchy of the magnitudes of sand displacements, i.e. the G82 and LAT which typically caused the highest disturbances also produced the highest extra gross thrusts (the highest tread factors). This thrust benefit was necessarily determined in a holistic manner from all of the data, as no simple methodology was able to separate the complex inter-relationships caused by the tyres. A close relationship was established between the tread factors and coefficients (equation 65) which enabled the percentage extra gross thrust that a tread with a given tread coefficient would be capable of achieving over a plain tread tyre on loose desert sand to be calculated.

The tread representation also allowed a relationship between the tread patterns and the sand displacements they caused to be determined. The significance of the trends was negligible at low slips, but at higher slips the treads with higher tread coefficients caused considerably more sand to be displaced, so the relationship was non-linear. As the treads with higher tread coefficients created more longitudinal sand flow, this explained why they derived both greater gross thrusts and increased wheel sinkages.

11.3 TYRE PERFORMANCE

11.3.1 Cyclical Slip and Thrust Behaviour

The modelling results confirmed that the gross thrusts achieved were dependent upon the wheel sinkage, load, contact area and slip, but providing 15% slip was exceeded the effect of slip on the gross thrust was considerably less significant than other factors. Instead slip had a much more significant influence on the wheel sinkage, and hence the rolling resistance, as increased slip sinkage notably increased the depth of operation. As the slip cyclically changed over the course of each test run, 80 mm to 100 mm variations in wheel sinkage were generated. These caused significant vertical accelerations of the test rig, as it drove (dug) itself into or out of the sand mass. These were equivalent to a 50% increase (or decrease) in dynamic loading ($\pm\frac{1}{2}$ g). The minimum loading occurred at minimum sinkage and vice versa. Therefore as the

sinkage increased the contact area was increased because it was surrounded by extra sand and because the extra loading caused an increased deflection of the tyre carcass.

The increased contact area (and loading) potentially produced a gross thrust benefit for the tyre. However, gross thrust was only one part of the relationship. Both the fixed slip and variable slip test runs that were conducted on the sand found that increased wheel slip led to extra sinkage, but not increased net thrust. This was because the increased sinkage also caused the tyre to face a greater mass of sand ahead of itself, which generated extra rolling resistance. Although the gross thrust output at low sinkages exceeded the rolling resistance, the rate of increase in resistance with increased sinkage exceeded the rate of increase in gross thrust as the sinkage increased (Figure 10.25). Therefore extra sinkage produced greater immobility. As the wheel slip exceeded 20% (which yielded good sand shear) the variation in the magnitude of the slip at higher slips did not greatly influence the gross thrust output. However, the slip sinkage governed the rolling resistance faced by the tyre instead and therefore the slip indirectly controlled the net thrust.

The combination of the variations in gross thrust and rolling resistance caused the net thrusts to cyclically vary between approximately +1 kN and -4 kN over a test run (for a 235/70 R16 tyre on sand). The peak net thrust output of +1 kN was authenticated by a whole vehicle test in which a similar net thrust was achieved on the same sand surface at a low sinkage. It was found that for both the fixed slip tests and the variable slip tests the maximum (positive) net thrusts were achieved at the lowest slips, and as the slip was increased the increased sinkage (resistance) caused the tyre to become immobilised. When higher slips occurred the transformation from mobility to immobility occurred more rapidly, as the tyre sank faster.

11.3.2 Sand Displacements

The sand displacement results highlighted that performance differences existed between the tread patterns. Two elements of the tyres contributed to the sand displacements, and therefore the recorded thrusts. These were (1) the tyre carcass structure and its dimensions, and (2) the tread pattern. The carcass was responsible for the main

quantities and patterns of sand displacement experienced, which occurred in all three-dimensions. The common disturbances due to the carcasses occurred across a 500 mm wide by 250 mm deep portion of the sand mass. In contrast, the treads only influenced a region of sand 200 mm wide by 200 mm deep. Within this region only variations in the displacement in the longitudinal (rearward) direction were significantly related to variations in the tread pattern, and more importantly the variation in the magnitude of gross thrust caused by each tread (up to 5% extra thrust over a plain tread tyre).

The directions of the sand displacements were significantly affected by the magnitude of wheel slip. Increased slip caused increased rearward sand displacements, so the displacements changed from being both downwards and rearwards, to mostly rearwards. This change was supported by the modelling results, which indicated that when passing from medium to high slips a changeover occurred, such that the sand came to be both sheared and thrown rearwards. The increased volume of displacement at higher slips that this created caused larger voids beneath the tyres, which in turn increased the lateral sand flows along the side of the tyre rut, as failure back towards the tyre and into the rut occurred. Carcass effects upon sand displacement were not investigated as a constant tyre size was tested, but it is more likely that changes to the tyre dimensions would have affected the magnitudes of the displacements, rather than their directions.

11.3.3 Tread Effects

The investigation of the effects of tread showed that the PT tread produced the least rearwards sand displacement. This displacement was used as a base line quantity of disturbance against which any extra longitudinal displacement produced by the other treads could be quantified. The treads that created the biggest disturbances (G82 and LAT) tended to generate the peak positive net thrusts. However, they also generated the peak negative net thrusts because they operated at slightly higher slips (up to +5%), which caused them to operate slightly deeper, especially at maximum slip.

When the extra gross thrusts produced by the treads during the displacement investigations were ranked by magnitude, their order agreed with a ranking based upon the magnitude of the displacements, i.e. greater displacement equalled a greater gross

thrust capability. The tread model developed by the author (equation 58) linked this effect to the tread, such that the treads with higher tread coefficients were those that were able to achieve more thrust. However, the increased thrust came at the expense of greater sand disturbance (sinkage), particularly at higher slips. This explained why at low slips and low sinkages the higher tread coefficient treads developed higher net thrusts (due to higher gross thrusts), yet why at high slips they offered the most negative net thrusts due to the extra resistance generated by the extra sinkage they caused.

This relationship showed that at the low forward speeds (5 km/h) tested on this poor mobility surface, continuous positive net traction would only be achieved if the wheel slip were limited to below 20%. If this setting was exceeded then high thrust would momentarily be achieved, but the tyre would soon become immobilised by the excessive sinkage generated by the high slip. At the tested forward speeds the experiment was comparable to the vehicle situation, as the processor resistance represented the resistance of the vehicle, which causes a wheel to spin and dig into the sand if high slips are rapidly applied, rather than drive the vehicle forward. At higher forward speed conditions (which were not investigated) it is suspected that the test methodology would become unrepresentative, as the processor would prevent the tyre rapidly propelling both itself and the vehicle (processor) forward when operating at high slips. Thus the tyre would be prevented from driving up the bow-wave (operating with reduced sinkage), in a manner similar to how dune racers operate. Instead, the resistance of the processor would limit the forward motion and force the tyre to sink into the rut that it would create beneath itself.

At slips of less than 20% the higher tread coefficient treads produced extra gross thrust. This was translated into extra net thrust because at low slips all the treads operated at comparable sinkages, so hence no rolling resistance penalty existed. The thrust results indicated that the maximum possible gross thrust benefit due to tread pattern would always be small in comparison to the total gross thrust generated by the rest of the tyre, but the maximum recorded thrust increase due to tread (+5% over a plain tread) was still sufficient enough to cause a significant effect.

11.3.4 Contact Patch Pressure Distributions

The pressure distributions were recorded for four of the treads at the point of greatest interest in the thrust/ slip cycle, when high slip (approx. 70%) was causing high sand displacement, which was the condition that resulted in tyre immobility. Reduced pressures were recorded at the tyre entry and exit points, whilst the highest pressures were recorded across the second quarter of the tread contact length and along the edges of tread features when the traction process concentrated the sand at these tread faces. These pressure distributions indicated that wide variations occurred in the pressures acting across the contact patch in all cases, which agreed with results presented by other previous authors. Although wide variations occurred within the pressure distributions experienced beneath all of the treads, in each case the recorded average pressure agreed with the expected average pressure, which was calculated based upon the measured contact area and acting normal load at the point in the thrust cycle under consideration.

The uneven pressure distributions meant that the treads did not produce uniform gross thrusts over their contact lengths. Assuming that the thrust at the tread interface was proportional to the normal load, then the bulk of thrust would have been generated where the maximum normal loads occurred. These positions were concentrated across the second quarter of the contact length, but they also appeared over the third quarter of the contact length. Less thrust would have been produced from the regions where the load was reduced, most notably the contact entry and exit points. The pressure also tended to be increased closer to the shoulder of the treads, rather than along the central portion. Thus, if lateral tread features were to be included on a tread to boost gross thrust performance, as indicated by the tread model, then these should be positioned toward the outer edges of the tyre to achieve the maximum possible thrust benefit.

Towards the end of the contact patch the load (pressure) on the sand reduced and therefore less effort was required to displace any sand located here that had direct contact with the treads. Thus the sand that was closest to the surface experienced the greatest rearward displacements. This effect was especially pronounced at the highest slips, when the sand tended to be both sheared and thrown rearwards, rather than being solely sheared rearwards as it was at lower slips. These changing displacement effects

accounted for why much higher sand displacements were recorded at the highest slips, than the medium or lower slips.

The possible longevity of the TekScan mats under exposure to harsh shear environments had always been questioned, and whilst the rubber covers offered mechanical protection, they could not prevent the multi-planar deformations that the mats endured during the contact event, which led to the connections being severed. Despite the mats' failures to withstand these extreme conditions, the preliminary tests undertaken at zero slip on a firm surface were all conducted satisfactorily, as less extreme deflection differentials were experienced. This functionality means that potentially some research applications could change from placing mats on the ground and driving over them, which still causes some mat damage, to instead encapsulating them onto experimental tyres. This could allow speedier data collection and enable greater mobility, as experimentation could occur upon a range of surfaces.

11.3.5 Combination of the Effects Upon Performance

The experimental results and subsequent modelling showed that tread pattern affected tyre performance in off road sand conditions, but its effect was small in comparison to the thrust achieved by the overall tyre dimensions and construction, i.e. the considerable increase in contact patch length that can be generated at low inflation pressures. As the tyre body, its carcass and dimensions, rather than the tread, generated the majority of this thrust, then thrust on sand could only be greatly increased by fitting larger tyres. As the tyre diameter has already been maximised within the bodywork and packaging constraints, and the width and stiffness are limited by handling and manoeuvrability constraints, the small thrust contribution (recorded as up to 5% gross thrust) that a tread can give becomes significant for the low mobility conditions under consideration.

At low slips (below 20%) and therefore low sinkages the tyre's gross thrust exceeded its rolling resistance and thus positive net thrust and forward progress ensued. This set of circumstances was stable until wheel slip was increased, a method which some drivers use in an attempt to increase thrust. However, extra slip produced extra slip sinkage and thus extra resistance, which exceeded the actual gross thrust benefit yielded. This

achieved negative net thrust and led to the tyre being immobilised. The only way to maintain mobility at low forward speeds tested on this surface was to limit the wheel slip to below 20%. This would not however prevent immobility on significantly softer sand conditions, where the initial sinkage due to bearing capacity failure would be significantly increased to the point where the resistance would exceed the maximum achievable gross thrust.

At higher forward speeds it may not be desirable to limit the slip. In these instances it is likely that the ability to achieve a large amounts of sand displacement becomes vital to the vehicle being able to generate sufficient thrust and momentum so that it can maintain its speed and keep on the crest of the bow-wave (reduced sinkage), leading to reduced sinkage. Speed (or momentum) effects were not investigated, nor were they were modelled, so although slip should be controlled at low speeds, the type of control required at high forward speeds is unknown.

Tread patterns influenced both the amount of gross thrust achieved and the rate at which sinkage (resistance) increased. The magnitude of the extra sinkage (resistance) generated by the tread increased as the wheel slip increased. Despite this relationship, if the slip was limited, then the maximum traction would be derived from a more laterally treaded (higher tread coefficient) tyre, which featured a high quantity of tread grooves. The tyres tested were capable of achieving up to 1 kN of net thrust on the sand surface at the forward speeds that were investigated, providing that the wheel slip was limited.

Although a range of different prototype treads were tested, it was found that the standard production G82 tread was capable of achieving the greatest percentage extra thrust (relative to a plain tread). This was not unexpected as this tread was developed for this purpose, and it achieved the highest tread coefficient score. It was interesting to prove that the quoted performance benefits achieved by the actual G82 tyre are not only due to both its shape and size, but also its tread pattern. So although the larger diameter tyres were able to generate the greatest net thrusts, a larger diameter tyre that featured the G82 tread pattern would deliver the maximum known performance.

Alternatively the tread model (equation 58) could be used to design a tread with a higher tread coefficient score (gross thrust potential) than the G82 tread, which would potentially deliver even higher thrusts. This possibility was not investigated, but such a tread would require tread grooves sufficiently wide (approximately 5 mm) to allow sand to enter them, whilst retaining sufficient block width to provide enough mechanical strength to shear the sand and maintain a typical block: groove ratio of between 60% to 70%. Extra thrust could also be developed by tread features to constrict the sand flow. Whilst this factors can be adjusted, equation 55 clearly demonstrated that slip exercised much greater control over the tyre performance than the tread, and thus any optimisation of tyre tread is of limited use without an adequate traction (slip) control system.

11.4 TYRE RECOMMENDATIONS AND IMPLICATIONS

The outcomes of the work showed that for traction to be maximised, wheel slip must be controlled. Land Rover has used this knowledge in the production of control strategies to govern the vehicle drive attributes through slip control and traction control systems for sand environments, irrespective of the tyre fitment. These allow the vehicle to derive maximum net thrust from the tyre and surface, by offering faster and more complex vehicle control than any driver is capable of achieving. These systems will help maintain Land Rover's brand value of off-road excellence, which will assist in justifying the premium price tag of its vehicles.

The current market trends exhibit increased competition in the 'high performance' premium sector of the 4x4 market, e.g. the new entrants of Volkswagen Touareg and Porsche Cayenne, alongside established brands such as Jeep and Toyota. Such vehicles need to be fitted with high quality, high performance road going tyres that are capable of delivering the grip necessary to keep these powerful vehicles, which inherently have a reduced dynamic capability (e.g. high centre of gravity) on the road. In many markets highways lead to the off-road environment, so the vehicles must be able to perform well on-road to safely reach an intended off-road destination. These requirements force OEM's to fit tyres capable of safely achieving the necessary on-road performance as the number one priority.

Market opportunities exist for selling dedicated off-road sand tyres in the replacement (custom) tyre market. These customers would be more likely to select tyres to suit their personal vehicle usage. Choosing these as a second set of dedicated off-road sand tyres could be useful for certain global regions and vehicle roles, i.e. expeditions, military vehicles and serious off-road enthusiasts. However, the size of modern 4x4 tyres (between 16 and 19 inch rims) make transporting and changing sets of them highly impractical, so most owners are likely to only fit one set of tyres for use in all instances. Therefore most tyre purchasers (either OEM or secondary) seek one set of tyres for their vehicle that will achieve the desired compromise between the levels of on-road versus off-road performance that they require.

Most manufacturers SUV's are road-biased, to suit the larger (road-going) market segments, so tyres that meet the on-road performance criteria are specified as a matter of priority. Contrastingly Land Rover's product (brand) targets demand that its vehicles achieve 'best in class' off road performance, which necessitates that the tyres fitted achieve both on-road, and off-road performance goals. In a similar manner, a secondary tyre purchaser has an opinion regarding the level of performance compromise they wish their vehicle to achieve. For any tyres to be eligible selections for either customer (an OEM or an end-user) then some minimum acceptable levels (baseline hygiene standards) of both on-road and off-road performance must be achieved. Failure to achieve either baseline will preclude a tyre's selection, but a tyre that cost effectively exceeds either, or preferably both, of the entry targets (hygiene standards) becomes desirable. Increasingly achieving the off-road target becomes more challenging as the necessary on-road performance levels become more stringent to enable the tyre to be a competitive fitment.

It is already known that traction on sand can be maximised by fitting the largest possible diameter tyres. Tyres currently fitted to Land Rover vehicles are already close to the achievable boundaries, given all the technical constraints and conflicting performance requirements, so this has already been exploited. Therefore given the necessities to maintain a given tyre size and construction, the only option remaining to improve the necessary performance compromise is the adjustment of the tread pattern. '*Serious*' off-

road drivers were shown to be capable of using their experience to choose tyres that would offer good off-road performance. However, a desire also existed to fit tyres that would 'look good' on their cars. High performance and 'good' looks are not mutually exclusive, but good off-road performance requires high profile tyres, which are deemed as less attractive and perform worse on road. Tread patterns can be adjusted for looks, but if the priority is performance, then a tyre should be designed to achieve the necessary on-road performance targets, after which the tread should, where possible, be optimised to give good thrust in the off-road environment.

The current G82 tread pattern from Goodyear was shown to offer the best gross thrust improvement gains (+5%) on the loose sand conditions that were tested. This was due to a good combination of lateral edges, a balance between the quantity and the width of the grooves, and a number of constricting tread features, all of which combined to promote sand/ sand shear and thus high thrusts. However, such large tread features potentially make a tyre too noisy and insufficiently capable at high speeds for the level of on-road performance currently required, so a more refined version would be necessary. Whilst the other tested treads were less capable, they helped determine important tread features for the delivery of good thrust performance. Therefore developments that Goodyear could make for improved off-road capability for on-road/ loose sand biased tyres would be to incorporate the maximum possible number of lateral tread edges, though these need not be continuous. Maintaining a groove of sufficient width to allow sand ingress (i.e. approximately 5 mm) between these edges is also a necessity and constricting tread features (apexes) can assist in achieving extra thrust.

The main benefit that this work delivered were the models (equation 55, 58 and 65) that allowed the effect of the interrelating of variables on desert sand to be understood. These showed that the tread effect was a small, but significant, consideration. Thus predictions can be made for future tread designs, for example, if Goodyear was considering two tread designs that offered similar levels of on-road performance for an SUV, these could be analysed using the models presented to determine which tread would offer the better performance on desert sand, and therefore warrant selection. The models and the test results in this thesis also have potential value in the development of

the computational models of vehicle (and terrain) off-road tractive performance models that will undoubtedly be created in the coming years, as vehicle development becomes further based in the virtual world to achieve extra cost savings.

Tread design is only one small decision to be made among many necessary tyre design considerations, and the results showed that the tread gross thrust effect was small (+5% maximum). For thrust to be maximised most effectively the construction must allow the tyre to freely deform under reduced inflation pressure so that the contact area is maximised. A better way to address the issue and improve vehicle performance both on-road and off-road would be to fit a CTIS system to Land Rover vehicles. This would allow tyre pressure to be adjusted on either surface and would allow tyre pressures to be reduced when off-roading, in the knowledge that they can be increased again, to make driving home safe. This would be a relatively straightforward development for Land Rover, as air inflation systems are already fitted to its products for the air suspension, whilst hollow axles and rim assemblies have been designed for military applications, so these would only need refining.

12 CONCLUSION

The conclusions drawn from the study were grouped into three sections:

12.1 TRACTION MODELLING

- The tyre carcass dimensions and construction accounted for approximately 95% of the gross thrust achieved by a tyre. In contrast the maximum gross thrust benefit achieved by any of the tested tread patterns was less than 5% (G82). However, if tyre dimensions and construction are constrained then the potential extra thrust achieved by a sand-biased tread becomes significant.
- A traction prediction model (equation 55) was developed from adaptations of Bekker's¹⁰⁵ tyre prediction methodologies. This enabled rolling resistance and gross thrust to be predicted for typical 4x4 tyres operating on desert sand to within an error of 7% and 8% respectively. Net thrust could then be derived from these values for constant or fluctuating conditions.
- The measured gross thrust benefit of a tread pattern was related to the quantity of tread grooves and lateral tread features on the tyre via the tread coefficient model developed by the author (equations 58 and 65). In combination these models enabled the prediction of the gross thrust performance of a tread pattern relative to a plain treaded tyre of similar properties, i.e. size and construction.
- The tyre tread performance model can be used for the optimisation of on-road tyres to offer better levels of off-road sand performance, which could enable designers to better meet the conflicting range of on-road and off-road performance requirements for desert tyres in markets situated in desert regions.

12.2 TYRE PERFORMANCE AND DESIGN IMPLICATIONS

- The modelling of the results showed that complex inter-relationships existed between the gross thrust, the wheel slip and the sinkage. Once 15% wheel slip was exceeded the gross thrusts were mainly dependent upon the applied load and contact area, which were both governed by the sinkage, rather than being directly affected by the slip. However, the slip directly governed the wheel sinkage, as increased slip caused increased sinkage, so it indirectly governed the thrust output.
- Positive net thrust was only achieved at low slip, when minimum sinkage (due to bearing capacity failure) occurred, which allowed the gross thrust to exceed the rolling resistance. The modelling proved that the rate of increase in resistance due to increased slip sinkage exceeded the rate by which the gross thrust increased, and thus why the net thrust reduced as slip increased. Therefore to prevent immobilisation on this surface at the 5 km/h (1.4 m/s) forward speed investigated, the wheel slip should be limited to below 20%, irrespective of the tread pattern.
- The tread patterns that produced the greatest quantities of longitudinal sand displacement also produced the most positive gross thrusts, and therefore the highest net traction at low slips. However, at higher slips (in excess of 20% slip) the same treads also caused the highest wheel sinkages, which resulted in rolling resistances that exceeded (nullified) the gross thrust benefit and which thus caused these treads to also be capable of achieving the greatest levels of immobility.
- Consumers indicated that they wanted 'aesthetically pleasing' tread patterns, but this wish was outweighed by their desire for off-road performance. If an 'unsightly' tread achieves sufficient off-road performance the market will always favour it over a more 'pleasing' tread that fails to deliver good thrust.
- For improved net thrust on loose desert sand a tread design should maximise the quantity of lateral tread edges and provide a space between blocks in excess of 5 mm to enable sufficient sand to be captured to maximise sand/ sand shear.

12.3 NOVEL INVESTIGATIVE TECHNIQUES

- A novel sand displacement measurement methodology was developed which enabled sand displacement occurring beneath driven wheels to be quantified to a resolution of ± 5.5 mm in three-dimensions by the application of RFID data tag technology.
- A novel application of TekScan pressure measuring hardware and software directly to the tyre surface enabled maps of the normal stress distributions beneath the tyres during some of the investigations to be determined for a dynamic situation on a deformable surface across the full contact area of the tyres.
- The methodologies, data and models developed from this study could potentially be applied when validating the computational models that will inevitably be developed within the automotive industry to predict off-road vehicle and tyre performance.

13 FUTURE RECOMMENDATIONS

No simple test rig design could deliver a constant torque on a variable soil surface, particularly under the effect of slip sinkage, as soil does not provide a consistent resistance. To account for this situation a closed loop torque control system, with a fast feedback, could be employed which would allow the wheel speed to be far more consistently controlled than was achieved with the presented test rig design.

The applications of the modelling techniques to different production tyre situations were outlined in the thesis. It would be useful to conduct further testing on this surface to widen the boundaries of the model in terms of different sized or shaped wheels and a wider range of normal loads, as this work only investigated a limited range of conditions.

The tread coefficient model (equation 58) produced a very useful means of quantifiably representing tread patterns. The elements of the model were based upon factors that were believed to be important for pure loose sand. The tread model could be used to determine an optimum tread for a sand tyre. This would have to be conducted in an iterative fashion, as the inputs rely on a number of inter-related factors, each of which has different limits, so it is not possible to adjust each variable individually in isolation to achieve the maximum tread coefficient. Instead a structured investigation of different potential tread combinations would be required.

To enable this model to be applied to a greater range of deformable surfaces it may be necessary to include extra terms to account for the interaction between the tread and surface, for instance in a very cohesive soil, the cleaning ability of the tread can become vital, but the representation of this effect was unnecessary for the application to sand traction and therefore ignored. Although in principle the approach detailed in this work would be applicable to a range of surfaces, further research will be necessary to establish what, if any, extra model terms are necessary to improve its representative capability.

The novel use of the TekScan system in this investigation has developed an investigative technique. Previously this system has been used statically beneath rolling tyres on hard surfaces. The new application of the mats directly onto the tyre surface has improved the flexibility of the system and proved its usefulness for investigating normal stress distributions beneath tyres on deformable surfaces. Therefore this approach could now be adopted in similar future investigations on deformable surfaces.

The proven application of the RFID technology to the quantification of sand displacement within soils is a powerful development. The small size of the tags allows them to be introduced into the soil surface with a very minimal disturbance to both the existing conditions and any subsequent soil flow. Whilst it is time consuming to subsequently locate a large number of such tags, careful choice of the boundaries of any such investigation can limit this issue. Irrespectively, this issue would be a criticism of any similar previous methodology, but which have been significantly less capable of reducing the interference of the additional particles on the soil deformation.

14 REFERENCES

- ¹ **Ji, X., Zhuang, J. & Qiu, X.** (1996) *A new type of off-road tire – Bionic Camel Foot Tire*. Proceedings of the 12th International Conference of the International Society of Terrain Vehicle Systems (ISTVS), 1, pp. 639-646.
- ² **Pemberton, M.** (2002) *Long-term forecasting: World Automotive Forum start-up – 31/05/2002*. Automotive Online News and Information. www.automotive-online.com/data_analysis/details.asp, 23/08/02.
- ³ **Hitzky, L. & Van Der Meer, A.** of GTC*L, Goodyear Ltd. (1999) *Personal meeting with the author*. Both light truck/ 4x4 tyre designers/ developers specialising in off-road performance.
- ⁴ **Rodgerson, C.** (1998) *Just Desert*. Land Rover Owner International, no. 8, July 1998, pp. 34-45.
- ⁵ **Sheppard, T.** (1994) *The Land Rover Experience – A user's guide to four-wheel driving, 2nd edition*. Land Rover Ltd.
- ⁶ **Franklin, E.** of Land Rover Ltd. (Various 1998-2002) *Personal communications with the author*. Senior tyre test/ tyre development engineer.
- ⁷ **Lechtenböhmer, A.** of GTC*L, Goodyear Ltd. (1998) *Tire technology – a training course*. Unpublished.
- ⁸ **Robinson, T.** (1998) *Foreword – Statistically speaking*. Tire Technology International, December 1998.
- ⁹ **Williams, M.** of Land Rover Ltd. (Various 2002) *Personal communications with the author*. Traction and modelling engineer.
- ¹⁰ **Micklethwaite, E. W. E.** (1944) *Soil mechanics in relation to fighting vehicles*. Military College of Science, Chertsey, UK.
- ¹¹ **Liu, J.** (1994) *The mechanism of sinkage of running gear on sand*. Journal of Terramechanics, 31 (3), pp. 185-195.
- ¹² **Goodyear GTC*L** (1996) *Basic Tyre Training, June 1996*. Unpublished technical report.
- ¹³ **Garbari, F.** (1964) *Rolling resistance of wheeled vehicles on deformable terrains*. Journal of Terramechanics, 1 (1), pp. 7-30.
- ¹⁴ **Wang, Z. & Reece, A.** (1984) *The performance of free rolling rigid and flexible wheels on sand*. Journal of Terramechanics, 21 (4), pp. 347-360.
- ¹⁵ **Ataka, H & Yamashita, F.** (1995) *Analysis and prediction of tire performance on sand*. Tire Science and Technology, TSTCA, 23 (1), pp. 52-67.
- ¹⁶ **Kemp, I.** of Dunlop Tyres Ltd. (Various 2000-2001) *Personal communications with the author*. Tyre research manager, Dunlop UK.
- ¹⁷ **Driven** (2002) *TV motoring programme screened on Channel 4*. Shown at 20.30, 18th April, 2002.

-
- ¹⁸ Zhuang, J., Wang, Z. & Liu, J. (1990) *Study on the dynamic characteristics of wheeled vehicles on sand*. Proceedings of the 2nd ASME Symposium on Transportation systems, ASME Winter Annual Meeting, Dallas, Texas.
- ¹⁹ Zhuang, J., Wang, Z. & Liu, J. (1991) *The ways to improve trafficability of vehicles on sand*. Proceedings of the 5th European Conference of the International Society of Terrain Vehicle Systems (ISTVS), 1, pp. 121-126.
- ²⁰ Bekker, M. G. (1960) *Off-the-road locomotion; research and developments in terramechanics*. University of Michigan Press, Ann Arbor.
- ²¹ Wismer, R. D. & Luth, H. J. (1973) *Off-road traction prediction for wheeled vehicles*. Journal of Terramechanics, 10 (2), pp. 49-62.
- ²² Piper, E. J. W. (2000) *Experimental design for the evaluation of the tractive performance of tyres in sand*. Unpublished BSc. Thesis, Cranfield University at Silsoe.
- ²³ Perera, R. (1979) *The effect of tread pattern and wheel shape on rolling resistance in sand*. Unpublished TEng. Thesis, Cranfield University at Silsoe.
- ²⁴ Gill, W. R. & Vanden Berg, G E. (1968) *Soil dynamics in tillage and traction*. Agricultural Handbook No. 316; Agricultural Research Service, United States Department of Agriculture.
- ²⁵ Gliemerth, G. (1953) *Investigations of compaction and displacement phenomenon in the soil under wheel and track vehicles*. Zeitschrift fur Acker und Pflanzenbau, 96, pp. 218-234.
- ²⁶ Payne, P. C. J. (1956) *Relationships between the mechanical properties of soil and the performance of simple cultivation implements*. Journal of Agricultural Engineering Research, 1, pp. 23-50.
- ²⁷ Bekker, M. G. (1958) *Performance improvement in track-type tractors*. Agricultural Engineering, 39, pp. 630-632.
- ²⁸ Wong, J. Y. & Reece, A. R. (1966) *Soil failure beneath rigid wheels*. Proceedings of the 2nd International Conference of the International Society for Terrain-Vehicle Systems (ISTVS), pp. 425-445.
- ²⁹ Wong, J. Y. (1967) *Behaviour of soil beneath rigid wheels*. Journal of Agricultural Engineering Research, 12 (4), pp. 257-269.
- ³⁰ Oliver, M. J. (2002) *Contact patch dynamics of pneumatic tyres in pure sand*. Unpublished EngD. Thesis, Cranfield University at Silsoe.
- ³¹ Shikanai, T., Hashiguvhi, K., Nohse, Y., Ueno, M. & Okayasu, T. (2000) *Precise measurement of soil deformation and fluctuation in drawbar pull for steel and rubber-coated rigid wheels*. Journal of Terramechanics, 37 (1), pp. 21-39.
- ³² Nohse, Y., Hashiguchi, K., Ueno, M., Shikanai, T., Izumi, H. & Koyama, F. (1991) *A measurement of basic mechanical quantities of off-the-road travelling performance*. Journal of Terramechanics, 28 (4), pp. 359-370.
- ³³ Hashiguchi, K., Nohse, Y., Ueno, M., Sumiyoshi, K., Uchiyama, K. & Yoshimaru, T. (1994) *Travelling performance of a wheel on a finite thickness ground*. Journal of Terramechanics, 31 (4), pp. 257-263.
-

-
- ³⁴ **Marantz P.** of Cranfield University (2000) *Personal communication with the author.* Expert in image processing and control, School of Industrial Manufacturing Science.
- ³⁵ **Reynolds, A. J. R.** of Cranfield University at Silsoe (Various 1998-2002) *Personal communications with the author.* Senior soil bin technician.
- ³⁶ **Abebe, A. T., Tanaka, T. & Yamazaki, M.** (1989) *Soil compaction by multiple passes of a rigid wheel relevant for optimisation of traffic.* Journal of Terramechanics, 26 (2), pp. 139-148.
- ³⁷ **Wood, R. K. & Wells, L. G.** (1985) *Characterizing soil deformation by direct measurement within the profile.* Transactions of the ASAE, 1985, 28 (6), pp.1754-1758.
- ³⁸ **Spoor, G. & Trein, C. R.** (1992) *A technique for quantifying soil strain and density change.* ASAE. Paper no. 92-1505, St. Joseph, MI.
- ³⁹ **Trein, C. R.** (1995) *The mechanics of soil compaction under wheels.* Unpublished PhD. Thesis, Cranfield University at Silsoe.
- ⁴⁰ **Yu, Qun, Jie, Shen, & Xianbin, Dia.** (1996) *Camera tracing and image processing system for soil deformation.* Journal of Terramechanics, 29 (4/5), pp. 423-431.
- ⁴¹ **Wells, L. G., Yaping, Jiang, & Xing, Zhang Xiao.** (1996) *Measuring three-dimensional soil deformation.* Journal of Terramechanics, 33 (6), pp. 281-292.
- ⁴² **Xing, Zhang Xiao, Wells, L. G., Yaping, Jiang & Shearer, S. A.** (1997) *Using image analysis to measure two-dimensional soil deformation.* Journal of Terramechanics, 34 (2), pp. 73-82
- ⁴³ **Burt, E. C., Reaves, C. A., Bailey, A. C. & Pickering, W. D.** (1980) *A machine for testing tractor tires in soil bins.* Transactions of the ASAE, 23 (3), pp. 546-552.
- ⁴⁴ **Wells, L. G. & Buckles, J. D.** (1987) *PC-controlled soil/ tire tester.* ASAE. Paper no. 87-1014, St. Joseph, MI.
- ⁴⁵ **Boyd, C. W & Windisch, S. J.** (1966) *A technique for measuring deformations within a sand under controlled wheel loads.* Proceedings of the 2nd International Conference of the International Society for Terrain-Vehicle Systems (ISTVS), 1, pp. 183-197.
- ⁴⁶ **Windisch E. J. & Yong, R. N.** (1970) *The determination of soil strain-rate behaviour beneath a moving wheel.* Journal of Terramechanics, 7 (1), pp. 55-67
- ⁴⁷ **Way, T. R., Bailey, A. C., Raper, R. L. & Burt, E. C.** (1993) *Tire lug height effect on soil stress measurements.* ASAE paper, no. 93-1033.
- ⁴⁸ **Way, T. R., Johnson, C. E. Bailey, A. C., Raper, R. L. & Burt, E. C.** (1996) *Soil stress state orientation beneath a tyre at various loads and inflation pressures.* Journal of Terramechanics, 33 (4), pp. 185-194.
- ⁴⁹ **Nichols, T. A., Bailey, A. C. Johnson, C. E. & Grisso, R. D.** (1987) *A stress state transducer for the soil.* Transactions of the ASAE, 30 (5), pp. 1237-1241.
- ⁵⁰ **Hammel, K.** (1994) *Soil stress distribution under lugged tyres.* Soil and tillage research, 32, pp. 163-181.
-

-
- ⁵¹ Freitag, D. R., Green, A. J. & Murphy, N. R. (1965) *Normal stresses at the tire soil interface in yielding soils*. Highway Research Record, No. 74, pp. 1-18.
- ⁵² Trabbic, G. W., Lask, K. V. & Buchele, W. F. (1959) *Measurement of soil-tire interface pressures*. Agricultural Engineering, Nov. 1959, pp. 678-681.
- ⁵³ Burt, E. C., Wood, R. K. & Bailey, A. C. (1992) *Some comparisons of average to peak soil-tire contact pressures*. Transactions of the ASAE, 35 (2), pp. 401-404.
- ⁵⁴ Oida, A., Satoh, A., Itoh, H., & Triratanasirihai, K. (1988) *Measurement and analysis of normal, longitudinal and lateral stresses in the wheel-soil contact area*. Proceedings of the 2nd Asia-Pacific Conference of the International Society for Terrain-Vehicle Systems (ISTVS).
- ⁵⁵ Krick, G. (1969) *Radial and shear stress distribution under rigid wheels and pneumatic tires operating on yielding soils, with considerable tyre deformation*. Journal of Terramechanics, 6 (3), pp. 73-98.
- ⁵⁶ Oida, A., Satoh, A., Itoh, H., & Triratanasirihai, K. (1991) *Three-dimensional stress distributions on a tire-sand contact surface*. Journal of Terramechanics, 28 (4), pp. 319-330.
- ⁵⁷ Smith, B. E., Burcham, T. N., To, F. S., Van Devender, K. W. & Matthes, R. K. (1994) *Mobile soil-tire interface measurement system*. Transactions of the ASAE, 37 (5), pp. 1633-1637.
- ⁵⁸ Burt, E. C., Bailey, A. C. & Wood, R. K. (1987a) *Effects of soil and operational parameters on soil-tire interface stress vectors*. Journal of Terramechanics, 24 (3), pp. 324-327.
- ⁵⁹ Burt, E. C., Wood, R. K. & Bailey, A. C. (1987b) *A three-dimensional system for measuring tire deformation and contact stresses*. Transactions of the ASAE, 30 (2), pp. 401-404.
- ⁶⁰ Assegedow, T. (1991) *An investigation into developing a conductive rubber transducer for tyre contact stress measurement*. Unpublished MSc Thesis, Cranfield University at Silsoe.
- ⁶¹ Haresign, S. (1993) *Development of transducers to determine normal and shear forces exerted on a rubber crawler track over the contact area*. Unpublished MSc Thesis, Cranfield University at Silsoe.
- ⁶² TekScan Inc. Website. (1999) www.tekscan.com
- ⁶³ Wong, J. Y. (1989) *Terramechanics and off-road vehicles*. Elsevier Science Publishers, B. V.
- ⁶⁴ Baladi, G. Y. & Rohani, B. (1984) *Development of a soil-wheel interaction model*. Proceedings of the 4th International Conference of the International Society for Terrain-Vehicle Systems (ISTVS), I, pp. 33-60.
- ⁶⁵ Upadhyaya, S. K. & Wulfsohn, D. (1990) *Review of traction prediction equations*. ASAE Paper No. 90-1573.
- ⁶⁶ Sharma, A. K. & Pandey, K. P. (1996) *A review on contact area measurement of pneumatic tyres on rigid and deformable surfaces*. Journal of Terramechanics, 33 (5), pp. 253-264.
-

-
- ⁶⁷ Freitag, D. R. (1965) *A dimensional analysis of the performance of pneumatic tires on soft soils*. Technical Report No. 3-688, U.S. Army Engineer Waterways Experiment Station, Vicksburg, Mississippi.
- ⁶⁸ Turnage, G. W. (1972) *Performance of soils under tire loads; application of test results to tire selection for off-road vehicles*. Technical Report No. 3-666, 8th September, U.S. Army Engineer Waterways Experiment Station, Vicksburg, Mississippi.
- ⁶⁹ Dwyer, M. J., Comely, D. R. & Evernden, D. W. (1975) *Development of the N.I.A.E. handbook of agricultural tyre performance*. Proceedings of the 5th International Conference of the International Society for Terrain-Vehicle Systems (ISTVS).
- ⁷⁰ Wismer, R. D. & Luth, H. J. (1974) *Off-road traction prediction for wheeled vehicles*. Transactions of the ASAE, 17 (1), pp. 8-14.
- ⁷¹ Godbole, R. & Alcock, R. (1995) *A device for the in situ determination of soil deformation modulus*. Journal of Terramechanics, 32 (4), pp. 199-204.
- ⁷² Reece, A. R. & Peca, J. O. (1981) *An assessment of the value of the cone penetrometer in mobility prediction*. Proceedings of the 7th International Conference of the International Society for Terrain-Vehicle Systems (ISTVS), III: A1-A33.
- ⁷³ Turnage, G. W. (1984) *Prediction of in-sand tire and wheeled vehicle drawbar performance*. Proceedings of the 8th International Conference of the International Society for Terrain-Vehicle Systems (ISTVS), I, pp. 121-150.
- ⁷⁴ Gee-Clough D. (1978) *A comparison of the mobility number and the Bekker approaches to traction mechanics and recent advances in both methods at N.I.A.E.* Proceedings of the 6th International Conference of the International Society for Terrain-Vehicle Systems (ISTVS), II, pp. 735-755.
- ⁷⁵ Wong, J. Y. (1984) *On the study of wheel-soil interaction*. Journal of Terramechanics, 21 (2), pp. 117-131.
- ⁷⁶ Dwyer, M. J., Comely, D. R. & Evernden, D. W. (1974) *The field performance of some tractor tyres related to soil mechanical properties*. Journal of Agricultural Engineering Research, 19, pp.35-50.
- ⁷⁷ Alcock, R. & Wittig, V. (1992) *An empirical method of predicting traction*. Journal of Terramechanics, 29 (4/5), pp. 381-394.
- ⁷⁸ Bekker, M. G. (1956) *Theory of land locomotion; the mechanics of vehicle mobility*. University of Michigan Press, Ann Arbor.
- ⁷⁹ Bekker, M. G. (1959) *Mobility of cross-country vehicles, 1; Thrust for propulsion*. Machine Design, December 24, pp. 93-98.
- ⁸⁰ Bekker, M. G. (1960) *Mobility of cross-country vehicles, 2; Flotation and motion resistance*. Machine Design, January 7, pp. 145-152.
- ⁸¹ Bekker, M. G. (1969) *Introduction to terrain-vehicle systems*. University of Michigan Press, Ann Arbor.
- ⁸² Dwyer, M. J. (1984) *The tractive performance of wheeled vehicles*. Journal of Terramechanics, 21 (1), pp. 19-34.
-

-
- ⁸³ **Onafeko, O. & Reece, A. R.** (1967) *Soil stresses and deformations beneath rigid wheels*. Journal of Terramechanics, 4 (1), pp. 59-80.
- ⁸⁴ **Wong, J. Y. & Reece, A. R.** (1967) *Prediction of rigid wheel performance based on the analysis of soil-wheel stresses, Part I. Performance of driven rigid wheels*. Journal of Terramechanics, 4 (1), pp. 81-98.
- ⁸⁵ **Wong, J. Y. & Reece, A. R.** (1967) *Prediction of rigid wheel performance based on the analysis of soil-wheel stresses, Part II. Performance of towed rigid wheels*. Journal of Terramechanics, 4 (1), pp. 81-98.
- ⁸⁶ **Reece, A. R.** (1965) *Principles of soil-vehicle mechanics*. Proceedings of the Institution of Mechanical Engineers, Automobile division, 1965-66, vol. 180, part 2a, no. 2, pp. 45-66.
- ⁸⁷ **Ziani, F. & Biarez, J.** (1990) *Pressure sinkage relationship for tyres on very loose sand*. Journal of Terramechanics, 27 (3), pp. 167-177.
- ⁸⁸ **Ji, X., Zhuang, J. & Qui, X.** (1996) *Effects of loadings patterns on the pressure-sinkage relation of dry loose sand*. Journal of Terramechanics, 33 (1), pp. 13-20.
- ⁸⁹ **Janosi, Z. & Hanamoto, B.** (1961) *The analytical determination of drawbar pull as a function of slip for tracked vehicles in deformable soil*. Proceedings of the 1st International Conference of the Mechanics of Soil-Vehicle Systems, Italy
- ⁹⁰ **Komandi, G.** (1999) *An evaluation of the concept of rolling resistance*. Journal of Terramechanics, 36 (2), pp. 159-166.
- ⁹¹ **Yong, R. N., Fattah, E. A. & Skiadas, N.** (1984) *Vehicle traction mechanics – developments in agricultural engineering 3*. Elsevier Science Publishers B.V.
- ⁹² **Godbole, R., Alcock, R. & Hettiaratchi, D.** (1994) *The prediction of tractive performance on soil surfaces*. Journal of Terramechanics, 30 (6), pp. 443-459.
- ⁹³ **Wulfsohn, D. & Upadhyaya, S. K.** (1991) *Traction of low-pressure pneumatic tires in deformable soil*. Transactions of the SAE, 100 (2), pp. 348-363.
- ⁹⁴ **Upadhyaya, S. K. & Wulfsohn, D.** (1990a) *Relationship between tire deflection characteristics and 2D tire contact area*. Transactions of the ASAE, 33 (1), pp. 25-30.
- ⁹⁵ **Upadhyaya, S. K. & Wulfsohn, D.** (1990b) *Determination of the 3D soil-tire contact profile*. ASAE Paper No. 90-1571.
- ⁹⁶ **Wulfsohn, D. & Upadhyaya, S. K.** (1992a) *Determination of dynamic three-dimensional soil-tyre contact profile*. Journal of Terramechanics, 29 (4), pp. 433-464.
- ⁹⁷ **Wulfsohn, D. & Upadhyaya, S. K.** (1992b) *Prediction of traction and soil compaction using 3D soil-tyre contact profile*. Journal of Terramechanics, 29 (5), pp. 541-564.
- ⁹⁸ **Upadhyaya, S. K., Wulfsohn, D. & Jubbal, G.** (1989) *Traction prediction equations for radial ply tires*. Journal of Terramechanics, 26 (2), pp. 149-175.
- ⁹⁹ **Upadhyaya, S. K., Wulfsohn, D. & Mehlschau, J.** (1993) *An instrumented device to obtain traction related parameters*. Journal of Terramechanics, 30 (1), pp. 1-20.
-

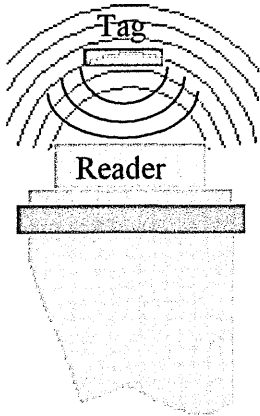
-
- ¹⁰⁰ **Upadhyaya, S. K. & Wulfsohn, D.** (1993) *Traction prediction using soil parameters obtained with an instrumented analogue device*. Journal of Terramechanics, 30 (2), pp. 85-100.
- ¹⁰¹ **Upadhyaya, S. K., Sime, M., Raghuwanshi, N. & Adler, B.** (1997) *Semi-empirical traction prediction equations based on relevant soil parameters*. Journal of Terramechanics, 34 (3), pp. 141-154.
- ¹⁰² **Gee-Clough, D.** (1978) *A comparison of the mobility number and Bekker approaches to traction mechanics and recent advances in both methods at the N.I.A.E.* Proceedings of the 6th International Conference of the International Society for Terrain-Vehicle Systems (ISTVS), II, pp. 735-755.
- ¹⁰³ **Gee-Clough D.** (1976) *The Bekker theory of rolling resistance to take account of skid and deep sinkage*. Journal of Terramechanics, 13 (2), pp. 87.
- ¹⁰⁴ **Hetherington, J. G. & Littleton, I.** (1978) *The rolling resistance of towed, rigid wheels in sand*. Journal of Terramechanics, 15 (2), pp. 95-105.
- ¹⁰⁵ **Bekker, M. G.** (1983) *Prediction of design and performance parameters in agro-forestry vehicles*. National Research Council of Canada Report No. 22880.
- ¹⁰⁶ **Yong, R. N. & Fattah, E. A.** (1976) *Prediction of wheel-soil interaction and performance using the finite element method*. Journal of Terramechanics, 13 (4), pp. 227-240.
- ¹⁰⁷ **Oida, A.** (1984) *Analysis of rheological deformation of soil by means of the finite element method*. Journal of Terramechanics, 21 (3), pp. 237-251.
- ¹⁰⁸ **Regli, G., Handke, A. & Bütikofer, M.** (1993) *Material laws as a basis for simulation models for the calculation of wheel-soil interaction examination using the finite element method*. Journal of Terramechanics, 30 (3), pp. 165-179.
- ¹⁰⁹ **Liu, C. H., Wong, J. Y. & Mang, H. A.** (2000) *Large strain finite element analysis of sand: model algorithm and application to numerical simulation of tire-sand interaction*. Computers and Structures, 74 (3), pp. 253-265.
- ¹¹⁰ **Uffelman, F. L.** (1961) *The performance of rigid cylindrical wheels on clay soil*. Proceedings of the 1st International Conference of the Mechanics of Soil-Vehicle Systems, Italy, pp. 111-125.
- ¹¹¹ **Reece, A. R & Wills, B. M. D.** (1961) *A Forced-slip wheel and track tester*. Proceedings of the 1st International Conference of the Mechanics of Soil-Vehicle Systems, Italy, pp. 387-399.
- ¹¹² **Del Rosario, C. R.** (1980) *Lateral force investigations on steered pneumatic tyres operating under soil condition*. Unpublished Ph.D. Thesis, Cranfield University at Silsoe.
- ¹¹³ **Soehne, W.** (1961) *Discussion of Reece & Wills paper, ref. no. ¹¹¹*. Proceedings of the 1st International Conference of the Mechanics of Soil-Vehicle Systems, Italy.
- ¹¹⁴ **Reed, I. F. & Berry, M. O.** (1949) *Equipment and procedures for farm tractor tyre studies under controlled conditions*. Agricultural Engineering, 30, pp. 67.
- ¹¹⁵ **Bailey, P. H.** (1954) *The N.I.A.E. single wheel tester; an apparatus for research on the performance of tractor wheels*. Report No. 40, N.I.A.E., Silsoe, UK.
-

-
- ¹¹⁶ **Billington, W. P.** (1973) *The N.I.A.E. Mk II single wheel tester*. Research Note, Journal of Agricultural Engineering Research, 18, pp 67-70.
- ¹¹⁷ **Upadhyaya, S. K., Mehlschau, J., Wulfsohn, D. & Glancey, J. L.** (1986) *Development of a unique, mobile, single wheel traction testing machine*. Transactions of the ASAE, 29 (5), pp. 1243-1246.
- ¹¹⁸ **Upadhyaya, S. K., Mehlschau, J., Wulfsohn, D. & Glancey, J. L.** (1985) *Development of a unique, mobile, single wheel traction testing device*. ASAE Paper no. 85-1554, St. Joseph, MI.
- ¹¹⁹ **Keen, A.** (1998) *Traction prediction on a sandy loam soil for a single wheel tester*. Proceedings of the 5th Asia-Pacific Conference of the International Society for Terrain-Vehicle Systems (ISTVS), Seoul, Korea, pp. 393-400.
- ¹²⁰ **Keen, A.** (2001) *The effect of wheel vibration on traction – an investigation using a single wheel tester*. Proceedings of the 6th Asia-Pacific Conference of the International Society for Terrain-Vehicle Systems (ISTVS), Bangkok, Thailand.
- ¹²¹ **Keen, A.** (2001) *The tyre and suspension characteristics of an off-road vehicle determined using a single wheel tester*. Proceedings of the EAEC European Automotive Congress, Bratislava.
- ¹²² **The Advertising Association.** (1995) *Regional marketing pocket book, 1995*. NTC Publications Ltd. Oxfordshire.
- ¹²³ **McDonald, M. & Dunbar, I.** (1998) *Market segmentation, How to do it, How to profit from it*. Macmillan Business, Hampshire.
- ¹²⁴ **British Standards. 1990. 1377: Part 2: Classification tests.** (1990) *Methods of test for classifying soils and for determining their basic physical properties*. B.S.I. London.
- ¹²⁵ **Terzaghi, K. Peck, R. B. & Mesri G.** (1996) *Soil mechanics in engineering practice, 3rd Edition*. J. Wiley & Sons, Inc. New York.
- ¹²⁶ **Osman, M. S.** (1964) *The measurement of soil shear strength*. Journal of Terramechanics, 1 (3), pp. 54.
- ¹²⁷ **Moseley, P.** (1999) *Soil incorporation of bio-solids into arable cropping*. Unpublished EngD. Thesis, Cranfield University at Silsoe.
- ¹²⁸ **Desboilles, J. M. A.** (1994) *Development of semi-empirical draught force models for tillage implements*. Unpublished PhD. Thesis, Cranfield University at Silsoe.
- ¹²⁹ **Hatherill, D. W.** (1993) *The design and development of a rigid tine implement for sub-soil slotting and chemical incorporation*. Unpublished PhD. Thesis, Cranfield University at Silsoe.
- ¹³⁰ **Van Bavel, C. H. M.** (1949) *Mean weight-diameter of soil aggregates as a statistical index of aggregation*. Soil Science Society Proceedings 1949, pp. 20-23.
- ¹³¹ **Bagnold, R. A.** (1965) *The physics of blown sands and desert dunes*. Methuen & Co. Ltd. London.
- ¹³² **Day, R. W.** (2001) *Soil testing manual, procedures, classification data, and sampling procedures*. McGraw-Hill, Inc. New York.
-

-
- ¹³³ **Taylor, D. W.** (1948) *Fundamentals of soil mechanics*. New York, John Wiley & Sons, Inc. London.
- ¹³⁴ **Godwin R. J. & Lovelace G.** (1992) *Soil mechanics laboratory sheet: A measurement of soil/ metal friction*. Unpublished experimental guidance notes, Cranfield University at Silsoe.
- ¹³⁵ **Siemens, J. C. & Weber, J. A.** (1964) *Soil bin and model studies on tillage tools and traction devices*. *Journal of Terramechanics*, 1 (2), pp. 56-67.
- ¹³⁶ **Wismer, R. D.** (1984) *Soil bin facilities: characteristics and utilization*. Proceedings of the 8th International Conference of the International Society for Terrain-Vehicle Systems (ISTVS), Cambridge, UK.
- ¹³⁷ **Hann, M. J. & Giessibel, J.** (1998) *Force measurement on driven discs*. *Journal of Agricultural Engineering Research*, 69 (2), pp. 149-158
- ¹³⁸ **Smith, D. L. O., Godwin, R. J., Spoor, G. S. & Kilgour, J.** (1987) *The new soil bin testing facilities at Silsoe College*. Internal Engineering Report, Silsoe College, Cranfield University, Beds, UK. Unpublished.
- ¹³⁹ **Godwin, R. J.** (1975) *An extended octagonal ring transducer for use in tillage studies*. *Journal of Agricultural Engineering Research*, 20, pp. 347-352.
- ¹⁴⁰ **Brighton, J. L. & Richards, T. E.** (2001) *Soil Dynamics Laboratory Whole Vehicle Test*. Unpublished Test Data, Cranfield University at Silsoe.

APPENDIX 1 – RFID TECHNOLOGY AND PRODUCTS

Background to RFID technology – Text copied from www.robotag.co.uk.



Radio **F**requency **I**dentification uses transponders, usually called tags, which have an aerial and a chip with memory. Its history can be traced back to 'friend or foe' transponders (*transmitter responders*) fitted to aircraft in World War II, through scientific developments during the 70's, to animal id tags introduced in USA and UK in the 80's. Rapid growth in the 90's occurred in two fields, access control (contact-less id passes) and car security. Additionally, the 'chipping' of pets under the 'Pet Passport' scheme has become one of the best known applications, whilst

others include automatic road toll collection, ski lift passes, timing in marathons (tags fitted into shoes) and electronic asset management/ tracking.

A typical RFID transponder is passive i.e. it does not have a battery. It is powered by the electromagnetic field generated by the reader when it 'talks' to the tag. Active transponders also exist. Both passive and active transponders can be read-only or read/write. As the name suggests the unique code in the memory of a read-only transponder cannot be changed, whereas a read/write memory can be changed, stored and then read again. Like the memory in mobile phone SIM cards, this memory is non-volatile and does not need continuous power.

RFID tags come in many shapes and sizes ranging from those implanted in pets (approximately the size of a grain of rice) to credit card sized active tags. The maximum range of a tag and reader system depends on the frequency of the system, the size of the tag and the size and power of the reader. At one extreme, battery powered handheld readers operating at low (125-135 kHz) or medium frequencies (13.56 MHz) have a maximum range of about 30-80 mm, whilst at the other extreme large mains powered high frequency (900 MHz or 2.45 GHz) units working with active tags can have a range of over 50 m.

Specific Destron Fearing tag and reader systems used

Information from www.destron-fearing.com

Destron Fearing has pioneered the development of syringe injectable, miniaturized microchip technology for injection under the skin of animals. The products and technology Destron Fearing manufactures and markets to the animal identification industry include a variety of radio frequency microchips or "tags," portable readers, stationary readers and microchip injecting devices. Destron microchips have their identification codes read by magnetic radio frequency signals generated from scanning devices. The microchip uses the energy from the magnetic field to power itself and transmit a return signal to the scanner, which is converted to the microchip's identification code. The alphanumeric identification code is displayed on the reader, or relayed via computer interface to other equipment. Destron's portable scanners are battery operated and feature similar electrical components, but differing hardware and packaging designs. The scanners considered for this project were the Pocket Reader, and the Pocket Reader EX.



Pocket Reader™



Pocket Reader EX®

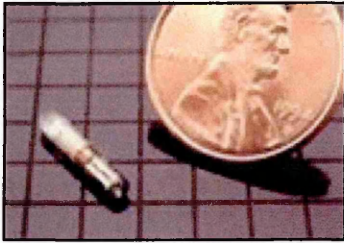
The Destron hand-held "Pocket" type scanners were designed specifically for use with companion animals in animal shelters or veterinary clinics. Both scanners have a one-function button for ease of operation and display only the tag's alphanumeric code. The Pocket Reader EX™ scanner is a universal scanner so it consistently read microchips from various manufacturers.

Pocket Reader Features

- **SMART™:** (Standard Memory And Re-Programmable Technology) The scanners can be re-programmed and through the use of SMART software, they can read current and future microchip technologies in 13 different languages.
- **Automatic Channel Searching:** The Pocket Reader line of products automatically searches for the presence of other manufacturers' microchips.
- **RF Surround:** The scanner's antenna is designed to surround the tag in a high intensity magnetic field. This optimises reading performance for any tag orientation.
- **RS 232 Compatible:** Interface with Serial Interface Link or Smart™ Kit allows the user to send ID codes directly from the scanner to a computer.
- **Low Cost:** The scanners are priced to be affordable for shelters and veterinarians.
- **Ergonomic:** The lightweight scanners are designed to fit easily into the hand of male or female operators to allow for effortless operation with the right or left hand.
- **Pocket Reader EX Only – Larger Antenna Size:** The antenna has a larger surface area designed to give greater read range, surface area coverage and speed.
- **Technical Specification:**

Operating Frequency:	125 kHz or ISO 134.2 kHz
Case Size:	170 mm L x 80 mm W x 32 mm H
Weight:	308 g
Material:	ABS Plastic
Operating Temperature:	0°-50°C or 32°-122°F
Humidity:	10 - 90% (non-condensing)
Storage Temperature:	-20° to 65°C or -4°to 149°F
Batteries:	4 AAA size 1.5-volt alkaline batteries
Display:	16-character LCD
Output Port:	Serial field-programmable port
RS 232 Port:	Compatible

TX1400L – Injectable Transponders (Miniature tags)



The Injectable Transponder is a passive radio-frequency identification tag, designed to work in conjunction with a compatible radio-frequency ID reading system. The transponder consists of an electromagnetic coil, tuning applicator and microchip sealed in a cylindrical glass enclosure.

The chip is pre-programmed with a unique ID code that cannot be altered; over 34 billion individual code numbers are available. When the transponder is activated by low frequency radio signal, it transmits the ID code to the reading system. Although specifically designed for injecting in animals, this transponder can be used for other applications requiring a micro-sized identification tag.

- **Technical Specification:**

Dimensions (nominal):	11 mm by 2.1 mm
Housing:	Bio-compatible glass
Average weight:	0.06g
Temperature range:	-40° to 70°C, operating and storage
Read range with the HS5105L Mini-Portable Reader ¹ :	10 cm (Maximum)
Read speed:	Approximately 1 meter per second
Vibration:	Sinusoidal; 1.5 mm peak-to-peak, 10 to 80 Hz, 3 axis
Vibration:	Sinusoidal; 10 g peak-to-peak, 80 Hz to 2 kHz, 3 axis
Injector needle size:	About 12 gauge
Operating frequency:	125 kHz
¹ in a benign noise environment with optimal orientation of transponder and scanner)	

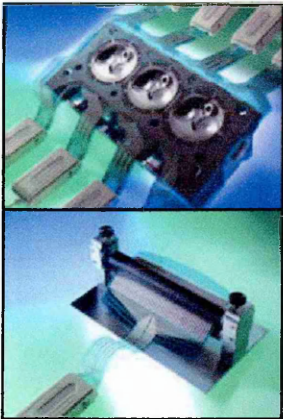
APPENDIX 2 – TEKSCAN SYSTEM DATA AND INFORMATION



Text taken from the company website (www.tekscan.com).

The Industrial Sensing (I-Scan) System – Overview

TekScan's pressure sensing technology is used worldwide to solve the toughest pressure measurement problems. The Industrial Sensing System (I-Scan) removes many of the obstacles to studying the pressure distribution between two mating surfaces, and thus provides insights into dynamic pressure events.



Applications range from soft seal applications with highly compliant materials at extremely low pressures, to extremely high-pressure applications such as engine gasket design. For example TekScan allows design engineers to evaluate fasteners, gaskets and seals; scientists to measure the force distribution in granular materials; ergonomists to develop improved automotive seating; and production engineers to adjust roller nip pressure to insure proper materials transport.

Each system is portable and comes with appropriate sensors and unique Windows™ based software. The software displays the pressure and force information in 'real time' on a computer screen in coloured 2D or 3D images. Dynamic tests can also be recorded as a "movie", and played back in a VCR style. Pressure data can be analysed using the I-Scan software, copied and pasted it into other applications, saved as text (ASCII) files and imported it into other analysis programs, or printed it out.

The Industrial Sensing (I-Scan) System – Hardware

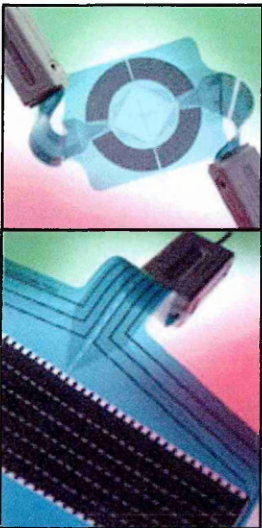
The TekScan Industrial Sensing (I-Scan) System is a complete kit that converts an IBM-compatible PC into an advanced pressure distribution measurement system. The I-Scan system consists of matrix-based sensors of various shapes, sizes, resolutions and

pressure ranges; an 8-bit A/D converter (handle) that connects to the sensors; a specially designed interface; and Windows™-based software.



For flexibility two hardware interfaces are supported; a PC Interface Board or a Parallel Interface. The PC Interface Board is a data acquisition card that inserts into a 16-bit ISA expansion slot, whilst the Parallel Interface shares the printer port. The hardware components - the handle and interface - collect pressure information from the sensor and make it available to the system software, which processes, displays, and analyses this data.

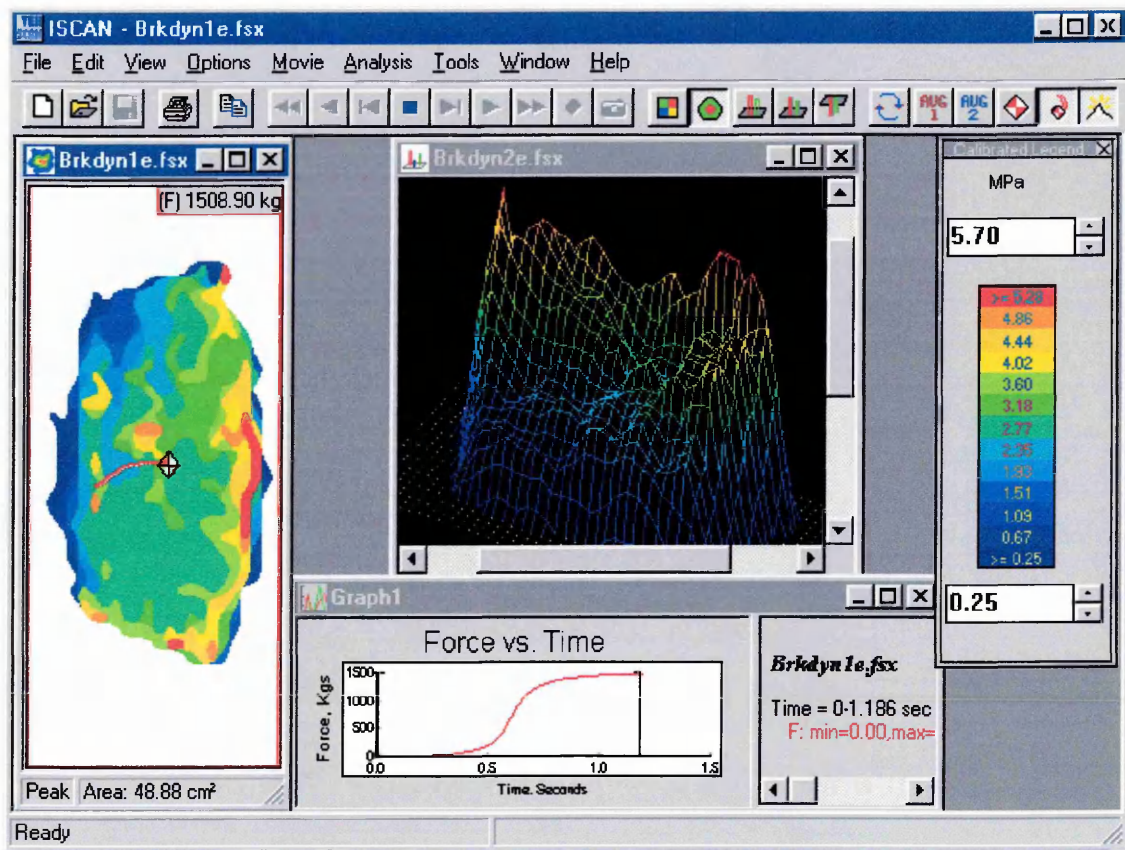
The Industrial Sensing (I-Scan) System – Software



The I-Scan system is capable of interfacing with a broad range of sensors from TekScan. The standard I-Scan sensor is a flexible printed circuit with up to 2288 individual pressure sensing locations, which can be close together (0.025"/ 0.6 mm) or far apart (0.5"/ 13 mm).

Due to the nature of the pressure sensitive layer inside the sensor, it is possible to produce sensors of varying sensitivity. Sensors with pressure ranges from as low as 0 - 2 PSI (14 kPa) up to as high as 0 - 25,000 PSI (175 MPa) have been produced.

The system software displays contact pressure or force in real time on the computer screen in coloured, easy to understand, 2-dimensional or 3-dimensional images. The software allows multiple windows to be opened and force and pressure information to be viewed in user-defined focus areas.



Data graphs and images can be printed for inclusion in reports. The system can also graph information in several ways, including force vs. time, pressure vs. time, peak pressure vs. time, and pressure profile vs. sensor length. The system can export data in bitmap or ASCII format for post-processing.

APPENDIX 3 – MOTOR SHOW QUESTIONNAIRE – OCT. 1998

DATE _____ / LOCATION _____ / INTERVIEWER _____

1. What area of the U.K. do you come from? _____ Male / Female
2. Age Group? <20 21-25 26-30 31-35 36-40 41-50 51-60 61+
3. What is your occupation? _____
4. What is your current vehicle?
 Make _____ Model _____ Age _____ Private / Company _____

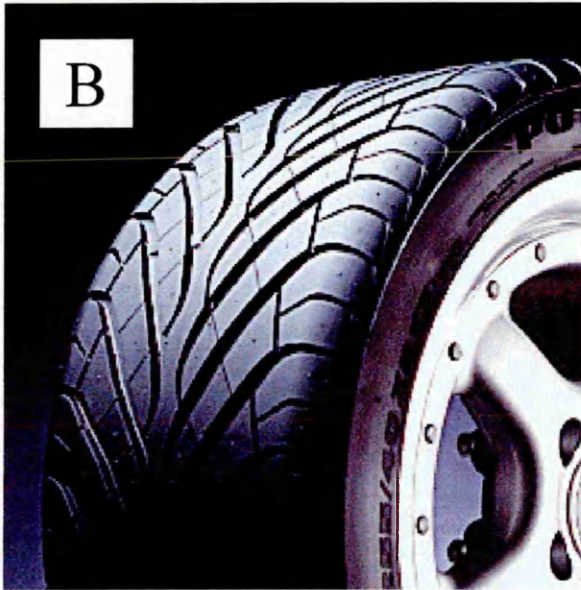
5. Rank the following tyre factors in order of importance, for driving on-road. (1-5)
 Performance _____ Aesthetics _____
 Noise _____ Cost _____
 Comfort _____
6. Choose and rank the 4 most important on-road tyre performance factors. (1-4)
 Load Capacity _____ Tread Pattern _____
 Handling _____ Grip _____
 Wear Rate _____ Wet Performance _____
7. Do you prefer wide or narrow tyres on your vehicle? _____ Wide / Narrow
8. Do you prefer low or high profile tyres on your vehicle? _____ Low / High
9. Which of these tyre types would you prefer to see on your vehicle? _____ A / B / C
 Why? _____
10. Which of these tyre styles would be most aesthetically suited to your vehicle? _____ D / E / F / G
 Why? _____
11. Do you prefer a chunky or smooth tread pattern on your tyres? Chunky / Smooth
12. Do you prefer plain black or raised white lettering? _____ Plain / White
13. Do you prefer black, white or coloured sidewall? _____ Black / White / Coloured _____
14. Which of these tyres would grip better on road? _____ H / I
15. Which brand of tyre offers the best performance? _____
16. Which brand offers the best value for money? _____
17. What mileage do you expect from your tyres? _____
18. Have you ever change a 4x4 wheel and tyre assembly due to a puncture? _____ Yes / No
 If yes - Rate the difficulty 1 – 10 (1=easy / 10=v. hard). _____
19. For a puncture would you use a breakdown organisation or D.I.Y? _____ B.O / D.I.Y
20. How often do you check your tyre pressures? _____
 Do you also check the spare tyre pressure? _____ Yes / No
21. Do you participate in off-road driving? _____ Yes / No

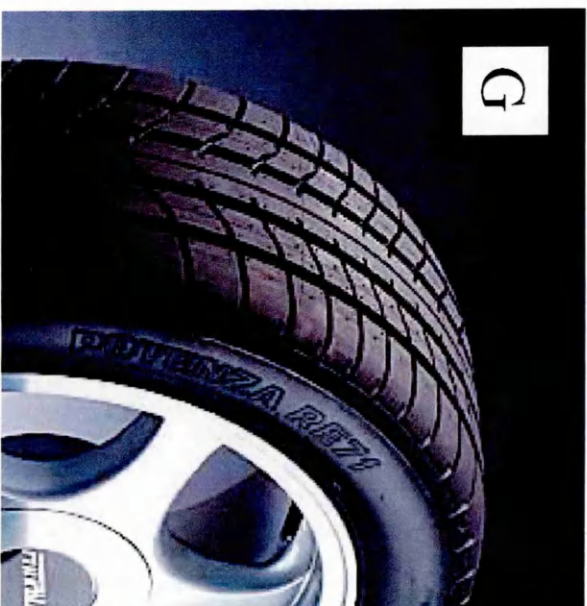
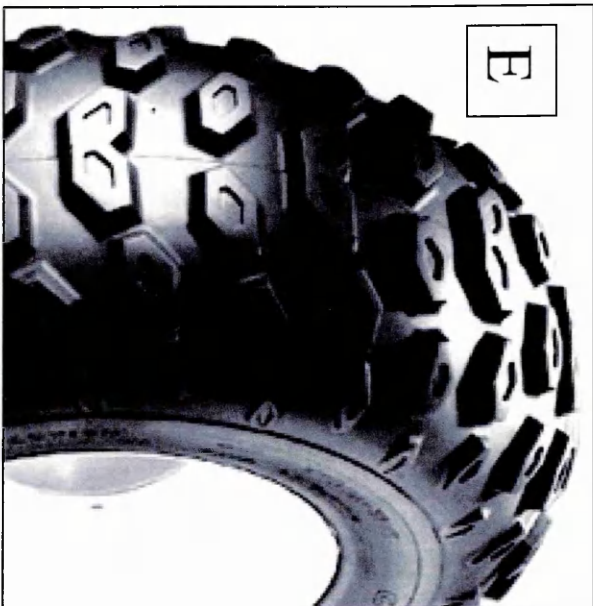
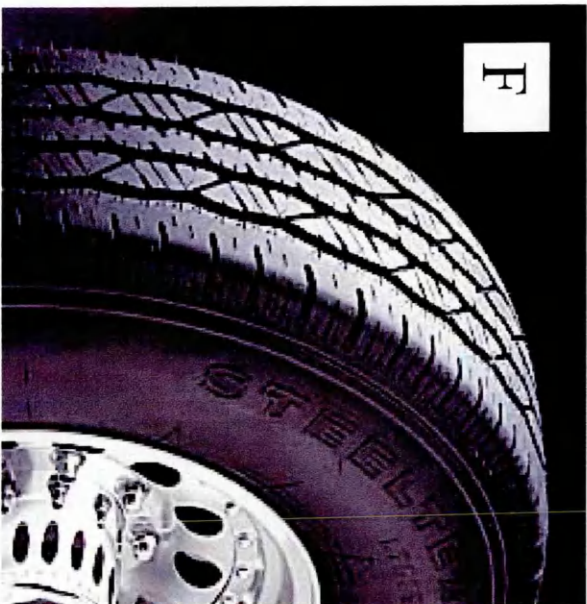
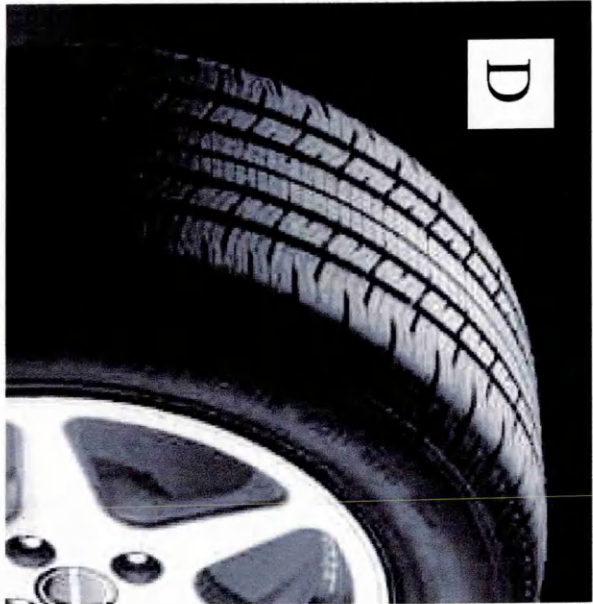
22. What vehicle do you use? _____ Make _____ Model _____

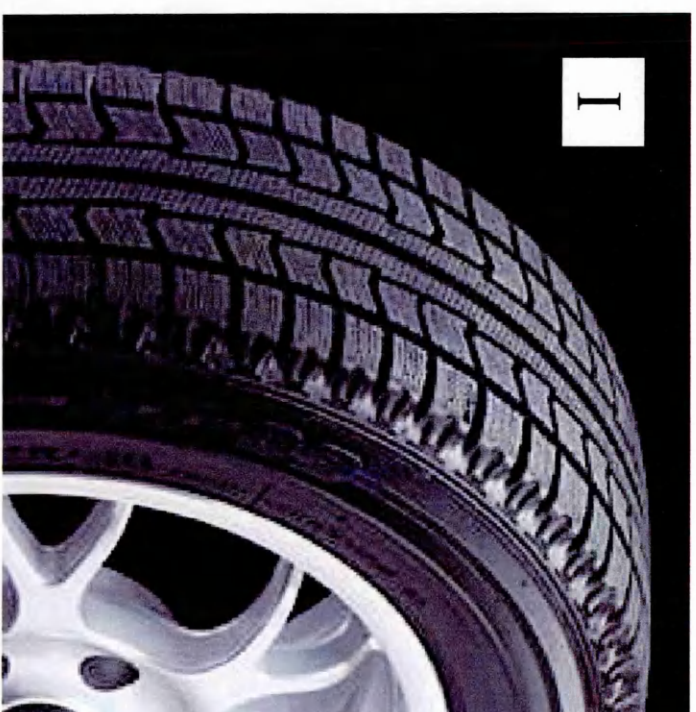
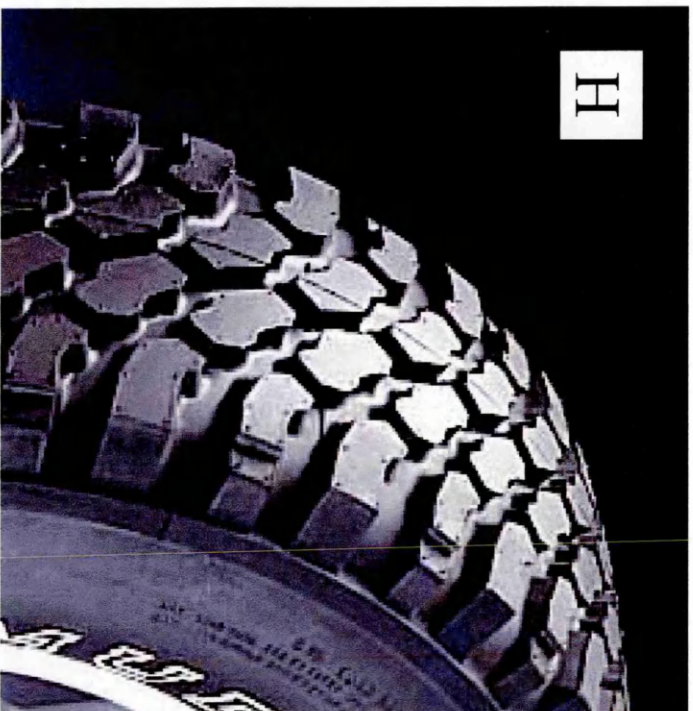
23. Is the use recreational or job related? Recreational / Job
24. On what terrain? Mud Sand Rock Snow Ice Wet Grass Other
25. How frequently? Daily Weekly Monthly Annually Other
26. What type / make of tyres do you use? _____
 Why? _____
27. Rank the following tyre factors in order of importance, for driving off-road. (1-5)
- | | | | |
|-------------|-------|------------|-------|
| Noise | _____ | Comfort | _____ |
| Performance | _____ | Aesthetics | _____ |
| Cost | _____ | | |
28. Choose and rank the **3 most important** off-road tyre performance factors. (1-3)
- | | | | |
|---------------|-------|---------------|-------|
| Handling | _____ | Load Capacity | _____ |
| Wear Rate | _____ | Grip | _____ |
| Tread Pattern | _____ | | |
29. Do you use the same tyres for both off-road and on-road driving? Yes / No
 If yes, would you consider using separate off-road tyres if they were available? Yes / No
30. Rank these 3 factors in order of importance when choosing specialist off-road tyres. (1-3)
- | | |
|---|-------|
| Extra cost for two sets of tyres | _____ |
| Ease of interchange between on and off-road tyres | _____ |
| Improved performance over on-road tyres | _____ |
31. If special off road tyres giving better off-road grip were available but only capable of 55 mph on road would you consider their purchase? Yes / No
32. If, as an extra, you could purchase a self-sensing tyre inflation system which automatically adjusted your tyre pressures to give maximum traction, would you be prepared to pay for this feature? Yes / No How much? £500, £1000, £2000, £4000?
33. Do you expect one set of tyres to exhibit good performance over all terrain's and conditions? Yes / No
34. Would you be prepared to purchase one set of tyres for on-road and one for off-road, if the off-road tyres gave a 30% improved performance for total off-road driving and cost £600 for a complete set of tyres. Why?
 Yes / No - too expensive / No - too little performance / No - don't go off-road

35. Should off-road tyres be low profile and wide section so they are similar to on-road tyres?
 Yes / No _____

36. When will you next change your vehicle? _____
37. Will your next vehicle be New or Used? _____
38. If private owner will you purchase outright or use finance? Purchase / Finance





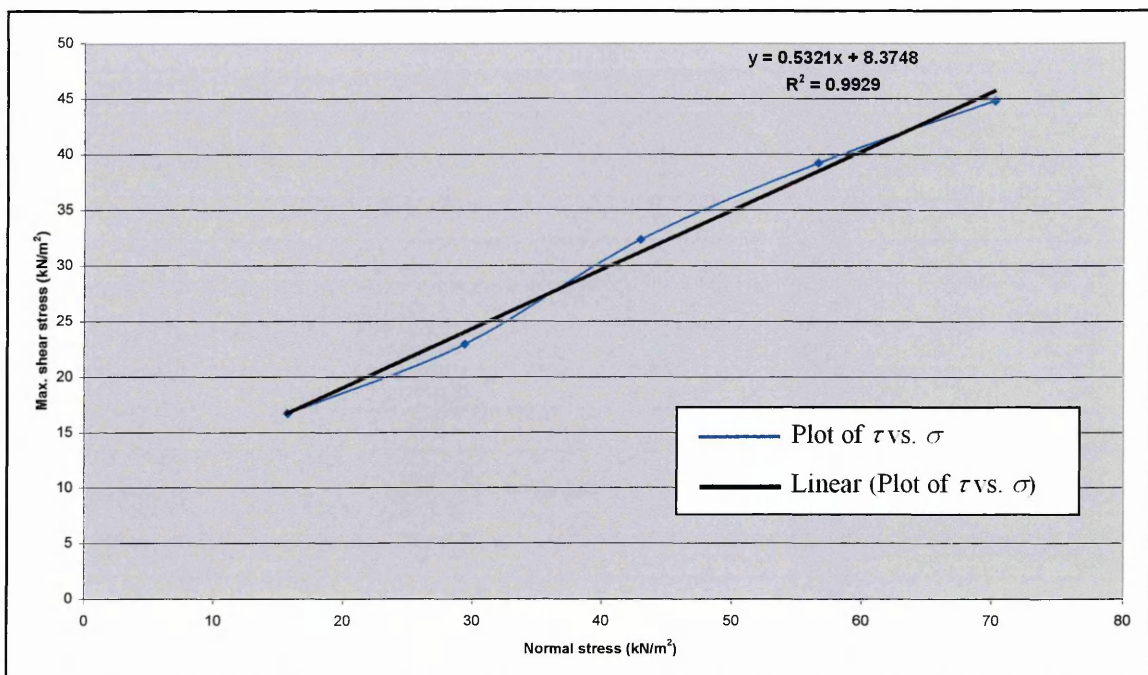


APPENDIX 4 – TRANSLATIONAL SOIL SHEAR TEST RESULTS

These tests were used to determine c and ϕ for the sandy loam soil used for the experiments, plotting values of the maximum shear stress (τ) achieved against values of normal stress (σ) at which the shear stress was achieved. The results can be seen in the table and figure below.

A table of maximum soil shear stresses recorded at different normal stresses

Normal Stress kN/m ²	Max. Shear Stress kN/m ²
15.64	16.69
29.33	22.96
42.89	32.36
56.53	39.22
70.17	44.82



A graph of maximum soil shear stresses recorded at different normal stresses

From the equation of the trend line shown on the graph it was possible to determine both c and ϕ . In this instance c equalled the intercept, 8.4 kN/m², whilst ϕ equalled \tan^{-1} of the gradient of the trend line, i.e. $\tan^{-1} 0.5321$, or 28°.

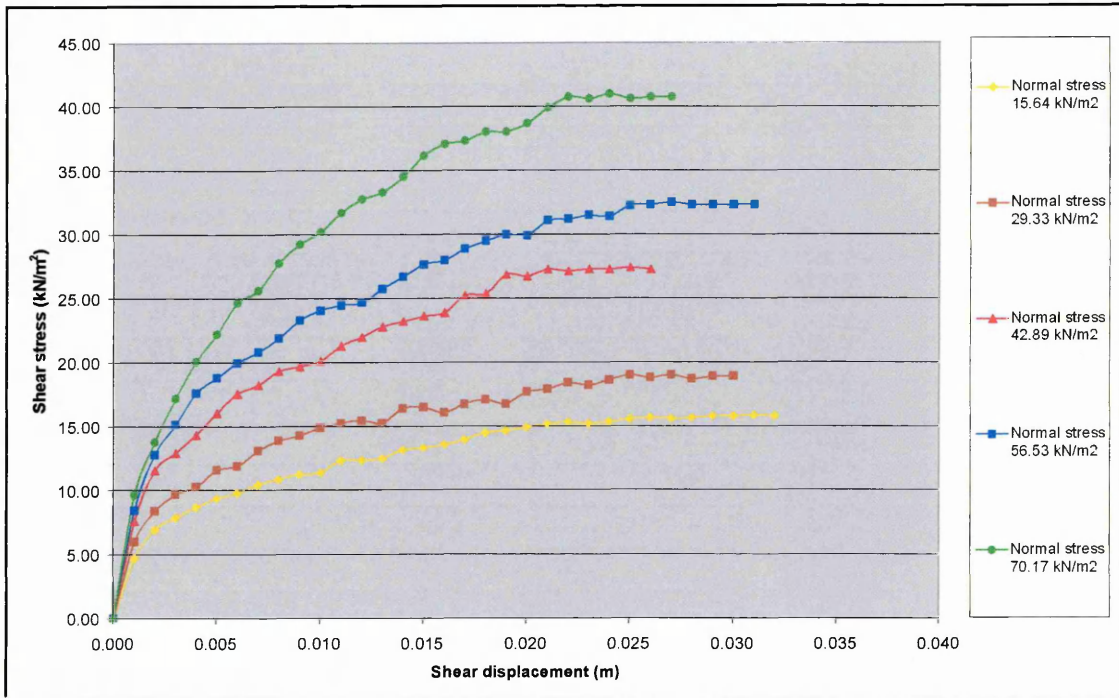
APPENDIX 5 – CALCULATION OF *K* (SOIL DEF. MODULUS)

To determine *K*, the procedure detailed in section 3.5.3.3 was used. The first stage of this was to conduct a number of shear box tests to determine the shear stress-shear displacement relationships for the sandy loam soil under varying normal loads. These results are shown in the table below:

A table of shear-stress/ shear deformation results for different normal loads

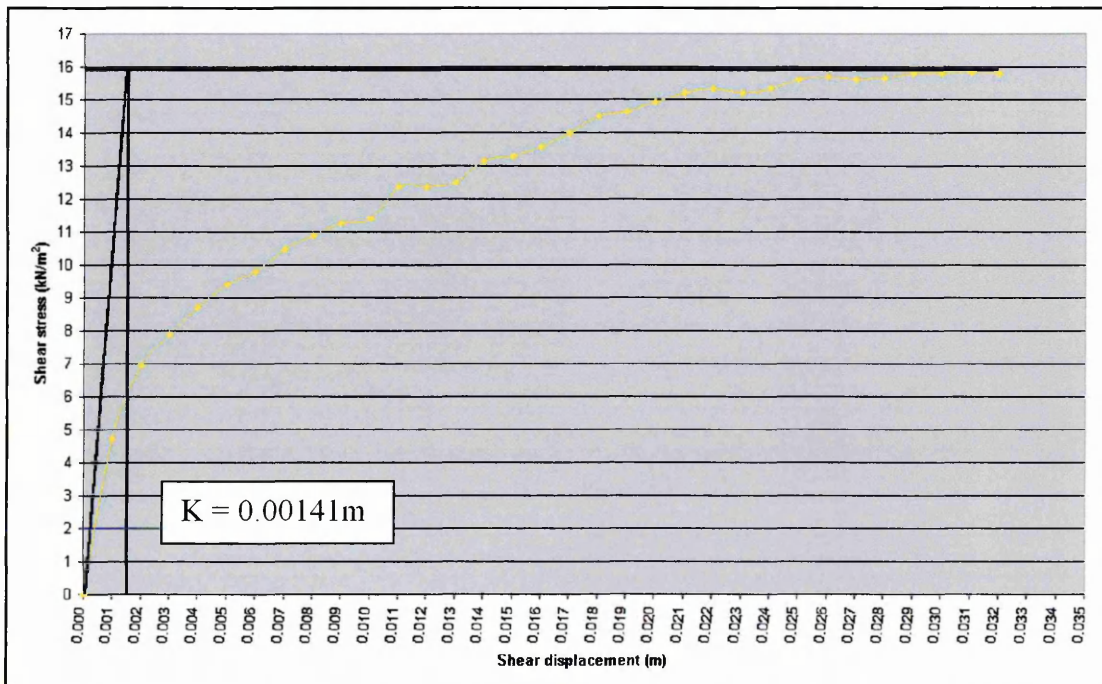
Sand Deformation m	Normal stress 15.64 kN/m ²	Normal stress 29.33 kN/m ²	Normal stress 42.89 kN/m ²	Normal stress 56.53 kN/m ²	Normal stress 70.17 kN/m ²
	Shear stress kN/m ²	Shear stress kN/m ³	Shear stress kN/m ⁴	Shear stress kN/m ⁵	Shear stress kN/m ⁶
0.000	0.00	0.00	0.00	0.00	0.00
0.001	4.72	6.00	7.66	8.47	9.65
0.002	6.97	8.40	11.61	12.84	13.80
0.003	7.91	9.70	12.96	15.13	17.20
0.004	8.72	10.30	14.36	17.60	20.07
0.005	9.40	11.60	16.07	18.80	22.22
0.006	9.80	11.90	17.56	20.00	24.66
0.007	10.48	13.10	18.24	20.80	25.60
0.008	10.88	13.90	19.31	21.90	27.77
0.009	11.29	14.30	19.69	23.30	29.25
0.010	11.42	14.90	20.12	24.10	30.20
0.011	12.37	15.30	21.32	24.50	31.69
0.012	12.37	15.50	22.02	24.70	32.77
0.013	12.51	15.30	22.83	25.80	33.31
0.014	13.18	16.40	23.23	26.70	34.53
0.015	13.32	16.50	23.64	27.70	36.17
0.016	13.59	16.10	23.91	28.00	37.10
0.017	13.99	16.80	25.26	28.90	37.37
0.018	14.53	17.10	25.40	29.50	38.04
0.019	14.67	16.80	26.88	30.00	38.04
0.020	14.94	17.70	26.75	29.94	38.72
0.021	15.21	17.90	27.29	31.10	39.94
0.022	15.35	18.40	27.16	31.20	40.75
0.023	15.21	18.20	27.29	31.50	40.61
0.024	15.35	18.63	27.29	31.40	41.00
0.025	15.62	19.03	27.42	32.27	40.65
0.026	15.70	18.80	27.29	32.35	40.75
0.027	15.62	19.02		32.50	40.75
0.028	15.65	18.70		32.33	
0.029	15.80	18.89		32.31	
0.030	15.80	18.89		32.33	
0.031	15.83			32.35	
0.032	15.80				

These results were then plotted to assess the relationships, as shown in the figure below, on which the expected curved relationship was produced.



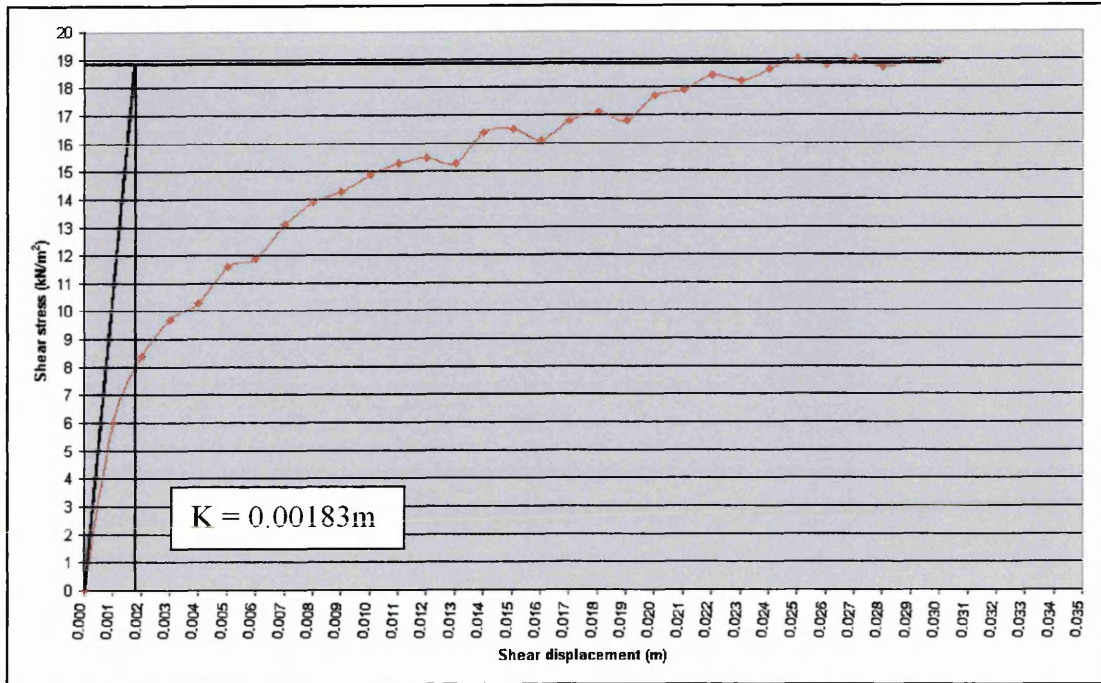
Shear-stress results plotted against shear-displacements for varying normal loads

The five plots were then considered separately to allow the tangents to be calculated. This graphical interpretation was conducted by hand on paper to achieve maximum accuracy, but representations of the results are presented on the following five graphs.

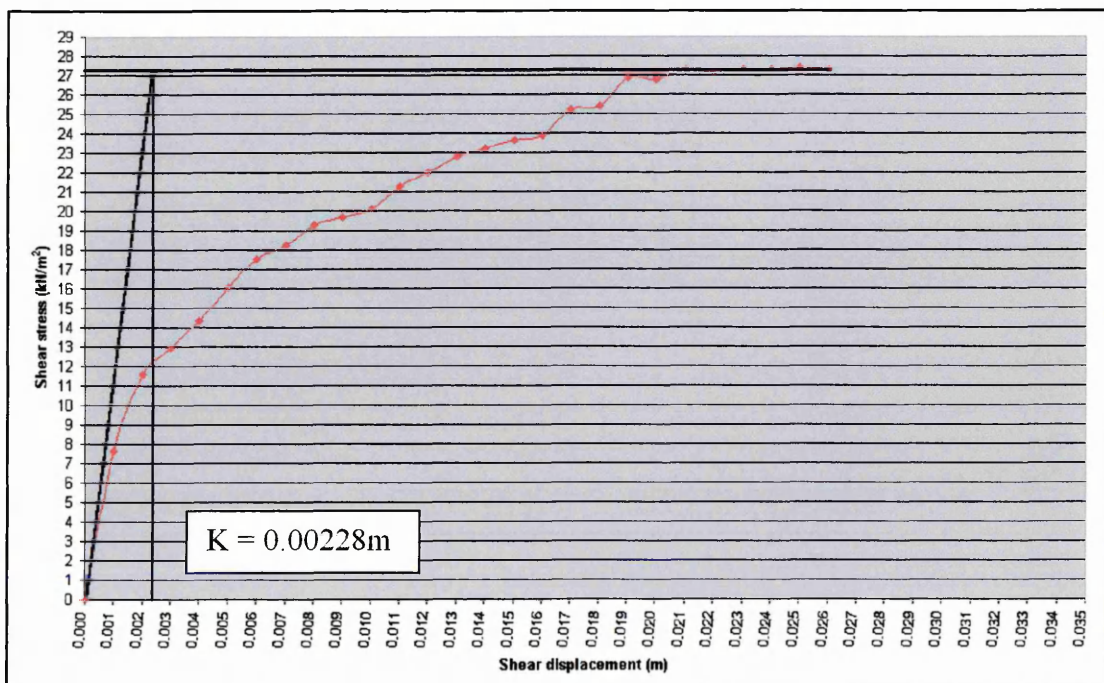


Calculation of soil deformation modulus (K) for a 15.64 kN/m^2 normal load

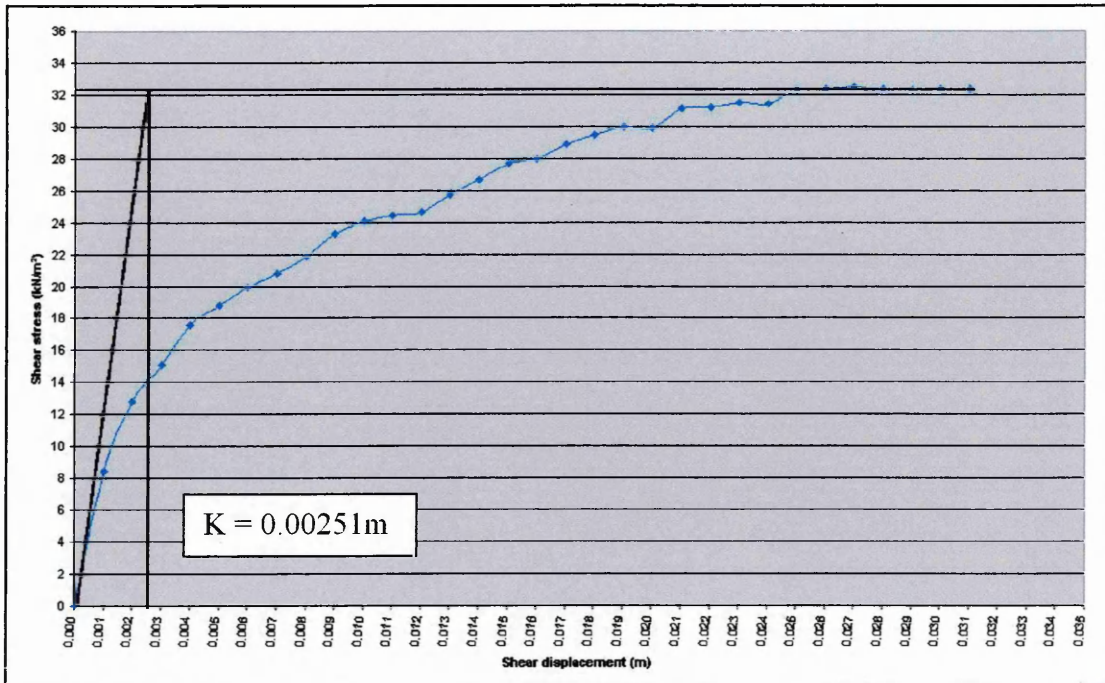
The value of K was read off these graphs at the point where the vertical line (which indicates the intercept of the horizontal line and tangent) intercepts the X-axis.



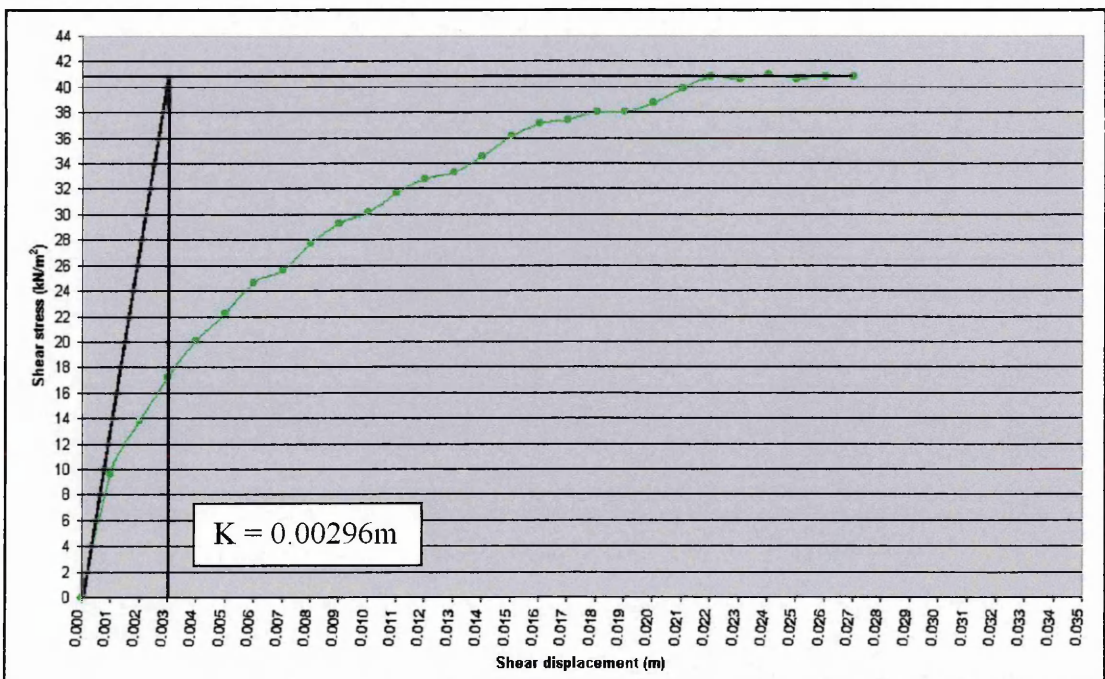
Calculation of soil deformation modulus (K) for a 29.33 kN/m^2 normal load



Calculation of soil deformation modulus (K) for a 42.89 kN/m^2 normal load

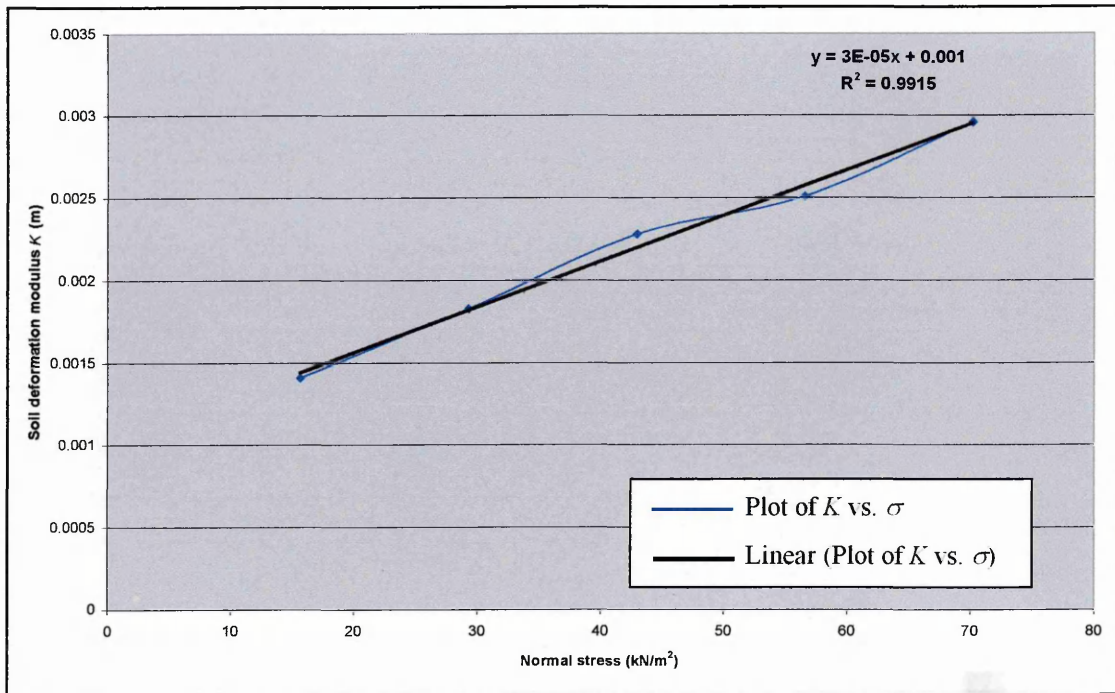


Calculation of soil deformation modulus (K) for a 56.53 kN/m^2 normal load



Calculation of soil deformation modulus (K) for a 70.14 kN/m^2 normal load

The results from this interpretation were plotted to allow the relationship between normal load and K to be determined, which is shown on the graph below.

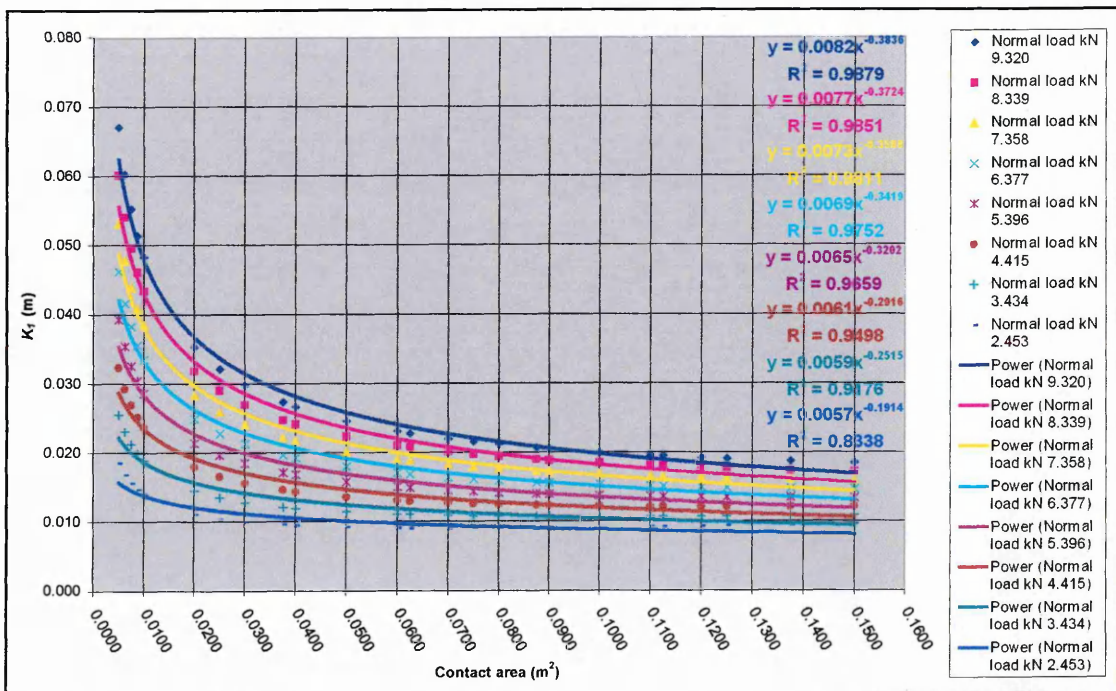


A graph of soil deformation modulus, K , against normal soil stress, σ

The graph showed that a linear relationship existed between σ and K . This took the form of $K = 0.00003\sigma + 0.001$. Thus the value of K at any given normal load (within the tested range) could be determined. Equation 16 $\left\{ \frac{K_1}{K_2} = \sqrt{\left(\frac{A_1}{A_2} \right)} \right\}$ showed that for soils experiencing similar normal stresses, but over varying areas A_1 (tyre contact) and A_2 (shear box), then through knowledge of K_2 then K_1 could be derived. This led to an analysis to determine values of K_1 for given normal stresses. However, it was only possible to determine a range of possible of K_1 values for any given soil load, because as the contact area size (as yet unknown) was increased then this altered both the normal stress, which was used to compute of K_2 , and also the ratio of areas $A_1 : A_2$. Thus for each load a range of K_1 values were produced, as the table and figure below indicate.

A table of K_1 values for different normal loads on the sandy loam soil

$K1 = K2 \text{ sqrt}(A1/A2)$ $K2 = 0.0009 (\text{sigma}) + 0.001$			Normal load kN							
K1 = tyre	K2 = box		9.320	8.339	7.358	6.377	5.396	4.415	3.434	2.453
A1 = tyre	A2 = box									
Contact length	Contact width	Contact area	Value of K_1							
m	m	m ²	m	m	m	m	m	m	m	m
0.05	0.10	0.0050	0.0671	0.0601	0.0532	0.0463	0.0393	0.0324	0.0255	0.0185
0.05	0.13	0.0063	0.0603	0.0541	0.0479	0.0416	0.0354	0.0292	0.0230	0.0168
0.05	0.15	0.0075	0.0552	0.0496	0.0439	0.0383	0.0326	0.0269	0.0213	0.0156
0.05	0.18	0.0088	0.0514	0.0461	0.0409	0.0356	0.0304	0.0252	0.0199	0.0147
0.05	0.20	0.0100	0.0483	0.0434	0.0385	0.0335	0.0286	0.0237	0.0188	0.0139
0.10	0.20	0.0200	0.0353	0.0318	0.0284	0.0249	0.0214	0.0180	0.0145	0.0110
0.15	0.20	0.0300	0.0298	0.0270	0.0241	0.0213	0.0185	0.0156	0.0128	0.0100
0.20	0.20	0.0400	0.0266	0.0242	0.0217	0.0193	0.0168	0.0144	0.0119	0.0095
0.25	0.20	0.0500	0.0246	0.0224	0.0202	0.0180	0.0158	0.0136	0.0114	0.0092
0.30	0.20	0.0600	0.0231	0.0211	0.0191	0.0171	0.0151	0.0131	0.0111	0.0091
0.35	0.20	0.0700	0.0220	0.0202	0.0183	0.0165	0.0146	0.0128	0.0109	0.0090
0.40	0.20	0.0800	0.0212	0.0195	0.0177	0.0160	0.0143	0.0125	0.0108	0.0090
0.45	0.20	0.0900	0.0205	0.0189	0.0173	0.0156	0.0140	0.0124	0.0107	0.0091
0.50	0.20	0.1000	0.0200	0.0185	0.0169	0.0154	0.0138	0.0123	0.0107	0.0091
0.55	0.20	0.1100	0.0196	0.0181	0.0166	0.0151	0.0137	0.0122	0.0107	0.0092
0.60	0.20	0.1200	0.0192	0.0178	0.0164	0.0150	0.0136	0.0121	0.0107	0.0093
0.10	0.25	0.0250	0.0321	0.0290	0.0259	0.0228	0.0197	0.0166	0.0135	0.0104
0.15	0.25	0.0375	0.0273	0.0248	0.0222	0.0197	0.0172	0.0146	0.0121	0.0096
0.20	0.25	0.0500	0.0246	0.0224	0.0202	0.0180	0.0158	0.0136	0.0114	0.0092
0.25	0.25	0.0625	0.0228	0.0208	0.0189	0.0169	0.0150	0.0130	0.0110	0.0091
0.30	0.25	0.0750	0.0216	0.0198	0.0180	0.0162	0.0144	0.0126	0.0108	0.0090
0.35	0.25	0.0875	0.0207	0.0190	0.0174	0.0157	0.0141	0.0124	0.0107	0.0091
0.40	0.25	0.1000	0.0200	0.0185	0.0169	0.0154	0.0138	0.0123	0.0107	0.0091
0.45	0.25	0.1125	0.0195	0.0180	0.0166	0.0151	0.0136	0.0122	0.0107	0.0092
0.50	0.25	0.1250	0.0191	0.0177	0.0163	0.0149	0.0135	0.0121	0.0107	0.0094
0.55	0.25	0.1375	0.0187	0.0174	0.0161	0.0148	0.0135	0.0121	0.0108	0.0095
0.60	0.25	0.1500	0.0185	0.0172	0.0160	0.0147	0.0134	0.0122	0.0109	0.0096



A graph showing the relationships between contact area and K_1 for the DA80F sand under different normal tyre loads

APPENDIX 6 – PLATE SINKAGE TESTS ON SOIL

These tests were used to determine values of the Bekker soil coefficients n , k_c and k_ϕ for the three sandy loam soil preparations used for the experiments, those being 1170 kg/m³ (0 rolls), 1270 kg/m³ (1 roll) and 1400 kg/m³ (4 rolls). The coefficients were derived

from knowledge of equation 8, $\rho = \left(\frac{k_c}{b} + k_\phi \right) z^n$

where: ρ = normal pressure beneath the plate (load/ area)

b = minimum plate dimension (width \square)

z = plate sinkage

k_c, k_ϕ & n = soil defining constants

This equation can be re-arranged, such that, $\ln \rho = n \ln z + \ln \left(\frac{k_c}{b} + k_\phi \right)$. Thus if $\ln \rho$ is plotted against $\ln z$ for several different plate sizes then the gradient of the lines will equal n , whilst the intercepts will equal $\ln \left(\frac{k_c}{b} + k_\phi \right)$. To determine these k coefficients then the inverse \ln 's of intercept values must be plotted against the appropriate $1/b$ values. When trend lines are fitted to this data a new line will be formed, with a gradient equal to k_c , and the intercept at $1/b = 0$ will equal k_ϕ .

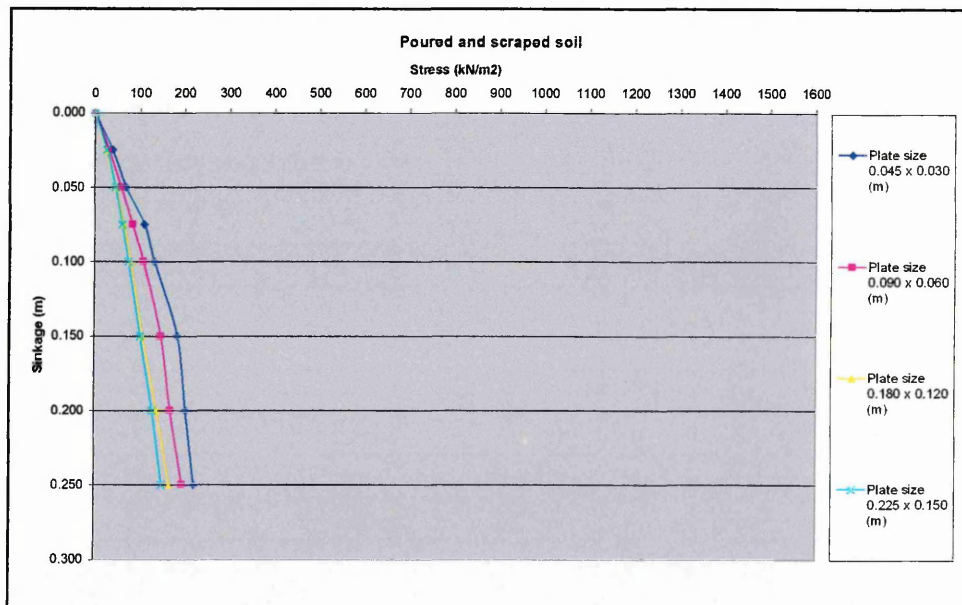
This investigation used four different sized rectangular plates that were hydraulically forced into the three soil preparations at a constant velocity of 0.025 m/s, and the resistive force upon each plate and its sinkage were recorded. Each test was replicated three times. The pressure acting on the soil/ plate and the plate sinkage was determined and the pressure sinkage relationships achieved from these tests are detailed on the following sets of tables and graphs.

Poured and scraped				
Rep 1	Rep 2	Rep 3	Plate size	0.045 x 0.030 (m)
ρ (kN/m ²)	ρ (kN/m ²)	ρ (kN/m ²)	Mean ρ (kN/m ²)	Sinkage (m)
0.000	0.000	0.000	0.000	0.000
33.979	45.872	35.678	38.509	0.025
66.259	80.257	60.259	68.925	0.050
107.034	106.582	115.528	109.715	0.075
122.324	139.314	135.916	132.518	0.100
175.258	190.258	185.470	183.662	0.150
190.282	203.258	212.590	202.043	0.200
214.067	219.164	228.258	220.497	0.250

Rep 1	Rep 2	Rep 3	Plate size	0.090 x 0.060 (m)
ρ (kN/m ²)	ρ (kN/m ²)	ρ (kN/m ²)	Mean ρ (kN/m ²)	Sinkage (m)
0.000	0.000	0.000	0.000	0.000
41.199	25.909	22.936	30.015	0.025
72.205	53.942	46.721	57.623	0.050
100.663	93.442	56.490	83.532	0.075
116.378	141.437	65.834	107.883	0.100
146.959	205.997	87.920	146.959	0.150
172.018	217.890	112.609	167.506	0.200
218.739	240.826	124.448	194.671	0.250

Rep 1	Rep 2	Rep 3	Plate size	0.180 x 0.120 (m)
ρ (kN/m ²)	ρ (kN/m ²)	ρ (kN/m ²)	Mean ρ (kN/m ²)	Sinkage (m)
0.000	0.000	0.000	0.000	0.000
27.319	18.077	27.319	24.238	0.025
51.240	32.552	51.240	45.011	0.050
72.511	47.299	72.511	64.107	0.075
90.520	59.259	90.520	80.100	0.100
119.674	80.802	119.674	106.717	0.150
156.371	101.325	156.371	138.022	0.200
179.817	140.061	179.817	166.565	0.250

Rep 1	Rep 2	Rep 3	Plate size	0.225 x 0.150 (m)
ρ (kN/m ²)	ρ (kN/m ²)	ρ (kN/m ²)	Mean ρ (kN/m ²)	Sinkage (m)
0.000	0.000	0.000	0.000	0.000
33.660	18.370	26.121	26.051	0.025
59.782	32.068	42.580	44.810	0.050
80.806	45.128	56.384	60.773	0.075
99.707	56.278	67.745	74.577	0.100
133.367	80.275	88.982	100.875	0.150
168.939	99.388	113.086	127.138	0.200
193.255	123.811	128.908	148.658	0.250

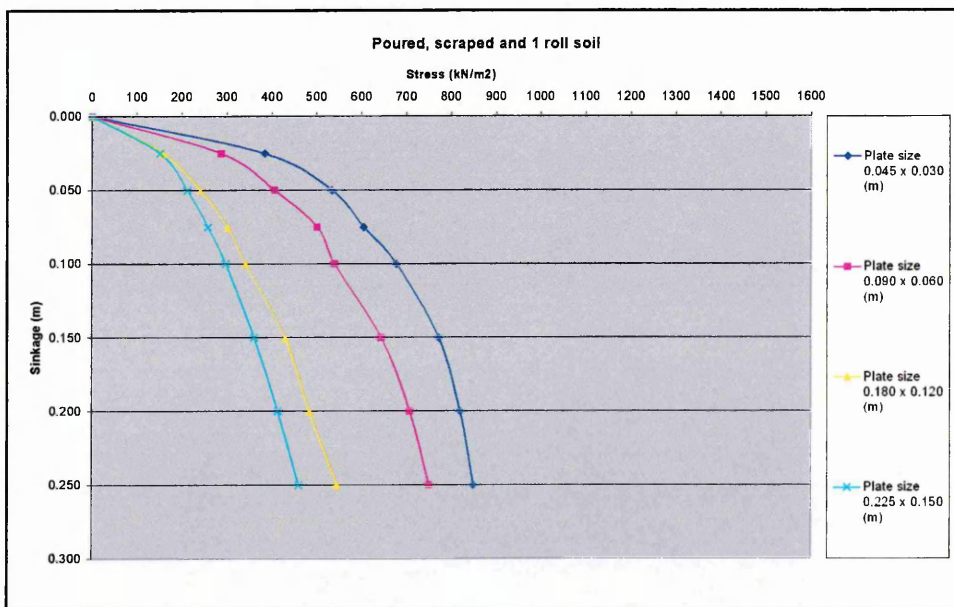


Poured, scraped and 1 roll				
Rep 1	Rep 2	Rep 3	Plate size	0.045 x 0.030 (m)
ρ (kN/m ²)	ρ (kN/m ²)	ρ (kN/m ²)	Mean ρ (kN/m ²)	Sinkage (m)
0.000	0.000	0.000	0.000	0.000
355.080	331.295	463.812	383.396	0.025
535.168	516.480	550.459	534.036	0.050
591.233	642.202	581.040	604.825	0.075
640.503	781.515	611.621	677.880	0.100
688.073	912.334	718.654	773.021	0.150
728.848	976.894	755.450	820.398	0.200
789.235	968.400	792.633	850.089	0.250

Rep 1	Rep 2	Rep 3	Plate size	0.090 x 0.060 (m)
ρ (kN/m ²)	ρ (kN/m ²)	ρ (kN/m ²)	Mean ρ (kN/m ²)	Sinkage (m)
0.000	0.000	0.000	0.000	0.000
254.642	269.164	338.321	287.376	0.025
379.052	392.338	448.135	406.508	0.050
479.871	501.468	521.942	501.094	0.075
509.490	543.276	567.679	540.148	0.100
686.374	613.320	635.406	645.033	0.150
766.225	674.907	683.401	708.178	0.200
791.284	752.633	709.310	751.076	0.250

Rep 1	Rep 2	Rep 3	Plate size	0.180 x 0.120 (m)
ρ (kN/m ²)	ρ (kN/m ²)	ρ (kN/m ²)	Mean ρ (kN/m ²)	Sinkage (m)
0.000	0.000	0.000	0.000	0.000
168.514	138.146	170.213	158.958	0.025
252.187	231.163	242.631	241.994	0.050
320.358	286.379	299.227	301.988	0.075
365.274	317.915	344.249	342.479	0.100
448.734	428.135	415.499	430.789	0.150
524.231	467.847	461.370	484.483	0.200
596.967	535.168	507.454	546.530	0.250

Rep 1	Rep 2	Rep 3	Plate size	0.225 x 0.150 (m)
ρ (kN/m ²)	ρ (kN/m ²)	ρ (kN/m ²)	Mean ρ (kN/m ²)	Sinkage (m)
0.000	0.000	0.000	0.000	0.000
156.439	147.197	149.303	150.980	0.025
212.980	220.795	201.903	211.893	0.050
272.851	256.405	243.085	257.447	0.075
307.781	304.995	278.899	297.225	0.100
374.312	377.166	332.518	361.332	0.150
423.989	441.590	375.671	413.750	0.200
489.025	472.035	420.455	460.505	0.250

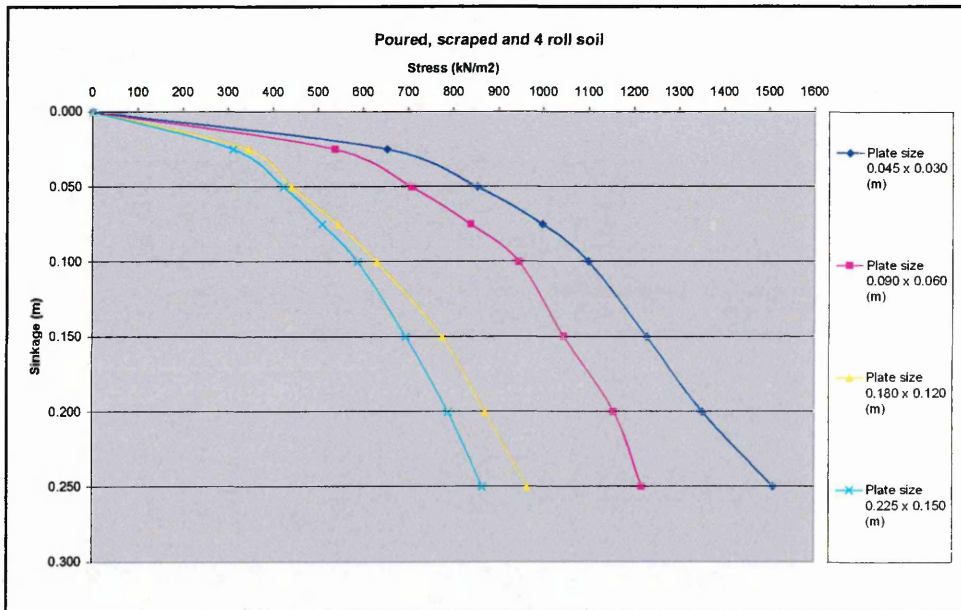


Poured, scraped and 4 rolls				
Rep 1	Rep 2	Rep 3	Plate size	0.045 x 0.030 (m)
ρ (kN/m ²)	ρ (kN/m ²)	ρ (kN/m ²)	Mean ρ (kN/m ²)	Sinkage (m)
0.000	0.000	0.000	0.000	0.000
643.073	655.063	658.977	652.371	0.025
872.722	725.450	961.604	853.259	0.050
1013.690	899.850	1078.831	997.457	0.075
1138.336	977.431	1182.080	1099.282	0.100
1257.757	1098.292	1328.479	1228.176	0.150
1373.286	1238.564	1442.846	1351.565	0.200
1527.890	1405.685	1592.577	1508.717	0.250

Rep 1	Rep 2	Rep 3	Plate size	0.090 x 0.060 (m)
ρ (kN/m ²)	ρ (kN/m ²)	ρ (kN/m ²)	Mean ρ (kN/m ²)	Sinkage (m)
0.000	0.000	0.000	0.000	0.000
574.105	533.803	501.614	536.507	0.025
704.370	727.429	689.772	707.190	0.050
830.785	880.479	806.575	839.280	0.075
925.926	1020.642	892.796	946.455	0.100
934.845	1148.063	1053.772	1045.560	0.150
1105.254	1200.306	1164.628	1156.729	0.200
1275.852	1230.887	1149.337	1218.692	0.250

Rep 1	Rep 2	Rep 3	Plate size	0.180 x 0.120 (m)
ρ (kN/m ²)	ρ (kN/m ²)	ρ (kN/m ²)	Mean ρ (kN/m ²)	Sinkage (m)
0.000	0.000	0.000	0.000	0.000
302.744	397.628	336.537	345.637	0.025
390.545	496.942	438.753	442.080	0.050
496.942	591.021	547.592	545.185	0.075
599.091	664.288	628.504	630.628	0.100
768.667	797.762	762.084	776.171	0.150
899.805	875.382	839.917	871.701	0.200
965.326	985.389	948.437	966.384	0.250

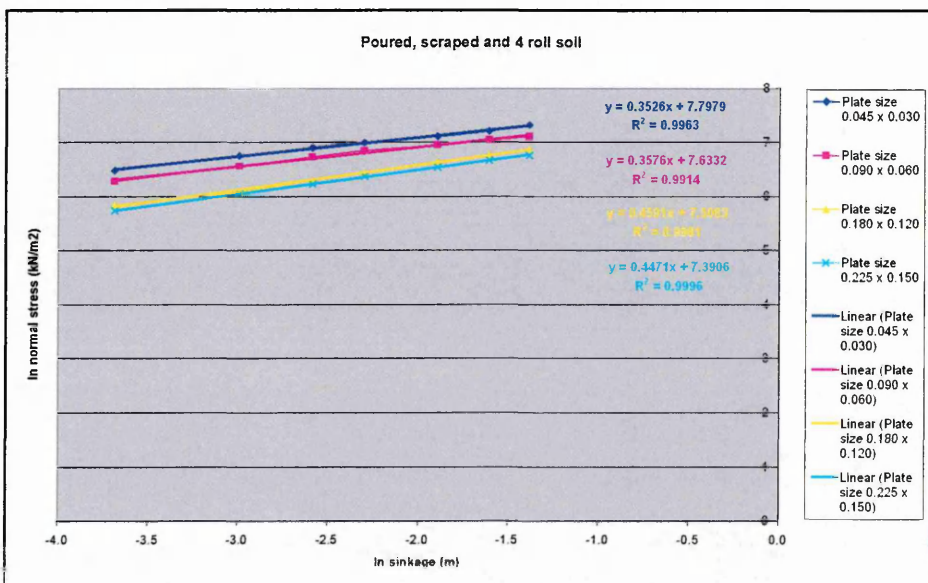
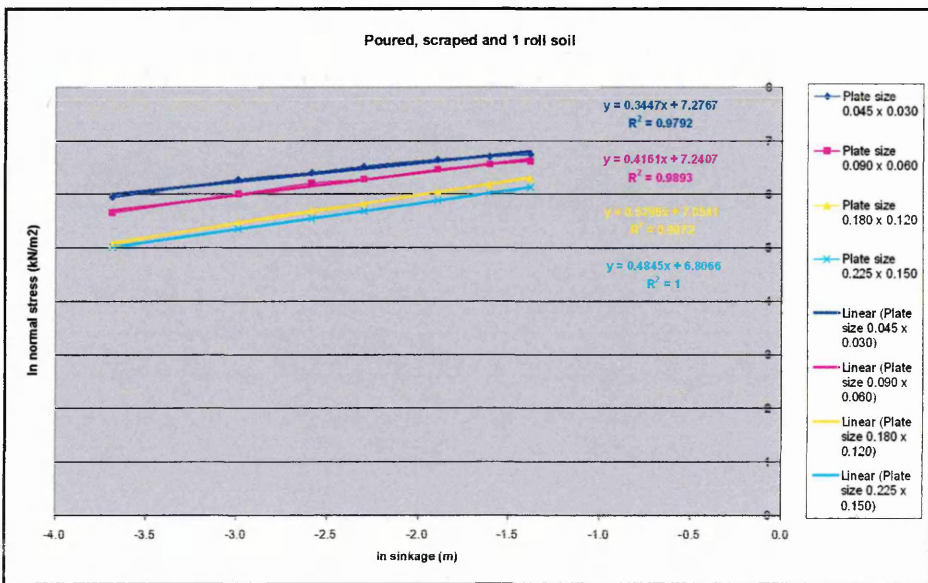
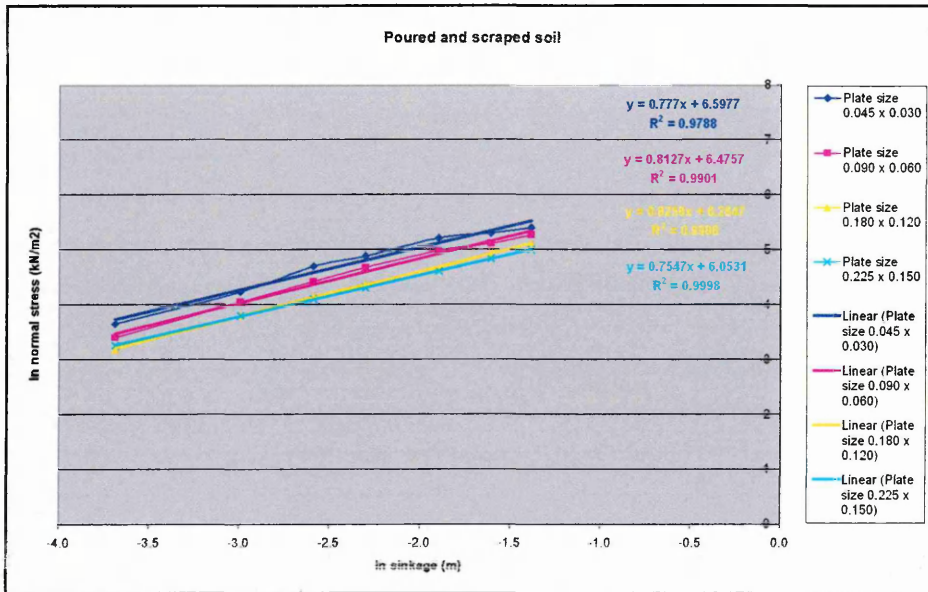
Rep 1	Rep 2	Rep 3	Plate size	0.225 x 0.150 (m)
ρ (kN/m ²)	ρ (kN/m ²)	ρ (kN/m ²)	Mean ρ (kN/m ²)	Sinkage (m)
0.000	0.000	0.000	0.000	0.000
296.024	364.526	270.880	310.477	0.025
417.465	457.900	394.224	423.196	0.050
507.305	536.120	482.909	508.778	0.075
604.893	597.350	559.701	587.315	0.100
719.062	701.393	663.541	694.665	0.150
817.261	780.632	768.739	788.878	0.200
870.549	863.677	861.706	865.310	0.250



These results were then transformed by taking natural logarithms of both axes to calculate $\ln \rho$ and $\ln z$. This produced the data shown in the table below, which was plotted to determine the gradients and the intercepts of trend lines fitted to the data.

Poured		1 Roll		4 Roll	
Plate size 0.045 x 0.030		Plate size 0.045 x 0.030		Plate size 0.045 x 0.030	
In depth m	In pressure kN/m ²	In depth m	In pressure kN/m ²	In depth m	In pressure kN/m ²
-3.689	3.651	-3.689	5.949	-3.689	6.481
-2.996	4.233	-2.996	6.280	-2.996	6.749
-2.590	4.698	-2.590	6.405	-2.590	6.905
-2.303	4.887	-2.303	6.519	-2.303	7.002
-1.897	5.213	-1.897	6.650	-1.897	7.113
-1.609	5.308	-1.609	6.710	-1.609	7.209
-1.386	5.396	-1.386	6.745	-1.386	7.319
Plate size 0.090 x 0.060		Plate size 0.090 x 0.060		Plate size 0.090 x 0.060	
In depth m	In pressure kN/m ²	In depth m	In pressure kN/m ²	In depth m	In pressure kN/m ²
-3.689	3.402	-3.689	5.661	-3.689	6.285
-2.996	4.054	-2.996	6.008	-2.996	6.561
-2.590	4.425	-2.590	6.217	-2.590	6.733
-2.303	4.681	-2.303	6.292	-2.303	6.853
-1.897	4.990	-1.897	6.469	-1.897	6.952
-1.609	5.121	-1.609	6.563	-1.609	7.053
-1.386	5.271	-1.386	6.622	-1.386	7.106
Plate size 0.180 x 0.120		Plate size 0.180 x 0.120		Plate size 0.180 x 0.120	
In depth m	In pressure kN/m ²	In depth m	In pressure kN/m ²	In depth m	In pressure kN/m ²
-3.689	3.188	-3.689	5.069	-3.689	5.845
-2.996	3.807	-2.996	5.489	-2.996	6.091
-2.590	4.161	-2.590	5.710	-2.590	6.301
-2.303	4.383	-2.303	5.836	-2.303	6.447
-1.897	4.670	-1.897	6.066	-1.897	6.654
-1.609	4.927	-1.609	6.183	-1.609	6.770
-1.386	5.115	-1.386	6.304	-1.386	6.874
Plate size 0.225 x 0.150		Plate size 0.225 x 0.150		Plate size 0.225 x 0.150	
In depth m	In pressure kN/m ²	In depth m	In pressure kN/m ²	In depth m	In pressure kN/m ²
-3.689	3.260	-3.689	5.017	-3.689	5.738
-2.996	3.802	-2.996	5.356	-2.996	6.048
-2.590	4.107	-2.590	5.551	-2.590	6.232
-2.303	4.312	-2.303	5.694	-2.303	6.376
-1.897	4.614	-1.897	5.890	-1.897	6.543
-1.609	4.845	-1.609	6.025	-1.609	6.671
-1.386	5.002	-1.386	6.132	-1.386	6.763

Plotting the data from the table above produced the graphs shown below. Each graph had trend lines fitted to represent the data and from the equations of these lines the gradients (n values) and intercepts $\left(\ln \left(\frac{k_c}{b} + k_\phi \right) \right)$ values were determined.

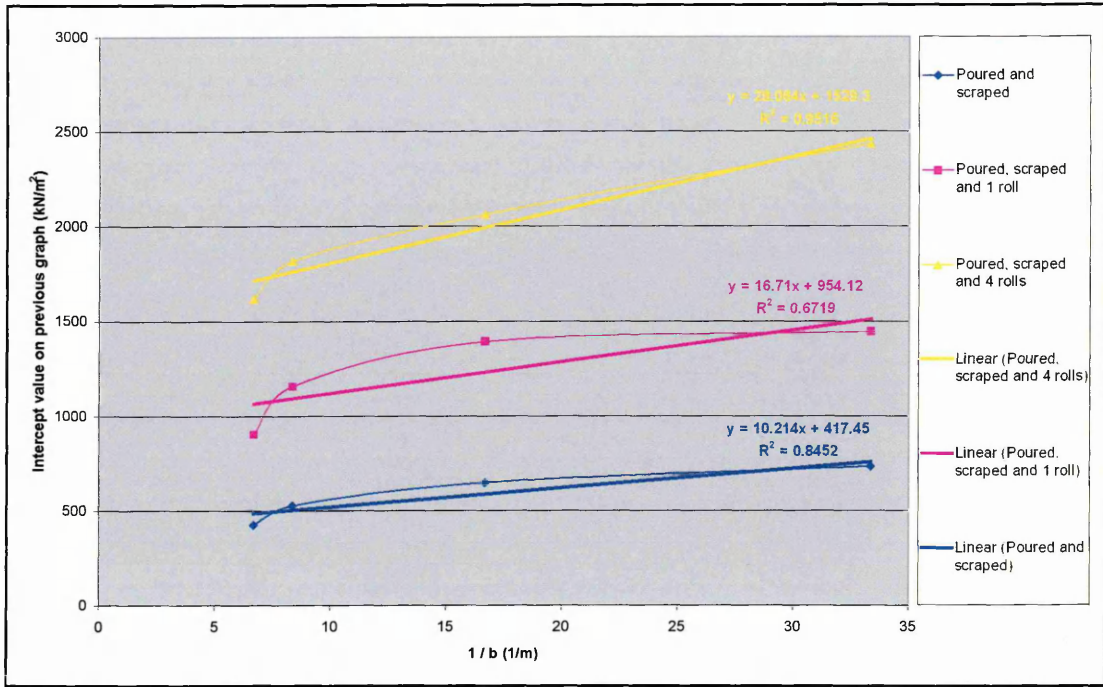


The equations generated for each of the trend lines are presented in the table below; from these equations the n coefficient for each soil type was determined by calculating the mean of the four gradients for the four plate sizes. Inverse natural logs of the intercept values were calculated to produce the values to plot against $1/b$ to allow the values of k_c and k_ϕ to be determined.

Soil type	Plate size m	Equation of the 'best fit' line	Gradient (n)	Intercept ln kN/m ²	Inverse ln of intercept kN/m ²
Poured and scraped	0.045 x 0.030	$y = 0.777x + 6.5977$	0.777	6.5977	733
Poured and scraped	0.090 x 0.060	$y = 0.8127x + 6.4757$	0.8127	6.4757	649
Poured and scraped	0.180 x 0.060	$y = 0.8258x + 6.2647$	0.8258	6.2647	526
Poured and scraped	0.225 x 0.150	$y = 0.7547x + 6.0531$	0.7547	6.0531	425
Average gradient (n)			0.793		
Poured, scraped and 1 roll	0.045 x 0.030	$y = 0.3447x + 7.2767$	0.3447	7.2767	1446
Poured, scraped and 1 roll	0.090 x 0.060	$y = 0.4161x + 7.2407$	0.4161	7.2407	1395
Poured, scraped and 1 roll	0.180 x 0.060	$y = 0.5296x + 7.0541$	0.5296	7.0541	1158
Poured, scraped and 1 roll	0.225 x 0.150	$y = 0.4845x + 6.8066$	0.4845	6.8066	904
Average gradient (n)			0.444		
Poured, scraped and 4 rolls	0.045 x 0.030	$y = 0.3526x + 7.7979$	0.3256	7.7979	2435
Poured, scraped and 4 rolls	0.090 x 0.060	$y = 0.3576x + 7.6332$	0.3576	7.6332	2066
Poured, scraped and 4 rolls	0.180 x 0.060	$y = 0.4591x + 7.5063$	0.4591	7.5063	1819
Poured, scraped and 4 rolls	0.225 x 0.150	$y = 0.4471x + 7.3906$	0.4471	7.3906	1621
Average gradient (n)			0.397		

This process produced the values shown in the table below, which were plotted to form the graph presented below, from which the gradients and intercepts were determined.

b (plate width) m	$1/b$ 1 / (plate width) m	Inverse ln of intercept kN/m ²
Poured and scraped		
0.03	33.33	733
0.06	16.67	649
0.12	8.33	526
0.15	6.67	425
Poured, scraped and 1 roll		
0.03	33.33	1446
0.06	16.67	1395
0.12	8.33	1158
0.15	6.67	904
Poured, scraped and 4 rolls		
0.03	33.33	2435
0.06	16.67	2066
0.12	8.33	1819
0.15	6.67	1621



From this graph both the values of k_c and k_ϕ were determined. All of these results enabled calculation of the actual Bekker coefficients, as detailed in the table below.

Soil type	Equation of the 'best fit' line	Gradient	Intercept	From previous equation
Notation		k_c	k_ϕ	n
Unit			kN/m^2	
Poured and scraped	$y = 10.214x + 417.45$	10.214	417	0.793
Poured, scraped and 1 roll	$y = 16.71x + 954.12$	16.71	954	0.444
Poured, scraped and 4 rolls	$y = 28.064x + 1529.3$	28.064	1529	0.397

APPENDIX 7 – DENSITY AND MOISTURE CONTENT STATISTICS

1170 kg/m³ soil – Density and Moisture Content

237 "Data taken from unsaved spreadsheet: New Data;1"

238 DELETE [Redefine=yes] _stitle_ : TEXT _stitle_

239 READ [print=*;SETNVALUES=yes] _stitle_

242 PRINT [IPrint=*] _stitle_ ; Just=Left

Data imported from Clipboard

on: 25-Jul-2002 12:35:24

243 DELETE [redefine=yes] Treatment,Rep,MC,Density

244 FACTOR [modify=yes;nvalues=90;levels=30] Treatment

245 READ Treatment; frepresentation=ordinal

Identifier	Values	Missing	Levels
------------	--------	---------	--------

Treatment	90	0	30
-----------	----	---	----

250 FACTOR [modify=yes;nvalues=90;levels=3] Rep

251 READ Rep; frepresentation=ordinal

Identifier	Values	Missing	Levels
------------	--------	---------	--------

Rep	90	0	3
-----	----	---	---

255 VARIATE [nvalues=90] MC

256 READ MC

Identifier	Minimum	Mean	Maximum	Values	Missing
------------	---------	------	---------	--------	---------

MC	7.350	9.326	11.25	90	0
----	-------	-------	-------	----	---

264 VARIATE [nvalues=90] Density

265 READ Density

Identifier	Minimum	Mean	Maximum	Values	Missing
------------	---------	------	---------	--------	---------

Density	1014	1172	1307	90	0
---------	------	------	------	----	---

276

277 "General Analysis of Variance."

278 BLOCK "No Blocking"

279 TREATMENTS Treatment
 280 COVARIATE "No Covariate"
 281 ANOVA [PRINT=aovtable,information,means,%cv,missingvalues; FACT=32;
 FPROB=yes; PSE=diff,\
 282 lsd,means; LSDLEVEL=5] Density

***** Analysis of variance *****

Variate: Density

Source of variation	d.f.	s.s.	m.s.	v.r.	F	pr.
Treatment	29	104725.	3611.	0.94	0.557	
Residual	60	229622.	3827.			
Total	89	334346.				

* MESSAGE: the following units have large residuals.

units 87 -155.9 s.e. 50.5

***** Tables of means *****

Variate: Density

Grand mean 1172.0

Treatment	1	2	3	4	5	6	7
	1144.5	1137.0	1229.4	1152.2	1138.7	1214.7	1197.8
Treatment	8	9	10	11	12	13	14
	1224.5	1159.9	1137.6	1128.1	1156.3	1142.4	1184.5
Treatment	15	16	17	18	19	20	21
	1218.5	1116.1	1231.2	1225.0	1173.6	1165.3	1159.7
Treatment	22	23	24	25	26	27	28
	1142.9	1143.0	1194.3	1149.9	1141.4	1180.4	1175.7
Treatment	29	30					
	1169.8	1225.4					

*** Standard errors of means ***

Table	Treatment
rep.	3
d.f.	60
e.s.e.	35.72

*** Standard errors of differences of means ***

Table	Treatment
rep.	3
d.f.	60
s.e.d.	50.51

*** Least significant differences of means (5% level) ***

Table	Treatment
rep.	3
d.f.	60
l.s.d.	101.04

***** Stratum standard errors and coefficients of variation *****

Variate: Density

d.f.	s.e.	cv%
60	61.86	5.3

283 "General Analysis of Variance."

284 BLOCK "No Blocking"

285 TREATMENTS Treatment

286 COVARIATE "No Covariate"

287 ANOVA [PRINT=aovtable,information,means,%cv,missingvalues; FACT=32;
FPROB=yes; PSE=diff,\

288 lsd,means; LSDLEVEL=5] MC

***** Analysis of variance *****

Variate: MC

Source of variation	d.f.	s.s.	m.s.	v.r.	F	pr.
Treatment	29	16.0886	0.5548	1.09	0.380	
Residual	60	30.5593	0.5093			
Total	89	46.6478				

* MESSAGE: the following units have large residuals.

units 21 1.507 s.e. 0.583

units 51 -1.637 s.e. 0.583

***** Tables of means *****

Variate: MC

Grand mean 9.326

Treatment	1	2	3	4	5	6	7
	9.000	9.587	8.853	9.823	9.813	9.253	9.123
Treatment	8	9	10	11	12	13	14
	8.743	9.077	9.680	9.250	9.040	9.720	8.810
Treatment	15	16	17	18	19	20	21
	8.923	9.897	8.987	9.167	9.113	9.713	9.120
Treatment	22	23	24	25	26	27	28
	10.043	9.047	8.627	9.997	8.887	9.947	9.683
Treatment	29	30					
	9.050	9.793					

*** Standard errors of means ***

Table	Treatment
rep.	3
d.f.	60
e.s.e.	0.4120

*** Standard errors of differences of means ***

Table	Treatment
rep.	3
d.f.	60
s.e.d.	0.5827

*** Least significant differences of means (5% level) ***

Table	Treatment
rep.	3
d.f.	60
l.s.d.	1.1656

***** Stratum standard errors and coefficients of variation *****

Variate: MC

d.f.	s.e.	cv%
60	0.7137	7.7

1270kg/m³ soil – Density and Moisture Content

37 "Data taken from unsaved spreadsheet: New Data;1"

38 DELETE [Redefine=yes] _stitle_ : TEXT _stitle_

39 READ [print=*;SETNVALUES=yes] _stitle_

42 PRINT [IPrint=*] _stitle_ ; Just=Left

Data imported from Clipboard

on: 25-Jul-2002 12:17:13

43 FACTOR [modify=yes;nvalues=21;levels=7] Treatment

44 READ Treatment; frepresentation=ordinal

Identifier	Values	Missing	Levels
Treatment	21	0	7

46 FACTOR [modify=yes;nvalues=21;levels=3] Rep

47 READ Rep; frepresentation=ordinal

Identifier	Values	Missing	Levels
Rep	21	0	3

49 VARIATE [nvalues=21] MC

50 READ MC

Identifier	Minimum	Mean	Maximum	Values	Missing
MC	7.930	8.727	9.600	21	0

53 VARIATE [nvalues=21] Density

54 READ Density

Identifier	Minimum	Mean	Maximum	Values	Missing
Density	1201	1270	1370	21	0

58

59 "General Analysis of Variance."

60 BLOCK "No Blocking"

61 TREATMENTS Treatment

62 COVARIATE "No Covariate"

63 ANOVA [PRINT=aovtable,information,means,%cv,missingvalues; FACT=32; FPROB=yes; PSE=diff,\

64 lsd,means; LSDLEVEL=5] Density

***** Analysis of variance *****

Variate: Density

Source of variation	d.f.	s.s.	m.s.	v.r.	F	pr.
Treatment	6	13394.	2232.	0.81	0.580	
Residual	14	38681.	2763.			
Total	20	52075.				

* MESSAGE: the following units have large residuals.

units 6 -102. s.e. 43.

***** Tables of means *****

Variate: Density

Grand mean 1270.

Treatment	1	2	3	4	5	6	7
	1256.	1303.	1262.	1239.	1279.	1243.	1307.

*** Standard errors of means ***

Table	Treatment
rep.	3
d.f.	14
e.s.e.	30.3

*** Standard errors of differences of means ***

Table	Treatment
rep.	3
d.f.	14
s.e.d.	42.9

*** Least significant differences of means (5% level) ***

Table	Treatment
rep.	3
d.f.	14
l.s.d.	92.1

***** Stratum standard errors and coefficients of variation *****

Variate: Density

d.f.	s.e.	cv%
14	52.6	4.1

65 AGRAPH [METHOD=lines] Treatment
 66 "General Analysis of Variance."
 67 BLOCK "No Blocking"
 68 TREATMENTS Treatment
 69 COVARIATE "No Covariate"
 70 ANOVA [PRINT=aovtable,information,means,%cv,missingvalues; FACT=32;
 FPROB=yes; PSE=diff,\

71 lsd,means; LSDLEVEL=5] MC

***** Analysis of variance *****

Variate: MC

Source of variation	d.f.	s.s.	m.s.	v.r.	F pr.
Treatment	6	0.6235	0.1039	0.76	0.616
Residual	14	1.9254	0.1375		
Total	20	2.5489			

* MESSAGE: the following units have large residuals.

units 3	0.627	s.e. 0.303
units 20	0.690	s.e. 0.303
units 21	-0.760	s.e. 0.303

***** Tables of means *****

Variate: MC

Grand mean 8.727

Treatment	1	2	3	4	5	6	7
	8.353	8.867	8.713	8.697	8.843	8.703	8.910

*** Standard errors of means ***

Table	Treatment
rep.	3
d.f.	14
e.s.e.	0.2141

*** Standard errors of differences of means ***

Table	Treatment
rep.	3
d.f.	14
s.e.d.	0.3028

*** Least significant differences of means (5% level) ***

Table	Treatment
rep.	3
d.f.	14
l.s.d.	0.6494

***** Stratum standard errors and coefficients of variation *****

Variate: MC

d.f.	s.e.	cv%
14	0.3708	4.2

1400kg/m³ soil – Density and Moisture Content

<i>Soil Density</i>		<i>Moisture Content</i>	
Mean	1398.958	Mean	8.691533
Standard Error	9.425736	Standard Error	0.122735
Median	1395.054	Median	8.75
Mode	#N/A	Mode	#N/A
Standard Deviation	28.27721	Standard Deviation	0.368206
Sample Variance	799.6006	Sample Variance	0.135576
Kurtosis	-0.27083	Kurtosis	-0.79536
Skewness	0.005337	Skewness	-0.26257
Range	92.28904	Range	1.134751
Minimum	1352.348	Minimum	8.085212
Maximum	1444.637	Maximum	9.219962
Sum	12590.62	Sum	78.22379
Count	9	Count	9
Confidence Level(95.0%)	21.7358	Confidence Level(95.0%)	0.283028

APPENDIX 8 – CONE INDEX STATISTICS (SOIL)

1170kg/m³ soil – Cone Index

28 "Data taken from unsaved spreadsheet: New Data;1"
 29 DELETE [Redefine=yes] _stitle_: TEXT _stitle_
 30 READ [print=*;SETNVALUES=yes] _stitle_
 33 PRINT [IPrint=*_stitle_]; Just=Left

Data imported from Clipboard

on: 10-Sep-2002 20:23:52

34 DELETE [redefine=yes] Treatment,Rep,CI
 35 FACTOR [modify=yes;nvalues=66;levels=22] Treatment
 36 READ Treatment; frepresentation=ordinal

Identifier	Values	Missing	Levels
Treatment	66	0	22

40 VARIATE [nvalues=66] Rep
 41 READ Rep

Identifier	Minimum	Mean	Maximum	Values	Missing
Rep	1.000	2.000	3.000	66	0

44 VARIATE [nvalues=66] CI
 45 READ CI

Identifier	Minimum	Mean	Maximum	Values	Missing
CI	95.97	138.8	197.9	66	0

57

58 "General Analysis of Variance."

59 BLOCK "No Blocking"

60 TREATMENTS Treatment

61 COVARIATE "No Covariate"

62 ANOVA [PRINT=aovtable,information,means,%cv,missingvalues; FACT=32;
 FPROB=yes; PSE=diff\

63 lsd,means; LSDLEVEL=5] CI

***** Analysis of variance *****

Variate: CI

Source of variation	d.f.	s.s.	m.s.	v.r.	F	pr.
Treatment	21	18102.9	862.0	1.78	0.054	
Residual	44	21332.6	484.8			
Total	65	39435.6				

* MESSAGE: the following units have large residuals.

units 4	46.2	s.e. 18.0
units 40	47.0	s.e. 18.0

***** Tables of means *****

Variate: CI

Grand mean 138.8

Treatment	1	2	3	4	5	6	7
	136.3	126.8	122.0	129.1	144.1	112.9	111.8
Treatment	8	9	10	11	12	13	14
	116.1	118.5	162.7	156.8	165.9	166.7	150.9
Treatment	15	16	17	18	19	20	21
	150.1	148.5	137.4	154.4	132.3	130.3	137.4
Treatment	22						
	143.4						

*** Standard errors of means ***

Table	Treatment
rep.	3
d.f.	44
e.s.e.	12.71

*** Standard errors of differences of means ***

Table	Treatment
rep.	3
d.f.	44
s.e.d.	17.98

*** Least significant differences of means (5% level) ***

Table	Treatment
rep.	3

d.f.	44
l.s.d.	36.23

***** Stratum standard errors and coefficients of variation *****

Variate: CI

d.f.	s.e.	cv%
44	22.02	15.9

1170 kg/m³ soil – Cone Index

GenStat Fifth Edition (Service Pack 1)
GenStat Procedure Library Release PL12.1

```
1 %CD 'P:/gen5ed/bin'
2 "Data taken from unsaved spreadsheet: New Data;1"
3 DELETE [Redefine=yes] _stitle_ : TEXT _stitle_
4 READ [print=*;SETNVALUES=yes] _stitle_
7 PRINT [IPrint=*] _stitle_ ; Just=Left
```

Data imported from Clipboard

on: 10-Sep-2002 20:16:00

```
8 DELETE [redefine=yes] Treatment,Rep,CI
9 FACTOR [modify=yes;nvalues=21;levels=7] Treatment
10 READ Treatment; frepresentation=ordinal
```

Identifier	Values	Missing	Levels
------------	--------	---------	--------

Treatment	21	0	7
-----------	----	---	---

```
12 VARIATE [nvalues=21] Rep
```

```
13 READ Rep
```

Identifier	Minimum	Mean	Maximum	Values	Missing
------------	---------	------	---------	--------	---------

Rep	1.000	2.000	3.000	21	0
-----	-------	-------	-------	----	---

```
15 VARIATE [nvalues=21] CI
```

```
16 READ CI
```

Identifier	Minimum	Mean	Maximum	Values	Missing
------------	---------	------	---------	--------	---------

CI	341.6	415.7	481.7	21	0
----	-------	-------	-------	----	---

```
21
```

```
22 "General Analysis of Variance."
```

```
23 BLOCK "No Blocking"
```

```
24 TREATMENTS Treatment
```

```
25 COVARIATE "No Covariate"
```

```
26 ANOVA [PRINT=aovtable,information,means,%cv,missingvalues; FACT=32;
FPROB=yes; PSE=diff,\
```

```
27 lsd,means; LSDLEVEL=5] CI
```

***** Analysis of variance *****

Variate: CI

Source of variation	d.f.	s.s.	m.s.	v.r.	F pr.
Treatment	6	2638.	440.	0.29	0.932
Residual	14	21182.	1513.		
Total	20	23819.			

* MESSAGE: the following units have large residuals.

units 7 -84.7 s.e. 31.8

***** Tables of means *****

Variate: CI

Grand mean 415.7

Treatment	1	2	3	4	5	6	7
	395.3	418.6	426.3	410.2	419.0	408.8	431.7

*** Standard errors of means ***

Table	Treatment
rep.	3
d.f.	14
e.s.e.	22.46

*** Standard errors of differences of means ***

Table	Treatment
rep.	3
d.f.	14
s.e.d.	31.76

*** Least significant differences of means (5% level) ***

Table	Treatment
rep.	3
d.f.	14
l.s.d.	68.12

***** Stratum standard errors and coefficients of variation *****

Variate: CI

d.f.	s.e.	cv%
14	38.90	9.4

APPENDIX 9 – SLED FRICTION ANOVA RESULTS

The angles of sand-rubber friction (δ) and value of adhesion (a) for all of the sand types and all of the five sleds were tested to ascertain if significant difference existed between the mean results for each of the five sleds.

Null Hypothesis: No significant difference exists between the means results for each sled (sample).

This hypothesis was tested for both (δ) and (a), for all of the following tests.

Test 1, ANOVA Results for (δ)

Null Hypothesis was tested at the 99% confidence level.

SUMMARY

<i>Groups</i>	<i>Sled</i>	<i>Count</i>	<i>Sum</i>	<i>Average</i>	<i>Variance</i>
Column 1	A	17	450.9	26.52353	0.860662
Column 2	B	17	480.3	28.25294	3.102647
Column 3	C	17	478.7	28.15882	2.713824
Column 4	D	17	477.7	28.1	2.7475
Column 5	E	17	470.2	27.65882	2.917574

ANOVA

<i>Source of Variation</i>	<i>SS</i>	<i>df</i>	<i>MS</i>	<i>F</i>	<i>P-value</i>	<i>F crit</i>
Between Groups	34.92659	4	8.731647	3.537312	0.010393	3.563116
Within Groups	197.4753	80	2.468441			
Total	232.4019	84				

The calculated F statistic does not exceed F *critical*, therefore the Null Hypothesis cannot be rejected.

Test 2, ANOVA Results for (a)

The Null Hypothesis was tested at the 95% confidence level.

SUMMARY

Groups	Sled	Count	Sum	Average	Variance
Column 1	A	17	584	34.35294118	385.617647
Column 2	B	17	1816	106.8235294	530.029412
Column 3	C	17	1369	80.52941176	322.264706
Column 4	D	17	1811	106.5294118	276.014706
Column 5	E	17	1884	110.8235294	192.404412

ANOVA

Source of Variation	SS	df	MS	F	P-value	F crit
Between Groups	70587.69412	4	17646.92353	51.71014518	1.9626E-21	2.485883
Within Groups	27301.29412	80	341.2661765			
Total	97888.98824	84				

The calculated F statistic exceeds F critical, therefore the Null Hypothesis can be rejected. It can therefore be stated with 95% confidence that significant difference exists between the sample means.

Test 3, ANOVA Results for (a), for sleds B, D & E

The Null Hypothesis was tested at the 95% confidence level.

SUMMARY

Groups	Sled	Count	Sum	Average	Variance
Column 1	B	17	1816	106.8235	530.0294
Column 2	D	17	1811	106.5294	276.0147
Column 3	E	17	1884	110.8235	192.4044

ANOVA

Source of Variation	SS	df	MS	F	P-value	F crit
Between Groups	195.6471	2	97.82353	0.293927	0.746663	3.190721
Within Groups	15975.18	48	332.8162			
Total	16170.82	50				

The calculated F statistic does not exceed F critical, therefore the Null Hypothesis cannot be rejected.

Test 4, ANOVA Results for (a), for sleds A and C

The Null Hypothesis was tested at the 95% confidence level.

SUMMARY

<i>Groups</i>	<i>Sled</i>	<i>Count</i>	<i>Sum</i>	<i>Average</i>	<i>Variance</i>
Column 1	A	17	584	34.35294	385.6176
Column 2	E	17	1369	80.52941	322.2647

ANOVA

<i>Source of Variation</i>	<i>SS</i>	<i>df</i>	<i>MS</i>	<i>F</i>	<i>P-value</i>	<i>F crit</i>
Between Groups	18124.26	1	18124.26	51.207	4.01E-08	4.149086
Within Groups	11326.12	32	353.9412			
Total	29450.38	33				

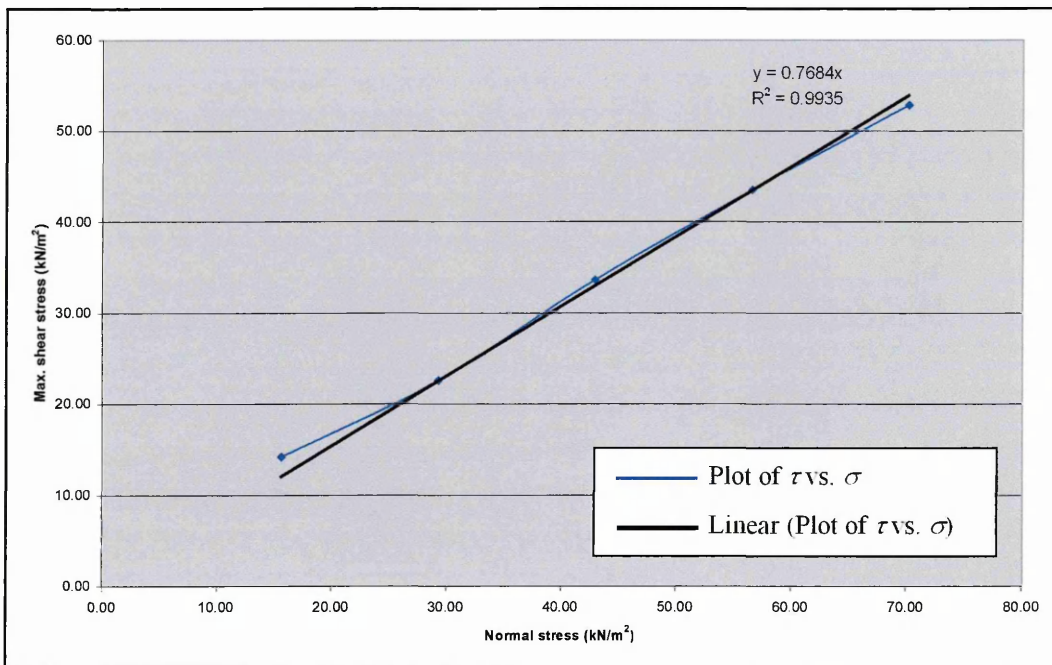
The calculated F statistic exceeds F critical, therefore the Null Hypothesis can be rejected. It can therefore be stated with 95% confidence that significant difference exists between the sample means.

APPENDIX 10 – TRANSLATIONAL SAND SHEAR RESULTS

These results demonstrate the methodology by which c and ϕ were determined for the DA80F replicate sand used for the experiments. Values of maximum shear stress (τ) achieved were plotted against values of normal stress (σ) at which the shear stresses were achieved, as the table and figure below detail.

A table of maximum soil shear stresses recorded at different normal stresses

Normal stress kN/m ²	Max. shear stress kN/m ²
15.64	14.19
29.27	22.58
42.89	33.66
56.52	43.53
70.14	52.86



A graph of maximum soil shear stresses recorded at different normal stresses

From the equation of the trend line shown on the graph, both c and ϕ were determined. In this instance c equalled the intercept, 0 kN/m², as expected, whilst ϕ equalled \tan^{-1} of the gradient of the trend line, i.e. $\tan^{-1} 0.7684$, or 37.5°.

APPENDIX 11 – SAND DENSITY RESULTS

These values were recorded from sand density tests throughout the duration of all of the sand testing. As the density was consistent, because of the close particle size distribution, only a limited number of tests were conducted solely to confirm that the soil processing did not affect the achieved density. A mean density of $1482 \text{ kg/m}^3 \pm 21 \text{ kg/m}^3$ was achieved.

Date of test	Sand Density kg/m^3
Wk 32, August 2000	1488
Wk 32, August 2000	1461
Wk 32, August 2000	1493
Wk 32, August 2000	1475
Wk 33, August 2000	1482
Wk 33, August 2000	1483
Wk 34, August 2000	1481
Wk 34, August 2000	1480
Wk 34, August 2000	1492
Wk 24, June 2001	1484
Wk 24, June 2001	1492
Wk 24, June 2001	1479
Wk 25, June 2001	1491
Wk 25, June 2001	1487
Wk 25, June 2001	1476
Wk 26, June 2001	1490
Wk 26, June 2001	1481
Wk 27, July 2001	1480
Wk 27, July 2001	1495
Wk 27, July 2001	1482
Wk 28, July 2001	1490
Wk 29, July 2001	1477
Wk 29, July 2001	1485
Wk 30, July 2001	1474
Wk 30, July 2001	1487
Wk 15, April 2002	1469
Wk 15, April 2002	1465
Wk 16, April 2002	1478
Wk 17, April 2002	1481
Wk 17, April 2002	1481
Wk 18, May 2002	1470
Mean Density	1482
Range (plus and minus)	21

APPENDIX 12 – CONE INDEX STATISTICS (REPLICATE SAND)

213 "Data taken from unsaved spreadsheet: New Data;1"

214 DELETE [Redefine=yes] _stitle_: TEXT _stitle_

215 READ [print=*;SETNVALUES=yes] _stitle_

218 PRINT [IPrint=*] _stitle_; Just=Left

Data imported from Clipboard

on: 10-Sep-2002 21:21:29

219 FACTOR [modify=yes;nvalues=75;levels=25] Treatment

220 READ Treatment; frepresentation=ordinal

Identifier	Values	Missing	Levels
------------	--------	---------	--------

Treatment	75	0	25
-----------	----	---	----

224 VARIATE [nvalues=75] Rep

225 READ Rep

Identifier	Minimum	Mean	Maximum	Values	Missing
------------	---------	------	---------	--------	---------

Rep	1.000	2.000	3.000	75	0
-----	-------	-------	-------	----	---

228 VARIATE [nvalues=75] CI

229 READ CI

Identifier	Minimum	Mean	Maximum	Values	Missing
------------	---------	------	---------	--------	---------

CI	98.57	128.7	170.6	75	0
----	-------	-------	-------	----	---

243

244 "General Analysis of Variance."

245 BLOCK "No Blocking"

246 TREATMENTS Treatment

247 COVARIATE "No Covariate"

248 ANOVA [PRINT=aovtable,information,means,%cv,missingvalues; FACT=32; FPROB=yes; PSE=diff,\

249 lsd,means; LSDLEVEL=5] CI

***** Analysis of variance *****

Variate: CI

Source of variation	d.f.	s.s.	m.s.	v.r.	F	pr.
Treatment	24	9229.5	384.6	1.60	0.080	

Residual	50	12010.3	240.2
Total	74	21239.7	

* MESSAGE: the following units have large residuals.

units 4	30.0	s.e. 12.7
units 64	37.9	s.e. 12.7
units 68	-32.2	s.e. 12.7
units 75	46.1	s.e. 12.7

***** Tables of means *****

Variate: CI

Grand mean 128.7

Treatment	1	2	3	4	5	6	7
	136.3	121.6	119.3	135.5	116.9	132.7	120.8
Treatment	8	9	10	11	12	13	14
	124.0	141.4	151.3	133.1	133.1	118.1	119.3
Treatment	15	16	17	18	19	20	21
	125.2	122.4	114.5	116.5	112.5	130.8	140.3
Treatment	22	23	24	25			
	128.9	147.9	151.0	124.5			

*** Standard errors of means ***

Table	Treatment
rep.	3
d.f.	50
e.s.e.	8.95

*** Standard errors of differences of means ***

Table	Treatment
rep.	3
d.f.	50
s.e.d.	12.65

*** Least significant differences of means (5% level) ***

Table	Treatment
rep.	3
d.f.	50
l.s.d.	25.42

***** Stratum standard errors and coefficients of variation *****

Variate: CI

d.f.	s.e.	cv%
50	15.50	12.0

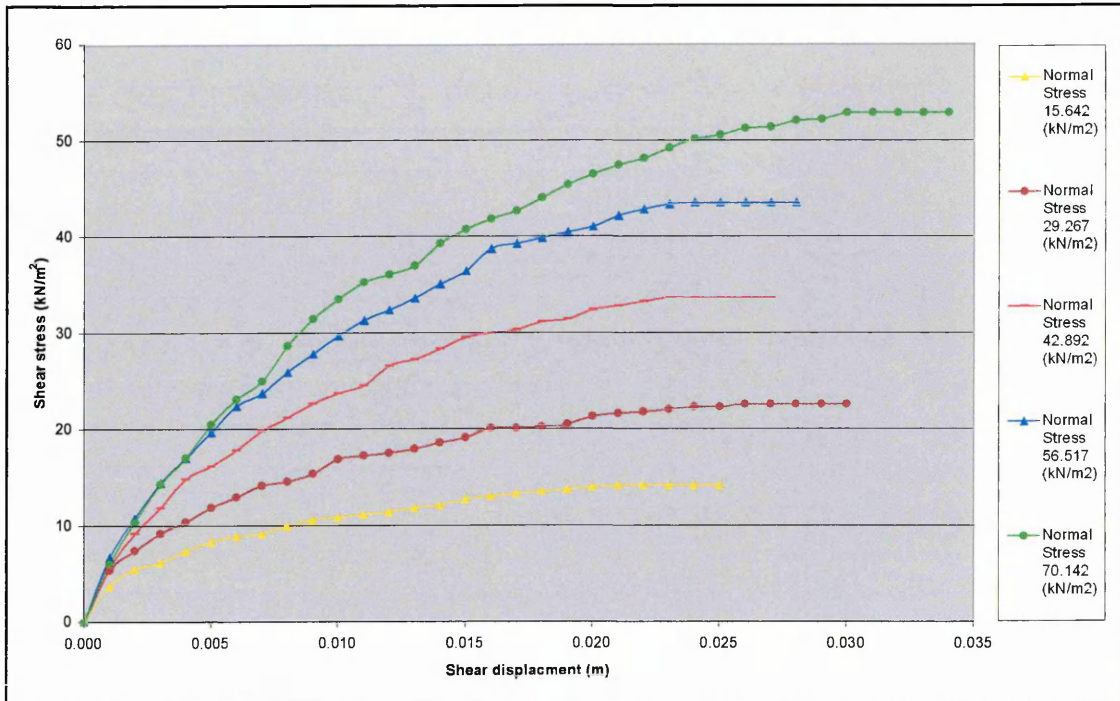
APPENDIX 13 – CALCULATION OF K (SAND DEF. MODULUS)

To determine K , the procedure detailed in section 3.5.3.3 was used. The first stage of this was to conduct a shear box tests to determine the shear stress – shear displacement relationships for the DA80F replicate sand under varying normal loads. The results of these experiments are detailed in the table below:

A table of shear-stress/ shear deformation results for different normal loads

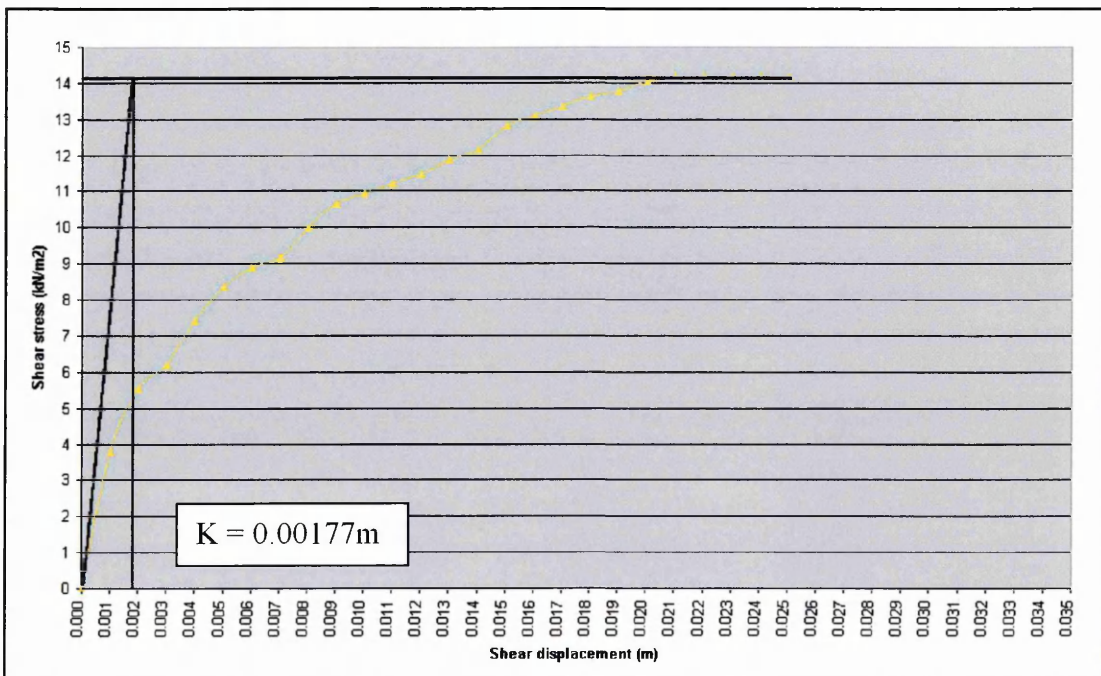
Sand Deformation m	Normal stress 15.64 kN/m ²	Normal stress 29.27 kN/m ²	Normal stress 42.89 kN/m ²	Normal stress 56.52 kN/m ²	Normal stress 70.14 kN/m ²
	Shear stress kN/m ²				
0.000	0.0	0.0	0.0	0.0	0.0
0.001	3.8	5.4	5.7	6.8	6.1
0.002	5.5	7.4	9.2	10.8	10.4
0.003	6.2	9.2	11.9	14.5	14.3
0.004	7.4	10.4	14.9	17.0	17.0
0.005	8.4	11.9	16.2	19.7	20.5
0.006	8.9	13.0	17.8	22.4	23.1
0.007	9.2	14.2	19.9	23.8	25.0
0.008	10.0	14.6	21.2	26.0	28.7
0.009	10.7	15.4	22.7	27.8	31.5
0.010	11.0	16.9	23.8	29.7	33.5
0.011	11.2	17.3	24.6	31.4	35.3
0.012	11.5	17.6	26.6	32.4	36.1
0.013	11.9	18.0	27.3	33.7	37.0
0.014	12.2	18.7	28.4	35.1	39.3
0.015	12.8	19.2	29.6	36.5	40.8
0.016	13.1	20.1	30.0	38.8	41.9
0.017	13.4	20.1	30.4	39.3	42.7
0.018	13.7	20.3	31.2	39.9	44.1
0.019	13.8	20.5	31.5	40.6	45.4
0.020	14.1	21.4	32.4	41.1	46.5
0.021	14.2	21.6	32.9	42.2	47.5
0.022	14.1	21.8	33.3	42.9	48.1
0.023	14.2	22.0	33.8	43.4	49.2
0.024	14.3	22.3	33.7	43.5	50.2
0.025	14.2	22.3	33.6	43.4	50.6
0.026	14.2	22.6	33.7	43.4	51.2
0.027		22.6	33.7	43.5	51.4
0.028		22.7		43.5	52.0
0.029		22.6			52.2
0.030		22.6			52.9
0.031					53.0
0.032					52.8
0.033					52.9
0.034					52.9

These results were then plotted to assess the relationships, as shown in the figure below, on which the expected curved relationship was produced.



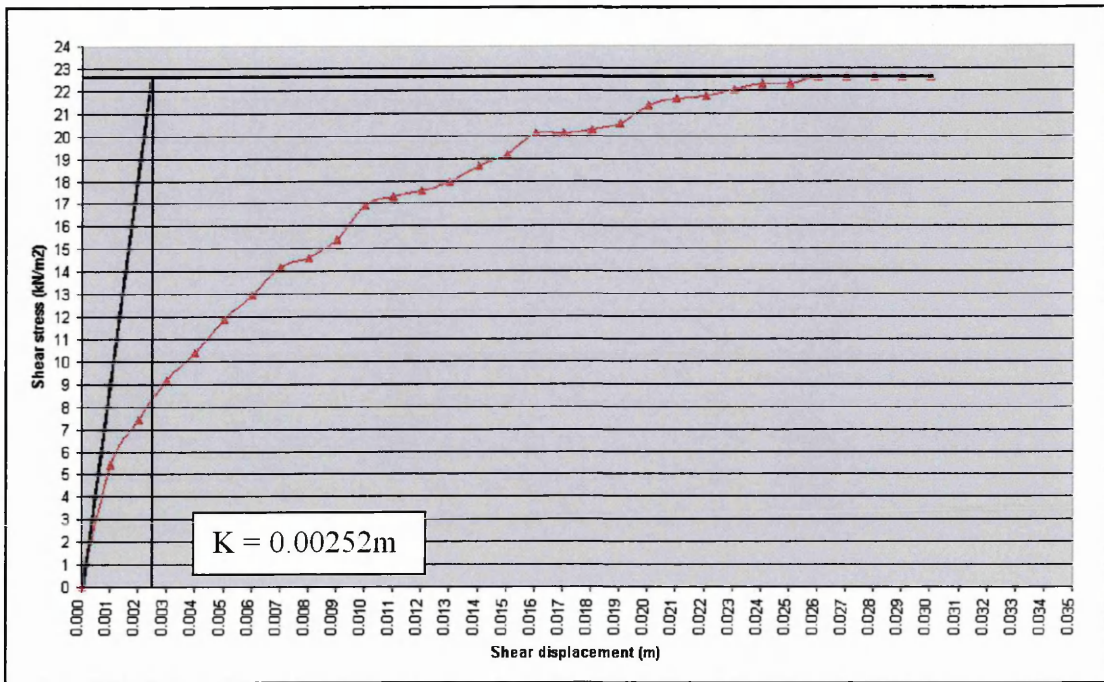
Shear-stress results plotted against shear-displacements for varying normal loads

The five plots were then considered separately to allow the tangents to be calculated. This graphical interpretation was conducted by hand on paper to achieve maximum accuracy, but representations of the results are presented on the following five graphs.

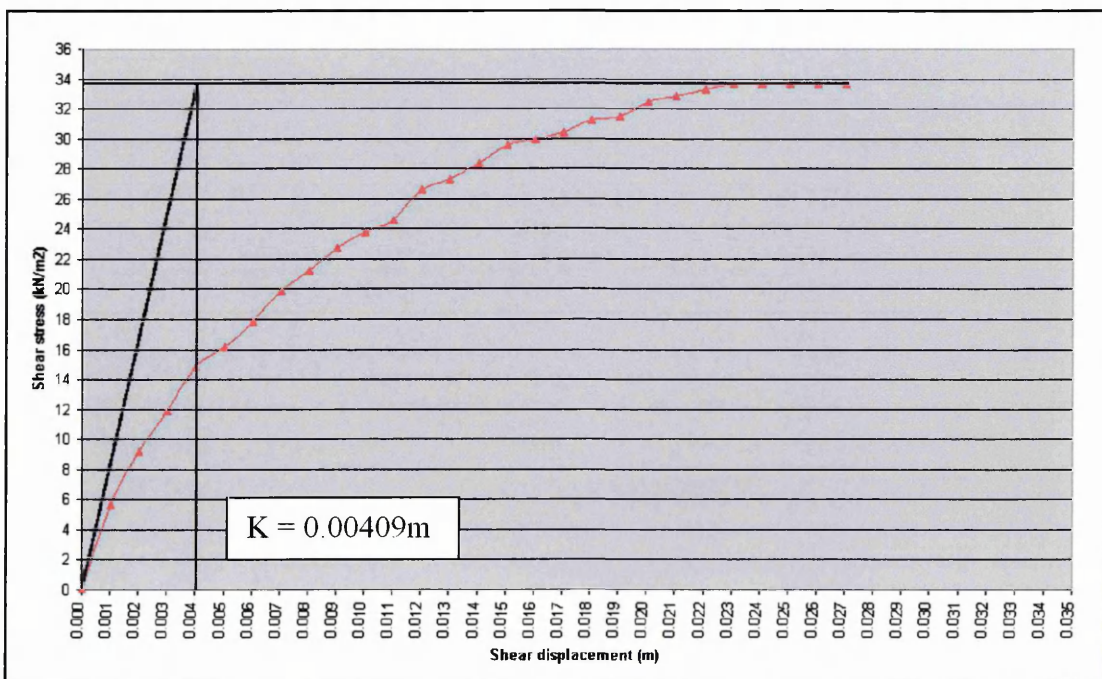


Calculation of sand deformation modulus (K) for a 15.64 kN/m² normal load

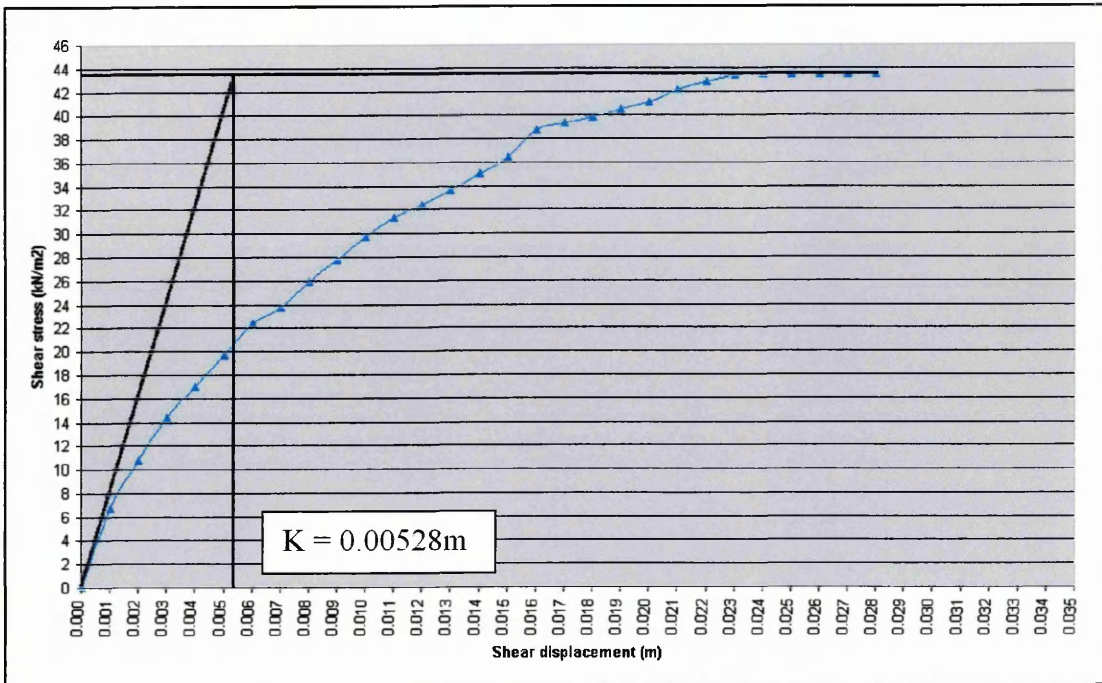
The value of K was read off these graphs at the point where the vertical line (which indicates the intercept of the horizontal line and tangent) intercepts the X-axis.



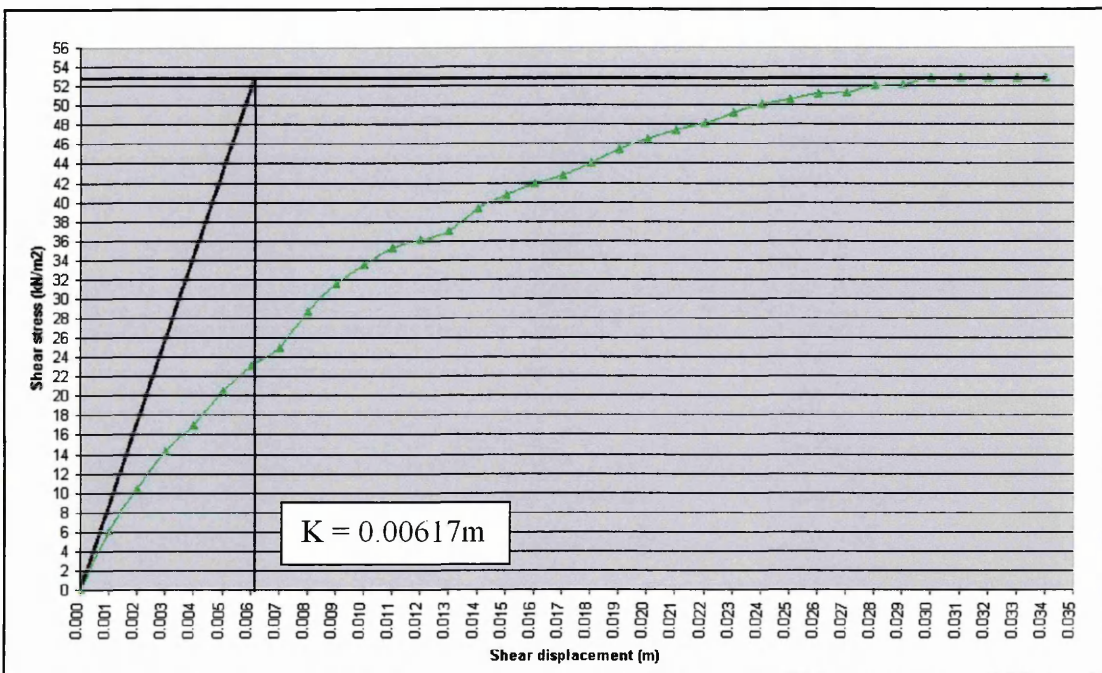
Calculation of sand deformation modulus (K) for a 29.27 kN/m² normal load



Calculation of sand deformation modulus (K) for a 42.89 kN/m² normal load

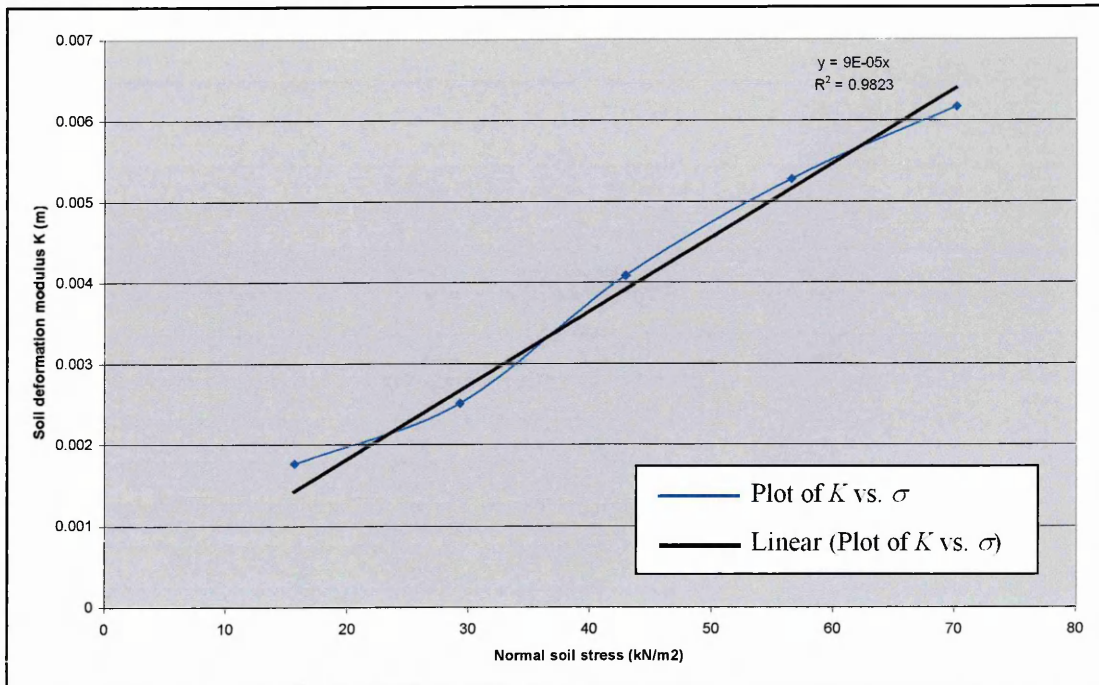


Calculation of sand deformation modulus (K) for a 56.52 kN/m² normal load



Calculation of sand deformation modulus (K) for a 70.14 kN/m² normal load

The results from this interpretation were plotted to allow the relationship between normal load and K to be determined, which is shown on the graph below.



A graph of sand deformation modulus, K , against normal soil stress, σ

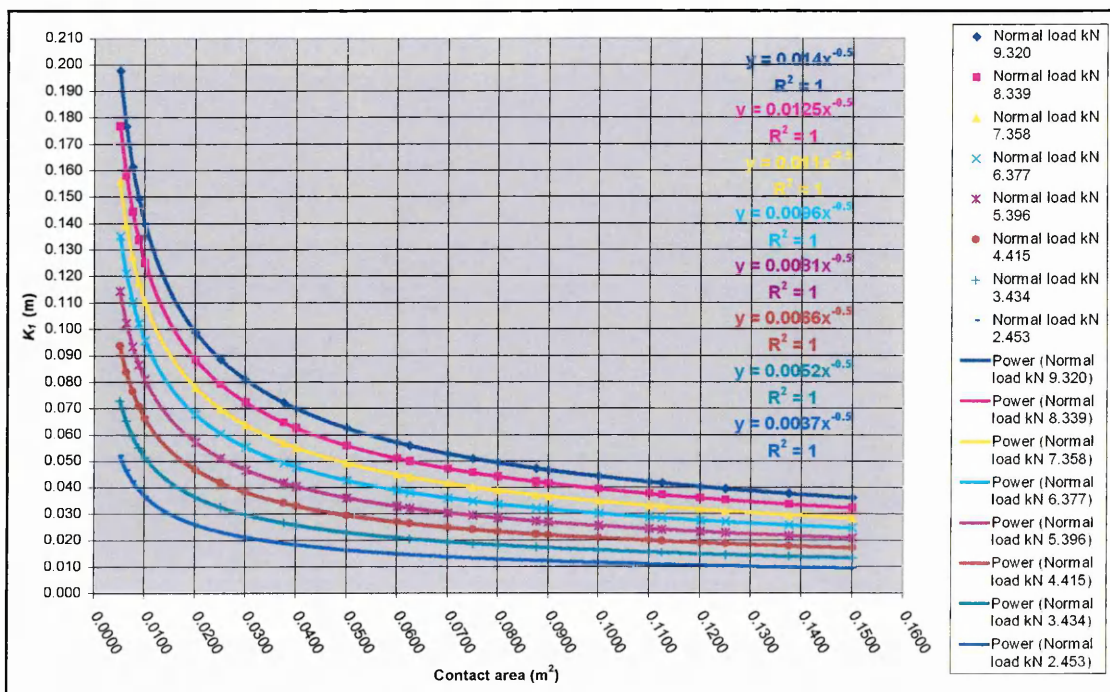
The graph showed that a linear relationship existed between σ and K . This took the form of $K = 0.00009\sigma$. Thus the value of K at any given normal load (within the tested

range) could be determined. Equation 16 $\left\{ \frac{K_1}{K_2} = \sqrt{\left(\frac{A_1}{A_2} \right)} \right\}$ showed that for sand

experiencing similar normal stresses, but over varying areas A_1 (tyre contact) and A_2 (shear box), then through knowledge of K_2 then K_1 could be derived. This led to an analysis to determine values of K_1 for given normal stresses. However, it was only possible to determine a range of possible of K_1 values for any given sand load, because as the contact area size (as yet unknown) was increased then this altered both the normal stress, which was used to compute of K_2 , and also the ratio of areas $A_1 : A_2$. Thus for each load a range of K_1 values were produced, as the table and figure below indicate.

A table of K_1 values for different normal loads on the DA80F sand

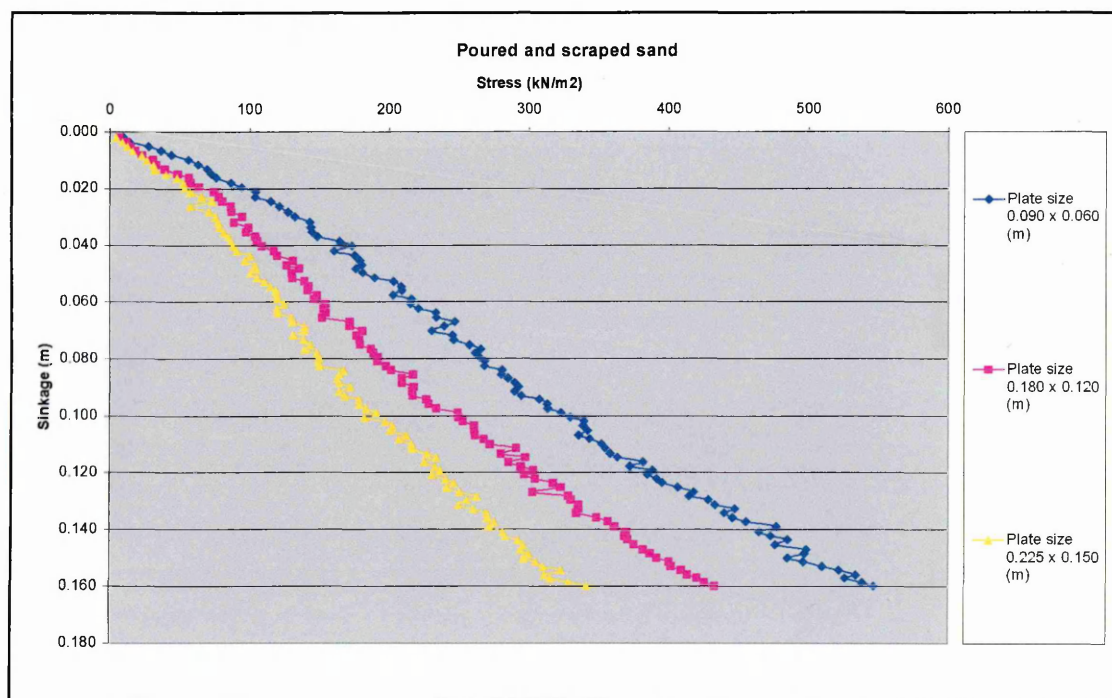
K1 = K2 sqrt (A1/A2)		Normal load kN								
K2 = 0.0009 (sigma)										
K1 = tyre	K2 = box	9.320	8.339	7.358	6.377	5.396	4.415	3.434	2.453	
A1 = tyre	A2 = box									
Contact length	Contact width	Contact area	Value of K1							
m	m	m ²	m	m	m	m	m	m	m	m
0.05	0.10	0.0050	0.1977	0.1769	0.1561	0.1353	0.1145	0.0936	0.0728	0.0520
0.05	0.13	0.0063	0.1768	0.1582	0.1396	0.1210	0.1024	0.0838	0.0651	0.0465
0.05	0.15	0.0075	0.1614	0.1444	0.1274	0.1104	0.0935	0.0765	0.0595	0.0425
0.05	0.18	0.0088	0.1494	0.1337	0.1180	0.1023	0.0865	0.0708	0.0551	0.0393
0.05	0.20	0.0100	0.1398	0.1251	0.1104	0.0956	0.0809	0.0662	0.0515	0.0368
0.10	0.20	0.0200	0.0988	0.0884	0.0780	0.0676	0.0572	0.0468	0.0364	0.0260
0.15	0.20	0.0300	0.0807	0.0722	0.0637	0.0552	0.0467	0.0382	0.0297	0.0212
0.20	0.20	0.0400	0.0699	0.0625	0.0552	0.0478	0.0405	0.0331	0.0258	0.0184
0.25	0.20	0.0500	0.0625	0.0559	0.0494	0.0428	0.0362	0.0296	0.0230	0.0165
0.30	0.20	0.0600	0.0571	0.0511	0.0451	0.0390	0.0330	0.0270	0.0210	0.0150
0.35	0.20	0.0700	0.0528	0.0473	0.0417	0.0362	0.0306	0.0250	0.0195	0.0139
0.40	0.20	0.0800	0.0494	0.0442	0.0390	0.0338	0.0286	0.0234	0.0182	0.0130
0.45	0.20	0.0900	0.0466	0.0417	0.0368	0.0319	0.0270	0.0221	0.0172	0.0123
0.50	0.20	0.1000	0.0442	0.0396	0.0349	0.0302	0.0256	0.0209	0.0163	0.0116
0.55	0.20	0.1100	0.0421	0.0377	0.0333	0.0288	0.0244	0.0200	0.0155	0.0111
0.60	0.20	0.1200	0.0404	0.0361	0.0319	0.0276	0.0234	0.0191	0.0149	0.0106
0.10	0.25	0.0250	0.0884	0.0791	0.0698	0.0605	0.0512	0.0419	0.0326	0.0233
0.15	0.25	0.0375	0.0722	0.0646	0.0570	0.0494	0.0418	0.0342	0.0266	0.0190
0.20	0.25	0.0500	0.0625	0.0559	0.0494	0.0428	0.0362	0.0296	0.0230	0.0165
0.25	0.25	0.0625	0.0559	0.0500	0.0441	0.0383	0.0324	0.0265	0.0206	0.0147
0.30	0.25	0.0750	0.0510	0.0457	0.0403	0.0349	0.0296	0.0242	0.0188	0.0134
0.35	0.25	0.0875	0.0473	0.0423	0.0373	0.0323	0.0274	0.0224	0.0174	0.0124
0.40	0.25	0.1000	0.0442	0.0396	0.0349	0.0302	0.0256	0.0209	0.0163	0.0116
0.45	0.25	0.1125	0.0417	0.0373	0.0329	0.0285	0.0241	0.0197	0.0154	0.0110
0.50	0.25	0.1250	0.0395	0.0354	0.0312	0.0271	0.0229	0.0187	0.0146	0.0104
0.55	0.25	0.1375	0.0377	0.0337	0.0298	0.0258	0.0218	0.0179	0.0139	0.0099
0.60	0.25	0.1500	0.0361	0.0323	0.0285	0.0247	0.0209	0.0171	0.0133	0.0095



A graph showing the relationships between contact area and K_1 for the DA80F sand under different normal tyre loads

APPENDIX 14 – PLATE SINKAGE TESTS ON SAND

These tests were used to determine values of the Bekker soil coefficients n , k_c and k_ϕ for the replicate sand preparation (poured and scraped) used for the experiments. The same methodology was used as was outlined in Appendix 5, except only three different sized rectangular plates were used. Each test was replicated three times. The pressure and sinkage results from these tests are shown on the following sets of tables and graphs.



Rep 1	Rep 2	Rep 3	Plate size	0.090 x 0.060 (m)	Rep 1	Rep 2	Rep 3	Plate size	0.090 x 0.060 (m)
ρ (kN/ μ 2)	ρ (kN/ μ 2)	ρ (kN/ μ 2)	Mean r (kN/m2)	Sinkage (m)	ρ (kN/ μ 2)	ρ (kN/ μ 2)	ρ (kN/ μ 2)	Mean r (kN/m2)	Sinkage (m)
11.118	10.166	5.624	9	0.002	255.231	284.533	302.100	281	0.084
8.930	17.004	14.515	13	0.003	278.988	284.218	276.585	280	0.085
15.699	36.906	29.442	27	0.005	285.923	287.122	281.505	285	0.087
30.394	45.201	32.780	36	0.007	284.388	291.299	293.028	290	0.088
31.613	52.218	47.100	44	0.008	282.444	298.850	295.832	292	0.090
51.469	62.966	52.200	56	0.010	292.885	289.603	286.227	290	0.091
56.964	71.842	58.806	63	0.012	293.967	298.519	291.225	295	0.093
65.847	75.606	65.709	69	0.013	300.082	311.151	310.801	307	0.094
73.613	75.191	67.936	72	0.015	330.083	314.827	294.432	313	0.096
61.368	84.165	81.453	76	0.016	309.056	313.867	316.646	313	0.097
76.258	88.926	92.451	86	0.018	319.481	329.501	319.474	323	0.099
80.468	103.811	97.324	94	0.019	348.711	329.996	309.862	330	0.100
103.327	109.953	97.373	104	0.021	356.997	342.134	319.186	339	0.102
100.322	112.383	97.110	103	0.023	358.423	339.266	318.528	339	0.103
110.627	122.018	111.305	115	0.024	333.884	346.660	345.456	342	0.105
118.384	130.274	113.524	121	0.026	305.850	339.793	361.360	336	0.107
120.709	129.829	130.454	127	0.028	332.107	351.230	346.853	343	0.108
117.032	136.679	141.999	132	0.030	370.845	354.119	330.980	352	0.110
146.271	147.473	134.108	143	0.032	318.357	363.405	381.575	354	0.111
133.426	149.796	146.796	143	0.033	355.659	364.184	354.904	358	0.113
145.092	151.557	135.434	144	0.035	375.633	372.770	341.681	363	0.115
143.235	149.252	151.428	148	0.037	402.733	383.004	358.726	381	0.116
146.291	168.810	176.359	164	0.038	391.945	374.504	349.920	372	0.118
174.321	181.426	162.415	173	0.040	380.153	392.992	391.757	388	0.119
156.333	167.012	156.655	160	0.042	374.780	391.736	388.443	385	0.121
177.278	175.759	171.501	175	0.043	407.227	398.905	368.037	391	0.122
157.159	185.889	192.001	178	0.045	418.834	395.456	371.761	395	0.123
176.298	179.766	183.217	180	0.047	424.183	412.959	382.195	406	0.125
178.917	182.607	165.052	176	0.048	438.190	422.622	393.001	418	0.127
190.426	181.514	169.808	181	0.050	376.768	420.637	446.299	415	0.128
172.589	190.945	203.466	189	0.051	386.860	436.884	461.041	428	0.129
200.335	208.407	199.354	203	0.053	453.461	438.358	407.157	433	0.131
202.402	210.342	211.556	208	0.054	473.932	447.495	420.674	447	0.133
213.882	215.835	196.186	209	0.056	430.722	445.486	443.289	440	0.134
190.108	211.105	205.791	202	0.057	407.098	450.098	479.764	446	0.136
225.367	218.022	202.428	215	0.059	477.352	460.433	428.143	455	0.137
193.229	220.149	231.363	215	0.060	496.204	486.371	448.592	477	0.139
219.302	225.102	217.184	221	0.062	457.443	468.245	468.029	465	0.141
226.910	242.435	229.655	233	0.064	427.551	481.982	509.056	473	0.142
213.315	235.495	251.194	233	0.065	473.291	493.741	488.701	485	0.144
242.960	253.193	243.059	246	0.067	432.219	484.256	512.941	476	0.145
246.113	246.073	224.706	239	0.068	451.942	507.038	536.731	499	0.147
210.949	231.446	247.604	230	0.070	523.709	500.032	467.386	497	0.148
218.321	252.927	263.753	245	0.072	442.790	490.282	522.230	485	0.150
239.676	248.348	249.197	246	0.073	492.708	496.808	499.943	496	0.151
227.463	267.125	276.816	257	0.075	505.095	511.387	513.426	510	0.153
265.810	267.815	261.795	265	0.077	513.603	526.799	525.386	522	0.154
238.021	264.455	281.230	261	0.078	523.510	540.536	537.208	534	0.156
266.391	265.726	261.041	264	0.079	522.787	532.282	522.517	526	0.157
268.148	271.344	264.729	268	0.081	568.494	540.437	506.279	538	0.158
268.774	270.225	264.482	268	0.082	546.447	550.620	543.516	547	0.160

Rep 1	Rep 2	Rep 3	Plate size	0.180 x 0.120 (m)		Rep 1	Rep 2	Rep 3	Plate size	0.180 x 0.120 (m)	
ρ (kN/ μ 2)	ρ (kN/ μ 2)	ρ (kN/ μ 2)	Mean r (kN/m2)	Sinkage (m)		ρ (kN/ μ 2)	ρ (kN/ μ 2)	ρ (kN/ μ 2)	Mean r (kN/m2)	Sinkage (m)	
8.277	5.535	6.770		7	0.002	213.321	182.348	207.519	201		0.084
13.446	10.689	11.829		12	0.003	222.507	214.191	214.030	217		0.085
16.855	12.504	14.389		15	0.005	216.926	203.257	205.936	209		0.087
21.603	13.366	17.922		18	0.007	225.782	188.368	212.256	209		0.088
27.158	17.780	23.031		23	0.008	232.200	199.016	221.002	217		0.090
31.160	35.291	25.208		31	0.010	231.771	197.285	219.895	216		0.091
33.412	38.056	27.716		33	0.012	218.480	220.202	211.323	217		0.093
40.868	37.580	38.448		39	0.013	236.653	209.749	232.886	226		0.094
52.883	42.594	48.933		48	0.015	238.026	211.377	234.386	228		0.096
60.764	50.388	56.966		56	0.016	234.159	238.147	228.135	233		0.097
63.718	49.481	58.015		57	0.018	254.903	246.089	245.541	249		0.099
64.709	67.082	57.878		63	0.019	262.216	230.179	255.882	249		0.100
76.574	72.215	72.923		74	0.021	265.223	233.356	258.974	253		0.102
78.752	81.451	72.084		77	0.023	267.826	256.817	257.133	261		0.103
82.501	78.379	78.849		80	0.024	261.661	264.983	255.305	261		0.105
90.253	75.155	92.389		86	0.026	276.085	240.215	267.835	261		0.107
87.098	91.036	81.050		86	0.028	278.249	260.121	263.861	267		0.108
101.081	85.905	95.832		94	0.030	283.883	253.635	278.444	272		0.110
91.662	86.166	87.155		88	0.032	307.087	268.456	297.456	291		0.111
104.285	86.583	105.119		99	0.033	295.450	258.242	286.530	280		0.113
101.854	86.203	103.713		97	0.035	300.050	300.295	292.155	298		0.115
105.482	107.161	98.304		104	0.037	293.121	281.363	281.561	285		0.116
107.353	107.636	99.477		105	0.038	314.807	268.689	299.047	294		0.118
114.724	95.364	114.728		108	0.040	324.839	276.527	308.205	303		0.119
124.203	102.942	123.257		117	0.042	304.438	292.692	292.660	297		0.121
122.419	117.668	117.669		119	0.043	318.087	284.041	310.749	304		0.122
134.470	128.781	129.023		131	0.045	328.825	299.659	323.927	317		0.123
131.304	122.431	124.358		126	0.047	326.038	324.772	317.388	323		0.125
141.866	122.299	141.767		135	0.048	320.805	279.566	307.695	303		0.127
132.394	132.441	124.400		130	0.050	335.600	325.487	324.006	328		0.128
133.852	128.429	128.547		130	0.051	336.958	327.518	325.666	330		0.129
140.788	142.715	133.734		139	0.053	336.879	340.310	330.577	336		0.131
148.584	128.799	148.376		142	0.054	345.988	329.776	331.199	336		0.133
141.707	146.234	135.953		141	0.056	340.300	332.912	329.948	334		0.134
156.755	132.840	154.482		148	0.057	349.951	352.687	343.301	349		0.136
150.590	143.405	144.090		146	0.059	369.282	338.155	363.403	357		0.137
162.814	139.517	160.850		154	0.060	381.259	336.082	367.643	362		0.139
157.961	148.945	150.418		152	0.062	391.001	342.987	376.175	370		0.141
157.316	156.629	148.955		154	0.064	389.823	341.586	374.853	369		0.142
163.904	136.965	154.198		152	0.065	393.225	342.711	377.173	371		0.144
182.273	154.030	177.836		171	0.067	394.653	349.907	381.593	375		0.145
178.976	157.486	177.916		171	0.068	401.814	356.135	388.455	382		0.147
187.821	175.459	178.047		180	0.070	407.538	359.999	393.370	387		0.148
182.557	171.917	173.732		176	0.072	408.041	368.928	398.169	392		0.150
183.941	175.102	175.971		178	0.073	412.243	393.973	395.135	400		0.151
188.973	162.263	185.302		179	0.075	422.487	374.967	408.702	402		0.153
195.262	171.066	192.849		186	0.077	431.858	380.167	416.170	409		0.154
199.027	171.902	195.149		189	0.078	420.211	412.959	408.345	414		0.156
197.663	187.877	188.957		191	0.079	434.219	400.244	426.916	420		0.157
191.763	196.661	186.195		192	0.081	436.017	421.816	420.433	426		0.158
207.581	181.406	204.178		198	0.082	442.434	429.954	427.567	433		0.160

Rep 1	Rep 2	Rep 3	Plate size	0.225 x 0.150 (m)		Rep 1	Rep 2	Rep 3	Plate size	0.225 x 0.150 (m)	
ρ (kN/ μ 2)	ρ (kN/ μ 2)	ρ (kN/ μ 2)	Mean r (kN/m2)	Sinkage (m)		ρ (kN/ μ 2)	ρ (kN/ μ 2)	ρ (kN/ μ 2)	Mean r (kN/m2)	Sinkage (m)	
4.052	4.328	4.472	4		0.002	161.273	156.896	183.115	167		0.084
8.123	8.130	9.451	9		0.003	161.288	159.610	171.268	164		0.085
11.885	8.963	15.872	12		0.005	156.925	151.979	177.903	162		0.087
15.688	17.234	14.561	16		0.007	157.012	155.205	179.767	164		0.088
21.821	18.611	26.888	22		0.008	169.868	162.924	183.238	172		0.090
25.613	22.292	31.092	26		0.010	163.842	153.561	174.582	164		0.091
30.395	29.999	32.233	31		0.012	165.787	159.516	179.026	168		0.093
31.691	31.905	31.816	32		0.013	169.082	168.688	196.426	178		0.094
39.370	38.429	41.522	40		0.015	177.558	167.785	190.298	179		0.096
47.073	46.056	49.705	48		0.016	175.218	172.180	202.025	183		0.097
51.963	50.840	53.869	52		0.018	184.273	179.099	208.542	191		0.099
51.878	47.811	60.220	53		0.019	173.369	171.997	200.844	182		0.100
55.755	50.832	64.100	57		0.021	194.809	185.818	210.146	197		0.102
63.136	59.845	71.518	65		0.023	192.401	190.801	222.846	202		0.103
72.577	69.507	75.965	73		0.024	195.798	196.649	209.454	201		0.105
56.136	54.895	59.258	57		0.026	206.201	208.209	221.176	212		0.107
69.241	63.356	78.731	70		0.028	195.444	196.509	227.935	207		0.108
73.030	68.260	83.621	75		0.030	213.249	203.376	230.394	216		0.110
74.310	71.642	84.877	77		0.032	206.804	205.604	236.125	216		0.111
77.311	74.694	81.546	78		0.033	219.683	213.604	247.869	227		0.113
80.032	78.620	84.675	81		0.035	221.793	221.088	257.552	233		0.115
84.012	80.478	88.568	84		0.037	217.574	211.786	245.660	225		0.116
85.521	82.339	90.464	86		0.038	226.415	228.835	242.973	233		0.118
86.680	85.122	91.693	88		0.040	232.023	230.534	246.873	236		0.119
87.556	83.378	99.404	90		0.042	218.490	218.297	254.008	230		0.121
99.228	94.628	105.087	100		0.043	229.984	225.779	265.044	240		0.122
95.780	91.467	101.369	96		0.045	245.625	229.483	263.291	246		0.123
101.876	94.076	114.368	103		0.047	239.173	226.396	257.926	241		0.125
102.702	100.840	108.633	104		0.048	249.447	233.951	267.954	250		0.127
98.865	95.560	105.407	100		0.050	255.586	258.444	274.345	263		0.128
102.600	102.509	109.469	105		0.051	242.372	241.741	281.530	255		0.129
107.939	107.673	115.075	110		0.053	243.750	244.694	260.689	250		0.131
112.882	111.316	119.657	115		0.054	259.591	242.404	278.415	260		0.133
117.990	112.094	125.465	119		0.056	260.852	254.834	294.218	270		0.134
117.505	114.992	124.086	119		0.057	261.005	255.553	294.709	270		0.136
115.688	111.504	132.121	120		0.059	265.352	260.643	300.018	275		0.137
119.932	115.704	137.032	124		0.060	271.401	252.970	291.002	272		0.139
117.635	115.982	124.684	119		0.062	273.250	277.713	294.056	282		0.141
116.976	116.641	124.684	119		0.064	281.348	264.727	303.210	283		0.142
125.407	120.435	142.966	130		0.065	287.097	284.957	305.313	292		0.144
123.127	124.334	143.908	130		0.067	294.306	276.636	317.198	296		0.145
131.869	131.641	153.241	139		0.068	280.423	277.180	324.267	294		0.147
133.747	130.607	152.844	139		0.070	283.826	289.019	326.370	300		0.148
123.579	124.176	144.078	131		0.072	274.215	287.750	326.804	296		0.150
137.699	130.552	146.934	138		0.073	286.347	292.339	336.528	305		0.151
136.398	135.446	158.087	143		0.075	299.075	308.089	324.051	310		0.153
136.307	135.549	145.093	139		0.077	323.178	300.223	346.706	323		0.154
147.833	138.974	157.372	148		0.078	294.296	300.781	338.876	311		0.156
147.501	144.933	156.076	150		0.079	295.289	303.232	348.062	316		0.157
143.412	140.061	163.599	149		0.081	303.472	320.421	362.817	329		0.158
145.590	139.236	164.359	150		0.082	329.863	338.780	356.863	342		0.160

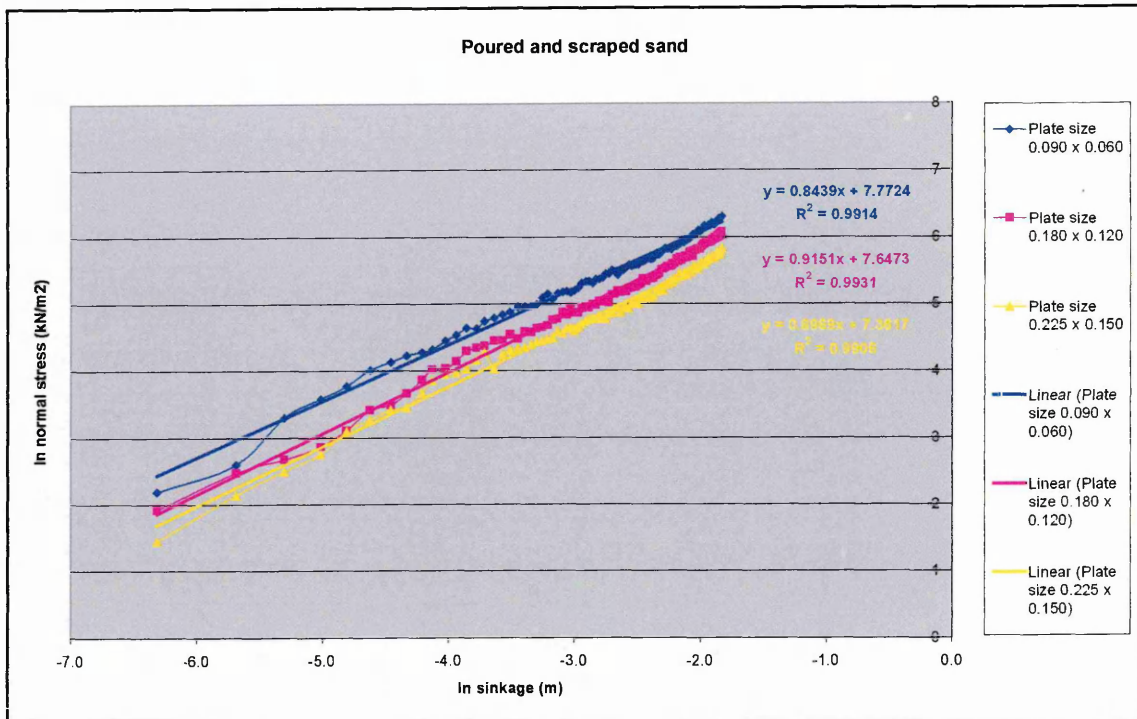
These results were then transformed by taking natural logarithms of both axes to produce data of $\ln \rho$ against $\ln z$, which is shown on the tables below.

		Plate size 0.090 x 0.060				Plate size 0.090 x 0.060	
Mean ρ kN/m ²	Sinkage m	In sinkage m	In pressure kN/m ²	Mean ρ kN/m ²	Sinkage m	In sinkage m	In pressure kN/m ²
9	0.002	-6.315	2.194	281	0.084	-2.479	5.637
13	0.003	-5.686	2.601	280	0.085	-2.461	5.635
27	0.005	-5.303	3.309	285	0.087	-2.445	5.652
36	0.007	-5.015	3.587	290	0.088	-2.428	5.668
44	0.008	-4.811	3.776	292	0.090	-2.410	5.678
56	0.010	-4.625	4.017	290	0.091	-2.393	5.668
63	0.012	-4.462	4.136	295	0.093	-2.377	5.686
69	0.013	-4.334	4.235	307	0.094	-2.363	5.728
72	0.015	-4.215	4.280	313	0.096	-2.345	5.747
76	0.016	-4.131	4.326	313	0.097	-2.329	5.747
86	0.018	-4.025	4.453	323	0.099	-2.314	5.777
94	0.019	-3.940	4.542	330	0.100	-2.299	5.798
104	0.021	-3.861	4.640	339	0.102	-2.285	5.827
103	0.023	-3.782	4.637	339	0.103	-2.269	5.825
115	0.024	-3.715	4.742	342	0.105	-2.253	5.835
121	0.026	-3.641	4.794	336	0.107	-2.237	5.816
127	0.028	-3.571	4.844	343	0.108	-2.225	5.839
132	0.030	-3.514	4.882	352	0.110	-2.208	5.864
143	0.032	-3.450	4.960	354	0.111	-2.195	5.871
143	0.033	-3.397	4.965	358	0.113	-2.179	5.881
144	0.035	-3.346	4.970	363	0.115	-2.167	5.895
148	0.037	-3.304	4.997	381	0.116	-2.153	5.944
164	0.038	-3.258	5.099	372	0.118	-2.139	5.919
173	0.040	-3.216	5.152	388	0.119	-2.127	5.962
160	0.042	-3.174	5.075	385	0.121	-2.115	5.953
175	0.043	-3.137	5.164	391	0.122	-2.103	5.970
178	0.045	-3.096	5.184	395	0.123	-2.092	5.980
180	0.047	-3.061	5.192	406	0.125	-2.079	6.007
176	0.048	-3.034	5.168	418	0.127	-2.065	6.035
181	0.050	-3.005	5.196	415	0.128	-2.055	6.027
189	0.051	-2.971	5.242	428	0.129	-2.045	6.060
203	0.053	-2.944	5.312	433	0.131	-2.031	6.071
208	0.054	-2.912	5.338	447	0.133	-2.020	6.103
209	0.056	-2.888	5.341	440	0.134	-2.009	6.086
202	0.057	-2.858	5.310	446	0.136	-1.996	6.100
215	0.059	-2.834	5.372	455	0.137	-1.987	6.121
215	0.060	-2.805	5.370	477	0.139	-1.974	6.168
221	0.062	-2.779	5.396	465	0.141	-1.961	6.141
233	0.064	-2.756	5.451	473	0.142	-1.950	6.159
233	0.065	-2.729	5.452	485	0.144	-1.941	6.185
246	0.067	-2.707	5.507	476	0.145	-1.929	6.166
239	0.068	-2.684	5.476	499	0.147	-1.917	6.212
230	0.070	-2.659	5.438	497	0.148	-1.908	6.209
245	0.072	-2.638	5.501	485	0.150	-1.897	6.184
246	0.073	-2.616	5.504	496	0.151	-1.889	6.208
257	0.075	-2.592	5.550	510	0.153	-1.878	6.234
265	0.077	-2.570	5.580	522	0.154	-1.869	6.258
261	0.078	-2.554	5.565	534	0.156	-1.859	6.280
264	0.079	-2.535	5.577	526	0.157	-1.852	6.265
268	0.081	-2.516	5.591	538	0.158	-1.842	6.289
268	0.082	-2.496	5.590	547	0.160	-1.834	6.304

		Plate size 0.180 x 0.120				Plate size 0.180 x 0.120	
Mean ρ kN/m ²	Sinkage m	In sinkage m	In pressure kN/m ²	Mean ρ kN/m ²	Sinkage m	In sinkage m	In pressure kN/m ²
7	0.002	-6.315	1.926	201	0.084	-2.479	5.304
12	0.003	-5.686	2.484	217	0.085	-2.461	5.379
15	0.005	-5.303	2.680	209	0.087	-2.445	5.341
18	0.007	-5.015	2.870	209	0.088	-2.428	5.341
23	0.008	-4.811	3.120	217	0.090	-2.410	5.382
31	0.010	-4.625	3.419	216	0.091	-2.393	5.377
33	0.012	-4.462	3.498	217	0.093	-2.377	5.378
39	0.013	-4.334	3.663	226	0.094	-2.363	5.422
48	0.015	-4.215	3.874	228	0.096	-2.345	5.429
56	0.016	-4.131	4.026	233	0.097	-2.329	5.453
57	0.018	-4.025	4.044	249	0.099	-2.314	5.517
63	0.019	-3.940	4.147	249	0.100	-2.299	5.519
74	0.021	-3.861	4.303	253	0.102	-2.285	5.531
77	0.023	-3.782	4.349	261	0.103	-2.269	5.563
80	0.024	-3.715	4.381	261	0.105	-2.253	5.563
86	0.026	-3.641	4.454	261	0.107	-2.237	5.566
86	0.028	-3.571	4.459	267	0.108	-2.225	5.589
94	0.030	-3.514	4.546	272	0.110	-2.208	5.606
88	0.032	-3.450	4.481	291	0.111	-2.195	5.673
99	0.033	-3.397	4.592	280	0.113	-2.179	5.635
97	0.035	-3.346	4.577	298	0.115	-2.167	5.695
104	0.037	-3.304	4.641	285	0.116	-2.153	5.654
105	0.038	-3.258	4.652	294	0.118	-2.139	5.684
108	0.040	-3.216	4.685	303	0.119	-2.127	5.714
117	0.042	-3.174	4.760	297	0.121	-2.115	5.692
119	0.043	-3.137	4.781	304	0.122	-2.103	5.718
131	0.045	-3.096	4.873	317	0.123	-2.092	5.760
126	0.047	-3.061	4.837	323	0.125	-2.079	5.777
135	0.048	-3.034	4.908	303	0.127	-2.065	5.713
130	0.050	-3.005	4.866	328	0.128	-2.055	5.794
130	0.051	-2.971	4.870	330	0.129	-2.045	5.799
139	0.053	-2.944	4.935	336	0.131	-2.031	5.817
142	0.054	-2.912	4.955	336	0.133	-2.020	5.816
141	0.056	-2.888	4.951	334	0.134	-2.009	5.812
148	0.057	-2.858	4.997	349	0.136	-1.996	5.854
146	0.059	-2.834	4.984	357	0.137	-1.987	5.878
154	0.060	-2.805	5.040	362	0.139	-1.974	5.891
152	0.062	-2.779	5.027	370	0.141	-1.961	5.914
154	0.064	-2.756	5.039	369	0.142	-1.950	5.910
152	0.065	-2.729	5.022	371	0.144	-1.941	5.916
171	0.067	-2.707	5.144	375	0.145	-1.929	5.928
171	0.068	-2.684	5.144	382	0.147	-1.917	5.946
180	0.070	-2.659	5.195	387	0.148	-1.908	5.958
176	0.072	-2.638	5.171	392	0.150	-1.897	5.971
178	0.073	-2.616	5.184	400	0.151	-1.889	5.993
179	0.075	-2.592	5.187	402	0.153	-1.878	5.997
186	0.077	-2.570	5.228	409	0.154	-1.869	6.015
189	0.078	-2.554	5.240	414	0.156	-1.859	6.025
191	0.079	-2.535	5.255	420	0.157	-1.852	6.041
192	0.081	-2.516	5.255	426	0.158	-1.842	6.055
198	0.082	-2.496	5.287	433	0.160	-1.834	6.071

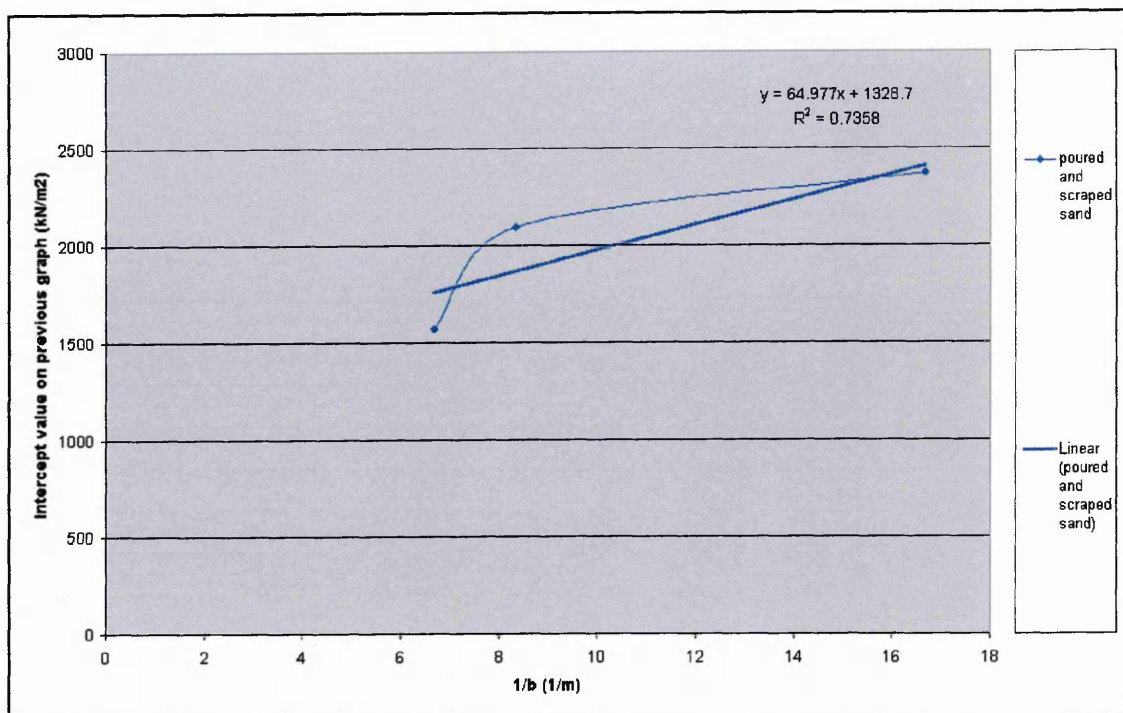
		Plate size 0.225 x 0.150				Plate size 0.225 x 0.150	
Mean ρ kN/m ²	Sinkage m	In sinkage m	In pressure kN/m ²	Mean ρ kN/m ²	Sinkage m	In sinkage m	In pressure kN/m ²
4	0.002	-6.315	1.455	167	0.084	-2.479	5.119
9	0.003	-5.686	2.148	164	0.085	-2.461	5.100
12	0.005	-5.303	2.505	162	0.087	-2.445	5.089
16	0.007	-5.015	2.762	164	0.088	-2.428	5.100
22	0.008	-4.811	3.111	172	0.090	-2.410	5.148
26	0.010	-4.625	3.271	164	0.091	-2.393	5.100
31	0.012	-4.462	3.430	168	0.093	-2.377	5.125
32	0.013	-4.334	3.460	178	0.094	-2.363	5.182
40	0.015	-4.215	3.683	179	0.096	-2.345	5.185
48	0.016	-4.131	3.863	183	0.097	-2.329	5.210
52	0.018	-4.025	3.956	191	0.099	-2.314	5.250
53	0.019	-3.940	3.976	182	0.100	-2.299	5.204
57	0.021	-3.861	4.041	197	0.102	-2.285	5.283
65	0.023	-3.782	4.172	202	0.103	-2.269	5.308
73	0.024	-3.715	4.286	201	0.105	-2.253	5.301
57	0.026	-3.641	4.039	212	0.107	-2.237	5.356
70	0.028	-3.571	4.255	207	0.108	-2.225	5.331
75	0.030	-3.514	4.317	216	0.110	-2.208	5.374
77	0.032	-3.450	4.343	216	0.111	-2.195	5.376
78	0.033	-3.397	4.355	227	0.113	-2.179	5.425
81	0.035	-3.346	4.396	233	0.115	-2.167	5.453
84	0.037	-3.304	4.435	225	0.116	-2.153	5.416
86	0.038	-3.258	4.456	233	0.118	-2.139	5.450
88	0.040	-3.216	4.475	236	0.119	-2.127	5.466
90	0.042	-3.174	4.501	230	0.121	-2.115	5.439
100	0.043	-3.137	4.602	240	0.122	-2.103	5.482
96	0.045	-3.096	4.566	246	0.123	-2.092	5.506
103	0.047	-3.061	4.639	241	0.125	-2.079	5.485
104	0.048	-3.034	4.645	250	0.127	-2.065	5.523
100	0.050	-3.005	4.605	263	0.128	-2.055	5.571
105	0.051	-2.971	4.653	255	0.129	-2.045	5.542
110	0.053	-2.944	4.703	250	0.131	-2.031	5.520
115	0.054	-2.912	4.742	260	0.133	-2.020	5.561
119	0.056	-2.888	4.775	270	0.134	-2.009	5.598
119	0.057	-2.858	4.778	270	0.136	-1.996	5.600
120	0.059	-2.834	4.786	275	0.137	-1.987	5.618
124	0.060	-2.805	4.822	272	0.139	-1.974	5.605
119	0.062	-2.779	4.783	282	0.141	-1.961	5.641
119	0.064	-2.756	4.783	283	0.142	-1.950	5.646
130	0.065	-2.729	4.864	292	0.144	-1.941	5.678
130	0.067	-2.707	4.871	296	0.145	-1.929	5.691
139	0.068	-2.684	4.934	294	0.147	-1.917	5.683
139	0.070	-2.659	4.935	300	0.148	-1.908	5.703
131	0.072	-2.638	4.872	296	0.150	-1.897	5.691
138	0.073	-2.616	4.930	305	0.151	-1.889	5.721
143	0.075	-2.592	4.965	310	0.153	-1.878	5.738
139	0.077	-2.570	4.934	323	0.154	-1.869	5.779
148	0.078	-2.554	4.998	311	0.156	-1.859	5.741
150	0.079	-2.535	5.007	316	0.157	-1.852	5.754
149	0.081	-2.516	5.004	329	0.158	-1.842	5.796
150	0.082	-2.496	5.009	342	0.160	-1.834	5.834

Plotting the data from the table above produced the graphs shown below. Each graph had trend lines fitted to represent the data and from the equations of these lines the gradients (n values) and intercepts $\left(\ln \left(\frac{k_c}{b} + k_\phi \right) \right)$ values were determined.



The equations generated for each of the trend lines are presented in the table below; from these equations the n coefficient was determined by calculating the mean of the three gradients for the three plate sizes. Inverse natural logs of the intercept values were calculated to produce the values to plot against $1/b$ to allow the values of k_c and k_ϕ to be determined.

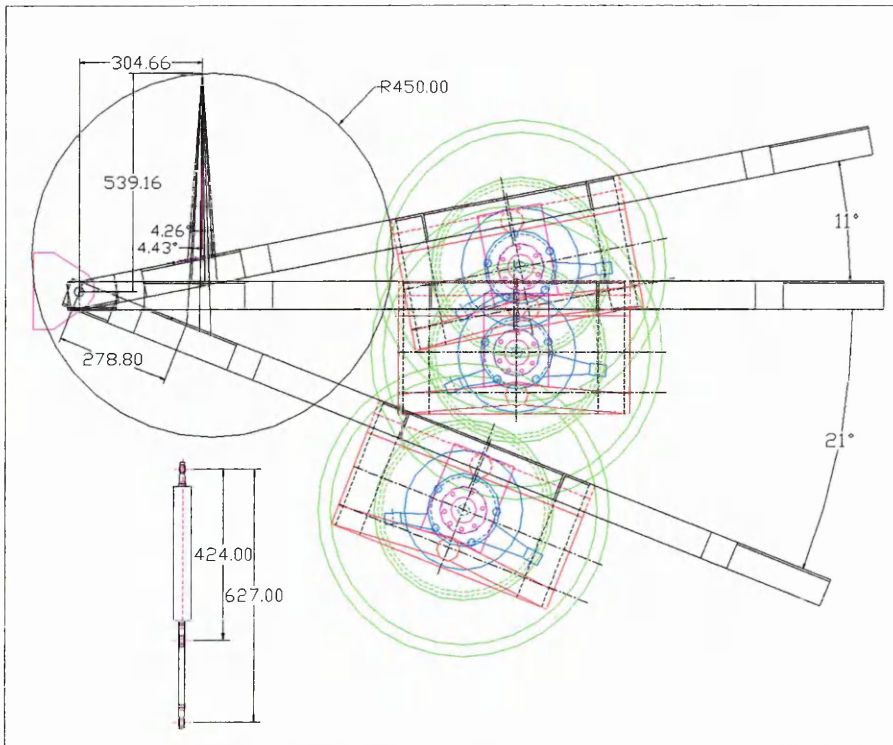
Plate size	Equation of the 'best fit' line	Gradient	Intercept	$1/b$	Inverse In
m		(n)	ln kN/m ²	1 / (plate width)	of intercept
				m	kN/m ²
0.090 x 0.060	$y = 0.8439x + 7.7724$	0.8439	7.7724	16.67	2374
0.180 x 0.120	$y = 0.9151x + 7.6473$	0.9151	7.6473	8.33	2095
0.225 x 0.150	$y = 0.8969x + 7.3617$	0.8969	7.3617	6.67	1575
	<i>Average gradient (n)</i>	0.885			



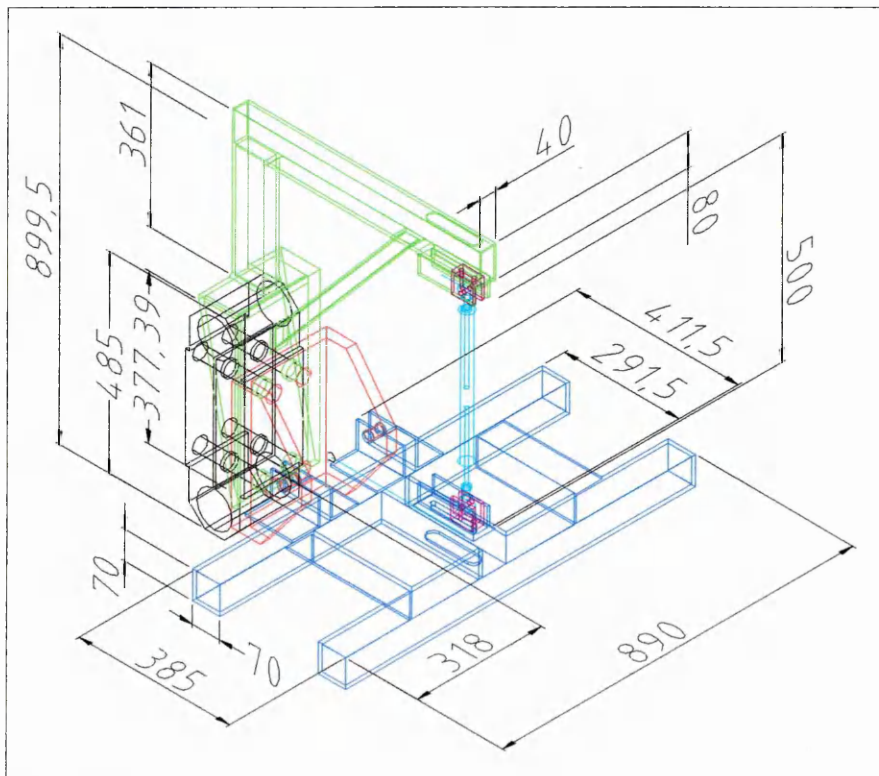
From this graph the values of k_c and k_ϕ were determined, and in combination all of these results produced the Bekker coefficients shown in the table below.

Equation of the 'best fit' line	Gradient	Intercept	From previous equation
Notation	k_c	k_ϕ	n
Unit		kN/m ²	
$y = 64.977x + 1328.7$	64.977	1329	0.885

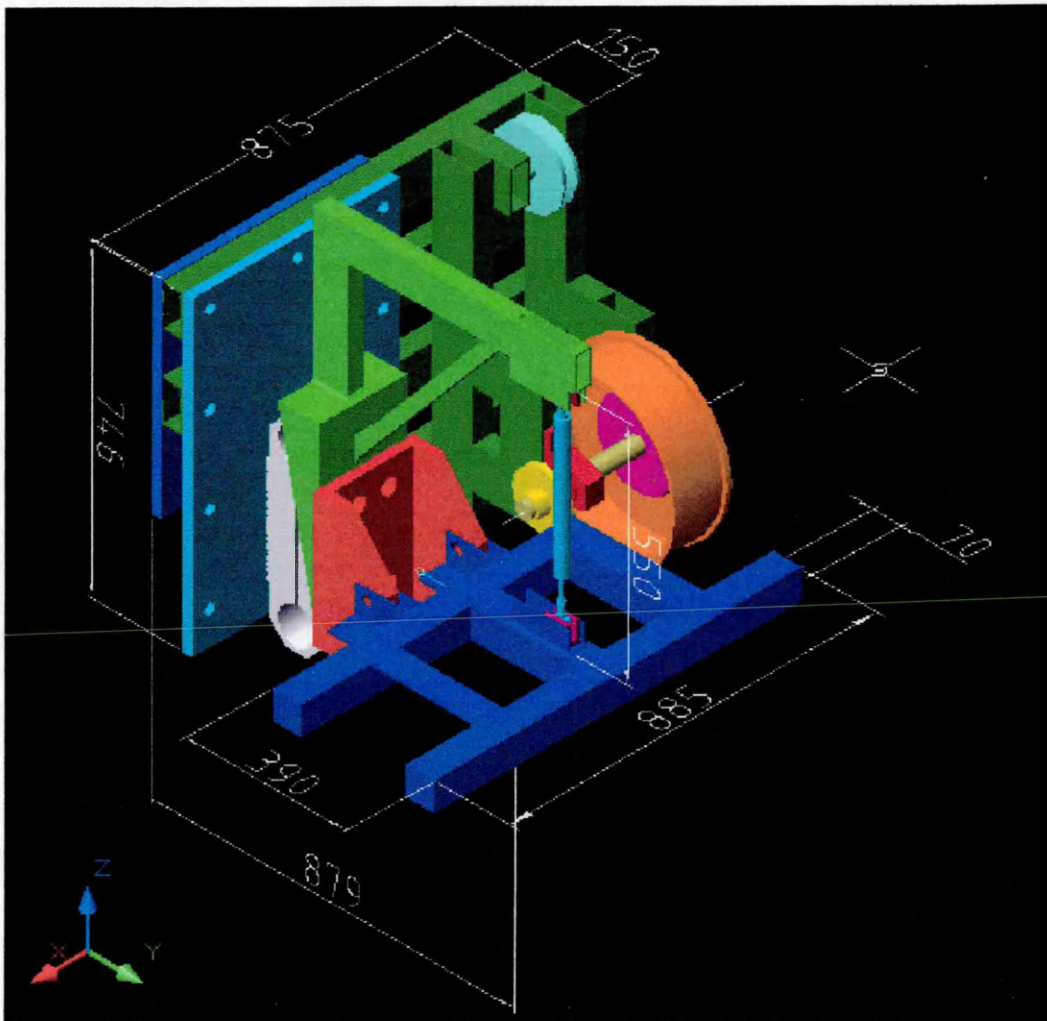
Angles of sinkage that the rig could achieve when fitted with the damper



The relative dimensions of the damper bracket, EORT, and the test rig mountings



The relative dimensions of the damper bracket, damper, EORT, and the test rig mountings, in conjunction with the mountings for fixed slip drive



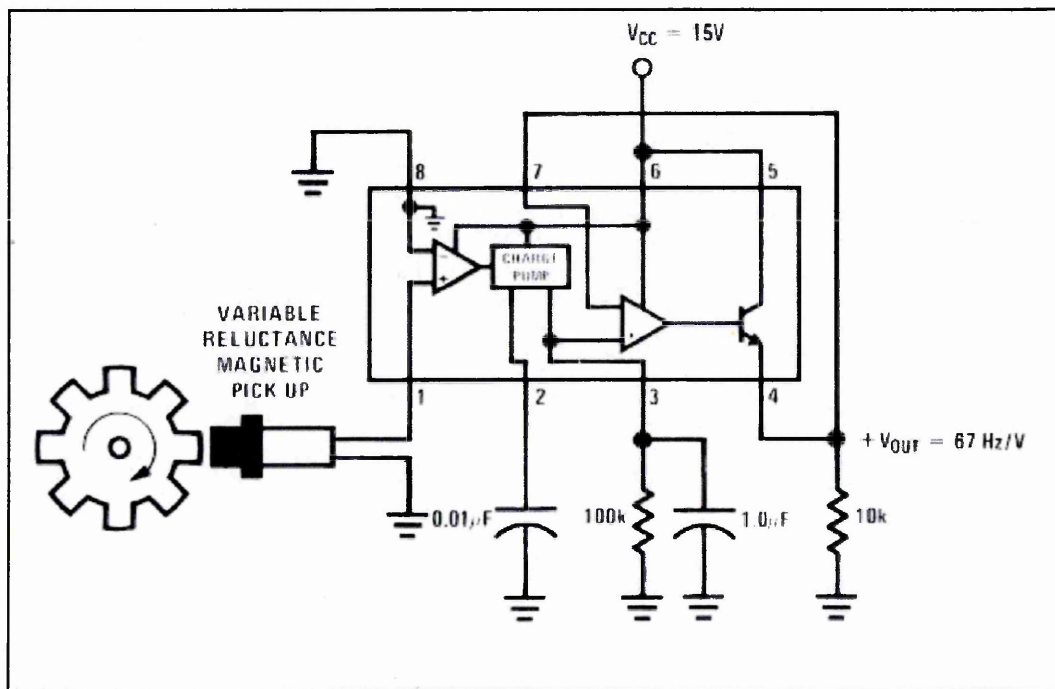
APPENDIX 16 – TEST RIG INSTRUMENTATION

Component	Details / Basic Specification
EORT	Manufactured to Cranfield University Soil Laboratory standard specification.
Tension Link	Military performance grade strain gauged tension link, capable of measuring up to 8 kN.
LVDT	300 mm stroke LVDT manufactured by RDP.
Drawstring transducer (short)	100 mm range device, comprising a high accuracy multi-turn potentiometer. Manufactured by Carlsbad – part no. LX-PA-10.
Tacho-generator	DC output tacho-generator, rated 6 V at 600 rpm.
Rotary Encoder	Hengstler optical rotary shaft encoder, 1024 ppr, 10-30 V DC.
Induction Switch	M12 inductive proximity switch, brass bodied, multi voltage.
Drawstring transducer (long)	1m range device, comprising a high accuracy multi-turn potentiometer. Manufactured by Carlsbad – part no. LX-PA-1000.

APPENDIX 17 – PULSE COUNTER CIRCUIT (WHEEL SPEED)

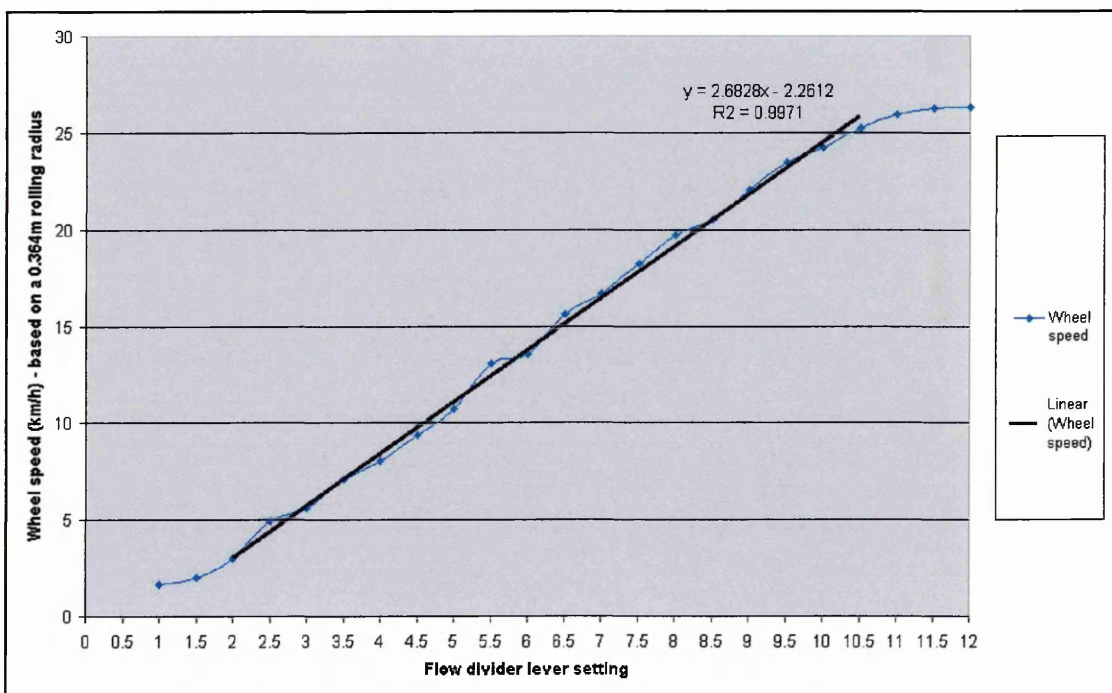
Encoder Frequency to Voltage Conversion Circuit

The frequency to voltage conversion circuit was based around an LM2917 operational amplifier. The encoder output was connected to the circuit shown below, which gave a varying voltage output, which was proportional to the pulse frequency output of the encoder (or test wheel speed).



APPENDIX 18 – VARIABLE SLIP RIG PERFORMANCE

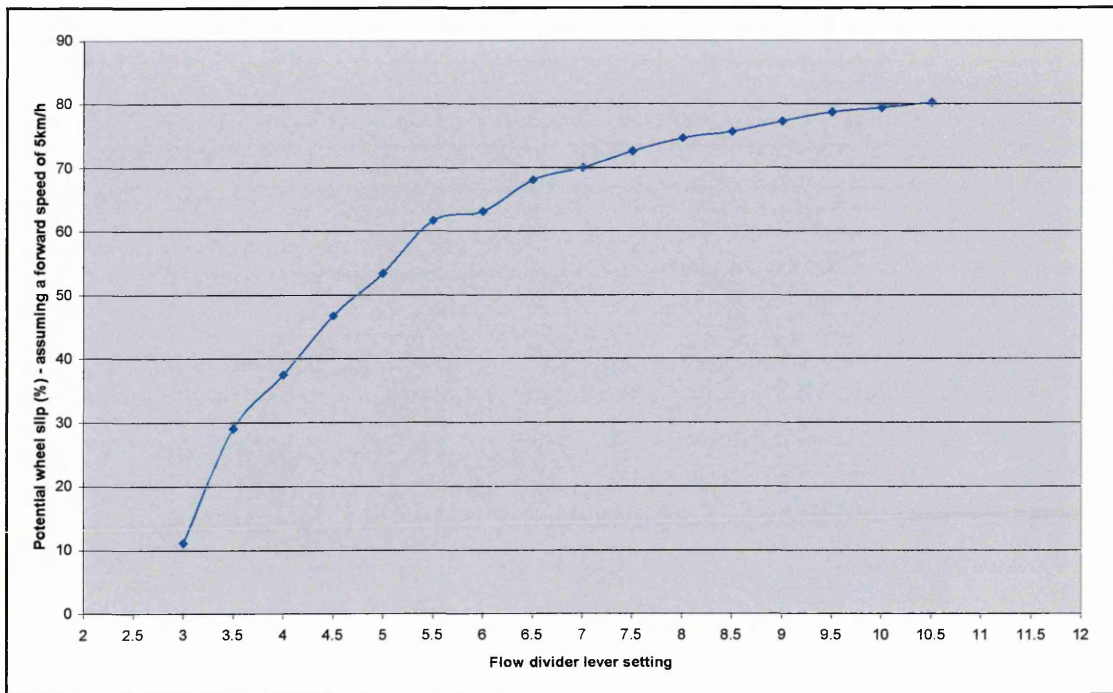
Stationary tests were conducted to confirm the capability of the variable slip test rig to achieve a range of wheel slips from 15% to 80% wheel slip. These tests involved suspending the wheel off the ground whilst the flow control was cycled through its marked range (1 to 12), which varied the speed of the wheel motor. As with the encoder calibration, the wheel speed measurements were taken once the wheel speed had stabilised after each adjustment, using an optical rev counter. These measurements produced a range of rotational speeds that were transformed into forward speeds by assuming a 0.364 m rolling radius. The results are shown in the figure below, upon which the trend line is plotted for flow divider settings between 2 and 10.5 (the region of linear response).



Wheel speeds produced by changing the flow divider setting

Linearity was not essential, as the wheel slip would always be measured, but it made the selection of a desired slip simpler. The data shown in the figure below developed the relationship further, by calculating wheel slips for the region of linear response (2.5 km/h to 25 km/h) based upon the calculated wheel speeds and an assumed forward

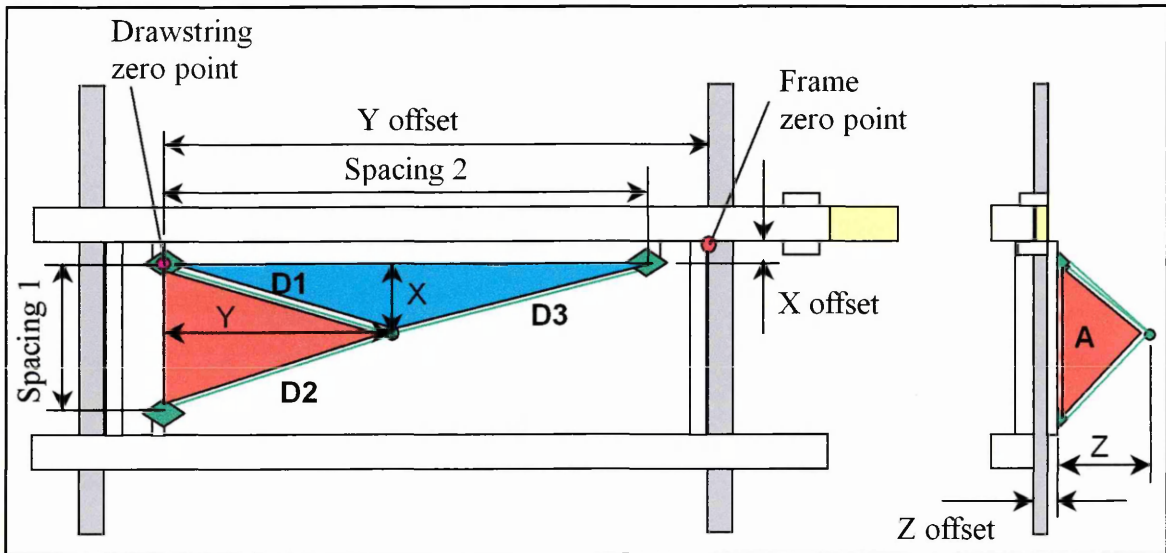
travel speed of 5 km/h. This showed this test rig was capable of achieving the desired slip range from 10% to 80% wheel slip.



Range of wheel slip that the variable slip rig could achieve

APPENDIX 19 – MATHEMATICS OF THE MEASURING FRAME

The mathematics used to calculate the orthogonal grid coordinates relative to the frame zero point from the three drawstring lengths took the following form. The diagram below shows all the measurements that were used in the calculation.



A schematic diagram of the data tag position measurement frame

The string lengths were calculated from the following equations, based upon the output voltages (V1, V2 and V3) from the drawstring transducers, which were recorded relative to the input voltages. The drawstrings were fitted with stops that would have prevented them being fully wound in, if the attachment to the pointer had failed. This left an offset between the end of the stop and the end of the pointer. This offset was added to the calculated length to determine the true string lengths. Thus the equations below determined the drawstring lengths (in mm).

$$\text{Length D1} = \left[\frac{(V1 - 11.307)}{(-0.0092)} \right] + 57.8$$

$$\text{Length D2} = \left[\frac{(V2 - 11.339)}{(-0.0092)} \right] + 49.39$$

$$\text{Length D3} = \left[\frac{(V3 - 11.313)}{(-0.0092)} \right] + 51.62$$

The calculation used these string lengths to determine the orthogonal coordinates relative to the drawstring zero point by applying Pythagoras's theorem, which was included in the equations presented below. The cosine term in the 'X' calculation accounts for the angular offset of 0.0028° from True Square of the three drawstring positions.

$$\text{Spacing 1} = 503.8580$$

$$\text{Spacing 2} = 497.8555$$

$$\text{Distance X} = \frac{D1 \left[\frac{(497.8555^2 + D1^2 - D3^2)}{(2 \times 497.8555 \times D1)} \right]}{\cos 0.0028}$$

$$\text{Distance Y} = (-)D1 \left[\frac{(503.858^2 + D1^2 - D2^2)}{(2 \times 503.858 \times D1)} \right]$$

$$\text{Distance Z} = \sqrt{\left(D1^2 - \left(\sqrt{(X^2 + Y^2)} \right)^2 \right)}$$

The offset distances were then included to determine the position relative to the frame zero point.

$$\text{X offset} = -25.4662$$

$$\text{Y offset} = 53.7814 + 1032 = 1085.7814$$

$$\text{Z offset} = 41.696$$

This methodology is clearer when studied in conjunction with the attached file *Measuring Frame Calculation* (on the enclosed data CD), which presents these equations in the form in which they were applied.

APPENDIX 20 – TRIAL COLUMN INSERTION RESULTS

These results were used to determine the accuracy of the tag positioning apparatus. A single column of tags was entered into the sand to a depth of 400 mm using the positioning apparatus. Tags were placed at 25 mm depth intervals over the full depth. These were not disturbed, but instead they were immediately excavated and their positions were measured using rulers, squares and clamps. This process was repeated six times in total. The measurements recorded are shown in the tables on the following two pages. These results showed that the accuracy of the placement apparatus was ± 1.5 mm to a depth of 300 mm and ± 2.5 mm between a depth of 325 mm and 400 mm, which are shown at the bottom of the second set of tables (below data from insertion 6).

Relative Depth	initial location from bin 0,0,0			measured location from bin 0,0,0			Difference in position		
	in x	in y	in z	in x	in y	in z	in x	in y	in z
Insertion 1									
400	150.50	830.00	664.00	150.29	828.50	664.35	0.21	1.50	-0.35
375	150.50	830.00	639.00	150.47	832.10	640.56	0.03	-2.10	-1.56
350	150.50	830.00	614.00	150.43	831.34	614.23	0.07	-1.34	-0.23
325	150.50	830.00	589.00	150.22	830.78	589.23	0.28	-0.78	-0.23
300	150.50	830.00	564.00	149.98	831.11	563.88	0.52	-1.11	0.12
275	150.50	830.00	539.00	151.45	831.25	538.67	-0.95	-1.25	0.33
250	150.50	830.00	514.00	149.99	830.69	515.11	0.51	-0.69	-1.11
225	150.50	830.00	489.00	150.90	831.34	488.38	-0.40	-1.34	0.62
200	150.50	830.00	464.00	151.21	830.19	463.60	-0.71	-0.19	0.40
175	150.50	830.00	439.00	150.44	831.29	439.34	0.06	-1.29	-0.34
150	150.50	830.00	414.00	150.53	830.11	412.99	-0.03	-0.11	1.01
125	150.50	830.00	389.00	149.93	829.79	388.97	0.57	0.21	0.03
100	150.50	830.00	364.00	149.15	830.82	364.33	1.35	-0.82	-0.33
75	150.50	830.00	339.00	150.29	831.32	340.22	0.21	-1.32	-1.22
50	150.50	830.00	314.00	150.44	830.33	315.00	0.06	-0.33	-1.00
25	150.50	830.00	289.00	149.58	831.29	289.78	0.92	-1.29	-0.78
Surface	150.50	830.00	264.00	150.24	829.56	263.19	0.26	0.44	0.81
Insertion 2									
400	150.50	830.00	664.00	151.03	828.22	662.99	-0.53	1.78	1.01
375	150.50	830.00	639.00	152.11	828.66	638.23	-1.61	1.34	0.77
350	150.50	830.00	614.00	149.24	828.99	613.83	1.26	1.01	0.17
325	150.50	830.00	589.00	152.33	831.14	591.00	-1.83	-1.14	-2.00
300	150.50	830.00	564.00	149.93	830.82	563.81	0.57	-0.82	0.19
275	150.50	830.00	539.00	149.74	831.19	539.01	0.76	-1.19	-0.01
250	150.50	830.00	514.00	149.05	830.83	513.79	1.45	-0.83	0.21
225	150.50	830.00	489.00	151.04	830.83	489.22	-0.54	-0.83	-0.22
200	150.50	830.00	464.00	151.83	830.33	464.30	-1.33	-0.33	-0.30
175	150.50	830.00	439.00	150.44	831.11	438.55	0.06	-1.11	0.45
150	150.50	830.00	414.00	151.29	830.22	414.01	-0.79	-0.22	-0.01
125	150.50	830.00	389.00	150.16	830.92	389.04	0.34	-0.92	-0.04
100	150.50	830.00	364.00	149.82	829.55	365.00	0.68	0.45	-1.00
75	150.50	830.00	339.00	149.83	829.73	338.94	0.67	0.27	0.06
50	150.50	830.00	314.00	151.01	831.04	313.02	-0.51	-1.04	0.98
25	150.50	830.00	289.00	150.05	830.94	289.92	0.45	-0.94	-0.92
Surface	150.50	830.00	264.00	151.49	831.30	264.10	-0.99	-1.30	-0.10
Insertion 3									
400	150.50	830.00	664.00	148.20	831.33	665.33	2.30	-1.33	-1.33
375	150.50	830.00	639.00	149.99	831.19	640.44	0.51	-1.19	-1.44
350	150.50	830.00	614.00	152.22	832.02	615.20	-1.72	-2.02	-1.20
325	150.50	830.00	589.00	152.71	830.39	590.29	-2.21	-0.39	-1.29
300	150.50	830.00	564.00	149.33	831.22	564.99	1.17	-1.22	-0.99
275	150.50	830.00	539.00	150.11	830.22	539.92	0.39	-0.22	-0.92
250	150.50	830.00	514.00	150.44	831.33	515.22	0.06	-1.33	-1.22
225	150.50	830.00	489.00	150.35	831.22	488.33	0.15	-1.22	0.67
200	150.50	830.00	464.00	151.11	830.22	464.92	-0.61	-0.22	-0.92
175	150.50	830.00	439.00	151.22	831.01	440.32	-0.72	-1.01	-1.32
150	150.50	830.00	414.00	151.22	829.22	414.93	-0.72	0.78	-0.93
125	150.50	830.00	389.00	151.28	829.48	388.99	-0.78	0.52	0.01
100	150.50	830.00	364.00	149.56	830.83	363.84	0.94	-0.83	0.16
75	150.50	830.00	339.00	150.94	829.48	340.44	-0.44	0.52	-1.44
50	150.50	830.00	314.00	149.04	831.33	313.02	1.46	-1.33	0.98
25	150.50	830.00	289.00	151.22	830.33	288.57	-0.72	-0.33	0.43
Surface	150.50	830.00	264.00	149.44	829.42	263.39	1.06	0.58	0.61

Insertion 4										
400	150.50	830.00	664.00	152.00	831.44	664.99	-1.50	-1.44	-0.99	
375	150.50	830.00	639.00	149.44	828.33	637.22	1.06	1.67	1.78	
350	150.50	830.00	614.00	152.89	832.07	613.22	-2.39	-2.07	0.78	
325	150.50	830.00	589.00	150.99	832.17	587.33	-0.49	-2.17	1.67	
300	150.50	830.00	564.00	150.83	831.38	564.39	-0.33	-1.38	-0.39	
275	150.50	830.00	539.00	150.24	831.28	540.00	0.26	-1.28	-1.00	
250	150.50	830.00	514.00	150.22	831.22	513.18	0.28	-1.22	0.82	
225	150.50	830.00	489.00	149.44	829.67	487.96	1.06	0.33	1.04	
200	150.50	830.00	464.00	149.94	830.48	465.29	0.56	-0.48	-1.29	
175	150.50	830.00	439.00	151.40	831.26	440.21	-0.90	-1.26	-1.21	
150	150.50	830.00	414.00	150.94	831.22	414.40	-0.44	-1.22	-0.40	
125	150.50	830.00	389.00	150.20	831.22	389.44	0.30	-1.22	-0.44	
100	150.50	830.00	364.00	150.33	829.39	364.19	0.17	0.61	-0.19	
75	150.50	830.00	339.00	151.29	831.22	339.39	-0.79	-1.22	-0.39	
50	150.50	830.00	314.00	150.11	830.33	314.96	0.39	-0.33	-0.96	
25	150.50	830.00	289.00	150.82	831.04	289.73	-0.32	-1.04	-0.73	
Surface	150.50	830.00	264.00	150.33	831.02	263.22	0.17	-1.02	0.78	
Insertion 5										
400	150.50	830.00	664.00	148.99	830.29	666.03	1.51	-0.29	-2.03	
375	150.50	830.00	639.00	150.32	832.27	639.59	0.18	-2.27	-0.59	
350	150.50	830.00	614.00	148.78	828.72	611.89	1.72	1.28	2.11	
325	150.50	830.00	589.00	152.39	827.68	590.89	-1.89	2.32	-1.89	
300	150.50	830.00	564.00	149.26	829.89	563.96	1.24	0.11	0.04	
275	150.50	830.00	539.00	149.67	830.18	539.84	0.83	-0.18	-0.84	
250	150.50	830.00	514.00	151.55	831.22	512.97	-1.05	-1.22	1.03	
225	150.50	830.00	489.00	150.47	830.76	490.47	0.03	-0.76	-1.47	
200	150.50	830.00	464.00	149.87	830.67	463.89	0.63	-0.67	0.11	
175	150.50	830.00	439.00	151.49	829.22	440.34	-0.99	0.78	-1.34	
150	150.50	830.00	414.00	150.84	831.13	415.00	-0.34	-1.13	-1.00	
125	150.50	830.00	389.00	150.59	831.33	389.95	-0.09	-1.33	-0.95	
100	150.50	830.00	364.00	151.54	831.20	364.89	-1.04	-1.20	-0.89	
75	150.50	830.00	339.00	149.62	831.30	339.67	0.88	-1.30	-0.67	
50	150.50	830.00	314.00	151.33	830.70	314.62	-0.83	-0.70	-0.62	
25	150.50	830.00	289.00	151.86	831.22	287.77	-1.36	-1.22	1.23	
Surface	150.50	830.00	264.00	151.39	831.39	264.56	-0.89	-1.39	-0.56	
Insertion 6										
400	150.50	830.00	664.00	152.20	832.02	664.92	-1.70	-2.02	-0.92	
375	150.50	830.00	639.00	152.55	828.44	638.10	-2.05	1.56	0.90	
350	150.50	830.00	614.00	152.33	830.22	612.22	-1.83	-0.22	1.78	
325	150.50	830.00	589.00	152.22	831.59	590.73	-1.72	-1.59	-1.73	
300	150.50	830.00	564.00	150.23	830.83	564.29	0.27	-0.83	-0.29	
275	150.50	830.00	539.00	151.29	830.49	539.44	-0.79	-0.49	-0.44	
250	150.50	830.00	514.00	150.44	830.34	514.22	0.06	-0.34	-0.22	
225	150.50	830.00	489.00	151.55	830.22	488.30	-1.05	-0.22	0.70	
200	150.50	830.00	464.00	150.39	831.22	464.93	0.11	-1.22	-0.93	
175	150.50	830.00	439.00	150.30	829.29	439.94	0.20	0.71	-0.94	
150	150.50	830.00	414.00	151.22	831.39	414.59	-0.72	-1.39	-0.59	
125	150.50	830.00	389.00	150.38	831.33	389.44	0.12	-1.33	-0.44	
100	150.50	830.00	364.00	149.48	829.47	364.44	1.02	0.53	-0.44	
75	150.50	830.00	339.00	150.48	831.33	340.44	0.02	-1.33	-1.44	
50	150.50	830.00	314.00	150.48	830.33	314.29	0.02	-0.33	-0.29	
25	150.50	830.00	289.00	150.54	830.55	287.93	-0.04	-0.55	1.07	
Surface	150.50	830.00	264.00	151.43	831.37	263.39	-0.93	-1.37	0.61	
							Max error (325 to 400 mm)	2.30	2.32	2.11
							Min error (325 to 400 mm)	-2.39	-2.27	-2.03
							Max error (0 to 300 mm)	1.46	0.78	1.23
							Min error (0 to 300 mm)	-1.36	-1.39	-1.47

APPENDIX 21 – TRIAL GRID INSERTION RESULTS

The results from this trial were used to determine the accuracy of the tag positioning and measurement apparatus as a total package. Three complete grids of tags (64 tags in each grid) were entered into the sand in the standard grid alignment. These were not disturbed, but instead they were immediately excavated and their positions were measured using the measurement frame. This produced the measurements recorded in the three tables below, which compared the measurements to the tags intended positions. These results showed that the accuracy of the placement and measurement apparatus in combination was ± 5.5 mm in any direction (as indicated in the top right corner of first table). The error in repeatability for measurements of the same grid position over the three grids was ± 3.5 mm. The full results, including the spatial calculations are copied on the enclosed data CD, see file: *3 trial tag grid insertions*.

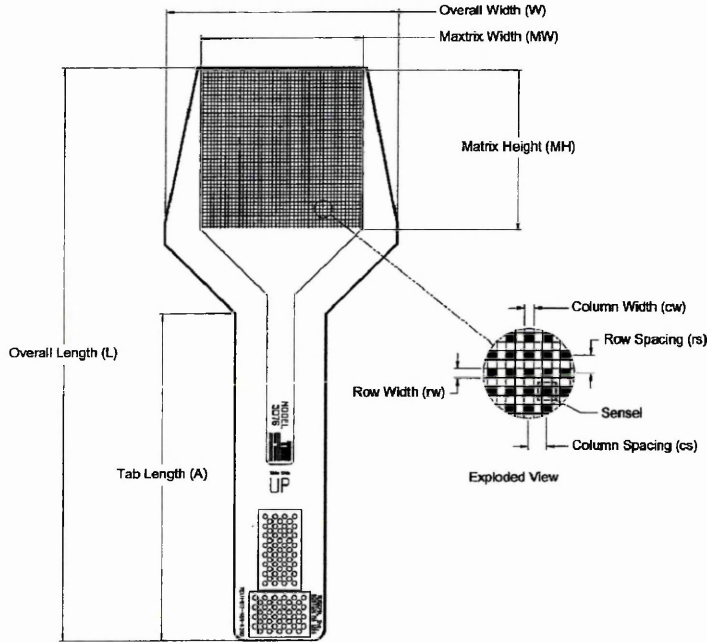
point	use Pexit, Pzero and Frame Zero			Frame Zero			Maximum Error			5.23	5.02	5.22
	Reading from pot (volts)			position from bin 0,0,0			initial location from bin 0,0,0			Difference in position		
	Orange	Purple	Brown	in x	in y	in z	in x	in y	in z	in x	in y	in z
										Positive (view down bin)		
										Back	Left	Down
1	8.5058	9.2054	6.3512	-61.62	865.78	263.51	-59.5	869	267	-2.12	-3.22	-3.49
2	8.3121	9.0559	6.3048	-57.38	871.12	291.28	-59.5	869	292	2.12	2.12	-0.72
3	8.1455	8.8586	6.2047	-56.42	870.85	318.97	-59.5	869	317	3.08	1.85	1.97
4	7.8614	8.5215	6.0014	-57.81	869.75	363.37	-59.5	869	367	1.69	0.75	-3.63
5	7.5165	8.1018	5.7085	-63.10	866.47	414.84	-59.5	869	417	-3.60	-2.53	-2.16
6	7.1589	7.7048	5.4845	-57.84	865.66	464.31	-59.5	869	467	1.66	-3.34	-2.69
7	6.3258	6.8514	4.9054	-54.33	870.19	568.96	-59.5	869	567	5.17	1.19	1.96
8	5.5014	5.9947	4.2437	-56.21	872.49	669.21	-59.5	869	667	3.29	3.49	2.21
9	8.2648	9.4048	6.4568	-60.70	898.57	264.08	-59.5	894	267	-1.20	4.57	-2.92
10	8.1132	9.1670	6.3244	-62.59	896.00	294.99	-59.5	894	292	-3.09	2.00	2.99
11	8.0547	9.0032	6.2534	-60.57	889.64	312.82	-59.5	894	317	-1.07	-4.36	-4.18
12	7.7211	8.6504	6.1000	-54.53	893.85	362.34	-59.5	894	367	4.97	-0.15	-4.66
13	7.3196	8.2007	5.8035	-58.19	896.31	419.26	-59.5	894	417	1.31	2.31	2.26
14	7.9302	7.8112	5.5543	-58.00	891.01	463.83	-59.5	894	467	1.50	-2.99	-3.17
15	6.2501	6.9567	4.9521	-59.42	893.02	565.22	-59.5	894	567	0.08	-0.98	-1.78
16	5.4390	6.0501	4.2965	-54.46	889.85	668.61	-59.5	894	667	5.04	-4.15	1.61
17	8.1232	9.4757	6.5024	-59.16	915.23	267.67	-59.5	919	267	0.34	-3.77	0.67
18	7.9121	9.2912	6.3806	-63.46	922.62	296.77	-59.5	919	292	-3.96	3.62	4.77
19	7.8043	9.1509	6.3533	-57.56	923.33	316.01	-59.5	919	317	1.94	4.33	-0.99
20	7.5600	8.7690	6.1603	-55.61	919.34	361.67	-59.5	919	367	3.89	0.34	-5.33
21	7.2001	8.2833	5.8534	-58.39	916.78	418.99	-59.5	919	417	1.11	-2.22	1.99
22	6.9001	7.9200	5.6128	-59.96	916.88	461.93	-59.5	919	467	-0.46	-2.12	-5.07
23	6.1324	7.0027	5.0060	-55.98	914.36	567.54	-59.5	919	567	3.52	-4.64	0.54
24	5.3121	6.1054	4.3098	-59.92	917.20	670.01	-59.5	919	667	-0.42	-1.80	3.01
25	7.6990	9.8012	6.6503	-58.97	973.55	262.26	-59.5	969	267	0.53	4.55	-4.74
26	7.6001	9.5921	6.5545	-59.42	971.61	286.74	-59.5	969	292	0.08	2.61	-5.26
27	7.4502	9.3696	6.4523	-59.04	973.31	314.13	-59.5	969	317	0.46	4.31	-2.87
28	7.2050	8.8547	6.2115	-55.18	963.53	371.10	-59.5	969	367	4.32	-5.47	4.10
29	6.9013	8.4554	5.9512	-59.37	965.84	417.59	-59.5	969	417	0.13	-3.16	0.59
30	6.5076	8.0065	5.6502	-62.76	973.22	470.41	-59.5	969	467	-3.26	4.22	3.41
31	5.8481	7.1555	5.1211	-55.11	971.94	565.97	-59.5	969	567	4.39	2.94	-1.03
32	5.1044	6.2544	4.4032	-63.81	970.69	665.26	-59.5	969	667	-4.31	1.69	-1.74
33	7.3560	9.9033	6.7155	-56.12	1014.05	267.22	-59.5	1019	267	3.38	-4.95	0.22
34	7.2511	9.6970	6.6071	-58.72	1014.24	290.55	-59.5	1019	292	0.78	-4.76	-1.45
35	7.1098	9.5006	6.5121	-59.43	1018.37	313.83	-59.5	1019	317	0.07	-0.63	-3.17
36	6.8560	9.0020	6.2498	-60.98	1014.38	368.72	-59.5	1019	367	-1.48	-4.62	1.72
37	6.5862	8.6221	6.0760	-55.60	1017.95	412.23	-59.5	1019	417	3.90	-1.05	-4.77
38	6.2522	8.1590	5.7921	-56.00	1020.76	463.86	-59.5	1019	467	3.50	1.76	-3.14
39	5.6122	7.2216	5.1501	-58.06	1013.87	565.91	-59.5	1019	567	1.44	-5.13	-1.09
40	4.9096	6.3521	4.5132	-57.45	1015.68	661.56	-59.5	1019	667	2.05	-3.32	-5.44
41	6.9320	9.9599	6.7112	-59.58	1064.24	270.65	-59.5	1069	267	-0.08	-4.76	3.65
42	6.8440	9.7511	6.5999	-62.69	1063.62	293.17	-59.5	1069	292	-3.19	-5.38	1.17
43	6.7221	9.5011	6.5332	-56.69	1063.79	321.46	-59.5	1069	317	2.81	-5.21	4.46
44	6.4548	9.0501	6.2904	-58.92	1067.32	370.86	-59.5	1069	367	0.58	-1.68	3.86
45	6.2126	8.5948	6.0110	-62.59	1064.07	420.13	-59.5	1069	417	-3.09	-4.93	3.13
46	5.9330	8.2017	5.8212	-55.67	1068.35	463.85	-59.5	1069	467	3.83	-0.65	-3.15
47	5.3121	7.3037	5.2029	-58.88	1068.76	561.55	-59.5	1069	567	0.62	-0.24	-5.45
48	4.5534	6.3072	4.4594	-60.95	1069.96	670.01	-59.5	1069	667	-1.45	0.96	3.01
49	6.0287	9.8189	6.6500	-59.97	1172.11	271.41	-59.5	1169	267	-0.47	3.11	4.41
50	5.9311	9.6071	6.5498	-60.93	1173.88	295.33	-59.5	1169	292	-1.43	4.88	3.33
51	5.9119	9.4492	6.5204	-55.14	1167.07	316.38	-59.5	1169	317	4.36	-1.93	-0.62
52	5.7100	8.9701	6.2511	-58.44	1163.60	371.10	-59.5	1169	367	1.06	-5.40	4.10
53	5.4139	8.4990	5.9513	-63.11	1170.70	421.79	-59.5	1169	417	-3.61	1.70	4.79
54	5.1502	8.0513	5.7340	-54.46	1171.76	472.18	-59.5	1169	467	5.04	2.76	5.18
55	4.5801	7.1521	5.1013	-57.97	1171.70	571.47	-59.5	1169	567	1.53	2.70	4.47
56	4.0570	6.3401	4.5039	-57.47	1163.58	661.96	-59.5	1169	667	2.03	-5.42	-5.04
57	5.2511	9.4195	6.4408	-63.77	1263.70	269.05	-59.5	1269	267	-4.27	-5.30	2.05
58	5.1487	9.2108	6.3302	-64.83	1266.28	295.49	-59.5	1269	292	-5.33	-2.72	3.49
59	5.0495	9.0514	6.2497	-64.59	1271.12	313.42	-59.5	1269	317	-5.09	2.12	-3.58
60	4.8462	8.6001	6.0021	-64.31	1269.87	372.18	-59.5	1269	367	-4.81	0.87	5.18
61	4.6311	8.1985	5.7613	-64.26	1271.44	420.84	-59.5	1269	417	-4.76	2.44	3.84
62	4.4000	7.8027	5.5500	-57.79	1273.76	467.93	-59.5	1269	467	1.71	4.76	0.93
63	3.8598	6.9101	4.8999	-62.53	1273.81	572.12	-59.5	1269	567	-3.03	4.81	5.12
64	3.3798	6.1398	4.3610	-55.43	1267.24	662.75	-59.5	1269	667	4.07	-1.76	-4.25

point	Reading from pot (volts)			position from bin 0,0,0			initial location from bin 0,0,0			Difference in position		
	Orange	Purple	Brown	in x	in y	in z	in x	in y	in z	in x	in y	in z
1	8.5018	9.2078	6.3510	-61.81	866.26	263.58	-59.5	869	267	-2.31	-2.74	-3.42
2	8.3127	9.0586	6.2999	-58.24	871.26	290.90	-59.5	869	292	1.26	2.26	-1.10
3	8.1386	8.8321	6.2008	-54.91	869.43	321.70	-59.5	869	317	4.59	0.43	4.70
4	7.8614	8.5215	6.0111	-56.42	869.75	363.51	-59.5	869	367	3.08	0.75	-3.49
5	7.5211	8.1053	5.7085	-63.43	866.33	414.28	-59.5	869	417	-3.93	-2.67	-2.72
6	7.1217	7.7138	5.4800	-59.48	870.74	465.69	-59.5	869	467	0.02	1.74	-1.31
7	6.3258	6.8514	4.9054	-54.33	870.19	568.96	-59.5	869	567	5.17	1.19	1.96
8	5.5022	5.9990	4.2467	-56.28	872.98	668.88	-59.5	869	667	3.22	3.98	1.88
9	8.2845	9.4013	6.4498	-61.41	896.68	262.87	-59.5	894	267	-1.91	2.68	-4.13
10	8.1132	9.1670	6.3423	-60.17	896.00	295.33	-59.5	894	292	-0.67	2.00	3.33
11	8.0600	9.0031	6.2534	-60.56	889.16	312.49	-59.5	894	317	-1.06	-4.84	-4.51
12	7.7312	8.6489	6.1000	-54.41	892.75	361.87	-59.5	894	367	5.09	-1.25	-5.13
13	7.3196	8.2007	5.7989	-58.87	896.31	419.20	-59.5	894	417	0.63	2.31	2.20
14	7.0302	7.8112	5.5543	-58.00	891.01	463.83	-59.5	894	467	1.50	-2.99	-3.17
15	6.2597	6.9767	4.9389	-64.08	894.15	562.99	-59.5	894	567	-4.58	0.15	-4.01
16	5.4646	6.0965	4.2965	-61.10	892.51	663.81	-59.5	894	667	-1.60	-1.49	-3.19
17	8.1322	9.4653	6.5078	-57.80	913.79	268.21	-59.5	919	267	1.70	-5.21	1.21
18	7.9378	9.2917	6.3863	-62.73	920.26	295.29	-59.5	919	292	-3.23	1.26	3.29
19	7.8087	9.1512	6.3421	-59.09	922.93	315.55	-59.5	919	317	0.41	3.93	-1.45
20	7.5612	8.7688	6.1598	-55.66	919.20	361.62	-59.5	919	367	3.84	0.20	-5.38
21	7.1999	8.2801	5.8546	-57.93	916.52	419.29	-59.5	919	417	1.57	-2.48	2.29
22	6.8989	7.9198	5.6019	-61.61	917.01	461.86	-59.5	919	467	-2.11	-1.99	-5.14
23	6.1298	7.0017	5.0058	-55.89	914.60	567.74	-59.5	919	567	3.61	-4.40	0.74
24	5.3118	6.1034	4.3079	-59.99	916.96	670.17	-59.5	919	667	-0.49	-2.04	3.17
25	7.6979	9.8002	6.6497	-59.00	973.60	262.41	-59.5	969	267	0.50	4.60	-4.59
26	7.5997	9.5916	6.5539	-59.47	971.62	286.80	-59.5	969	292	0.03	2.62	-5.20
27	7.4476	9.3688	6.4516	-59.08	973.53	314.31	-59.5	969	317	0.42	4.53	-2.69
28	7.2050	8.8547	6.2010	-56.63	963.53	370.97	-59.5	969	367	2.87	-5.47	3.97
29	6.9007	8.4533	5.9512	-59.19	965.74	417.81	-59.5	969	417	0.31	-3.26	0.81
30	6.5063	8.0048	5.6498	-62.65	973.22	470.61	-59.5	969	467	-3.15	4.22	3.61
31	5.8481	7.1555	5.1203	-55.24	971.94	565.96	-59.5	969	567	4.26	2.94	-1.04
32	5.1022	6.2529	4.4032	-63.60	970.84	665.47	-59.5	969	667	-4.10	1.84	-1.53
33	7.3499	9.9036	6.7079	-57.10	1014.72	267.26	-59.5	1019	267	2.40	-4.28	0.26
34	7.2505	9.6963	6.6083	-58.52	1014.26	290.66	-59.5	1019	292	0.98	-4.74	-1.34
35	7.1078	9.5002	6.5014	-60.81	1018.57	313.75	-59.5	1019	317	-1.31	-0.43	-3.25
36	6.8573	9.0021	6.2476	-61.29	1014.24	368.64	-59.5	1019	367	-1.79	-4.76	1.64
37	6.5859	8.6216	6.0755	-55.63	1017.94	412.28	-59.5	1019	417	3.87	-1.06	-4.72
38	6.2513	8.1589	5.7890	-56.46	1020.87	463.86	-59.5	1019	467	3.04	1.87	-3.14
39	5.6008	7.2195	5.1495	-57.92	1015.32	566.35	-59.5	1019	567	1.58	-3.68	-0.65
40	4.9089	6.3499	4.5122	-57.33	1015.50	661.79	-59.5	1019	667	2.17	-3.50	-5.21
41	6.9321	9.9601	6.7012	-60.86	1064.24	270.44	-59.5	1069	267	-1.36	-4.76	3.44
42	6.8442	9.7524	6.6041	-62.22	1063.67	293.10	-59.5	1069	292	-2.72	-5.33	1.10
43	6.7119	9.5001	6.5347	-56.43	1064.97	321.68	-59.5	1069	317	3.07	-4.03	4.68
44	6.4534	9.0509	6.2923	-58.72	1067.56	370.81	-59.5	1069	367	0.78	-1.44	3.81
45	6.2016	8.6011	6.0211	-61.67	1066.07	419.63	-59.5	1069	417	-2.17	-2.93	2.63
46	5.9297	8.2003	5.8216	-55.48	1068.68	464.03	-59.5	1069	467	4.02	-0.32	-2.97
47	5.3112	7.3038	5.2019	-59.05	1068.92	561.53	-59.5	1069	567	0.45	-0.08	-5.47
48	4.5532	6.3068	4.4601	-60.77	1069.94	670.07	-59.5	1069	667	-1.27	0.94	3.07
49	6.0197	9.8201	6.6503	-60.00	1173.43	270.76	-59.5	1169	267	-0.50	4.43	3.76
50	5.9298	9.6064	6.5511	-60.72	1174.02	295.39	-59.5	1169	292	-1.22	5.02	3.39
51	5.9131	9.4512	6.5215	-55.12	1167.02	316.17	-59.5	1169	317	4.38	-1.98	-0.83
52	5.6987	8.9718	6.2586	-57.54	1165.37	370.57	-59.5	1169	367	1.96	-3.63	3.57
53	5.4178	8.5110	5.9601	-62.86	1171.12	420.38	-59.5	1169	417	-3.36	2.12	3.38
54	5.1496	8.0529	5.7289	-55.37	1172.01	471.89	-59.5	1169	467	4.13	3.01	4.89
55	4.5817	7.1518	5.1025	-57.74	1171.39	571.57	-59.5	1169	567	1.76	2.39	4.57
56	4.0569	6.3399	4.5051	-57.23	1163.58	661.99	-59.5	1169	667	2.27	-5.42	-5.01
57	5.2505	9.4201	6.4419	-63.66	1263.84	268.88	-59.5	1269	267	-4.16	-5.16	1.88
58	5.1499	9.2117	6.3310	-64.78	1266.15	295.46	-59.5	1269	292	-5.28	-2.85	3.46
59	5.0502	9.0399	6.2488	-63.88	1270.19	315.68	-59.5	1269	317	-4.38	1.19	-1.32
60	4.8443	8.5988	6.0010	-64.36	1270.08	372.22	-59.5	1269	367	-4.86	1.08	5.22
61	4.6302	8.1998	5.7599	-64.59	1271.72	420.52	-59.5	1269	417	-5.09	2.72	3.52
62	4.4007	7.8001	5.5511	-57.36	1273.37	468.44	-59.5	1269	467	2.14	4.37	1.44
63	3.8612	6.9131	4.9001	-62.86	1273.91	571.72	-59.5	1269	567	-3.36	4.91	4.72
64	3.3815	6.1410	4.3620	-55.42	1267.07	662.66	-59.5	1269	667	4.08	-1.93	-4.34

point	Reading from pot (volts)			position from bin 0,0,0			initial location from bin 0,0,0			Difference in position		
	Orange	Purple	Brown	in x	in y	in z	in x	in y	in z	in x	in y	in z
1	8.5085	9.2097	6.3521	-61.79	865.86	262.89	-59.5	869	267	-2.29	-3.14	-4.11
2	8.3154	9.0599	6.3122	-56.66	871.13	290.81	-59.5	869	292	2.84	2.13	-1.19
3	8.1475	8.8608	6.2089	-56.01	870.84	318.71	-59.5	869	317	3.49	1.84	1.71
4	7.8700	8.5211	6.0121	-56.24	868.91	363.01	-59.5	869	367	3.26	-0.09	-3.99
5	7.5198	8.1032	5.7100	-63.01	866.26	414.55	-59.5	869	417	-3.51	-2.74	-2.45
6	7.1603	7.7079	5.4897	-57.36	865.83	464.05	-59.5	869	467	2.14	-3.17	-2.95
7	6.3311	6.8578	4.9101	-54.33	870.28	568.24	-59.5	869	567	5.17	1.28	1.24
8	5.5036	5.9978	4.2445	-56.51	872.60	668.88	-59.5	869	667	2.99	3.60	1.88
9	8.2689	9.4100	6.4589	-60.76	898.55	263.31	-59.5	894	267	-1.26	4.55	-3.69
10	8.1167	9.1690	6.3212	-63.16	895.83	294.50	-59.5	894	292	-3.66	1.83	2.50
11	8.0598	9.0022	6.2578	-59.89	889.11	312.66	-59.5	894	317	-0.39	-4.89	-4.34
12	7.7224	8.6499	6.0986	-54.69	893.69	362.28	-59.5	894	367	4.81	-0.31	-4.72
13	7.3196	8.2007	5.8033	-58.22	896.31	419.25	-59.5	894	417	1.28	2.31	2.25
14	7.0312	7.8103	5.5528	-58.14	890.80	463.83	-59.5	894	467	1.36	-3.20	-3.17
15	6.2498	6.9588	4.9499	-60.05	893.31	565.05	-59.5	894	567	-0.55	-0.69	-1.95
16	5.4390	6.0501	4.2965	-54.46	889.85	668.61	-59.5	894	667	5.04	-4.15	1.61
17	8.1272	9.4797	6.5012	-59.56	915.12	266.98	-59.5	919	267	-0.06	-3.88	-0.02
18	7.9210	9.2993	6.3892	-62.84	922.32	295.62	-59.5	919	292	-3.34	3.32	3.62
19	7.8089	9.1573	6.3519	-58.19	923.34	315.13	-59.5	919	317	1.31	4.34	-1.87
20	7.5599	8.7699	6.1598	-55.75	919.42	361.59	-59.5	919	367	3.75	0.42	-5.41
21	7.1998	8.2889	5.8518	-59.14	917.31	418.49	-59.5	919	417	0.36	-1.69	1.49
22	6.8987	7.9198	5.6432	-55.31	917.03	462.36	-59.5	919	467	4.19	-1.97	-4.64
23	6.1388	7.0087	5.0012	-57.50	914.21	566.71	-59.5	919	567	2.00	-4.79	-0.29
24	5.3181	6.1101	4.3121	-60.17	916.92	669.40	-59.5	919	667	-0.67	-2.08	2.40
25	7.7001	9.8002	6.6499	-58.97	973.38	262.30	-59.5	969	267	0.53	4.38	-4.70
26	7.6011	9.5000	6.5512	-54.27	965.99	295.89	-59.5	969	292	5.23	-3.01	3.89
27	7.5010	9.3101	6.4000	-62.11	964.19	316.93	-59.5	969	317	-2.61	-4.81	-0.07
28	7.2101	8.8700	6.2112	-56.40	964.13	369.43	-59.5	969	367	3.10	-4.87	2.43
29	6.9021	8.4522	5.9543	-58.65	965.48	417.90	-59.5	969	417	0.85	-3.52	0.90
30	6.5045	8.0100	5.6511	-62.96	973.94	470.19	-59.5	969	467	-3.46	4.94	3.19
31	5.8564	7.1567	5.1223	-55.06	970.89	565.61	-59.5	969	567	4.44	1.89	-1.39
32	5.1078	6.2589	4.4078	-63.60	970.76	664.79	-59.5	969	667	-4.10	1.76	-2.21
33	7.3560	9.9033	6.7112	-56.67	1014.05	267.15	-59.5	1019	267	2.83	-4.95	0.15
34	7.2567	9.6984	6.6099	-58.43	1013.70	290.27	-59.5	1019	292	1.07	-5.30	-1.73
35	7.1108	9.4999	6.5019	-60.72	1018.21	313.71	-59.5	1019	317	-1.22	-0.79	-3.29
36	6.8543	9.0018	6.2542	-60.36	1014.57	368.85	-59.5	1019	367	-0.86	-4.43	1.85
37	6.5847	8.6225	6.0742	-55.89	1018.16	412.20	-59.5	1019	417	3.61	-0.84	-4.80
38	6.2523	8.1600	5.7965	-55.45	1020.84	463.80	-59.5	1019	467	4.05	1.84	-3.20
39	5.6112	7.2201	5.1498	-57.94	1013.84	566.08	-59.5	1019	567	1.56	-5.16	-0.92
40	4.9076	6.3501	4.5155	-56.77	1015.75	661.82	-59.5	1019	667	2.73	-3.25	-5.18
41	6.9310	9.9601	6.7132	-59.34	1064.37	270.68	-59.5	1069	267	0.16	-4.63	3.68
42	6.8438	9.7501	6.6002	-62.60	1063.59	293.29	-59.5	1069	292	-3.10	-5.41	1.29
43	6.7255	9.5045	6.5322	-57.03	1063.58	321.03	-59.5	1069	317	2.47	-5.42	4.03
44	6.4567	9.0505	6.3219	-54.66	1067.10	371.21	-59.5	1069	367	4.84	-1.90	4.21
45	6.2158	8.5955	6.0121	-62.49	1063.70	420.04	-59.5	1069	417	-2.99	-5.30	3.04
46	5.9321	8.2001	5.8255	-54.89	1068.33	464.08	-59.5	1069	467	4.61	-0.67	-2.92
47	5.3133	7.3041	5.2059	-58.44	1068.62	561.53	-59.5	1069	567	1.06	-0.38	-5.47
48	4.5561	6.3053	4.4609	-60.42	1069.23	670.23	-59.5	1069	667	-0.92	0.23	3.23
49	6.0291	9.8190	6.6511	-59.84	1172.06	271.43	-59.5	1169	267	-0.34	3.06	4.43
50	5.9318	9.6098	6.5510	-60.93	1173.94	295.00	-59.5	1169	292	-1.43	4.94	3.00
51	5.9122	9.4501	6.5232	-54.83	1167.08	316.31	-59.5	1169	317	4.67	-1.92	-0.69
52	5.7104	8.9767	6.2525	-58.74	1164.02	370.23	-59.5	1169	367	0.76	-4.98	3.23
53	5.4143	8.5000	5.9521	-63.08	1170.73	421.67	-59.5	1169	417	-3.58	1.73	4.67
54	5.1510	8.0524	5.7356	-54.32	1171.74	472.07	-59.5	1169	467	5.18	2.74	5.07
55	4.5811	7.1534	5.1022	-57.98	1171.68	571.33	-59.5	1169	567	1.52	2.68	4.33
56	4.0450	6.3410	4.5044	-57.51	1165.94	661.56	-59.5	1169	667	1.99	-3.06	-5.44
57	5.2533	9.4301	6.4416	-64.33	1264.02	267.22	-59.5	1269	267	-4.83	-4.98	0.22
58	5.1497	9.2115	6.3302	-64.88	1266.17	295.46	-59.5	1269	292	-5.38	-2.83	3.46
59	5.0448	9.0511	6.2501	-64.52	1271.86	312.97	-59.5	1269	317	-5.02	2.86	-4.03
60	4.8465	8.6010	6.0041	-64.10	1269.90	372.08	-59.5	1269	367	-4.60	0.90	5.08
61	4.6319	8.1998	5.7619	-64.29	1271.42	420.69	-59.5	1269	417	-4.79	2.42	3.69
62	4.4033	7.8041	5.5519	-57.64	1273.31	467.97	-59.5	1269	467	1.86	4.31	0.97
63	3.8603	6.9120	4.9002	-62.71	1273.94	571.84	-59.5	1269	567	-3.21	4.94	4.84
64	3.3810	6.1412	4.3615	-55.54	1267.19	662.60	-59.5	1269	667	3.96	-1.81	-4.40

APPENDIX 22 – TEKSCAN DATA SHEETS AND RESULTS

MAP AND SENSOR MODEL NUMBER: 5051, 5076, 5101
NAME: I-SCAN



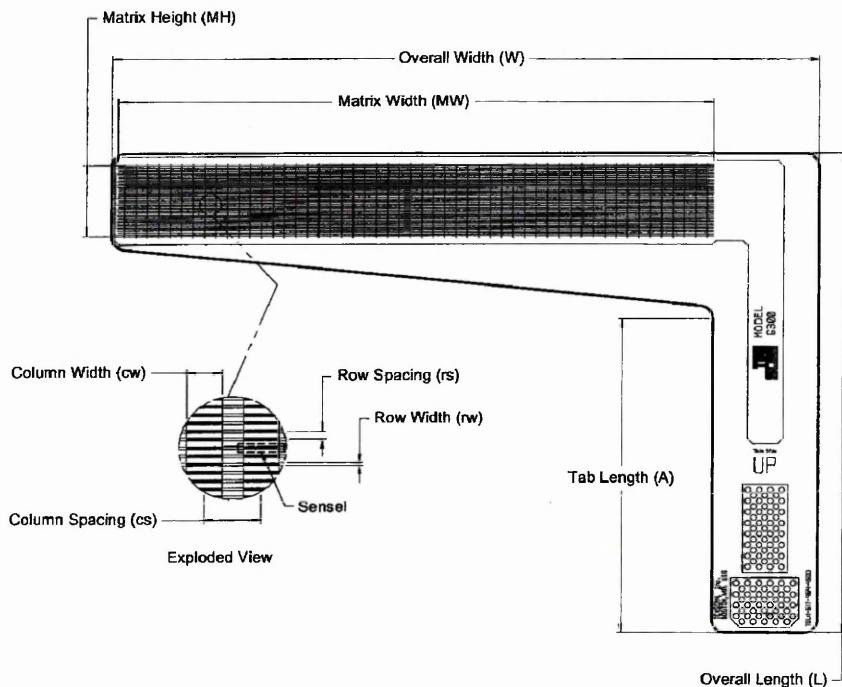
Model Number	General Dimensions			Sensing Region Dimensions						Summary			
	Overall Length <i>L</i>	Overall Width <i>W</i>	Tab Length <i>A</i>	Matrix Width <i>MW</i>	Matrix Height <i>MH</i>	Columns			Rows		No. of Sensels	Sensel Density	
	<i>L</i>	<i>W</i>	<i>A</i>	<i>MW</i>	<i>MH</i>	<i>CW</i>	<i>CS</i>	<i>Qty.</i>	<i>RW</i>	<i>RS</i>	<i>Qty.</i>		(sensel per sq-in)
US	(in)	(in)	(in)	(in)	(in)	(in)	(in)		(in)	(in)			(sensel per sq-in)
5051	9.9	3.2	6.6	2.2	2.2	0.03	0.05	44	0.03	0.05	44	1936	400
5076	12	4.8	6.9	3.3	3.3	0.04	0.075	44	0.04	0.075	44	1936	178
5101	13.4	5.9	6.5	4.4	4.4	0.05	0.1	44	0.05	0.1	44	1936	100
Metric	(mm)	(mm)	(mm)	(mm)	(mm)	(mm)	(mm)		(mm)	(mm)			(sensel per sq-cm)
5051	251	81	168	56	56	0.76	1.27	44	0.76	1.27	44	1936	62.0
5076	305	122	175	84	84	1.02	1.91	44	1.02	1.91	44	1936	27.6
5101	340	150	165	112	112	1.27	2.54	44	1.27	2.54	44	1936	15.5

Application Example: Excellent for general purpose uses.

Special Feature: Wide range of available pressures.

Tekscan, Inc., 307 West First Street, South Boston, MA 02127 Phone: 617-464-4500 Fax 617-464-4266 Website: www.tekscan.com

MAP AND SENSOR MODEL NUMBER: 6300
SENSOR NAME: STRIP



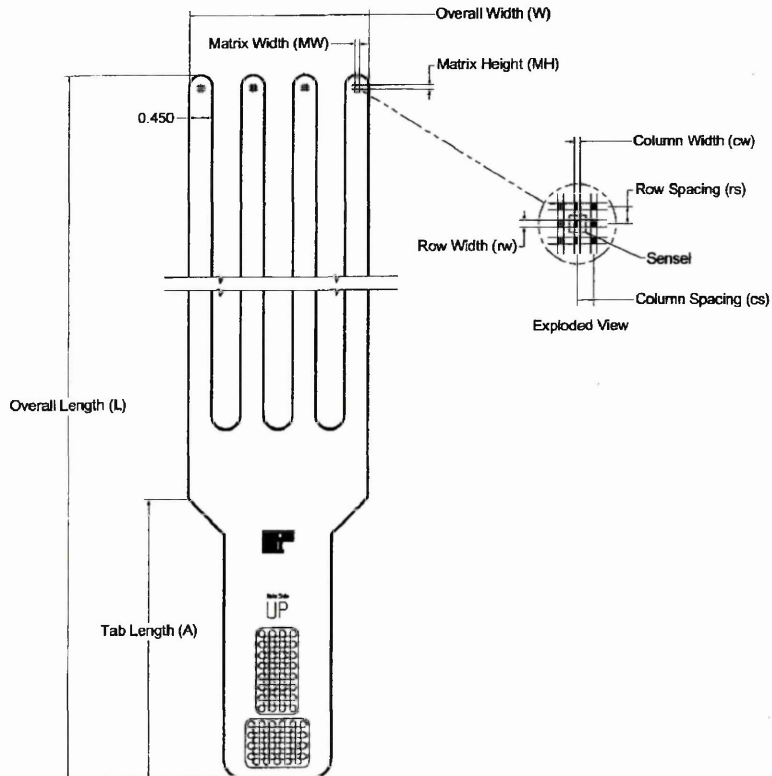
Model Number	General Dimensions			Sensing Region Dimensions							Summary	
	Overall Length <i>L</i>	Overall Width <i>W</i>	Tab Length <i>A</i>	Matrix Width <i>MW</i>	Matrix Height <i>MH</i>	Columns			Rows		No. of Sensels	Sensel Density
	(in)	(in)	(in)	(in)	(in)	<i>CW</i>	<i>CS</i>	<i>Qty.</i>	<i>RW</i>	<i>RS</i>	<i>Qty.</i>	(sensel per sq-in)
US 6300	8.73	12.385	5.71	10.4	1.32	0.125	0.2	52	0.01	0.03	44	166.667
Metric	(mm)	(mm)	(mm)	(mm)	(mm)	(mm)	(mm)		(mm)	(mm)		(sensel per sq-cm)
6300	222	315	145	264	34	3.18	5.08	52	0.25	0.76	44	25.833

Application Examples: Car door seals, oil pan seals and roller roundness measurements.

Special Feature: Sensor can be cut from either edge to make it shorter or narrower without affecting the output.

Tekscan, Inc., 307 West First Street, South Boston, MA 02127 Phone: 617-464-4500 Fax 617-464-4266 Website: www.tekscan.com

MAP AND SENSOR MODEL NUMBER: 6911
SENSOR NAME: QUAD



Model Number	General Dimensions			Sensing Region Dimensions								Summary	
	Overall Length	Overall Width	Tab Length	Matrix Width	Matrix Height	Columns			Rows		No. of Sensels	Sensel Density	
	L	W	A	MW	MH	CW	CS	Qty.	RW	RS			Qty.
US 6911	(in) 24	(in) 3.45	(in) 4.5	(in) 0.12	(in) 0.12	(in) 0.015	(in) 0.04	3	(in) 0.015	(in) 0.04	3	9	(sensel per sq-in) 625
Metric 6911	(mm) 610	(mm) 88	(mm) 114	(mm) 3	(mm) 3	(mm) 0.38	(mm) 1.02	3	(mm) 0.38	(mm) 1.02	3	9	(sensel per sq-cm) 96.9

Application Example: Sensing for human fingertips.

Special Feature: Four independent sensing fingers.

Tekscan, Inc., 307 West First Street, South Boston, MA 02127 Phone: 617-464-4500 Fax 617-464-4266 Website: www.tekscan.com

The data used to produce the pressure maps for the comparison of the performance of the three different pressure maps is included on the data CD, in files: *TekScan results 6911 (22)*, *TekScan results 5051 (22)* and *TekScan results 6300 (22)*. Results are presented for all three mats, 6911, 5051 and 6300. To allow their inclusion limited processing has been conducted, as every TekScan test generated a very large quantity of data. Even these short test runs produced too much data to enable its direct inclusion; therefore the data corresponding to when the mats were out of ground contact has been omitted. The 6911 mats had significantly fewer cells on each mat, so it was possible to present the pure results for this mat, for all three repetitions of the tests. For the other two mats mean results of the three repetitions were included to reduce the quantity of data presented.

APPENDIX 23 – SAND DISPLACEMENT STATISTICS

The statistical analysis that was conducted on these results produced a large quantity of data; therefore copies of the output files have been included on the enclosed data CD. The files included have been separated by the variable for which they were analysed e.g. wheel slip. The following files are included:

Sand tag displacement stats – Force

Sand tag displacement stats – Tyre Depth

Sand tag displacement stats – Tyre Slip

Sand tag displacement stats – X Direction

Sand tag displacement stats – Y Direction

Sand tag displacement stats – Z Direction

APPENDIX 24 – MODELLING SPREADSHEETS

All of the modelling (thrust and tread) was completed using models created in Excel. These have been included on the data CD, to allow their construction and application to be fully understood. They are located in the files detailed in the table below.

DATA	FILENAME
Net Thrust modelling (derived from Gross Thrust and Rolling Resistance modelling)	<i>Net thrust model – GT + RR</i>
Rolling Resistance modelling	<i>Rolling Resistance model</i>
Tread Coefficient modelling	<i>Tread Coefficient model</i>

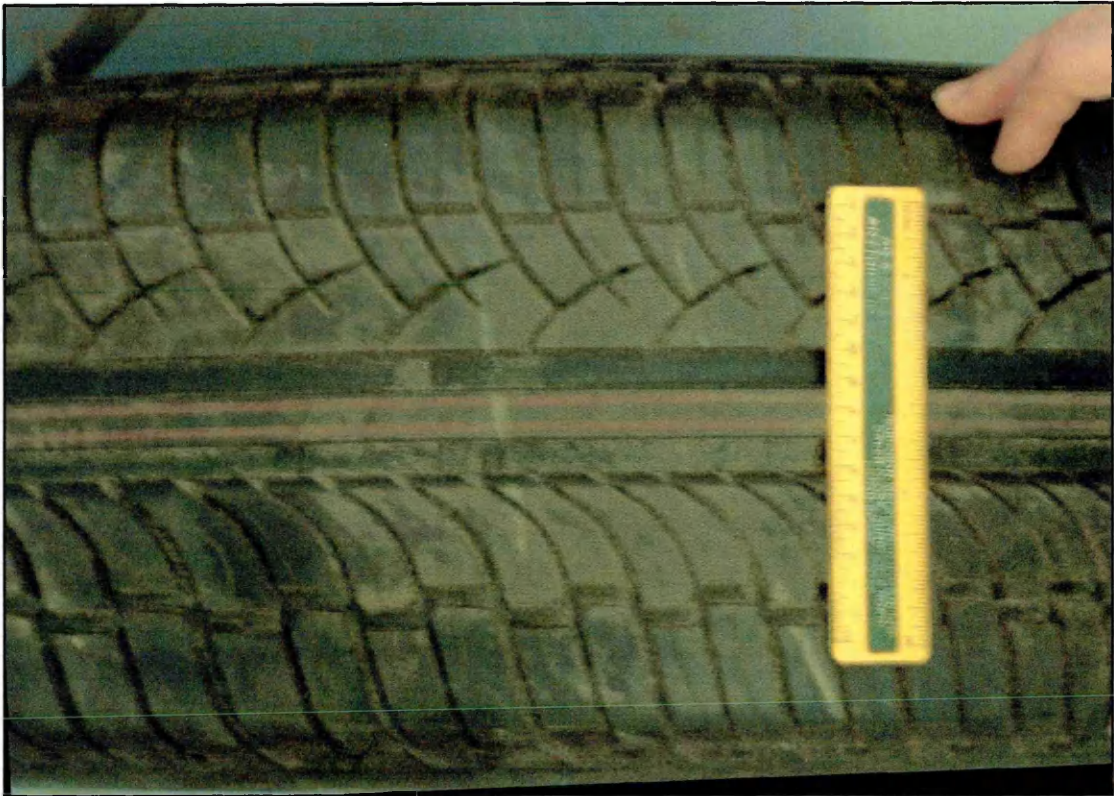
APPENDIX 25 – CALCULATION OF TREAD COEFFICIENTS

Tread coefficients were calculated for all the treads. This information is presented on the three tables below for the three sets of treads, prototype, 235/70 R16 production and 255/55 R19 production. The complete calculations used to derive these calculations are included on the data CD in file: *Tread coefficient calculations*. Photographs of the three 255/55 R19 production treads from which the tread information was derived are included. The graphs from which the percentage gross thrust benefits of all the production treads were calculated are also included in this Appendix.

Tread coefficients	Factor	PT	LON	45F	45B	LAT
Fraction of full width	Wff	2	2	2	2	2
Fraction of unit length	Lfu	1	1	1	1	1
Tread to void ratio	Tvr	1	0.6	0.6	0.6	0.6
Number of edges	Qte	1	4	8	8	12
Tread factor	E x Tvr	1	2.4	4.8	4.8	7.2
Width adjuster		2	4.8	9.6	9.6	14.4
Length adjuster		2	4.8	9.6	9.6	14.4
Tread factor		0.693	1.569	2.262	2.262	2.667
Lat groove width	Wg	30	30	30	30	30
Lon groove length	Lg	0	150	125	125	90
Groove area	Wg x Lg	0	4500	3750	3750	2700
No. grooves	Qg	0	2	4	4	6
Width adjuster		0	4	8	8	12
Length adjuster	10000	0	4	8	8	12
Groove factor		0.000	1.800	3.000	3.000	3.240
Lat groove width	Wg	N/A	N/A	N/A	N/A	N/A
Lon groove length	Lg					
Groove area	Wg x Lg					
No. grooves	Qg					
Width adjuster						
Length adjuster	10000					
Groove factor						
Tread angle	At	0	0	45	135	90
Sine tread angle	sin At	0.000	0.000	0.707	0.707	1.000
No. lat/ angled edges	Ql	0	0	4	4	6
Lateral edge length	Lle	0	0	90	90	90
Total edge length	20	0	0	360	360	540
No. trap points	5	0	0	-3	2	0
Weightings		0	0	3	28	27
Width adjuster		0	0	6	56	54
Length adjuster		0	0	6	56	54
Edge factor		0.000	0.000	1.946	4.043	4.007
Constant 1	0.8					
Constant 2	1					
Constant 3	0.2					
Numerical calc per area	1	0.555	3.055	5.199	5.618	6.175
TREAD COEFFICIENT	1	0.000	2.500	4.644	5.064	5.621

Tread coefficients	Factor	G82	HP	UG
Fraction of full width	Wff	2	2	2
Fraction of unit length	Lfu	1	1	1
Tread to void ratio	Tvr	0.6	0.75	0.75
Number of edges	Qte	24	60	24
Tread factor	E x Tvr	14.4	45	18
Width adjuster		28.8	90	36
Length adjuster		28.8	90	36
Tread factor		3.360	4.500	3.584
Lat groove width	Wg	25	8	8
Lon groove length	Lg	45	125	45
Groove area	Wg x Lg	1125	1000	360
No. grooves	Qg	8	4	8
Width adjuster		16	8	16
Length adjuster	10000	16	8	16
Groove factor		1.800	0.800	0.576
Lat groove width	Wg	25	15	12
Lon groove length	Lg	45	150	150
Groove area	Wg x Lg	1125	2250	1800
No.grooves	Qg	8	1	2
Width adjuster		16	2	4
Length adjuster	10000	16	2	4
Groove factor		1.800	0.450	0.720
Tread angle	At	60	45	35
Sine tread angle	sin At	0.866	0.707	0.574
No. lat/ angled edges	Ql	12	32	16
Lateral edge length	Lle	30	40	30
Total edge length	20	360	1280	480
No. trap points	5	6	0	0
Weightings		48	64	24
Width adjuster		96	128	48
Length adjuster		96	128	48
Edge factor		4.575	4.860	3.892
Constant 1	0.8			
Constant 2	1			
Constant 3	0.2			
Numerical calc per area	1	7.203	5.822	4.941
TREAD COEFFICIENT	1	6.649	5.267	4.387

Tread coefficients	Factor	DIA- LH	DIA - RH	HP	TG31
Fraction of full width	Wff	2	2	2	2
Fraction of unit length	Lfu	1	1	1	1
Tread to void ratio	Tvr	0.8	0.8	0.75	0.8
Number of edges	Qte	90	52	60	65
Tread factor	E x Tvr	72	41.6	45	52
Width adjuster		144	83.2	90	104
Length adjuster		144	83.2	90	104
Tread factor		4.970	4.421	4.500	4.644
Lat groove width	Wg	5	5	8	5
Lon groove length	Lg	110	130	125	20
Groove area	Wg x Lg	550	650	1000	100
No. grooves	Qg	8	6	4	20
Width adjuster		16	12	8	40
Length adjuster	10000	16	12	8	40
Groove factor		0.880	0.780	0.800	0.400
Lat groove width	Wg	12	12	15	8
Lon groove length	Lg	150	150	150	150
Groove area	Wg x Lg	1800	1800	2250	1200
No.grooves	Qg	1	1	1	2
Width adjuster		2	2	2	4
Length adjuster	10000	2	2	2	4
Groove factor		0.360	0.360	0.450	0.480
Tread angle	At	20	20	45	0
Sine tread angle	sin At	0.342	0.342	0.707	0.000
No. lat/ angled edges	Ql	44	12	32	0
Lateral edge length	Lle	25	60	40	0
Total edge length	20	1100	720	1280	0
No. trap points	5	0	0	0	0
Weightings		55	36	64	0
Width adjuster		110	72	128	0
Length adjuster		110	72	128	0
Edge factor		4.710	4.290	4.860	0.000
Constant 1	0.8				
Constant 2	1				
Constant 3	0.2				
Numerical calc per area	1	6.158	5.535	5.822	4.596
TREAD COEFFICIENT	1	5.603	4.981	5.267	4.041
Average of DIA-LH and DIA-RH			5.292		



A photograph of the Michelin Diamaris Tread

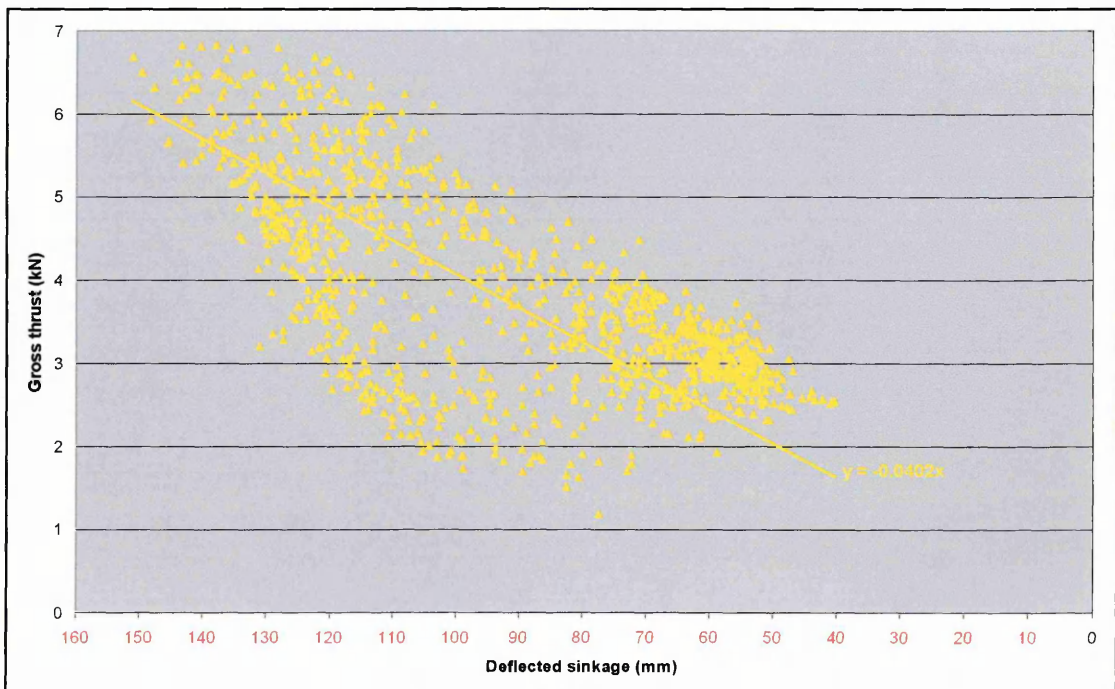


A photograph of the Dunlop TG31 Tread

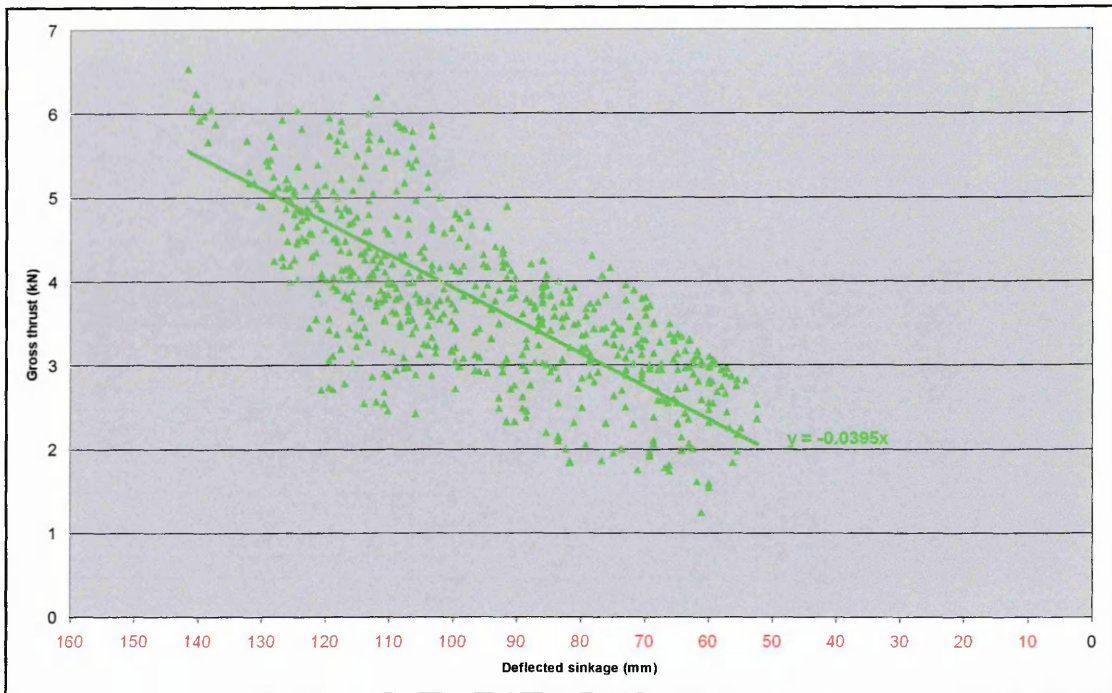


A photograph of the Goodyear Wrangler HP Tread

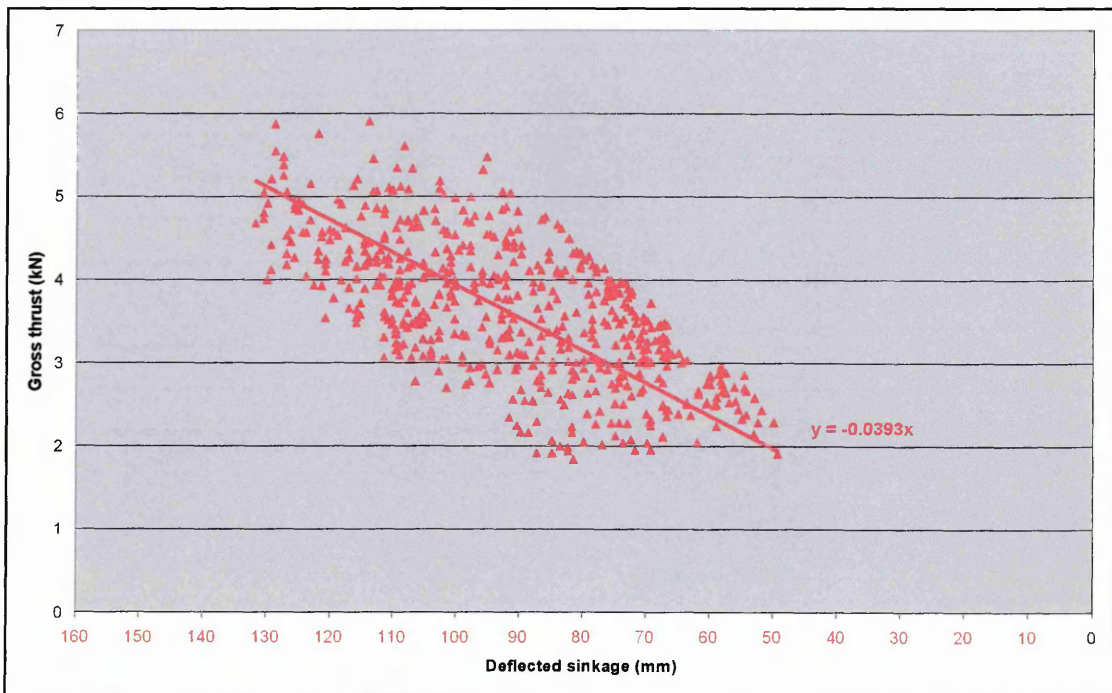
Gross thrust benefits of the 235/70 R16 production treads



Gross thrusts achieved by the G82 tread during the displacement experiments



Gross thrusts achieved by the HP tread (235/70 R16) during traction experiments



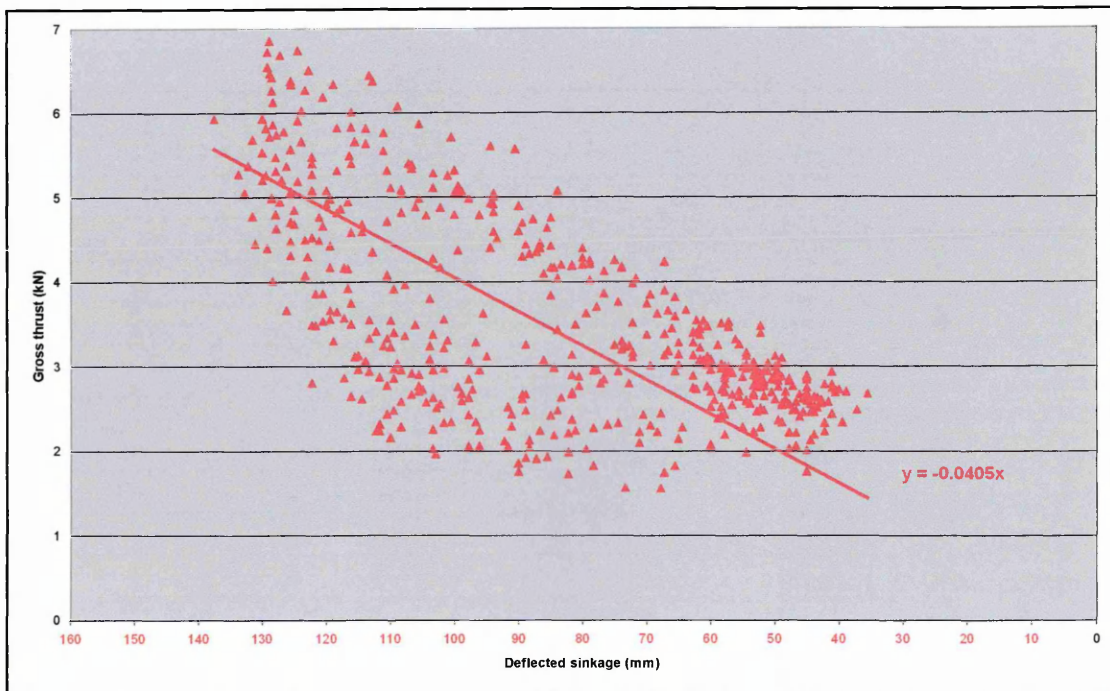
Gross thrusts achieved by the UG tread during traction experiments

The gradients of these results were used to calculate the gross thrust benefits generated by each of these treads, which are shown on the table below:

Percentage extra gross thrusts achieved by the 235/70 R16 production treads

Tread Type	% Extra Gross Thrust
PT	0.00
G82	5.24
HP	3.40
UG	2.88

Gross thrust benefits of the 255/55 R19 production treads

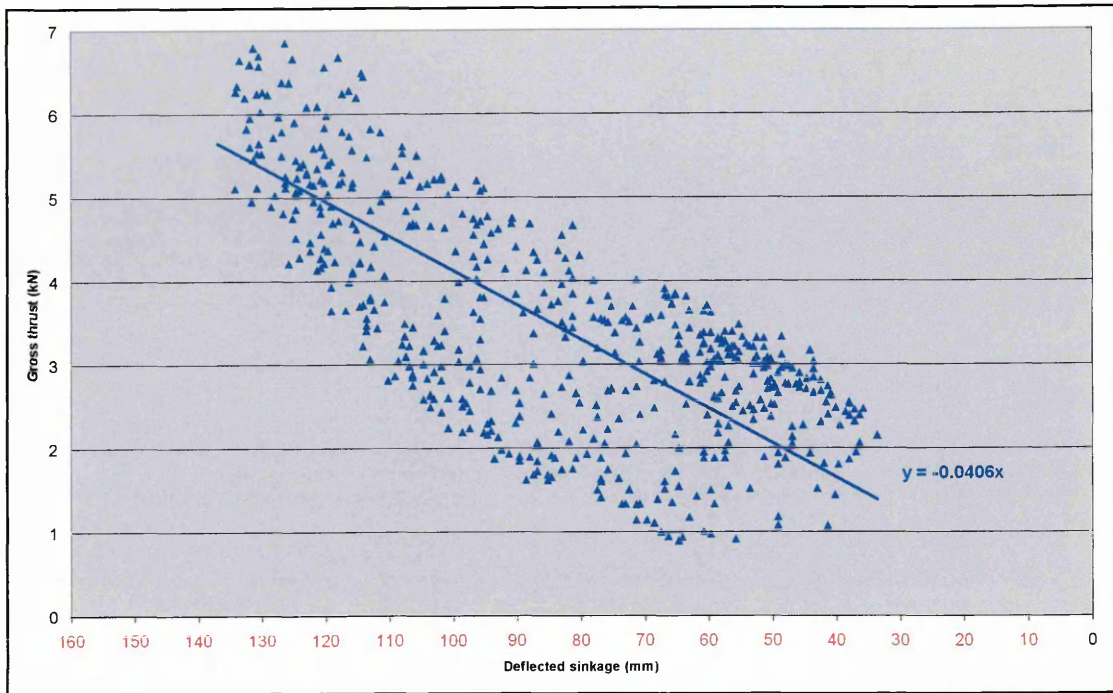


Gross thrusts achieved by the Diamaris tread during traction experiments

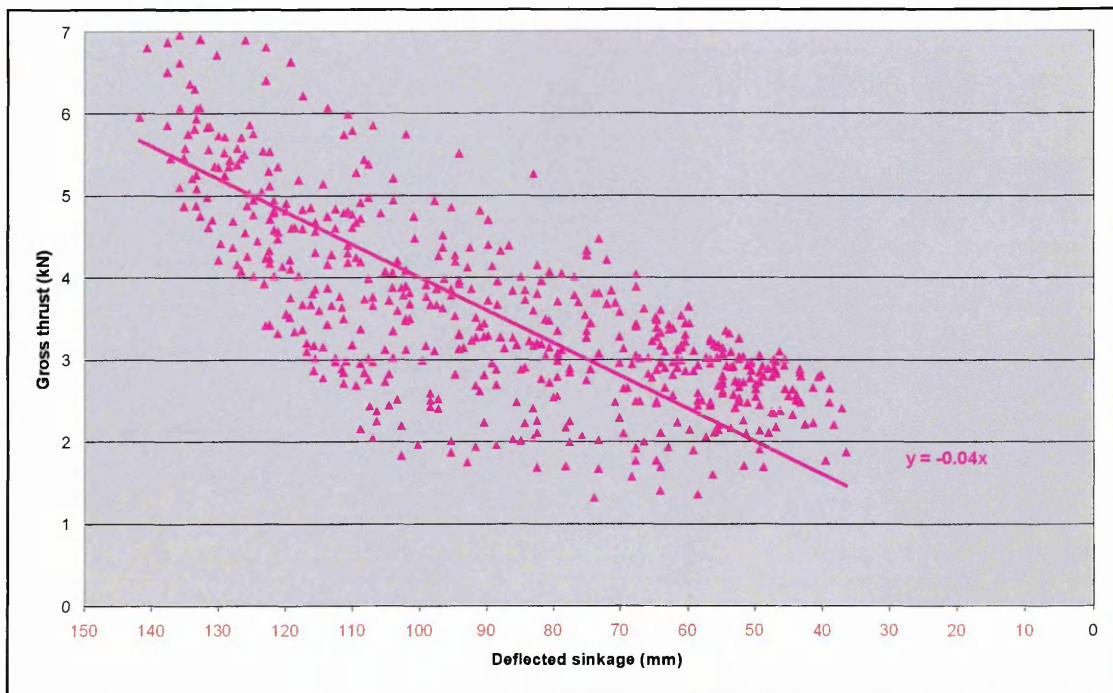
Again the gradients of these results were used to calculate the gross thrust benefits generated by each of these treads, relative to a larger diameter plain tread tyre. These results are shown on the table below:

Percentage extra gross thrusts achieved by the 255/55 R19 production treads

Tread Type	% Extra Gross Thrust
PT	0.00
DIAMARIS	3.85
HP	4.10
TG31	2.56



Gross thrusts achieved by the HP tread (255/55 R19) during traction experiments



Gross thrusts achieved by the TG31 tread during traction experiments

APPENDIX 26 – DISPLACED SAND VOLUMES

The calculation of the volumes of longitudinal sand displacement beneath the treads at each of the three replicates, for the eighteen treatments investigated, produced the results shown on the table below. As the volumes of longitudinal displacement were only measured under half of each tyre (tread), the mean volume had to be doubled to calculate the volume of displacement beneath a whole tyre.

Volume of Sand Displacement m ³						
Tread Slip	Rep 1	Rep 2	Rep 3	Mean	Total (2 x Mean)	
G82 L	0.0008	0.0010	0.0009	0.0009	0.00183	
45F L	0.0014	0.0011	0.0003	0.0009	0.00189	
LAT L	0.0011	0.0007	0.0012	0.0010	0.00207	
45B L	0.0006	0.0019	0.0007	0.0011	0.00212	
PT L	0.0013	0.0010	0.0012	0.0012	0.00230	
LON L	0.0014	0.0015	0.0008	0.0012	0.00248	
PT M	0.0010	0.0021	0.0010	0.0014	0.00276	
LON M	0.0014	0.0016	0.0017	0.0016	0.00311	
45F M	0.0009	0.0025	0.0013	0.0016	0.00311	
G82 M	0.0012	0.0014	0.0025	0.0017	0.00340	
LAT M	0.0015	0.0016	0.0023	0.0018	0.00352	
45B M	0.0016	0.0025	0.0017	0.0019	0.00389	
PT H	0.0026	0.0028	0.0022	0.0025	0.00508	
45B H	0.0045	0.0024	0.0038	0.0035	0.00710	
LON H	0.0050	0.0047	0.0036	0.0044	0.00887	
45F H	0.0053	0.0053	0.0033	0.0046	0.00922	
G82 H	0.0050	0.0045	0.0057	0.0051	0.01014	
LAT H	0.0039	0.0061	0.0058	0.0053	0.01056	

APPENDIX 27 – MODELLING NET THRUST RESULTS

All of the net thrust modelling was completed using models created in Excel. All of the models that produced the predicted sand performance results used in the thesis for comparison against net thrust results are included on the data CD in the following files:

235 45F on sand

235 45B on sand

235 G82 on sand

235 HP on sand

235 LAT on sand

235 LON on sand

235 PT on sand

235 UG on sand

255 DIA on sand

255 HP on sand

255 TG on sand